IAHR AIRH

International Association for Hydro-Environment Engineering and Research

Hosted by
Spain Water and IWHR, China

1st IAHR Young Professionals Congress

Online. 17 - 18 November 2020

Proceedings

Editors: José María Carrillo | Eva Fenrich
David Ferràs | Silke Wieprecht

IAHR YPN

Hosted by
Spain Water and IWHR, China

ISBN: 978-90-82484-6-63

The papers included in this volume were part of 1st IAHR Young Professionals Congress cited on the cover and title page. Papers were selected and subject to review by the editors and International Scientific Committee. The papers published in these proceedings reflect the work and thoughts of the authors and are published herein as submitted. The publisher is not responsible for the validity of the information or for any outcomes resulting from reliance thereon.

Proceedings of the 1st IAHR Young Professionals Congress

Online. 17-18 November 2020

Editors: José María Carrillo, Eva Fenrich, David Ferràs, Silke Wieprecht

Published by:

International Association for Hydro-Environment Engineering and Research -IAHR-

Pª Bajo Virgen del Puerto, 3 28005 Madrid, SPAIN

A-1 Fuxing Road, Haidian District, 100038, Beijing, CHINA

ISBN: 978-90-82484-6-63

IAHR publications follow the Ethical Guidelines and Codes of Conduct provided by the Committee of Publication Ethics (COPE).

IAHR, founded in 1935, is a worldwide independent member-based organization of engineers and water specialists working in fields related to the hydro-environmental sciences and their practical application. Activities range from river and maritime hydraulics to water resources development and eco-hydraulics, through to ice engineering, hydro informatics, and hydraulic machinery.
IAHR consists of two offices: Madrid Office, Spain and Beijing Office, China.

Table of contents

Foreword.....VIII

Session 1: Climate change adaptation

Data fusion of precipitation products based on triple collocation method.....11

Climate change projections and water level decrease in a brazilian multipurpose reservoir 13

The socio-quantitative analysis of water-energy-food-climate nexus in india 15

Influence of climate change on future water availability in the mapacho river sub-basin, Cuzco - Peru, using swat model abstract.....17

Caracterization of the variability of flows in the sub-basin of cirí grande, until the Cañones Hidrometric Station for the period (1988- 2017).....19

Analysis of recent climate change research on water resources in the Korean Peninsula.....21

Drought risk index for nationwide comparison in South Korea 23

Valorising driftwood transported by rivers from waste to an anode in sodium-ion battery.....25

The role of the agulhas system in the global climate by using the lagrangian.....27

Session 2: Fluvial hydraulics

A satellite-based analysis of the geomorphological efficiency of river plumes 30

Modelling erosion of pre-embankment breaches in coversand ridges in the Ijssel floodplain due to major flood events in medieval times.....32

Data-driven modelling of high flow-related poor water quality events in the mid-Brisbane river 34

A method for simulation of reactive solute transport in natural rivers 36

How good are 2D-morphodynamic models in reproducing bed morphology of meandering channels? Analyzing the strengths and limitations of three popular 2D models 38

Identification of contaminant source using truncated breakthrough curves in rivers.....40

Water quality modeling of Parana river, between the Yacyreta dam and its junction with the Paraguay river. 42

Vertically-integrated and moment equations for non-hydrostatic flow modelling Matlab platform.....44

Session 3: Hydroinformatics

Improving rainfall fields in data scarce basins: a comparison of downscaling, interpolation and merging schemes 47

Initial development of a citizen science-based river flood monitoring and forecasting for the Rimac River in Lima Peru ..49

Assessment of maximum storm precipitation changes over last decades 51

Phet platform to support the teaching of fluid mechanics during the covid-19 pandemic.....53

Analysis of the performance of a commercial software for pipe burst detection.....55

Gis based multicriteria decision analysis for flash flood hazard mapping using frequency ratio in Bavaria 57

Climatological analysis for the agroecological zoning of the peach tree in San Pablo de Pillao, Huánuco 59

A hydrodynamic model as input for a spatial planning tool. Case study: Delta of the Paraná river (Argentina). 61

Analysis of urbanization induced land cover change and impact on land surface temperature with landsat, modis and era 5 imagery.....63

Session 4: Urban drainage

Hydraulic model of stormwater drainage system using different methods for defining the catchment area 66

Computational fluid dynamics (CFD) study of the biological reactor of the wastewater treatment plant of Roldán, Lo Ferro and Balsicas (Spain) 68

Stochastic modeling of storm precipitation scenarios.....70

CDF model development and sensitivity analysis for water-air flow in a close conduit sewer pipe. 72

Comprehensive benefit assessments of green infrastructure 74

Comparison of urban basin application between gr4j (snu-cahl) and swmm.....76

An experimental study of sediment accumulation, erosion and transport processes in combined sewer pipes 78

Database design and graph-based analysis for swmm urban modelling 80

Experimental characterization of a permeable pavement using simulated rain.....82

Session 5: Water resources management

Water balance of the estibaná sub-catchment in Panama 85

Evaluating historical drought using different drought indices and data processing schemes 87

Application of the hydrological model mgb-iph at the Seridó river basin (Brazil).....89

Flow regulation by water reservoir for irrigation use 91

Characterization of meteorological droughts in continental ecuador during the period 1902-2017.....93

Modelling actual evapotranspiration using optimized enn methods 95

Departmentalization as a tool for water governance in The Philippines 97

Multi-objective optimal operation of cascade hydropower plants based on water-energy nexus: a water footprint

approach 99

Water budget using regional hydrological modelling and gis techniques in Peruvian Amazon: case study in Yuracyacu Watershed- Mayo river 101

Session 6: Coastal engineering and groundwater hydraulics

Numerical simulation of dissolved oxygen in coastal lagoons case study: El Gouna, Egypt 104

Developing an efficient modelling framework to evaluate nature- based solutions to counteract estuarine salt intrusion 106

Coastal area classification using total suspended matter concentration 108

Initial findings of microplastics concentration in three coastal environments: a case study in the Peruvian Coast 110

Dilution of plunging jets used for desalination brine disposal 112

Simulation of seawater intrusion area using feedforward neural network in Longkou 114

Vertically-averaged coastal flow modelling using moment equations 116

Coastal erosion in beaches of the coast of Buenos Aires, Argentina 118

Ground water depletion trends and the need for remediation in Punjab, India: 2000-2019. 120

Session 7: Sediment transport, experimental methods and instrumentation

Effects of land cover/use changes on the Ethiopian Fincha dam capacity 123

Les two-phase modelling of suspended sediment transport using a two-way coupled euler-lagrangian approach 125

Wastewater quality estimation through led spectrophotometry by means of statistical models 127

Comparing lidar with common free-surface measurement methods in aerated hydraulic jumps 129

Debris-flow susceptibility assessment using the index entropy model in the viso catchment 131

Experimetnal study on transport of microplastis in coastal sediment with an oscillating water tunnel 133

Influence of surge wave on carrying capacity and tranport of macroplastics 135

Balancing flushing efficiency and duration: proof of concepts 137

Efficiency of sediment flushing for different sediment mixtures 139

Session 8: Transient flows and hydraulic machinery

Study of turbulent structures and air entrainment patterns in surge waves 142

Numerical modal analysis of a Kaplan turbine runner 144

TSNet: transient simulation in water networks 146

Chasing transients in a water transmission main in Milan, Italy 148

A preliminary low-frequency pressure analyis towards high- frequency transients monitoring in the Padua water distribution system 150

Unsteady friction computation in commercial hydraulic software 152

The effect of the functioning conditions on the transient behaviour of a water distribution system: laboratory tests 154

A well-balanced non-hydrostatic pressure model for steady and unsteady shallow 156

Time reversal of waves in pressurized pipelines 158

Session 9: Flood risk management

Beyond inner slope instability: a method to quantify the residual dike strength by wave overtopping 161

Flood disaster and adaptation measures in Brisbane Australia 163

Statistical analysis of precipitation data for hydrological and hydraulic modeling of flash floods 165

Simulation of hydrological and morphodynamical processes in a mountain catchment of the Central Pyrenees 167

Evaluation of floodplains along the Danube in Austria with the floodplain evaluation matrix - comparison of 1D and 2D models 169

A procedure for human safety assessment during hydropeaking events 171

Assessment of land cover changes of Marikina watershed, Philippines to river Runoff and flooding 173

Coupled hydrodynamic and hydrologic modelling using telemac-2D 175

Optimization and visualization of numerical models of flash floods in steep Norwegian rivers 177

Session 10: Hydraulic structures

Measurement of void fraction and velocity profiles in rectangular free-falling jets 180

Influence of length of micro groins on bed morphology in a straight channel 182

The influence of berms and roughness on wave overtopping at rock- armoured dikes 184

Numerical modelling of impulse wave forces on dams 186

Experimental and numerical methods in investigations of sustainable deep scours as fish habitat 188

Damping of ship-induced waves in Groyne Fields 190

Energy dissipation for flow over the Gabion Weir 192

Level set based modeling of local scouring in the vicinity of a submerged arch bridge 194

Formulae to estimate peak effluent flows from brasilian dams break in 21th century 196

Session 11: Ecohydraulics

Estimating the resistance of a porous media that numerically represents a floating treatment wetland 199

Plastics in streams: transport dynamics and open questions 201

Tracking fish swimming behaviour in response to a vertical axis turbine 203

Bursting phenomena dowsntream aquatic plants growing in natural conditions 205

Eco-hydraulic impact of plastic flow over the mouth of the Magdalena river and adjacent beaches 207

Phytoremediation of contaminated soil with heavy metals applying Plateau native species: Fuerte Simalva Echinata and Lupinus Ballianus 209

Velocity profiles on a grass-lined spillway in supercritical flow 211

Attracting silver perch into a tube fishway: preliminary results 213

Hydro-environment 215

Least disturbed rivers in the altai mountains can reveal environmental guiding principles for Alpine Rivers: a case study from the Biya river 217

Session 12: Fluid mechanics

Concepts for performance improvements of shallow water flow simulations 220

Bottom gravity currents and stratified exchange flows in a rotating channel 222

Interaction of gravity currents with slopes and overhangs 224

The influence of a grid structure on hydraulic river modelling outcomes of schematised river meanders 226

Numerical study of meandering effect on confluence channel flow by Openfoam 228

A well-balanced dg scheme for the resolution of the shallow water equations 230

Turbulent flow structure upstream of an isolated boulder: implications for sediment deposition 232

Applicability of telemac-3D for fine-scale hydraulics 234

Optimization of the transport velocity for ale-sph scheme 236

Foreword

Humankind tends to adopt a negative vision of its reality; this is a defense and adaptation mechanism. We are living in a very dynamic world, constantly bombarded by the news media that daily reminds us how bad we are to the environment, to our overpopulated earth, how we have produced mass extinctions, global warming, deforestation… you name it! We are milking the earth. How we deal with nature is probably the cause of the 2020 pandemic. No doubt this has been a very dark year for humanity. Based on this logic, the Armageddon should be right at the corner. But this is not new, more than 200 years ago the demographer Thomas Robert Malthus stated human needs would soon outweigh the world's resources. Covid-19 may has struck us, nevertheless in 2021 the life expectancy almost doubles the one from Malthus' times. Science and technology made this possible, we have altered nature up to the point that we have called our period the Anthropocene. Yet, there is plenty of room for life in the Anthropocene and its quality highly depends on us, on how we address and how we deploy science and technology. These proceedings are just a sample of the world's youth caring and working for a better hydro-environment.

The context of 2020 has brought us the chance to develop and foster our skills on remote working. Many events have been postponed, others have gone online, and new initiatives have emerged. One of them has been the 1st IAHR Online Congress for Young Professionals, where 109 research contributions have been presented to an audience of 924 young researchers and practitioners connected from 88 different countries. Without the physical travelling constraints of the face-to-face congresses, the virtual congress enabled the exchange of scientific advance among the IAHR youth community at an unprecedented scale. Modern world problems related with the UN Sustainable Development Goals have been tackled in special sessions such as the one on Climate Change Adaptation, Water Resources Management and Global Water Security. A keynote lecture on the topic was also provided by Angelos Findikakis (IAHR Liaison to UN Water). The congress has also brought to light scientific contributions on the classic fields of hydraulics research, such as the ones presented in the special sessions on Fluid Mechanics, Fluvial Hydraulics or Hydraulic Structures. Even the newly created working group on Transient Flows has had a special session with great participation. Moreover, emergent disciplines like the ones on Ecohydraulics or Hydroinformatics have proved consolidation among the IAHR youth.

An International Scientific Committee (ISC) formed by 45 prestigious researchers representing the 19 IAHR Technical Committees have supported the congress with a high-quality peer-review process. The ISC members have been also involved as chairs moderating the congress sessions. Their role has been crucial to make lively discussions with authors and attendees, bringing added value to the extended abstracts and presented posters. Fostering mentoring by means of connecting IAHR senior researchers to young

professionals has been as well one of the aims of the congress. The benevolent willingness of the ISC members to help young professionals made this possible. The role of IAHR Madrid secretariat has been also decisive. They have provided the framework, as they always do, but this time the challenge was especial, the conference venue was virtual. From the conceptualization of the online congress idea until its final execution, passing by the peer-review platform, communications, venue and the present proceedings. The support from IAHR Madrid secretariat has been incalculable.

Hydro-environmental research and engineering does not understand of nationality nor age or gender, but unfortunately its development and deployment does depend on them. The organizers hope to have contributed on bringing these constraints down. We are taking a long list of takeaways out from this enriching first experience. We wish the proceedings readers to have a joyful read and hope to (e)meet you again in the next 2nd IAHR Online Congress for Young Professionals.

José María Carrillo, Eva Fenrich, David Ferràs and Silke Wieprecht

Editors

IAHR AIRH

International Association for Hydro-Environment Engineering and Research

Hosted by
Spain Water and IWHR, China

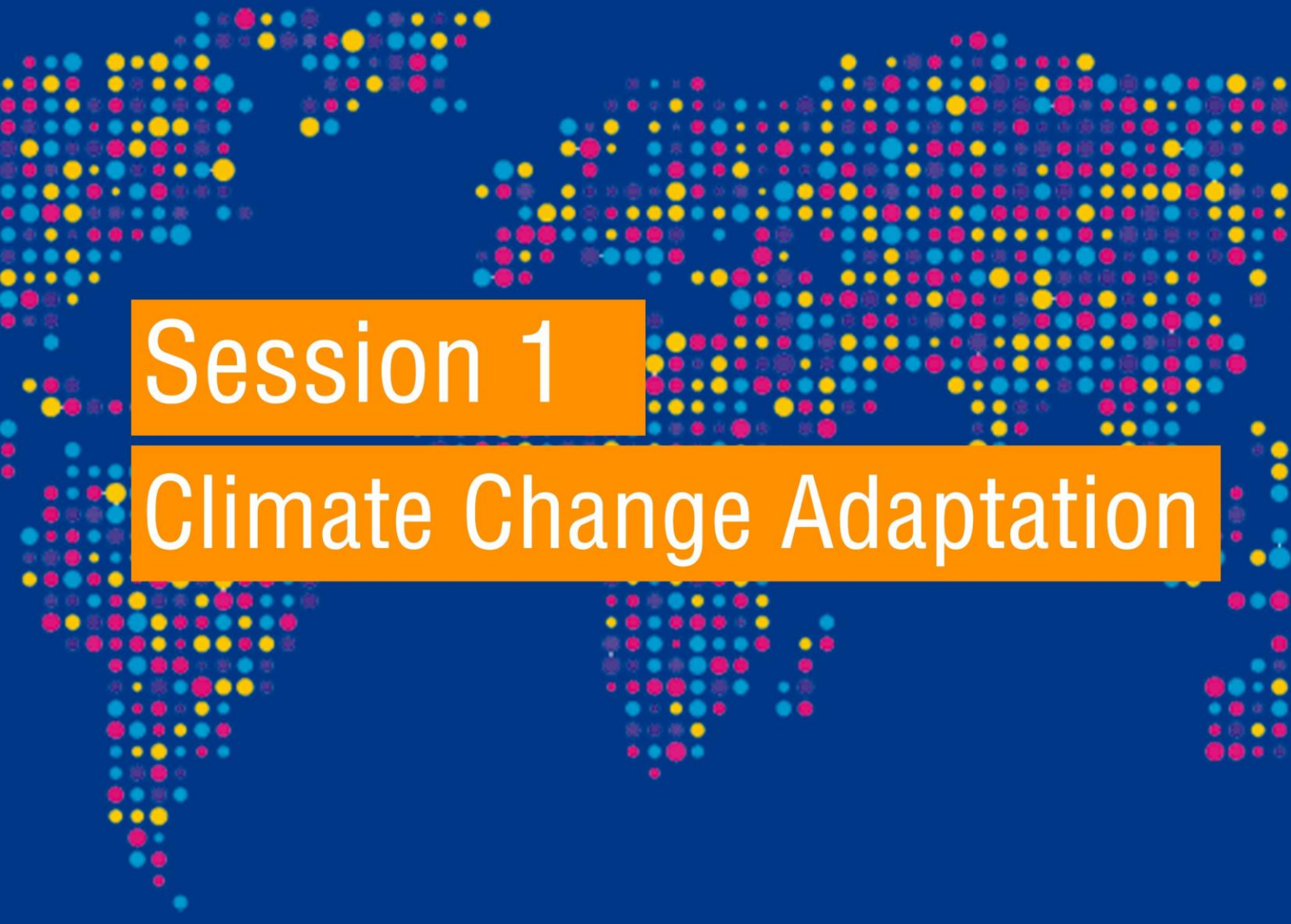

Session 1
Climate Change Adaptation

IAHR YPN

Hosted by
Spain Water and IWHR, China

Proceedings of the 1st IAHR
Young Professionals Congress
17-18 November 2020

DATA FUSION OF PRECIPITATION PRODUCTS BASED ON TRIPLE COLLOCATION METHOD

Chen Cheng [1,2]

[1] Center for Eco-Environmental Research, Nanjing Hydraulic Research Institute, Nanjing, China, e-mail (chencheng@nhri.cn)
[2] College of Water Conservancy and Hydroelectric Power, Hohai University, Nanjing, China

ABSTRACT

This study proposed a triple collocation (TC) method for data fusion of daily precipitation products (GPM IMERG, SM2RAIN and ERA) over Yangtze River basin from 2015 to 2018. The original precipitation products and data fusion result were validated using the rain gauge data. Results showed that the data fusion results by TC method had better performance compared to the original three collocated inputs, with large correlation coefficient (CC) and small root mean square error (RMSE). This study demonstrates the effectiveness and great application potential of TC method for data fusion to improve precipitation accuracy.

Keywords: triple collocation, data fusion, precipitation, Yangtze River basin.

1 INTRODUCTION

Accurate precipitation estimates are crucial for agricultural irrigation and flood prevention. Data fusion is critical to improving the accuracy of multiple precipitation observations for practical applications, however, it faces the challenge of poor ground-based observations, especially over the regions where reliable and dense rain gauge data is absent or unavailable. Triple collocation (TC) was originally proposed by Stoffelen (1998) to assess the error of ocean wind speed products, which provides an efficient way for error estimation without knowing the true value and thus has a potential for multiple-source data fusion, while it has not been well investigated. Compared to the traditional method (the rain gauge data was used as the ground reference to assess the error), TC method can quantify the errors in three independent products without knowing the true value (Alemohammad et al., 2015). Since TC method can solve the error statistics of three independent measurements without the reliance of gauge observations, it has the potential to be incorporated into data fusion/merging algorithms. However, there are very few studies on TC-based precipitation data fusion method (Lyu et al., 2020). To fill the aforementioned knowledge gap, this study conducted a comprehensive study on data fusion of three precipitation products based on TC method over Yangtze River basin.

2 MATERIAL AND METHODS

2.1 Study area and datasets

The Yangtze River basin was selected as the study area of this study. The Yangtze River basin is the largest river basin in China with a latitude of 24°30' -35°45' N and a longitude of 90°30'-124°30' E. The average annual precipitation is approximately 1100 mm. Three independent precipitation products at daily scale over Yangtze River basin from 2015 to 2018 were used in this study, including satellite-based 0.1° IMERG (Integrated Multisatellite Retrievals for Global Precipitation Measurement), reanalysis-based 0.25° ERA (the interim-European Centre for Medium-Range Weather Forecasts ReAnalysis), and soil moisture-based 10 km (~0.1°) SM2RAIN (Soil Moisture to Rain-Advanced SCATterometer) precipitation products. The 0.25° ERA data was resampled into 0.1° spatial grids to make it comparable. In addition, 737 rain gauge stations with daily precipitation measurements from 2015 to 2018 was also obtained and interpolated to 0.1° resolution for validation.

2.2 Methods

TC can be used to quantify the error variance of geophysical variables using three independent measurements without the requirement of ground references or “true values” (Lyu et al., 2020). TC method is

established based on the mathematical assumptions that three collocated variables have zero mean residual errors and are uncorrelated with each other and with the true values. More details can be found in Alemohammad et al. (2015).

A least squares based data fusion method was utilized to calculate the weight of each collocated estimate in this study. Based on the TC estimates, the basic function of data fusion is shown as follows:

$$\mathbf{P}_f = \omega_1\mathbf{P}_1 + \omega_2\mathbf{P}_2 + \omega_3\mathbf{P}_3 \quad s.t.\ \omega_1+\omega_2+\omega_3 = 1 \qquad [1]$$

$$\omega_1 = \frac{\sigma^2_{\mathbf{P}_2}\sigma^2_{\mathbf{P}_3}}{\sigma^2_{\mathbf{P}_1}\sigma^2_{\mathbf{P}_2} + \sigma^2_{\mathbf{P}_1}\sigma^2_{\mathbf{P}_3} + \sigma^2_{\mathbf{P}_2}\sigma^2_{\mathbf{P}_3}} \qquad [2]$$

$$\omega_2 = \frac{\sigma^2_{\mathbf{P}_1}\sigma^2_{\mathbf{P}_3}}{\sigma^2_{\mathbf{P}_1}\sigma^2_{\mathbf{P}_2} + \sigma^2_{\mathbf{P}_1}\sigma^2_{\mathbf{P}_3} + \sigma^2_{\mathbf{P}_2}\sigma^2_{\mathbf{P}_3}} \qquad [3]$$

$$\omega_3 = \frac{\sigma^2_{\mathbf{P}_1}\sigma^2_{\mathbf{P}_2}}{\sigma^2_{\mathbf{P}_1}\sigma^2_{\mathbf{P}_2} + \sigma^2_{\mathbf{P}_1}\sigma^2_{\mathbf{P}_3} + \sigma^2_{\mathbf{P}_2}\sigma^2_{\mathbf{P}_3}} \qquad [4]$$

where, $\mathbf{P}_i$ and ω_i (i=1, 2, 3) represent the *ith* precipitation estimate and weight of each collocated estimate, respectively; $\mathbf{P}_f$ is the desired fused precipitation estimation; $\sigma_{\mathbf{P}_i}$ represents the standard variance estimated by TC.

3 Results and discussion

Compared to IMERG data (Table 1), ERA and SM2RAIN had better performances. ERA had the largest CC and SM2RAIN had the smallest RMSE. It is because that the SM2RAIN approach is very good in obtaining low RMSE values owe to its capacity to accurately reproduce accumulated rainfall consistently over time. Data fusion results by TC method had better performance (CC=0.61, RMSE=6.11 mm) when compared to the original three collocated inputs. It indicates the effectiveness of the TC-based data fusion method.

Table 1. Validation results of original three collocated inputs and data fusion results obtained by TC.

Precipitation data	CC	RMSE (mm)
GPM IMERG	0.48	8.70
SM2RAIN	0.50	6.73
ERA	0.59	6.95
DATA FUSION BY TC	0.61	6.11

4 CONCLUSIONS

A comprehensive study on data fusion of multiple source precipitation products by TC method was carried out over Yangtze River basin from 2015 to 2018. ERA and SM2RAIN had better performances when compared to the GPM IMERG precipitation product. Data fusion results by TC method showed consistency with rain gauge data and had obvious improvement than the original three collocated inputs, demonstrating the effectiveness of TC method for data fusion of multiple precipitation products.

REFERENCES

Alemohammad, S. H., McColl, K. A., Konings, A. G., Entekhabi, D., Stoffelen, A. (2015). Characterization of precipitation product errors across the US using multiplicative Triple Collocation. *Hydrology & Earth System Sciences*, 12(2).

Stoffelen, A. (1998). Toward the true near‐surface wind speed: Error modeling and calibration using triple collocation. *Journal of Geophysical Research: Oceans*, 103(C4), 7755-7766.

Lyu, F., Tang, G., Behrangi, A., Wang, T., Tan, X., Ma, Z., Xiong, W. (2020). Precipitation Merging Based on the Triple Collocation Method Across Mainland China. *IEEE Transactions on Geoscience and Remote Sensing*.

Proceedings of the 1st IAHR
Young Professionals Congress
17-18 November 2020

CLIMATE CHANGE PROJECTIONS AND WATER LEVEL DECREASE IN A BRAZILIAN MULTIPURPOSE RESERVOIR

CAROLINA CERQUEIRA BARBOSA [1], LAURA MELO VIEIRA SOARES [1] & MARIA DO CARMO CALIJURI [1]

[1] Hydraulic and Sanitation Department, University of São Paulo at São Carlos School of Engineering, São Carlos, Brazil,
e-mail: carolina.cbarbosa@usp.br; laurasoares@usp.br; calijuri@sc.usp.br

ABSTRACT

Data from climate projections were used to analyze the possible climate change effects on the water level of a Brazilian multipurpose reservoir for the 2050s. Two scenarios based on optimistic (RCP 4.5) and pessimistic (RCP 8.5) climate change projections concerning greenhouse gas emissions were simulated using a one-dimensional hydrodynamic model. In comparison with the baseline simulation (2009-2018), it was identified water level decrease trends, especially regarding the rainfall reduction. Such behavior may affect water availability and impair the reservoir uses, which may also demand adaptive management strategies for the reservoir operation.

Keywords: Hydrodynamic modeling, climate change assessment, Itupararanga Reservoir, water resources management.

1 INTRODUCTION

Climatic extremes are already being reported worldwide (Reichstein et al., 2013). Data generated by regionalized climate models (RCM) have been used to assess likely impacts on local ecosystems and decision-making. In the present study, data from an RCM were used as input to a one-dimensional hydrodynamic model to compare probable water level fluctuations in a Brazilian multipurpose reservoir.

2 METHODS

2.1 Study site

Itupararanga Reservoir is located in an urbanized region in São Paulo State, Brazil, built for many purposes, mainly to drinking water supply and power generation. The reservoir surface area is 29.9 km² and the basin drainage area is 936.5 km². The regional climate is warm temperate with dry winter and hot summer (Cwa, Kottek et al., 2006).

2.2 Modeling procedure

The one-dimensional General Lake Model (GLM) (Hipsey et al., 2019) was used to simulate the water level of Itupararanga Reservoir. The model requires hydrological and meteorological data, reservoir's bathymetry and the water temperature and salinity in the reservoir and in its tributaries. Those data were provided by the energy company, and governmental agencies (INMET, 2019; CETESB, 2019).

The model was calibrated from 2009 to 2013 and validated from January 2014 to March 2019. A performance assessment was applied using the Root Mean Squared Error (RMSE) and the Pearson correlation coefficient(*r*).

Climate change projections from The Hadley Centre Global Environmental Model (HadGEM2-ES) regionalized by the ETA model (Chou et al., 2014) were coupled to GLM for generating scenarios from January 2050 to December 2059 for two representative concentration pathways (RCPs) of the greenhouse gases emissions (GHG): RCP 4.5 and RCP 8.5. Those data included: short-wave radiation (SW), air temperature (AT), air relative humidity (RH), wind speed (WS) and rainfall (rain). The baseline simulation (2009-2018) of water level was compared with the simulated projection (2050s decade) considering the alterations in all meteorological forcing variables and in each meteorological variable individually.

3 RESULTS AND DISCUSSION

The model was able to accurately represent the water level (RMSE<0.7m, *r*=0.8). Climate change projections revealed an increase in AT and SW and a rain decrease for the 2050s (Table 1).

In this way, the climatic trends influenced the reservoir's water level. The simulated water level would drop in both rain scenarios and for the set of all predicted climatic variables (Figure 1a). Such a decrease in the average water level (falling to the dead storage in the middle and the end of 2050s decade) (Figure 1b) could generate serious damage to the water supply and power generation. Uncertainties remain regarding lake levels fluctuations in the future, however it is certain that more climatic extremes will arise around the world (Woolway et al., 2020).

Table 1: Climate variables daily average and standard deviation for the baseline and future projections.

Meteorological Data	Baseline	RCP 4.5	RCP 8.5
SW (W m^{-2})	213.9 (61.2)	217.2 (59)	223.6 (51)
AT (°C)	20.6 (2.7)	22.3 (4.2)	23.6 (3.1)
RH (%)	75.2 (7.2)	85.3 (11.5)	73.3 (13.8)
WS (m s^{-1})	2.2 (0.8)	2.3 (0.8)	2.4 (0.6)
Rain (mm d^{-1})	3.2 (5.0)	2.5 (6.0)	1.9 (3.1)

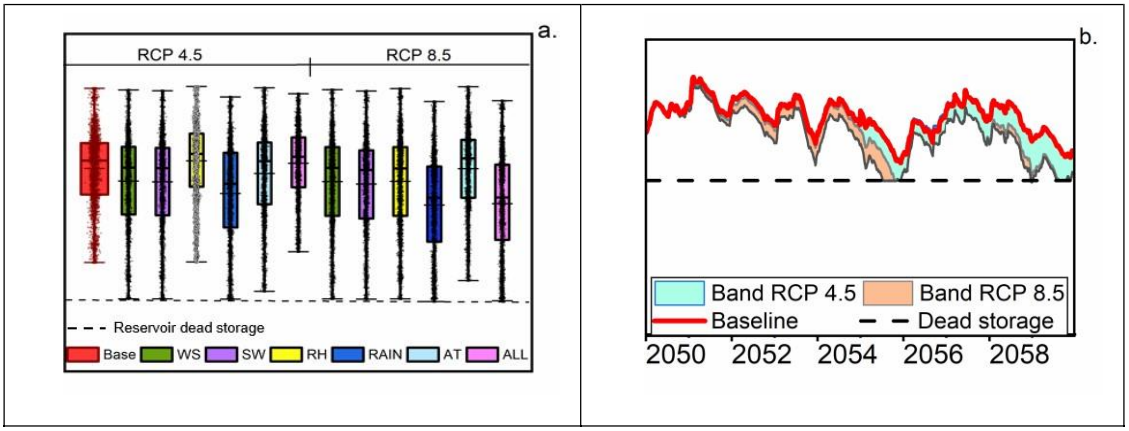

Figure 1: Simulated water level (m): a. Average value and outliers for each scenario; b. Minimum water level for climate change scenarios.

4 CONCLUSIONS

Data from climate change projection for the 2050s were coupled to the GLM model to compare water level simulations with a baseline. The projections indicate water level drop, which might require adaptive management strategies for reservoir operation to avoid possibility of water rationing in the near future.

ACKNOWLEDGEMENTS

We would like to thank INMET, UFSCAR and CETESB for the available data, and the Coordenação de Aperfeiçoamento de Pessoal de Nível Superior (CAPES) for the financial support.

REFERENCES

CETESB (2019). Infoáguas Database. https://sistemainfoaguas.cetesb.sp.gov.br/. (Accessed 25 Oct 2019).

Chou, S. C., Lyra, A., Mourao, C., Dereczynski, C., Pilotto, I., Gomes, J., Bustamante, J., Tavares, P., Silva, A., Rodrigues, D., Campos, D., Chagas, D., Sueiro, G., Siqueira, G., Marengo, J. (2014). Assessment of Climate Change over South Downscaling Scenarios. *American Journal of Climate Change,* 3, 512–27.

Hipsey, M. R., Bruce, L. C., Boon, C., Busch, B., Carey, C. C., Hamilton, D. P., Winslow, L. A. (2019). A General Lake Model (GLM 3.0) for linking with high-frequency sensor data from the Global Lake Ecological Observatory Network (GLEON). *Geosc. Model Development*, *12*(1), 473–523.

INMET (2019). Automatic monitoring stations. http://www.inmet.gov.br. (Accessed 06 Dec 2019).

Kottek, M., Grieser, J., Beck, C., Rudolf, B., Rubel, F. (2006). World map of the Köppen-Geiger climate classification updated. *Meteorologische Zeitschrift*, *15*(3), 259–263.

Reichstein, M., Bahn, M., Ciais, P., Frank, D., Mahecha, M. D., Seneviratne, S. I.; Wattenbach, M. (2013). Climate extremes and the carbon cycle. *Nature*, *500*(7462), 287–295.

Woolway, R. I., Kraemer, B. M., Lenters, J. D., Merchant, C. J., O'Reilly, C. M., Sharma, S. (2020). Global lake responses to climate change. *Nature Reviews Earth & Environment*, 1, 388–403.

Proceedings of the 1st IAHR
Young Professionals Congress
17-18 November 2020

THE SOCIO-QUANTITATIVE ANALYSIS OF WATER-ENERGY-FOOD-CLIMATE NEXUS IN INDIA

Purnanjali Chandra [1], KS Kasiviswanathan [2], B Soundharajan[3] & Claudia Teutschbein[4]

[1] Tata Institute of Social Sciences, Mumbai, India
chandrapurnanjali11@gmail.com
[2] Indian Institute of Technology, Roorkee, India
k.kasiviswanathan@wr.iitr.ac.in
[3] Amrita Vishwa Vidyapeetham, Coimbatore, India
bsoundharajan@gmail.com
[4]Uppsala University, Uppsala, Sweden
claudia.teutschbein@geo.uu.se

ABSTRACT

The climate change effects have been evolving as a global phenomenon with a major hurdle in accomplishing the sustainable management of resources and development. These require to be dealt with an integrated nexus approach rather than in silos. As the quantitative and policy analysis of climate change effects have often been discreetly handled in food-water-energy (FWE) sectors, this paper examines the climate change impacts on the nexus of FEW for suggesting viable solutions to mitigate the effects. The temporal and graphical data, stakeholder and policy analysis were utilized to make the comparison between the Global and Indian context mainly to provide a broader framework of solutions and also to establish the "global to local" connection.

Keywords: climate change, water-energy-food nexus, drought, biofuels

1 INTRODUCTION

The water, energy, and food (WEF) sectors are dynamically intertwined (Albrecht et al., 2018) with one another, where a rise or decline in consumption of one sector, impacts the other sectors simultaneously. They operate as the motor wheels of an engine and the "drivers" create friction posing serious challenges to the nexus goals fulfillment (Hoff, 2011).

Climate Change, is one of the most inevitable "drivers", that triggers major trade-offs within the WEF nexus dynamics subsiding the synergies of the system. The expanding population and rising demand for energy, water and food add to the menace. (Andrews-Speed et al., 2019). The work, thus, highlights on interlinking the understanding of water energy and food nexus with climate change, that will ensure better adaptation and water-energy-food resource security in India.

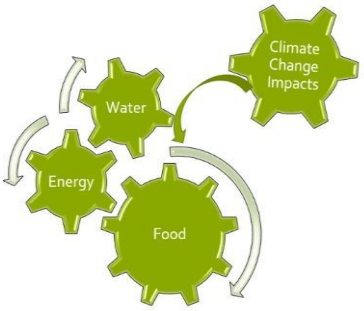

Figure 1. The water-energy-food nexus

It focuses on the complexities that arise on isolated approach to manage the challenges induced by climate change impacts on WEF nexus. There are multiple practices in India with regard to agriculture, drought mitigation methods or even ways of cutting down carbon emissions that are dealt in silos, thereby, aggravating trade-offs over synergies.

2 METHODOLOGY

The information obtained from reports, published articles, policy documents and literature on existing infrastructures were used to develop a comparative study on the nexus discourse between India and other nations. These components also aided in identifying the gaps of sectoral approach to resource management. The study distinctly highlights the extent of interconnectedness among the sectors of food,water and energy which is otherwise overlooked while managing losses or mitigating climate change impacts in India.

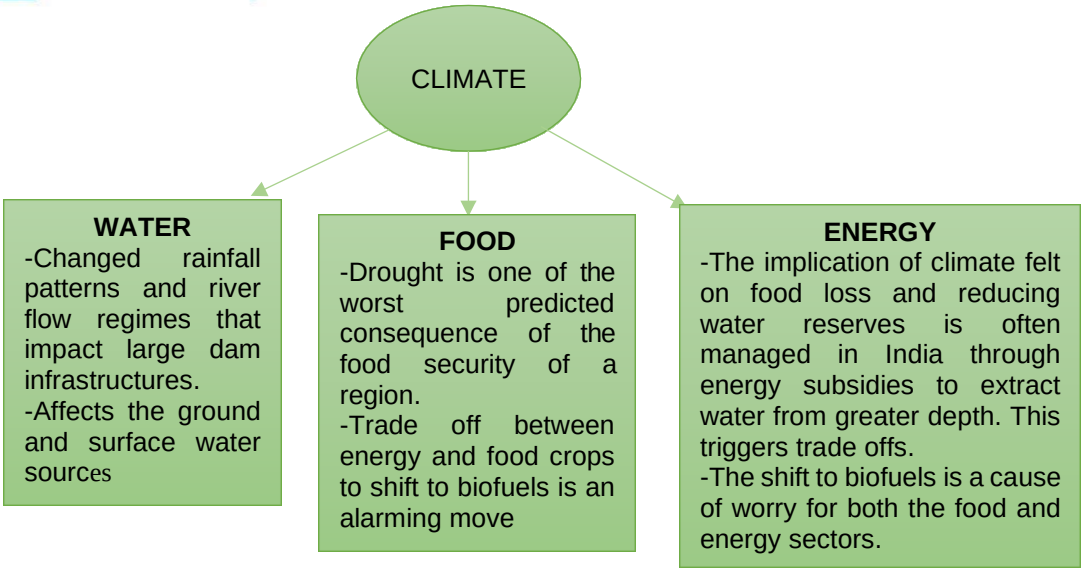

Figure 2. The water-food-energy-climate nexus

3 DISCUSSION

The work identifies some major gaps in the nexus approach for resource management in India. The policies such as the National Biofuel Policy, 2009, has a discrete approach to cut down on GHG emissions with a shift to first generation biofuels. However, in the Indian cotext, the introduction of flex crops like maize, used in other nations, can be a serious threat to the food and water security of a region. It, therefore, highlights the need for a cross-sectoral approach to sustainably utilize the huge river potential in India. With diverse geographic conditions and altered rainfall patterns, dams require an integrated management approach such that it caters to multiple needs for food,water, and energy, efficiently. It also reflects upon the importance of making the discourse of nexus more inclusive by enabling the stakeholders at the grassroots come up with their understandings. In India, such an approach to incorporate nexus idea, not just at the bureaucracy but also on ground, can enable its true implementation in WEF resource management and security.

4 SUMMARY

The work comments on mechanisms to strengthen cross-sectoral interactions in India and highlights policy modifications. It suggests a potential improvisation of ideas on green economy and infrastructures as well as stakeholder participation among other measures to adapt to climate change impacts on WEF nexus security.

ACKNOWLEDGEMENT

The first author would like to acknowledge the funding agency Swedish Research Council for supporting part of this work (Grant No: VR 2018-05848).

REFERENCES

Albrecht, T. R., Crootof, A., & Scott, C. A. (2018). The Water-Energy-Food Nexus: A systematic review of methods for nexus assessment. *Environmental Research Letters*, *13*(4). https://doi.org/10.1088/17489326/aaa9c6

Andrews-Speed, P., Zhang, S., Andrews-Speed, P., & Zhang, S. (2019). The Water-Energy-Food Nexus. *China as a Global Clean Energy Champion*, 215–243. https://doi.org/10.1007/978-981-13-3492-4_9

D'Odorico, P., Davis, K. F., Rosa, L., Carr, J. A., Chiarelli, D., Dell'Angelo, J., Gephart, J., MacDonald, G. K., Seekell, D. A., Suweis, S., & Rulli, M. C. (2018). The Global Food-Energy-Water Nexus. *Reviews of Geophysics*, *56*(3), 456–531. https://doi.org/10.1029/2017RG000591

Hoff, H. (2011). Understanding the Nexus. *Background Paper for the Bonn2011 Conference: The Water, Energy and Food Security Nexus.*, *November*, 1–52.

Rasul, G., & Sharma, B. (2014). *Water , Food , and Energy Nexus in South Asia : Implications for Adaption to Climate Change Why is Nexus-Based Adaptation*

Proceedings of the 1st IAHR
Young Professionals Congress
17-18 November 2020

INFLUENCE OF CLIMATE CHANGE ON FUTURE WATER AVAILABILITY IN THE MAPACHO RIVER SUB-BASIN, CUZCO - PERU, USING SWAT MODEL ABSTRACT

Yaranga Lázaro, David[1,2], Espinoza Varillas, Kithner [3,4] & Jiménez Yanasupo, Andrés [5]

[1] *Master's Programme in Water Resources – National Agrarian University La Molina, Lima, Peru,*

[2] *National Meteorological and Hydrological Service Peru, Lima, Peru,*
davidyar7@gmail.com

[3] *Master's Programme in Water Resources –National Agrarian University La Molina, Lima, Peru,*

[4] *Scientific Research Assistant at the Geophysical Institute of Peru, Lima, Peru,*

alfonso.e08@gmail.com

[5] *Faculty of Agricultural Engineering – National Agrarian University La Molina, Lima, Peru,*
andresjimenezy310@gmail.com

ABSTRACT

The study analyzed the impacts of climate change on future water availability in the Mapacho river sub-basin, Cuzco - Perú; evaluating three different global climate models (GCM) CSIRO.Mk3.6.0, GFDL-ESM2M and MIROC5 under emission scenarios RCP4.5 and RCP8.5. This approach used the Soil and Water Assessment Tool (SWAT), simulating the daily discharge in two scenarios: near future (2020-2050) and far future (2070-2100). The statistics show an acceptable performance in the calibration period (NSE = 0.68, RMSE = 13.5 and PBIAS = 1.5%) and validation (NSE = 0.64, RMSE = 27.44 and PBIAS = -18.3%). It is concluded that the annual discharges, for the near future period, present a variation from -14.4 % to 14.30% and from -7.55% to 19.89%, for RCP4.5 and 8.5, respectively.

Keywords: Water availability, Climate change, PISCO v.2.1, Flows, SWAT.

1 INTRODUCTION

Climate change proves to be the most complex problem for societies in the next years, due to the significant impacts on flow regimes. Its incidence would exacerbate the current water availability problem that affects different exploitation activities. Soto et al. (2010), shows that during the years 2000 and 2010, 163 drought events were recorded in Peru, of which 78% occurred on the coast, 15% in the highlands and 7% in the jungle, reflecting the first impact of climate change.

2 OBJECTIVE

Evaluate the impact of climate change on the future water availability of the Mapacho River Sub-basin, using SWAT modeling considering two scenarios: near future (2020-2050) and far future (2070-2100).

3 MATERIALS AND METHODS

3.1 Study area

The Mapacho River Sub-Basin is a tributary of the Urubamba River with an extension of 5496.6 km², it is located between an altitude from 494 to 5988 masl and located between 12.32º and 13.85º of South latitude and 71.06º and 72.87º of West longitude. The average annual discharge (2007-2018) in the headwater of the sub-basin (Paucartambo hydrological station) is 35.98 m3/s, a high water period between the months of December to April, with an average flow of 64.67 m3/s and a low water period in the months of May to November, with an average flow of 15.49 m3/s.

3.2 Data

3.2.1 Observed , gridded climatological information and Hydrometric

There were a total of 21 meteorological stations distributed in the Mapacho River Sub-Basin. Likewise, were used the monthly gridded information PISCO-Precipitation v2.1 and maximum and minimum temperature

v1.1, with a spatial resolution of 0.1 ° (10km).(Aybar et al., 2019).
GCM data download (P, T.max, T.min) was performed from NASA's NEX database. Of the 21 CMIP5 models downloaded, 3 of them were selected considering the representativeness of precipitation and temperature with respect to the historical PISCO data; for two scenarios (RCP 4.5 and RCP 8.5), with a resolution of 0.25º (25km - 25km). Spatial scaling of the GCM using IDW interpolation, selection of the GCM based on the RMSE and R2 indicators, and correction of the bias of the selected GCMs (Shrestha M. 2015). Hydrometric information for the calibration and validation process covers the period 2008 -2018.

3.2.2 DEM, Land Use and Soil Type

The DEM was downloaded from the Geoserver of the Ministry of Environment of Peru. The vegetation cover was downloaded from GlobeLand30 (Chen et al., 2015), 30 meter resolution and the soil map used was from FAO (Food and Agriculture Organization of the United Nations), year 1995 at a scale of 1:5 000 000.

3.3 Methodology

SWAT Hydrological Model
SWAT (Neitsch, Arnold, Kiniry, & Williams, 2011) or Soil and Water Assessment Tool. It is a model of a river basin in continuous and semi-distributed time. The process of uncertainty analysis, automatic calibration and validation of the model was used SWATcup (Abbaspour et al., 2015).
The efficiency of the model will be evaluated considering statistics such as the Nash-Sutclife efficiency method (NSE), the percentage bias method (PBIAS) and the RSR method by RMSE-Observations Standard Deviation. According (D.N. Moriasi et al. 2007) estimated as satisfactory if NSE> 0.5, RSR≤0.70 and PBIAS = ± 25% for flow and NSE> 0.5, RSR≤0.70 and PBIAS = ± 55% for sediment.

4 RESULTS

For the months of December to March (high water period), discharges were obtained for RCP 4.5 in the near and far future, variations ranging from -12.3% to 7.1% and from 7.4% to 10.8%, respectively; while for the months of April to November (low water period), discharges were obtained in the near and distant future, variations from -17.5% to 54.7% and from -16.4 to 18.9%.
On the other hand, in RCP8.5 in the wet season, discharges were obtained in the near and fur future, variations ranging from -6.7% to 19.9% and from -24.1% to 90.9%, respectively; while for the dry season the variations in the near and distant future were from -5.8% to 25% and from -5.7 to 132.1%.

5 CONCLUSIONS

The projections of annual discharges in the far future for RCP 8.5 indicate a probable increase of 15.58% to 99.2% in the water supply, while in the wet season variations from 24.1% to 90.9% could be obtained, which it could cause possible floods. However, for RCP 4.5 the annual discharges in the near and far future are very varied, that is, there would be variations that could generate underestimations or overestimations with respect to the historical flow period (2008-2018), in the order of -14.14 to 14.30% and -11 to 11.43, for the near and distant future, respectively.

REFERENCES

Abbaspour, K. C., Rouholahnejad, E., Vaghefi, S., Srinivasan, R., Yang, H., & Kløve, B. (2015). A continental-scale hydrology and water quality model for Europe: Calibration and uncertainty of a high-resolution large-scale SWAT model. *Journal of Hydrology*. https://doi.org/10.1016/j.jhydrol.2015.03.027

Aybar, C., Fernández, C., Huerta, A., Lavado, W., Vega, F., & Felipe-Obando, O. (2019). Construction of a high-resolution gridded rainfall dataset for Peru from 1981 to the present day. *Hydrological Sciences Journal*. https://doi.org/10.1080/02626667.2019.1649411

Chen, J., Chen, J., Liao, A., Cao, X., Chen, L., Chen, X., … Mills, J. (2015). Global land cover mapping at 30 m resolution: A POK-based operational approach. *ISPRS Journal of Photogrammetry and Remote Sensing*. https://doi.org/10.1016/j.isprsjprs.2014.09.002

D. N. Moriasi, J. G. Arnold, M. W. Van Liew, R. L. Bingner, R. D. Harmel, & T. L. Veith. (2007). Model Evaluation Guidelines for Systematic Quantification of Accuracy in Watershed Simulations. *Transactions of the ASABE*. https://doi.org/10.13031/2013.23153

Neitsch, S. ., Arnold, J. ., Kiniry, J. ., & Williams, J. . (2011). *Soil & Water Assessment Tool: Theoretical Documentation Version 2009*. *Texas Water Resources Institute, TR-406*. https://doi.org/10.1016/j.scitotenv.2015.11.063

Shrestha M. (2015). Data analysis relied on Linear Scaling bias correction (V.1.0) Microsoft Excel file.

Proceedings of the 1st IAHR
Young Professionals Congress
17-18 November 2020

CARACTERIZATION OF THE VARIABILITY OF FLOWS IN THE SUB-BASIN OF CIRÍ GRANDE, UNTIL THE CAÑONES HIDROMETRIC STATION FOR THE PERIOD (1988-2017)

OMAR JESÚS PÉREZ BOUTET

[1,3] Universidad de Panamá , Chiriquí, Panamá
Ing.op12@hotmail.com

ABSTRACT

The need of the Panama Canal Authority, to guarantee the existence of water resources for the operation of this global business, makes it necessary to deepen hydrological studies so that they allow a more precise knowledge of the contributions of all water sources available, for this reason the characterization of flow variability was carried out, which is a tool that allows, through a set of analysis of its daily, monthly or annual flows.
For this hydrological study, methodologies recommended by the Department of Hydrometereology of ACP were followed, which included aspects of the geomorphological part of the study area, to be able to characterize the different general parameters of the basin.
As results we can point out that for the 1988-2017 study period, the forest cover has been improved (%), and it was possible to verify that the existing data on the water contributions is reliable, therefore the water performance of the sub-basin of Cirí Grande is stable.

Keywords: Hydrology, Panama Canal Basin, Cirí Grande Sub-basin, Flow variability, Geomorphology.

1 INTRODUCTION

One of the various changes in water behavior that occur in a basin or sub-basin are the variabilities of the different flows, for that the Los Cañones Hydrometric Station has been selected, belonging to the sub-basin of the Cirí Grande River, to which the will carry out a hydrological study in a period of 30 years (1988-2017). In Panama, there are various problems related to the availability of water resources due to climate-related factors (Climate Change, Climate Variability such as ENSO, Deforestation and Burning), all this has been caused by anthropogenic problems in a higher percentage, which brings with it climate change that is reflected over the years, in such a way that we are affected as human beings, and most of the hydrological processes, fauna and flora are also being affected.
The increases in river flows can be due to extreme events (La Purísima-2010 and Huracán Otto-2016), which have consequences in the morphometric part of the riverbed.
It was established that in order to classify the wet, average and dry years, the average flow of the multi-year flow group must be taken into account, and then proceed to calculate the standard deviation, and through the ranges that result from these, the can say that if the flows exceed the deviation (+) they are wet years, if they are below the standard deviation (-) they are considered to be dry years, but if the flows remain within the range of the deviations (±), they are average years (Castañeda, O. 1984).
In the Cirí Grande-Los Cañones Hydrometric Station sub-basin, it was determined that there are three wet years (1996, 2016, 2017), and only two dry years resulted (1997, 2015), and the rest were average years.

2 MATERIALS AND METHODS

The compilation of hydrometerological information to carry out this work was obtained from the database of the Operational Hydrology Unit, Water Resources Section, Vice Presidency of Water and Environment, Panama Canal Authority, which is based on the methodology of the Practical Guide of the World Meteorological Organization No. 168, and that of the United States Geological Survey.

3 PARAMETERS AND VARIABLES TO ANALYSE IN THE HYDROLOGICAL STUDY

3.1 Basin morphometry

i. General parameters of the Basin.
ii. Basin shape parameters.
iii. Relief parameters.
iv. Drainage parameters
v. Flow analysis
vi. Rainfall analysis

3.2 Hypsometric curve

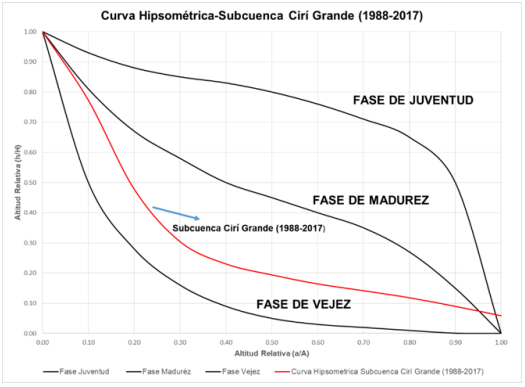

4 CONCLUSIONS

According to the analyzed flow and rainfall data, they show that the Cirí Grande sub-basin is very stable in the hydrological part from the year 1988-2017.
It is a sub-basin with an elongated shape, where its concentration times are fast, which indicates that the water quickly infiltrates the subsoil, and the runoff occurs in the same fast way, continuing the entire process of the hydrological cycle.

REFERENCES

ACP (Autoridad del Canal de Panamá, Panamá). 2010. Agua y Bosques en la Cuenca del Canal: Tendencias a Largo Plazo. Ciudad de Panamá, Panamá. 106 p.

Bermúdez, F. Díaz, A. (1987). Morfometría de Redes Fluviales: Revisión Crítica de los Parámetros más utilizados y aplicación al Alto Guadalquivir. Consultado: 29 de julio de 2019. Disponible en: https://revistas.um.es/geografia/article/view/42391/40741

CICH, 2008. Plan de Manejo de las Subcuencas Cirí Grande y Trinidad. Consultado: 5 de abril de 2019. Disponible en: http://www.cich.org/Publicaciones/05/vol-iii-plan-de-manejo-ciri-grande-2008.pdf

Proceedings of the 1st IAHR
Young Professionals Congress
17-18 November 2020

ANALYSIS OF RECENT CLIMATE CHANGE RESEARCH ON WATER RESOURCES IN THE KOREAN PENINSULA

Ji Heun Kim [1], Jae Kyoung Lee [2] & Young-Oh Kim [3]

[1,3] Dept. of Civil and Environmental Engineering, Seoul National University, Seoul, Korea
e-mail: wlgms94@snu.ac.kr [1], yokim05@snu.ac.kr [3]
[2] Innovation Center for Engineering Education, Daejin University, Pochoen-si, Gyeonggi-do, Korea
e-mail: myroom1@daejin.ac.kr

ABSTRACT

With a significant role of uncertainty in future climate change projection, the results may vary according to the choice of General Circulation Models (GCMs), Regional Circulation Models (RCMs) and downscaling methods. Thus, analyzing the ensemble of climate change simulation results is essential to make an inclusive decision-making. In this study, by filtering 13 Korean domestic journals and reports according to keywords and titles from 2014 to 2019, total of 161 pieces of research are chosen. Keywords treated in the research are classified into 3 groups: atmospheric variables, hydrologic variables, and environmental groups. Afterwards, the results were sorted into 4 chapters: (1) Observed Changes and their Causes, (2) Future Climate Change, Risks and Impacts, (3) Primary Causes of Future Vulnerability, and (4) Adaptation Options. Agreement on the results were derived into 3 scales: Substantial Agreement (SA), Moderate Agreement (MA), and Restricted Agreement (RA). Research trends of each chapters are also presented.

Keywords: climate change, flood, drought, uncertainty, adaptation, Korea climate change assessment report

1 INTRODUCTION

The role of uncertainty concept is significant in climate change science (Wilby and Harris,2006; Kay et al., 2009). For instance, future projection results vary by the choice of General Circulation Models (GCMs), Regional Circulation Models (RCMs) and the downscaling methods. Hence, gathering and analyzing the ensemble of climate change research results in the Korean peninsula is crucial for inclusive decision-making. Korea Ministry of Environment (ME) and Korea National Institute of Environmental Sciences (NIER) have organized expert groups, gathered climate change research in various fields. Consequently, the outcomes were published under the name of 'Korea Climate Change Report' in 2010, 2014 (ME and NIER, 2010; ME and NIER, 2014). To summarize the latest research results, a total of 161 pieces of recent studies published from January 2014 to June 2019 were used in this study. The objective of this study is to analyze the results, provide the research trends and the agreement of the results.

2 METHODS

To filter the appropriate research of 13 Korean domestic journals and numerous reports published from January 2014 to June 2019, keywords and titles were used. Then the variables dealt within the research are classified into three groups: atmospheric variables, hydrologic variables, and environmental variables. Results of these variables were then classified into four chapters: (1) Observed Changes and their Causes, (2) Future Climate Change, Risks and Impacts, (3) Primary Causes of Future Vulnerability, and (4) Adaptation Options. To evaluate the agreement level of the results, three criteria are used: Substantial Agreement (SA), Moderate Agreement (MA), and Restricted Agreement (RA).

3 Result

3.1 Research trends

The overall research trends are as follows. In 'Observed Changes and their Causes', rainfall data were analyzed with statistical trends, spatial-temporal variability of evapotranspiration was analyzed with remote sensing and flux-tower data. Verifying new drought indicators or to combine numerous hydrological and meteorological drought indicators were mainly proceeded in drought studies. Stochastic modeling was used to assess the increase in probable rainfall, design flood. The expected damage of flood was estimated by using occurrence scale and flood frequency concepts.
In the 'Future Climate Change, Risks and Impacts' chapter, almost all the studies have applied the Representative Concentration Pathways (RCP) instead of Special Report on Emission Scenario (SRES) according to the Intergovernmental Panel on Climate Change (IPCC) 5th Assessment. The number of drought research has surpassed that of the flood, uncertainty assessment research has grown rapidly. In the 'Primary Causes of Future Vulnerability' section, flood vulnerability research has been widened to include regional vulnerability due to sudden floods in creeks, mountain areas, and urban flooding. Decision-making research has occupied most of the portion in 'Adaptation Options', still more active research and meaningful information were required.

3.2 Agreements on the results

Annual precipitation has generally increased; summer rainfall has clearly increased, along with the frequency of extreme rainfall over the past thirty years (SA). The maximum rainfall, probable rainfall, design rainfall, and extreme rainfall were projected to increase (SA). Future discharge tends to increase in general particularly in summer (MA) where evaporation also expected to increase (MA). Also, both the frequency and intensity of the future flooding were likely to grow (MA). The frequency and scale of drought will generally increase in the future, in particular, drought damage was projected to exacerbate in the Han River and the southern part of the country (MA). Research on river water pollution has been conducted in some areas, showing that the water pollution will increase in general (RA). However, the uncertainty increased as the projection time period increased, hence the result varied (SA).

4 Conclusion

By gathering the climate change water resource studies from 2014 to 2019 in the Korean peninsula, common results of the research are presented in three agreement scales. Furthermore, research trends are also given. Precipitation continues to increase and the risk of flooding and drought continues to rise on the Korean peninsula. Compare to the prior two climate change reports which are limited to projecting the future possible flood and drought, research topics have become more various and the amount of vulnerability, risk assessment studies have increased. As the series of 'vulnerability analysis-vulnerability projection-decision making' process settled down in water resource fields recently, more balanced studies are encouraged.

REFERENCES

Kay, A.L, Davies, H.N, Bell, V.A, and Jones, R.G. (2009). Comparison of uncertainty sources for climate change impacts: Flood frequency in England, *Climatic Change*, 92(1-2), 41-63.

Ministry of Environment (ME), National Institute of Environmental Research (NIER). (2010) Korean climate change assessment report 2010 (in Korean).

Ministry of Environment (ME), National Institute of Environmental Research (NIER). (2014) Korean climate change assessment report 2014 (in Korean).

Wilby, R.L, and Harri, I. (2006). A framework for assessing uncertainties in climate change impacts: Low-flow scenarios for the River Thames, *Water Resources Research*, 42(2), 02419, doi:10.1029/2005WR004065.

Proceedings of the 1st IAHR
Young Professionals Congress
17-18 November 2020

DROUGHT RISK INDEX FOR NATIONWIDE COMPARISON IN SOUTH KOREA

Heewon Jee [1], Young-Oh Kim [2], Tae-Ho Kang [3] & Daeho Kim

[1,2] Seoul National University, Seoul, Republic of Korea,
heewon.jee@snu.ac.kr [1], yokim05@snu.ac.kr [2], bigtiger94@snu.ac.kr [4]
[3] Kongju National University, Kongju, Republic of Korea,
kangth@kongju.ac.kr [3]

ABSTRACT

Drought indices for the assessment of the potential hazard have been developed focusing on meteorological drought. However, these indices do not reflect the social aspects parting of socio-economic drought. To deal with this problem, we considered the factor of society and recommended the Drought Risk Index (DRI). DRI is comprised of three components, which are hazard, exposure, and capacity. Hazard is computed by climate characteristics (e.g. monthly precipitation), while Exposure depends on the water demand of agricultural, industrial, and municipal sectors. Capacity is divided into adaptive and coping capacities. DRI was conducted for regional comparison and projection for future DRI performed using HadGEM3-RA under RCP 4.5 and 8.5. In conclusion, the highest drought risk appears near the metropolitan area in the entire 21st century.

Keywords: drought, drought risk assessment, hazard, exposure, capacity

1 INTRODUCTION

Since drought risk is difficult to evaluate quantitatively, the conceptual model has applied for drought risk assessment. The relative comparison of risk is essential to determine the priorities of the region for disaster management. Drought damage caused by climate change is increasing worldwide. The frequency of droughts, in South Korea, increased from 0.36 times per year (1904~2000) to 0.72 times per year (2001~2018). In 2015, the Boryeong dam recorded the lowest storage level, and the Chungnam Province delivered emergency water supplies. Moreover, more than 9,000 people suffered from limited and transported water supplies in 2019. For managing drought, International expert institutions, such as World Meteorological Organization, National Drought Mitigation Center, are stressing to understand disaster risk. However, the government of South Korea is not considered the concept of risk actively. Therefore, this study conducts new drought risk assessment focusing on the suitability for regional comparison and the clarity for improving the awareness of people.

2 METHODOLOGY

2.1 Drought risk assessment

In this study, drought risk defines as the probability of potential damage causing drought affected by climate change and categorizes to three indicators, hazard, exposure, and capacity. First, hazard indicates the causation for drought and explains using drought index such as the standardized precipitation index (SPI) and Palmer Drought Severity Index (PDSI). Exposure is the objects (e.g. people, assets) exposed to drought. Lastly, capacity means the ability of society to cope with or adapt drought.

2.2 Drought risk index

Applied the drought risk assessment, Drought Risk Index (DRI) is the result to clearly show the comparison between the regions. DRI ranging from 0 to 1 is conducted using Eq. [1] where H, E, and C, presenting the indicators of risk, calculated by the representative components. The three indicators are multiplied and if one value of the indicator is 0, it means that there is no risk.

$$\mathrm{DRI} = f(H, E, C) = H^{1/3} \times E^{1/3} \div C^{1/3} \qquad [1]$$

3 APPLICATION

3.1 Data

The drought risk assessment is applied at 113 basins in South Korea and collects the 22 data sets. In hazard indicator, precipitation is single components and calculates to SPI, proposed by Mckee et al. 1993, with 12 months for long term drought. Additionally, for predicting future drought risk, HadGEM3-RA based on RCP 4.5 and 8.5 is used. And the exposure indicator is derived from the water demand to use (municipal, agricultural, and industrial). Lastly, socio-economic data for the local government are used for capacity indicator. Coping capacity is using water resources infrastructure data (e.g. emergency water supply facilities, multi-regional and local water supply system, dam and reservoir storage) and adaptive capacity is socio-economic status and ability (e.g. per capita personal income, financial self-reliance ratio, research and development costs, gross regional domestic product).

3.2 Weight

To improve the validity of DRI, each component is assigned the weight using the method of Kim et al. 2019. This method conjugates Pearson correlation coefficients between the components and disaster damage. Due to the complexity of figuring out the drought damage, the Water Deficit Ratio (WDR) used to assume the quantify the drought damage in this study. WDR means the ratio of the supply against demand, therefore explains the quantity of water use. In this method, the higher the correlation, the higher the weight. The weight range from 1 to 7 through trial and error.

4 RESULTS AND CONCLUSIONS

The past period DRI is verified with Spearman correlation analysis. The results of future DRIs are shown in Table 1 and Table 2. Under RCP 4.5, the mean of future DRI will increase only in the early 21st century and then decrease in the further future. While under RCP 8.5, the future DRI in mid 21st century is higher than past period DRI. Although the mean of future DRIs increases or decreases according to the future period, it is confirmed that the all maximums of future DRIs are higher values than in the past period. For the spatial comparison, the increasing trend indicates the regions near the metropolitan cities including Seoul, while the decreasing trend shows near the southeast area of South Korea.

Table 1. Future DRI statistics and ratio against past DRI with HadGEM3-RA under RCP 4.5

	PAST	2030	2050	2080
MEAN	0.7014	0.7203 (+2.69%)	0.6632 (-5.45%)	0.6869 (-2.07%)
MAX	0.8240	0.9509 (+15.40%)	0.8289 (+0.59%)	0.8761 (+6.43%)

Table 2. Future DRI statistics and ratio against past DRI with HadGEM3-RA under RCP 8.5

	PAST	2030	2050	2080
MEAN	0.7014	0.6948 (-0.94%)	0.7206 (+2.74%)	0.6813 (-2.87%)
MAX	0.8240	0.9219 (+11.88%)	0.9275 (+12.56%)	0.8643 (+4.89%)

REFERENCES

Daeho, Kim., Young-Oh, Kim., Hee Won, Jee., and Tae-Ho, Kang. (2019). Development of index for flood risk assessment on national scale and future outlook. J. Korea Water Resour. Assoc., 53(5), 323-336.

Mckee, T.B., Doesken, N.J., and Kleist, J. (1993). The relationship of drought frequency and duration to time scale. *In Proceedings of the 8th Conference on Applied Climatology,* 17(22), 179-183.

Proceedings of the 1st IAHR
Young Professionals Congress
17-18 November 2020

Valorising driftwood transported by rivers from waste to an anode in sodium-ion battery

Abdullah F. Qatarneh[1], Capucine Dupont[1], Hervé Piégeay[2], Virginia Ruiz-Villanueva [3], Mario J. Franca[*1,4]

[1]IHE Delft, Delft, Netherlands
[2]ENS Lyon, Lyon, France
[3]University of Lausanne, Lausanne, Switzerland
[4]TU Delft, Delft, Netherlands

*Correspondance : abdullah.qatarneh@gmail.com

1 INTRODUCTION

A large volume of wood is transported by rivers in many parts around the world. The wood is usually referred to as large wood or driftwood. It is generally supplied through floods and is of different types and shapes. Their sources are mainly natural and include most notably the riparian zone (Le Lay *et al.*, 2013). Driftwood plays a beneficial role in geomorphology and ecology of the river, and they impact the dynamics of particulate organic matter storage, aquatic life and bedload transport in rivers (Gurnell *et al.*, 2002).

On the other hand, driftwood can have a negative impact by increasing the destructive power of floods. Accumulation of wood at bridges and weirs may block a river cross-section increasing structural loading and scouring of bridges foundations (Parola *et al.*, 2000; Lagasse *et al.*, 2010). In dams, driftwood can cause damages to the hydropower stations; as a result, they are often collected and removed for safety reasons.

Collected driftwood is often combusted or landfilled (Bartocci *et al.*, 2017). Previous studies investigating driftwood have only considered driftwood without identification of its type for energy recovery applications. Hydrothermal carbonization (HTC) is an active area of research providing a favourable option for lignocellulosic biomass with high moisture content (Heidari *et al.*, 2019). Hydrochar produced by HTC has a high-value potential as battery anodes.

The research aims to evaluate the feasibility of driftwood as a high added value material used as an anode in an innovative sodium-ion battery. The study identifies the different genre of driftwood collected from Génissiat dam and to characterize driftwood physicochemical properties. Moreover, the study examines the behaviour of different driftwood genre for hydrochar production in order to optimize hydrochar production. The electrochemical performance of produced hydrochar is then evaluated as a hard carbon anode in sodium-ion batteries.

2 CASE STUDY

The research is focused on the case of Génissiat dam located on the Rhône River in France 50 km downstream from Geneva (Switzerland) and 160 km upstream from Lyon. The driftwood at Génissiat is supplied mainly during floods. It consists of wood stored within the fluvial corridor and wood recruited from bank erosion along the Rhône River and its two main tributaries; the Arve and Valserine Rivers. The woods coming from upstream of Génissiat dam from the Arve and Valserine Rivers are is blocked since the river has no overflow pathway (Benacchio *et al.*, 2017).

3 MATERIALS AND METHODS

The driftwood samples were collected from the storage facility in Lyon. Sampling was random to represent different genre, lengths and diameter. Identification of samples' genera was then based on the wood anatomical

Table 1: Standards used in the analysis of driftwood

Type of analysis	Standard
High heating value	UNI 14918:2009
Proximate analysis/Ash content	UNI 14775:2010
Ultimate analysis (C, H, N)	UNI 15104:2011

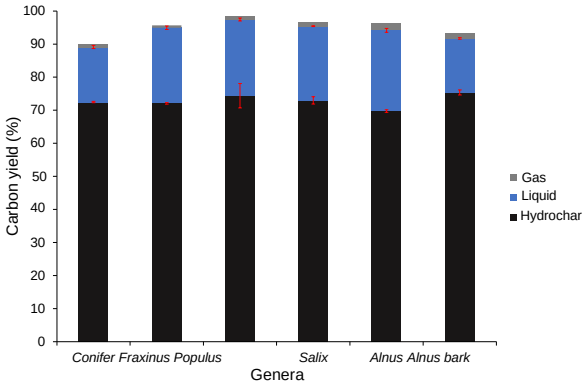

Figure 1: Carbon yield of HTC of five driftwood genera and Alnus bark for the raw driftwood and the hydrochar produced following HTC at a temperature of 200 C and a residence time of 11.5 h above: the carbon losses could be

characteristic, i.e. cell patterns and wood features of polished samples using a microscope (Schweingruber *et al.*, 2007). Table 1 provides a summary of the major analysis conducted and the corresponding standards that was followed for driftwood and hydrochar characterization. All measurements were done in triplicates.

4 RESULTS

Five genera of driftwood were identified including *Alnus*. Characterization of the different driftwood reflected the different properties of driftwood. Driftwood has a low ash content ,which is beneficial for different application and most notably for hydrochar production. Figure shows the carbon fate during HTC of different genera. Hydrochar produced by hydrothermal carbonization provides a carbon sink that is produced in an environmentally friendly technology where approximately less than 5% of the original carbon is transferred to CO_2. In addition, hydrothermal carbonization lead to a lower ash content, high carbon content and higher surface area.

5 CONCLUSIONS

The physicochemical properties of five genera of driftwood samples including *Alnus* collected from Génissiat dam were analyzed. Hydrochar produced by hydrothermal carbonization of driftwood improved its characteristics. Produced hydrochar has a potential for production of hard carbon in sodium-ion batteries.

References

Bartocci P., Barbanera M., D'Amico M., Laranci P., Cavalaglio G., Gelosia M., Ingles D., Bidini G., Buratti C., Cotana F., *et al.* (2017). Thermal degradation of driftwood: Determination of the concentration of sodium, calcium, magnesium, chlorine and sulfur containing compounds. *Waste Management 60*, 151–157.

Benacchio V., Piégay H., Buffin-Bélanger T., Vaudor L. (2017). A new methodology for monitoring wood fluxes in rivers using a ground camera: Potential and limits. *Geomorphology 279*, 44–58.

Gurnell A., Piégay H., Swanson F., Gregory S. (2002). Large wood and fluvial processes. *Freshwater Biology 47*(4), 601–619.

Heidari M., Dutta A., Acharya B., Mahmud S. (2019). A review of the current knowledge and challenges of hydrothermal carbonization for biomass conversion. *Journal of the Energy Institute 92*(6), 1779–1799.

Lagasse P. F., Zevenbergen L. W., Clopper P. E. (2010). Impacts of debris on bridge pier scour. In *Scour and Erosion*, pp. 854–863.

Le Lay Y.-F., Piégay H., Moulin B., *et al.* (2013). Wood entrance, deposition, transfer and effects on fluvial forms and processes: problem statements and challenging issues. *Treatise on geomorphology 12*, 20–36.

Parola A. C., Apelt C. J., Jempson M. A. (2000). *Debris forces on highway bridges*. Number 445. Transportation Research Board.

Schweingruber F. H., Börner A., Schulze E.-D. (2007). *Atlas of woody plant stems: evolution, structure, and environmental modifications*. Springer Science & Business Media.

Proceedings of the 1st IAHR
Young Professionals Congress
17-18 November 2020

The role of the Agulhas system in the global climate by using the Lagrangian approach

Jacopo Busatto[1,2], Claudia Adduce[1], Federico Falcini[2], Chunxue Yang[2]

[1]Roma Tre University, Rome, Italy
[2]ISMAR - CNR, Rome, Italy

*Correspondance : jacopo.busatto@uniroma3.it

ABSTRACT

Agulhas Current is the western boundary current of the Southern Indian Ocean; it has a mean transport of $\sim 70 Sv$; it flows along the coast of Mozambique and South Africa. Arrived to the homonymous Cape Agulhas the current changes direction (Agulhas Retroflection) and start flowing eastward along the Sub-Tropical Front. Due to instability, it sheds (Agulhas Leakage) eddies in the Atlantic Ocean (Agulhas Rings). This study aim to identify the the influence of Agulhas Leakage on the Atlantic Meridional Overturning Circulation. Satellite data of Sea Surface Temperature, geostrophic velocity and Heat fluxes are used. A positive trend in the eddy kinetic energy and in the surface temperature is found indicating an increase in the leakege.

Keywords: Aghulas Current, Satellite data, Climate.

1 INTRODUCTION

Agulhas Current follows the slope of the continental shelf. Having passed the Agulhas Bank, the Agulhas Current, flows back into the South Indian Ocean (Agulhas Retroflection) as the Agulhas Return Current. A major leakage of water from the Indian Ocean to the South Atlantic occurs due to a process of ring shedding (Agulhas Ring). Agulhas Rings entering the Atlantic lower density surfaces and instigate the propagation of planetary waves, causing short term variability and possibly interannual to decadal oscillations. Agulhas Leakage waters strengthen the Atlantic Meridional Overturning Circulation enhancing the Atlantic meridional pressure gradient and preconditioning North Atlantic for deep convection [Beal *et al.* (2011)].

2 METHODS

Satellite data will be used to analyse surface proprieties of the water masses: Sea surface temperature (SST), geostrophic velocities and surface heat fluxes are used up to now. Resolution of every data set is $0.25^\circ \times 0.25^\circ$. Climatology will be the time mean of the data set; trends will be the slope of a linear interpolation performed for every pixel. Source of data: Sea surface temperature is obtained from ESACCI 1982-2018. Geostrophic velocities come from CMEMS 1993-2019. Heat fluxes come from ERA5 1979-2019. For heat fluxes: net heat flux is the sum of latent heat flux, sensible heat flux, solar and thermal radiation. Eddy, or turbulent, kinetic energy is defined as the variance of the (horizontal) velocity field: $EKE = < \vec{u}^2 > - < \vec{u} >^2$:

3 RESULTS

Sea surface temperature climatology shows the position of the cold and relatively fresh Sub-tropical front, that flows eastward at $\sim 40^\circ S$ (fig. 1(a)). Sea surface temperature trend map (fig. 2(b)) highlights a growing behavior in the retroflection region, meaning a south-shifting of the sub-tropical front implying a wider gap between Africa

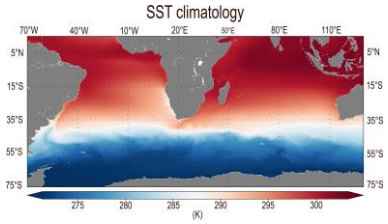

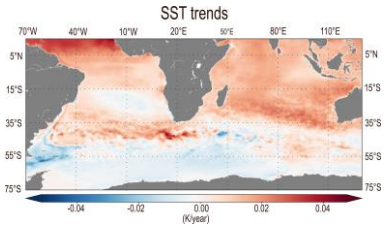

((a)) ((b))

Figure 1: Sea surface temperature climatology (a) and trends (b).

and the Antarctic Circumpolar Current. This increases Agulhas Leakage [Beal *et al.* (2006)]. Agulhas retroflection region is clearly turbulent and a brighter shade of higher eddy kinetic energy sheds into

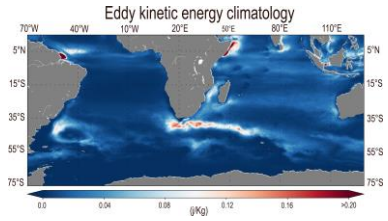

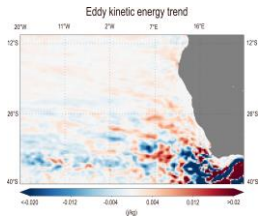

((a)) ((b))

Figure 2: Eddy kinetic energy climatology (a) and trends (b).

the South Atlantic (fig. 2(a)). There an average positive trend in eddy kinetic energy has been evaluated (fig. 2(b)) (see also [Beal et Elipot (2016)]). Sub-Tropical Front south-shifting and an eddy kinetic energy positive trend in the South Atlantic are proofs of an increase in the Agulhas Leakage, since it means that more Agulhas rings are shed. Net surface heat flux (fig. 3) indicate a strong heat loss in the Agulhas retroflection region(fig.

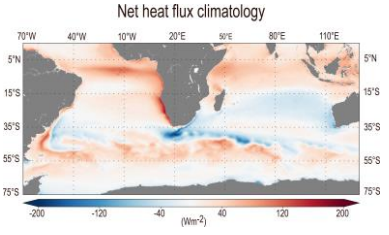

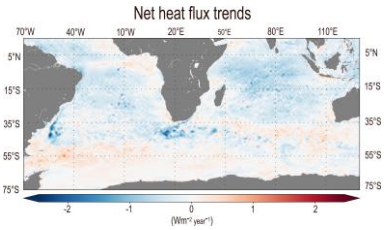

((a)) ((b))

Figure 3: Net surface heat flux climatologies (a) and trends (b).

3(a)). Trends (fig. 3(b)) shows a further ingreasing (negatively) behaviour indicating a growing heat loss during time. Warm water diffusion in the Atlantic can compete with the Greenland contribute: one strengthening and one reducing the Atlantic Meridional Overturning Circulation [Beal *et al.* (2011)].

References

Beal L. M., Chereskin T. K., Lenn Y. D., Elipot S. (2006, 11). The Sources and Mixing Characteristics of the Agulhas Current. *J. P. O. 36*(11), 2060–2074. URL: https://doi.org/10.1175/JPO2964.1, doi:10.1175/JPO2964.1.

Beal L. M., De Ruijter W., Biastoch A. e. a. (2011). On the role of the Agulhas system in ocean circulation and climate. *Nature 472*, 429–436. URL: https://doi.org/10.1038/nature09983, doi:10.1038/nature09983.

Beal L. M., Elipot S. (2016). Broadening not strengthening of the Agulhas Current since the early 1990s. *Nature 540*(7634), 570–573. URL: https://doi.org/10.1038/nature19853, doi:10.1038/nature19853.

IAHR AIRH

International Association for Hydro-Environment Engineering and Research

Hosted by
Spain Water and IWHR, China

Session 2
Fluvial Hydraulics

IAHR YPN

Hosted by
Spain Water and IWHR, China

Proceedings of the 1st IAHR
Young Professionals Congress
17-18 November 2020

A SATELLITE-BASED ANALYSIS OF THE GEOMORPHOLOGICAL EFFICIENCY OF RIVER PLUMES

Rossella Belloni [1], Claudia Adduce [1], Federico Falcini [2], Vittorio Ernesto Brando [2] & Marco Bracaglia[2]

[1] Roma Tre University, Rome, Italy
email: rossella.belloni@uniroma3.it, claudia.adduce@uniroma3.it
[2] National Research Council - Research Institute of Marine Sciences (CNR-ISMAR), Rome, Italy
email: federico.falcini@cnr.it, vittorio.brando@cnr.it, marco.bracaglia@artov.ismar.cnr.it

ABSTRACT

River plumes play a fundamental role in coastal areas affecting both the morphology and the ecology. In this study, the geomorphological efficiency of the Po River, the main Italian river flowing into the northern Adriatic Sea, is investigated. To this end, a statistical analysis of high spatial resolution turbidity maps obtained from Sentinel-2 (S2) images was performed to evaluate the spatio-temporal variability of river plume morphologies. River plume images captured by S2 were then linked to the main environmental forcings that affect the dispersal of suspended sediments in the study area. In this regard, river discharge and wind data were used in the attempt to assess how streamflow and meteo-marine conditions affect the overall structure of river plumes. The analysis showed plume morphologies with a moderate spatio-temporal variability and confirmed the major role of wind and river discharge in affecting their overall structure.

Keywords: River plumes, Remote sensing, Coastal geomorphology, Coastal dynamics.

1 INTRODUCTION

River plumes are generated by river freshwater flowing into the coastal zone where they significantly affect circulation, water properties and morphology of coastal areas. The analysis of the main processes affecting their dispersal into the coastal waters is therefore of strong scientific interest and practical importance. River plumes show characteristic patterns based largely on coastal morphology and on the magnitude of the river discharge, however, external forcings, such as wind and wave action, may strongly modify the overall structure of the plume and therefore their influence on coastal areas (Horner-Devine et al., 2015; Falcini et al., 2012).

The analysis of phenomena occurring in a highly dynamic and complex environment, such as that of coastal waters, requires monitoring techniques that provide data with a spatio-temporal resolution consistent with the characteristic scales of the phenomena examined. The most direct method of deriving such information involves satellite imagery. Specifically, in this study, the potential of high spatial resolution satellite data to investigate the coastal geomorphological efficiency of the Po River, the main Italian river flowing into the northern Adriatic Sea, was examined through a statistical analysis of high-resolution turbidity maps obtained by processing Sentinel-2 images. Moreover, river discharge and wind data in the area of interest were used for assessing how river discharge and meteo-marine conditions affect river plume dynamics in northern Adriatic Sea and, therefore, their coastal sediment supply.

2 MATERILAS AND METHODS

In this study, a time series of Level-1C Sentinel-2 images for the area of the northern Adriatic Sea was collected and processed to investigate the geomorphological efficiency of Po River. The images were collected for the period June 2015 - April 2018, excluding those with a remarkable cloudiness and sun glint and those not showing any clearly visible river plume. The images so selected were later processed using an automatic processor developed for atmospheric correction of Landsat (5/7/8) and Sentinel-2 (A/B) imagery on coastal and inland waters (Vanhellemont and Ruddick, 2014, 2015): ACOLITE (Atmospheric Correction for OLI 'lite'). The processor allows, furthermore, the calculation of many reflectance-derived parameters. In this study, the

ACOLITE-derived water leaving reflectance was converted in turbidity (FNU) using the algorithm developed by Dogliotti et al. (2015).

The time series of turbidity images were used to investigate the spatio-temporal variability of the plume morphologies of the analyzed river. In this regard, for each available satellite image, the overall coastal area affected by the dispersal of the river plume was identified comparing the satellite-derived turbidity data with a threshold value established by considering the Adriatic Sea background turbidity (approximately 6 FNU). In the end, the geomorphological efficiency of the river plumes was evaluated considering the frequency of the suspended sediments dispersal in the alongshore direction.

River plumes images were furthermore linked to the main environmental forcings that affect the dispersal of suspended sediments in the northern Adriatic Sea: wind and river discharge. In this regard, considering that the dynamic observed through a satellite image depends on the evolution of the environmental forcings in the antecedent period, discharge and wind data referred to a temporal window of 72 hours before the satellite acquisition were considered, as suggested by Braga et al. (2017).

3 RESULTS AND CONCLUSIONS

The analysis showed plumes morphologies with a moderate spatio-temporal variability. The dispersal of suspended sediments in the alongshore direction occurred, indeed, just a few times, consequently impacting the geomorphological efficiency of the river (Figure 1).

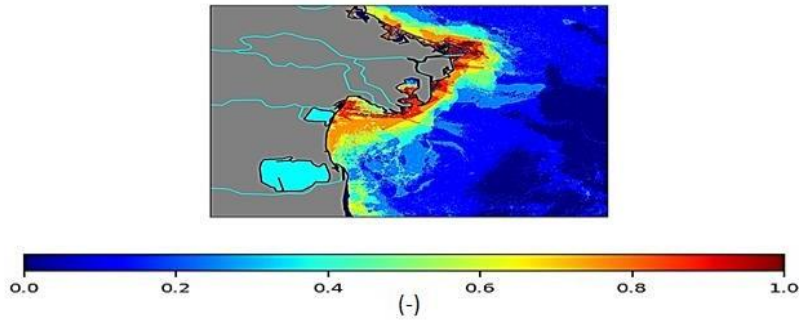

Figure 1. Relative frequency maps of turbidity values: Po River.

The results obtained were confirmed by the qualitative analysis of true color images. Indeed, many different plume structures were identified and the major role of river discharge and wind in affecting their overall structure was confirmed. In particular, the role of wind forcing strictly depends on wind direction with respect to the coastal orientation. For instance, long-lasting northerly winds tend to generate narrow coastal plume patterns that facilitate sediment supply along the coast.

REFERENCES

Braga F, Zaggia L, Bellafiore D, Bresciani M, Giardino M, Lorenzetti G, Maicu F, Manzo C, Riminucci F, Raviaioli M, Brando VE (2017) Mapping turbidity patterns in the Po river prodelta using multi-temporal Landsat 8 imagery. *Estuarine, Coastal and Shelf Science*, 198, 555–567.

Dogliotti A, Ruddick K, Nechad B, Doxaran D, Knaeps E (2015) A single algorithm to retrieve turbidity from remotely-sensed data in all coastal and estuarine waters, *Remote Sensing of Environment*, 156, 157–168.

Falcini F, Khan NS, Macelloni, L, Horton BP, Lutken, CB, McKee KL, Santoleri R, Colella S, Li C, Volpe G, D'Emidio M, Salusti A, Jerolmack DJ (2012) Linking the historic 2011 Mississippi River flood to coastal wetland sedimentation, *Nature Geoscience*, 5(11), 803-807.

Horner-Devine AR, Hetland RD, MacDonald DG (2015) Mixing and transport in coastal river plumes, *Annual Review of Fluid Mechanics*, 47, 569–594.

Vanhellemont Q, Ruddick K (2014) Turbid wakes associated with offshore wind turbines observed with Landsat 8. *Remote Sensing of Environment*, 145, 105–115.

Vanhellemont Q, Ruddick K (2015) Advantages of high quality swir bands for ocean colour processing: examples from Landsat-8, *Remote Sensing of Environment*, 161, 89–106.

Proceedings of the 1st IAHR
Young Professionals Congress
17-18 November 2020

Modelling erosion of pre-embankment breaches in coversand ridges in the IJssel floodplain due to major flood events in medieval times

Roy Dierx[1*], Anouk Bomers[1], Kim Cohen[2], Suzanne Hulscher[1]

[1]University of Twente, Water Engineering and Management, Enschede, the Netherlands
[2]Utrecht University, Physical Geography, Utrecht, the Netherlands

*Correspondance : roy.dierx@hotmail.com

ABSTRACT

Coversand ridges are natural elevated areas that formed in the last part of the glacial period due to wind transport. Some coversand ridges created a watershed between the Rhine and IJssel floodplain. Erosion of these coversand ridges was of major influence for the formation of the river IJssel as a Rhine delta distributary. A coupled hydrodynamic-erosion model is set up to simulate potential coversand ridge breach scenarios at different locations along the coversand ridges during flood events. Computed flow velocities and water depths from the hydrodynamic model were exported to an erosion model. This coupled modelling approach gives insight in the hydrodynamic conditions of different breaches during various floods. The first results imply that breaches in the coversand ridges located at the current location of the river IJssel are the most favourable for a breach to expand. This result gives insight in the landscape development of the Netherlands.

Keywords: Coversand ridge, Erosion model, Flood events, River formation, River IJssel.

1 INTRODUCTION

Rivers flow through their floodplains (river basins) like they have been there all the time, but rivers form, change and can run dry over time. A trigger for a change in the course of a river is often an extreme flood wave. A successful river change requires both reach-scale cross-channel flow potential energy exceeding a threshold, and the availability of a more favorable path at landscape-scale on its floodplain (Hajek et Wolinsky, 2012).

This case study focuses on the formation of the river IJssel, a distributary of the river Rhine in the Netherlands. Research showed that the river IJssel came into existence between 300 and 750 AD (Cohen et Stouthamer, 2012). Before that time, the IJssel floodplain was not part of the Rhine floodplain and had a separate drainage. A local higher elevated area created a watershed that splitted both floodplains. This higher elevated area consisted of coversand and is called a coversand ridge. The formation of the river IJssel is related to some flood waves, that had the potential to overtop these coversand ridges, initiated the erosion on the crests of the coversand ridges and eventually resulted in two breaches that can be found today (Cohen *et al.*, 2009). The first breach is located at the current river IJssel (referred to as the easterly breach) and the second breach is located approximately one kilometer West of the current river (referred to as the westerly breach). Where the easterly breach expanded and became part of the river IJssel; the westerly breach eventually silted. Understanding the annexation process of the IJssel floodplain by the river Rhine by the formation of the river IJssel is of archeological-historical interest and can offer an opportunity to quantify major historical floods of the river Rhine. The objective of this research is to find the hydrodynamic differences between both breaches during flood waves.

2 MODEL SET-UP

A Digital Elevation Model (DEM) of the Rhine and IJssel floodplain for the situation before the existence of the river IJssel is set up by Van der Meulen *et al.* (2020) and is used as a starting point in the static hydrodynamic modelling set-up in this research. In this approach several static moments in time during a developing breach in a coversand ridge are constructed and implemented in the DEM. A hydrodynamic model is set up with these pre-defined breaches, analogous to Bomers *et al.* (2019). The output of the hydrodynamic model, consisting of the flow velocity and water depth, is exported to an erosion model. These two models together form the coupled

hydrodynamic-erosion model. The erosion model computes the erosion velocity (v_e) in m s^{-1} and erosion rate (E) in kg m^{-2} s^{-1} in the pre-defined breaches with the following equation (van Rhee, 2010):

$$v_e = \frac{E}{\rho_s(1-n_0)}, \text{ where } \quad E = 0.00033\rho_s[(s-1)gd_{50}]^{0.5}(D_*)^{0.3}f_D \left(\frac{\theta-\theta_{cr}}{\theta_{cr}}\right)^{1.5} \tag{1}$$

In these equations ρ_s is the sediment density in kg m^{-3}, s is the relative density between sediment and water, g is the gravitational acceleration in m s^{-2}, D_{50} is the median grain size in m, D_* is the dimensionless grain size parameter, f_D is a damping factor for super critical flow, θ is the grain-related Shields parameter, θ_{cr} the critical Shields parameter and n_0 the in-situ porosity.

3 FIRST RESULTS

Two flood waves are used for the hydrodynamic simulations: (1) A flood wave with a peak discharge of 14,000 m^3 s^{-1} in Andernach, Germany, which is the most probable trigger to overtop and erode the coversand ridges (first hypothesized in Cohen et Lodder (2007) based on geological grounds; supported by hydrodynamic modelling by van der Meulen *et al.* (In Prep)). (2) And a flood wave of 10,000 m^3 s^{-1} to simulate subsequent floods of a more moderate magnitude.

Table 1: Erosion velocity in the pre-defined breaches [m s^{-1}] for various breach widths, depths and flood waves

Width [m]	**Depth** [m]	**Discharge** [m^3 s^{-1}]	**Max. erosion velocity westerly breach** ($*10^{-3}$) [m s^{-1}]	**Max. erosion velocity easterly breach (IJssel location)** ($10*^{3}$) [m s^{-1}]
50	**2**	**10000**	12.3	16.6
50	**2**	**14000**	13.8	17.6
50	**4**	**10000**	11.7	14.1
50	**4**	**14000**	13.3	15.3
100	**4**	**10000**	7.8	11.9
100	**4**	**14000**	9.3	12.9

Next to the higher erosion velocities in the easterly breach (Table 1), the flood wave reaches the easterly breach approximately twelve hours earlier. During this time period the erosion velocity that occurs in the easterly breach already reaches approximately 2 to 3 $*10^{-3}$ m s^{-1}, triggering this breach to expand in depth and in width.

4 CONCLUSIONS

From the results it can be concluded that in the easterly breach larger erosion velocities occur during a flood wave (Table 1) and that these flow velocities occur earlier during the flood wave. The hydrodynamic conditions at that location are more favourable for a breach to expand. The results from this study substantiate why the river IJssel formed at the location where it still flows today. The results are of archeological-historical interest.

5 ACKNOWLEDGEMENTS

This research is supported by the Netherlands Organisation for Scientific Research (NWO, project 14506) which is partly funded by the Ministry of Economic Affairs and Climate Policy. Furthermore, the research is supported by the Ministry of Infrastructure and Water Management and Deltares.

References

Bomers A., Schielen R. M. J., Hulscher S. J. M. H. (2019). Application of a lower-fidelity surrogate hydraulic model for historic flood reconstruction. *Environmental Modelling and Software 117* (February), 223–236. doi:10.1016/j.envsoft.2019.03.019.

Cohen K. M., Lodder Q. J. (2007). *Paleogeografie en veiligheid tegen overstromen*.

Cohen K. M., Stouthamer E. (2012). Digitaal basisbestand paleogeografie van de Rijn-Maas delta. dans. doi:10.17026/dans-x7g-sjtw.

Cohen K. M., Stouthamer E., Hoek W. Z., Berendsen H. J. A., Kempen H. F.J. (2009). *Zand in Banen*. Province of Gelderland & Utrecht University.

Hajek E. A., Wolinsky M. A. (2012). Simplified process modeling of river avulsion and alluvial architecture: Connecting models and field data. *Sedimentary Geology 257-260*, 1–30. doi:10.1016/j.sedgeo.2011.09.005.

van der Meulen B., Bomers A., Cohen K., Middelkoop H. (In Prep). Late holocene flood dynamics and magnitudes in the lower Rhine river valley and upper delta resolved by two-dimensional hydraulic modelling. *Earth Surface Processes and Landforms*.

Van der Meulen B., Cohen K. M., Pierik H. J., Zinsmeister J. J., Middelkoop H. (2020). Lidar derived high resolution palaeo DEM construction workflow and application to the early medieval lower Rhine valley and upper delta. *Geomorphology* (370).

van Rhee C. (2010). Sediment Entrainment at High Flow Velocity. *Journal of Hydraulic Engineering 136*(September), 572–582. doi:10.1061/(ASCE)HY.1943-7900.0000214.

Proceedings of the 1st IAHR
Young Professionals Congress
17-18 November 2020

DATA-DRIVEN MODELLING OF HIGH FLOW-RELATED POOR WATER QUALITY EVENTS IN THE MID-BRISBANE RIVER

Edoardo Bertone [1,2,3], Martin Luna Juncal [1], Khoi Nguyen[1] & Dapo Kufeji[4]

[1] School of Engineering and Built Environment, Griffith University, Parklands Drive, Southport QLD 4222, Australia
e.bertone@griffith.edu.au , martin.lunajuncal@griffithuni.edu.au , k.nguyen@griffith.edu.au

[2] Cities Research Institute, Griffith University, Southport QLD 4222, Australia

[3] Australian Rivers Institute, Griffith University, 170 Kessels Road, Nathan QLD 4111, Australia

[4] Seqwater, 117 Brisbane Street, Ipswich QLD 4305, Australia
dapo.kufeji@seqwater.com.au

ABSTRACT

Due to the availability of high-frequency flow and water quality data at multiple stations, opportunities for a data-driven prediction and optimization model for Australia's Mid-Brisbane river were explored. This river receives water from Wivenhoe dam and a number of tributaries, with raw water drawn for drinking water treatment and supply to the Brisbane region. A number of poor raw water quality events regularly occur, and such model would look at predicting and minimizing them. At this stage, a preliminary flow prediction model, including lag times among locations along the river, was developed. It was also established that high turbidity events can be predicted based on flows from certain tributaries, and that conductivity events are strongly related to the flow of a minor, but impactful, tributary. Future work will link the water quality modelling component to existing flow predictions, while also suggesting coping strategies (e.g. dam releases) and their best timing to minimize water quality issues at the treatment plant.

Keywords: Data-driven modelling; Floods; Mid-Brisbane River; Water treatment optimization

1 INTRODUCTION

The Mount Crosby drinking water treatment plant (DWTP), which in fact combines two separate plants (East Bank and West Bank), collects water from the Mid-Brisbane River, and can treat and supply up to 800 ML/day of drinking water to the Brisbane and Ipswich regions, in South-East Queensland, Australia. The efficacy of its treatment processes (which are traditional coagulation, flocculation, sedimentation, filtration and disinfection methods) is challenged at times (Khan et al 2017), especially when heavy rain causes high flows at upstream locations. It seems that the location of heavy rainfall also impacts the risk of poor water quality events, with certain tributaries (e.g. Lockyer's Creek) believed to be the main turbidity inputs and others (e.g. Black Snake Creek) to be the cause of high conductivity events at the DWTP. Consequently, due to the capacity of adjusting flow releases from the upstream Wivenhoe dam, there is potential to increase such flows in order to effectively dilute any poor-quality flows from tributaries. Given the installation, in the last decade, of a number of high-frequency water quality monitoring stations at several locations along the river, the collected historical data (combined with rain and flow data) provides an opportunity to better understand relationships between flows at different locations and tributaries, lag times, and water quality.

2 MATERIALS AND METHODS

Following a stakeholder workshop which assisted in understanding the issues, system behavior and data sources, such data was collected and pre-processed. Hourly flow data for seven river locations during a period ranging from 2009 to 2020 was collected, as well as hourly water quality data (with a focus on turbidity and conductivity) at six of these locations starting between 2012 and 2016. However, missing/unreliable data occurring between 1% and 74% of the entire time period, depending on parameter and station, was present after pre-processing. The data analysis included a visual inspection, time series analysis, and linear/nonlinear regression analysis. We also looked at turbidity/flow hysteresis loops (Evans and Davies, 1998) to characterize the type of runoff event. As a result of the data analysis, short-term flow forecasting models were developed. Previous (medium-term) flow models were developed by the author with a probabilistic approach (Bertone et al., 2017). For this study, such models were developed based on three different approaches, including machine learning (i.e. long short-term memory regression), statistical model (i.e. state-space approach) and multi-variate regression. Depending on the flow rate of input data, the relevant model is automatically selected. In order to

obtain the highest accuracy, the system also allows the user to choose different sources of input data/stations for the forecasting task. Work is underway to also develop water quality models with methods such as artificial neural networks, random forest, decision tree and extreme gradient boosting models.

3 RESULTS

Clear, strong relationships were identified between historical flow rates of subsequent stations moving downstream of the catchment. The ratios between peak flows at different locations have correlations with rain-dependent variables (e.g. total rain in the past 6 months; rainfall heterogeneity within the catchment). Based on such correlations, the flow prediction model was developed, with a user-friendly interface created in MATLAB. Presented in Figure 1 is the predicted downstream flow at the Mount Crosby reservoir 10 hours ahead during an extreme event occurred in 2011. Based on the inflow magnitude at two upstream stations, the multivariate regression model was employed by the algorithm to yield a very close prediction (black line) compared to the actual inflow (blue line) with a RMSE of 165 m^3/s, which is about 2% of the average flow rate of that 10-hour period.

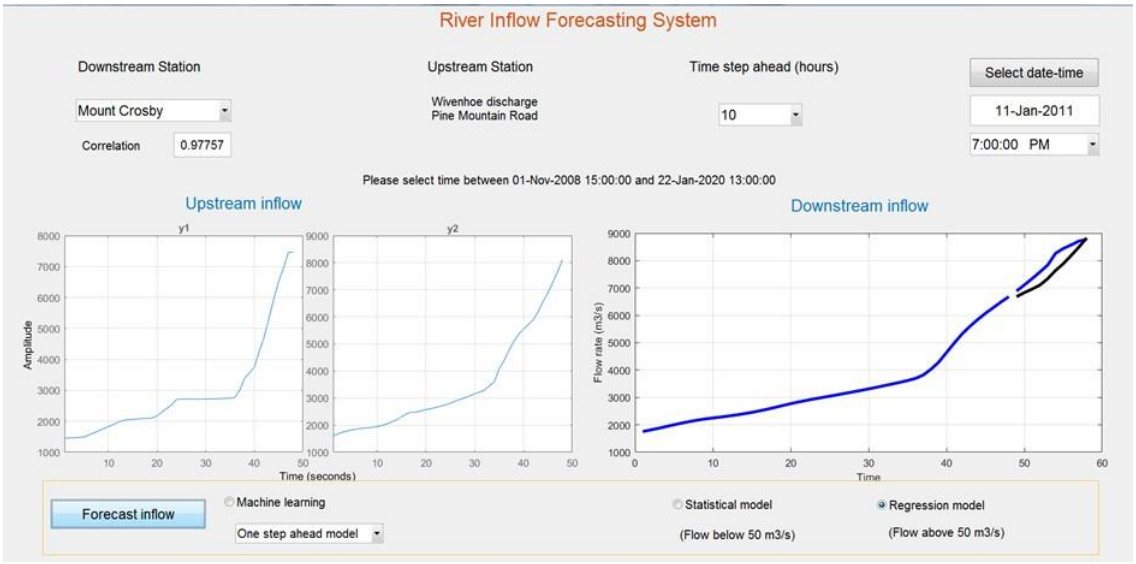

Figure 1. Graphical interface for flow forecasting model, Mid Brisbane River.

From a water quality perspective, paucity of accurate data did not allow an achievement of similarly accurate models at this stage. However, there seems to be potential to predict the magnitude and timing of turbidity based on flow predictions, with turbid flows recorded both before and after the flow peak, depending on the flow magnitude. It seems also highly feasible to predict true colour (whose data frequency was only daily) based on turbidity, and also conductivity drops (i.e. rainfall event causing dilution and outflow) from a small tributary (Black Snake Creek) anticipating conductivity peaks at the DWTP.

4 CONCLUSIONS

A combined, preliminary data-driven water quantity (flow) – quality model was developed for the Mid-Brisbane river with good accuracy achieved thus far for the flow component. The final, refined model has the potential to predict the sources, timing and magnitudes of poor water quality events reaching the Mount Crosby DWTP.

ACKNOWLEDGEMENTS

Griffith University and Seqwater co-fund this project through a Griffith University Postdoctoral Fellowship.

REFERENCES

Bertone, E., O'Halloran, K., Stewart, R.A., & de Oliveira, G. F. (2017). Medium-term storage volume prediction for optimum reservoir management: A hybrid data-driven approach. *Journal of Cleaner Production*, 154, 353-365.

Evans, C., Davies, T.D. (1998). Causes of concentration/discharge hysteresis and its potential as a tool for analysis of episode hydrochemistry. *Water Resources Research*, 34(1), 129-137.

Khan, S.J., Deere, D., Leusch, F.D., Humpage, A., Jenkins, M., Cunliffe, D., Fitzgerald, S.K. & Stanford, B.D., (2017). Lessons and guidance for the management of safe drinking water during extreme weather events. *Environmental Science: Water Research & Technology*, 3(2), pp.262-277.

Proceedings of the 1st IAHR
Young Professionals Congress
17-18 November 2020

A METHOD FOR SIMULATION OF REACTIVE SOLUTE TRANSPORT IN NATURAL RIVERS

Byunguk Kim [1], Siyoon Kwon[2], Il Won Seo [3]

[1,2,3] *Seoul National University, Seoul, Republic of Korea*
e-mail kim.byunguk@snu.ac.kr; ksy92@snu.ac.kr; seoilwon@snu.ac.kr

ABSTRACT

For several decades, solute transport models have been used in order to predict behavior of solute in rivers. However, most previous studies assumed that the subject solute is conservative, and few of studies taking account of decay terms into the models which mostly employed optimization methods to determine decay parameters. In this study, we added two decay terms to the Transient Storage Model (TSM) representing volatilization and biodegradation, and proposed the method to estimate the decay parameters based on chemodynamics theories. Using this advanced model, the reactive solute transport simulation was carried out at natural river of Gam Creek, South Korea in 2020. The results revealed that there was considerable difference in resulting breakthrough curve depending on the type of chemicals.

Keywords: *reactive solute transport model, parameters, volatilization, biodegradation, tracer test*

1 INTRODUCTION

Solute transport models have been used to predict the behavior or the fate of released solute into riverine domain. Even though majority of chemicals has its reactivity in water, most of the studies assumed that the solute is conservative because of the difficulty of experimental field-application with actual toxicant chemicals.

Runkel and Broshears (1991) produced OTIS model which includes the first-order decay term to consider the mass loss of the solute in rivers. In later studies, however, the decay parameters have been mostly determined by optimization method which has local problems, namely, the optimized decay parameters cannot be used for other various types of chemicals.

To supplement the deficiency of previous studies, we considered the phenomenon of volatilization and biodegradation of a chemical in rivers, and proposed the method to theoretically estimate the decay parameters using inherent properties of a chemical representing its volatility and biochemical reactivity. Furthermore, we evaluated how the decay parameters function in the model with sensitivity analysis, and suggested the significant regime of the parameters using Damkohler number.

2 TRANSIENT STORAGE PARAMETER OPTIMIZATION

In this study, the governing equations were suggested as:

$$\frac{\partial C}{\partial t} + \frac{Q}{A}\frac{\partial C}{\partial x} = \frac{\partial}{\partial x}\left(K\frac{\partial C}{\partial x}\right) + \alpha(C_s - C) + \lambda_v C + \lambda_b C \quad (1a)$$

$$\frac{\partial C_s}{\partial x} = \alpha\frac{A_F}{A_S}(C - C_s) + \lambda_b C \quad (1b)$$

where C and C_S (g m^{-3}) denote solute concentration within the surface flow and storage zone, respectively, Q (m^3 s^{-1}) denotes volumetric flow rate, A_F and A_S (m^2) denote cross-section area of surface flow and storage zone, respectively, K (m^2 s^{-1}) denotes longitudinal dispersion coefficient, α (s^{-1}) denotes mass exchange rate coefficient between the surface flow zone and the storage zone, t (s) denotes time variable, λ_v and λ_b denote volatilization rate and biodegradation rate, respectively. The x -coordinate was taken to be approximately streamwise distance.

The numerical modeling for these governing equations was conducted by spatial-temporally discretizing of the concentration variables using Finite Difference Method (FDM) and Crank-Nicolson method. Since the estimation of the transient storage parameters should be preceded the determination of decay parameters, a trace test was carried out at Gam Creek, South Korea in 2020. The flow properties and numerical simulation information were summarized in Table 1. The transient storage parameters were optimized to the measured concentration data from the tracer test, and resulting simulation result yielded over 0.991 of determination coefficient (R^2).

Table 1. Flow properties surveyed from the tracer tests and information for numerical simulation

Sub-reach	Flowrate (m3 s-1)	Sub-reach length (m)	Mean depth (m)	Mean width (m)	Mean velocity (m s-1)	Bed slope	Sinuosity	Grid size (m)	Time step (sec)
RC1(S1-S2)	2.17	954	0.305	20.75	0.305	0.000825	1.07	10	4
RC2(S2-S3)	2.17	1,798	0.388	15.45	0.317		1.05	10	4
RC3(S3-S4)	2.17	1,105	0.395	16.75	0.315		1.02	10	4

3 DECAY PARAMETER ESTIMATION

The volatilization can be interpreted as a first-order mass transfer between two-phase boundary layer that is refer to as the Two film theory (Whitman, 1923). In this theory, it is assumed that concentration gradient within the quiescent boundary layers is linear due to molecular diffusion. Therefore, the molecular diffusivity dominates the volatilization rate(λ_v) based on the Fick's law, and the λ_b can be determined by relating with reaeration rate. The biodegradation rate can be also referred to as the half-life kinetics. To determine the λ_b, we employed the BIOWIN model which is a biodegradation half-life estimator for a chemical.

4 RESULT AND DISCUSSION

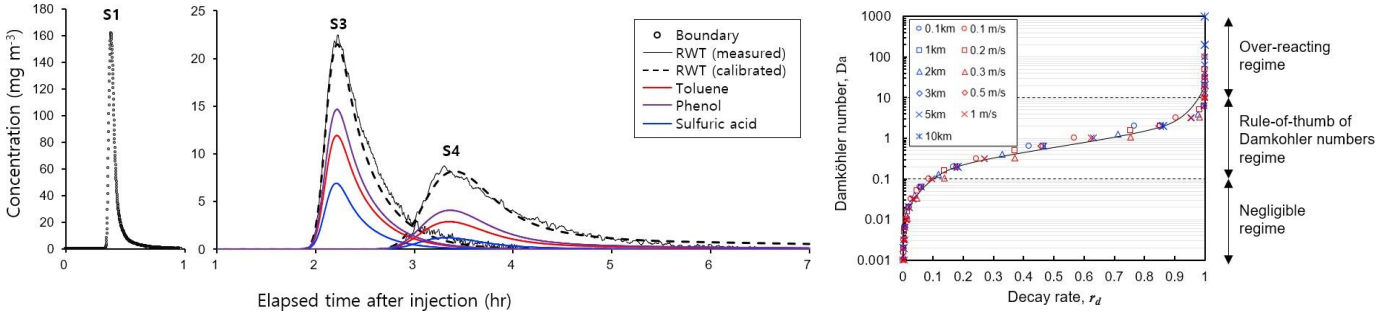

Figure 1. (a) Resulting breakthrough curves for conservative solute, toluene, phenol, and sulfuric acid. S1, S3, and S4 are the cross-sections 820m, 2,850m, 4,850m away from the injection point, respectively. (b) the relation between the Damkohler number and decay rate.

We simulated the transport of Toluene, Phenol, and Sulfuric acid at the 4.85km reach of the Gam Creek. As shown in Fig.1a, the simulation results for three chemicals were considerably different indicating the inappropriateness of the conservation assumption. In addition, we found out that the relation between the Damkohler number and the mass loss is independent on flow velocity and travel distance as shown in Figure 1b. Accordingly, the estimated decay parameters can be evaluated by the Damkohler number.

ACKNOWLEDGEMENTS

This research was supported by Korea Ministry of Environment (MOE) as "Chemical Accident Response R&D Program (2018001960001)", and the BK21 PLUS research program of the National Research Foundation of Korea.

REFERENCES

Runkel, R. L., & Broshears, R. E. (1991). One-dimensional transport with inflow and storage (OTIS): a solute transport model for small streams (p. 85). CADSWES, Center for Advanced Decision Support for Water and Environmental Systems, Department of Civil Engineering, University of Colorado.

Whitman, W. G. (1923). The two-film theory of gas absorption. Chem. Metall. Eng., 29, 146-148.

Proceedings of the 1st IAHR
Young Professionals Congress
17-18 November 2020

HOW GOOD ARE 2D-MORPHODYNAMIC MODELS IN REPRODUCING BED MORPHOLOGY OF MEANDERING CHANNELS? ANALYZING THE STRENGTHS AND LIMITATIONS OF THREE POPULAR 2D MODELS

Saroj Karki [1], Hajime Nakagawa [2] & Yaoxin Zhang [3]

[1] Ministry of Physical Infrastructure Development, Province 1, Biratnagar, Nepal
sarojioe@gmail.com

[2] Disaster Prevention Research Institute, Kyoto University, Kyoto, Japan
nakagawa@uh31.dpri.kyoto-u.ac.jp

[3] National Center for Computational Hydroscience and Engineering, The University of Mississippi, Oxford, USA
yzhang@ncche.olemiss.edu

ABSTRACT

Several morphodynamic models have been developed which are being increasingly used to support the decision and planning of different river management works. In the current study, the applicability of three widely used 2D morphodynamic models: Telemac2D, Nays2DH and CCHE2D in replicating meander bed morphology are investigated. The models were applied to simulate an experimental case of a sine-generated meandering channels from the previous works available from the literatures. Simulation results showed that each model is capable of satisfactorily reproducing the meander bed morphology but there exist significant differences in capturing particular bed features like point bar, outer bank scour, etc. However, further analysis under different flow and other hydraulic conditions might be necessary to get more detailed insights of the various aspects of the morphodynamic models.

Keywords: Morphodynamic models, meander morphology, Telemac2D, Nays2DH, CCHE2D.

1 INTRODUCTION

Several models have been developed in the recent years with a capability to simulate various river morphological processes. These models are being increasingly used to better understand the river morphological characteristics which support planners and river engineers to prevent river disasters, design and operation of hydraulic structures, maintain and improve river ecosystem, etc. (Jang and Shimizu, 2005). In this context, the reproduction of meander morphology using 2D numerical models is a tricky issue as it involves parametrization in sediment transport, secondary flow adjustment, etc. It is therefore important to evaluate the strength and limitations of the models so that the users have prior knowledge regarding the choice of any particular model. Against this backdrop, this study is aimed at comparative evaluation of the performance of the three popularly used 2D morphodynamic models in meandering channels. The reason for the selection of these three models are basically due to their wide applicability and validity in both experimental and real field cases.

2 METHODOLOGY

An experimental case is chosen from the available literatures from the past and three widely used 2D morphodynamic models are applied to simulate the experimental case. The performance of each of the models in reproducing the experimental results are investigated. The experimental data used to validate the model was derived from the works of Ferrera da Silva and El-Tahawy (2008). Their experiment was performed in a sine-generated meandering channel consisting of two full meander length with a deflection angle 70^0. The inlet was connected to a straight channel measuring 2m in length. Constant steady discharge of 9.8l/s (inflow boundary condition) with average flow depth 5cm (outflow boundary condition) was supplied to the inlet rectangular channel of width 80cm having fixed banks. Non-uniform sand having median diameter d_{50}=0.65mm was used as bed material in the channel of bed slope of 1:250 along the centerline. The experiment was conducted for a duration of 170 minutes.

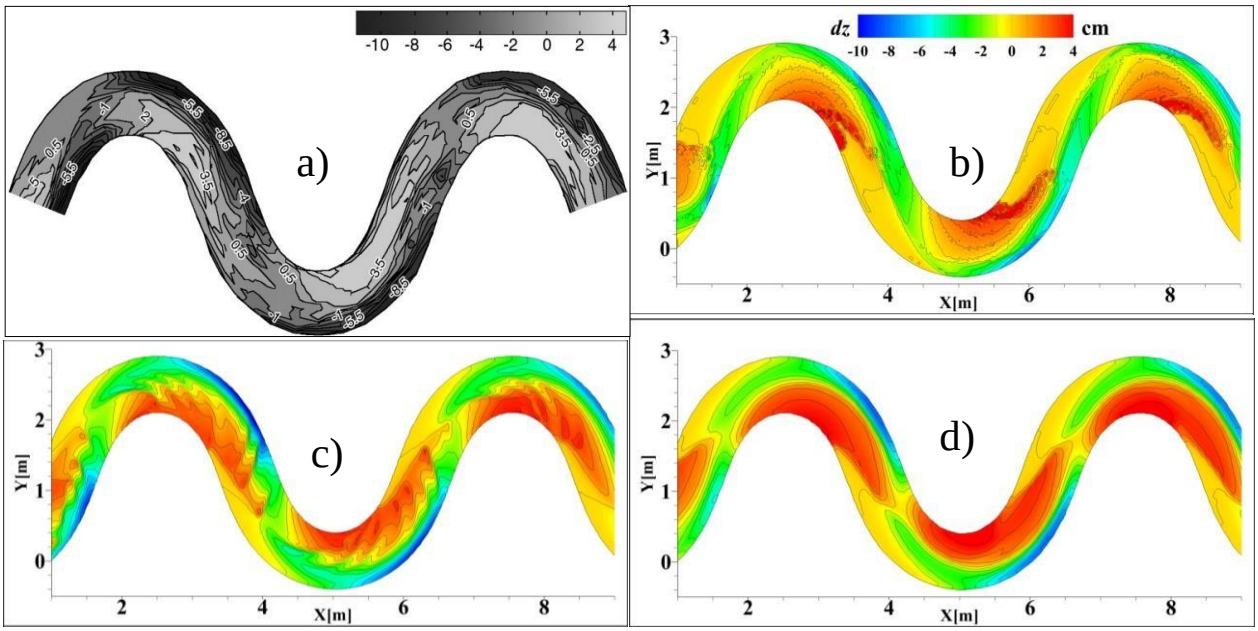

Figure 1. Change in bed morphology at the end of the 170minutes; a) Experiment, derived from Ferrera da Silva and El-Tahawy (2008) b) Telemac2D c) Nays2DH and d) CCHE2D.

3 MODELS USED

The three popularly used morphodynamic models Telemac2D, Nays2DH and CCHE2D are applied in the current study.Telemac2D solves the shallow water equations (momentum and continuity) using the finite-element approach in an unstructured (triangular elements) computational mesh. The sediment transport model sisyphe and the hydrodynamic model Telemac2D are internally coupled. Nays2DH is a computational model within IRIC interface for simulating unsteady horizontal (2D) flow, sediment transport, and morphological changes of bed and banks in rivers. It is based on general curvilinear coordinates.CCHE2D is also a depth-integrated 2D model for simulating free-surface turbulent flows, sediment transport, and morphological change. This is a finite element-based model of the collocation method using quadrilateral mesh. The governing equations solving the flow are two-dimensional depth-integrated Reynolds equations in the cartesian coordinate system. The secondary flow correction parameter was adopted in each of the models. The average size of the mesh was about 4cm.

4 RESULTS AND FUTURE WORKS

The comparison of the change in bed morphology in the experiments and simulation using three models are depicted in Figure 1. In general, all the models satisfactorily reproduced the various bed morphological features obtained in the experiments like deep scour along the outer banks as well as the point bar along the inner bank. The erosion-deposition pattern, extent and the location of the maximum erosion were well mimicked by all models. Comparatively, Nays2DH better captured the length including the depth of erosion along the concave banks. But the length and the size of the formation of point bar on the convex bend was better reproduced by CCHE2D. However, the location of the beginning of the point bar on the convex bend matched close to the experiment in Nays2DH and Telemac2D. The scour depth along the outer bank including the size of the point bar was slightly underestimated in case of Telemac2D. The performance of the Telemac2D lied in between the Nays2DH and the CCHE2D model. It can be concluded that each model, in general, is capable of satisfactorily reproducing the meander bed morphology but there exist differences in capturing particular bed features like point bar, outer bank scour, etc.
However, further analysis under different flow conditions might be necessary to get more detailed insights of the various aspects of the morphodynamic models.

REFERENCES

Jang, Chang-Lae and Shimizu, Y. (2005). Numerical Simulation of Relatively Wide, Shallow Channels with Erodible Banks. *Journal of Hydraulic Engineering,* 131 (7), 565-575.

Ferrera da Silva AM and El-Tahawy T (2008). On the location in flow plan of erosion-deposition zones in sine-generated meandering streams. Journal of Hydraulic Research 46, 49–60.

Proceedings of the 1st IAHR
Young Professionals Congress
17-18 November 2020

IDENTIFICATION OF CONTAMINANT SOURCE USING TRUNCATED BREAKTHROUGH CURVES IN RIVERS

Siyoon Kwon [1], Il Won Seo [2] & Hyoseob Noh [3]

[1,2,3]Dept. of Civil & Environmental Engineering, Seoul National University,
1 Gwanak-ro, Gwanak-gu, Seoul, South Korea 151-744,
ksy92@snu.ac.kr, seoilwon@snu.ac.kr, hyoddubi1@snu.ac.kr

ABSTRACT

When accidental spills of the contaminant occur in natural rivers, it is necessary to identify the contaminant source to minimize the damage from the contamination. Thus, we proposed new data-driven models to identify the pollution source location and spill mass in the river system. The models used the Breakthrough Curve (BTC) obtained from the downstream section as input data. Besides, both Whole Breakthrough Curve (WBTC) and Truncated Breakthrough Curve (TBTC) are capable of input data, which enhances the efficiency of accident response. For developing the models, a large number of numerical simulations under many spill cases with various hydraulic conditions were implemented by the Transient Storage zone Model (TSM). Finally, the performances of six Machine Learning (ML) models for WBTC and TBTC were compared.

Keywords: Contaminant Source identification; Contaminant transport; Transient storage zone; Machine learning

1 INTRODUCTION

When the contaminant spill accidents occur in rivers, predicting contaminant source is an ill-posed problem due to the lack of the observed data, and the complexity of the mixing processes. In order to overcome the lack of real tracer test data, contaminant spill scenarios were generated in this study. The transient storage zone model (TSM) was employed for the synthetic scenarios. In the TSM, the storage zone equation is modeled as well as the advection-dispersion equation for the main flow zone. This model doable the shape of the breakthrough curves (BTC) to a steep slope in the rising part and a long tail in the falling part, which is caused by storage effect. Accordingly, the contaminant spill scenarios were simulated with potential contaminant spill scenarios according to sensor location, spill location, spill mass, flowrate, and some hydromorphic data.

The source identification models have been developed by Machine Learning (ML) approaches from several researchers in groundwater and surface water (Singh et al. 2004, Khorsandi et al. 2014). However, these models have lacked practical researches to apply in surface water. In detail, optimization approaches (Zang & Xin 2017) were much more performed in surface water. These methods had drawbacks to regard as feasible models due to constitutionally sizeable computational load. Therefore, this study carried out Machine Learning (ML) models to identify both spill location and spill mass of contaminant source. For developing the models, the contaminant spill scenarios were generated from TSM numerical model. Then, Breakthrough Curves (BTC) of spill scenarios were extracted into both Whole Breakthrough Curve (WBTC), and Truncated Breakthrough Curve (TBTC) features. Both types of BTC features were served as input variables of ML models, respectively. From this framework, six ML models, Decision Tree (DT), Random Forest (RF), Xgboost, Ridge regression, linear Support Vector Machine (SVM), nonlinear Support Vector Machine (SVM), were compared for both quick and accurate pollutant source identification.

2 Methodology

2.1 Contaminant spill scenarios

To estimate TSM parameters, empirical equations, derived from the Principle Components Regression (PCR), were adopted. The contaminant spill scenarios were simulated in Gam Creek of South Korea. The numerical model used the finite difference method and the Crank-Nicolson method. The validation results of this model showed 0.9 R^2 by the field tracer test data. The model domain consists of 39 km with 30 potential spill locations.

2.2 Machine Learning (ML) models

In this study, six ML models, Decision Tree (DT), Random Forest (RF), Xgboost, Ridge regression, linear Support Vector Machine (SVM), nonlinear Support Vector Machine (SVM), were applied to find the most efficient algorithm for spill location and mass. Figure. 1 (b) and (c) show both WBTC and TBTC, which featured as BTC features as input variables of ML models. The training data set was given by 80% of total spill scenarios. Also, 20% of these scenraios were used to validate the ML models.

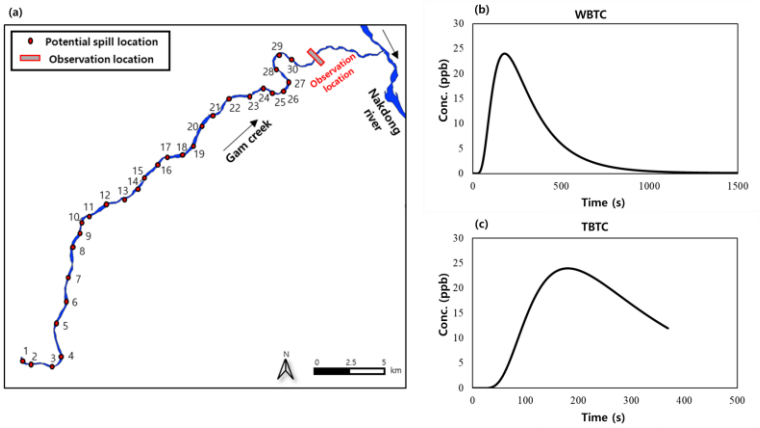

Figure 1. (a) Location of potential spill locations in Gam creek, (b) shape of WBTC, and (c) shape of TBTC

3 RESULTS

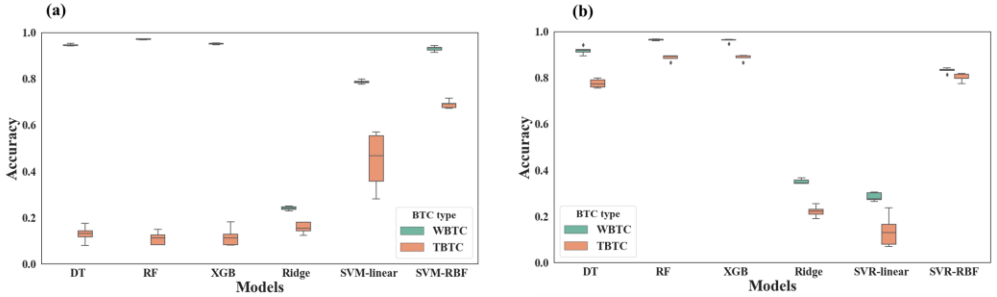

Figure 2. Comparison of 5-fold cross-validation results according to BTC type by each ML to predict (a) spill location and (b) spill mass

As shown in Figure. 2, DT based models outperformed other models when WBTC is used to predict the spill location and mass. However the tree-based models failed to predict spill location using TBTC features. Only SVM-RBF showed accuracy over 0.7. The reason can be explained by the relative importance of each ML algorithms. Since the tree-based models highly depend on the slope of the tail calculated only in WBTC, these models are difficult to predict well with less contributed TBTC features. In the case of SVM, the overall feature importance is more distributed than the tree-based model. Thus, using only the TBTC features significantly contributes to the prediction. Consequently, nonlinear-SVM is the most optimal model for both spill location and mass.

ACKNOWLEDGEMENTS

This research was partially supported by the BK21 PLUS research program of the National Research Foundation of Korea, Ministry of Environment (MoE) as “Chemical Accident Response R&D Program (2018001960001)”, and the Korea Agency for Infrastructure Technology Advancement(KAIA) grant funded by the Ministry of Land, Infrastructure, and Transport (Grant 19DPIW-C153746-01

REFERENCES

Singh, R.M., Datta, B. & Jain, A. (2004). Identification of unknown groundwater pollution sources using artificial neural networks. *J Water Res PL Asce* 130: 506–514.

Srivastava, D., Singh, R.M. (2014). Breakthrough curves characterization and identification of an unknown pollution source in groundwater system using an artificial neural network (ANN). *Environ Forensic* 15(2):175–189.

Zhang, S. & Xin, X. (2017). Pollutant source identification model for water pollution incidents in small straight rivers based on genetic algorithm. *Applied Water Science* 7(4): 1955–1963.

Proceedings of the 1st IAHR
Young Professionals Congress
17-18 November 2020

WATER QUALITY MODELING OF PARANA RIVER, BETWEEN THE YACYRETA DAM AND ITS JUNCTION WITH THE PARAGUAY RIVER.

Ing. Dayana Pita

Young Professional Network, Venezuela.
dayanapita1993@gmail.com

ABSTRACT

The following work shows the results of the study of the dispersion capacity of six hypotheticals pollutants and the variation of their concentration along a section of the Paraná River, between the Yacyretá dam and the confluence with the Paraguay River, making use of the water quality module in HEC-Ras software.

Key Words: Pollutant, dispersion, advection, diffusion, decay, Paraná River, HEC-Ras[i].

1 INTRODUCTION

Water quality modeling is a very useful tool for the correct management of water resources, since it allows estimating and characterizing the assimilation ability of different water bodies, analyzing the impact of discharges and identifying the spatial and temporal variability of water quality, among others. The fundamental objective of this work is, through the use of the water quality module in HEC - Ras, to evaluate the dispersion capacity of a section of the Parana River. Six different hypothetical pollutants were used simulating the entry of each one into the river at the Yacyretá dam. The Paraná River is a river in east-central South America that flows through Brazil, Paraguay, and Argentina. It is 4880 km long and has an average flow of 17,300 m^3/s

2 POLLUTANTS DISPERSION

When a pollutant with a concentration "C" enters a water body, a dispersion process occurs, which will cause the concentration "C" to decrease for a time "t" and a distance "X". The dispersion of a pollutant is given by the advection process and the diffusion process, the first depends on the flow velocity of the receiving body, and the second is how the mass is transported due to the concentration difference and it depends on the coefficient of molecular diffusion. Another parameter is the decay coefficient "K" of the pollutant, which is proportional to its concentration. If it is equal to zero, the pollutant is conservative and its concentration will not change; this coefficient depends on the reactions that pollutants undergo (physical, chemical, or biological), which can modify their mass over time. On the other hand, the pollutant discharge can be punctual, variable, or constant.

3 MODELING IN HEC-Ras.

The data was obtained from a practical case seen in the subject Maths Models, from the specialization course Sanitary Engineering of the University of Buenos Aires.

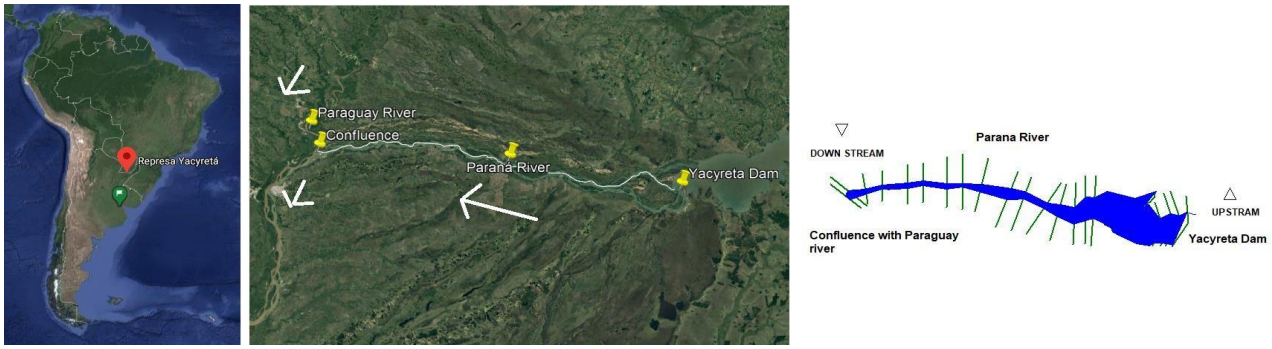

Figure 1. Section of the Paraná River under study, between the Yacyretá dam and its confluence with the Paraguay River- The sections loaded in HEC- Ras are shown on the right. The distance between the study points is 190.054 meters.

Once the geometry and hydrodynamics had been loaded, it was necessary to load the quality parameters, concentrations, decay coefficients and type of discharge. The following table shows the characteristics of each pollutant under study:

Table1. Pollutant type, initial and boundary conditions for modeling – Pollutant input: Yacyretá Dam.

POLLUTANT	TYPE OF POLLUTANT		COEFFICIENT OF DECAY (K=-1/d)	INITIAL CONDITIONS - CONCENTRATION (ml/l)	EDGE CONDITIONS -CONCENTRATION (mg/l)								
					DAY 1	DAY 2	DAY 3	DAY 4	DAY 5	DAY 6	DAY 7	DAY 8	DAY 9
P-1	Constant	conservative	0	10	10	10	10	10	10	10	10	10	10
P-2	Constant	Non conservative	-1	10	10	10	10	10	10	10	10	10	10
P-3	Variable	conservative	0	10	10	8	6	4	10	8	6	12	20
P-4	Variable	Non conservative	-1	10	10	8	6	4	10	8	6	12	20
P-5	Punctual	conservative	0	0	0	0	0	0	10	0	0	0	0
P-6	Punctual	Non conservative	-1	0	0	0	0	0	10	0	0	0	0

4 RESULTS AND CONCLUSIONS

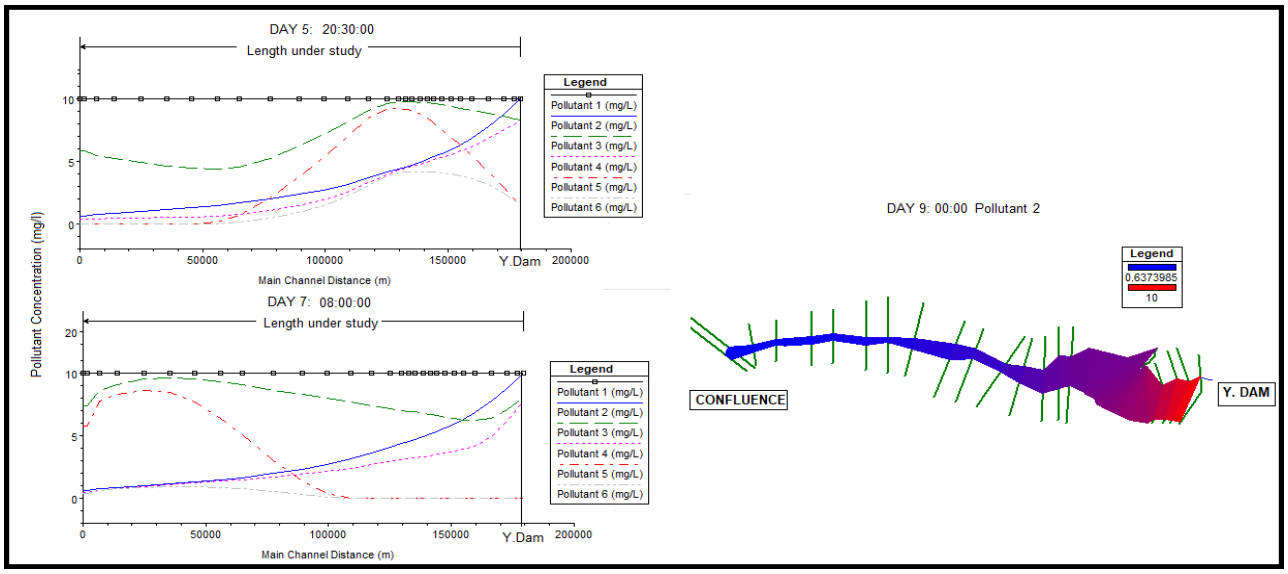

Figure 1. Pollutant concentration vs channel length for days 5, 7 and 9.

Pollutants 2, 4 and 6, being non-conservative, have smaller curve areas than pollutants 1, 3 and 5 respectively, this is due to the fact that when having a decay rate "K", the concentration decreases over time, while conservatives are only diluted by dispersion. Point pollutants have graphs in Gaussian form, where the peak moves by advection and decreases by diffusion. In the case of the conservative pollutants, the area under the curve remains constant throughout the entire route and in the case of the non-conservatives the area decreases according to the decay rate "K". As can be seen in the previous graphs, the HEC-Ras water quality module allows us to represent the processes that occur in nature and simulate different future scenarios in order to establish the most probable behavior of water bodies in the face of different variations in the input data, since it allows evaluating the concentrations variation in space and time of a pollutant with determined characteristics.

ACKNOWLEDGEMENTS

Thanks to my parents, my professor's college, and specially Karol Sánchez, President of YPN Venezuela, for trust and give me the motivation for make this paper.

REFERENCES

James L. Martin, Steven C. McCutcheon (2018). Hydrodynamics and Transport for Water Quality Modeling. CRC press Taylor & Francis.

Ministerio de Ambiente y Desarrollo Sostenible - Dirección de gestión integral del recurso hídrico (2018). Guía nacional de modelación del recurso hídrico para aguas superficiales continentales. Bogotá, D.C.

Steven C. Chapra. (2008). Surface Water Quality Modeling- Waveland Press Inc.

[i] HEC-RAS has been developed for the U.S. Army Corps of Engineers (USACE).

Proceedings of the 1st IAHR
Young Professionals Congress
17-18 November 2020

VERTICALLY-INTEGRATED AND MOMENT EQUATIONS FOR NON-HYDROSTATIC FLOW MODELLING MATLAB PLATFORM

Pedro Gamero [1], Rafael J. Bergillos [2], Francisco N. Cantero-Chinchilla [3] & Oscar Castro-Orgaz [4]

[1,2,4] Hydraulic Engineering Area, Department of Agronomy, University of Córdoba, Rabanales Campus, Leonardo da Vinci Building, 14071 Córdoba, Spain
e-mail (Corresponding author): rafael.bergillos@uco.es (R.J. Bergillos)
[3] Soil and Water Division, IAS-CSIC, Spanish National Research Council, Alameda del Obispo s/n, 14004 Córdoba, Spain

ABSTRACT

The majority of the software platforms designed for non-hydrostatic shallow water flow modelling rely on the solution of computational-costly three-dimensional flow models or depth-averaged Boussinesq-type models that require optimization of dispersive terms. In this field, an unexplored but reliable alternative is the Vertically-Averaged and Moment (VAM) equations model. This work presents a MATLAB software platform for one-dimensional non-hydrostatic flow modelling using the VAM model. First, the VAM governing equations are introduced, which use the weighted residual method to account for the non-hydrostatic and non-uniform characteristics of flow. Then, the structure of the user-friendly graphical interface is described. Finally, the model is applied to two nearshore and open-channel non-hydrostatic flow tests. The comparison of the results with experimental data highlights the accuracy of the VAM model and the potential of the present software for modelling non-hydrostatic flows.

Keywords: non-hydrostatic flows, depth-integrated model, software platform, coastal applications, open-channel tests.

1 INTRODUCTION

The use of non-hydrostatic models is often required to provide realistic predictions in coastal and open-channel flows, where the development and use of depth-integrated simulation models is a common practice. Three families of vertically-averaged models have been developed so far to simulate non-hydrostatic flows: (i) the Boussinesq-type equations (Castro-Orgaz and Hager, 2017), (ii) the multilayer non-hydrostatic extension of the shallow water equations (Casulli, 1999), and (iii) the vertically-averaged models based on the use of the weighted residual (WR) method to derive the vertically-averaged and moment (VAM) equations from the Reynolds-Averaged Navier-Stokes (RANS) equations, known as VAM equations model (Cantero-Chinchilla et al., 2018). Despite it was recently demonstrated to be accurate for predicting a number of river and coastal flows (Cantero-Chinchilla et al., 2018), the VAM model is a physical system of equations that is still unfamiliar to the scientific community to some extent and hardly settled by using a user-friendly platform for practical applications. The purpose of this work is presenting a user-friendly MATLAB software platform to apply the VAM model to simulate non-hydrostatic flows in a number of coastal and open-channel flow cases. The platform is freely available on GitHub (https://github.com/Frncch/VAM_Model_Software).

2 BASICS OF THE VAM MODEL

The governing equations for the VAM model are derived using the WR method into the depth-averaging process of the RANS equations. First, predictors for the field variables containing perturbation parameters are used to prescribe the non-hydrostaticy and non-uniformity of flow, increasing the number of independent variables in the depth-averaged equations. Then, a weighting function involving moments around the centroid of a section is selected to derive moment equations, providing mathematical closure to the system. The system of equations is solved by using a hybrid finite volume-finite difference numerical scheme, where the MUSCL-TVD-4th is applied to reconstruct the variables at the interfaces and the HLLC approximate Riemann solver is employed to compute the numerical fluxes. To grant the C-property, the WSDGM method and a proper discretization of the gravity term are applied. The solution is then evolved in time using a one-step forward Euler scheme plus an iterative Newton-Raphson method. Details can be consulted in Cantero-Chinchilla et al. (2018) and Gamero et al. (2020).

3 DESCRIPTION AND APPLICATION OF THE SOFTWARE PLATFORM

The initial window of the software platform allows the user to select between coastal or open-channel flow applications (Fig. 1a). The open channel flow application enables the numerical experimentation on Favre waves and flow over Gaussian obstacles (Fig. 1b). The coastal flow application models the solitary wave propagation over horizontal bed and the solitary wave propagation with run-up (Fig. 1c). All the applications include numerous editable options to customize the desired numerical experiment.

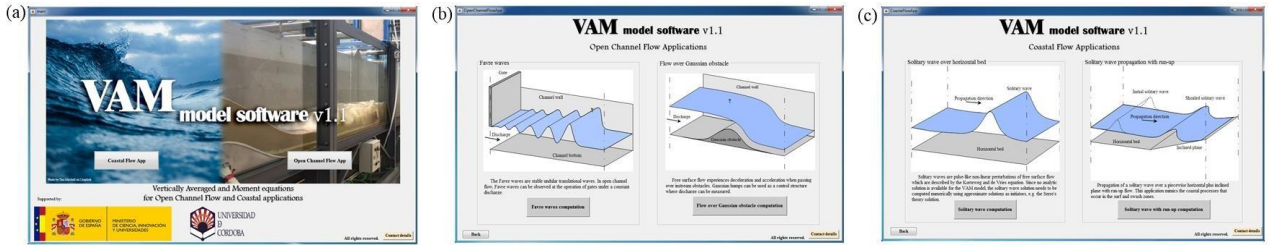

Figure 1. Software platform screens: (a) main menu, (b) open-channel flow app, and (c) coastal flow app.

Fig. 2 shows the applications for flow over a Gaussian obstacle and solitary wave propagation with run-up using the experimental data of Sivakumaran (1981) and Synolakis (1986), respectively. As compared to the standard Saint-Venant model solution, the VAM model yields more accurate results for both tests.

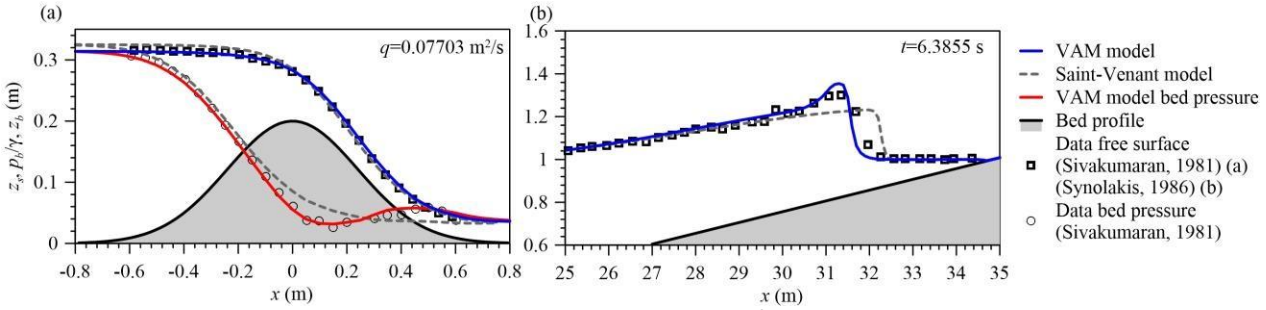

Figure 2. (a) Flow over a Gaussian bed with q = 0.07703 m^2/s (Sivakumaran, 1981), (b) solitary wave propagation and run-up over a beach profile at t = 6.3855 s (Synolakis, 1986), where z_s is free surface level, p_b is bed pressure, z_b is bed level, γ is specific weight of water, x is longitudinal distance and t is time.

4 CONCLUSIONS

The easy-to-use environment and the accuracy of the results highlight the potential of this user-friendly MATLAB software platform for modeling open-channel and nearshore flows, where non-hydrostatic pressure and non-uniform velocity shall be accounted for. This entails a useful hydraulic tool suitable for teaching and research purposes.

ACKNOWLEDGEMENTS

This work was supported by the research project CTM2017-85171-C2-1-R (State Research Agency, Spain) and the research group AGR-127. RB and FNCC were partly funded by the Spanish Ministry of Science, Innovation and Universities through research contracts FJCI-2017-31781 and FJCI-2016-28009, respectively.

REFERENCES

Cantero-Chinchilla, F.N., Castro-Orgaz, O. and Khan, A.A. (2018). Depth-integrated nonhydrostatic free-surface flow modeling using weighted-averaged equations. *International Journal for Numerical Methods in Fluids*, 87(1), 27-50.

Castro-Orgaz, O. and Hager, W.H. (2017). *Non-hydrostatic free surface flows*. Springer, 696 pp.

Casulli, V. (1999). A semi-implicit finite difference method for non-hydrostatic, free-surface flows. *International Journal for Numerical Methods in Fluids*, 30(4), 425-440.

Gamero, P., Bergillos, R.J., Cantero-Chinchilla, F.N. and Castro-Orgaz, O. (2020). A MATLAB software platform for modelling vertically-integrated non-hydrostatic flows with moment equations. *Environmental Modelling & Software*, 104674.

Sivakumaran, N.S. (1981). Shallow-flow over curved beds. Doctoral Thesis, Asian Institute of Technology, Bangkok, Thailand.

Synolakis, C. E. (1986). The runup of long waves. Doctoral dissertation, California Institute of Technology.

IAHR AIRH

International Association for Hydro-Environment Engineering and Research

Hosted by
Spain Water and IWHR, China

Session 3
Hydroinformatics

IAHR YPN

Hosted by
Spain Water and IWHR, China

Proceedings of the 1st IAHR
Young Professionals Congress
17-18 November 2020

IMPROVING RAINFALL FIELDS IN DATA SCARCE BASINS: A COMPARISON OF DOWNSCALING, INTERPOLATION AND MERGING SCHEMES

Nicolás Duque-Gardeazabal[1] & Erasmo A. Rodríguez.[1]

[1]Universidad Nacional de Colombia, Grupo de Investigación en Ingeniería de los Recursos Hídricos (GIREH), Bogotá, Colombia; nduqueg@unal.edu.co; earodriguezs@unal.edu.co

ABSTRACT

Reduction of *in situ* precipitation measurements increases the uncertainty of rainfall fields. To tackle this problem we use alternative data sources, but not only remote sensed rainfall. We performed rain gauge interpolations, downscaling of the MSWEP dataset based on vegetation data, simple linear downscaling, and a merging between MSWEP and rain gauge data. We present a comparison of the performance of rainfall fields produced with different network densities, which mimics precipitation data availability in a basin. We found that interpolation methods highly deteriorate their performance when the network density is artificially reduced. Using vegetation indices with a simple approach can reduce the error of the MSWEP, yet the highest reduction is achieved by blending the MSWEP with the rain gauge data. A combination of downscaling and merging methods can further reduce the error in low network densities.

Keywords: MSWEP, Kernel Smoothing, Enhanced Vegetation Index, Rain gauge density, Satellite Precipitation

1 INTRODUCTION

A proper estimation of the distributed rainfall field in a basin is paramount. It affects the estimation of water discharge in rainfall-runoff models, the calculation of indices in water planning and management, among other studies. There exist many methodologies to perform this estimation, yet the most popular techniques are based on rain gauge observations that are then interpolated. However, according to García, Rodríguez, Wijnen, & Pakulski (2016), there has been a global decrease in the *in situ* precipitation measurements in recent decades.

To improve the rainfall estimation in regions with data limitations, alternative sources such as satellite and reanalysis data bring support and robustness to calculations. There is remote sensed data of rainfall but also data associated with the influence of rainfall in other environmental variables. For instance, remote sensed vegetation variables that have been exploited in the field of ecohydrology. Although these alternative products, associated with rainfall quantification, have good spatial and temporal coverage, they suffer from bias and temporal consistency. Several downscaling and merging algorithms have been proposed (Li & Shao, 2010).

The Double Smoothing (DS) algorithm is a statistical merging approach which is not based on gaussian or geostationary assumptions (Li & Shao, 2010). It is a simple and flexible method that only requires the coordinates and time series of the rain gauge and satellite products, allowing to easily add, retrieve or modify the datasets used in the analysis. The purpose of this work is to compare the performance of the DS algorithm against traditional interpolation and simple downscaling methodologies. In the analysis, the available rain gauge information, inside a data rich watershed in the tropical Andes was constrained, allowing to explore the model´s performance at different station densities.

2 DATA AND METHODS

The case study was the Sogamoso river basin in Colombia, which has 219 rain gauges, from where 156 were selected for the analysis (those with more than 50% of missing daily rainfall data in the period 1980-2012 were excluded). We used the Multi-Source Weighted-Ensemble Precipitation (MSWEP) (Beck et al., 2017) as rainfall support product (rain gauges utilize in its creation were discarded). Estimates of the Enhanced Vegetation Index (EVI) from the MODIS sensor on board of both the Terra and Aqua satellites (Didan, 2015), were used at 1km resolution to perform a simple downscaling based on ecohydrological concepts. A 90 m resolution Digital Elevation Model (DEM) was employed to bolster an interpolation method, coming from the SRTM mission.

We explored different levels of rain gauge network density and different configurations, via random sampling. The performance of interpolation, downscaling and merging methods was calculated against the observed data in the basin, using cross validation (CV) and independent validation (IV) methods. Due to the availability of EVI measurements, the period chosen to conduct the goodness of fit was from 2000 to 2005.

The DS merging was conducted with the modified rainmerging R package, which allowed calibrating the model parameters (Duque-Gardeazábal, Zamora, & Rodríguez, 2018). We also made use of the ordinary, universal, external drift and regression Kriging, and IDW interpolators and chose to only show the best results for

comparison (regression Kriging and IDW). We downscaled the precipitation of the MSWEP by monthly averaging the EVI time series, upscaling the 1 km satellite images to 25 km, making a regression between the 25 km MSWEP and EVI values lagged 1 month (based on the experiments of López López, Immerzeel, Rodríguez, Sterk, & Schellekens (2018)), applying the regression to the 1 km EVI values and finally disaggregating the monthly rainfall into daily values. Likewise, we used a simple bilinear downscaling of the MSWEP data.

3 RESULTS

Figure 1 shows that a bilinear downscaling can slightly reduce the RMSE of the MSWEP. However, the reduction is higher if the analysis considers the cumulative influence of rainfall on vegetation, through the use of EVI. These results are present for both comparison methodologies (CV and IV), and for almost every rain gauge network density and configuration. This behavior is also reported by the Percent Bias (not shown here).

Figure 2 shows a lower estimation error by using the interpolation methods than the performed downscalings. Yet some of them highly suffer when the density of measurement is reduced (e.g. regression kriging). The lowest error is consistently produced by merging the MSWEP with local rain gauges, even if the network density is below 1 gauge/1000km^2.

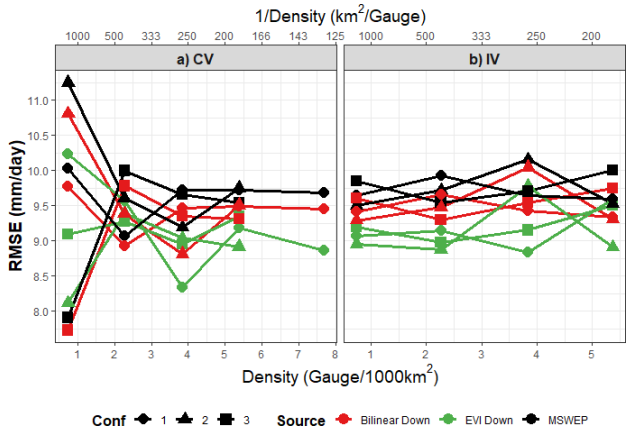

Figure 1. Performance of MSWEP and its downscalings, against the rain gauge networks configuration

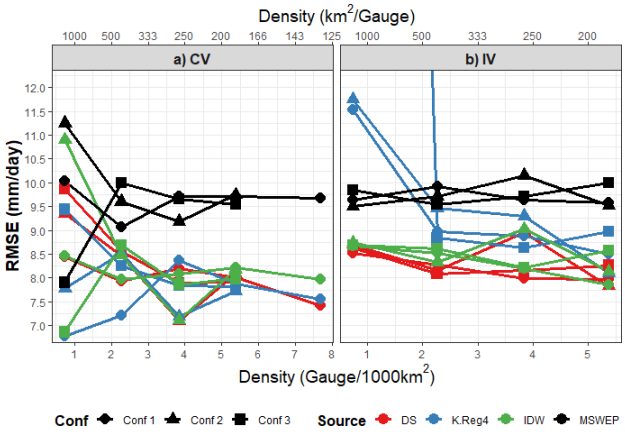

Figure 2. Performance of MSWEP, interpolations and DS merging method

4 CONCLUSIONS

This research evidenced that the lowest rainfall error among the used methods was the merging between the MSWEP and the rain gauges observations. This occurred not only for high density networks but also for experiments mimicking a data scarce basin. It was also demonstrated that considering ancillary environmental information can decrease the error. Even a simple regression with the EVI produced a higher error reduction compared with a simple methodology. However, it did not outperform the merging with a low number of rain gauges. More specialized downscaling methodologies such as the Geographic Weighted Regression and the combination with other ancillary variables can improve even more the error of the rainfall field estimations. The error can be further reduced if the rain gauge data is merged with a product that has been firstly downscaled with the previously mentioned procedures.

REFERENCES

Beck, H. E., Van Dijk, A. I. J. M., Levizzani, V., Schellekens, J., Miralles, D. G., Martens, B., & de Roo, A. (2017). MSWEP: 3-hourly 0.25° global gridded precipitation (1979-2015) by merging gauge, satellite, and reanalysis data. Hydrology and Earth System Sciences, 21(1), 589–615. https://doi.org/10.5194/hess-21-589-2017

Didan, K. (2015). MYD13A2 MODIS/Aqua Vegetation Indices 16-Day L3 Global 1km SIN Grid V006 [Data set]. https://doi.org/10.5067/MODIS/MYD13A2.006

Duque-Gardeazábal, N., Zamora, D., & Rodríguez, E. (2018). Analysis of the Kernel Bandwidth Influence in the Double Smoothing Merging Algorithm to Improve Rainfall Fields in Poorly Gauged Basins. 13th International Conference on Hydroinformatics, 3(July), 635–626. https://doi.org/10.29007/2xp6

García, L. E., Rodríguez, D. J., Wijnen, M., & Pakulski, I. (2016). Earth Observations for Water Resources Management: current use and futute opportunities for the water sector. Washington D.C.: International bank for recostruction and development/ The world Bank.

Li, M., & Shao, Q. (2010). An improved statistical approach to merge satellite rainfall estimates and raingauge data. Journal of Hydrology, 385(1–4), 51–64. https://doi.org/10.1016/j.jhydrol.2010.01.023

López López, P., Immerzeel, W. W., Rodríguez, E. A., Sterk, G., & Schellekens, J. (2018). Spatial downscaling of satellite-based precipitation and its impact on discharge simulations in the Magdalena River basin in Colombia Impact of high spatial resolution precipitation on streamflow simulations. Frontiers in Earth Science, 6(June). https://doi.org/10.3389/feart.2018.00068

Proceedings of the 1st IAHR
Young Professionals Congress
17-18 November 2020

INITIAL DEVELOPMENT OF A CITIZEN SCIENCE-BASED RIVER FLOOD MONITORING AND FORECASTING FOR THE RIMAC RIVER IN LIMA PERU

Maria Paz Garcia [1], Diego Velayarce[1], Andrea Tipe [1], Chiara Manassero[1], Camila Timana[1] & Daniel Horna [1,2]

[1]Universidad de Ingeniería y Tecnología - UTEC, Lima, Perú
[2] Centro de Investigación y Tecnología del Agua - CITA, Universidad de Ingeniería y Tecnología - UTEC, Lima, Perú

ABSTRACT

The present study describes the initial efforts of building a citizen science-based monitoring river system for flood forecasting in the Rimac River located in Lima, Peru, a city that is severely affected by flooding, especially during El Niño events. This system will be based on videos recorded of the Rimac River taken by regular citizens at accessible bridges when the water level begins to rise. Then, the videos will be uploaded to the system database for processing and getting useful results to alert the population in the case of flooding. In order to validate the system, the research team recorded videos at three bridges along the Rimac River and compared them with official data. The recorded videos were processed using Large Scale Particle Image Velocimetry (LSPIV) to obtain free-surface velocity, to then obtain corresponding flowrates.

Keywords: LSPIV, citizen science, El Niño, Rimac River.

1 INTRODUCTION

The Rimac River is the most important river that passes through Lima, Peru, a city that is severely affected by floods and mudslides especially during El Niño years. This situation causes significant economic losses and endangers the citizens settled in the Rimac riverbanks and its tributary streams (Comeca et al., 2019). The uncertainty of the event and the high levels of vulnerability in the affected regions still represents a high risk (French & Mechler, 2017). Likewise, the hydrometeorological information is insufficient to build any kind of early warning system. During high flow, it is dangerous for the operators to make intrusive measurements, furthermore, the values will possibly be affected by floating debris and transported sediment (Moramarco, et al., 2017). Within this context, the processing of river videos using LSPIV to obtain flowrate data represents an extra source of information which will allow the elaboration of an early warning system that is built on the collaboration of the vulnerable population to achieve their own safety.

2 METHODOLOGY

2.1 Field data collection

Three bridges along the Rimac basin were selected to record videos of the river free surface with a conventional cell phone camera (Table 1). These were chosen based on the distance from the bridge to a city of importance, the curvature of the river, the flatness of the free surface, and accessibility. To assure data collection validity, the videos had to show four known location control points during their entire length (minimum 1 minute). The processing algorithm requires visible particles on the water surface to obtain a direction of the velocity profile. Natural particles on the surface of a river are commonly used as tracers. However, artificial particles such as wood sawdust can provide a more accurate image analysis, because they form a unique pattern on the free surface to be followed by the PIV algorithm (Gharahjeh et al., 2016). Thus, wood sawdust particles were thrown at the surface in two study sites (San Mateo 1 and Chosica) for a better video processing accuracy.

2.2 Data analyzing

The recorded videos were analyzed using Large Scale Particle Image Velocimetry (LSPIV) to extract the river mean velocity by comparing pairs of images and contrasting the displacement of the river current. The RivER program (Patalano and García, 2006) identifies the current lines in the delimited area and calculates the speed vectors along the cross-sectional area to obtain the discharge velocity (Figure 1). For that purpose, it is commonly used for the natural channels a velocity index of 0.85 to convert free surface velocity into mean velocity in the vertical, which assumes a logarithmic vertical velocity distribution (Rantz, 1982). Moreover, an initial cross section was estimated with an approximation that the river length must be twenty times the river depth (Rodriguez et al., 2004).

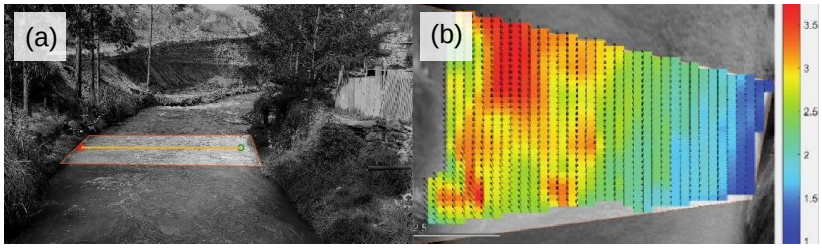

Figure 1. (a) Cross section of the original image (b) Vector and magnitude velocities of the rectified image.

3 RESULTS

The flowrates obtained are shown in Table 1 and compared with the official values provided by a nearby hydrometric station managed by The National Water Authority (ANA, by its acronym in Spanish). For San Mateo 1, the flowrate calculated with the wood sawdust particles (artificial tracers) on the surface is closer to the hydrometric value. However, the result with natural tracers also matches the official flowrate. In Chosica, the calculated flowrate with natural tracers on the surface exceeds the official value while the one with artificial tracers is considerably lower. Hence, it is not possible to identify if the LSPIV processing underestimates or overestimates the actual flowrate value.

Table 1. Flowrates at each measurement point (m^3/s)

Bridge	Latitude (°)	Longitude (°)	Natural tracers	Artificial tracers	Hydrometric value	Relative Error N.T	Relative Error A.T
San Mateo 1	-11.755820	-76.295911	9.49	10.93	11.62	18.3 %	5.94%
San Mateo 2	-11.760115	-76.301058	6.08	*	11.62	47.7%	*
Chosica	-11.935066	-76.692523	25.34	16.70	22.00	15.2%	24.1%

∗ Video was not recorded because the access to the bridge hindered sawdust transportation.

CONCLUSIONS

To create a system that is based on citizen participation, the communities that live along the Rimac River must be informed about the study relevance to understand their role on prevention. The system is accessible and practical and can be scaled to enrich the database and obtain extensive validation. Another approach that will enhance the system is to install more LSPIV camera chambers since there are only a few active cameras on the Rimac basin (CITA UTEC, 2019). This will generate an interconnected network of all the data that can be correlated with other hydraulic and environmental attributes to validate the system with greater precision. Finally, as future work, a hydrodynamic model in HEC-RAS will be developed to predict flood propagation along the river network and estimate the most affected sections. Furthermore, the final aim is to develop an application that achieves the automatic processing of the videos to maintain an active response to the population needs.

REFERENCES

Centro de Investigación y Tecnología del Agua CITA (2019). *Cuenca del río Rímac cuenta con nueva Estación LSPIV que permitirá su monitoreo y reducción del riesgo de desastres*. Cita.utec.edu.pe.

Comeca, M. Á., Cruz, F. M., Durand, D. M., Rojas, T., La Torre, F. M., & Comeca, L. M. (2019). El Niño Costero y la ocupación del territorio, cuenca del río Rímac. Caso: Chosica. *Investigaciones Sociales*, *22*(41), 105-120.

French, A., Mechler, R. (2017). Managing el Niño risks under uncertainty in Peru: Learning from the past for a more disaster-resilient future. *International Journal of Disaster Risk Reduction*.

Gharahjeh, S., Aydin, I. (2016). *Application of video imagery techniques for low cost measurement of water surface velocity in open channels, 79 -94.*

Moramarco, T., Barbetta, S., & Tarpanelli, A. (2017). From Surface Flow Velocity Measurements to Discharge Assessment by the Entropy Theory. *Water*, *9*(2), 120.

Patalano, A., García, C. (2006). RIVeR—towards affordable, practical and user-friendly toolbox for large scale PIV and PTV techniques. In: IAHR RiverFlow Conference, St. Louis, Missouri, USA

Rantz, S. E. (1982). *Measurement and computation of streamflow* (USGS Numbered Series No. 2175; Water Supply Paper). U.S. G.P.O.

Rodriguez, J. F., Bombardelli, F. A., García, M. H., Frothingham, K. M., Rhoads, B. L., & Abad, J. D. (2004). High-resolution Numerical Simulation of Flow Through a Highly Sinuous River Reach. *Water Resources Management*, *18*(3), 177-199.

Proceedings of the 1st IAHR
Young Professionals Congress
17-18 November 2020

ASSESSMENT OF MAXIMUM STORM PRECIPITATION CHANGES OVER LAST DECADES

Aleksandra Bazheeva

Russian state agrarian university - Moscow agricultural academy named after K.A. Timiryazev, Department Meteorology, Moscow, Russia,
bazheeva.al@yandex.ru

ABSTRACT

Different criteria have been considered for evaluation of storm precipitation change during the last several decades in respect to different geographical zones of the European territory of Russia.

Keywords: climate change, storm precipitation; Mann Kendall's test

1 INTRODUCTION

An increase of maximum daily precipitation during storm rains has been observed recently at many meteorological stations around the world (Groisman et al, 2005; Ilinich 2016 et al; Zolina,2012; etc,). The appearance of heavy precipitation is primarily due to an increase in air temperature and increased pollution in the urban areas, and other causes (Groisman et al, 2005; Ilinich 2016 et al; etc.). The main purpose of the research is to analyze the possible criteria for assessment of change of storm precipitation during last decades.

2 MATERIALS AND METHODS

The object of the study is data from stations located in various natural zones: the foothills of the North Caucasus (Mineral Waters), the forest zone (Bryansk), the Steppe zone (Volgograd). Chronological changes in the maximum daily precipitation are shown in Fig. 1.

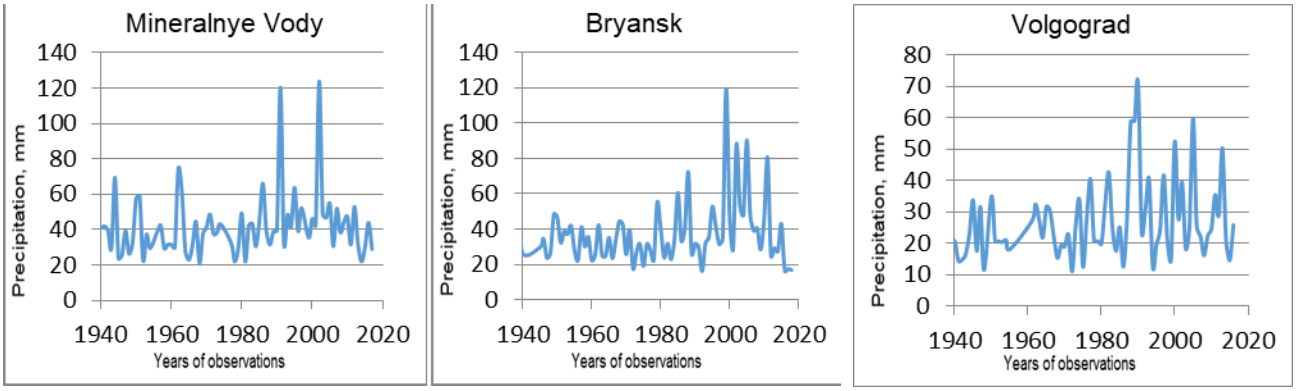

Figure 1. Examples of long-time observation at different meteorological stations.

There is a positive trend of changes at all the stations studied. However, the obtained graphs are not sufficient for a full assessment of changes in precipitation. Man Kendall's numerical criterion (Mann 1945) has been used for estimation of storm precipitation's trend. The procedure of estimation is based on using chronological series from n data. The size of differences is determined by comparing the data value from a later (Xi) time period to data value from an earlier (Xj) time period. The difference between them takes on values 1, 0, or -1. Value 1 is assigned if Xj-Xi > 0; 0 if Xj-Xi = 0; -1 if Xj-Xi < 0. The S parameter is calculated according to the formula 1.

$$S = \sum_{i=1}^{n-1} \sum_{j=i+1}^{n} \operatorname{sgn}\left(x_j - x_i\right); \qquad \text{Sgn}(\qquad (1)$$

A positive value of S parameter means that the observations have a positive trend. The following values of the criteria were obtained: Mineralnye Vody +255; Bryansk +205; Volgograd +429. Similar estimations were made for other time windows: a) 1950–2017 and b) 1960 – 2017. The following S-parameters were obtained correspondently a) 129; 118; 157 and b) 188; 219; 111.

The next criterion takes into account the quantiles of maximum daily precipitation, which is determined with help of Weibull formula (Dmowska el al., 2011). The obtained results are represented in figure 2. The figure shows that the values of the second series of observations are higher than the ones on the first, which means that there is an increase in storm precipitation.

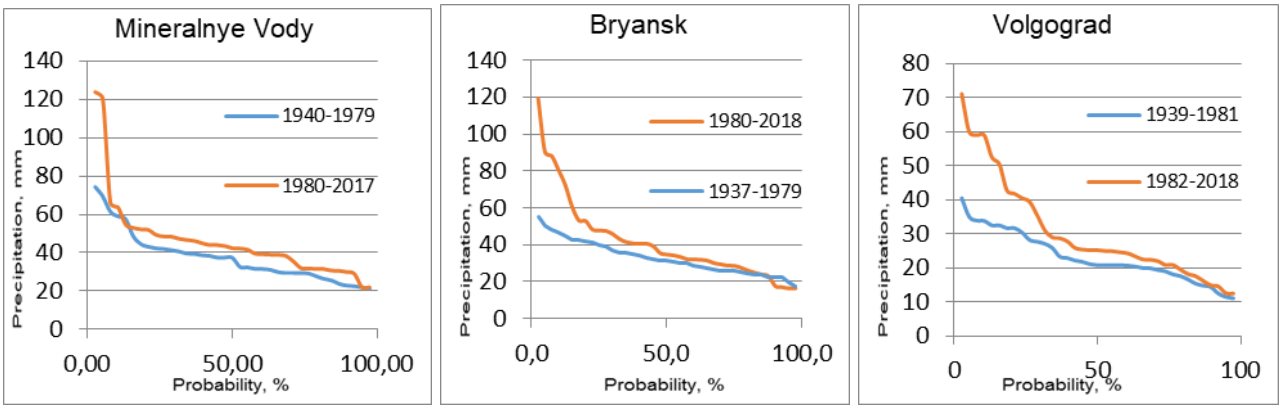

Fig. 2. Points of quintile values of empirical probabilistic curves

3 RESULTS AND DISCUSSION

All analyzed aspects allow us to conclude that there is an increase in maximum daily storm precipitation during the last several decades at all studied stations. It is necessary to note that the values of Man Kendall's numerical criterion are very significant even such value is located within 10-20 we believe that there is a clear positive test. Also we have to note that almost all quantiles of maximum daily precipitation during the last several decades are above the quantiles of previous decades. The differences are much more significant for smaller probabilities (3-5%).

4 CONCLUSIONS

All the considered criteria for assessing the increase in maximum daily precipitation validate each other; respectively, we can conclude that they are quite objective. Since the design standards for hydraulic structures on small rivers, both in Russia and in many other countries, take into account the maximum daily precipitation, we can conclude that the reliability of all such structures from the last century has been decreased due to increased rainfall. Empirical dependences (fig.2) between precipitation and of their probability (for the last decades) can be used for projecting small hydraulic structures within 5 - 10% of probability.

REFERENCES

Groisman P.U., Knight R.W., Easterling T.R., Hegerl G.G., Razuvaev V.N. Trends in intense precipitation in climate record// J. Climate. 2005.18.1326-1350.

Dmowska, Ed.R. & Hartman D. & Rossby H.T. 2011. Statistical methods in the Atmospheric Sciences. Inter. Geoph. Series Vol.1. Oxford, OX51GB, UK, P. 668.

V. Ilinich, E. Akulova, V. Belchihina and K. Ponomarchuk. Estimation of Statistical Characteristics for Storm Precipitation with Long-term Data to Assess Climate Change. Journal of Climate Change, Vol. 2, No. 2 (2016), pp. 83–87. DOI 10.3233/JCC-160019.

Ilinich V.V., Larina T.D. Evaluation of changes storm Precipitation during century for the modeling of floods. In the book: Sustainable Hydraulics in the Era of Global Change – Erpicum et al. (Eds.) © 2016 Taylor & Francis Group, London, ISBN 978-1-138-02977-4, p. 928 – 934.

Mann H.B. (1945) Non-parametric Test against Trend, Econometrica: 13, p. 245-249.

Proceedings of the 1st IAHR
Young Professionals Congress
17-18 November 2020

PHET PLATFORM TO SUPPORT THE TEACHING OF FLUID MECHANICS DURING THE COVID-19 PANDEMIC

Daniel Rios [1] & Tania Grisales [2]

[1] Professor of the Cooperative University of Colombia, Medellín, Colombia
juan.riosar@campusucc.edu.co

[2] Student of the Cooperative University of Colombia, Medellín, Colombia
tania.grisales@campusucc.edu.co

ABSTRACT

This research work presents the results obtained to use the PhET platform for teaching of fluid mechanics during the COVID-19 pandemic in the Cooperative University of Colombia. The PhET Interactive Simulations Project is distributing under the Creative Commons-Attribution 3.0 license and the Creative Commons GNU General Public License. The most important finding is the connection development between the students and platform due to the confinement condition, the use of PhET platform was like to "game" and improve the mood of the students. We conclude that PhET platform is excellent tool for teaching of fluid mechanics during the COVID-19 pandemic if the student has a good computer equipment.

Keywords: PhET Interactive Simulations, COVID-19, fluid mechanics, teaching.

1 INTRODUCTION

The COVID-19 pandemic has changed the traditional education in the Universities around the world due to social distance and confinement condition however the Professors and Universities has looking for new methodologies and strategies to continue teaching. One big difficult have been the practices and laboratories the which required to be in physical spaces, in response to this difficult the Professors has finding support in the digital and web platform to simulate process and continue teaching Engineering.

In the Cooperative University of Colombia at Medellín we used in general the hydraulics laboratory for the practices and laboratories of fluid mechanics (viscosity, density, Bernoulli equation, loss energy…) and hydraulic courses, however the COVID-19 pandemic change this routine and we decided to use PhET platform to perform the loss energy practices in the fluid mechanics courses of the Civil Engineering program on remote way and continue with biosecurity protocols.

2 MATERIALS AND METHODS

We use the PhET Interactive Simulations platform that is distributing under the Creative Commons-Attribution 3.0 license and the Creative Commons GNU General Public License by University of Colorado at Boulder. For the laboratory practice 10 flow rates (discharges) were selected in the range between 1000 and 10000 (l / s), later for the constant pipe area equal to 3.1 m², velocities to full tube (Table 1) were calculate corresponding to each flow rate (discharges) selected and finally the curve Flow (m³ / s) vs Velocity (m / s) was constructed.

Table 1. Relation of discharges and Velocities.

Flow (m³ / s)	1.679	2.053	3.269	4.532	5.608	6.169	7.666	8.040	9.069	9.911
Velocity (m / s)	0.54	0.66	1.05	1.46	1.81	1.99	2.47	2.59	2.93	3.20

3 RESULTS

The most important finding is the connection development between the students and platform due to the confinement condition, the use of PhET platform was like to “game” and improve the mood of the students. We conclude that PhET platform is excellent tool for teaching of fluid mechanics during the COVID-19 pandemic if the student has a good computer equipment. In addition, the concepts of discharge, velocity and unit energy loss that were explained in class are apply by student for PVC material in appropriate form (Figure 1).

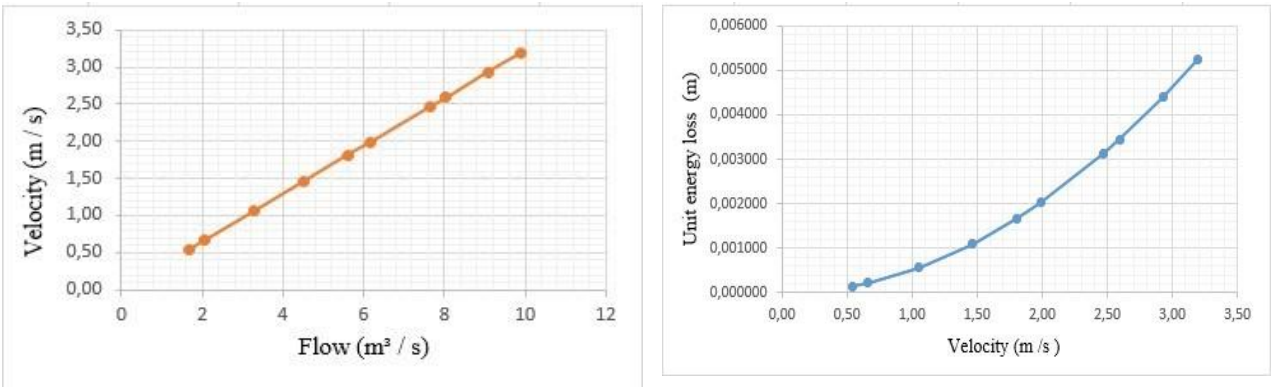

Figure 1. Relationship between discharge and velocity (left) and relationship between velocity and unit energy loss (right).

4 CONCLUSIONS

We conclude that PhET platform is excellent tool for teaching of fluid mechanics during the COVID-19 pandemic and normal condition because is interactive and easy for all students, therefore we recommended this platform for digital laboratory practice and examples during the COVID-19 pandemic and for the time post pandemic.

ACKNOWLEDGEMENTS

We thanks to:

- University of Colorado at Boulder for share PhET Interactive Simulations platform to academic community.
- Students of Cooperative University of Colombia for your interest and efforts in the laboratory practice.

REFERENCES

University of Colorado. (2004-2013). PhET Interactive Simulations platform.

Proceedings of the 1st IAHR
Young Professionals Congress
17-18 November 2020

ANALYSIS OF THE PERFORMANCE OF A COMMERCIAL SOFTWARE FOR PIPE BURST DETECTION

Nicole Friedrich Neumann [1], David Ferras, PhD.[1], Martijn Bakker, PhD. [2] & Maria Kennedy, PhD.[1]

[1] IHE Delft: Institute for Water Education, Delft, The Netherlands,
e-mail nifneumann@gmail.com

[2] Royal HaskoningDHV, Amersfoort, The Netherlands,

ABSTRACT

In developing countries, 35% of treated water is lost before reaching households. Thus, more water needs to be abstracted, energy is wasted, and water supply is interrupted. Therefore, detecting more and faster pipe bursts reduces the physical losses. Aquasuite© BURST Alert is a data-driven heuristic model, easy to implement once it does not require the installation of new sensors at the distribution system. It uses as inputs (i) the prediction of flow and pressure from another model; (ii) measurements from WDS. The main objective of this research was to investigate deeper which variables influence the computation of a burst alarm, and then determine their best setup. Statistical tests have been performed to analyze the parameters at an offline environment in Python. Results showed that adding weather data to BURST Alert would not improve significantly the software detection; however, they indicated the influence of DVG's average flow.

Keywords: water distribution systems, pipe burst, heuristic detection model, water demand forecasting.

1 INTRODUCTION

Projections indicate that by 2050, almost 6 billion people will experience severe water scarcity. Therefore, the usage of water needs to be efficient and its losses minimized. Leakages in water distribution systems (WDS) increases the water stress, since a higher volume will have to be abstracted to meet the demand. The pipe burst is the event for which a leak starts; hence detecting bursts is primary to avoid the development of leaks in WDS's.

Aquasuite© BURST Alert is a data-driven heuristic model, easy to implement once it does not require the installation of new sensors at the distribution system (Bakker *et al*., 2014). The program developed by Royal HaskoningDHV uses the prediction of flow and pressure and it compares with real-time data. If the deviation is too high (*e.g*., the flow measured is higher than the threshold), a burst or leak most likely occurred, triggering an alarm to the water company. However, improvements are still needed to decrease the number of false alarms whilst detecting the maximum possible number of bursts. This research aimed to find the best parameters values for enhancing the performance of Aquasuite BURST Alert software. With the right parameter's setup, the underlying algorithm software will be able to detect extra burst events and without increasing too much the number of false alarms. The specific objectives are (i) to determine the performance of the software during 2019 at sub-supply areas (DVGs) of the water company Oasen; (ii) to investigate the influence of weather variables at burst occurrence.

2 METHODOLOGY

BURST Alert was reproduced in Python code, generating thresholds for flow and pressure and alarms. Using the output of the code, logistic regressions were done at *R* software to model dichotomous outcome of a burst event: 0 = no burst, 1 = burst registered by the water company. The outcome tested if the burst event (dependent variable) could be explained by a combination of independent variables: temperature, humidity, diameter, DVG's average flow and cause of burst (spontaneous or due to consequential damage).

3 RESULTS & DISCUSSION

The code in Python reproduces the functionality of BURST Alert, generating flow/pressure thresholds and triggering an alarm. However, it presents some limitations. Firstly, to generate the thresholds, 90 days of data are required, so they were calculated only from the 4th month onwards. Also, the thresholds generated by the code are slightly different from the historian data, which also implies at different alarm triggering. It was expected that the error increased during the night, since at this period the flow is mainly composed by leakage flow (Soldevila *et al.*, 2016; Salguero, Cobacho and Pardo, 2019). However, the error has a high variation both during the day and at night.

The water company Oasen provided an Excel file with all the service orders realized during 2019. This data is considered as the real burst data; thus, it was used for validating the bursts triggered by the Python code and for evaluating the performance of BURST Alert in 2019, at each DVG. Two methods were used to evaluate the performance of BURST Alert at Oasen's DVGs in 2019. The first , method-1, considered a burst as a single event; a true alarm is the one triggered inside the range of initial - end time of Oasen and it is visible on flow trends (Table 1)

Table 1. Performance evaluation of BURST Alert by method-1.

\	Average flow (m^3/h)	Bursts reported by Oasen	Bursts detected by BURST Alert	Detection probability (%)	Number of false alarms	Total number of alarms	Days without burst	Rate of false alarms (%)
Alblasserdam	320	9	3	33.3	12	15	340	3.5
Alblasserwaard en Vijfheerenlanden	1250	93	0	0.0	10	10	148	6.8
Alphen	500	31	4	12.9	65	69	297	21.9
Gouda	1900	126	2	1.6	12	14	159	7.6
Hazerswoude	525	59	5	8.5	12	17	149	8.0
Lekkerkerk	339	32	7	21.9	69	76	214	32.2
Nieuwkoop	300	31	8	25.8	32	40	270	11.8
Ridderkerk	323	15	3	20.0	30	33	330	9.1
Zwijndrecht	438	28	6	21.4	8	14	318	2.5
whole Oasen	5895 Total	424 Total	38 Total	16.2 Average	250 Total	288 Total	236 Average	11.5 Average

By analyzing Table 1, BURST Alert had a better performance at DVGs with average flows < 500 m^3/h. On average, the software has a low DP and RF. The second method, namely method-2, was an exploratory analysis, where all the observations (288 datapoints/day) are considered. Both true positive and true negative events are considered correct events. This method demonstrates that the software triggered less alarms than expected (average of 99% of correct answers), thus having a high precision at the moments without bursts. The software was also compared to other detection methods (Kim *et al.*, 2016; Romano, Kapelan and Savić, 2012; Mounce, Mounce and Boxall, 2011). BURST Alert has a lower DP, but the best RF amongst them. This means that the software has a low sensitivity to burst events, but a high precision. In addition, this study has a much wider sample with 424 real-life bursts, being majority of low flow, thus hard to detect. As other studies were carried different areas and burst events, a direct comparison might be misleading.

Daily measurements for temperature and humidity variables were retrieved from the Koninklijk Nederlands Meteorologisch Instituut website, for the period of 2019. Logistic regressions were done with two bases: (i) all the observations, (ii) only bursts. At first, all the variables (Tavg, Tmax, Tmin, deltaT, Uavg, Umax, Umin, deltaU, diameter, DVG's average flow, cause of burst) were included in the model one by one, and a stepwise was done to find the best model. For the complete base, the best adjustment had an Akaike information criterion (AIC) of 305, and it was using average humidity, average temperature, diameter and cause of leakage. However, the effects were small (small estimates), and no statistical significance was found (p-value>0.05). For the event base, the best fit model was using only diameter (AIC = 94), but no significant effect on burst was found. The second-best model (AIC = 1150) indicated a significant effect on the DVGs Alblasserwaard en Vijfheerenlanden, Gouda, Hazerswoude and Nieuwkoop. Thus, the bigger the DVG the higher is the burst occurrence.

4 CONCLUSIONS

The research aimed to improve the detection of bursts by the software BURST Alert. Firstly, the software reproduced it in Python. Then, the performance of the software at 9 DVGs in The Netherlands was evaluated by two methods: (i) considering burst as single event, (ii) and considering the true negative observations. The choice of method leads to different results: DP=16.2%, RF=11.5% (low sensitivity, medium precision) *versus* 99% of right observations (low sensitivity, high precision). The logistic regressions showed that DVG's size has a significant influence at burst occurrence, while the weather variables were not significant. Future research should use weather data with more observations (*e.g.*, T and U hourly measurements).

ACKNOWLEDGEMENTS

The authors would like to thank the European Commission for sponsoring the Erasmus Master IMETE, and Royal HaskoningDHV for sharing the data about BURST Alert.

REFERENCES

Bakker, M., Vreeburg, J. H. G., *et al.* (2014) 'Heuristic burst detection method using flow and pressure measurements', *Journal of Hydroinformatics*, 16(5), pp. 1194–1209. doi: 10.2166/hydro.2014.120.
Kim, Y. *et al.* (2016) 'Robust leak detection and its localization using interval estimation for water distribution network', *Computers and Chemical Engineering*. Elsevier Ltd, 92, pp. 1–17. doi: 10.1016/j.compchemeng.2016.04.027.
Mounce, S. R., Mounce, R. B. and Boxall, J. B. (2011) 'Novelty detection for time series data analysis in water distribution systems using support vector machines', *Journal of Hydroinformatics*, 13(4), pp. 672–686.
Romano, M., Kapelan, Z. and Savić, D. A. (2012) 'Automated detection of pipe bursts and other events in water distribution systems', *Journal of Water Resources Planning and Management*, 140(4), pp. 457–467.
Salguero, F. J., Cobacho, R. and Pardo, M. A. (2019) 'Unreported leaks location using pressure and flow sensitivity in water distribution networks', *Water Science and Technology: Water Supply*, 19(1), pp. 11–18. doi: 10.2166/ws.2018.048.
Soldevila, A. *et al.* (2016) 'Leak localization in water distribution networks using a mixed model-based/data-driven approach', *Control Engineering Practice*. Elsevier, 55, pp. 162–173. doi: 10.1016/j.conengprac.2016.07.006.

Proceedings of the 1st IAHR
Young Professionals Congress
17-18 November 2020

GIS BASED MULTICRITERIA DECISION ANALYSIS FOR FLASH FLOOD HAZARD MAPPING USING FREQUENCY RATIO IN BAVARIA

Junqi Mao

Technical University of Munich, Munich, Germany
e-mail junqi.mao@tum.de

ABSTRACT

A flash flood is an emergency that develops rapidly at an hourly timescale between rainfall and the onset of flooding. This study intends to assess flood conditioning factors by introducing a new multicriteria decision making (MCDM) method, which applies and further develops frequency ratio (FR) based on standing water records in real events. Standing water record databases were generated using the frequency ratio method by counting record numbers in each index layer under a GIS framework. The frequency ratio results were then applied to weighting index. Flash flood hazard maps were generated for visualization and for comparing different conditioning indices, together with sensitivity analysis, calibration and validation. Subsequently, an evaluation framework of flash flood hazard, named as MCDM-FR, was developed that is not only relevant for the catchments with recorded events but which also serves as flash flood hazard analysis for Bavaria.

Keywords: flash flood; weighting index; frequency ratio

1 INTRODUCTION

A flash flood is a rapid disaster with limited response time (a few hours or even less), and usually occurs after high-intensity rainfall that can no longer infiltrate the soil and is available as surface runoff. In recent years, the most significant German flash flood event was in May and June 2016, when exceptional precipitation fell over Bavaria (Mayr et al., 2020). After the 2016 flash flood, the Bavarian state office set up the HiOS (Hinweiskarten Oberflächenabfluss & Sturzflut) project to enhance the current hydrological software for prevention and mitigation of flash floods, and to ensure the public's sense of security (HiOS, 2020). In this context, creation of a hazard map for Bavarian flash floods is considered urgent in order to provide decision making tools for land use planning following precautionary management principles. Ten typical flash flood events from 2002 to 2016 from ten catchments across Bavaria were chosen to represent flash floods in recent decades (Figure 1a). The weighting orders of parameters were examined for each catchment and holistically for Bavaria. Afterwards, a ready-to-use and repeatable tool was developed to visualize the hazard maps using the Geographical Information System (GIS) as ArcGIS Pro 2.4.

2 MATERIALS AND METHODS

This study used four indices for decision making: slope, land use, soil type and flow accumulation. Each index was classified into several classes. Frequency ratio can be expressed as the proportion of flooded area to non-flooded area in the total study area (equation 1) (Samanta et al, 2018). The effect of each category in an index is classified under five different hazard classes: very high, high, moderate, low and very low (Mentzafou et al., 2017). Each hazard index is attributed with a weight referring to its influence on the flood processes. The flood-hazard map can then be generated using the weighted sum of frequency ratio values (equation 2).

$$FR = (E/F)/(M/L) \quad (1)$$

where E is the number of flood records for each index; F is the total number of flood records; M is the number of pixels per subclass of effective flash flood factors; L is total number of pixels in a region (Pham et al., 2020).

$$S = \sum_i^i w_i x_i \quad (2)$$

where S: the hazard index, w_i: the weight of factor i, and x_i: the rate of factor i. The hazard value S for each pixel was expressed as the weighted sum of frequency ratio values by using weight multiplied FR values.

3 RESULTS AND DISCUSSION

Each pixel in the study site can form a specific hazard value following equation 2. Thus, a flash flood hazard map could be built up using hazard value information as Figure 1b. For hazard classification, the Jenks optimization method is to determine the best arrangement of values into different classes (Stefanidis et al., 2013). The raw hazard map was classified into a map with five hazard levels (Figure 1c). For the whole of Bavaria, the average values of indicators were obtained from the ten catchments to draw a hazard map (Figure 1d) based on weighting index. Sensitivity analysis methods were carried out to check the proper utility and weight of each index. For validation, the seed cell areas index (SCAI), as the ratio of area extent of hazard class to flood in each hazard class, can be used as an indicator to test the reliability of flood hazard maps (Khosravi et al., 2016). More than 80% of standing water records with inundation depth >0.25m are included in high hazard and very high hazard regions together with high frequency ratio values and low SCAI values.

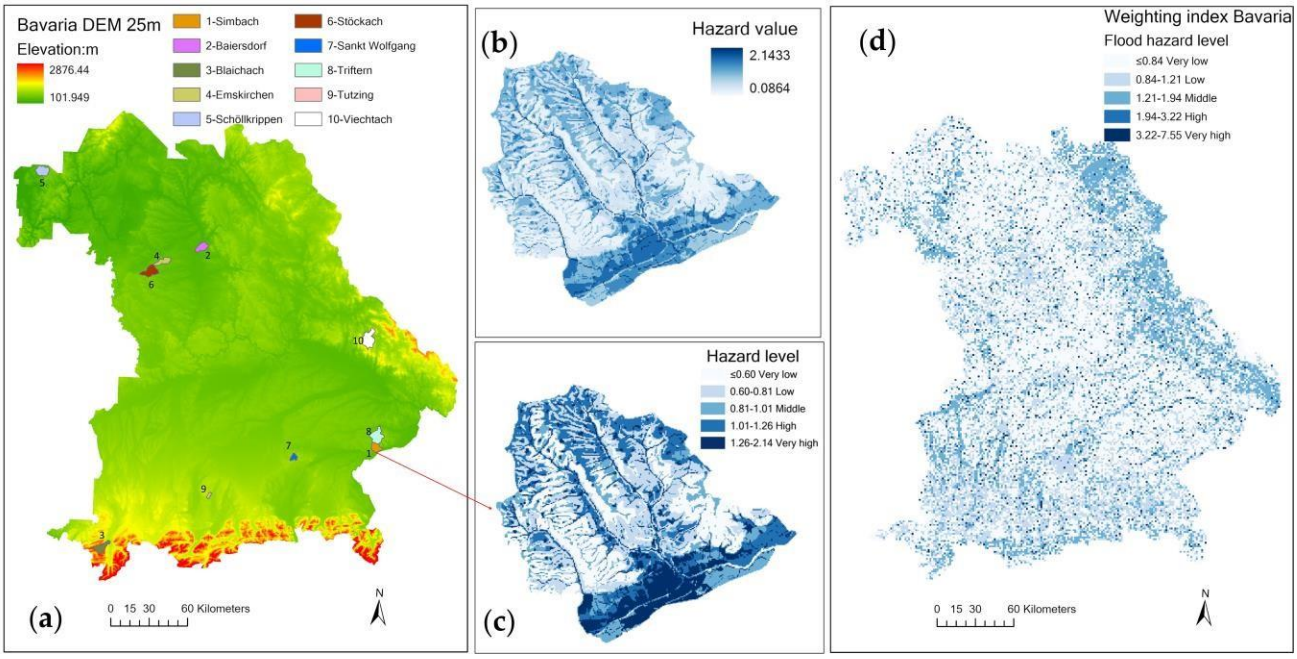

Figure 1. (a) The location of ten study catchments in Bavaria; (b) hazard map of Simbach catchment; (c) hazard map of Simbach catchment after Jenks natural break; (d) hazard map of Bavaria

4 CONCLUSIONS

The analysis and evaluation for flash flood is needed for more efficient management and response to the emergency. This framework of MCDM is recommended for hazard planning as it promotes the interaction between real events and topographic/human factors, explores the representative measure to draw maps from city-scale to state-scale, while frequency ratio/SCAI values are found to be effective measures.

REFERENCES

HiOS. (2020). Inundation in Germany due to heavy rain. Retrieved from HiOS Project website: http://www.hios-projekt.de/.

Khosravi, K., Nohani, E., Maroufinia, E. and Pourghasemi, H. R. (2016). A GIS-based flood susceptibility assessment and its mapping in Iran: a comparison between frequency ratio and weights-of-evidence bivariate statistical models with multi-criteria decision-making technique. *Natural Hazards*, 83(2), 947–987.

Mayr, B., Thaler, T., & Hübl, J. (2020). Successful Small-Scale Household Relocation after a Millennial Flood Event in Simbach, Germany 2016. *Water*, 12, 156.

Mentzafou, A., Markogianni, V. and Dimitriou, E. (2017). The Use of Geospatial Technologies in Flood Hazard Mapping and Assessment: Case Study from River Evros. *Pure and Applied Geophysics*, 174(2), 679–700.

Pham, B. T., Avand, M., Janizadeh, S., Phong, T. Van, Al-Ansari, N. and Ho, L. S. (2020). GIS based hybrid computational approaches for flash flood susceptibility assessment. *Water*, 12(3). 683.

Samanta, S., Pal, D. K. and Palsamanta, B. (2018). Flood susceptibility analysis through remote sensing, GIS and frequency ratio model. *Applied Water Science*, 8(2), 1–14.

Stefanidis, S. and Stathis, D. (2013). Assessment of flood hazard based on natural and anthropogenic factors using analytic hierarchy process (AHP). *Natural Hazards*, 68(2), 569–585.

Proceedings of the 1st IAHR
Young Professionals Congress
17-18 November 2020

CLIMATOLOGICAL ANALYSIS FOR THE AGROECOLOGICAL ZONING OF THE PEACH TREE IN SAN PABLO DE PILLAO, HUÁNUCO

Leonardo Gutierrez [1]

[1] La Molina National Agrarian University, Lima, Perú,
e-mail: leonardogl1497@gmail.com

ABSTRACT

Planning in the distribution of crops in rural areas through the Agroecological Zoning (ZAE), has become a useful tool for precision agriculture and sustainable development. With this purpose, in the district of San Pablo de Pillao with an area of 59,284.20 ha and located in the center of the department of Huanuco in Peru, the optimal areas for the cultivation of peach trees were determined, a crop with a stable value in the market and in Huanuco. To do this, the method of the Analytical Process Hierarchical (APH) was applied, which is usually used in multi-criteria analysis for the determination of areas of the ZAE according to the level of aptitude for the agroecological development of the peach tree.

Keywords: Climate analysis, Agroecological Zoning, San Pablo de Pillao, Drought, Peach tree.

1 INTRODUCTION

In this research it is proposed to identify and evaluate the variability climatic for planting the peach tree, specifically of the variety huayco rojo, due to its high acceptance in the market and agroclimatic requirements present in the study area, higher value economic in the market. In addition, the peach tree is chosen based on the recommendations of specialists from *Sierra y Selva Exportadora*, which is a public executing agency attached to the Ministry of Agriculture - Perú.

The application of the Multicriteria Analysis Method of Decisions, using remote sensing resources and geographic information systems, will allow us to know the spatial distribution of the optimal potentialities of the study area for the peach tree. This method allows identifying the territorial surfaces with optimal edaphological, physiographic and climatic characteristics to achieve the maximum yield of the peach tree, the red huayco variety.

Planning in the distribution of crops in rural areas through Agroecological Zoning (ZAE), has become a useful tool for precision agriculture and sustainable development. For this purpose, in the district of San Pablo de Pillao with an area of 59,284.20 ha and located in the center of the department of Huánuco in Peru, the optimal areas for peach cultivation were determined, a crop with a stable value in the market and highest profitability in Huánuco. To do so, the Hierarchical Analytical Process (AHP) method was applied, which is frequently used in multi-criteria analysis to determine areas of the ZAE based on the level of aptitude for the agroecological development of a given crop. To apply the various determining sub-criteria in the ZAE, such as elevation, slopes, precipitation, temperature, cold hours, relative humidity, salinity, organic matter content, soil acidity and textural class, the spatial tools and statistics of Geographic Information Systems (GIS).

2 STUDY AREA

The research study area was developed in the district of San Pablo de Pillao which is politically located in the department of Huanuco, province of Huanuco and district of San Pablo de Pillao. The study district has an area of 59,284 ha, with a range of altitudes from 784.93 to 3664.63 masl.

3 DATA AND METHODS

3.1 Data

The various raster data are used to prepare the base maps of each sub-criterion, the climate maps are based on the information of the PISCO product of monthly rainfall and monthly temperatures, prepared by SENAMHI. The PISCO product of precipitation analyzed in the study area is within the period from 1990 to 2019, while the PISCO product of temperature was analyzed during the period from 1987 to 2016.

3.2 Interpolation methods

The monthly information was extracted for the study area and interpolated with the geostatistical techniques of Inverse Distance Weighting (IDW) for temperature and Ordinary Kriging for precipitation.

3.3 Trend analysis

The precipitation and temperature data averaged for the study area, the analysis of this monthly and annual time series was made with box plots, histograms. In addition, a trend analysis was performed with the non-parametric Mann-Kendall test on the annual data

3.4 Standardized Index of Precipitation

The analysis of intensities and identification of droughts was estimated with the Standardized Precipitation Index (SPI), which is based on the probability of precipitation for a given time scale (3, 6 and 9 months).

4 RESULTS AND DISCUSSION

Regarding the annual precipitation series, according to the boxplot, there is a high variability of accumulated precipitation with a range from 1500 to 2160 mm / year. The frequency histogram indicates that the range with the highest probability of the most frequent annual precipitation is 1900 to 2000 mm / year. A general trend was determined to increase the annual accumulated precipitation throughout the study area. The accumulated annual precipitation series analyzed describe an incremental trend of 9.59 mm / year with a confidence level of 95%.

Regarding the annual temperature series, there is a low temperature variability with a range from 17.6 to 18.8 °C. The frequency histogram indicates that the most frequent range with the highest probability of annual temperature is 18 to 18.2 °C. A generalized trend towards an increase in the annual average temperature was determined throughout the study area. The average of the mean temperature series in the study area describes an incremental trend of 0.019 °C / year with a confidence level of 99%.

The identification of extremely dry droughts with the SPI index at 3 months, recorded these events in the years 1992, 1995, 1998 and 2016. While with the SPI index at 6 months and 12 months, these extreme long-term events were recorded. duration in 1992 and a shorter one in 1993; From this year there were no more extreme droughts.

In general, the SPI-12 indicator has a higher probability of occurrence of droughts, with respect to the spatial distributions obtained with the SPI-6 and SPI-3 indicators, on average the probability of occurrence of SPI-6 is 16.4%, for moderate droughts, 6.65% for severe droughts and 1.72% for extreme droughts.

5 CONCLUSIONS

The multi-annual climatic variability show a trend significative to increase the annual average precipitation at a rate of 9.59 mm / year, which favors the peach tree; moreover, show a trend significative to increasing the average temperature at a rate of 0.023 ° C / year, which would not significantly affect the peach tree, since it has a wide range of adaptation to the variability of maximum and minimum temperatures. While the probability of occurrence of extreme droughts in the study area is less than 4%, therefore, it does not represent a danger for the agricultural development of the peach tree.

REFERENCES

Ashraf, M., Routray, J., and L (2015). Spatio-temporal characteristics of precipitation and drought in Balochistan Province, Pakistan. Natural Hazards, 77(1):229–254.

Aybar, C. C., Lavado, C.W., Huerta, J. A., Fernández, P. C., Vega, J. F., Sabino Rojas, E., and Felipe Obando, O. G. (2017). Use of the grilled product pisco of precipitation in studies, investigations and operational systems of monitoring and hydrometeorological forecast.

Baíza, A. V. (2004). Peach cultivation technical guide. Technical report, IICA, San Salvador Ministerio de Agricultura y Ganadería.

Huerta, J. A., Aybar, C. C., and Lavado, C. W. (2018). PISCO temperature.

Vega, F. (2015). Regionalization and characterization of droughts in Peru.

Proceedings of the 1st IAHR
Young Professionals Congress
17-18 November 2020

A HYDRODYNAMIC MODEL AS INPUT FOR A SPATIAL PLANNING TOOL. CASE STUDY: DELTA OF THE PARANÁ RIVER (ARGENTINA).

Mayra Morale*[1], Martín Sabarots Gerbec [2], & Pablo García [3],

[1] Instituto Nacional del Agua, Ezeiza, Argentina.
*mmorale@ina.gob.ar

ABSTRACT

The Paraná Delta in Argentina is considered a unique and vast mosaic of wetlands of international importance. To support decision-making for the sustainable spatial planning of the Paraná Delta, a planning kit and a two-dimensional hydrodynamic model are developed with a defined domain in the territory of the Delta. The model, implemented in Delft3D FM, is built from a flexible mesh, incorporating topography and rail and road structures. The link between INA and Deltares made possible the implementation and validation of the 2D model and the simulation of the hydrological and anthropological change scenarios in the short term. According to the results, the greatest effects on the water level growth are due to anthropological interventions associated with dikes.

Keywords: Delta, 2D Model, simulation, fluvial.

1 INTRODUCTION

The Paraná Delta Covers more than 17500 km2 and its key characteristics include the rich biodiversity and valuable range of ecosystem goods and services provided by the wetlands of the Delta; the proximity to the highly urbanized and industrial corridor of Buenos Aires province; the extensive modification of the natural system in the lower delta; and a slowly decreasing population living in the Delta.

This work aims to describe the implementation of 2D modelling that is carried out to evaluate the impact of anthropic interventions-mainly infrastructure- in the Paraná Delta.

2 HYDRODYNAMIC MODEL

2.1 Implementation and Methodology

As initial contributions, the INA provided the pre-existing information; bathymetries, cross sections, hydrometric variables, and Deltares Delft 3D FM software, training, and technical support.

The domain includes the middle and front of the Delta. The topobatymetry was taken from the Digital Elevation Model (DEM) carried out at INA (Sabarots Gerbec, et al, 2017). The rugosity coefficient value used was: 0.015 for rivers and 0.1 in alluvial plains according to the literature. The upstream boundary conditions used in the Paraná River by the Arroyo Seco were according to 1D model developed by INA (Sabarots Gerbec, 2014) and levels were included in the downstream boundary in front of the Delta. A flexible mesh was developed in the defined domain with quadrilateral cells and triangular cells.

2.2 Validation

Observed and simulated levels were compared at observation stations. The selected scenarios for this stage included flows of 17,100 and 25,000 m^3/s and average levels in the Río de la Plata.

2.3 Simulation scenarios

The simulations were carried out in a permanent regime in all cases. The first runs were validation runs to adjust the model. Two temporary conditions were proposed and four situations of anthropic variations to the

environment according to the base scenario. 1)Hydrological changes: Current Scenario and Climate Change Scenario. 2)Anthropic Variations: New Route Trace, Open Dock, and Polders.

The 50-year climate change scenario was considered based on an increase in levels in the Rio de la Plata according to Badano, et al. (2012) and an 20% increase in income flows. The simulation scenarios with anthropic variations were obtained from the reports (Castro, et al, 2018 a). It also included the existing dikes according to the survey carried out and published in 2010 by the University of San Martin. (Kandus, et al 2010).

3 RESULTS & CONCLUSIONS

To evaluate the most critical hydrological conditions, the historical flood of the Paraná River was defined as the base scenario. The results of the simulations express that all the scenarios that represent anthropic modifications raise the water levels, somehow, compared to the simulation without interventions. In the simulation the highest effects on the levels are visualized with dikes and a combination of interventions. As for the minimum impact, it occurred for the intervention of the Nueva Palmira International Connection (CINP).

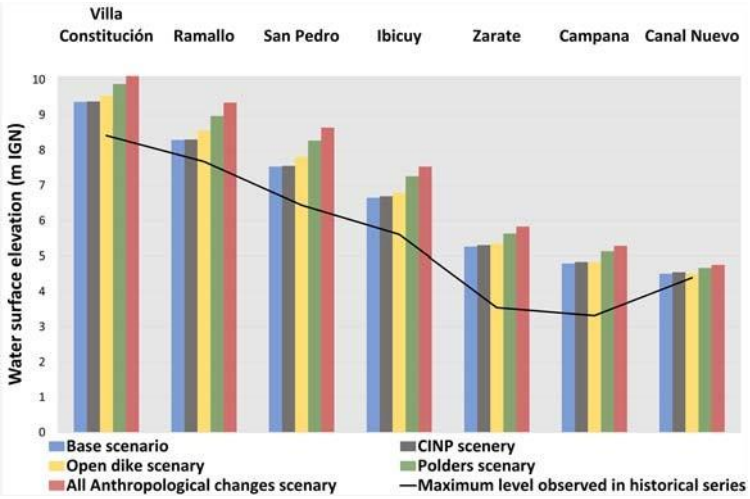

Figure 1. Impact on the levels in the observation stations.

The implementation of a two-dimensional hydrodynamic model on Delft 3D FM is an optimal tool to assess flood impacts inanthropic interventions. The joint experience between INA and Deltares was, not only enriching both academically and professionally, but also enabled this work done in just seven weeks.

ACKNOWLEDGEMENTS

To the Instituto Nacional Del Agua, especially Pablo Spaletti, Julio De Lio. To the great technical and human team of the Computational Hydraulics Program. To Deltares in Delft, Netherlands, especially Anke Becke, Begoña Arellamo Jaimerena, Paricia Trambauer and Kymo Slager.

REFERENCES

Badano, N. D., Sabarots Gerbec, M., Re, M., Menéndez, A. N., Garcia, 2012. A coupled hydrosedimentologic model to assess the advance of the Parana River Delta Front. Proceedings of the Sixth International Conference on Fluvial Hydraulics, San José, Costa Rica.

Castro, L. S., Garcia, P.E., Menéndez, A.N., Sabarots Gerbec, M., 2018. Final report, Paraná Delta: Strategic projects for sustainable development. INA.

Kandus, P., Minotti, Priscilla., 2010. Distribution of embankments and designated areas in the Paraná Delta region. Chapter 2. Endowments and embankments in the Paraná Delta: situation, environmental effects and legal framework. Wetlands International.

Sabarots Gerbec, M., 2014. Study of the surface dynamics of the channel network of the Middle Delta of the Paraná River. 2nd Meeting of researchers in training in water resources

Sabarots Gerbec, M., Re, M., Garcia, P.E., Storto, L., 2017. Digital Elevation Model of the Paraná River Delta. Final report. Proyect INA 373. Report LHA 01-373-17.

Proceedings of the 1st IAHR
Young Professionals Congress
17-18 November 2020

ANALYSIS OF URBANIZATION INDUCED LAND COVER CHANGE AND IMPACT ON LAND SURFACE TEMPERATURE WITH LANDSAT, MODIS AND ERA 5 IMAGERY

Alejandra Tancara [1]; Freddy Ángel Soria [2]

[1,2] Centro de Investigación en Agua, Energía y Sostenibilidad (CINAES), Universidad Católica Boliviana "San Pablo", La Paz – Bolivia.
[1] moraleta1698@gmail.com, [2] fsoria@ucb.edu.bo

ABSTRACT

Bolivia's cities continue developing among size and population. Metropolitan areas have a significant impact on Urban heat islands (UHI's) affecting environmental conditions and human comfort. Vegetation indicators are widely used to estimate the relationship between Land Surface Temperature (LST) and vegetation coverage based on remote sensing. Therefore, this research uses Google Earth Engine to demonstrate a multitemporal correlation between land cover change and LST in the three most important cities of Bolivia using NDVI and EVI indexes. This study used MODIS, Landsat and ERA satellites. The results show that an increase of LST and air temperature when there is a decrease in NDVI and EVI depending on the geographical location.

Keywords: Urban Heat Island, sustainable development goals, Google Earth Engine, Land Surface Temperature.

1 INTRODUCTION

More than 60% of Bolivia's population lives in urban areas, where La Paz, Santa Cruz de la Sierra and Cochabamba are the most populated cities in the country (INE, 2015). Urbanization process replaced natural vegetation to artificial surface. Land surface temperature (LST) is the skin temperature of the ground. It is a fundamental element for monitoring vegetation, surface energy change and climate change (Kayet & et.al, 2016), which is commonly used to quantify UHI's. UHI's can affect human health and comfort, alter environmental conditions and increase the energy consumption (Peng & et.al, 2016). Google Earth Engine (GEE) is a public computing platform that allows users to run geospatial analysis on its infrastructure without downloading any information. The main purpose of this study was to demonstrate the correlation between land cover change and land surface temperature (LST) using vegetation indexes with GEE in the cities mentioned

2 MATERIALS AND METHODS

The study region was on the metropolitan areas of La Paz, Cochabamba and Santa Cruz from 2001 to 2019. These cities are located in different regions (high plateau, plain and valley respectively) and environmental conditions. GEE was used to pre-process and process data. The LST was computed using the Statistical Mono-Window Algorithm (Ermida & et.al, 2020) using Landsat satellites 5,7,8. Emissivity was calculated with ASTER GED satellite, then we figured atmospheric data applying NCEP/NCAR data. The data from the Landsat series are considered consistent and inter-calibrated, and all bands have a 30 m spatial resolution (Ermida & et.al, 2020). Enhanced Vegetation Index (EVI) and Normalized Difference Vegetation Index (NDVI) were acquired from MODIS Terra Vegetation Indices whose resolution is 250 m. ERA5 dataset was acquired to obtain average air temperature at 2m height (monthly average). Overpass times of MODIS Terra and Landsat series are daily and every 16 days, respectively. MODIS Terra and ERA5 datasets in GEE have the quality of being ready to obtain the information that is needed without previous algorithm or other process. It only necessary select the band and filter the date.

3 RESULTS AND DISCUSSION

A graphic was executed for LST, air temperature, NDVI and EVI over the years (2001-2019). Lineal regression was performed for LST and air temperature. For LST, in La Paz we calculated a 0.15°C increase per year; in Santa Cruz 0.17 °C per year and in Cochabamba 0.11°C per year. For air temperature, on the other hand, in La Paz and Cochabamba we computed a 0.04 °C per year; in Santa Cruz 0.03°C per year. NDVI and EVI indices were classified according to the scale of values proposed by Bahadur in 2018, where 0 mean water

bodies and 1 is abundance of vegetation. La Paz presented in average 0.12 NDVI which means a bare vegetation or barren rocks. Santa Cruz in average had 0.32 and Cochabamba with 0.21 which represent shrubs and grasslands or senescing crops. Results show an increase of LST and air temperature when there is a decrease in NDVI and EVI indices in most of the years. Both indicators were considered in order to better understand the relationship between LST and land cover, in terms of vegetation abundance. Each city has different results such may have occurred due to the diverse geographic locations and environmental conditions. The increase in LST in cities may be due to the growth of built-up areas, which replace the current natural vegetation cover. La Paz has the lowest vegetation coverage due to it is located in a plateau region with an altitude of 3600 meter above the sea.

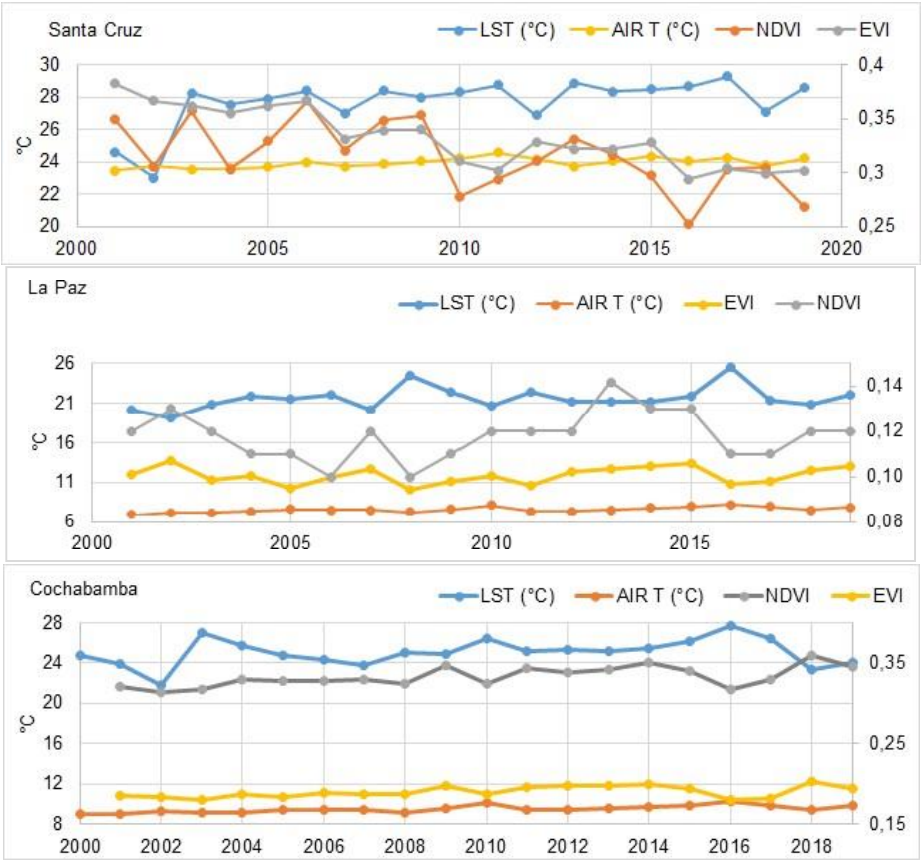

Figure 1. Time series of LST, air temperature, NDVI and EVI from 2001 to 2019

4 CONCLUSIONS

This study is focused on the relationship among LST, air temperature, NDVI and EVI over the time using GEE. NDBI and EVI has an inverse correlation with LST in the three cities. It is observed that LST has increased over the years on the metropolitan areas. Assessment of LST provides important information for surface energy, land cover change and climate change. In addition, these indexes are useful to analyze time series due to the facility to calculate and precision in the results no matter the geographical areas.We suggest to compare these spatial measurements with in situ ones to accurate it.

REFERENCES

Kshetri, Tek (2018) NDVI, NDBI & NDWI Calculation Using Landsat 7, 8. *Researchgate.net,* 327971920.

Ermida, S; Soares, P; Mantas, V; Göttsche, F and Trigo, I. (2020) Google Earth Engine Open-Source Code for Land Surface Temperature Estimation from the Landsat Series. *Remote Sensing,* 12 (9) 1471

Kayet, N; Pathak, K; Chakrabarty, C; Sahoo,S (2016) Urban heat island explored by co-relationship between land surface temperature vs multiple vegetation indices. *Spatial Information Research* 24, (515–529)

Ma, W; Chen,Y; Zhou, J; Gong, A. (2008) Quantitative analysis of land surface temperature-vegetation indexes relationship based on remote sensing. The International Archives of the Photogrammetry, Remote Sensing and Spatial Information Sciences 37.

Peng, F; Weng, Q (2016) A time series analysis of urbanization induced land use and land cover change and its impact on land surface temperature with Landsat imagery. *Remote Sensing of Environment* 175, 15 (205-214)

IAHR AIRH

International Association for Hydro-Environment Engineering and Research

Hosted by
Spain Water and IWHR, China

Session 4
Urban Drainage

IAHR YPN

Hosted by
Spain Water and IWHR, China

Proceedings of the 1st IAHR
Young Professionals Congress
17-18 November 2020

HYDRAULIC MODEL OF STORMWATER DRAINAGE SYSTEM USING DIFFERENT METHODS FOR DEFINING THE CATCHMENT AREA

Ana Grupcheva [1]

[1] Ss. Cyril and Methodius University, Faculty of Civil Engineering, Skopje, North Macedonia
anagrupceva@gmail.com

ABSTRACT

The stormwater drainage system is an infrastructure facility that accumulates the rainwater, protecting the urban areas from flooding. An important parameter for these systems in urban areas is the size, shape and type of catchment area. According to current practice the catchment area can be determined by: classical methods- where the catchment area can be defined using a roof symmetry by links and modern methods in which the definition of the catchment area is made by the elevation differences, natural water barriers, slope, etc. by using break lines and different characteristic catchment width.

Subject of this hydraulic analysis is to apply the classical and modern methods in order to show their advantages and disadvantages with a further comparison and recommendations for designing the stormwater drainage system.

Keywords: analysis, stormwater, catchment

1 INTRODUCTION

The amount of water flow that appears in the stormwater drainage system is highly variable throughout the year. During dry periods it is equal to zero, while during heavy rains its value can be quite high. The stormwater drainage system collects the water flows from the natural water processes such as: rainfalls, melting snow, ground water, etc.

According to previously stated, the water flow in the stormwater drainage system depends on various parameters, giving a lead role to the size and type of the catchment area due to creating a hydraulic model and its analysis, using the rational method.

$Q = C \cdot i \cdot A$ (C- runoff coefficient, i- storm intensity(defined by IDF-curves), A- area)

2 CATCHMENT AREA AND DEFINING METHODS

Catchment areas are hydrologic units of land whose topography and drainage system elements direct surface runoff to a single discharge point. While making a hydraulic model, the size of the catchment area and its parameters can be defined using the two methods - classical method and modern methods.

2.1 Classical method

To define the catchment area using the classical method mean that the boundary conditions will be determined by the method of roof symmetry by links (Roof symmetry method) or by distributing it in equal parts at all nodal points of points of the hydraulic model (Thiessen polygon).

2.2 Modern method

Defining the catchment areas using the modern method generates the topography of the terrain, with a main note on its: slope, groundwater, its use, elevation, geometric change, embankments, etc. The boundary elements defining these catchments are called "break lines" (or break points), placed at elevation differences, natural water barriers, slope changes, etc.

3 HYDRAULIC MODEL

For the purpose of the hydraulic analysis, a hydraulic model has been developed that will simulate the runoff conditions of the stormwater drainage system, using the SWMM (Storm Water Management Model) software package according to the two methods. The return period from the inserted IDF-curves was chosen for 2 years to be in accordance with the designing law for stormwater drainage systems. The hydraulic model is made for

the city of Ohrid, North Macedonia – applying the methods on the existing stormwater system using different runoff coefficients on every formed catchment area.

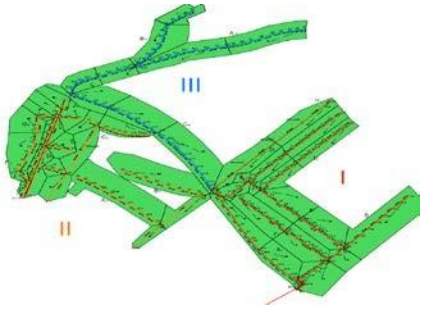

Figure 1. Classical method

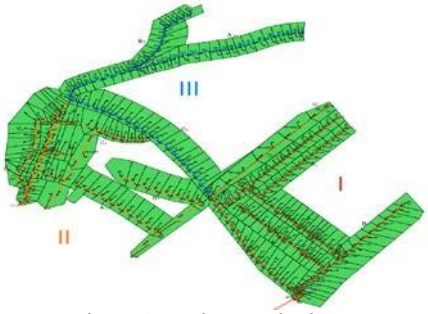

Figure 2. Modern method

4 RESULTS

To make a comparison between the accuracy of the two analysis of the hydraulic model, one can see the difference in the flow rate of the links, depending on the amount of water they receive from the catchment areas. This is further illustrated by means of hydrograms, where The flow Q is expressed in [l/s], and the time T is expressed in [min].

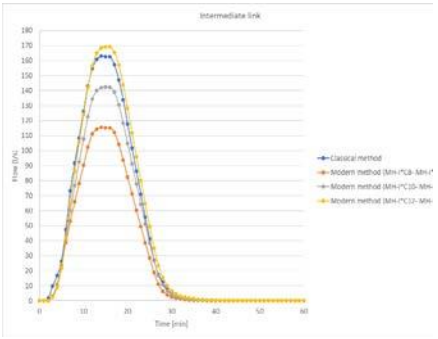

Figure 1. Hydrograms for upstream link

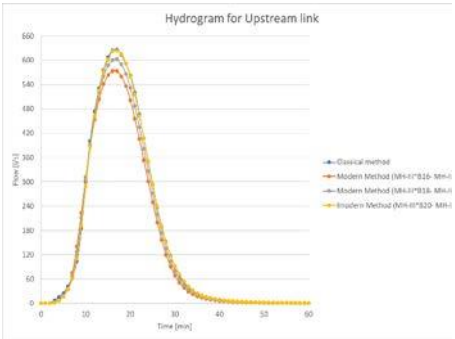

Figure 2. Hydrograms for intermediate link

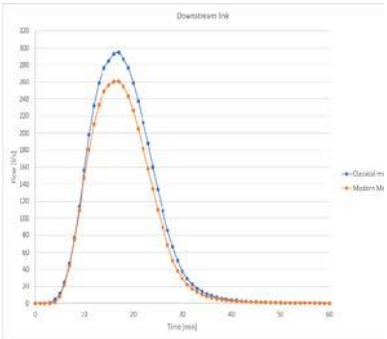

Figure 3. Hydrograms for downstream link

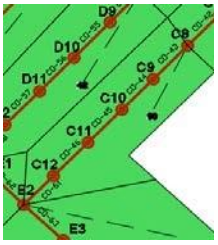

Figure 4. Classical method

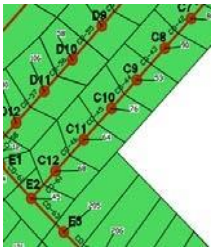

Figure 5. Modern method

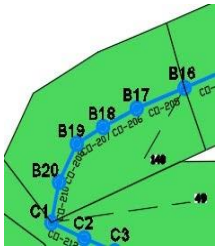

Figure 6. Classical method

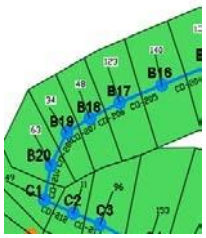

Figure 7. Modern method

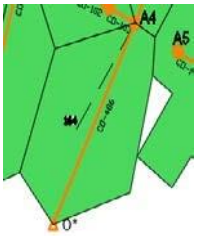

Figure 8. Classical method

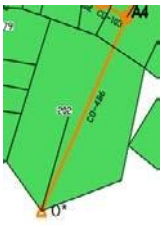

Figure 9. Modern method

5 CONCLUSION

When analyzing a stormwater systems, the modern method can be said to be better for upstream parts because they allow optimization of the pipe diameters (due to its peak flows). With the help of diametric optimization, lower economic cost of current projects would be obtained. In the case of the intermediate and downstream parts of stormwater drainage systems, it can be said that both the classical and modern methods are suitable for the use of catchment area definitions, as the difference in hydrograms is minimal. These recommendations would apply to urban, predominantly plain areas.

REFERENCES

Ana Grupcheva' *"Hydraulic Model of Stormwater Drainage System Using Different Methods for Defining the Catchment Area",* Master thesis, Skopje, North Macedonia, 2019

Thewodros K. Gebermariam Ph.D., P.E., D. WRE. "*Urban Drainage Infrastructure Design Model Calibration and Output Uncertainty Minimization"*, 2014, New York University Polytechnic School of Engineering, Department of Civil & Urban Engineering, NY 11201, USA, 2347-3878

David B. Thompson "*The Rational Method"*, September, 2006, Civil Engineering Department, Texas Tech University (in PDF)

Proceedings of the 1st IAHR
Young Professionals Congress
17-18 November 2020

COMPUTATIONAL FLUID DYNAMICS (CFD) STUDY OF THE BIOLOGICAL REACTOR OF THE WASTEWATER TREATMENT PLANT OF ROLDÁN, LO FERRO AND BALSICAS (SPAIN)

Alicia Ros-Bernal[1], José M. Carrillo[1] & Juan T. García[1]

[1]Civil Engineering and Mining Engineering School, *Universidad Politécnica de Cartagena, Cartagena, Spain.*
alicia.ros@edu.upct.es, jose.carrillo@upct.es, juan.gbermejo@upct.es

ABSTRACT

The hydrodynamic study of a biological reactor allows the detection of dead zones or preferential flow paths that reflect hydrodynamic deficiencies in its operation. It is crucial to identify and optimize its behavior. If the required hydrodynamic conditions are provided, the efficiency of the purification process will substantially increase. Therefore, the purpose of this study is to evaluate the hydrodynamic behavior, for the design flow, of a biological reactor type A2O of the Roldán, Lo Ferro and Balsicas Wastewater Treatment Plant, located in Torre Pacheco (Spain). The FLOW-3D software has been selected to analyze the three-dimensional operation of the anaerobic chamber for an inlet flow of 2,750 m^3/day. The influence of the turbulence model and the mesh size in the hydraulic retention time has been investigated.

Keywords: *Wastewater Treatment Plant (WWTP), biological reactor, hydrodynamic, Computational Fluid Dynamics (CFD)*

1 INTRODUCTION

Computational Fluid Dynamics (CFD) is a growing tool in the field of wastewater treatments. Karpinska & Bridgeman (2016) consider the use of CFD as a powerful and necessary tool for the optimization of water treatment systems. The works carried out so far show the influence of the geometry of biological reactors on the flow pattern, which is why hydrodynamic modeling has gained relevance in optimization designs. Traditionally, the key parameters have been taken into account for the volume of these units, trying to determine the required hydraulic retention time (HRT) with which the expected reduction levels are achieved. This supposes a homogeneous renewal rate of the fluid and it can present great deficiencies since this simplification does not contemplate the real hydraulic behavior. For this reason, among others, the expected efficiency is not achieved on many occasions, highlighting the interest raised by three-dimensional hydraulic analysis. CFD modeling helps to detect anomalous flow behaviors, dead zones, hydraulic short circuits or preferential flow paths, facilitating the proposal of more efficient geometric alternatives that allow the total volume of the reactor to be efficient.

2 MATERIALS AND METHODS

The biological reactor presented in the following figure belongs to the Roldán, Lo Ferro and Balsicas Wastewater Treatment Plant, WWTP (Spain). The anaerobic chamber has dimensions of 6.40 m long and 20 m wide. The chamber is communicated with the anoxic part by two bottom orifices of 0.2 x 0.4 m^2. For the design flow, there is not upper overflow. The entrance to the biological reactor takes place through a section of 0.3 x 0.3 m^2 located at the beginning of the anaerobic chamber, being the design flow of 2,750 m^3/day.

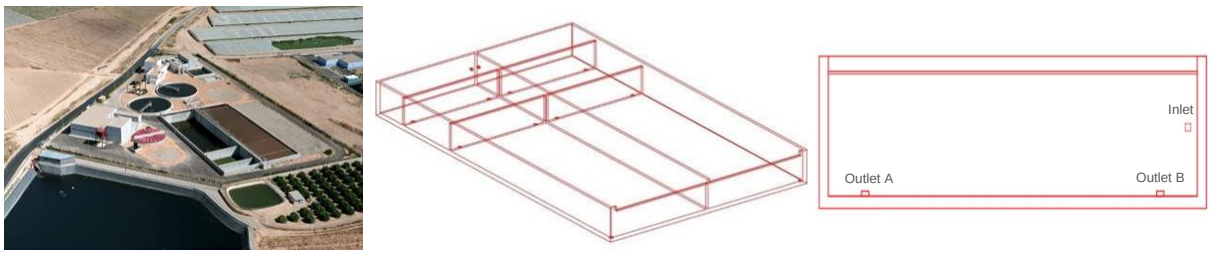

Figure 1. Plan view of the WWTP (left), 3D view (center) and front view (right) of the biological rector

A three-dimensional numerical model has been developed in FLOW-3D for the anaerobic chamber, solving the Navier-Stokes equations for water through the finite difference method. A structured mesh of rectangular cells is used to define the computational domain, studying different mesh sizes (0.6 m, 0.5 m, 0.4 m), in addition to nested mesh blocks with a mesh size of 0.1 m located in the bottom orifices and in the inlet. Regarding the boundary conditions, a constant flow condition equals to 0.032 m^3/s is established in the inlet, which is the design flow expressed in m^3/s for each treatment line. In the outlet condition, a hydrostatic pressure type condition has been specified, considering the fluid elevation at 5.49 m. All simulations have been carried out using the "Volume of Fluid" method proposed by Hirt and Nichols (1981) for modeling the free surface. For the turbulence model, two types have been considered: the turbulence model *k-ε* and the Re-Normalisation Group (RNG) *k-ε*. The laminar flow behavior has been also analyzed. To analyze the results, two numerical probes A and B have been placed in each bottom orifice.

3 RESULTS AND DISCUSSION

Considering the results obtained in Figure 2, the retention time in the two outlets of the anaerobic chamber is different. The reduction of the mesh size tends to diminish the HRT in the probe A and to increase the retention time in the probe B. This effect may be observed with the three turbulence models analyzed. Regarding the turbulence models comparison, the RNG *k-ε* tends to obtain the larger retention times in the outlet B, while the laminar flow cases obtain the higher HRT for the finer meshes in probe A. Comparing each model with their finest mesh, differences between mesh sizes of 0.5 and 0.4 m are smaller than 5% in all the cases.

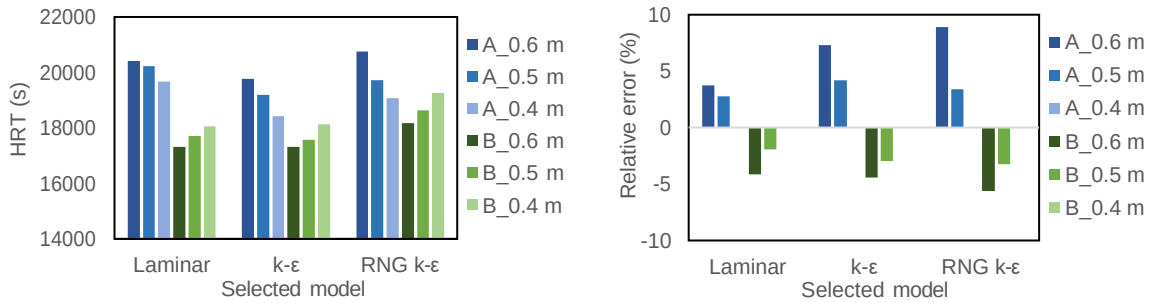

Figure 2. Hydraulic retention time in the probes as a function of the mesh size and the turbulence model (left) and relative error with respect to the finest mesh (right)

Similar retention time distributions may be observed for the *k-ε* model and the RNG *k-ε* models, with a large dead zone in the vicinity of the outlet B due to the recirculation of the flow (Figure 3). This may explain that there are similar residence times in both cases, even though outlet B is located in front of the inlet.

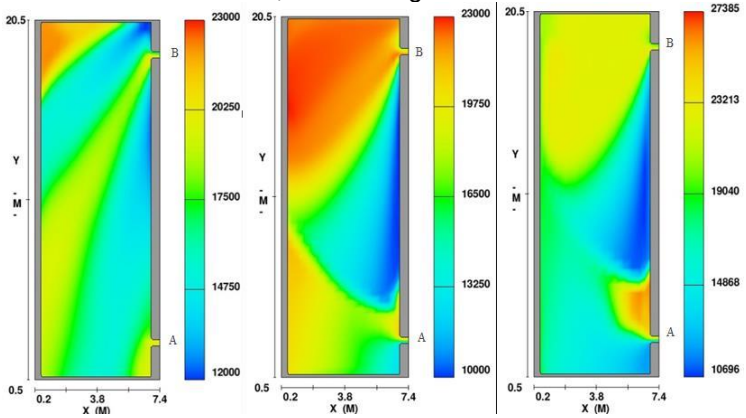

Figure 3. Hydraulic retention time for a horizontal plane located at the bottom outlets level with mesh size of 0.4 m: laminar model (left), *k-ε* model (center), RNG *k-ε* model (right)

REFERENCES

Hirt, C., & Nichols, B. (1981). Volume of fluid (VOF) method for the dynamics of free boundaries. *Journal of Computational Physics, 39*, 201-225.

Karpinska, A., & Bridgeman, J. (2016). CFD-aided modelling of activated sludge systems – A critical review. *Water Research, 88*, 861-879.

Proceedings of the 1st IAHR
Young Professionals Congress
17-18 November 2020

STOCHASTIC MODELING OF STORM PRECIPITATION SCENARIOS

Ivan Kuznetsov

Russian state agrarian university - Moscow agricultural academy named after K.A. Timiryazev, Department Meteorology, Moscow, Russia,
ivan_sosnovitsy_452_069@mail.ru

ABSTRACT

The article is dedicated to stochastic modeling of storm precipitation. The presented scientific study tests the main hypothesis about the sufficient adequacy of the main statistical characteristics of the observed and modeled storm precipitation using a special algorithm of the Monte Carlo method.

Keywords: storm precipitation; stochastic modeling; North Caucasus.

1 INTRODUCTION

At the moment storm precipitation modeling is one of the most important tasks in the field of meteorology and climatology. Due to the global warming, which we can observe nowadays, the evaporation from the surfaces of water bodies increases, so does the amount of moisture in the air and, as a result, the extremeness of precipitation grows as well (Groisman et al., 2005; Ilinich et al., 2016; Zolina et al, 2012). Therefore, the climate normals used in the past for safe living are outdated now and the regulatory documentation needs improvement. Stochastic modeling allows considering all potential storm precipitation scenarios for calculation of the maximal rivers discharge and the corresponding levels of territorial floods using different types of precipitation-runoff models.

The test of the hypothesis about the consistency of the presented method for modeling storm precipitation was based on the next implemented goals: to determine the main statistical characteristics in relation to the main elements of the observed rainfall graphs; to obtain modeled rainfall graphs based on a special algorithm using the Monte Carlo method; to assess the adequacy of the main statistical characteristics of the observed and modeled storm precipitation in relation to their main elements. The novelty of the study stems from the regional features of the storm precipitation formation and modeling.

2 MATERIALS AND METHODS

The baseline information for modeling is the observation data collected at the meteorological station in Tuapse, a city in the southern piedmont region of Russia in the North Caucasus. Many floods occur in the city on the Tuapse river. The baseline statistical series includes 69 rains, each with total daily precipitation greater than 30.0 mm. Each rain has its own duration (from 1 to 24 hours, in steps of 1 hour). The intensity of precipitation of each rain varies considerably. The peak of precipitation intensity can occur at any hour. Accordingly, 69 rainfall scenarios were obtained. For each hour there is a certain proportion “K” of the total precipitation for a given rain. All the scenarios graphs have been aligned in relation to the hour with maximum precipitation. The first stage of modeling using the Monte Carlo method is based on a series of 500 values of the equal distribution of random numbers ξ ($0 \le \xi \le 100$), where each number matches a random value of probability in percent (Ilyinich et al. (2016)). The modeled values of probability correspond to the specific amount of precipitation according to the Pearson binomial distribution (type III) that has possibility to represent different asymmetries of random values. At the next stage, each value of the modeled series of the daily precipitation Xd is multiplied by the “K” coefficients of the randomly modeled precipitation scenario number. In this way 500 scenarios of daily precipitation have been obtained.

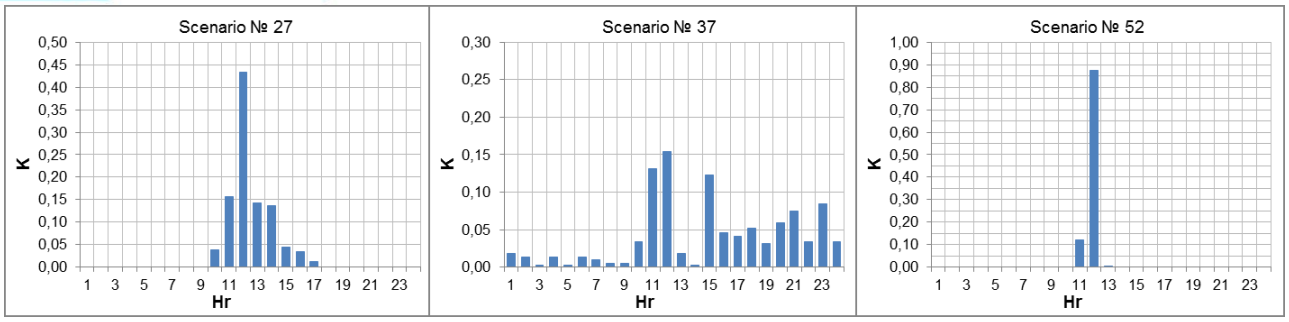

Figure 1. Examples of different rainfall scenarios.

3 RESULTS AND DISCUSSION

To assess the consistency of the presented modeling method, the statistical characteristics of the observed and modeled series were calculated. Such statistical characteristics as mean values and variation coefficient Cv were determined for amount of the rainfall (Xd), for the hour when the maximum precipitation was registered (Xmh), for the previous hour (Xmh – 1 hr) and for the next one (Xmh + 1 hr). In addition, the difference between the observed and modeled series was calculated, as well as the root mean square error. The results are presented in tables 1 and 2.

Table 1. Mean values for observed and modeled series

	Observed data, mm	Modeled data, mm	Difference, %	Root mean square error, %
Xd	48,0	47,8	0,410	5,441
Xmh	23,2	22,5	3,317	6,922
Xmh–1hr	4,7	5,3	11,754	14,121
Xmh+1hr	7,1	6,7	6,236	15,349

Table 2. Values for variation coefficient for observed and modeled series

	Observed data	Modeled data	Difference, %	Root mean square error, %
Xd	0,452	0,419	7,876	9,232
Xmh	0,575	0,573	0,349	9,635
Xmh–1hr	1,173	1,214	3,414	12,152
Xmh+1hr	1,275	0,958	33,031	12,606

Analysis of the tables shows that we can use the presented method for modeling scenarios of storm precipitation because the results are quite accurate and an inaccuracy appears just in one case (value for the variation coefficient at the hour following the hour when the maximum precipitation was registered).

4 CONCLUSIONS

The presented method for modeling scenarios of storm precipitation on the Tuapse river basin is enough accurate. It can be used in “precipitation – runoff” models for dangerous floods.

REFERENCES

Groisman P.U., Knight R.W., Easterling T.R., Hegerl G.G., Razuvaev V.N. Trends in intense precipitation in climate record// *J. Climate*. 2005.18. pp. 1326 – 1350.

Ilinich V., Akulova E., Belchihina V. and Ponomarchuk K. Estimation of Statistical Characteristics for Storm Precipitation with Long-term Data to Assess Climate Change. *Journal of Climate Change*, Vol. 2, No. 2 (2016), pp. 83 – 87. DOI 10.3233/JCC-160019.

Ilinich V., Belolubtcev A., Cavalli A., Veliev I., Lapushkin M. Modeling of storm precipitation. *Proceedings of the 11th Int. Conference on Urban Drainage Modeling*, 23-26 Sep. 2018, Palermo (ITALY). Ed. Prof. Giogio Manina, pp. 466 – 469.

Zolina O. Changes in European Extreme Precipitation.// UK: IAHS Press, 2012, In: “*Changes of Flood Risk in Europe*”, edited by Zbyszek Kundzewicz, pp. 97 – 120.

Proceedings of the 1st IAHR
Young Professionals Congress
17-18 November 2020

CFD MODEL DEVELOPMENT AND SENSITIVITY ANALYSIS FOR WATER-AIR FLOW IN A CLOSE CONDUIT SEWER PIPE.

Abhinav Dixit[1], Dr. Katharina Teuber[2], Prof. Dr. Dietmar Stephan[1], Prof. Dr.-Ing. Matthias Barjenbruch[1], Prof. Dr.-Ing. Reinhard Hinkelmann[1]

[1] Institute of Civil Engineering, Technische Universität Berlin, Berlin, Germany,
abhinav.dixit@wahyd.tu-berlin.de

[2] Research and Development, Berliner Wasserbetriebe, Berlin, Germany,
katharina.teuber@bwb.de

ABSTRACT

Biological corrosion of sewers networks and treatment plants constitutes a problem for asset management, and its effects result in the loss of billions of dollars per year. Hydrogen sulfide (H_2S) gas is the major contributor to the odour and corrosion occurring in the sewer networks. H_2S gas is formed by the breakdown of organic matter in the sewer under anaerobic conditions. These emissions not only increase the cost of maintenance but also pose a threat to human health of sewer workers. To understand and to be able to estimate transformation processes at the air-water interface, it is important to study the hydraulics and flow patterns in sewers. For this purpose, a model has been set up in the open source platform OpenFOAM, which is aimed to improve the data basis for a numerical model of natural sewer ventilation.

Keywords: OpenFOAM, sewer-networks, CFD, volume of fluid, air phase velocity

1 INTRODUCTION

Corrosion of concrete caused by hydrogen sulfide has been recognized as a serious problem in collection systems for the past century (Okabe et al., 2007). In some of the worst cases, the lifetime of sewer pipes and pumping stations has been reduced to less than ten years (Hvitved-Jacobsen, 2002). When designing urban sewer systems, common practice is to only consider the transport of wastewater and runoff water without giving any thought to the air phase in the systems (Edwini-Bonsu et al., 2004). Consequently, the airflow is generally uncontrolled, potentially malodorous and causes formation of corroding compounds (hydrogen sulfide) during transport of the wastewater. For this purpose, a two-phase CFD model is set up in the open source software OpenFOAM using the built-in solver interFoam, to verify and analyze the air-water flow in a closed conduit rectangular pipe which can later deliver the groundwork for models for natural sewer ventilation.

2 MODEL CONCEPT

A two-phase flow model is set up in order to study the impact of the two phases on each other inside a closed rectangular system of length 5 m, width 0.3 m and height 0.26 m under the following flow conditions:

i. Stagnant air with water flow due to inlet flow of 7.2 L/s;
ii. Stagnant water with air flow due to a pressure difference of 0.001 kgm/s^2
iii. With both phases flowing with the conditions mentioned above.

It was observed that for the chosen water velocity and pressure difference, impact of air flow on stagnant water is negligible when compared to the impact of flowing water on stagnant air. For the validation of the flow the experimental works of Bentzen et al. (2016) shown in Figure 1 were used. The experimental duct measures 15 m * 0.3 m * 0.26 m and has a water flow at the inlet. The sidewalls of the duct consisted of glass and the top wall of painted wood to have a minimum impact of wall friction. Air flow was measured at different points to generate a vertical profile that was used to validate the airflow for the CFD model. In the study it was observed that the induced flow in the air-phase is laminar hence using the k-epsilon model for this purpose would lead to inconstancies. For this purpose, the interFoam solver with a laminar flow model was used and the results abided with the experimental data.

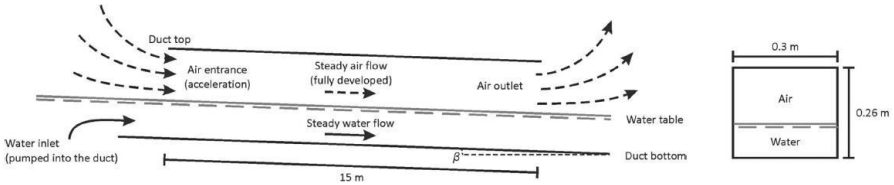

Figure 1. Experimental setup showing the flows involved and the dimensions (Bentzen et al., 2016).

3 Sensitivity analysis

A sensitivity analysis is a good way to ensure the accuracy of the mesh, time-steps, and various other parameters. After plausibility tests, the model was subjected to a sensitivity analysis based on changing viscosities and mesh resolution at the air-water interface. Because of the formulation of the interFoam solver is based on solving one set of Navier-Stokes equations with the phases described by an indicator function (Volume of Fluid approach), no friction approaches are applied at the interface between air-water and were therefore not considered in the sensitivity analysis. It was found that though there was an increase in the density of the data and plot for the air velocity profile, there was no significant change in the data when changing the mesh resolution. Secondly the impact of changing viscosity (v_{air} & v_{water}) was studied using seven different combinations of the two viscosities listed in the Table 1 with root mean square error between the experimental values and the results from different cases.

Table 1. Different combinations used to study the impact of changing viscosities with RMES

		Exp. values	Standard	Case 1	Case 2	Case 3	Case 4	Case 5	Case 6
v (m^2/s)	Water	1.00E-06	1.00E-06	1.00E-06	1.00E-06	1.00E-06	1.00E-04	1.00E-05	1.00E-07
	Air	1.51E-05	1.51E-05	1.51E-03	1.51E-04	1.51E-06	1.51E-05	1.51E-05	1.51E-05
	RMSE	---	0.005	0.075	0.077	0.078	0.122	0.035	0.071

It was observed that increasing the air viscosity in case 1 and 2 caused the velocity profile to change significantly from a s-shaped profile to almost a linear line. While reducing the viscosity of air in case 3 lead to s-shaped profile with a linear drop in the middle. Meanwhile increasing or decreasing the viscosity of water did not cause any significant change in the water and air velocity. All the profiles are shown in Figure 2.

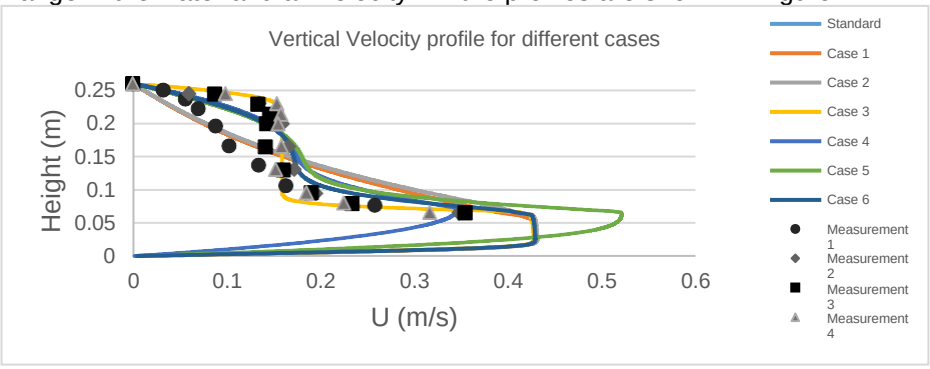

Figure 2. Vertical velocity profile for different viscosities

ACKNOWLEDGEMENTS
The Deutsche Forschungsgemeinschaft supports current research within the Research Training Group Urban Water Interfaces (RTG 2032/1 and 2032/2).

REFERENCES

Bentzen, T., Østertoft, K., Vollertsen, J., Fuglsang, E., and Nielsen, A. (2016). Airflow in Gravity Sewers–Determination of Wastewater Drag Coefficient. Water Environment Research, 239–256.
Edwini-Bonsu, S. and Steffler, P. (2004). Air Flow in Sanitary Sewer Conduits due to Wastewater Drag: A Computational Fluid Dynamics Approach. Journal Environmental Eng. Sci., 331-342.
Hvitved-Jacobsen, T. (2002). Sewer Processes – Microbial and Chemical Process Engineering of Sewer Networks. CRC Press, Boca Raton, Florida, USA.
Okabe, S. M., Odagiri, T. anf Satoh, H. (2007). Succession of sulphur-oxidizing bacteria in the microbial community on corroding concrete in sewer systems. Applied and Environmental Microbiology, 971-980.

Proceedings of the 1st IAHR
Young Professionals Congress
17-18 November 2020

Comprehensive benefit assessments of green infrastructure

Qian Yu[1], Na Li [2] & Gaohu Sun[3]

[1,2] Research Center on Flood & Drought Disaster Reduction of the Ministry of Water Resources, Beijing, China
e-mail: yqcherie@126.com

[1,2,3] China Institute of Water Resources and Hydropower Research, Beijing, China

ABSTRACT

Green infrastructure (GI), a resilient solution, could effectively solve water problems in urban areas. Compared to the single function of grey infrastructures, controlling rainfall runoff volumes, the comprehensive benefits of GI are more significant. In this study, a comprehensive benefit assessment system of 5 different GI, including 18 indicators from disaster reduction benefits, economic benefits, environmental benefits and social benefits, has been established. The new established performance assessment system has been applied to Jinan Daminghu Sponge City Construction pilot area. The results indicate: (1) under the 24h design storm with 5-year, 10-year and 20-year return period, the corresponding inundation area reduction rates are 11.02%, 9.32% and 8.02%, (2) the corresponding direct flood loss reduction rates are 13.86%, 4.28% and 4.09%, and (3) the corresponding groundwater recharge volumes are 2.23 million m^3, 2.86 million m^3 and 2.87 million m^3, respectively, (4) the constructed green roofs could reduce 0.38-0.61 t/yr NO_2, 0.74-1.17 t/yr O_3, 0.29-0.52 t/yr SO_2 and 0.14-0.17 t/yr PM10.

Keywords: urban water management; green infrastructure; comprehensive benefit assessment; Sponge City; Jinan.

In the last few decades, urbanization has almost swept across China. The population growth, urban density changes, and land cover changes accompany with urbanizations and urban developments. The traditional development paradigm raises the imperviousness rate. In addition, it also results in increased surface runoff volume and diminished infiltration rate in consequence (Ahiablame et al. 2012). The adverse impact is the increase of urban flood risks, which would also bring other negative impacts such as water quality deterioration, economics loss and even casualty. Green infrastructure (GI), a resilient solution, is an effective measure to reduce negative impacts caused by urbanizations and adapt to climate change by storing, detaining, infiltrating, and purifying rainfall runoff at source (Benedict et al. 2017). However, the public still have doubts over the benefits of GI due to the frequent occurrences of pluvial flooding in China. In addition to reducing rainfall runoff, GI can improve water quality of runoff, positively impact the air quality, reduce energy consumptions and enhance aesthetics, which is a great advantages compared to single-purpose grey infrastructure.

Different kinds of GI have different structures and functions. In this study, we establish a comprehensive benefit assessment system of 5 different GI within the urban context. The 5 kinds of GI are green roofs, bioretentions, permeable pavement, rainfall harvesting and bioswales, respectively. The system includes 18 indicators (Table 1) from disaster reduction benefits (No.1-5), economic benefits (No.6-9), environmental benefits (No.10-15) and social benefits (No.16-18).

We apply this comprehensive benefit assessment system to Daminghu District, which is a Sponge City Construction pilot area in Jinan city, China. The study area is about 39 km^2. The terrain is higher in the south, lower in the north, higher in the east and lower in the west. The 24h design storm with 5-year, 10-year and 20-year return period are shown in Figure 1. The 3 kinds of GI were designed in this area. They were green roofs (0.26km^2), sunken greenbelts (0.31km^2) and porous pavement (0.18 km^2), respectively.

In view of the characteristics of study area and existing data, 4 indicators were selected to evaluate the comprehensive performances of GI, i.e., reduces inundation area, reduces direct economic loss, increases groundwater recharge volumes and improves air quality. The flood simulation numerical model and flood risk analysis software (FRAS) and flood damage assessment software developed independently by IWHR were adopted to evaluate the first two indicators. For the increases of groundwater recharge volumes and air quality improvement, the empirical equations were used to calculate the values.

Table 1. Comprehensive performance evaluation indicators of GI.

	1	2	3	4	5	6	7	8	9
	Volume capture ratio of annual	Reduces inundation area	Reduces affected population	Reduces affected GDP	Reduces direct economic loss	Reduces grey infrastructure needs	Increases avaliable water supply	Reduces water treatment	Reduces energy use
Green roofs	●	●	●	●	●	●	✖	○	●
Bioretention	●	●	●	●	●	●	✖	○	○
Permeable pavements	●	●	●	●	●	●	✖	○	✖
Rainfall harvesting	●	●	●	●	●	●	●	○	✖
Bioswales	○	○	○	○	○	○	○	○	○
	10	11	12	13	14	15	16	17	18
	Reduces non-point source pollution	Improves habitat	Increases groundwater recharge	Improves air quality	Mitigates urban heat island	Reduces noise pollution	Improves aesthetics	Improves community cohesion	Enhances public education
Green roofs	●	●	✖	●	●	●	●	○	●
Bioretention	●	●	●	●	●	○	●	●	●
Permeable pavements	●	✖	○	✖	✖	●	✖	✖	●
Rainfall harvesting	●	✖	✖	✖	✖	✖	✖	✖	●
Bioswales	●	●	○	●	●	○	●	○	●

● Yes ○ Maybe ✖ No

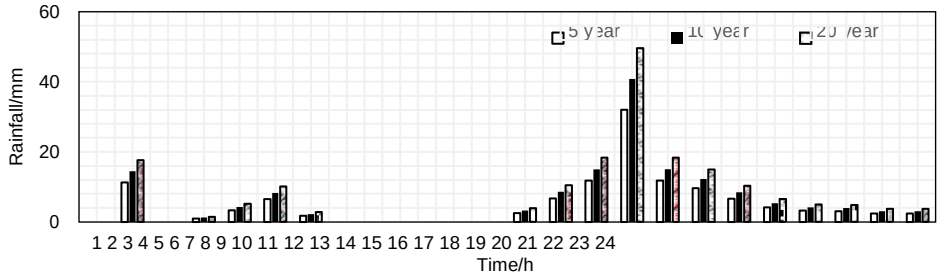

Figure 1. 24h design precipitation process in Jinan.

The results show that the inundation area reduction rates are 11.02%, 9.32% and 8.02%, and the direct economic loss reduction rates are 13.86%, 4.28% and 4.09% under the 24h design storm with 5-year, 10-year and 20-year return period, respectively. With the increase of rainfall volumes, the corresponding effectiveness of GI on rainfall runoff reduction decreases. However, the groundwater recharge volumes increase with the increases of rainfall volumes. The corresponding groundwater recharge volumes are 2.23 million m^3, 2.86 million m^3 and 2.87 million m^3 under three different rainfall return periods. In addition, the constructed green roofs could reduce 0.38-0.61 t/yr NO_2, 0.74-1.17 t/yr O_3, 0.29-0.52 t/yr SO_2 and 0.14-0.17 t/yr PM10. GI also improves the aesthetics of living environment. In Yingxiongshan Road of Daminghu pilot area, the former impervious surface are replaced by rain gardens and bioretentions, which significantly improve the environment, and increase recreational opportunities.

ACKNOWLEDGEMENTS

The research is financially supported by National Natural Science Foundation of China (51909273), Open Research Fund Program of State Key Laboratory of Hydroscience and Engineering (sklhse-2019-B-06) and Water Resources Technology Demonstration Project (SF-201903).

REFERENCES

Ahiablame, L. M., Engel, B. A., Chaubey, I. (2012). Effectiveness of low impact development practices: literature review and suggestions for future research. *Water Air & Soil Pollution*, 223(7):4253-4273.

Benedict, M., Mcmahon, E., Fund, T.C., et al (2017). Green infrastructure: linking landscapes and communities. *Natural Areas Journal*, 22(3): 282-283.

Proceedings of the 1st IAHR
Young Professionals Congress
17-18 November 2020

COMPARISON OF URBAN BASIN APPLICATION BETWEEN GR4J (SNU-CAHL) AND SWMM

Hyeonju Kim [1], Young-Oh Kim [2]

[1,2] Department of Civil and Environmental Engineering, Seoul National University, Seoul, South Korea,
E-mail: rtguswn@snu.ac.kr [1], yokim05@snu.ac.kr [2]

ABSTRACT

Owing to the generation of high peak flow, the increase in impermeable areas due to urbanization is a critical problem. To manage this inevitable issue, forecasting and analyzing runoff is essential. This study aims to make a more accurate urban basin prediction using the Seoul National University-Climate Change Impact Assessment for Hydrology Library (SNU-CAHL), which obtains runoff results generated by the GR4J model. Prior to this, a comparison of runoff results between the Storm Water Management Model (SWMM), which is an urban rainfall-runoff model, and GR4J was conducted. Both models were simulated using daily rainfall scenarios and daily rainfall observations. Compared to time-series data, the two models exhibited similar patterns but different flow duration curves. To improve the ability prospects of urban basin runoff, it is expected that in further studies, GR4J will be fit into SWMM together with a parameter adding section.

Keywords: SNU-CAHL, GR4J, SWMM, urban basin, runoff.

1 INTRODUCTION

Owing to climate change and severe urbanization, the impermeable area of the urban watershed will increase in the future. Urbanization generates a high peak flow and an increase in surface runoff, which leads to urban flood damage (Kim et al., 2019). Therefore, for urbanization and climate change adaptation, runoff prediction and analysis in the urban basin is crucial.

The runoff results depend on the hydrological model used. Owing to its ability to set various characteristic values of urban basins, Storm Water Management Model (SWMM) is generally used when simulating the urban basin runoff. However, Seoul National University-Climate Change Impact Assessment for Hydrology Library (SNU-CAHL) has the advantage of automated convenience. Therefore, the objective of this study is to improve the urban basin projection performance of GR4J in SNU-CAHL by comparing it with SWMM.

Seoul National University-Climate Change Impact Assessment for Hydrology Library (SNU-CAHL) was created to support calculations that are normally required in climate change research by connecting various models and input/output data effectively. Before applying the hydrological model, the entire process of creating the input data was automated. Regional Climate Model (RCM) data was used to generate daily averages for each basin and then inputted into SNU-CAHL to obtain potential evaporation. Runoff is obtained through the hydrological model GR4J or Tank (Park, 2016).

2 METHODS AND RESULTS

GR4J and SWMM models were compared to make a more accurate urban basin prediction in SNU-CAHL. The runoff results of the two models were obtained using the Representative Concentration Pathway (RCP) 4.5 Korea Meteorological Administration (KMA) precipitation scenarios for the basin, containing Bundang-gu in South Korea, from 2041 to 2070. The minimum, maximum, and average values of the runoff for the entire period are 0 mm, 327.11 mm, and 1.35 mm, respectively, for the SWMM, and 0.01mm, 383.54 mm, and 1.30 mm, respectively, for the GR4J. The following time series curve exhibits a similar pattern between the two models. Figure 2 shows a flow duration curve with relative frequency on the horizontal axis and flow rate on the vertical axis, in order of magnitude, for analyzing the discharge. A slight difference between the two models is evident.

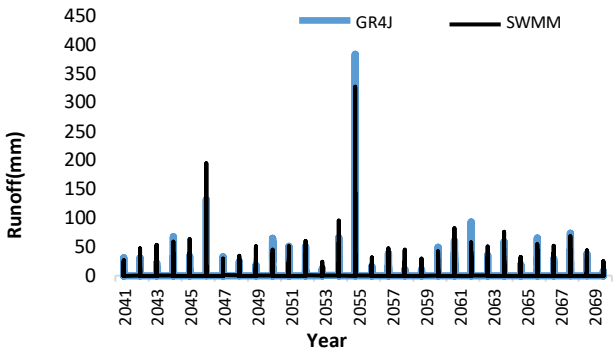

Figure 1. Time series curve

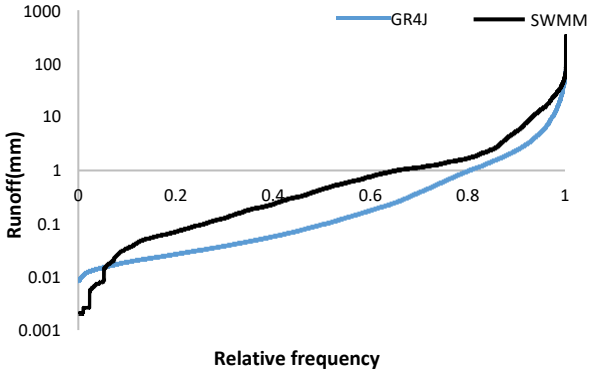

Figure 2. Flow duration curve

In order to effectively evaluate the performance of the two models, comparing these simulations with monitoring data is needed. For simulations, rainfall observations from 2009 to 2015 in South Korea, named Bundang-gu were obtained by the Water Resources Management Information System (WAMIS). The minimum, maximum and average values of the observed flow rate for the same observation site are 0.98mm, 175.29mm, and 4.42mm. The result values of the two simulated models are 0mm, 260.13mm, and 3.85mm for SWMM and 0.01mm, 76.22mm, and 1.01mm for GR4J in order of minimum, maximum, and average. When comparing the observed flow rate and the simulated flow rate values of the two models, it can be seen that the SWMM has a value closer to the observed value.

To analyze the cause of this difference, we need to take a closer look at the composition of the GR4J and SWMM models. First, in the GR4J model, the input values are precipitation and potential evapotranspiration. There are four parameters, namely the capacity of production store X1, the water exchange coefficient X2, the maximum capacity of the routing store X3, and the time parameter for unit hydrograph X4 (Ling Zeng et al., 2019). Unlike GR4J, SWMM can set values for each sub-catchment according to the following components: slope, area, width, percent impervious area, roughness, infiltration, and CN, which are features that can be set for each sub-catchment. The values of location, height, slope, roughness, and form can be assigned according to junctions and conduits. The rainfall parameters include intensity, duration, and frequency (Sahar Babaei et al., 2018).

As previously mentioned SWMM has the advantage of being able to set various conditions. This way, SWMM can set different characteristic values for each sub-catchment and accurately analyze runoff in urban basins. Considering the increase in impermeable area, which is the main effect of urbanization, the percent impervious area among the sub-catchment features of SWMM should be added as a parameter of GR4J.

3 CONCLUSIONS AND DISCUSSION

The overall runoff was similarly derived for the GR4J and SWMM models. Because the characteristics of urban basins are not efficiently applied in the GR4J model, the difference between the models in the flow duration curve was evident. For further research, we suggest that percent impervious area should be added as a parameter to the GR4J model, such that new runoff results will be simulated by the percent impervious area parameter applied to the GR4J model. Applying the calibrated GR4J model to SNU-CAHL is expected to be beneficial in representing the outflow of the urban watershed.

ACKNOWLEDGEMENTS

The Institute of Engineering Research at Seoul National University provided research facilities for this work.

REFERENCES

Kim, B.S, Lee S.J, Lim, S.H. (2019). Analysis of runoff by LID application in Busan eco delta city using SWMM. *Journal of Civil Engineering*, 237-239.

Park, D.K. (2016). Development of an open source software tool for climate change assessment in hydrology, SNU-CAHL. Master thesis, Seoul National University, Seoul.

Babaei, S., Ghazavi, R., Erfanian, M. (2018). Urban flood simulation and prioritization of critical urban sub-catchments using SWMM model and PROMETHEE II approach. *Physics and Chemistry of the Earth*, 105, 3-11.

Zeng, L., Xiong, L., Liu, D., Chen and Kim, J.S. (2019). Improving parameter transferability of GR4J model under changing environments considering nonstationarity. *Water*, 11(10), 2029.

Proceedings of the 1st IAHR
Young Professionals Congress
17-18 November 2020

AN EXPERIMENTAL STUDY OF SEDIMENT ACCUMULATION, EROSION AND TRANSPORT PROCESSES IN COMBINED SEWER PIPES

Manuel Regueiro-Picallo [1], Jose Anta [1], Joaquín Suárez [1] & Jerónimo Puertas [1]

[1] Universidade da Coruña, Water and Environmental Engineering Research Team, Elviña, 15071 A Coruña, Spain.
e-mail (manuel.regueiro1@udc.es)

ABSTRACT

The analysis of the sediment accumulation, erosion and transport processes in combined sewers is a key issue within urban drainage systems. Sewer sediments represent the main source of pollution in sewer systems to the receiving environment. To better understand these processes, an experimental campaign was design and carried out in a Flume Test Facility, in which wastewater flow conditions could be provided. New techniques and methodologies were developed in this facility to increase the accuracy in the measurement of the accumulation and transport of in-sewer sediments, such as the Structure from Motion (SfM), as well as to analyse their physicochemical properties. Furthermore, experiments were also performed on small-scale models to characterise the concentration and size of suspended particles by using acoustic sensors. As a result, a large dataset was obtained to develop advanced strategies for the design, operation and maintenance of combined sewer systems.

Keywords: sewer sediments, bed load transport, biodegradability, photogrammetry, acoustic turbidity.

1 INTRODUCTION

The accumulation, erosion and transport of sediments in combined sewer systems are important sources of pollution in urban areas. Secondary sewer networks (pipe diameter < 400 mm) significantly contribute to the production of these depositions mainly due to insufficient flow velocities during long-term dry weather periods. The accumulation of bed deposits reduces the pipe cross-section and increases the bed roughness. Consequently, the discharge capacity decreases, leading to progressive or sudden blockages. The persistence of sediment accumulation contributes to the generation of gasses and odours, such as methane and hydrogen sulphide, and increases the frequency of flooding and combined sewer overflow (CSO) episodes (Ashley et al., 2004). The release and mobilization of these depositions during rainfall episodes can overload sewer systems, thus influencing receiving aquatic environments (Regueiro-Picallo, 2020).

2 MATERIAL AND METHODS

Several experimental campaigns were conducted to understand the accumulation, erosion and transport of sediments in combined sewer pipes. For this purpose, a Flume Test Facility was set up in the Bens wastewater treatment plant (WWTP) of A Coruña (Spain). This facility allows different sewer pipe geometries to be tested under close-to-real conditions by supplying wastewater from the WWTP (600,000 inhabitants). Moreover, the facility controls, measures and characterizes wastewater and sediment discharges (Regueiro-Picallo et al., 2020). As for experiments, new methodologies were implemented to characterize sediments deposited in pipes. For instance, Structure from Motion (SfM), a photogrammetric correlation technique, was applied to determine the sediment bed morphology in accumulation and transport episodes. In addition, the sediment biodegradability and its influence on sediment transport was analysed by adapting analytical techniques to determine the chemical oxygen demand (COD) or the oxygen uptake rate (OUR). Furthermore, the facilities of Eawag (Dübendorf, Switzerland), were available to apply ultrasonic acoustic techniques to determine the concentration and size distribution of suspended particles through the acoustic turbidity measurements.

3 RESULTS AND DISCUSSION

The following results were obtained from the experiments performed in the above mentioned facilities. In the Flume Test Facility, tests were focused on accumulation, erosion and transport of sediments in different drainage pipes under different flow and slope conditions. In the development of these experimental campaigns,

the SfM photogrammetric technique has been applied to measure the structure of bed sediments deposited during the accumulation periods or after the erosion and transport tests. This technique provided a 3D reconstruction of the bottom of the pipe, which increased the accuracy to obtain the volume of sewer sediments and the analysis of bed forms regarding one-single point or transversal profiling measurements (Figure 1a). In addition, methodologies have been developed for sampling and analysis of the physicochemical properties of the sewer sediments (Regueiro-Picallo et al., 2018). This analysis showed differences in the results depending on the time of sampling. The organic fraction values decreased as the accumulation time increased (Figure 1b). This allowed establishing a correlation between the degradation in the organic fraction of the sediments, their cohesion and the capacity to be eroded when an increase in the flow rate conditions was induced (Regueiro-Picallo et al., 2020).

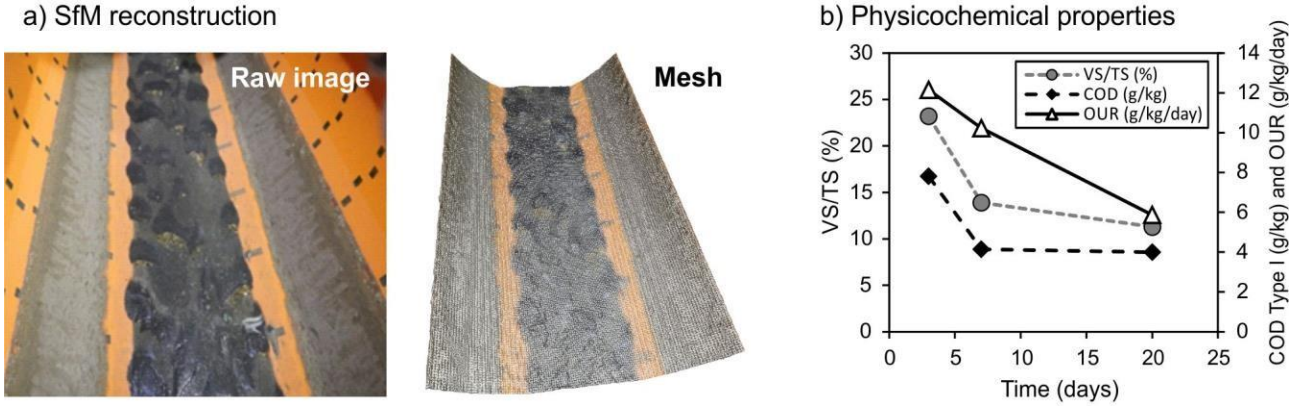

Figure 1. Picture of the deposited sediment in the pipe and mesh resulting from the SfM reconstruction (a), and time-evolution of the sediment physicochemical properties for different accumulation test periods (b). Figures taken from Regueiro-Picallo et al. (2018 and 2020).

On the other hand, several tests have been carried out in small-scale models with multi-frequency acoustic sensors to characterize the suspended solids. These tests have been carried out with different types of materials (plastic spheres and sand), and different suspend solid concentrations and particle sizes. Preliminary results were obtained that showed the dependence between the signal received by the sensors and the established conditions (Regueiro-Picallo, 2020). Thus, as the concentration or size increased, the signal recorded by the acoustic sensor was greater. These results can be used to calibrate acoustic turbidity models that predict sediment characteristics (size, density and concentration).

4 CONCLUSIONS

The use of experimental facilities allowed the application of novel techniques and the development of methodologies to improve the accuracy of the volume of deposited sediments measurements and the characterization of their physicochemical properties, respectively. In addition, multi-frequency acoustic sensors were sensitive to different suspended solid concentrations and particle grain sizes but further studies will be required in order to characterise wastewater suspended particles.

ACKNOWLEDGEMENTS

This research was financed by the projects ‘SEDUNIT’ Ref. CGL2015-69094-R and ‘OVALPIPE II’ Ref. RTC-2016-4987-5 (MINECO/FEDER, EU). The authors would like to thank the companies EDAR Bens SA, EMALCSA and ABN Pipe Systems S.L.U. for their assistance with the experimental work.

REFERENCES

Ashley, R.M., Bertrand-Krajewski, J.L., Hvitved-Jacobsen, T., and Verbanck, M.A. (2004). *Solids in sewers*. Scientific & Technical Report 14, IWA Publishing, London, UK.

Regueiro-Picallo, M. (2020). *Characterization of sediment accumulation, erosion and transport processes in combined sewer pipes*. PhD Thesis, Universidade da Coruña, A Coruña, Spain.

Regueiro-Picallo, M., Anta, J., Suárez, J., Puertas, J., Jácome, A., and Naves, J. (2018). Characterisation of sediments during transport of solids in circular sewer pipes. *Water Science and Technology*, *2017*(1), 8-15.

Regueiro-Picallo, M., Suárez, J., Sañudo, E., Puertas, J., and Anta, J. (2020). New insights to study the accumulation and erosion processes of fine-grained organic sediments in combined sewer systems from a laboratory scale model. *Science of The Total Environment*, 716, 136923.

Proceedings of the 1st IAHR
Young Professionals Congress
17-18 November 2020s

DATABASE DESIGN AND GRAPH-BASED ANALYSIS FOR SWMM URBAN MODELLING

Martín Ríos[1,2], Leandro D. Kazimierski[*1,2], Marina Lagos[1,2], Mariano Re[1,2]

[1]National Institute for Water (INA), Hydraulics Laboratory, Ezeiza, Argentina
[2]School of Engineering, University of Buenos Aires (UBA), Buenos Aires, Argentina

*Correspondance : marios@fi.uba.ar

ABSTRACT

This work illustrates the steps on the development of a graph-based approach for the analysis of a high-resolution urban 1D hydrological-hydraulic model. The basin of San Juan - Jimenez (SJJ, Buenos Aires, Argentina) is used as a test case, where the model was previously calibrated and validated. A database with the data (.INP file) and results (.OUT file) of the EPA-SWMM model is built in PostgreSQL. The database is used to build a graph network of the hydraulic system, allowing a deeper analysis over the sub-basins of each node.

Keywords: hydroinformatics, urban flooding, surrogate modelling, database, graphs

1 INTRODUCTION

SJJ basin of 75 km^2 in the Metropolitan Region of Buenos Aires (RMBA) has suffered numerous heavy rainfall events usually result in urban flooding. The development of 1D High-Resolution (1DHR) urban flood model of the dual-drainage system with EPA-SWMM, calibrated and validated with direct and indirect information (Re *et al.*, 2019; Ortiz *et al.*, 2017) allowed an advanced understanding of the flood dynamics in the basin. A forecast of water levels in streams during intense rain events in the basins of the RMBA is a demand of civil protection and local governments. These needs are requested to the Hydro and Meteorological National Services to generate strategies for their development. 1DHR models developed are not suitable for short-term forecasting due to their high computational cost.

The main objective of the whole project is the development of surrogate model (Bermúdez *et al.*, 2018) using graph neural networks for real-time operation on intense precipitation events. Surrogate models aim to increase speed forecasting with minimal loss in quality. Multiple simulations of the HR model for different scenarios are going to be used as input for the training of the neural network model (Berkhahn *et al.*, 2019). In this work, the first step in this development is presented, which includes the assembly of a database and the graph implementation.

2 METHODOLOGY

SSJ 1DHR model has over 19.000 nodes, 25.000 links and 18.000 subcatchments which generates an output file of about 4GB. For the simulation result, EPA-SWMM outputs a binary file (.OUT file), which makes the data-extraction a complex and time consuming process. A database in PostgreSQL was built, where all the data in the output file was extracted with the *swmmtoolbox* [1] library; the data in the model file (.INP file) and the meteorological data is stored. A Python script automates the extraction and loads the data on the database using the *psycopg2* library. The motivation to implement a graph is to achieve an alternative representation of the data extracted from the EPA-SWMM and the future design of a graph neural network model. A graph consists of nodes connected by edges, where each one of this elements have attributes. This approach appears to be suitable for modeling the behaviour of a basin, adding the constraint of the water flow direction at a given

[1]https://timcera.bitbucket.io/swmmtoolbox/docsrc/index.html

time. Thus, a directed graph is build mapping analog elements between them: nodes on the graph represent the EPA-SWMM's nodes (junctions and storage units) and the directed edges on the graph represent the EPA-SWMM's links (streets, channels and conduits). The properties on the EPA-SWMM's elements such as water level, velocity, roughness, are added as attributes of the nodes and links on the graph.

3 RESULTS

The database reduces the access time during operation from 5 seconds, directly from the binary file, to 10 milliseconds (a 500x reduction) querying from the database; the time consuming extraction is done once and the data remain accessible through a SQL interface in a more structured way. The database has 23 tables including: model version, rainfalls registry; sub-catchments, nodes and links of the model, geometric properties and the time series outputs of the model simulations. Once the graph is built, it can also generate the corresponding sub-graphs for a node of the model at any given time (Figure 1). This sub-graphs are composed by the predecessor tree and the chosen node as outlet of the sub-basin, with aggregated data such as accumulated precipitation, mean impervious area and the area associated to the sub-basin (Table 1). This data will be useful as features for the neural network model.

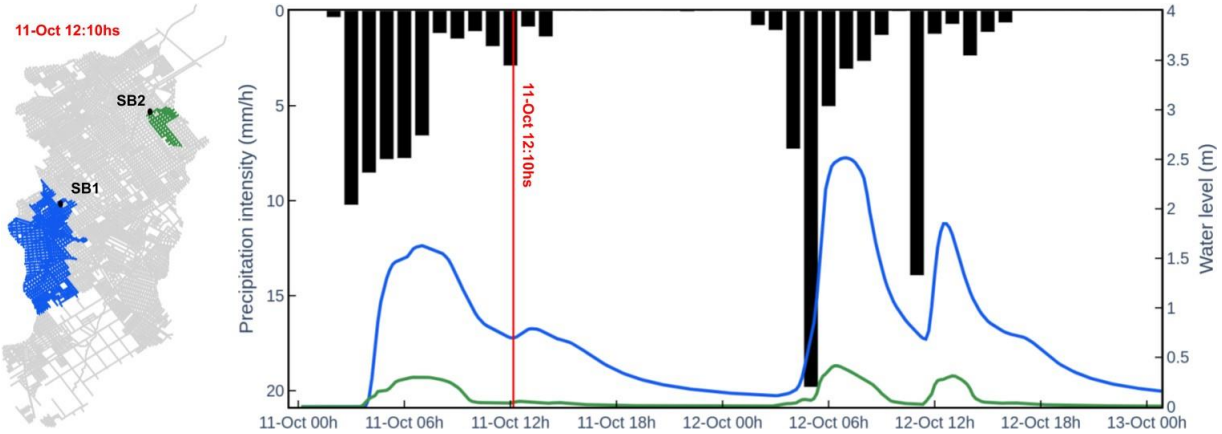

Figure 1: SSJ 1DHR model topology in grey and sub-basins associated to two nodes. Temporal series of water level and precipitation intensity every 1 hour in the two nodes with the time of analyses of the sub-basins properties in red.

Table 1: Attributes of the two sub-basins shown in Figure 1.

	SB1	SB2
Sub-basin Area [Ha]	751	99
Impervious Area [%]	47	68

4 CONCLUSIONS

During this work a database to manage the results of the simulation by the EPA-SWMM software was designed and implemented. Also, an exploratory analysis of the results and model performance was possible after the important reduction on access time. By querying the database, a graph of the basin for any node at any time was built, with detailed properties and variables time series. Finally, this information will be provided as input for a graph neural network which will aim to forecast water levels as a result of rainfall events.

References

Berkhahn S., Fuchs L., Neuweiler I. (2019). An ensemble neural network model for real-time prediction of urban floods. *Journal of Hydrology 575*, 743 – 754.

Bermúdez M., Ntegeka V., Wolfs V., Willems P. (2018). Development and comparison of two fast surrogate models for urban pluvial flood simulations. *Journal of Water Resources Management 32*(8), 2801–2815.

Ortiz N., Re M., Kazimierski L. D., Garcia P. E. (2017). Characterization of the impact associated with different flood types on an urban basin (in spanish). In *CONAGUA 2017*, Volume 1. Congreso Nacional del Agua, Argentina.

Re M., Kazimierski L. D., Badano N. D. (2019). High-resolution urban flood model for risk mitigation validated with records collected by the affected community. *Journal of Flood Risk Management 12*(S2), e12524.

Proceedings of the 1st IAHR
Young Professionals Congress
17-18 November 2020

EXPERIMENTAL CHARACTERIZATION OF A PERMEABLE PAVEMENT USING SIMULATED RAIN

Juan Naves [1], Jose Anta [1], Joaquín Suárez [1] & Alfredo Jácome [1]

[1] Universidade da Coruña, Water and Environmental Engineering Group (GEAMA), A Coruña, Spain, juan.naves@udc.es

ABSTRACT

Permeable pavements are among the most common Sustainable urban Drainage Systems (SuDS) techniques implemented on urban catchments, but their long-term performance has not been yet studied deeply and there is a great uncertainty about permeable pavements clogging and its effect on stormwater management. This study assessed the impact of retrofitting an impermeable concrete surface using a porous asphalt superficial layer. Initial records of the runoff routed to the drainage system during simulated rainfalls of 5 minutes and different intensities (30, 50 and 80 mm/h) over a full-scale street section physical model have been compared before and after surface retrofitting. In the next steps of the research, the long-term performance of the porous asphalt will be assessed both in terms of runoff peak reduction and pollution mobilization.

Keywords: Urban drainage, SuDS, permeable pavement, rainfall simulator.

1 EXTENDED ABSTRACT

The increase in impervious areas because of urban expansion leads to higher runoff volumes and flow discharges and increases the total pollutants load and peak concentrations during rainfall events. In this context, Sustainable urban Drainage Systems (SuDS) have become an increasingly common solution for the management and treatment of stormwater (CIRIA, 2015). Permeable pavements are among the most common SuDS techniques, being their effectiveness extensively demonstrated. However, their long-term performance considering clogging by surface sediments and other pollutants such as microplastics have not been yet analyzed in depth. In this study, the impact of permeable pavements on the hydrology and the mobilization of pollutants is assessed by comparing the obtained results against conventional impervious pavements, this being a first step to study their long-term performance under laboratory-controlled experiments.

Figure 1. (a) Permeable pavement placed over a street section physical model of 36 m^2 and detail of the surroundings of gully pot 1. (b) Rainfall simulator of 1 m^2 for the analysis of the pollutant removal efficiency of the permeable pavement.

The experimental setup consists of a full-scale street section physical model of 36 m^2 (Figure 1a) that uses a dripper-based rainfall simulator to generate three realistic and uniform precipitations of 30, 50 and 80 mm/h of rain intensity. The rainfall-runoff generated is drained through two gully pots and a downstream lateral channel where flow discharges and sediment concentrations are measured by using v-notches in lower deposits and by grabbing manual samples. A detailed description of this facility and the rain characteristics can be consulted in Naves et al. (2020a, 2020b). The impervious concrete road surface of the facility, which were previously used to perform high definition hydraulic, wash-off and sediment transport experiments (Naves et al., 2020c), has been retroffited using a permeable asphalt layer based on uniform granulometry to comparatively assess the influence of this type of SuDS in the quantity and quality of stormwater flowing into drainage networks. A detailed image of the permeable pavement in the surroundings of gully pot 1 is included in Figure 1a.

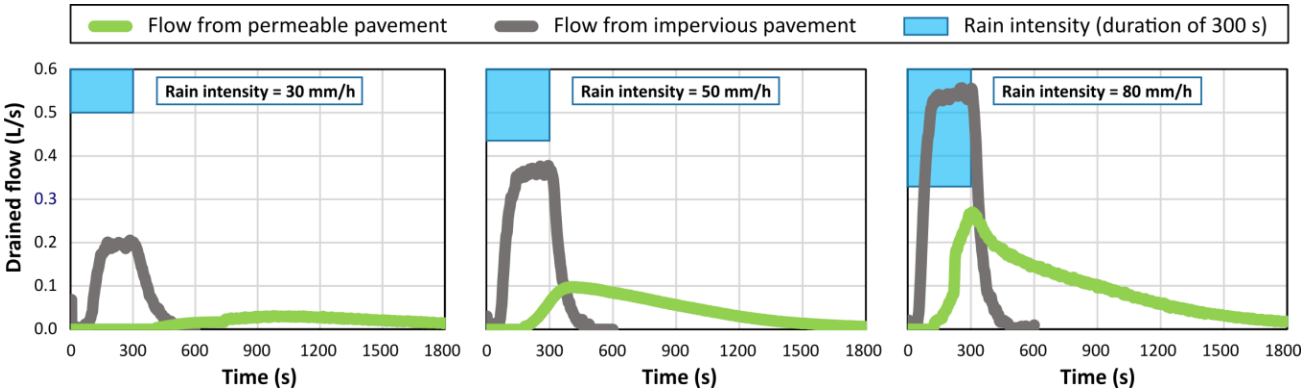

Figure 2. Comparison between the flow drained through the gully pots from the street section with and without the permeable pavement for the three rain intensities that the rainfall simulator can generate (30, 50 and 80 mm/h).

Figure 2 presents the water flow drained from the facility before and after the road surface retrofitting in three experimental cases where the rain intensities of 30, 50 and 80 mm/h were simulated during 300 s, this representing a range from medium to high intensity rain events. These first results obtained showed that the permeable pavement layer disposed over the street concrete surface reduces by 50% the peak of the drained flow in the worst case studied (rain intensity of 80 mm/h during 300 s). In addition, the hydrographs measured with the permeable pavement presented a lag in the runoff peak of more than 3 minutes in case of the highest rain intensity tested. These first results confirmed and quantified the benefits of this permeable pavements in urban stormwater management.

Next research will focus on the pollutant removal efficiency of the permeable pavement and the influence of clogging in hydraulic, sediment wash-off and water quality results. To do this, a 1 m^2 test facility (Figure 1b) has been developed to carried out preliminary studies considering pollutants where the initial state of the permeable pavement of the street physical model be not compromised, and allowing to develop tailored experimental and measurement methodologies. The final objective is to evaluate the long-term performance of permeable pavements in controlled laboratory experiments at full-scale physical model towards more efficient implementations and maintenance strategies.

ACKNOWLEDGEMENTS

This research was funded by the Spanish Ministry of Science, Innovation and Universities under POREDRAIN project RTI2018-094217-B-C33 (MINECO/FEDER-EU).

REFERENCES

CIRIA (2015). *The SuDS Manual*. C573. London: Ciria

Naves, J., Anta, J., Suárez, J., and Puertas, J. (2020a). Hydraulic, wash-off and sediment transport experiments in a full-scale urban drainage physical model, *Sci. Data*, 7, 44. https://doi.org/10.1038/s41597-020-0384-z.

Naves, J., Anta, J., Suárez, J., and Puertas, J. (2020b). Development and calibration of a new dripper-based rainfall simulator for large-scale sediment wash-off studies. *Water*, 12(1), 152, https://doi.org/10.3390/w12010152.

Naves, J., Rieckermann, J., Cea, L., Puertas, J., and Anta, J. (2020c). Global and local sensitivity analysis to improve the understanding of physically-based urban wash-off models from high-resolution laboratory experiments. *Sci. Total Environ.,* 709, 136152. https://doi.org/10.1016/j.scitotenv.2019.136152.

IAHR AIRH

International Association for Hydro-Environment Engineering and Research

Hosted by
Spain Water and IWHR, China

Session 5

Water Resources Management

IAHR YPN

Hosted by
Spain Water and IWHR, China

Proceedings of the 1st IAHR
Young Professionals Congress
17-18 November 2020

WATER BALANCE OF THE ESTIBANÁ SUB-CATCHMENT IN PANAMA

Arcenio A. Martínez [1], Zuri S. Rodríguez [1] & María G. Castrellón Romero [2, 3]

[1] *Facultad de Ingeniería Civil, Universidad Tecnológica de Panamá*

[2] *Centro de Investigaciones Hidráulicas e Hidrotécnicas, Universidad Tecnológica de Panamá*

[3] *Departamento de Gestión del Conocimiento e Investigación, Universidad del Istmo, Panamá*

E-mail: arcenio.martz@gmail.com, zuri.rodriguez@utp.ac.pa, mariag.castrellon@gmail.com

ABSTRACT

The Estibaná sub-catchment (ESC) has an area of 296 km^2, and is located within the Dry Arc region, in south-central Panama. The main water uses for ESC are human consumption and agriculture. Due to an increase in water consumption and more extreme weather, probably due to climate change, the need for water security has become imperative for this region. Therefore, and within the scope of a more comprehensive work, a water balance has been calculated for this sub-catchment for the 2018-2019 hydrological year. The water balance shows that Precipitation is the only water input, and that Evapotranspiration (ETR) corresponds to 67% of the precipitation. Consequently, during the dry season (December-April) deficit between supply and demand exists. This situation makes securing water availability in this region, a function of effective water saving policies, based on an integrated water resource management (IWRM).

Keywords: *Water Balance, Panama, Catchment Hydrology, Tropical Hydrology, Evapotranspiration.*

1 INTRODUCTION

The total freshwater availability in Panama has been estimated at $119.5\ x\ 10^9\ m^3/year$ out of which nearly 25.8% is currently being used mainly in non-consumptive uses such as transportation and energy production. By 2050 it is estimated that the national average water demand will double, reaching over 50% of the available resources (MIAMBIENTE, 2016). However, Panama's water supply is not equally distributed neither spatially nor temporally. Thus, regions in the country such as the Dry Arc frequently experience a decrease in streamflow during the dry season (December-April), with reports of shallow wells going dry (Castrellon Romero, 2018). The Estibaná sub-catchment (ESC) is located within La Villa River Watershed in the heart of the Dry Arc Region of Panama and has an area of 296 km^2. ESC's main economic activities are agriculture and cattle farming, making its population very dependent on water (Castrellon Romero et al., 2019). Lack of forest cover, poor soil conditions, and high temperatures, among other reasons, aggravate this situation, leading to longer periods of water scarcity. Also, climate change projections seems to indicate more extreme situation within the country (Fabrega R. et al., 2013) and for this region (MIAMBIENTE, 2018). Therefore, to face the current situation and to secure water availability in the face of climate change, a precise knowledge of water supply and demand in this area is essential. To assess the current situation in the ESC, a water balance was calculated for the 2018-2019 hydrological year. This assessment suggested possible actions to sustainably manage the water resources of this region and mitigate the effects of future droughts.

2 METODOLOGY

Data from the Department of Hydrometeorology of the Electrical Transmission Company of Panama (ETESA for its acronym in Spanish) were used to calculate the precipitation and the potential evapotranspiration (ETP). For the precipitation, data was retrieved from 5 ETESA meteorological stations located bordering the sub-catchment. Cumulative monthly and annual rainfall was calculated using the Thiessen method, and the results were verified with data from rain gauges installed inside the sub-catchment. For ETP, data from one station based on the Penman-Monteith Method and located outside the study area was available from ETESA. Consequently, the resulting ETP data were adjusted based on a conversion factor calculated from an average ETP map of the study area. Actual or real evapotranspiration (ETR) was then calculated using FAO's crop coefficient methodology (Allen et al., 2006). Runoff was calculated using water level data from the Estibaná River, measured by ETESA. Infiltration was estimated based on soil type and the hydraulic conductivity. For water demand, domestic, agricultural and livestock water consumption were considered. Domestic demand was estimated based on a water per capita consumption of 30 gallons per person per day (ANAM, 2008). Agricultural demand was calculated using ETR of the main crops, and its corresponding crop area and irrigation coefficients. Livestock water demand was calculated using graphs of cattle daily water consumption vs time based on growth rate, age and ambient temperature (Duarte, 2011).

3 RESULTS AND DISCUSSION

Figure 1 shows the monthly distribution of the water inputs and outputs in the ESC. Precipitation is the only input to the water balance. The highest precipitation occurred in June 2018, which is abnormal considering the historical rain pattern. ETR is the largest output and corresponds to 67% of the precipitation, which is within the 60 to 70% range reported by other studies conducted in tropical watersheds (Aponte-Hernández, 2013; Brooks et al., 1997). Total water demand amounts to only 1% of the annual water availability.

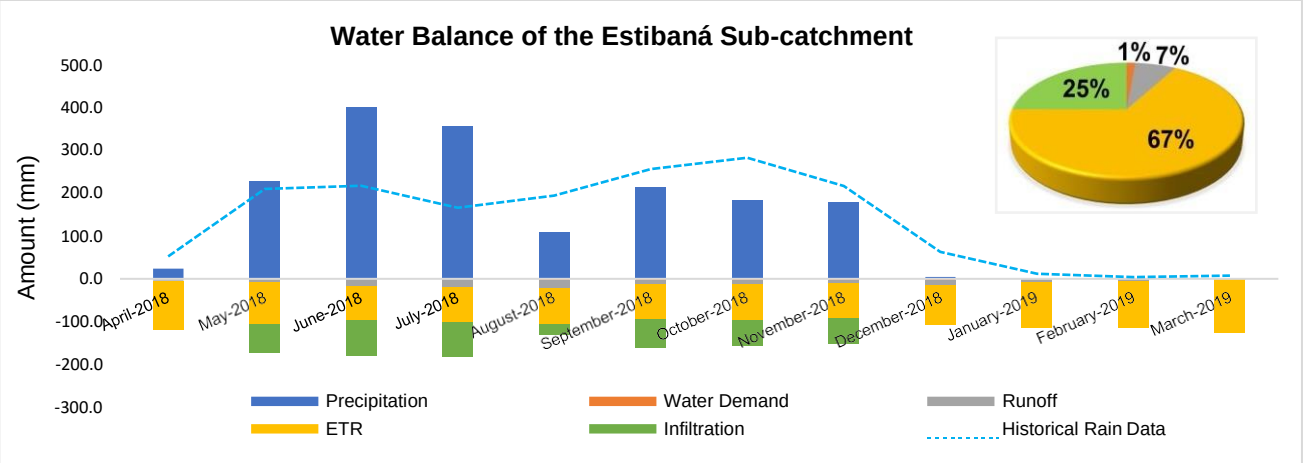

Figure 1. Water Balance of the Estibaná Sub-catchment.

4 CONCLUSIONS

The water balance indicates that dry season months have a deficit between supply and demand. Abnormal variations in precipitation due to climate change will likely worsen this deficit in the future. Therefore, efficient water saving policies during the dry season should be the first step to achieve water sustainability. These policies should include incentives to the employment of different water sources and capacity building actions, in order to acquire the necessary water related infrastructure to ensure a water secure region.

ACKNOWLEDGEMENTS

We thank the Secretaría Nacional de Ciencia, Tecnología e Innovación (SENACYT), for financing this project, the Ministerio de Desarrollo Agropecuario (MIDA), the Centro de Investigaciones Hidráulicas e Hidrotécnicas (CIHH) of the Universidad Tecnológica de Panamá (UTP), especially Dr. José Fábrega, for their collaboration and support.

REFERENCES

Allen, R., Pereira, L., Raes, D., Smith, M., 2006. Evapotranspiración del cultivo. Guía para la determinación del requerimiento de agua del cultivo, Organización de las Naciones Unidas para la agricultura alimentación.

ANAM, 2008. Cuenca Hidrográfica 128, Río La Villa, Evaluación de las Componentes del Balance Hídrico 37.

Aponte-Hernández, N.O., 2013. Metodología para evaluar la disponibilidad de agua y sus costos bajo los escenarios de cambio climático.

Brooks, K.N., Ffolliott, P.F., Gregersen, H.M., DeBano, L.F., 1997. Hydrology and the Management of Watersheds, Second. ed. Iowa State.

Castrellon Romero, 2018. Characterization and Modeling of a Tropical Groundwater System : La Villa Watershed , Panama.

Castrellon Romero, M.G., FABREGA, J.R., FOGLIA, L., MOJICA, A., RUIZ, A., SAAVEDRA, S., 2019. Groundwater Model of a Fractured Rock System As a Tool for Groundwater Management: the Estibaná Sub-Catchment, Azuero Peninsula, Panama. 38th IAHR World Congr. - «Water Connect. World» 38, 1959-1968. https://doi.org/10.3850/38wc092019-1794

Duarte, E., 2011. Uso del Agua en establecimientos agropecuarios. Planificación del sistema de abrevadero. Rev. Plan Agropecuario. 140, 38-43.

Fabrega R., J.R., T. Nakaegawa, R.P., K. Nakayama, O.A., Group, S.T.-C. modeling, 2013. Hydroclimate projections for Panama in the late 21st Century. Hydrol. Res. Lett. 7, 23-29. https://doi.org/10.3178/hrl.7.23

MIAMBIENTE, 2018. Tercera Comunicación Nacional sobre Cambio Climático Panamá, Mi Ambiente Panamá.

MIAMBIENTE, 2016. Plan Nacional de Seguridad Hídrica 2015-2050: Agua para Todos. Panamá: MiAMBIENTE/CONAGUA/Comité de Alto Nivel de Seguridad Hídrica. Panamá. https://doi.org/10.29327/15276.1-3

Proceedings of the 1st IAHR
Young Professionals Congress
17-18 November 2020

EVALUATING HISTORICAL DROUGHT USING DIFFERENT DROUGHT INDICES AND DATA PROCESSING SCHEMES

Tesfaye B. Senbeta[1] & Renata J. Romanowicz[1]

[1] Institute of Geophysics Polish Academy of Sciences, Warsaw, Poland

e-mail tsenbeta@igf.edu.pl

ABSTRACT

Drought is a natural phenomenon significantly affecting society, economy, and the natural environment. Precipitation deficit is the most important drought driving factor. Drought propagates from atmosphere to land, affecting soil moisture, groundwater, and surface water. The three most widely used drought indices: The Standardized Precipitation Index (SPI), the Effective Reconnaissance Drought Index (eRDI), and the Streamflow Drought Index (SDI) were used for evaluating historical meteorological, agricultural, and hydrological droughts. Two data processing systems were used for the drought analysis: (1) weighted mean area using a Thiessen polygon of drought indices calculated at individual meteorological stations; and (2) drought indices calculated from initially area - weighted averages of precipitation and evapotranspiration. Historical droughts have occurred in the Pilica River basin with different severities ranging from mild to severe. The study shows that there is no significant disagreement in the two data processing systems in identifying the severity of drought and the drought duration, but with the uncertainty considered the results may be different.

Keywords: drought indices, historical drought, data processing systems.

1 INTRODUCTION

Drought is a complex and costly natural phenomenon affecting more widespread areas than other natural hazards. Drought can be characterized by its severity, duration, areal extent, and spatial dimensions. It affects different components of the hydrological cycle, including precipitation, runoff, streamflow, soil moisture, evaporation, and groundwater. It extends spatially from the local catchment scale to the global and temporally from a few months to several years. Drought is classified into three main categories: meteorological drought (precipitation deficit, higher evapotranspiration); hydrological drought (reduction in surface and groundwater yield); and agricultural drought (soil moisture deficit, damage of crops). Drought indices are tools for characterizing and monitoring different types of drought, as found in Tigkas et al. (2015).

2 STUDY AREA AND DATA

The study area, the Pilica River basin, is the left tributary of the Vistula River basin, Poland. It drains a basin area of 8665 km^2. Daily streamflow data at the Bialobrzegi gauging station, and meteorological variables from nine stations inside and neighbouring the river basin from 1951 to 2019, were acquired from the Institute of Meteorology and Water Management, Poland. The quality of data was checked for accuracy and completeness, and missing values were filled by using a normal ratio method.

3 APPROACH

The three most widely used indices: The Standardized Precipitation Index (SPI), McKee et al. (1993), the Enhanced Reconnaissance Drought Index (eRDI), and the Streamflow Drought Index (SDI), were calculated using Drought Indices Calculator. According to Tigkas et al. (2015) droughts are characterized based on drought index as mild drought (0 to -0.99), moderate drought (-1 to -1.49), severe drought (-1.5 to -1.99), and extreme drought (-2.0 or lower). The same drought characterization ranges were used for all indices.

Two processing schemes were used: weighted mean of indices calculated at individual meteorological stations, and weighted precipitation and potential evapotranspiration. Potential evapotranspiration was calculated using the FOA-Penman Monteith method, Allen et al. (1998), using temperature, wind speed and relative humidity data.

4 RESULTS AND DISCUSSIONS

The study has shown that the SPI, eRDI and SDI identified historical meteorological, agricultural, and hydrological droughts, which occurred in the Pilica River basin ranging from mild to extreme droughts, as shown in Figure 1. The finding shows that the two weighted areal averaging methods applied to drought indices give similar results. Precipitation deficits, defined as a cumulative balance between precipitation and evapotranspiration, have occurred in the basin resulting in meteorological droughts specifically in 1959, 1969, 1976, 1982, 1991, 2003, 2015, 2019, which was confirmed by all three indices. As seen from Figure 1, the eRDI and SDI are close together whilst the SDI incorporates catchment processes which have influence on the drought accumulation and timing. All three indices are affected by the numerical errors resulting f rom the evaluation procedures.

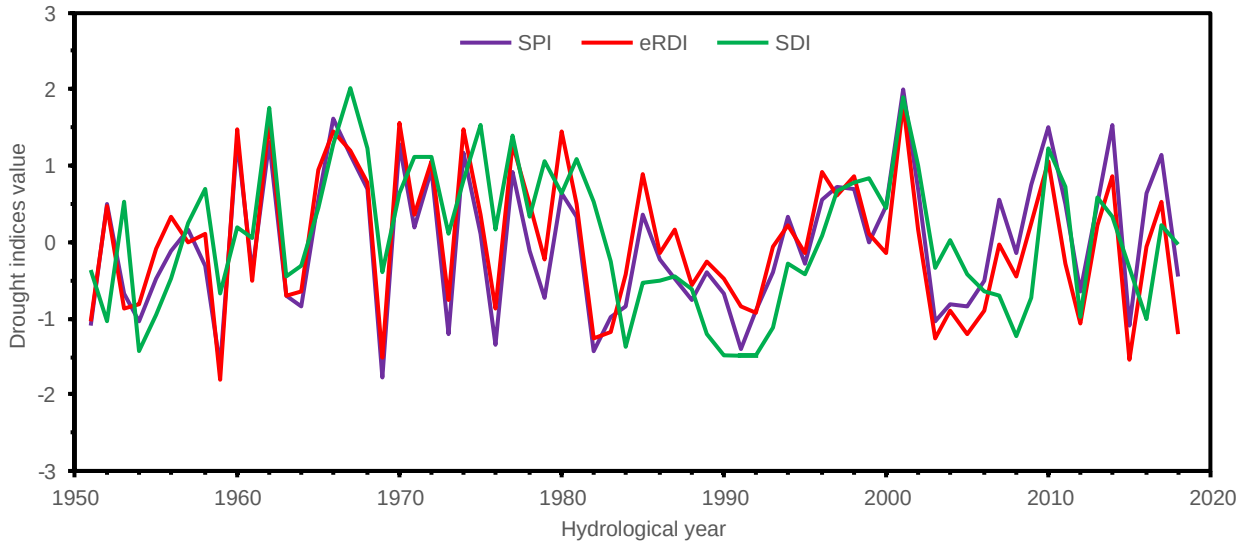

Figure 1. The historical drought severity indices for the Pilica River basin: SPI, eRDI and SDI.

5 CONCLUSIONS

Historical droughts have occurred in the Pilica watershed with severities ranging from mild to severe. The two approaches compared gave similar results, but with uncertainty considered the results may be different. Further work is planned to include an analysis of uncertainty.

ACKNOWLEDGEMENTS

This work was supported by the project HUMDROUGHT, carried out in the Institute of Geophysics Polish Academy of Sciences, funded by National Science Centre (contract 2018/30/Q/ST10/00654). The hydro-meteorological data were provided by the Institute of Meteorology and Water Management (IMGW), Poland.

REFERENCES

Allen, R.G., Pereira, L.S., Raes, D., & Smith, M. (1998). FAO Irrigation and Drainage Paper No. 56 - Crop Evapotranspiration. January 1998.

Mckee, T.B., Doesken, N.J., & Kliest, J. (1993). The relationship of drought f requency and duration of time scales. The preceeding of Eight Confirence on Applied Climatology, 17-22, Januarry 1993,p.179-184, Ariaheim, California.

Tigkas, D., Vangelis, H., & Tsakiris, G. (2015). DrinC: a software for drought analysis based on drought indices. Earth Science Informatics, 8(3), 697–709. https://doi.org/10.1007/s12145-014-0178-y

Proceedings of the 1st IAHR
Young Professionals Congress
17-18 November 2020

APPLICATION OF THE HYDROLOGICAL MODEL MGB-IPH AT THE SERIDÓ RIVER BASIN (BRAZIL)

Beatriz M. F. Negreiros[1,2] **and Joana Darc F. de Medeiros**[2]

[1]Institute for Modelling Hydraulic and Environmental Systems, Stuttgart, Germany
[2]Universidade Federal do Rio Grande do Norte, Natal, Brazil

*Correspondance : beatriz.negreiros@iws.uni-stuttgart.de

ABSTRACT

Hydrological modeling is a powerful tool for ensuring sustainable water resources management. The present study applied the large-scale rainfall-runoff model MGB-IPH (the acronym for Large Basins Model and Institute of Hydraulic Research) for modeling a river basin named Seridó. The Seridó river basin is located in the semi-arid Northeast region of Brazil, where water shortage is a frequent problem. The model is calibrated for the period between 1990 and 2000. The model successfully simulates the seasonality of the basin and the contrast between dry and rainy years. However, the discharge values are not adequately predicted by the model. One of the possible reasons for that difference is the presence of many reservoirs in the basin, which are not considered by the model. In conclusion, the present study reveals future research needs in the scope of hydrological modeling of river basins in semi-arid regions.

Keywords: Hydrological modeling, semi-arid region, MGB-IPH, calibration.

1 INTRODUCTION

The hydrological model MGB-IPH (Collischonn *et al.*, 2007) has been applied in several studies of South American basins (Paiva *et al.*, 2013; Fan *et al.*, 2014; Pontes *et al.*, 2017). Arid and semi-arid regions are drastically affected by changes in precipitation patterns and land use. In these areas, modeling can be an important tool for a more reasonable assessment and prediction of the supply capacity of the basins, which in turn frequently consist of intermittent rivers. Therefore, the goal of the present study is to apply the MGB-IPH and, thus, to build a hydrological model of the Seridó river basin.

2 MATERIALS AND METHODS

The Seridó river basin comprises a drainage area of approximately 10,080 square kilometers (Figure 1). The basin has a semi-arid climate and high evapotranspiration rates of the order of 1,786 mm/year. Precipitation is concentrated in short events that happen mainly from February to May, and are followed by long periods of drought. The mean annual precipitation is 500 mm.

The pre-processing of the Seridó River Basin is performed using the plugin *IPH Hydro Tools* coupled with the geoprocessing software *MapWindow*. The drainage system is obtained from the Digital Elevation Model (DEM). The basin is discretized in tree sub-basins: two with steeper topography and one with the flattest topography (Figure 1). The selected calibration period is between 1990 and 2000. From the available 81 rain gauges only 26 contain datasets for the selected time period (Figure 1). For the same reason, only 3 of the 46 stream gauges in operation are considered. Calibration is performed by manually adjusting the most sensitive parameters. The simulated flows are assessed with the Nash-Sutcliffe coefficient (NS) according to Nash et Sutcliffe (1970).

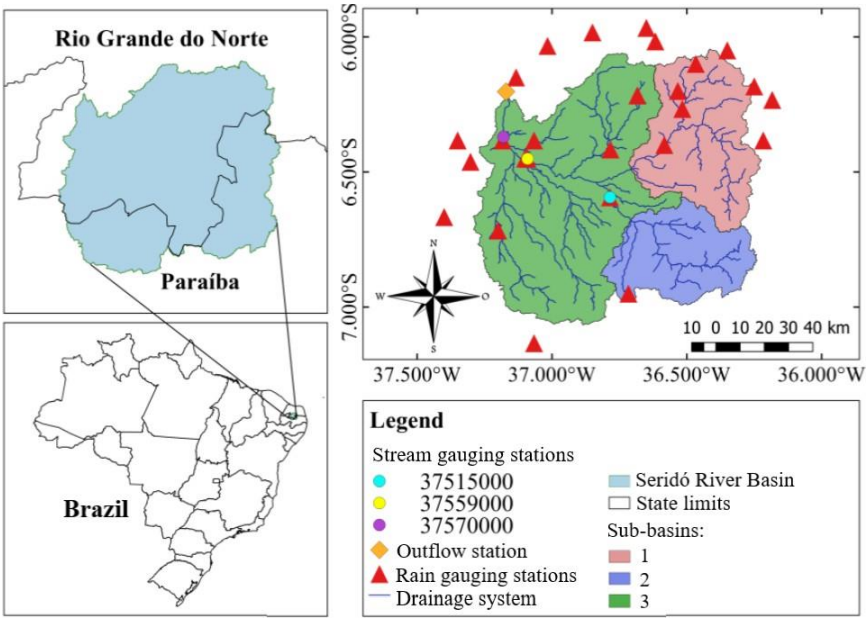

Figure 1: Location of the study area

3 RESULTS AND DISCUSSION

The analysis of the simulated and observed hydrographs indicates that the model reproduces the seasonality of the river basin and the contrast between dry and wet years. Nevertheless, the overall trend suggests that the model overestimates runoff. The reason is suspected to be the effect of several reservoirs. There are at least five reservoirs in the catchment area (in total more than 250,000,000 m^3 of storage capacity). These hold water that in turn never reaches the drainage system. Because the model does not account for this accumulated water, the simulation of the peak flows is compromised. The lack of sufficient rainfall and stream gauge data are additional challenges that may have hindered the calibration. Jørgensen et Bendoricchio (2001) points out that poor data quality may make proper calibration impossible. The present model obtains acceptable performance at only one stream gauge (NS = 0.246), while at the other two gauges the NS values indicate unsatisfactory efficiency (NS = -0.127 and -0.42).

4 CONCLUSIONS AND FUTURE RESEARCH NEEDS

The presence reservoirs, which are not considered in the MGB-IPH, is believed to be one of the causes for the inadequate model performance. In addition to that, the lack of sufficient data, specially stream measurements for the calibration step, is a major challenge. For future research, the implementation of reservoir operation in the MGB-IPH model is suggested. In conclusion, the present study conveys knowledge for further modeling of similar regions.

References

Collischonn W., Allasia D., Da Silva B. C., Tucci C. E. (2007). The MGB-IPH model for large-scale rainfall—runoff modelling. *Hydrological Sciences Journal 52*(5), 878–895. doi:https://doi.org/10.1623/hysj.52.5.878.

Fan F. M., Pontes P. R. M., Beltrame L., Collischonn W., Buarque D. C. (2014). Operational flood forecasting system of the Uruguay River basin using the hydrological model MGB-IPH. *ICFM-6 proceedings. São Paulo, Brasil*.

Jørgensen S. E., Bendoricchio G. (2001). *Fundamentals of ecological modelling*, Volume 21. Elsevier.

Nash J. E., Sutcliffe J. V. (1970). River flow forecasting through conceptual models part I— a discussion of principles. *Journal of hydrology 10*(3), 282–290. doi:https://doi.org/10.1016/0022-1694(70)90255-6.

Paiva R. C., Collischonn W., Buarque D. C. (2013). Validation of a full hydrodynamic model for large-scale hydrologic modelling in the Amazon. *Hydrological Processes 27* (3), 333–346. doi:https://doi.org/10.1002/hyp.8425.

Pontes P. R. M., Fan F. M., Fleischmann A. S., de Paiva R. C. D., Buarque D. C., Siqueira V. A., Jardim P. F., Sorribas M. V., Collischonn W. (2017). MGB-IPH model for hydrological and hydraulic simulation of large floodplain river systems coupled with open source GIS. *Environmental Modelling & Software 94*, 1–20. doi:https://doi.org/10.1016/j.envsoft.2017.03.029.

Proceedings of the 1st IAHR
Young Professionals Congress
17-18 November 2020

FLOW REGULATION BY WATER RESERVOIR FOR IRRIGATION USE

Ilyyas Veliev[1]

[1] Russian state agrarian university - Moscow agricultural academy named after K.A. Timiryazev
Moscow, Russia,
email: spp.sion@gmail.com

ABSTRACT

The research is dedicated flow regulation by water reservoir for rice plantations in conditions of dry years. Simulation of water reservoir control is carry out with help of stochastic programming methods.

Keywords: water reservoir; irrigation, stochastic modeling.

1 INTRODUCTION

The main goal of the research is decreasing of volume and duration of the water deficits for the rise paddies on the base of imitative simulation of water reservoir operation with help of stochastic programming. The next problems were decided for achivment of the goal: the choice of algoritm and corresponding PC program; adaptation and development of the simulative mathematical model for the irrigated water reservoir; modelling of the water reservoir storages and its drafts in conditions dry year; comparison results of the offered model (new model) and of the existing model (old model) for water reservoir regulation.

2 MATERIALS AND METHODS

Algorithm for water reservoir control of “fair concessions” (Voropaev et.al., 2003) and the corresponded PC program “IT balans” (Ismaiilov et al., 2014) were used for the search of effective rules of runoff regulation by water reservoir. The mathematical record of the task represented by minimizing the following functional:

$$\Phi(V,U,t) = \min \max \left| \sum_{t=1}^{t=T} \frac{U - U_{opt}}{U_{opt}} \right| \quad (1)$$

and the next conditions must be made:

$$\vec{V} = A\vec{\vec{W}} + B\vec{U} \quad (2)$$

$$\vec{\underline{V}} \le \vec{V} \le \vec{\bar{V}} \quad (3)$$

$$\vec{U} \ge 0 \quad (4)$$

$$\vec{V} \ge 0 \quad (5)$$

for t = 0, $\vec{V} = \vec{V}_0$, where $\vec{V}$– vector of the water reservoir storage (or level vector); $\vec{\underline{V}} = \vec{V}$, accordingly low limit – Dead storage and the upper limit - Full water reservoir storage; $\vec{U}$– vector of the plan drafts from water reservoir; $\vec{U}_t$ – vector of the real drafts at the moment t, which involves all water supply requirements of downstream (main - supply rise irrigation) and ecological water discharge; $\vec{U}_{opt}$ –optimum draft values; $\vec{\vec{W}}$ - vector of runoff to the water reservoir; t– time during the year (in our variant – numbers of pentads, maximum T=72); A and B - matrix system conditions.

The Krasnodar water reservoir was chocen for the research. The reservoir is situated on the Cuban river, its catchment is located in the foothills of the North Caucasus and has water regime of torrential floods during vegetation period, however, there is significant probability of long time dry period. Main water user is rice irrigation. The data about the object contained dependence between level and the storage volumes of the water reservoir and its main parametersare: Dead storage capacity196 mln m^{3}and corresponding Dead storage level

(DSL) 25.85 m; Full storage capacity 1798 mln m^3 and corresponding Normal level (NL) 32.75 m. Data about runoff to the reservor contain daily discharges with begining 1994 year.

Simulative model for the reservoir control have been made for the years of low water, in particularly for 1994 year (fig.1). According to the simulative model (Ismaiilov et al., 2014) of water reservoir were determined: graphs of water reservoir levels and water consumptions and water drafts during year (graph of fig.1); then the year sum of deficits, most pentad deficit (for 5 days), , amount of the deficit pentads were calculated. Same characteristics were determined with help of traditional water reservoir control according to dispatcher graph realized by PC program (Veliev, 2019). Results are represented table 1..

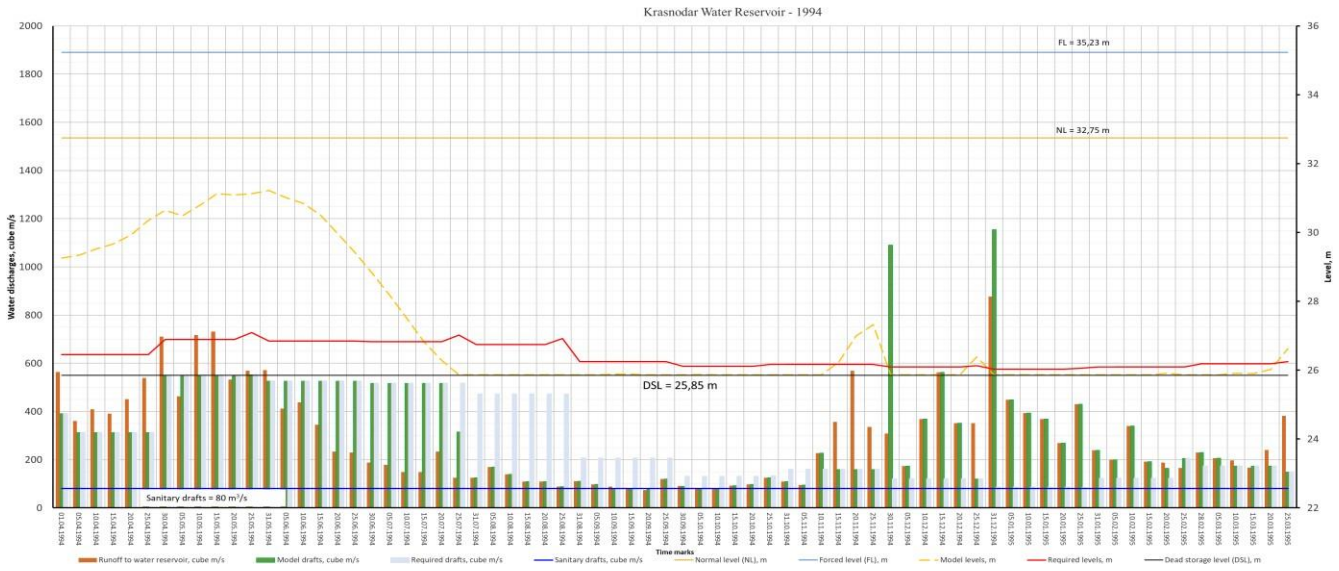

Figure 1. Examples of different rainfall scenarios.

3 RESULTS AND DISCUSSION

The results of comparison represent in table 1. They have showed that all main characteristics of new model are better old model.

Table 1. Results of model research for 1994 year

Models	The year sum of deficits, mln m^3	Most deficit, mln m^3	Quantity of deficit pentads during year
Old model	3579,2	442/25.08 - 31.08	33
New model	1474	198/25.08 - 31.08	21

4 CONCLUSIONS

The results of research have showed that the new model is much more profitable than the old model, but it works according to the well-known runoff hydrograph to the water reservoir. Therefore, the new model may be useful for the decision maker in the presence of short-term and long-term forecasts of runoff.

REFERENCES

VoropaevG.V., Ismaiilov G. Kh., Fedorov V.M. (2003) Problems of Water Resourses Control of Aral-Caspian Region. St.-Peterburg,.426 pp, (Rus).
Ismaiilov G. H., Perminov A. (2014) «Algorithm of the operation mode of water reservoir systems of seasonal and long-term regulation of river». Prirodoobustroistvo, 4, 2014. Moscow. 69-73 p. (Rus).
Veliev I.G. Modeling of elements of water balance of irrigation reservoir. In the book Agrometeorology of XXI century, part 2, 170-174 p, 2019 (Rus).

Proceedings of the 1st IAHR
Young Professionals Congress
17-18 November 2020

CHARACTERIZATION OF METEOROLOGICAL DROUGHTS IN CONTINENTAL ECUADOR DURING THE PERIOD 1902-2017

Ronnie Araneda-Cabrera [1], María Bermúdez [2] & Jerónimo Puertas [3]

[1,3]Water and Environmental Engineering Group, University A Coruña, A Coruña, Spain
ronnie.aranedac@udc.es, jeronimo.puertas@udc.es

[2] Environmental Fluid Dynamics Group, Andalusian Institute for Earth System Research, University of Granada, Granada, Spain
mariabermudez@ugr.es

ABSTRACT

Droughts in Ecuador are related to precipitation and temperature, varying their characteristics considerably across the country. Using the Standardized Precipitation and Evapotranspiration Index (SPEI), we have divided the country into three homogeneous drought regions that are similar to the country's geographical divisions. In these homogeneous drought regions, a characterization of the droughts during the periods 1906-1961 and 1962-2017 was performed. All three regions showed an increase in the frequency of droughts for all the temporal aggregations of SPEI. In the Coastal and Andean regions, the duration, intensity and severity also increased in the second period. The results point to increased pressure on water resources in recent years.

Keywords: drought; regionalization; SPEI; climate change; drought maps; Ecuador.

1 INTRODUCTION

Meteorological droughts, understood as the deficit of precipitation (P) with respect to its average, are slow onset events and difficult to quantify, constituting a problem that will be aggravated by climate change (WMO, 2006). For its monitoring and characterization, the Standardized Precipitation and Evapotranspiration Index (SPEI) proposed by Vicente-Serrano, Beguería, & López-Moreno, 2010 has been widely used, enabling the characterization of the phenomenon in the short and long term.

Due to its geography and climatology, Ecuador is frequently affected by drought events of variable duration and intensity. In recent years, strong relationships have been identified between P, temperature (T) and drought patterns over the entire territory (Vicente-Serrano et al., 2017). The objectives of this study were threefold: i) to identify the homogeneous drought regions of the country from the point of view of meteorological drought; ii) to analyze the change in the characteristics of droughts in two time periods of equal length: 1906 to 1961 and from 1962 to 2017 over the different regions; iii) to map drought characteristics across the country. The results can serve as a basis for developing risk management strategies and plans in Ecuador.

2 DATA AND METHODS

Monthly series from 1902 to 2017 of precipitation (P) and potential evapotranspiration (ETP) were downloaded from the Climate Research Unit, CRU TS3.10, of the University of East Anglia (UK), on a grid of 0.5°x0.5° over the whole Ecuadorian territory (106 cells). First, the SPEI was calculated on each of the CRU cells according to Vicente-Serrano et al. (2010) in 6-time windows: 3, 6, 12, 24, 36 and 48 months. Later, we used the minimum annual value of each SPEI to define homogenous drought regions and perform drought analysis. The regionalization analysis was conducted applying the k-means clustering method; the optimal number of regions was defined with the silhouette method. The statistical homogeneity test (H) was used to consider if the resulting regions were statistically homogeneous. In each region and period of analysis, the frequency of occurrence of droughts and the characteristics of duration, intensity and severity were computed based on the "run theory". Drought characteristics were mapped to facilitate spatial analysis. We defined drought as SPEI lower than -1 for at least 2 consecutive months.

3 RESULTS

Three homogeneous drought regions were identified in Ecuador (Coast, Andean and Amazon), which coincide approximately with the country's geographic regions. The H statistical test showed that the three regions were acceptably homogeneous (H < 1). SPEI time series were averaged in each region and drought characteristics were analyzed in each period (Table 1 shows the results for SPEI-12). The SPEI time series revealed drought events were in general more severe and intense (maximum intensity). In the Coastal and Andean regions, the higher the temporal aggregation of the SPEI, the higher the rate of change of the average characteristics between the first and second period, suggesting greater negative changes in the characteristics of hydrological droughts (river or aquifer flows). However, the Coast showed its drought characteristics slightly more affected than the Andean. In the Amazon region, the frequency of droughts was lower in the second period analyzed for the higher SPEI aggregations (12 and 24 months), and the average durations decreased when analyzing lower SPEI time periods (3 and 6 months). The average drought characteristics were mapped considering the SPEI time series over each CRU cell. It could be observed that the results found at the regional level are maintained (with small spatial variations) at the national level. In addition, the maps allowed us to identify smaller areas where droughts are more frequent, severe and intense.

Table 1. Average drought characteristics for the three drought regions of Ecuador using the SPEI-12.

SPEI ≤ -1.00	Coast		Andean		Amazon	
	1906 - 1961	**1962 - 2017**	**1906 - 1961**	**1962 - 2017**	**1906 - 1961**	**1962 - 2017**
Frequency [%]	1.04	2.23	1.34	2.38	2.08	1.79
Duration [N° months]	5.57	8.73	4.67	7.81	5.79	8.17
Intensity	-1.31	-1.56	-1.34	-1.48	-1.36	-1.45
Severity	-6.88	-12.93	-5.87	-10.82	-7.26	-10.97

4 CONCLUSIONS

The major conclusions of this study are: i) The SPEI index calculated with data from CRU detects as homogeneous drought regions the usual geographical regions of Ecuador, with contrasting climate regimes. ii) in the three regions of drought, the second half of the study period generally showed an increase in the frequency of drought; and, iii) the events tended to last longer and showed a higher intensity and severity, especially the long-term indices, suggesting that the main effects of droughts could be felt in river flows and groundwater. This work can serve as a basis for the development of drought and water management plans in Ecuador.

ACKNOWLEDGEMENTS

Ronnie Araneda gratefully acknowledges financial support from the Spanish Regional Government of Galicia (Xunta de Galicia) and the European Union through the predoctoral grant (reference ED481A-2018/162). María Bermúdez was supported by the EU H2020 research and innovation program under the Marie Skłodowska-Curie Grant Agreement No. 754446 and the Research and Transfer Fund of the University of Granada - Athenea3i.

REFERENCES

Vicente-Serrano, S. M., Beguería, S., & López-Moreno, J. I. (2010). A multiscalar drought index sensitive to global warming: The standardized precipitation evapotranspiration index. *Journal of Climate*, *23*(7), 1696–1718. https://doi.org/10.1175/2009JCLI2909.1

Vicente-Serrano, S. M., Martínez, E. A. R., Aguilar, E., Martínez, R., Martín-Hernández, N., Azorin-Molina, C., Sanchez-Lorenzo, A., Kenawy, A. El, Tomás-Burguera, M., Moran-Tejeda, E., López-Moreno, J. I., Revuelto, J., Beguería, S., Nieto, J. J., Drumond, A., Gimeno, L., & Nieto, R. (2017). The complex influence of ENSO on droughts in Ecuador. *Climate Dynamics*, *48*(1–2), 405–427. https://doi.org/10.1007/s00382-016-3082-y

WMO. (2006). Drought monitoring and early warning : concepts , progress and future challenges. *World Meteorological Organization*, *1006*, 24. http://www.wamis.org/agm/pubs/brochures/WMO1006e.pdf

Proceedings of the 1st IAHR
Young Professionals Congress
17-18 November 2020

MODELLING ACTUAL EVAPOTRANSPIRATION USING OPTIMIZED ENN METHODS

Jingran Liu [1*] , Xiankuan Meng [1] , Yingjie Ma [2] , Xin Liu [1]

1 Hebei University of Engineering, Handan, China; 2 Xinjiang Agricultural University, Urumqi , China

*Correspondence JL e-mail: 502560720@qq.com

ABSTRACT

Canopy temperature(Tc) was introduced using the Elman Neural Network (ENN) optimized by Mind Evolutionary Algorithm (MEA) and Genetic Algorithm (GA) methods to improve the predicting accuracy of evapotranspiration(ET). The improving planting methods, rainwater harvesting partial plastic film mulching and regulated deficit irrigation (MFR-RDI) with straw mulling, had been employed to save irrigation water. The results indicated that the Tc can well improve the accuracy of both MEA-Elman and GA-Elman models in predicting ET under the condition of MFR-RDI. Furthermore, the results showed that the performance of MEA-Elman was better than GA-Elman model under the same factors. Based on the above results, different input factors in different growth periods of crops has been adopted using the MEA-Elman4 model to further improve the predicting accuracy of ET. Indeed, MEA-Elman4 model exerted the best performance, which should be given priority to predict the ET.

Keywords: Evapotranspiration; Canopy temperature; Elman Neural Network; Mind Evolutionary Algorithm; Genetic Algorithm

1 INTRODUCTION

The high pressure areas of water resources in China are mainly distributed in North China. Irrigation water, accounting for nearly 70% of fresh water, has been over-exploited and over-used in many areas, leading to the water is becoming one of shortage resources in the world, especially in the arid and semiarid areas of northern China. It is particularly important to forecast actual crop evaportranspiration (ET), in order to alleviate the shortage of fresh water resources.

2 METHODS

The rainwater harvesting partial plastic film mulching and regulated deficit irrigation (MFR-RDI) with straw mulling, had been employed to save irrigation water.

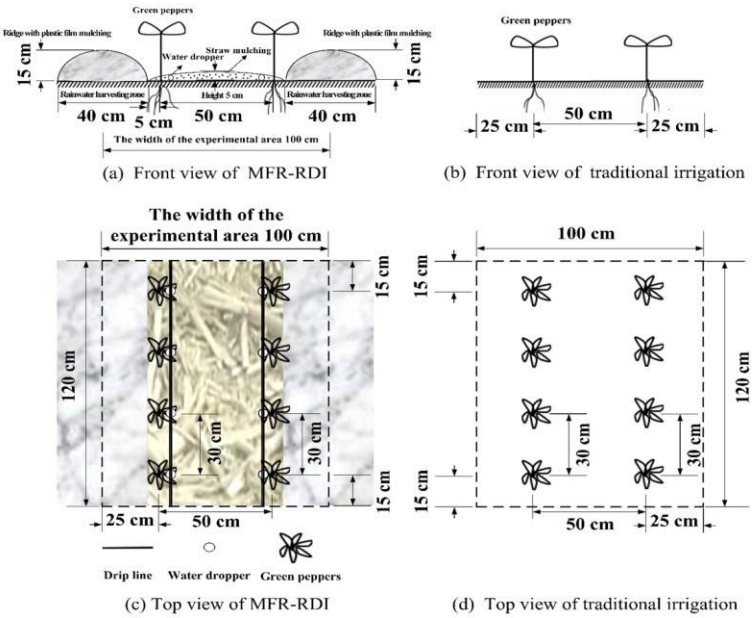

Figure 1.A schematic diagram of MFR-RDI system and traditional irrigation taking green pepper as an example.

The soil water balance method was used to determine ET.

$$ET = I + P \pm \Delta SW - D_P - R_{off} \quad [1]$$

where *ET* is evapotranspiration (mm); *I* is the amount of irrigation water applied (mm); *P* is the precipitation (mm); *ΔSW* is the change in the soil water content (mm); D_p is the deep percolation (mm); and R_{off} is the amount of runoff (mm). D_p and R_{off} always be ignored, given that the amount of irrigation water was only sufficient to bring the water deficit to field capacity and the experiment was carried out in the plot of precision irrigation experimental field.

Canopy temperature, Leaf area index and plant Heights were measured.Elman Neural Networks optimized by GA and MEA. Data from 2014 to 2017 were used for training, and data from 2018 were used for prediction and evaluation.Root mean square error (RMSE), mean absolute error (MAE) and Nash-Sutcliffe coefficient (NS) were used to evaluate the model performance.

3 RESULTS

Rainwater harvesting of straw mulching cultivation mode (MFR-RDI) can provide more suitable for crop growth of soil temperature and maintained high soil moisture content for crop growth. MFR-RDI can improve water use efficiency. The canopy temperature can well improve the accuracy of both MEA-Elman and GA-Elman models in predicting ET under MFR-RDI planting mode. The MEA-Elman model was better than the GA-Elman
model when the same variables were input. Selecting different input variables in different growth stages of crops played a positive role in improving the accuracy of ET prediction.

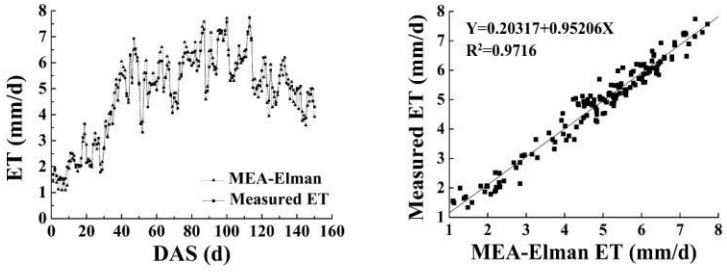

Figure 2. Comparison and analysis of the measured and predicted ET in selecting different input variables in different growth stages of crops.

4 CONCLUSIONS

MFR-RDI can improve water use efficiency. Leaf area index and canopy temperature had a large influence on the prediction of ET. Canopy temperature could be used as one of the important factors to predict ET. In case of the same input factors, the MEA-Elman model wasgenerally better than the GA-Elman model. Different
factors were selected as input variables for different growth periods to predict ET of crops, and the prediction effect was good.

ACKNOWLEDGEMENTS

The work was supported by Graduate Innovation Funding Projects of Hebei Province ,China, etc.

REFERENCES

Allen, R.G., Pereira, L.S., Raes, D., Smith, M., 1998. Crop Evapotranspiration. Guide Lines for Computing Crop
Evapotranspiration. FAO Irrigation and Drainage Paper no. 56, Rome 300, D05109.

Feng, Y., Jia, Y., Cui, N., Zhao, L., Li, C., Gong, D., 2017.Calibration of Hargreaves model for reference evapotranspiration estimation in Sichuan basin of southwest China.Agric. Water Manage. 181, 1-9.

Ferreira, L.B., Cunha, F.F., Oliveira, R.A., Filho, E.I.F.,2019. Estimation of reference evapotranspiration in Brazil with limited meteorological data using ANN and SVM–A new approach. J. Hydrol. 572, 556-570.

Proceedings of the 1st IAHR
Young Professionals Congress
17-18 November 2020

DEPARTMENTALIZATION AS A TOOL FOR WATER GOVERNANCE IN THE PHILIPPINES

Ivan Harris Tanyag[1]

[1] University of the Philippines, Diliman, Quezon City, Philippines
itanyag@up.edu.ph

ABSTRACT

Prospects of departmentalizing water service in the Philippines emerge as the country faced a series of water shortages, affecting the economic and social lives of the Filipinos. This however, would require a series of sweeping reforms in the country's water demand management. Overlapping functions and responsibilities amongst government agencies affect the water distribution. Water privatization has contributed to rising water rates in Metro Manila. Limited investments in the water economy has resulted to inadequacy of water infrastructure throughout the country. To identify whether the process of departmentalization contributes to water development, a series of fixed-effects correlation were made using three key-parameters namely, water accessibility, amount of water assistance received, and the level of permanent water bodies' extent in 162 countries, where 73 of which has a water department. The research suggests that the formation of a water department agency may significantly improve the level of water management in the community, as it has the institutional capacity to deploy water supply enhancements such as building dams and watersheds. The latter part of the research provides some recommendations prior to the imminent role of departmentalization in water governance around the globe.

Keywords: departmentalization, water governance, water resource management, Philippines

1 INTRODUCTION

In this paper, I look into the Philippines' case where the House of Representatives proposed a resolution suggesting the creation of a water department in the country as a mean to meet its water demands while ensuring a safe, clean, and affordable drinking water to Filipinos. The current water management structure in the Philippines, as of the writing of this paper, is composed of four agencies managed by different government departments namely, the Metropolitan Water and Sewerage System (MWSS), the Local Water Utilities Administration (LWUA), the National Water Resources Board (NWRB), and the National Irrigation Administration (NIA). Whilst the management structure varies amongst these agencies, its role and responsibilities are similar in nature however. That is, to effectively distribute water to all parties concerned. This perplexing structure creates a confusion among bureaucrats and policy-makers in reference to the adoption of water demand management strategies throughout the country. Prospects of creating a water department in the Philippines emerge soon after its capital region, Metro Manila, together with nearby provinces in the Central and Southern Luzon, experienced severe water interruptions as a result of water shortages recorded in the country's major dam reservoirs. This paper aims to address two key questions plaguing the narrative of water governance in the Philippines. One, would departmentalizing water distribution address the water shortage in the country? And two, can it resolve the long-standing issue of mismanagement and privatization of its water sector?

2 METHODOLOGY

This essay looks whether the creation of a *water department* would ensure the efficiency of water distribution across the country. Any other government agencies, including government-owned and controlled corporations, regulatory bodies, and autonomous agencies are not included in the research proper. A comparative analysis on the state of water governance was made using three parameters, which are vital in sustaining an effective and efficient water governance. One, the public's accessibility to a clean and safe drinking water. Two, the government's ability to receive and/or request an official aid from international organizations, private entities, and other stakeholders. Finally, the level of permanent water bodies' extent throughout the country. The paper analyzed more than 162 countries, 73 of which has a water department. All datasets considered in the research were gathered from the United Nations Water (UN Water). The scope of this research only covers the period of

2000 to 2017. Any other indicators in the UN Water's datasets were disregarded due to several factors, such as the incomplete or missing data values on datasets in some countries, and the limitations of *R* itself.[1]

3 RESULTS AND ANALYSIS

An in-depth analysis on the relationship between the parameters to the presence of a cabinet-level water agency is indicated at *Table 1*. Two separate tests were done using *R* to check whether there has been a change in the relationship between the parameters to the presence of a water department. The first test observes the presence of an agency *across* the countries observed, while the second test looks *within* the countries from a given period of 2000 to 2017. These tests identify the relationship between the unobserved variable, in this case, the presence of a water department, and the observed independent variable, which is the country. By observing *within* the countries, the presence of a cabinet-level water agency has a positive relationship to the level of water accessibility *within* the observed countries. However, as soon as these observations focused *across* these countries, it has produced a negative relationship between the two variables. This only means that the creation of a water department is more of a *needs-based* approach rather than the *charity* or *rights-based* approach. Water is distributed not because the government nor the provider considers it as a right, but because it is an essential need which has its own costs and risks. Similarly, countries who have a water department agency would not necessarily mean that it has the power nor the capacity to expand the level of permanent water body extent in its areas of concern, as it has no jurisdiction to utilize these, theoretically speaking, unless otherwise the public allows the government to utilize these water bodies for the greater good of the community. This of course would depend on the country's institutional and legal arrangement. As there is an agent who has the power to formulate and implement water supply enhancements, the amount of water and sanitation-related assistance increases as soon as the country departmentalizes its water distribution and management. Aside from increasing the level of institutional capacity, departmentalizing water distribution and management would also encourage the level of engagement and participation between the government and the civil society sector through public consultation, information dissemination, and knowledge-building capacity.

Table 1. Fixed Effects Correlation Between the Water Accessibility, the Level of Water Related Assistance Received, and the Level of Permanent Water Bodies' Extent to the Presence of a Water Department, Within and Across 162 Countries[1].

		Water Accessibility		Level of Water-Related Assistance Received		Level of Permanent Water Bodies' Extent	
		Across	Within	Across	Within	Across	Within
Intercept	Coefficient	75.312	58.062	29.167	55.936	2.398e+02	6.699e+02
	Standard Error	0.662	1.127	2.087	12.880	2.110e+02	3.525e+02
Slope***	Coefficient	-7.892	4.618	48.352	29.454	-1.8126e+04	8.114e-01
	Standard Error	1.438	0.580	3.601	5.056	3.929e+03	1.406e+02
Fixed Effects		No	Yes	No	Yes	No	Yes

ACKNOWLEDGEMENTS

I would like to thank Asst. Prof. Francis Joseph Dee (University of the Philippines, Diliman) for helping me with the statistical treatment of the data using R. I am extremely grateful for the insights I've learned from you.

REFERENCES

Dumol, M. *The Manila Water Concession: A Key Government Official's Diary of the World's Largest Water Privatization*. Washington, D.C.: The World Bank. 2000.
Fayol, H. "The Administrative Theory in the State." *Papers on the Science of Administration*. 1937: 99-114.
Gulick, L. "Notes on the Theory of Organization." *Classics of Organization Theory* 3, No. 1937, 1937: 87-95.
Soussan, J. *Water and Poverty in the Third World Water Forum.* Manila: Asian Development Bank. 2004.

[1] The research used a fixed-effects correlation, a type of statistical model that deals with the correlation between the independent variable and specific individual effects, which has its own limitations when using it at R.

Proceedings of the 1st IAHR
Young Professionals Congress
17-18 November 2020

MULTI-OBJECTIVE OPTIMAL OPERATION OF CASCADE HYDROPOWER PLANTS BASED ON WATER-ENERGY NEXUS: A WATER FOOTPRINT APPROACH

Lei Yu[1,2], Benyou Jia[1], Xiufeng Wu[1], Shiqiang Wu[1]&Peng Xu[1]

[1] State Key Laboratory of Hydrology-Water Resources and Hydraulic Engineering, Nanjing Hydraulic Research Institute, Nanjing, China
yulei0405@foxmail.com(L. Yu), byjia@nhri.cn (B. Jia), xfwu@nhri.cn(X. Wu), sqwu@nhri.cn(S. Wu) & xupeng1124@foxmail.com(P. Xu)

[2] College of Water Conservancy and Hydropower Engineering, Hohai University, Nanjing, China

ABSTRACT

Hydropower is the key component of the water-energy nexus, which can meet the energy demand and mitigate the greenhouse effect. This paper constructs an optimal operation model for cascade hydropower plants considering water footprint, quantifies the tradeoff relationship between power generation and water consumption (reservoir water footprint). The preliminary application in the Yalong River case has shown that (1) there are clear tradeoffs between hydropower generation and water consumption and (2) scheme 2 is the optimal scheme from the water-energy nexus for both two scenarios in a normal year.

Keywords: Multi-objective operation, Cascade hydropower plants, Water footprint, Benefit tradeoffs, Yalong River.

1 INTRODUCTION

The nexus is an advanced concept, which can improve system efficiency and performance through holistic understanding and coordination allocation of resources, and it also is the current research hotspot(Dai et al. 2018). Hydropower has the dual attributes of water-energy, on the one hand, hydropower generates clean and renewable energy to meet the energy demand and mitigate the greenhouse effect; on the other hand, the storage of water in reservoirs generates a lot of water consumption through the evaporation from open water surfaces (OWS) of reservoirs(Zhang et al. 2018). Therefore, how to balance these two attributes is a research problem. At present, most researches on the optimal operation of cascade hydropower plants (HHPs) focus on flood control and power generation benefits and ignore the impact on the ecological environment and water consumption. The water footprint is an indicator used to quantify the water consumption caused by human activities, which can be better applied to hydropower research(Hoekstra 2003). However, most of the available literature concerns only static the water footprint of hydropower, ignoring its temporal characteristics. To do so, based on the water-energy nexus, this paper takes the water footprint as an objective function, constructs an optimal operation model for cascade HHPs, and takes the lower reach of the Yalong River (China) as a research case-study, quantifies the tradeoffs relationship between power generation and water consumption (reservoir water footprint), and analyses the temporal variation characteristics of the water footprint. The present research results can provide scientific evidence for the sustainable development of hydropower and the improvement of resource utilization efficiency.

2 METHODS

This study employs the reservoir WF (water evaporated from OWS of reservoirs) and hydroelectric WF (the water consumption per unit of electricity production) to evaluate the consumption of water by hydropower for cascade HHPs (Mekonnen and Hoekstra 2012). Also, this paper constructs an optimal operation model for cascade HHPs and uses NSGA-II(Deb et al. 2002) algorithm to solve it. Finally, a sensitivity index is used to analyze the sensitivity of the hydroelectric WF. The flow chart through the methods used in this study is shown in Figure 1.

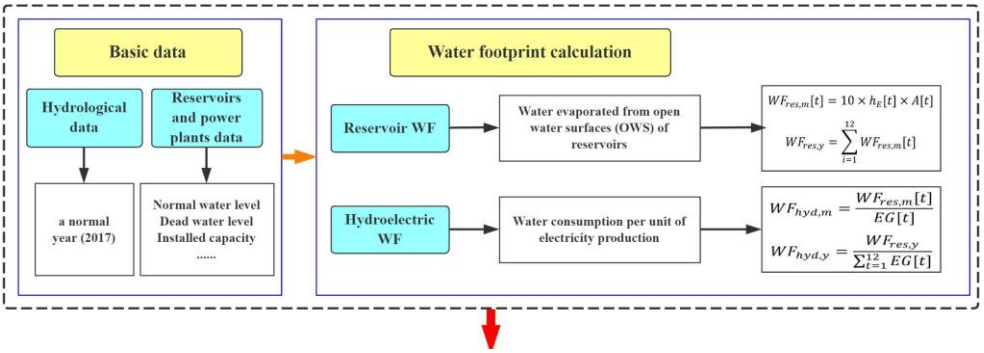

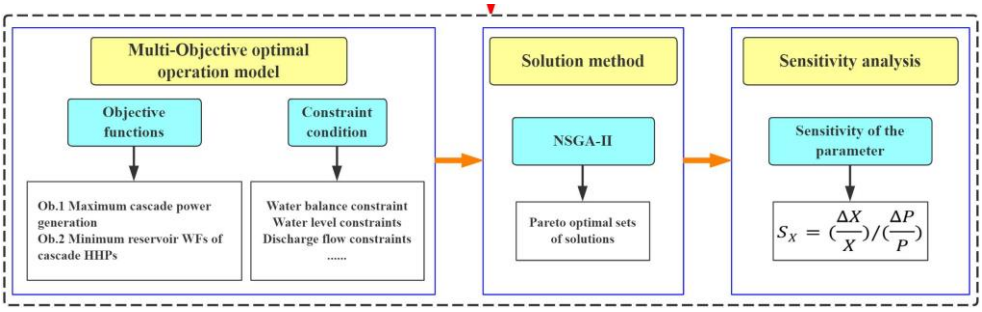

Figure 1. The flow chart through the methods used in this study.

3 RESULTS AND DISCUSSION

In this paper, a normal year is analyzed as a representative, and two scenarios are set: S1 (with the ecological flow) and S2 (without the ecological flow).

The Pareto optimal solution set of two scenarios is shown in Figure 2(a), and three schemes are selected as the recommended programs: scheme 1 (maximum cascade power generation), scheme 2 (minimum hydroelectric reservoir WFs of cascade HHPs), and scheme 3 (minimum reservoir WFs of cascade HHPs), as shown in Figure 2(b). We find that a clear tradeoff between hydropower generation and water consumption and the scheme with the maximum cascade power generation (Scheme 1) has the largest reservoir water footprint at some time. This is mainly because reservoirs usually operate at high water levels to pursue power generation benefits, which leads to a larger OWS. Therefore, scheme 2 is the optimal scheme from the water-energy nexus based on water footprint approach. And for scenario S1, the power generation and the reservoir WFs of the cascade HHPs of scheme 2 are 775.23×10^8 kWh and 159803.61×10^3 m^3, respectively; for scenario S2, they are 800.65×10^8 kWh and 159922.22×10^3 m^3, respectively.

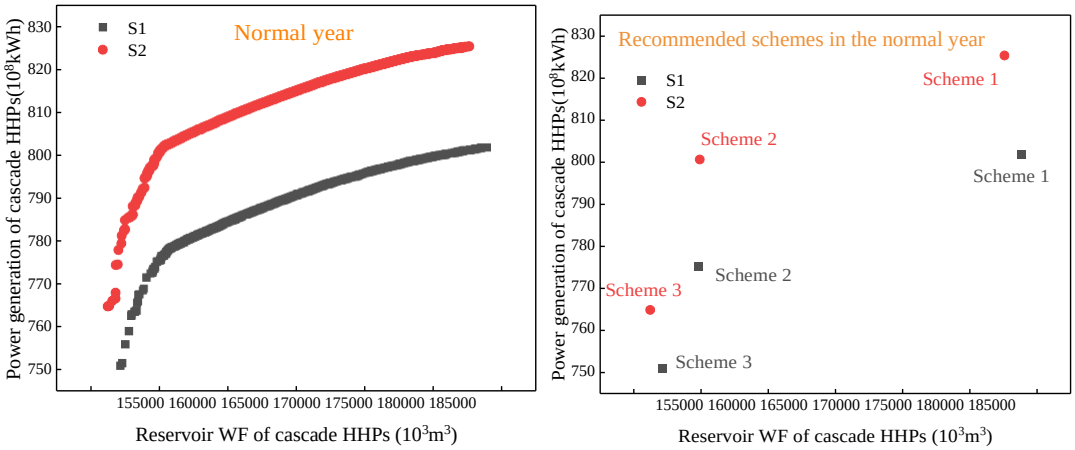

Figure 2. The Pareto optimal set of solutions under scenarios S1 and S2 in the normal year.

4 CONCLUSIONS

The following conclusions are drawn from this study:(1) there are clear tradeoffs between hydropower generation and water consumption and (2) scheme 2 is the optimal scheme from the water-energy nexus for both two scenarios in a normal year.

ACKNOWLEDGEMENTS

This study was supported by the National Key R & D Program of China (2017YFC0404605).

REFERENCES

Dai, J., S. Wu, G. Han, J. Weinberg, X. Xie, X. Wu, X. Song, B. Jia, W. Xue & Q. Yang (2018) Water-energy nexus: A review of methods and tools for macro-assessment. *Applied Energy*, 210**,** 393-408.

Deb, K., A. Pratap, S. Agarwal & T. Meyarivan (2002) A fast and elitist multiobjective genetic algorithm: NSGA-II. *IEEE Transactions on Evolutionary Computation*, 6**,** 182-197.

Hoekstra, A. H., P.Q. (2003) Virtual water trade: A quantification of virtual water flows between nations in relation to international crop trade. *Water Science and Technology*, 49**,** 203-209.

Mekonnen, M. M. & A. Y. Hoekstra (2012) The blue water footprint of electricity from hydropower. *Hydrology and Earth System Sciences*, 16**,** 179-187.

Zhang, X., H.-Y. Li, Z. D. Deng, C. Ringler, Y. Gao, M. I. Hejazi & L. R. Leung (2018) Impacts of climate change, policy and Water-Energy-Food nexus on hydropower development. *Renewable Energy*, 116**,** 827-834.

Proceedings of the 1st IAHR
Young Professionals Congress
17-18 November 2020

WATER BUDGET USING REGIONAL HYDROLOGICAL MODELLING AND GIS TECHNIQUES IN PERUVIAN AMAZON: CASE STUDY IN YURACYACU WATERSHED-MAYO RIVER

Walter Gómez Lora [1], Victor Gallo Ramos [2] & Katherine Camacho Zorogastúa [3]

[1,2,3] Instituto Especializado de Investigación y Gestión del Agua, Lima, Perú
[1,2,3] Facultad de Ingeniería Geográfica, Ambiental y Ecoturismo, Universidad Nacional Federico Villarreal, Lima, Perú
jgomez@unfv.edu.pe, 2012000392@unfv.edu.pe; 2016313001@unfv.edu.pe

ABSTRACT

In a context of paucity hydrometeorological data in the Peruvian Amazon as one of the main problems for Peru, added that this doesn't allow to know the water yield of it's basins. We propose a regional hydrological modelling approach to estimate the water availability over to 1989-2015 period applied in the Yuracyacu watershed, tributary of the Mayo river. This allowed relating physical catchment characteristics with hydrometeorological variables, thus offering a regional perspective for ungauged areas (e.g. others catchment of the Altomayo region).Differential Tests are used to assess the regional hydrological modelling robustness, showing a satisfactory flow simulate defined for Nash–Sutcliffe, Kling-Gupta efficiency and bias criteria.

Keywords: Regional hydrological modelling, Water budget, Water availability, Watershed.

1 INTRODUCTION

The water resource in the Peruvian Amazon basin has unique characteristics which give rise to the existence of regions that lack water for much of the year and others with overabundance in a short time, which can be explained by the topographical configuration and climatic variation of Peru.

(Emanuel & Escurra, 2000)mentioned that the Amazon River basin has almost 99% of the total water resources existing in the Peruvian territory and a study carried out by (UNESCO, 2006) considers that the net annual availability of water is 2696 mm.

However, there is limited information on hydrology in the Amazon of Peru. In this sense, (Lavado Casimiro, Labat , Loup Guyot, Ardoin-Bardin, & Ordoñez Galvez, 2011) told that there is paucity availability of rainfall information in the Amazon basin. This makes it difficult to determinate the water Budget and availability for different uses.

Therefore, (Olden, J.D., Kennard, M.J. , & Pusey, B.J, 2012) affirm that in regions where the information is limited, regionalization techniques and hydrological models are used to estimate the water balance, with many approaches that will depend on the availability of dataset and the purpose of the study to be executed.

Against this background, this study aims to (a) determinate the physical characteristics of the Yuracyacu watershed using G.I.S. and remote sensing techniques and (b) quantify the main hydrometeorological variables involved in the water balance to obtain annual, monthly and different frequency flows for water use purposes.

2 MATERIALS AND METHODS

2.1 Hydrometeorological dataset

The database includes monthly precipitation and temperature for the 1980-2019 period from 12 stations (see Figure 1) managed by the National Meteorological and Hydrological Service of Peru (SENAMHI). Available data for streamflow observations were 2001-2010 period (Yuracyacu gauging station). The precipitation and temperature series followed the usual homogenization and validation procedures.

2.2 Cartographic and Satellite data

Were used two maps (12-i and 13-i) managed by National Geography Institute (I.G.N.), digital elevations models of ALOS satellite and a Sentinel satellite image of 03/07/2019.

2.3 Method

Were established mathematical-deterministic models through simple and multiple regressions. The data was interpolate by Ordinary Krigging in 12.5 m x 12.5 m pixels considering altitudinals gradients. Potential evapotranspiration was calculate according to (Thornthwaite & Matter, 1967), (Turc, 1961)and runoff deficit regression functions. Finally, the streamflow were calculate using monthly water balance and the KGE (Gupta, Kling, Yilmaz, & Martinez, 2009), Nash Sutcliffe (NSE) (Nash & Sutcliffe, 1970), Pearson Correlation Coefficient and BIAS percentage (PBIAS) metrics were evaluated between the observed and simulated series.

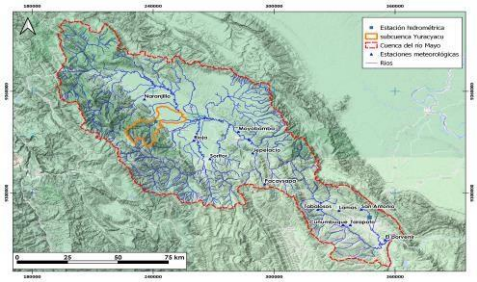

Figure 1 Spatial distributions of hydrometeorological stations – Mayo river basin

3 RESULTS

Regional hydrological modelling allowed equations to be defined to determinate annual and monthly values of the main hydrometeorological variables: $P = 252.39\ (H)^{-0.2579}$, $T = 51.83\ (H)^{-0.117}$, $E = 0.0002\ (H)^{2.0564}$, where P is annual precipitation (mm) T is annual average temperature and E is annual runoff (mm). In addition, monthly models estimated precipitations and runoff values (see Figure 2). Efficiency metrics showed KGE and NSE values equal to 0.9. Also, were found highly significant relationships (R > 0.8) between precipitation and runoff. Finally, the annual duration curve was generated (see Figure 3) in order to flow at different persistence for water availability purposes.

4 CONCLUSIONS

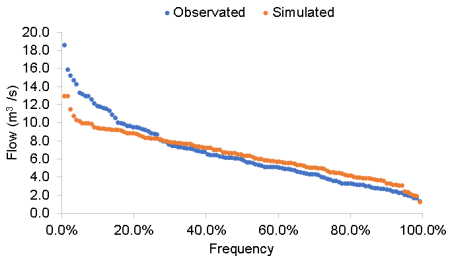

Figure 2 frequency curve

Regional models can quantify mean values of hydrometeorological variables involved in the water balance with an error of 3%, which is acceptable in regional studies and can be used in hydrological similar regions.
Of the results it was observed that 50% of the precipitated volume is generate in the altitudinal range of 1600 to 2100 m asl. On the other side, our results show high robustness in regional hydrological modelling to produce streamflow, in terms of KGE and NSE acceptable.

5 REFERENCES

Emanuel, C., & Escurra, J. (2000). *Informe nacional sobre la gestión del agua en el Perú.* Lima: Comité asesor técnico de America del sur - SAMTAC- Global Water Pathership (GWP).

Gupta, H. V., Kling, H., Yilmaz, K. K., & Martinez, G. F. (2009). Descomposition of the mean squared error and NSE performance criteria: Implications forr improving hydrological modelling. *Journal of Hydrology*, 80-91.

Lavado Casimiro, W., Labat , D., Loup Guyot, J., Ardoin-Bardin, S., & Ordoñez Galvez, J. (2011). Modelos de balance hídrico mensual en la cuenca hidrográfica del Amazonas en Perú: cuenca del río Ucayali. *Revista peruana Geo-atmosférica RPGA*, 84-92.

Nash, J. E., & Sutcliffe, J. V. (1970). River flow forecasting through conceptual models part I — A discussion of principles. *Journal of Hydrology*, 282-290.

Olden, J.D., Kennard, M.J. , & Pusey, B.J. (2012). A framework for hydrologic classification with a review. *Ecohydrology*, 503–518.

Thornthwaite, C., & Matter, J. (1967). The water balance. *Climatology*, 5-15.

Turc, L. (1961). Estimation of irrigation water requirements, potencial evapotranspiration: asimple climate formula wnvolved up to date. *Annals of Agronomy*, 13-49.

UNESCO. (2006). *Balance hídrico del Perú a nivel multianual.* Programa Hidrológico Nacional.

IAHR AIRH

International Association for Hydro-Environment Engineering and Research

Hosted by
Spain Water and IWHR, China

Session 6

Coastal Engineering and Groundwater Hydraulics

IAHR YPN

Hosted by
Spain Water and IWHR, China

Proceedings of the 1st IAHR
Young Professionals Congress
17-18 November 2020

NUMERICAL SIMULATION OF DISSOLVED OXYGEN IN COASTAL LAGOONS CASE STUDY: EL GOUNA, EGYPT

Omnia Abouelsaad [1,2], Kerlos Abdallah [1], Elena Matta[3], Gwendolin Porst [1], Mohie Omar [4], Reinhard Hinkelmann [1]

[1] Technische Universität Berlin, Chair of Water Resource Management and Modeling of Hydrosystems, Germany
e-mail: o.abouelsaad@campus.tu-berlin.de

[2] Mansoura University, Egypt

[3] *Post-doc Research Fellow*, Politecnico di Milano - Department of Electronics, Information, and Bioengineering

[4] National Water Research Center, Egypt

ABSTRACT

Preservation of water quality in coastal areas has become an urgent challenge especially upon considering the increasing anthropogenic impacts, the expansion of urban areas and the predicted climate change in the upcoming decades. Dissolved oxygen (DO) may be considered the most important parameter to study the quality of water, in which the preservation of a reasonable rate of DO is essential for a healthy aquatic life. Herein, the water quality considering dissolved oxygen in coastal lagoons located in El Gouna, Egypt, is investigated using the TELEMAC-2D WAQTEL module. The simulation focused on the effects of the increasing water temperature on the quantity of DO, as lower levels of DO are expected in case of high temperatures. Studying the DO values and the sensitivity analysis of the affecting parameters helps to prevent and control anoxic problems in shallow areas, which occur if the DO concentration is less than 0.5 mg/l.

Keywords: TELEMAC-2D, water quality, dissolved oxygen, coastal lagoons, WAQTEL.

1 INTRODUCTION

Dissolved oxygen (DO) is considered a crucial indicator of water quality, being an essential element of aquatic systems and is involved in all metabolic processes (Gattuso et al., 2006). It enters the water through the air or is produced as a byproduct of photosynthetic processes from phytoplankton, algae, seaweed and other aquatic plants (Watt, 2000). On the other hand, DO is consumed by respiration by aquatic animals or the decomposition process of the organic and ammoniacal load from wastewater. In the touristic city El Gouna located in the southeast of Egypt, there are interconnected lagoons with contact to the Red Sea. These lagoons are getting affected by pollution of wastewater disposal from hotels, boat leakage and the nearby desalination outflow (Al-Jabari, 2018). Moreover, the predicted increase in global temperature may also hinder water quality preservation in such coastal lagoons (Anthony et al., 2009). The domain under study consists of two connected lagoons with a perimeter of approximately 4700 m and an area of 23000 m^2 with shallow water having about 2-3 m water depth. A two-dimensional TELEMAC-2D model coupled with the O2 WAQTEL module was set up to assess the DO concentrations in the lagoons and analyze its sensitivity.

2 MODEL DATA

The lagoons under study exchange their water with the Red Sea through three water inlets as indicated in Figure 1. The bathymetric data come from a previous field survey carried out by Al-Jabari (Al-Jabari, 2018). The lagoons are subjected to a tidal wave, which may be simulated as a sinusoidal wave, wherein every tide wave lasts about 12 hours with 0.6 m amplitude). The mean elevation of 12m was used in the lagoons. Also, a previous study on wind data during the period 2016 – 2018 indicated a mean wind of 5.84 m/s in the direction of 322º (Al-Jabari, 2018). Field data about water quality in the studied lagoons is not available. Consequently, the background value of dissolved oxygen is considered from a previous field study in a section of the Red Sea beside the lagoons (Fahmy et al., 2016). Janet (Smile Consult GmbH; Lippert, 2001) mesh generation's software was used to transform the layout and bathymetric data into a suitable fine mesh. The final triangular

unstructured grid counts in a total of 2693 nodes and 4820 triangular elements. The mentioned chosen mesh resolution obtained the grid convergence and gave no changes when compared to a refined grid.

3 HYDRODYNAMIC AND WATER QUALITY MODEL

First, the hydrodynamics of the lagoons were investigated using the TELEMAC-2D module for calculating the water depth, velocity and tracer variations in the lagoons. The module was then coupled with the O_2 water quality module, which determines the source term in the tracer transport equation (Lang et al., 2014). The lagoons were investigated under the effect of two different water temperatures: 20°C and 30°C. The increase in temperature negatively affected the quantity of dissolved oxygen in the lagoons. Figure 1 shows the DO values in the lagoons after eight days of simulation. As reported in the figure, the DO decreased in the lagoons to reach a value less than 6 mgO_2/l at an area in the north-eastern part due to an increase in water temperature, while in case of lower temperatures, the minimum DO value was above 8 mgO_2/l. The average DO value in the lagoons decreased from 9.87 to 8.43 mgO_2/l in the scenario with higher temperatures. Later, a sensitivity analysis of different oxygen producing and consuming parameters has been conducted; e.g., the lagoons were investigated under different photosynthesis values to observe their effects on the DO concentration. Photosynthesis values of 0.0, 0.3, 1, 9 mgO_2/l were applied neglecting the effect of the organic load and the ammoniacal load. It can be concluded that photosynthesis plays a relevant role in DO production: e.g. considering a high photosynthesis production (P = 9.0 mgO_2/l), the average DO reached a value that is approximately three times the initial value.

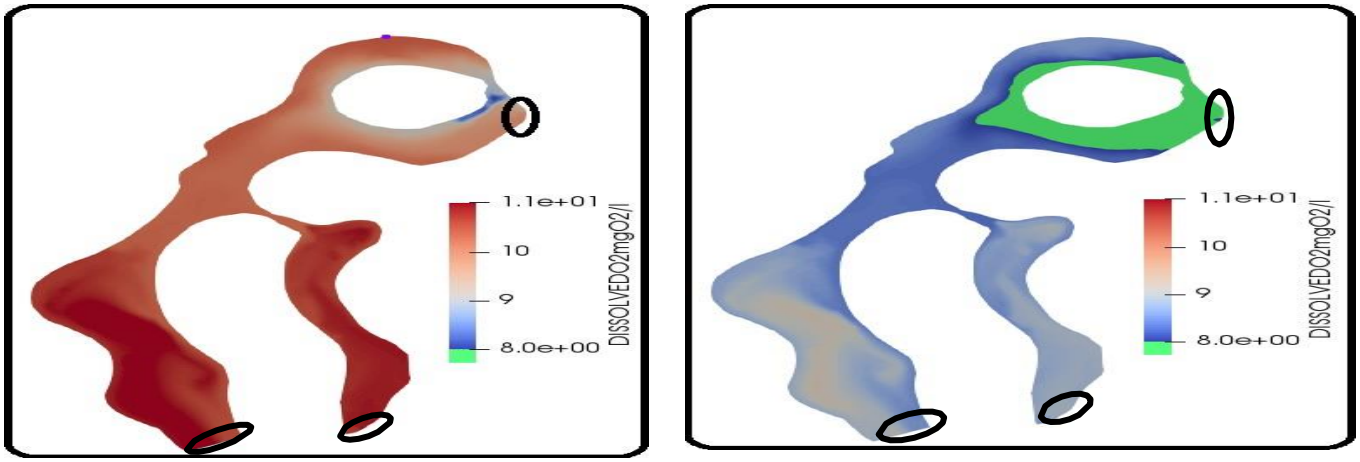

Figure 1. DO concentration in the lagoons after eight days of simulation at 20°C (left) and 30°C (right), respectively.

ACKNOWLEDGEMENTS
We gratefully acknowledge the Egyptian Missions for their regular support and funding.

REFERENCES

Al-Jabari, M. (2018). Numerical simulation of exchange processes between lagoons and the Red Sea in El Gouna, Egypt, Master Thesis in Water Engineering Department, Technische Universität Berlin.

Anthony, A., Joshua, A., Peter, A., Carrie, B., Stanley, C., Cheryl, F., Crystal, F., Arthur, G., Kifle, H., Leanna, H., Kimberly, L., James, J. O., Candace, O., Anna, P., Nicole, R., Leslie, S., Tiffany, S., Judith, S., and Nathan, V. (2009). Coastal lagoons and climate change: ecological and social ramifications in U.S. Atlantic and Gulf Coast ecosystems. Ecology and Society 14(1).

Fahmy, M. A., Laila, M. A. F., Ahmed, M. A., Mohamed, A. A., Ehssan, M. A., Hoda, H. A., Ahmed, H., Ahmed, A., and Mohamed A. S. (2016). Evaluation of the quality for the egyptian Red Sea coastal waters during 2011-2013. Journal of Environmental Protection 07(12):1810–34.

Gattuso, J. P., Gentili, B., Duarte, C. M., Kleypas, J. A., Middelburg, J. J., and Antoine, D. (2006). Light availability in the coastal ocean: impact on the distribution of benthic photosynthetic organisms and contribution to primary production. Biogeosciences 3(4):489–513.

Lang, P., Jonathan, D., ATA, R., Goeury, C. and Hervouet J. M. (2014). TELEMAC-2D software. 7(December):134.

Lippert, C. (2001). Preprocessor Janet, user guide. Smile Consult GmbH, Hanover.

Watt, M. K. (2000). A hydrologic primer for New Jersey watershed management (No. 4140). US Department of the Interior, US Geological Survey.

Proceedings of the 1st IAHR
Young Professionals Congress
17-18 November 2020

DEVELOPING AN EFFICIENT MODELLING FRAMEWORK TO EVALUATE NATURE-BASED SOLUTIONS TO COUNTERACT ESTUARINE SALT INTRUSION

Rutger Siemes [1], Trang Minh Duong [1], Bas Borsje [1] & Suzanne Hulscher [1]

[1] University of Twente, Enschede, Netherlands,
e-mail: r.w.a.siemes@utwente.nl

ABSTRACT

Estuaries connect our rivers and oceans, and support densely populated regions worldwide. These estuaries are increasingly threatened by salt intrusion due to climate change and side effects of human interventions, limiting freshwater availability. Nature-based solutions (NBSs), e.g. sand waves or wetlands, show potential to increase mixing of fresh- and salt water and have shown to be adaptable to a changing climate. Hence, they may provide a resilient way to reduce salt intrusion, while also supporting important ecosystem services. An efficient modelling framework will be developed, that is able to evaluate NBSs to counteract salt intrusion, estuarine wide, including CC. It will be applied to establish a knowledge base around the interactions between estuarine ecomorphology, related to NBSs, and salt intrusion. This way, the proposed research will improve understanding and provide modelling tools on the interaction between NBSs and estuarine wide salt intrusion.

Keywords: estuaries, salt intrusion, ecomorphology, nature-based solutions, numerical model

1 INTRODUCTION

In many and often densely populated regions worldwide, rivers meet with seas. Within these water systems, called estuaries, salt water can intrude far inland during extreme events, such as storm surges and river droughts. During recent periods of drought in the Netherlands (2003, 2011, 2018 & 2019), the intrusion of salt water severely limited freshwater availability, threatening the supply of fresh water for agricultural and industrial use. Moreover, estuarine regions are increasingly threatened by salt intrusion due to climate change (CC) and side effects of human interventions, further threatening freshwater supply in the future.

Due to the difference in density between fresh- and salt water, salt water intrudes inland as a plume over the estuarine bed. Nature-based measures, like artificial sand waves, wetlands or oyster beds, are proposed to reduce this salt intrusion. These measures impose a roughness on the flow of water, due to which they increase the mixing of the stratified fresh- and salt water flows. In addition, these ecosystems have dynamics on their own due to which they can adapt to a changing climate. Consequently, they may provide a resilient way to reduce salt intrusion. However, the various interactions between NBSs and salt intrusion are not yet understood.

Moreover, a modelling framework that is able to evaluate NBSs to counteract salt intrusion, under long-term development, is missing. This framework needs to include processes acting on vast spatial and temporal scales, resulting in substantial computational efforts. Surrogate approaches are available to improve modelling efficiency, e.g. Artificial Neural Networks (Bomers et al., 2019) and multi-fidelity approaches (Berends et al., 2018), but these methods are often novel and not yet applied to study long-term estuarine ecomorphodynamics.

The objective of this research is to develop a computationally efficient modelling framework to evaluate the impacts of NBSs on estuarine salt intrusion under ecomorphological development, on an estuary wide scale, for the present till the next century, taking into account CC,.

2 METHOD

To accomplish the set objective, a modelling framework will be created (within the process-based, numerical modelling software Delft3D-FM) in which the impact of estuarine ecomorphological development, related to NBSs, on salt intrusion can be assessed efficiently. However, when assessing the impact of long-term estuarine development on salt intrusion, various relevant timescales are identified (Figure 1).

To improve efficiency within the framework, the various timescales are separated when modelling. Firstly, an idealized ecomorphological model will be developed to study the impact of NBSs on estuarine development, on an engineering timescale (1 to 10 years). Herein, scenarios will be implemented within the estuary, representing NBSs. E.g., at the estuarine bed, scenarios ranging from flatbed to sand waves of equilibrium height or, at the estuarine sides, wetlands with various sizes and vegetation characteristics are implemented. Subsequently, an idealized salt intrusion model will be developed. Within this model, salt intrusion is studied for extreme scenarios (up to several days), before and after the previously simulated ecomorphological development. Hence, the impact of NBSs on salt intrusion, under estuarine development, can be assessed. For these models, surrogate approaches will be tested and applied to reduce computational efforts, e.g. ANNs or multi-fidelity approaches.

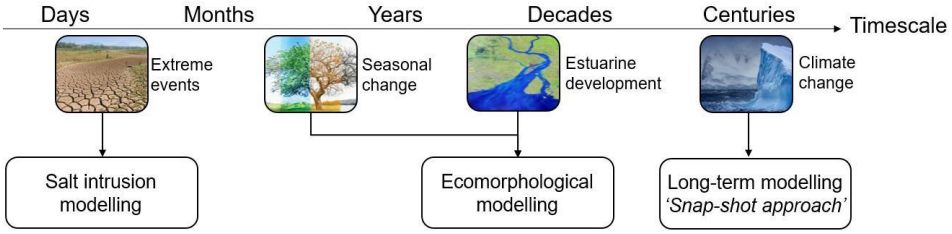

Figure 1. Temporal processes relevant to the study, and the modelling tools applied for these processes.

Next, salt intrusion due to NBSs will be assessed within a real study area of the Rhine-Meuse Delta (RMD), under CC till 2100. However, to study the long-term development due to CC (decadal+ timescale), regular, process-based modelling will lead to infeasible computational efforts. Therefore, the snap-shot approach will be applied, as proposed by (Duong et al., 2016). In addition, surrogate approaches which are successfully applied previously within the idealized models, will be applied within this framework. The complete modelling framework for a real case study, including all temporal scales (Figure 1), will be as follows:

1. Construct and validate a salt intrusion- and ecomorphological model for present day conditions.
2. Perform salt intrusion modelling of extreme events (several days) for present day conditions.
3. Apply the snap-shot approach to create future scenarios at the desired year (e.g. 2050, 2100) from the present day conditions, following (Duong et al., 2018). This is performed for the ecomorphological model and the salt intrusion model.
4. Perform ecomorphological modelling (1 year) of the future scenario created in the previous step.
5. Perform salt intrusion modelling of extreme events (several days) after the simulated future ecomorphological development (step 4). Comparison of these results with those of step 1 will show the impact of long-term estuarine development on salt intrusion.

This framework will be applied to study the impact of CC and its uncertainty within the RMD, by applying different CC scenarios. Also, scenarios representing NBSs are implemented within the framework, similarly as within the idealized models, as mentioned earlier. These NBSs will be implemented in both present and future simulations.

3 EXPECTED RESULTS

By reaching the research objective, an efficient modelling framework is constructed and will successfully be applied to predict the impact of a wide range of predetermined NBSs on estuarine development and salt intrusion within the RMD, under CC up to the next century. Insights will be gained on estuarine wide development due to various NBSs, and understanding on how this development affects salt intrusion will be improved. In addition, various novel surrogate approaches will be tested and successfully applied within the modelling framework to reduce computational restraints.

REFERENCES

Berends, K., Warmink, J., & Hulscher, S. (2018). Efficient uncertainty quantification for impact analysis of human interventions in rivers. *Environmental modelling & software, 107*, 50-58.

Bomers, A., van der Meulen, B., Schielen, R., & Hulscher, S. (2019). Historic flood reconstruction with the use of an Artificial Neural Network. *Water Resources Research, 55*(11), 9673-9688.

Duong, T. M., Ranasinghe, R., Thatcher, M., Mahanama, S., Wang, Z. B., Dissanayake, P. K., . . . Roelvink, D. (2018). Assessing climate change impacts on the stability of small tidal inlets: Part 2-Data rich environments. *Marine Geology, 395*, 65-81.

Duong, T. M., Ranasinghe, R., Walstra, D., & Roelvink, D. (2016). Assessing climate change impacts on the stability of small tidal inlet systems: Why and how? *Earth-science reviews, 154*, 369-380.

Proceedings of the 1st IAHR
Young Professionals Congress
17-18 November 2020

Coastal area classification using total suspended matter concentration

Hyoseob Noh[1], Yong Sung Park[*1,2], Minjae Lee[1]

[1]Department of Civil and Environmental Engineering, Seoul National University, 1 Gwanak-ro, Gwanak-gu, Seoul 151-744, Korea
[2]Integrated Research Institute of Construction and Environment, Seoul National University, Seoul 151-742, Korea

*Correspondance : dryspark@snu.ac.kr

ABSTRACT

Localities of various ocean physical features cause regional differences in sediment transport mechanisms. Hence, the regional analysis of the total suspended matter (TSM) in coastal zones helps to manage coastal areas. This work presents a new classification basis of the total suspended matter (TSM) sampling stations in coastal areas in South Korea using a newly introduced robust clustering protocol, iterative toroidal SOM-k-means, which reduced uncertainties in clustering analysis. Two location variables (longitude, latitude) and four concentrations (surface TSM in February and August, bottom TSM in February and August) in the 425 TSM sampling stations have been divided into six groups using iterative toroidal SOM-k-means. The systematic analysis showed that the surface sediment distribution, ocean currents, and tidal currents match with the clustering results.

Keywords: total suspended matter, clustering, toroidal self-organizing map, k-means, coastal area

1 INTRODUCTION

In coastal management, total suspended matter (TSM) is a great concern. However, understanding the governing factors of TSM variation is not easy since energy forcings affecting coastal sediment transport spatially and seasonally vary. The locality of TSM has been provoking the needs of regional analysis of TSM transport mechanisms in coastal development or ocean remote sensing.

A regional analysis of TSM can be conducted by applying unsupervised machine learning algorithms. Self-organizing map (SOM) Kohonen (1990) is one of the widely used methods for cluster analysis (Riveros *et al.*, 2019). Generally, the SOM network lattice has a lot of nodes. Thus, the two-staged approach, which performs k-means clustering into the network, can be applied in order to determine a reasonable number of clusters.

This study's main objective is to classify the TSM sampling stations based on the physical analysis of data clustering. The clustering was conducted using a newly proposed 2-staged SOM-k-means algorithm. Accordingly, we investigated the relationships between resulting clusters and three physical features: sediment distribution, ocean currents, tidal currents.

2 ITERATIVE TOROIDAL SOM-K-MEANS

We suggest a two-staged clustering protocol, the iterative toroidal SOM-k-means, which systematically determines the number of clusters and overcomes the local minima problem. At the first stage, the toroidal SOM trains the network without the edge effect (Mount et Weaver, 2011), and k-means separate the network. The sub-clustering procedure and the SOM network are repeated in user-specified iteration times. The algorithm repeats varying the cluster number from 2 to user-defined maximum cluster number to find optimal cluster number. The algorithm finds the best clustering result by finding the result with the smallest Davies-Bouldingindex (DBI) (Davies et Bouldin, 1979) among the iterations.

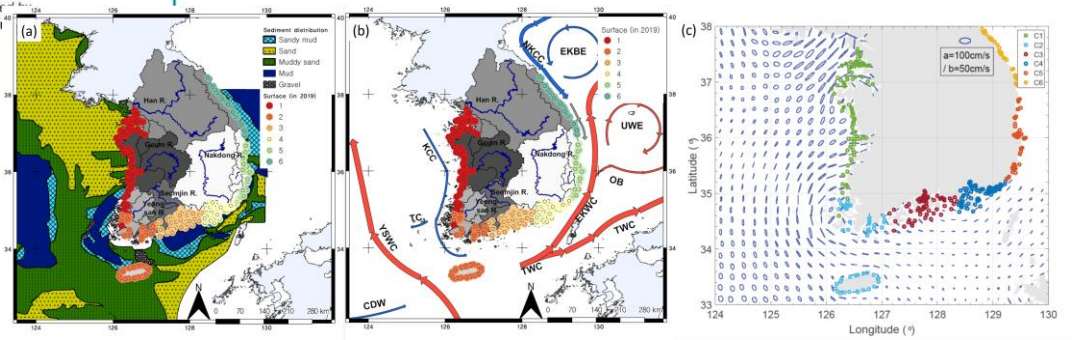

Figure 1: Physical features with clustering result; (a) sediment distribution map; (b) ocean currents map; (c) M_2 tidal current map.

3 RESULT

The cluster analysis was conducted using the iterative toroidal SOM-k-means algorithm described in the above section. The six variables longitude, latitude, TSM concentrations in August and February sampled at the surface and bottom layers, respectively, in 425 TSM sampling stations in South Korean coastal areas were used in cluster analysis. The smallest DBI was observed where the cluster number is 6.

Figure 1 presents the clustering results over the sediment distribution, ocean currents, M_2 tidal current maps. The boundary of Clusters 1 and 2 is in the middle of the Heuksan mud belt, but where the transversal current (TC) bifurcates in winter. The central south sea mud is distributed over Cluster 3. The Nakdong River disperse the sediment through the east Korean warm current and offshore branch to Cluster 4, and Nakdong River originated sediment reaches to Cluster 5 with seasonal variation. In between Clusters 5 and 6, summertime upwelling resulting in high surface TSM concentration occurs. The computed M_2 tidal ellipses from simulation result of (Nguyen et Lee, 2020) in Figure 1 (c) shows the distinguishing trend at Cluster 2.

4 CONCLUSION

The TSM sampling stations in South Korea were regionally divided in this study. In order to cluster the stations, the two-level clustering approach, iterative toroidal SOM-k-means, was proposed and applied. The resulted regions, clusters, were analyzed with the sediment distribution, ocean currents, and tidal currents. The demarcations of clusters are expected to be used as reference lines of downscaled sediment transport assessment.

5 ACKNOWLEDGEMENTS

This research work was conducted at the Institute of Engineering Research at in Seoul National University, Seoul, Korea. This research was partially supported by the BK21 PLUS research program of the National Research Foundation of Korea, and Korea Environment Industry & Technology Institute(KEITI) through Service Program for Demand-Responsive Water Supply, funded by Korea Ministry of Environment(MOE).(2020002650001)

References

Davies D. L., Bouldin D. W. (1979). A cluster separation measure. *IEEE transactions on pattern analysis and machine intelligence PAMI-1*(2), 224–227.

Kohonen T. (1990). The self-organizing map. *Proceedings of the IEEE 78*(9), 1464–1480.

Mount N. J., Weaver D. (2011). Self-organizing maps and boundary effects: quantifying the benefits of torus wrapping for mapping som trajectories. *Pattern Analysis and Applications 14*(2), 139–148.

Nguyen V. T., Lee M. (2020, June). Effect of Open Boundary Conditions and Bottom Roughness on Tidal Modeling around the West Coast of Korea. *Water 12*(6), 1706. URL: https://www.mdpi.com/2073-4441/12/6/1706, doi:10.3390/w12061706.

Riveros N. A. M., Espitia B. A. C., Pico L. E. A. (2019). Comparison between k-means and self-organizing maps algorithms used for diagnosis spinal column patients. *Informatics in Medicine Unlocked 16*, 100206.

Proceedings of the 1st IAHR
Young Professionals Congress
17-18 November 2020

INITIAL FINDINGS OF MICROPLASTICS CONCENTRATION IN THREE COASTAL ENVIRONMENTS: A CASE STUDY IN THE PERUVIAN COAST

Camila Timana [1], Andrea Tipe [1], Pedro Cahuana [1], Mauricio Rivas [1], Ryuji Segami [1], Tania Meza [1] & Daniel Horna [1,2]

[1]Universidad de Ingeniería y Tecnología - UTEC, Lima, Perú
[2] Centro de Investigación y Tecnología del Agua - CITA, Universidad de Ingeniería y Tecnología - UTEC, Lima, Perú

ABSTRACT

This paper presents the results of a comparative field study to determine the concentration of microplastics in three coastal environments in the coast of Peru. Samples were taken in both sand and sea water using a sieve and a neuston net, respectively. Three study sites were selected in the coast of Lima, Peru: Naplo (South of Lima), Los Yuyos (in Lima) and Chancay (North of Lima). It was found that Naplo beach presented the highest number of micropollutants, most of them were pellets with size ranges of 1-4mm and 0.5-4mm on the sea and seashore respectively, whereas Yuyos presented the lowest number of microplastics in both sand and sea. Few studies have been made to gather data regarding the Peruvian coast making these results difficult to extrapolate for a more general understanding of microplastics pollution in the Peruvian coast. Thus, further investigation on the matter must be performed to create a useful database.

Keywords: microplastic, seashore, micropollutants, marine debris.

1 INTRODUCTION

Microplastics refers to any plastic fragment which has 0.1µm to 5mm in length (NOAA, 2016). These might appear to be insignificant due to its size; however, as a result, the marine debris can be found not only within the stomachs of diverse marine life, but also floating at surface level water (Jovanović, 2017). Consequently, this can cause damage to the local ecosystem along with cross-contamination with human beings (Wieczorek et al., 2018) due to the ingestion of these plastics through fish consumption as additives might move up the food chain (Jovanović, 2017).

The main source of this pollution appears to be the gear used in economic activities within the affected area like fishing nets; as well as, products used daily, such as clothes, degraded plastic items, cosmetics, and others. (Coppock et al., 2017). Regarding microplastics pollution in the Peruvian coast, only one paper was found in the literature (Purca and Henostroza, 2017). The objective of this study is to assess the concentration of microplastic in three coastal environments in Lima, Peru that have not been studied previously.

2 METHODOLOGY

2.1 Field measurement (in-situ)

Three beaches were studied along the Peruvian coast in Lima's region: Naplo beach (South of Lima), Los Yuyos beach (near Lima), and Chancay beach (North of Lima) (Table 1). Sand and water samples were collected from April to June 2019. Each beach was divided in quadrants for sand samples, a 0.5 by 0.5m frame was used to delimit the quadrants (Purca and Henostroza, 2017). For seawater samples, equidistant points were distributed in the area, no further than two kilometers from the seashore. A neuston net of 300 microns of opening size was deployed and joined to a sample flask in which the seawater was accumulated (Kovač Viršek et al., 2016). Approximately 35 samples were collected at sand and 10 samples at seawater.

2.2 Data processing

After filtering, data processing was done using a microscope for sea water samples, and a portable method to separate microplastics from sediments with the sand samples (Coppock et al., 2017).

3 RESULTS

The results table (Table 2) shows a higher amount of microplastics in the Naplo sea when compared to the other two. A likely explanation can be the influence of anthropogenic and industrial activities as main sources of microplastics, which are then carried by small-scale ocean currents to the Naplo bay. As a result, these suspended micropollutants enter a recirculating region, caused by a blockage of ocean currents due to a land and rock formation, and they can be adhered to the Naplo seashore sediments due to high tides. These natural phenomena, in conjunction with the plastic bottling factory in the area may explain the reason why it is the most polluted one. As the second most polluted, the Chancay sea area may also be influenced by the large anthropogenic and fishing industry presence. This might be compounded by the presence of smallish-scale ocean currents, similar to those in Naplo but to a lesser degree. The seashore, on the other hand, seems to be contaminated mainly due to a lack of proper waste disposal practices around the food stalls. Regarding Los Yuyos beach, it is located far enough from the closest rivers, so a lower microplastic abundance was expected.

Table 1. Geospatial features for each beach evaluated

Beach	Latitude (°)	Longitude (°)	Total length (m)	Width (m)	Nearest dock (m)
Naplo	-12.479440	-76.793597	500	40	450
Los Yuyos	-12.153290	-77.024977	250	55	1350
Chancay	-11.584491	-77.272268	1157∗	185	0

∗ 200 m were used for the study area

Table 2. Features of sampled microplastics for each beach location

Beach	Features	Location	
		Sand	Seawater
Naplo	No. microplastics	103	703
	Shape	fragment, fiber	fragment, fiber, pellet
	Size	<0.5 - 4 mm	<1 - 5 mm
Los Yuyos	No. microplastics	23	96
	Shape	Not determined	fragment, fiber
	Size	Not quantified	<1 - 8 mm
Chancay	No. microplastics	85	361
	Shape	fragment, fiber	fragment
	Size	0.5 - 5 mm	0.5 - 5 mm

4 CONCLUSIONS

Three beaches in the coast of Lima, Peru were studied to assess the concentration of microplastics in their environment, concluding that the highest concentration was found south of Lima (Naplo), whereas the lowest concentration was found near Lima (Los Yuyos). The data was obtained at one field campaign, thus further campaigns are needed to complement the results from this study. Moreover, results can be further complemented with numerical model results. This is necessary to enable more accurate predictions of the spread of these micropollutants throughout seashores and the sea itself. Likewise, the type of polymer should be analyzed in order to enhance the understanding of the possible sources of these pollutants as well as their relative danger to the marine ecosystem, even more so, given the ever increasing warnings of a possible systems collapse that relates to SDG 14 “Life Below Water”.

REFERENCES

Coppock, R. L., Cole, M., Lindeque, P. K., Queirós, A. M., & Galloway, T. S. (2017). A small-scale, portable method for extracting microplastics from marine sediments. *Environmental Pollution*, *230*, 829-837.

Jovanović, B. (2017). Ingestion of microplastics by fish and its potential consequences from a physical perspective. *Integrated Environmental Assessment and Management*, *13*(3), 510-515.

Kovač Viršek, M., Palatinus, A., Koren, Š., Peterlin, M., Horvat, P., & Kržan, A. (2016). Protocol for Microplastics Sampling on the Sea Surface and Sample Analysis. *Journal of Visualized Experiments: JoVE*, *118*.

National Oceanic and Atmospheric Administration - U.S. Department of Commerce (2016) What are microplastics? National Oceanic and Atmospheric Administration “Facts”.

Purca, S., & Henostroza, A. (2017). Presencia de microplásticos en cuatro playas arenosas de Perú. *Revista peruana de Biología*, *24*(1), 101–106.

Wieczorek, A., Morrison, L., Croot, P., Allcock, L., MacLoughlin, E., Savard, O., Brownlow, H. & Doyle, T. (2018). Frequency of Microplastics in Mesopelagic Fishes from the Northwest Atlantic.

Proceedings of the 1st IAHR
Young Professionals Congress
17-18 November 2020

DILUTION OF PLUNGING JETS USED FOR DESALINATION BRINE DISPOSAL

Ishita Shrivastava [1,2], Aaron C. Chow [3], E. Eric Adams [1], Bader Al-Anzi [1,4] & Jongyoon Han [1]

[1] Massachusetts Institute of Technology, Cambridge, USA.
[2] ishita@mit.edu
[3] New York University, Abu Dhabi, UAE.
[4] Kuwait University, Kuwait.

ABSTRACT

We explore plunging liquid jets for disposal of reject brine from desalination plants. Compared to offshore submerged outfalls that rely on momentum to induce mixing, plunging jets released above the surface utilize both momentum and negative buoyancy. Also, plunging jets introduce air into the water column which, when dissolved, can reduce the possibility of hypoxic or anoxic zones. We measured dilution in lab experiments of both unconfined and confined plunging jets. Generally, the dilution of an unconfined jet exceeds that of a confined jet under similar conditions. For confined jets, the effects of the diameter and depth of the confining tube were also explored and dilution with narrow confining tubes with small depth was found to be comparable to that of an unconfined jet.

Keywords: plunging jet, desalination, brine, aeration, multiphase flow.

1 INTRODUCTION

Seawater desalination is a major source of freshwater for many parts of the world. A by-product of desalination is reject brine, which is typically discharged back to the sea. Reject brine can have twice the salinity of seawater and, unless highly diluted, can significantly impact the marine environment. Best dilution results when brine is discharged using high momentum submerged outfalls (Shrivastava and Adams, 2019) resulting in rapid mixing of brine with ambient water. However, negatively buoyant diluted brine tends to spread on the seafloor leading to density stratification, which inhibits vertical mixing and can lead to depleted near bottom dissolved oxygen (DO) (Hodges et al., 2011).

We evaluate plunging liquid jet reactors (PLJRs) as potential outfalls to both dilute reject brine and minimize pockets of low DO. Such reactors involve vertically downward discharge of brine from a jet located above the receiving water surface. As the jet falls through the headspace, it entrains air, which is injected to the water column. The downward momentum and negative buoyancy of the jet provide mixing with the receiving water and the entrained air promotes reaeration.

A variant of the PLJR is the confined plunging liquid jet reactor (CPLJR; Figure 1). CPLJRs can provide better mass transfer than PLJRs by confining the bubbly jet region and increasing jet penetration depth thus increasing contact time between the gas and the liquid phase (Al-Anzi et al., 2006; Cumming et al., 2002). Measurements of dilution for unconfined and confined plunging jets are presented, focusing on the effects of jet length (L_j), diameter (D_c) and depth of submergence below receiving water surface (H_c) of the confining tube.

2 EXPERIMENTAL SETUP, RESULTS AND DISCUSSION

A 4.8 m long x 1.2 m wide tank filled with fresh water to a depth of 50 cm acted as the receiving water. Brine with salinity of 10 psu was directed vertically downward to the tank through a 30 cm long x 1 cm diameter nozzle. Brine flow rate was 160 cm^3/s and jet length varied between 0 and 60 cm. For confined jets, clear acrylic pipes were used as the confining tube. Fluorescent dye (Rhodamine 6G) was added to the brine and a fluorometer (Turner Designs Cyclops 7) placed at the tank bottom (depth of 50 cm) at radial distance (R) of 50 cm from the nozzle measured dilution.

For the four jet lengths tested, the lowest and highest measured dilutions were for L_j/d_0 = 15 and 60, respectively (Figure 2(a)). Larger L_j implies higher downward momentum; thus increased dilution with L_j is expected.

However, the observed trend can be explained by considering the loss in jet momentum as it impacts the water surface. For $L_j/d_0 = 15$, the momentum loss is more than the momentum increase due to longer jet length.

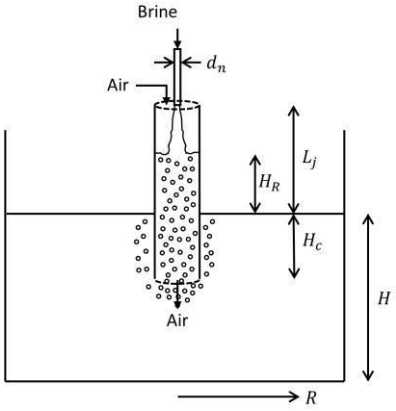

Figure 1. Definition sketch for a confined plunging jet reactor.

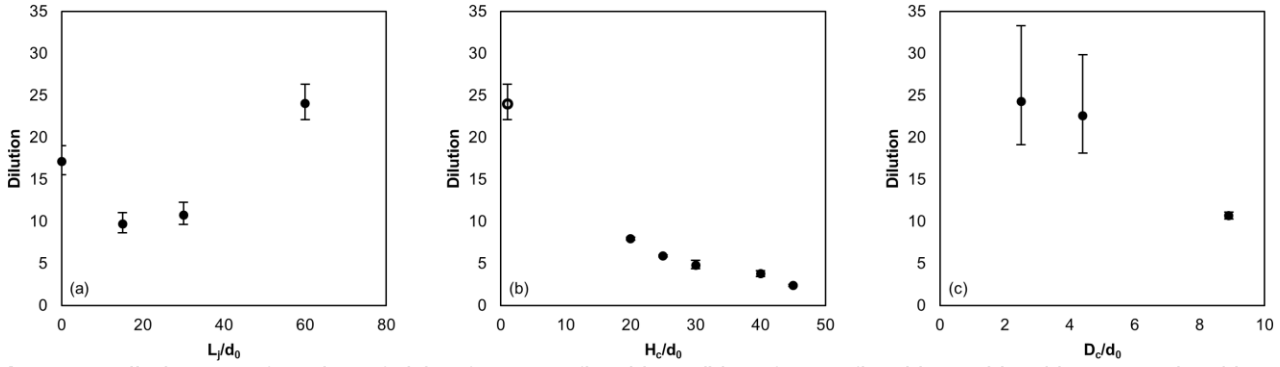

Figure 2. Dilution as a function of: (a) L_j for unconfined jets; (b) H_c for confined jets with $L_j/d_0 = 60$ and $D_c/d_0 = 4.4$; and (c) D_c for confined jets with $L_j/d_0 = 60$ and $H_c/d_0 = 15$. For (b) and (c), unconfined jet dilution = 24±2 (shown in (b) as an open circle at $H_c/d_0 = 0.1$). For $L_j/d_0 = 60$, $H_p/d_o = 20$ cm for an unconfined jet.

A CPLJR designed to increase aeration over that of a PLJR would have a larger depth of submergence than the depth to which bubbles penetrate (H_p) for an unconfined jet. However, the dilution of the confined jet with such a design is less than the dilution of the unconfined jet because the downcomer limits the amount of ambient water available for dilution (Figure 2(b)).

Figure 2(c) shows variation of dilution with downcomer diameter. For the diameters tested, dilution decreases with increasing D_c for constant H_c. This is likely because the jet exiting from the bottom of a narrow downcomer is stronger than that from a wide downcomer. However, confined jets with very wide confining tubes should behave as unconfined jets and get higher dilution than CPLJR with $D_c/d_0 = 9$.

ACKNOWLEDGEMENTS

This work was supported by Kuwait-MIT Center for Natural Resources and the Environment (CNRE), which was funded by Kuwait Foundation for the Advancement of Sciences (KFAS).

REFERENCES

Al-Anzi, B., Cumming, I.W., and Rielly, C.D., 2006. Air entrainment rates in a confined plunging jet reactor. 10th International Conference on Multiphase Flow in Industrial Plants, Italy, 71-82.

Cumming, I.W., Rielly, C.D., and Mason, A.J., 2002. Hydraulic performance of an annular plunging jet reactor. *Chemical Engineering Research and Design*, 80, 543-549.

Hodges, B.R., Furnans, J.E., and Kulis, P.S., 2011. Thin-Layer Gravity Current with Implications for Desalination Brine Disposal. *Hydraulic Engineering*, 137(3), 356-371.

Shrivastava, I., and Adams, E.E., 2019. Effect of shallowness on dilution of unidirectional diffusers. *Hydraulic Engineering*, 145 (12), 06019013.

Proceedings of the 1st IAHR
Young Professionals Congress
17-18 November 2020

SIMULATION OF SEAWATER INTRUSION AREA USING FEEDFORWARD NEURAL NETWORK IN LONGKOU

Daiyuan Li [1,2,3], Yongxiang Wu [1,2,*], Erkun Gao 2, Gaoxu Wang[1,2], Yi Xu [1,2], Huaping Zhong [1,2] & Wei Wu [1,2]

[1] State Key Laboratory of Hydrology-Water Resources and Hydraulic Engineering, Nanjing 210029, China
[2]Hydrology and Water Resources Department, Nanjing Hydraulic Research Institute, Nanjing 210029, China
[3]College of Hydrology and Water Resource, Hohai University, Nanjing 210098, China
[*]Correspondence: yxwu@nhri.cn

ABSTRACT

Reliable simulation of seawater intrusion (SI) is necessary for sustainable groundwater utilization. As a powerful tool, feedforward neural network (FNN) was applied to study seawater intrusion area (SIA) fluctuations in Longkou, China. In the present study, changes of groundwater level (GWL) were modeled by FNN Model 1. Then, FNN Model 2 was developed for fitting the relationship between GWL and SIA. Finally, two models were integrated to simulate SIA changes in response to climatic and artificial factors. The sensitivity analysis of each impact factor was conducted by the "stepwise" method to quantify the relative importance for SIA and GWL. The results from the integrated model indicated that this method could accurately reproduce SIA fluctuations when the Nash–Sutcliffe efficiency coefficient was 0.964, the root mean square error was 1.052 km2, the correlation coefficient was 0.983, and the mean absolute error was 0.782 km2. The results of sensitivity analysis prove that precipitation and groundwater pumping for agriculture mainly affect fluctuations of SIA in the study area. It can be concluded that FNN is effectively used for modeling SI fluctuations together with GWL, which can provide enough support for the sustainable management of groundwater resources with consideration of crucial impact factors of seawater intrusion (SI).

Keywords: seawater intrusion area; simulation; feedforward neural network; sensitivity analysis

1 INTRODUCTION

SI, as well as groundwater level (GWL), is generally affected by natural and anthropogenic factors, such as precipitation, surface water level, groundwater pumping, and artificial recharge. Most of the previous researches focused on chloride concentration changes, which are an important indicator to directly represent SI process. However, the chloride concentrations at some points are not stable and often have the extreme value from monitoring or simulation, which can increase the uncertainty in SI management. To accurately predict SI developing trends, there is a need for monitor station networks with wide distribution and high density. Besides, the chloride concentration monitoring of groundwater is quite expensive. As an alternative, fluctuations of seawater intrusion area (SIA) can be explored to represent SI process in this study, which might provide an easier and more straightforward tool for coastal water management.

During the past several years, numerical models have a good performance in many cases, but these methods require a large amount of data and many parameters describing the groundwater system and physical properties for the governing equation of groundwater flow and solute transport. It is generally known that a groundwater system is a highly complex and nonlinear system. Thus, a great quantity of data can cause tremendous computational burden and an increase in model uncertainty. Hence, the adaptability of numerical models is poor due to the lack of abundant hydrogeological information. Fortunately, the artificial neural network (ANN) is a strong tool for dealing with the complicated and uncertain system, which demands only time series data for input variables without fully understanding physical or hydrogeological properties.

Although ANN has some drawbacks such as overfitting and risk of using unrelated data, the features including simplicity of use and high-speed run with acceptable accuracy have led many researchers to apply it. ANNs can be also developed as surrogate models to approximate complex numerical variable density models. This study

focused on the application of the feedforward neural network (FNN) in SIA simulation, which is a typical and frequently used ANN structure.

2 Method

In this paper, changes of SIA together with GWL were simulated based on FNN, and Figure 1 depicts the model structure, in which n represents the number of input variables. The steps of the model are as follows:

1. The FNN Model 1 is built to simulate GWL changes effected by climatic factors and human activities.

2. The FNN Model 2 is developed to simulate the relationship between GWL of three zones and SIA.

3. FNN Model 1 and FNN Model 2 are integrated, which means that the results of the FNN Model 1 are viewed as the input data of the FNN Model 2. The integrated model can help managers understand SIA changes in response to natural and artificial factors.

4. The sensitivity of each factor is studied by the "stepwise" method, in which input variables are deleted one at a time and the corresponding model is developed and validated. Then, the relative importance ranks are obtained by comparison of model performance criteria, and crucial impact factors are identified for SIA and GWL.

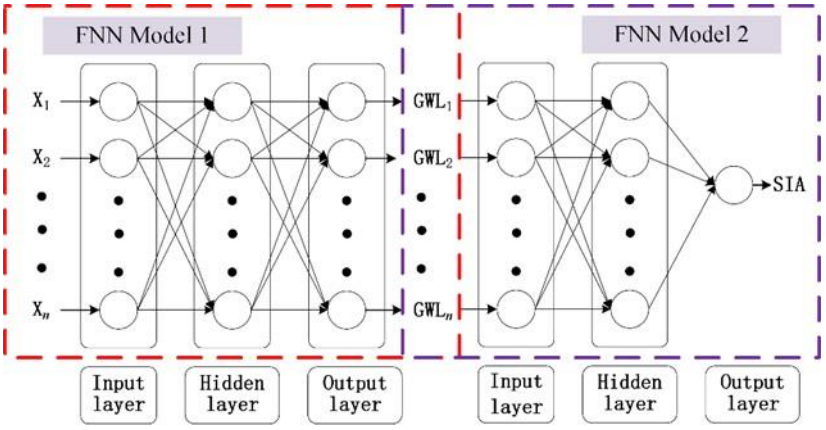

Figure 5. Configuration of the model for SIA simulation

3 Results

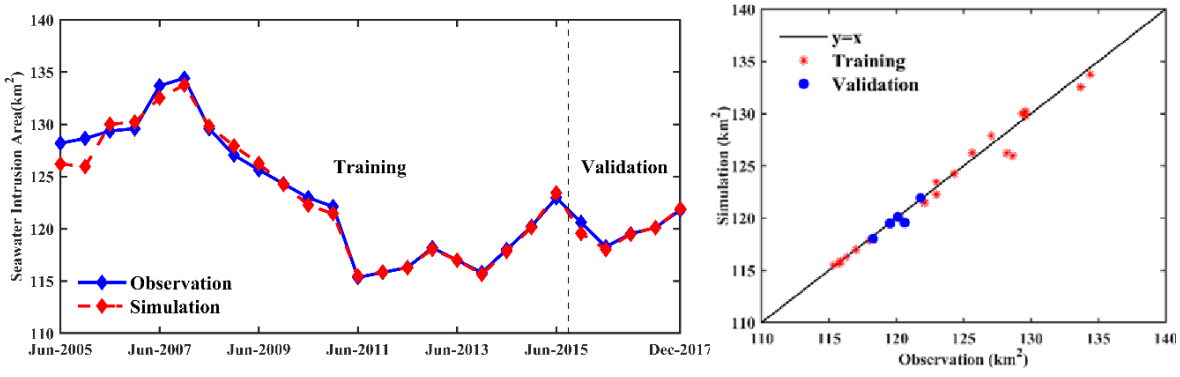

(a) (b)

Figure 2. Comparison between observation and simulation of six-monthly SIA using FNN Model 2: (a) line plot of results; (b) scatter plot of results.

Proceedings of the 1st IAHR
Young Professionals Congress
17-18 November 2020

VERTICALLY-AVERAGED COASTAL FLOW MODELLING USING MOMENT EQUATIONS

Francisco N. Cantero-Chinchilla [1], Rafael J. Bergillos [2] & Oscar Castro-Orgaz [3]

[1] Soil and Water Division, IAS-CSIC, Spanish National Research Council, Alameda del Obispo s/n, 14004 Córdoba, Spain
e-mail (Corresponding author): fncantero@ias.csic.es

[2,3] Hydraulic Engineering Area, Department of Agronomy, University of Córdoba, Rabanales Campus, Leonardo da Vinci Building, 14071 Córdoba, Spain

ABSTRACT

Among the available type of models in the literature, the vertically-averaged modelling of coastal flow processes is frequently accomplished resorting to Boussinesq-type equations. These models account for non-hydrostatic flow effects through the inclusion of dispersive extra terms in the governing equations, demanding high numerical accuracy while implementing the discrete form of derivatives in these extra terms. An useful alternative to Boussinesq-type models are the Vertically-Averaged and Moment (VAM) equations, where the extra degrees of freedown are mathematically closed in a Galerkin-type framework. This work presents the evaluation of a VAM model for simulating complex one-dimensional coastal flows. A challenging test comprising non-linear wave propagation, wave breaking, bore propagation and reflection is selected. The accuracy of the results as compared to the experimental data highlights the utility of VAM models as alternative tools to Boussinesq-type models in coastal flow modelling.

Keywords: Depth-integrated modelling, weighted residuals method, coastal flow, wave breaking, reflection.

1 INTRODUCTION

To investigate and manage coastal areas, it is essential to understand all the hydrodynamic processes from a physical viewpoint. Coastal flows may be subjected to dispersive effects depending on the environmental conditions, thereby involving non-hydrostatic and non-linearity during wave propagation, and, thus, requiring suitable mathematical modelling. Given the still high computational cost of three-dimensional models to simulate large domains, the vertically-integrated non-hydrostatic models, in which the vertical coordinate is removed from the governing equations, are widely in use. Vertically-integrated non-hydrostatic modelling from intermediate to shallow water in coastal flows can be accomplished using three related families of models, namely the Boussinesq-type models (Castro-Orgaz and Hager, 2017), the multilayer extension of the shallow water equations models (Casulli, 1999), and the weighted residual method based models (Steffler and Jin, 1993), also known as VAM models. Albeit the Boussinesq-type models are widely used in this field of research, which account for non-hydrostatic effects by implementing dispersive terms in the momentum balance, discretization of high-order dispersive terms requires extreme numerical accuracy. Further, simulation of waves in intermediate water depths can only be accomplished by optimization of the linear frequency dispersion relation. In contrast, the VAM models are capable of simulating dispersive waves from intermediate to shallow water without optimization, and the numerical schemes are settled based on robust discretization of first-order derivatives involving the field variables (Steffler and Jin, 1993). Wave breaking is automatically accounted for by the VAM model, while Boussinesq equations require a breaking sub-model to produce the transition from undular to broken waves. However, the VAM model has been shortly evaluated in coastal environments and hardly ever to complex coastal flows. Therefore, the objective of this work is to investigate the potential of the VAM model to simulate coastal flows in surf and swash zones comprising non-linear wave propagation, wave breaking, bore propagation and wave reflection.

2 PHYSICS OF THE VAM MODEL

To derive the VAM model equations, several mathematical steps must be considered. First, predictors involving a set of perturbation parameters of both the velocity and pressure fields are prescribed into the vertically-averaged RANS equations. Then, the weighted residual method is used to produce additional

vertically-averaged equations and resolve the extra degrees of freedown introduced by the perturbation parameters. In Cantero-Chinchilla et al. (2020) the system of equations is described in detail.

3 NUMERICAL MODEL

The VAM model is a system of 6 time-dependent PDE equations with 6 independent variables, involving the water depth, discharge and perturbation parameters of the velocity and pressure fields. In this work, the system is solved by applying a semi-implicit hybrid finite volume-finite difference scheme to tackle both the hyperbolic and elliptic parts of the equations. First, the flow variables are reconstructed in the cell interfaces using the MUSCL-TVD-4th method with the WSDGM method to grant the C-property. Then, the numerical fluxes are computed using the HLLC approximate Riemann solver. Later, the solution is evolved in time using the one-step forward Euler formula, with an implicit determination of non-hydrostatic effects using a Newton-Raphson algorithm. Finally, the viscous effects are implemented explicitly. The details of the numerical method can be consulted in Cantero-Chinchilla et al. (2020).

4 APPLICATION OF THE VAM MODEL TO A COMPLEX COASTAL FLOW TEST

Fig. 1 shows the results of the VAM model compared with those obtained by a Boussinesq-type model (Castro-Orgaz and Hager, 2017) for the experimental test of Roeber (2010), in which a solitary wave is propagated from deep water to a steep slope with a reef crest and a dry flat inland shore. The results show the ability of the VAM model to tackle wave breaking without external tuning, in contrast with the result of the Boussinesq-type model (Fig. 1a). In addition, once the wave is reflected by the vertical wall located at the right boundary, the VAM model is also able to accurately predict the free surface of the flow (Fig. 1b).

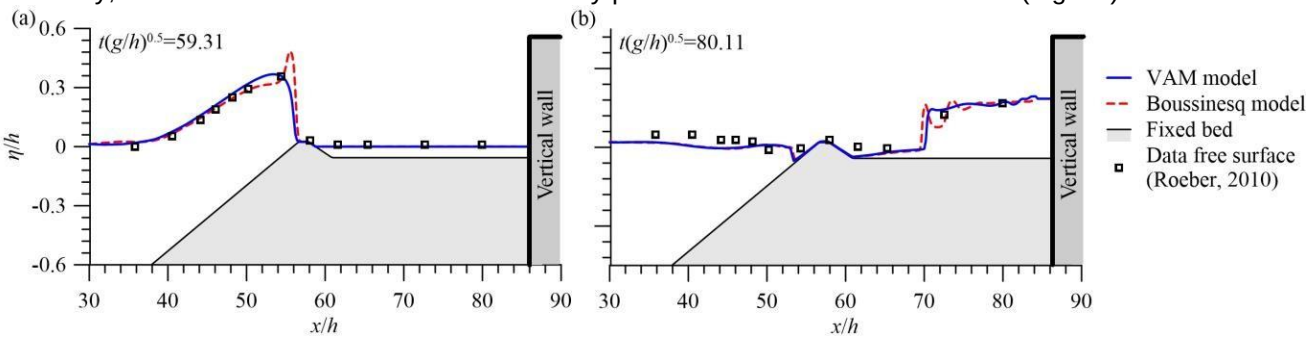

Figure 1. VAM model results as compared to a Boussinesq-type model using the data by Roeber (2010) at (a) $t(g/h)^{0.5}$ = 59.31 and (b) $t(g/h)^{0.5}$ = 80.11, where h = 2.5 m is the still water depth, η is the water elevation over the still water depth, g is the gravitational acceleration, x is the longitudinal distance and t is time.

5 CONCLUSIONS

The high-resolution, depth-averaged non-hydrostatic VAM model has been proved to be accurate to tackle complex coastal flows using automatic wave breaking detection. These results highlight the potential of the VAM model as a suitable alternative to Boussinesq-type models for maritime and coastal engineering applications.

ACKNOWLEDGEMENTS

This work was supported by the research project CTM2017-85171-C2-1-R (State Research Agency, Spain) and the research group AGR-127. RB and FNCC were partly funded by the Spanish Ministry of Science, Innovation and Universities through research contracts FJCI-2017-31781 and FJCI-2016-28009, respectively.

REFERENCES

Cantero-Chinchilla, F. N., Bergillos, R. J., and Castro-Orgaz, O. (2020). Nearshore coastal flow processes using weighted-averaged equations. *Ocean Engineering*, *211*, 107480.

Castro-Orgaz, O. and Hager, W.H. (2017). *Non-hydrostatic free surface flows*. Springer, 696 pp.

Casulli, V. (1999). A semi-implicit finite difference method for non-hydrostatic, free-surface flows. *International Journal for Numerical Methods in Fluids*, 30(4), 425-440.

Roeber, V. (2010). Boussinesq-type model for nearshore wave processes in fringing reef environment. Ph.D. dissertation, University of Hawaii at Manoa, Honolulu.

Steffler, P. M., and Jin, Y. C. (1993). Depth averaged and moment equations for moderately shallow free surface flow. *Journal of Hydraulic Research* 31(1), 5−17.

Proceedings of the 1st IAHR
Young Professionals Congress
17-18 November 2020

COASTAL EROSION IN BEACHES OF THE COAST OF BUENOS AIRES, ARGENTINA

Federico Haspert[1]

[1]Instituto Nacional del Agua – LH-INA, Ezeiza, Argentina, fhaspert@gmail.com

ABSTRACT

By using a simple and highly diffused model such as Bruun rule, a projection for the recession of the coastline was estimated along the entire maritime coastline of the province of Buenos Aires. For this, the sea levels corresponding to the 2045 and 2100 horizons were considered under the climate change scenarios RCP 4.5 and 8.5. By 2045, the calculated mean coastline recession values over the entire study area were 17.8 m (RCP 4.5) and 19.6 m (RCP 8.5). For the year 2100, mean recession values of 47.4 m (RCP 4.5) and 69.7 m (RCP 8.5) were obtained. The highest values of coastal recession were estimated in the coastal section between the districts of Pinamar and General Pueyrredón

Keywords: Bruun rule, mean sea level rise, climate change scenarios.

1 INTRODUCTION

In its more than 600 km of extension, the maritime coastline of the province of Buenos Aires (Argentina) exhibits a situation of more or less generalized advance of erosion. This is mainly explained by the rise in mean sea level, which has two components linked to global warming: the water added by the melting of glaciers and the polar ice caps and the expansion of sea water as its temperature increases (Mengel et al., 2016). The consequences of this phenomenon are none other than a worsening of processes that have already been occurring for several decades in coastal areas, such as lowland flooding, beach erosion, saltwater intrusion and wetland loss (Fitzgerald, 2008). The importance of coastal areas is that they have a high socioeconomic value associated with recreation, tourism and ecosystem services (Vousdoukas et al., 2020). That is why it is always desirable to estimate possible future scenarios in relation to the state of these areas in order to make planning decisions. The objective of this work is to estimate the effect of the increase in mean sea level on the maritime coastline of the province of Buenos Aires under different climate change scenarios.

2 MATERIALS AND METHODS

To study the changes on the equilibrium profile of a beach, the Bruun rule (1962; Eq. 1) was used, which determines erosion due to changes in sea level and depth of closure. As a complement, the formula of Hallermeier (1981; Eq. 2) was used to calculate the depth of closure h.

$$R = S\frac{L}{B + h} \quad [1]$$

where,
R: coastline recession (m).
S: sea level rise (m).
L: profile length between B and h (m).
B: dune height or other elevation estimate for the eroded area (m).
h: depth of closure (m).

$$h = 2{,}28.\ H_{e,t} - 68{,}5.\ \left(\frac{H_{e,t}^{\ 2}}{g.\ T_{e,t}^{\ 2}}\right) \quad [2]$$

where, $H_{e,t}$: significant wave height with a probability of

exceedance of 0,137% (m).
g: acceleration of gravity (m/s^2).
$T_{e,t}$: wave period associated with $H_{e,t}$ (s).

Parameters B (height of dune) and L (profile length) were obtained from the geometry of the beach profiles that were surveyed in a total of 53 locations along the entire coast. The parameter $H_{e,t}$ was calculated from the wave data for the period 1979-2018 (obtained from 16 virtual buoys). For the application of the formulas, the expected values of mean sea level rise for 2045 and 2100 corresponding to the climate change scenarios RCP 4.5 and RCP 8.5 (IPCC, 2014) were used (Figure 1a).

3 RESULTS

Figure 1b summarizes the results obtained in this work. By 2045, the calculated mean recession values of the coastline throughout the study area were 17.8 m (RCP 4.5; scenario 1) and 19.6 m (RCP 8.5; scenario 3). For the year 2100, mean recession values of 47.4 m (RCP 4.5; scenario 2) and 69.7 m (RCP 8.5; scenario 4) were obtained. The section with the highest values of coastal recession is the one between the districts of Pinamar and General Pueyrredón. To a lesser extent, some sectors of the districts of La Costa and Tres Arroyos also stand out.

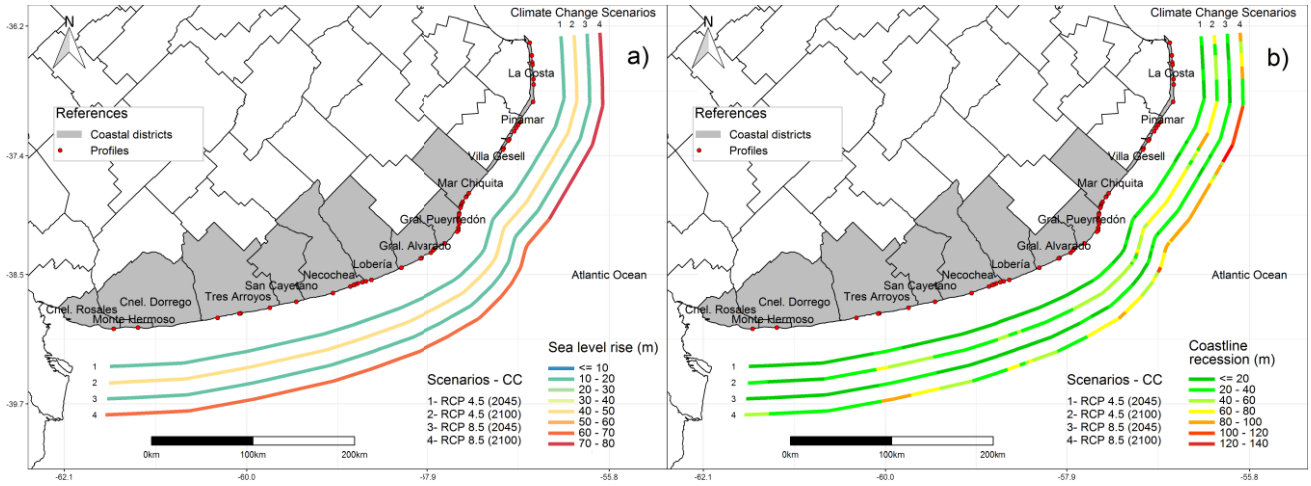

Figure 1. Mean sea level rise (a) and coastline recession (b) for the 2045 and 2100 horizons under different climate change scenarios.

4 CONCLUSIONS

Under the scenarios proposed, the Bruun model was helpful to identifying the areas of the coast of Buenos Aires that will potentially be most affected by the rise in mean sea level for horizons 2045 and 2100. This future diagnosis of the problems provides useful information that allows think about the development of a comprehensive management plan aimed at protecting coastal resources.

REFERENCES

Bruun, P. (1962). Sea Level Rise as a Cause of Shore Erosion, Journal of Waterway, Port, Coastal and Ocean Engineering, American Society of Civil Engineers, Vol. 88: 117-130.

Fitzgerald, D. M., Fenster, M. S., Argow, B. A. y Buynevich, I. V. (2008). Coastal Impacts Due To Sea-Level Rise. Annual Review of Earth and Planetary Sciences Vol. 36: 601-647.

Hallermeier, R. (1981). A Profile Zonation for Seasonal Sand Beaches from Wave Climate. Coastal Engineering Vol. 4: 253-277.

IPCC (2014). Climate Change 2014: Synthesis Report. Contribution of Working Groups I, II and III to the Fifth Assessment Report of the Intergovernmental Panel on Climate Change [Core Writing Team, R.K. Pachauri and L.A. Meyer (eds.)]. IPCC, Geneva, Switzerland, 151 pp.

Mengel, M., Levermann, A., Frieler, K., Robinson, A., Marzeion, B. y Winkelmann, R. (2016). Future sea level rise constrained by observations and long-term commitment. Proc Natl Acad Sci U.S.A. 2016 Vol. 113(10): 2597-2602.

Vousdoukas, M. I., Ranasinghe, R., Mentaschi, L. y Plomaritis, T. A. (2020). Sandy coastlines under threat of erosion. Nature Climate Change Vol. 10(3): 260-263.

Proceedings of the 1st IAHR
Young Professionals Congress
17-18 November 2020

Ground water depletion trends and the need for remediation in Punjab, India: 2000-2019.

Singh, R.[1] Sharma, K.[2]

Postgraduate Institute of Medical Education and Research, Chandigarh, India.

[1]roniedr.singh@gmail.com [2]kush.vashishtha@gmail.com

Abstract: Changes in the climate have influenced precipitation amounts, timings and intensity rates which directly affects surface and subsurface water resources. The groundwater level has been declining at a rapid rate (0.5 mbgl/year) due to excessive groundwater extraction from increased number of tube wells from 10.73 lac since 2000-01 to 14.76 lac in 2018-19. Erratic rainfall patterns have also affected the level of ground water recharge. The varying trends of rainfall being predominantly in the range of 400 to 700 mm/ year. In the past two decades, highest declines of 1.28mbgl and 1.47mbgl recorded in the year 2001 and 2016 respectively. However, immediate remedial measures are needed to reverse the declining trend of groundwater table. It is recommended that broader framework is needed on Integrated Water Resources Management for the state to align water use patterns with the needs and demands of different users taking the environmental changes into consideration for sustainable groundwater recharge and management.

Keywords: Climate Change, Groundwater remediation, Groundwater depletion, Water Resources Framework, Sustainable development.

Extended Abstract:

Introduction: Globally, water withdrawals have increased at almost twice the rate of population in the twentieth century. Changes in the climate have influenced precipitation amounts, timings and intensity rates which directly affects surface and subsurface water resources. Even without climate change, 15% of India's groundwater resources are overexploited. The water demand in India in the year 2000 was 634 BCM (billion cubic meters) and demand is expected to be 1093 BCM by the year 2025. Unfortunately, due to rampant drawing of the subsurface water, the water table in many regions of the Punjab has dropped significantly in the recent years resulting in threat to groundwater sustainability. More than 80 percent of the total water used for crop irrigation is extracted from groundwater resources and this number could be above 90 percent in drier years. Groundwater exploitation has grown exponentially in scale and intensity over recent decades. While intensification of groundwater use has contributed to improved livelihoods of millions of rural people, it has also resulted in long-term aquifer depletion and groundwater pollution with heavy metals in the state. Groundwater is currently and will continue to be a critical resource for the agricultural state of Punjab. It is important to assess the current and future status of our groundwater resources. Appropriate policy decisions regarding groundwater use and management can only occur when supported by sound, scientific information regarding our groundwater supplies. The ground water is being exploited exceeding to limit at annual recharge to meet increasing demand of water for diverse purposes i.e. intensive irrigation, drinking, industry, power generation etc. With such an important resource available to the state, the objective of this paper is to highlight changes in the

ground water reservoir and influence the state to continue investment in recovery, distribution and maintenance, carefully considering environmental social and economic factors influencing the further depletion of its ground water resources.

Methodology: This study examines long-term changes in rainfall and groundwater level trends in the last two decades from 2000-2019. The yearly data on rainfall and groundwater level from 2000-2019 in the state of Punjab was obtained from Water Source Information System, India (India-WRIS) being collected from the monitoring stations all across the state.

Results: The data reveals that water table levels are in the range of 10 to 20 mbgl (Metres below Ground Level) in major parts of the state. However, around major cities like Amritsar, Jalandhar, Ludhiana, Patiala, Barnala and Sangrur, water levels are 20 to 40 meters deep. The trends of the state show a decline from the level of 8.35 mbgl in the year 2000 to 17.84 mbgl in the year 2019 with a lowest depth of 18.27 mbgl recorded in the year of 2018. In the past two decades, highest declines of 1.28mbgl and 1.47mbgl recorded in the year 2001 and 2016 respectively. The varying trends of rainfall being predominantly in the range of 400 to 700 mm/ year. The highest being 953 mm in 2008 and 925 mm in 2011 that were followed by a slightly improved ground water level. Based on the last five years of precipitation the risk remains high affecting the groundwater through withdrawals considering the five years moving average between these as the highest decline was observed in 2016 in the last five years.

Conclusion and Recommendation: The groundwater level has been declining at a rapid rate (0.5 mbgl/year) due to excessive groundwater extraction from increased number of tube wells from 10.73 lac since 2000-01 to 14.76 lac in 2018-19. When water tables exhibit long-term declines, this is commonly referred to as "mining the resource." Erratic rainfall patterns have also affected the level of ground water recharge. The current state of development and management of groundwater resources has serious implications for the future groundwater availability in the state. In 2009, Punjab became the first state in the country to enact a law banning the sowing of rice before a stipulated date. This is reflected on the slightly improved rate of decline in the last decade from 0.58mbgl/year during 2000-2009 to 0.42Mbgl/year during 2010-2019. However, immediate remedial measures are needed to reverse the declining trend of groundwater table. It is recommended that broader framework is needed on Integrated Water Resources Management for the state to align water use patterns with the needs and demands of different users, including watershed management, quality monitoring, aquifer remediation. Mechanisms of decentralised local rainwater-harvesting and micro-watershed development can be a preferred route for water augmentation and management in view of technical and social feasibility in the state. A broader framework to tackle scarcity must include collective efforts to conserve the water through protection of conventional water resources by rejuvenating the rivers, harvesting of rainwater through ancient traditions of underground water storage tank systems, increasing capacity of storage through de-silting and deepening of the water resources, desalination units for the seawater, reuse of water from the canals, and limiting the dependency on groundwater use making Punjab a water surplus and a sustainable state.

IAHR AIRH

International Association for Hydro-Environment Engineering and Research

Hosted by
Spain Water and IWHR, China

Session 7

Sediment Transport Experimental Methods and Instrumentation

IAHR YPN

Hosted by
Spain Water and IWHR, China

EFFECTS OF LAND COVER/USE CHANGES ON THE ETHIOPIAN FINCHA DAM CAPACITY

Motuma Shiferaw Regasa [1,2] & Michael Nones [2]

[1] Affiliation Institution 1, Wollega University, Nekemte, Ethiopia
motumashiferaw@gmail.com
2Institute of Geophysics - Polish Academy of Sciences, Warsaw, Poland
mnones@igf.edu.pl

ABSTRACT

Ethiopia, as well as the downstream countries of Sudan and Egypt, are highly dependent on the water coming from the Nile, in particular from its tributary Blue Nile. In the last decades, an increasing human pressure, combined with climate change, altered the natural environment, with significant consequences on the local water resources and population. Indeed, the combined effect of soil degradation due to Land Use / Land Cover (LULC) changes and more frequent extreme rainfall events caused severe erosion and sediment transport, which contribute to negative impacts on downstream flooding, pollution and effective capacity of reservoirs. Using the Ethiopian Fincha River as a case study, this paper provides a general overview on the actual knowledge of LULC changes in the basin, proposing future studies that are needed for the future management of sedimentation within the Fincha Dam reservoir.

Keywords: ArcSWAT, Fincha River, LULC changes, siltation, reservoir management

1 INTRODUCTION

Since millennia the whole Nile Basin benefited from the water coming from the Ethiopian highlands, particularly from the Blue Nile. Besides Ethiopia, the downstream people living in Sudan and Egypt used the water in multiple and sometimes concurrent ways; agriculture, livestock, industry and power generation. To maximize the benefits, the local populations altered the natural environment, changing the coverage and the use of the majority of the land, particularly close to watercourses.

Therefore, evaluating the future effects of Land Use/ Land Cover (LULC) changes is important to generate and provide helpful information to policymakers and development practitioners (Ayana et al., 2014), specifically in the case of countries highly dependent from the local environment, such as Ethiopia. Indeed, bare land expansion, increased surface runoff production and soil erosion are major environmental damages attributed to LULC in the Fincha River basin (Gessesse & Bewket, 2014; Dibaba et al., 2020), north-western from the capital city Addis Ababa. These degradation processes have adverse impacts on the local agricultural productivity, water resource availability and food security. In addition, the increasing frequency of heavy rains due to climate change can cause severe erosion and sediment transport, which ultimately leads to the degradation of soil and contributes to negative impacts on downstream flooding, pollution and siltation of water bodies and reservoirs (Yan et al., 2013). LULC changes may result in a high rate of soil erosion and increased sediment transport by changing the magnitude and pattern of runoff, peak flow, sediment yield and groundwater levels, adversely affecting the useful life of reservoirs (Leta et al., 2017). Using, as a case study, the Fincha Dam, the present work will emphasize how LULC changes affect the sediment yield and its consequences on the reservoir capacity, tackling a series of objectives:

- quantification of the sediment yield deriving from different LULC types within the river basin;
- assessment of the correlation between sediment yield and topography, flow discharge, drainage basin characteristics, and channel geometry;
- evaluation of the impact of LULC changes on water flow and sediment yield at the catchment scale;
- quantification of sediment volume entering the reservoir and evaluation of the effect on the useful lifetime of the dam;

- development of recommendations and guidelines and consulting to policymakers on appropriate mitigation measures aiming to reduce the sediment yield in the watershed, and consequently the reservoir siltation.

2 PROJECT FLOWCHART

The proposed study, which will start in October 2020 and last for around four years, will assess the sediment yield and siltation impacts on the Fincha reservoir under LULC changes at the catchment scale. This will be performed combining spatially integrated hydrological parameters, digital elevation models (DEMs), land use and soil maps with the ArcGIS interface Soil and Water Assessment Tool (ArcSWAT). Remote sensed data like DEMs and LCLU maps will be acquired through the United State Geological Survey website, while additional information on the local climate, streamflow and soil conditions will be collected from different governmental offices in Ethiopia. To integrate and calibrate the remotely sensed information, field data will be also collected along the Fincha River and within the reservoir.

Employing multiple simulations, the research will provide water managers and policymakers with multiple future scenarios forced by different LULC, and associated management strategies and mitigation measures for reducing the siltation in the Fincha Dam reservoir, and consequently extending the useful lifetime of the dam. The use of satellite remote sensing and Markov modeling will found to be beneficial in describing and analyzing the direction, rate and spatial pattern of LULC change to generate scenarios for the next decades (e.g., 2030-2040-2050).

To achieve the main objectives of the project, some research questions will be tackled:

- What is the actual sediment yield, based on the present LULC conditions of the basin?
- How is the sediment yield affected by watershed characteristics (topography, LULC, etc.), the river flow discharge, the channel geometry, the local climate?
- What is the impact of LULC changes on the sediment yield of the catchment, and do these effects vary seasonally? Is there any temporal trend, that could be linked to the local hydro-meteorological conditions?
- Is the ArcSWAT model able to reproduce the observed sediment yield? If not, what additional data are needed for calibrating/validating the code?
- What are the possible management strategies and mitigation measures that can be applied for reducing the sediment load coming from the basin hillslopes and consequently the siltation in the Fincha Dam reservoir?

ACKNOWLEDGEMENTS

This work is developed under the project “Assessing Catchment Sediment Yield and Siltation Impacts on Reservoir Capacity under Land Cover/Use Changes: The Case Study of the Fincha Dam, Ethiopia”, funded by the National Science Centre, Poland, within the PreludiumBis-1 call, grant n. 2019/35/O/ST10/00167.

REFERENCES

Ayana, A.,B., Edossa, D.,C., and Kositsakulchai, E. (2014). Modeling the effects of land use change and management practices on runoff and sediment yields in Fincha watershed, Blue Nile. OIDA International Journal of Sustainable Development, 07(11), 75-88.

Dibaba, W.T., Demissie, T.A.,and Miegel, K. (2020). Drivers and Implications of Land Use/Land Cover Dynamics in Finchaa Catchment, Northwestern Ethiopia. Land, 9, 113.

Gessesse, B., and Bewket, W. (2014). Drivers and Implications of Land Use and Land Cover Change in the Central Highlands of Ethiopia: Evidence from Remote Sensing and Socio-demographic Data Integration. Ethiopian Journal of the Social Sciences and Humanities, 10(2), 1-23.

Leta, M.K., Demissie, T.A., & Koriche, S.A. (2017). Impacts of Land Use Land Cover Change on Sediment Yield and Stream Flow:A Case of Finchaa Hydropower Reservoir, Ethiopia. International Journal of Science and Technology, 6(4), 763–781.

Yan, B., Fang, N.F., Zhang, P.C., and Shi, Z.H. (2013). Impacts of land use change on watershed stream flow and sediment yield: An assessment using hydrologic modelling and partial least squares regression. Journal of Hydrology, 484, 26–37.

Proceedings of the 1st IAHR
Young Professionals Congress
17-18 November 2020

LES TWO-PHASE MODELLING OF SUSPENDED SEDIMENT TRANSPORT USING A TWO-WAY COUPLED EULER-LAGRANGIAN APPROACH

Daniel Wildt[*1,2] **and Michael Tritthart**[1,2]

[1]Christian Doppler Laboratory for Sediment Research and Management,
University of Natural Resources and Life Sciences, Vienna, Austria
[2]Institute of Hydraulic Engineering and River Research, Department of Water, Atmosphere and Environment,
University of Natural Resources and Life Sciences , Vienna, Austria

*Correspondence : daniel.wildt@boku.ac.at

ABSTRACT

A two phase LES model using Euler-Lagrangian two-way coupling has been developed in OpenFOAM. The model shall be used for the analysis of the interaction between particles and their surrounding fluid. Validation of the model has been performed using data from physical experiments.

Keywords: suspended sediment, computational fluid dynamics, large eddy simulation, Euler-Lagrangian two-way coupling.

1 INTRODUCTION

Efficient sediment management requires detailed process understanding of sediment transport in rivers. Despite this fact current literature is still lacking information on that subject. Models of suspended sediment transport are often based on simple advection-diffusion equations (Hauer *et al.*, 2018). The aim of this study is to set up a high fidelity CFD model for studying the particle-fluid interaction in turbulent channel flow.

2 METHODS

2.1 Governing equations and modelling approach

The development of a sediment plume in turbulent channel flow is studied using a two-phase LES model. Fluid flow is governed by the three-dimensional Navier-Stokes equations. The equations are solved on a structured mesh with 5.2 million cells (Yücesan *et al.*, 2020).

The movement of the dispersed phase (particles) is governed by Newton's law of motion and modelled using the Lagrangian approach. Momentum exchange between fluid and particles is two-way coupled. The entire model is solved using a modified version of the OpenFOAM-solver MPPICFoam (Greenshields, 2018).

2.2 Validation and test case

Validation of the model of suspended sediment transport in turbulent channel flow is carried out on the basis of physical experiments by Worf *et al.* (2019). In this experiment sediment is continuously released into a laboratory channel with turbulent flow with an average velocity of 0.5 m s^{-1}. The main parameter for the validation is the fall velocity derived from the (x, y)-positions of the particles. x is the direction of the bulk fluid velocity and the gravitational acceleration is pointing in negative y direction.

To study particle-fluid interactions 3,375 particles (density ρ_S = 2,650 kg m^{-3}, diameters d uniformly distributed: 0.51 mm $< d <$ 0.70 mm, shape factor: 0.45) are simultaneously released from the upper area close to the inlet of the channel. One second after the particles have been released the particle velocities are compared against the velocity of the surrounding fluid.

3 RESULTS

Worf *et al.* (2019) measured a fall velocity in the range of 0.03 m s^{-1} to 0.06 m s^{-1} for particles described above in turbulent channel flow with an average flow velocity of 0.5 m s^{-1}. The fall velocity in the numerical simulation of this experiment was determined as 0.06 m s^{-1}.

In Figure 1 the velocity of each individual particle is plotted against the velocity of its surrounding fluid. Looking at the x and z component of the velocities there appears to be no difference between the particle and fluid velocity apart from a random variation. As a result of particle settling, the y component of the particle velocity is lower than the y component of the fluid velocity.

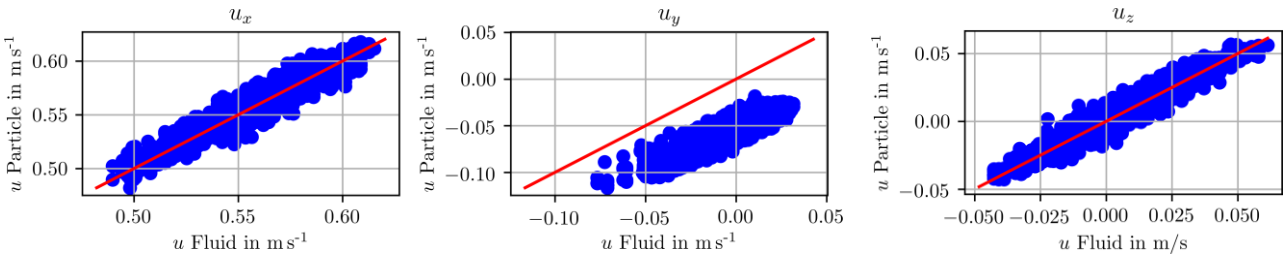

Figure 1: Comparison of the particle velocity and the velocity of its surrounding fluid 1 s after release into turbulent channel flow; each point represents one particle.

4 CONCLUSIONS

In this study the development of a sediment plume in turbulent channel flow has been numerically modelled and the velocity difference between particles and fluid has been analysed. In the next step, the model shall be used to study the different components of the forces acting on the particles and their contribution to the particle trajectory. This should yield more accurate models of suspended sediment transport also on larger scales.

5 ACKNOWLEDGEMENTS

This paper was written as a contribution to the Christian Doppler Laboratory for Sediment Research and Management. In this context, the financial support by the Christian Doppler Research Association, the Austrian Federal Ministry for Digital and Economic Affairs and the National Foundation for Research, Technology and Development is gratefully acknowledged. The computational results presented have been achieved using the Vienna Scientific Cluster (VSC).

References

Greenshields C. J. (2018). *OpenFOAM*. The OpenFOAM Foundation. URL: http://openfoam.org.

Hauer C., Wagner B., Aigner J., Holzapfel P., Flödl P., Liedermann M., Tritthart M., Sindelar C., Pulg U., Klösch M., Haimann M., Donnum B. O., Stickler M., Habersack H. (2018). State of the art, shortcomings and future challenges for a sustainable sediment management in hydropower: A review. *Renewable and Sustainable Energy Reviews 98*, 40–55. doi:10.1016/j.rser.2018.08.031.

Worf D., Schobesberger J., Lichtneger P., Habersack H., Sindelar C. (2019). Sedimentation velocity of saualm crystalline using image processing methods. In *16th International Symposium on Water Management and Hydraulic Engineering*.

Yücesan S., Schobesberger J., Sindelar C., Hauer C., Habersack H., Tritthart M. (2020). Large eddy simulation of a sediment particle under entrainment conditions. *Journal of Hydraulic Research*. revised.

Proceedings of the 1st IAHR
Young Professionals Congress
17-18 November 2020

WASTEWATER QUALITY ESTIMATION THROUGH LED SPECTROPHOTOMETRY BY MEANS OF STATISTICAL MODELS

Daniel Carreres-Prieto[1], Juan T.García[1], José M. Carrillo[1], Luis G. Castillo Elsitdié[1]

[1] Civil Engineering and Mining Engineering School. *Universidad Politécnica de Cartagena* (*Spain*)
daniel.carreres@upct.es, *juan.gbermejo@upct.es,* jose.carrillo@upct.es, luis.castillo@upct.es

ABSTRACT

Regulatory developments emanating from the European Union (EU) in the last decade in the environmental field have placed emphasis on halting water degradation and combating illegal discharges. Continuous, real-time, reliable information about the pollutants in the input sewage is key to fulfil EU environmental policies. The current methods of analysis make difficult to carry out a real time analysis, since they are based on punctual samples, which are subjected to diverse treatments and require chemical substances in laboratory. This research work has been focused on the development of a cost-effective equipment for the calculation of several variables such as COD, BOD_5, TSS, P, TN, and NO_3-N, from spectrophotometry data (380-700 nm). Measurements are carried out in real time and without the need of chemical or pre-treatment, with the aid of different statistical models all through a new spectrophotometer based on LED technology that does not require the use of optical elements to work.

Keywords: Chemical Oxygen Demand (COD), statistical models, real time monitoring.

1 WATER QUALITY ANALYSIS EQUIPMENT

In order to know the evolution of the pollutant load in sewage systems, this research work is focused on the development of a low-cost, low-consumption and small-sized equipment for the estimation of COD, BOD_5, TSS, P, TN, and NO_3-N from a spectrophotometric analysis based on LED technology. This equipment can be placed anywhere in the sewage network to carry out an analysis in almost real time.

The main characteristic of the equipment is that it does not require the use of incandescent lamps to generate the working spectrum or the use of optical elements to diffract the light, being possible to carry out an analysis between 380-700nm, with very close results to those obtained by commercial equipment based on incandescent lamps. Those results have enabled us to develop a much smaller, cost-effective and lower consumption equipment. Details of the research are available in Carreres-Prieto et al., (2019, 2020).

Figure 1a shows a simplified scheme of the main block of analysis of the equipment, where it consists of a wide-spectrum photodiode as a sensor, which is aligned with the samples to be analyzed (taken automatically), and the light source. The latter is composed of a system of 34 limited-bandwidth LED that are aligned with the sample, whose peak wavelengths are between 380-700nm. Figure 1b shows a 3D view of the equipment.

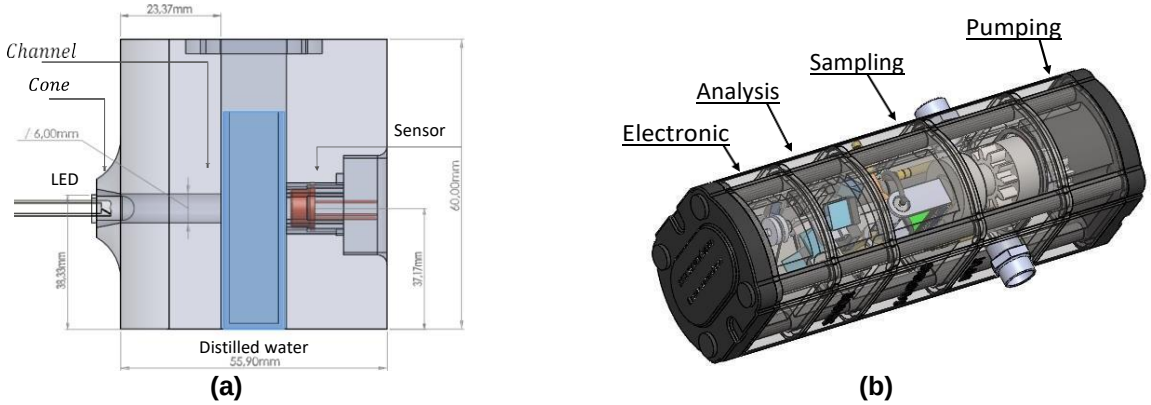

Figure 1. **(a)** Basic scheme of equipment analysis block. **(b)** 3D view of the equipment.

and BOD_5, that is, higher than 700mg/l and 450mg/l respectively, and with treated water (COD < 50mg/l and BOD_5 < 10), as shown in Figure 2a and b, respectively.

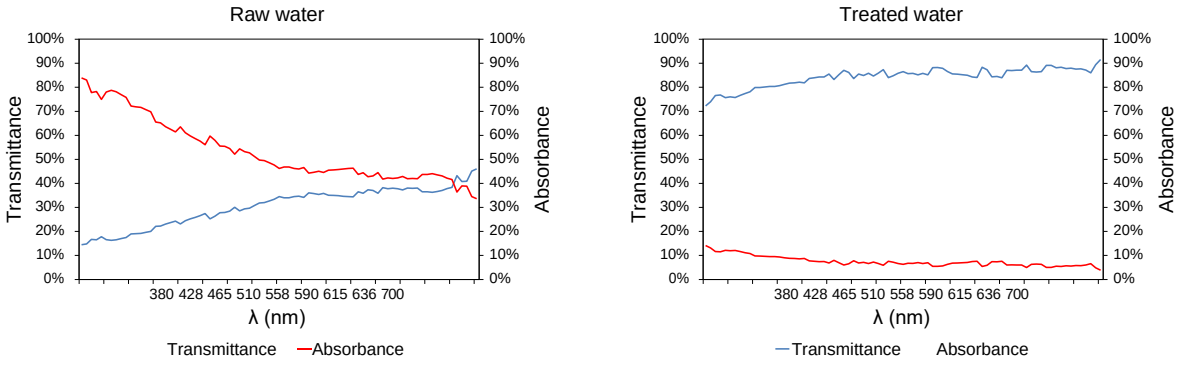

(a)

Figure 2. Spectral response (transmittance and absorbance) measur
entrance of the treatment plant (raw water), and **(b)** plant

2 LOAD POLLUTION ESTIMATION MODELS

From the spectrophotometric information, several models have been developed to calculate COD, BOD5, TSS, P, TN, and NO_3-N. These models have been calculated using genetic algorithms (deep learning) from more than 200 samples analyzed in a treatment plant in the Region of Murcia (Spain) during the period June 2019 to April 2020. The models are based on the search for correlations between the spectrophotometric values of the water samples and the contaminating parameters analyzed in the treatment plant's laboratory.

One of the characteristics of genetic algorithms is that they can provide multiple equally valid solutions. Eq. [1] shows, as an example, the estimated formula for the Chemical Oxygen Demand (COD).

$$COD = ((1.958 \cdot A_{420} - 1.663 \cdot A_{575}) \cdot \frac{0608 \cdot T_{522}}{1.059 \cdot T_{445}} \cdot (1.988 \cdot A_{385} - 1.663 \cdot A_{575}) \cdot 0.272 \cdot T_{461} + 35659 - 26.168) \quad [1]$$

where A_x and T_x are the absorbance and transmittance values measure at *x* wavelength.
These models are valid for both raw water and treated water, without the need to subject the samples to pre-treatment or chemicals. All the calculated models for estimating the water quality have shown an error of less than 4%. For instance, Figure 3 shows a comparison between the values of COD measured in the laboratory by traditional methods of analysis (blue) and the values estimated by the model during the training process (red), as well as the values calculated with test data, i.e. with data not used during the model generation process.

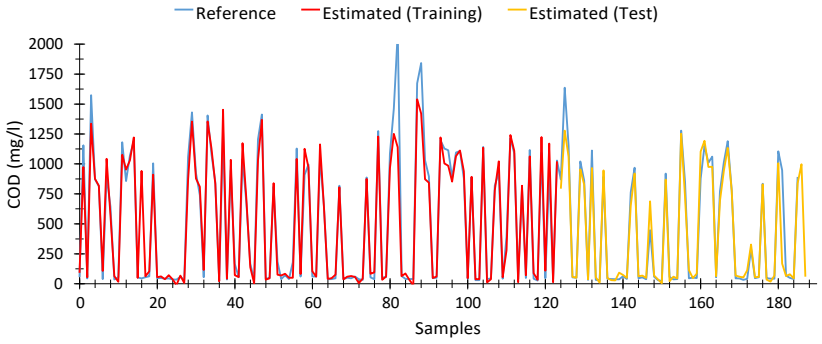

Figure 3. Comparison between COD values measured by the wastewater treatment plant laboratory and the values calculated from spectrophotometric data.

REFERENCES

Carreres-Prieto, D., García, J. T., Cerdán-Cartagena, F., & Suardiaz-Muro, J. (2020). Performing Calibration of Transmittance by Single RGB-LED within the Visible Spectrum. *Sensors*, 20(12), 3492.
Carreres-Prieto, D., García, J. T., Cerdán-Cartagena, F., & Suardiaz-Muro, J. (2019). Spectroscopy Transmittance by LED Calibration. *Sensors*, 19(13), 2951.

Proceedings of the 1st IAHR
Young Professionals Congress
17-18 November 2020

COMPARING LIDAR WITH COMMON FREE-SURFACE MEASUREMENT METHODS IN AERATED HYDRAULIC JUMPS

Rui Li[1#], Kristen D. Splinter[1] & Stefan Felder[1]

[1]Water Research Laboratory, School of Civil and Environmental Engineering, UNSW Sydney, NSW 2052, Australia
[#]r.li@unsw.edu.au

ABSTRACT

The free-surface of aerated hydraulic jumps is characterized by three-dimensional time-varying motions. LIDAR technology allows for continuous and quasi-synchronous recordings of the air-water free-surface with high-spatial resolution providing better understanding of free-surface features. To assess the comparative performance of LIDAR against commonly applied free-surface measurement methods (acoustic displace meter and wire gauge), free-surface properties were simultaneously recorded with these instruments in hydraulic jumps showing close agreement in distributions of free-surface properties. The average difference of the mean free-surface elevations and fluctuations measured with LIDAR and traditional instruments were less than 17 mm (13%) and 2.7 mm (12%), respectively. LIDAR demonstrated the advantage of simultaneous jump toe tracking which provided more precise mean jump toe positions than visual observations. Similar results in free-surface properties, while providing continuous high-spatial resolution data including the jump toe position, suggest that the LIDAR is superior compared to traditional instrumentation for the observation of free-surface processes of aerated hydraulic jumps.

Keywords: Acoustic displacement meter, air-water flows, free-surface, physical modelling, remote sensing.

1 INTRODUCTION AND METHODOLOGY

Air-water flows are common in many hydraulic structures and natural channels including hydraulic jumps. Traditional methods to measure free-surface properties in aerated hydraulic jumps include pointer gauges, conductivity probes, acoustic displacement meter (ADM) and wire gauge (WG). For continuous measurement of free-surface motions, ADMs and WGs are used but these have limitations including the point source measurement and the inference of a visually observed mean jump toe. Recently, LIDAR has been explored as a novel method to record free-surface features of air-water flow phenomena comprising channel junctions (Rak et al. 2017), hydraulic jumps (Montano et al. 2018), stepped spillway (Kramer et al. 2019) and stilling basin (Li et al. 2020a). LIDAR shows advantages of high spatial and temporal resolution providing continuous and quasi-synchronous measurements (Montano et al. 2018). Montano et al. (2018) have shown that LIDAR data were consistent with previously reported free-surface properties recorded with ADMs, video cameras and WGs. However, a direct comparison of measurements methods is needed to clarify reported differences and to eliminate the effects of inflow conditions, scale effects and other experimental bias (Li et al. 2020b).

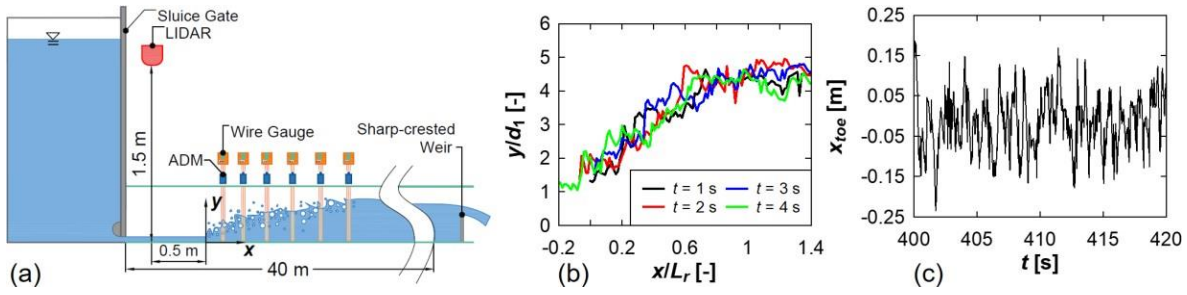

Figure 1. Experimental setup and exemplary raw LIDAR data (d_1 = inflow depth, L_r = roller length, x = horizontal distance from jump toe, y = elevation): (a) experimental setup; (b) dimensionless free-surface profiles y/d_1 (Inflow Froude number Fr_1 = 3.5); (c) instantaneous jump toe position x_{toe} (Fr_1 = 8).

An experimental study to compare LIDAR with common fast-sampling instruments, ADMs and WGs, was conducted at the UNSW Water Research Laboratory. The free-surface of hydraulic jumps with inflow Froude numbers Fr_1 of 3.5, 5 and 8 corresponding to Reynolds numbers Re = 9.2×10^4, 1×10^5 and 1.2×10^5 were simultaneously recorded for up to 30 minutes using LIDAR along the centreline and ADMs and WGs on each side with an offset of 0.07 m (Figure 1a). An example of instantaneous free-surface profiles y/d_1 of Fr_1 = 3.5 recorded with LIDAR is shown in Figure 1b. LIDAR also demonstrated the ability to simultaneously track the jump toe position x_{toe} while recording the free-surface (Figure 1c).

2 RESULTS AND DISCUSSION

A comparison of mean free-surface elevations and standard deviations simultaneously recorded with LIDAR, ADM and WG is shown in Figure 2a. Overall there was strong agreement between the three instruments over the Froude numbers tested with respect to basic free surface properties. The mean free-surface profiles measured with LIDAR were on average 9.5 mm (6%) lower than ADM measurements and 17 mm (13%) lower than WG measurements. The average difference in standard deviations y' was 2.7 mm (12%) between LIDAR and ADM and 1.4 mm (10%) between LIDAR and WG. The relative differences in free-surface properties can be explained with the different measurement principles of the three instruments including a larger spot size of the ADM compared to the LIDAR and potential wetting and drying processes of the intrusive WG. More detailed and advanced comparison of free-surface features of the three instruments is presented in Li et al. (2020b).

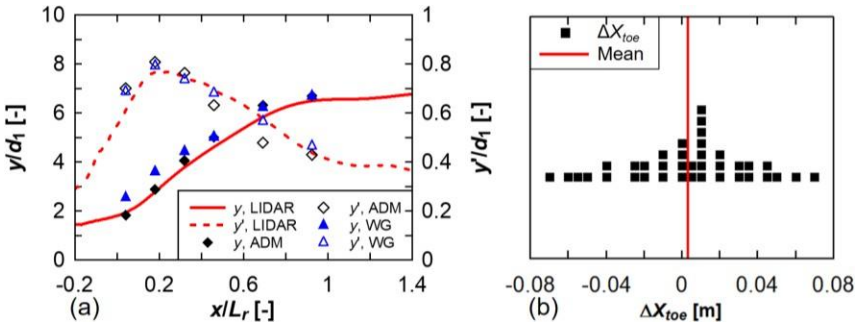

Figure 2. Results of free-surface and jump toe measured with LIDAR, ADMs and WGs: (a) free-surface profile and fluctuations (Fr_1 = 5); (b) difference between visual observations and LIDAR measurements of the mean jump toe position ΔX_{toe} (38 experiments for Fr_1 = 3.5, 5 and 8).

A key advantage of LIDAR over ADM and WG is the ability to track the time-varying jump toe (Figure 1c). In previous studies using traditional instruments, such as ADM, the mean jump toe position was visually determined. However, it is difficult to precisely visualise the mean jump toe position due to strong jump toe oscillations. In the present experiments, the best-visual estimates of mean jump toe position were compared against the mean jump toe position recorded with LIDAR. The differences between the visual observations and LIDAR measurements of mean jump toe position (ΔX_{toe}) of the three hydraulic jumps are shown in Figure 2b. Although the average ΔX_{toe} of all repeated experiments is close to 0, a ΔX_{toe} up to 70 mm can be observed. Free-surface data adjusted relative to the LIDAR jump toe position provided very close agreement between instruments (Figure 2a). The consistency in free-surface data measured with LIDAR compared to traditional instrumentation and the ability of the LIDAR to continuously track the free-surface with high-spatial resolution including the jump toe motions shows that LIDAR technology provides new opportunities to better understand complex air-water flows.

REFERENCES

Kramer, M., Chanson, H., and Felder, S. (2020). Can we improve the non-intrusive characterization of high-velocity air–water flows? Application of LIDAR technology to stepped spillways. *Journal of Hydraulic Research*, 58(2), 350-362.

Li, R., Splinter, K., and Felder, S. (2020a). Free-surface mapping of air-water flows in a stilling basin. *Proc. 8th IAHR International Symposium on Hydraulic Structures*, 12-15 May, Chile.

Li, R., Splinter, K., and Felder, S. (2020b). Time-varying free-surface properties of hydraulic jumps: a comparative analysis of experimental methods. arXiv preprint arXiv:2007.05128.

Montano, L., Li, R., and Felder, S. (2018). Continuous measurements of time-varying free-surface profiles in aerated hydraulic jumps with a LIDAR. *Experimental Thermal and Fluid Science*, 93, 379-397.

Rak, G., Hocevar, M. and Steinman, F. (2017). Measuring Water Surface Topography Using Laser Scanning. *Flow Measurement and Instrumentation,* 56, 35-44.

Proceedings of the 1st IAHR
Young Professionals Congress
17-18 November 2020

DEBRIS-FLOW SUSCEPTIBILITY ASSESSMENT USING THE INDEX ENTROPY MODEL IN THE VISO CATCHMENT

Jeancarlo Escalante[1,2], Cesar Sanchez[1,2], David Gonzalez[2,3], Jefferson Castillo[1,2], Bill Zorrilla[1,2,4]

[1]National University of Engineering, Lima, Peru
[2]Institute for the Mitigation of the Effects of El Niño Phenomenon (IMEFEN), Lima, Peru
[3]Technological University of Peru, Lima, Peru
[4]Royal Academy of Engineering (RAEng), London, The United Kingdom

*Correspondence : jescalantep@uni.pe

ABSTRACT

Debris Flow is one of the most typical natural hazards in the mountainous areas of Chosica in Peru, which causes significant damages to people and infrastructure, thus affecting lives and the economy. It is essential to research this phenomenon to understand its behaviour and mitigate its effects, thus building resilient cities. Therefore a model was developed for regional susceptibility assessments using geographic information system (GIS) and an index entropy model adapted for sensitivity analysis of several impact factors of debris flows such as slope gradient, slope aspect, precipitation, normalized difference vegetation index (NDVI), geology, and developmental stages of the Viso catchment. The success rate of debris flow prediction by the model is 72.7% based on area-under-the-curve (AUC) cross-validation of the model.

Keywords: Debris-flow, index entropy model, susceptibility assessment.

1 INTRODUCTION

Debris flows are natural phenomena, which usually come up in mountain regions with intense rainfall. One of the main approaches to develop hazard reduction strategies is creating debris-flow susceptibility maps to mitigate risk and avoid future situations (preventive measure). Moreover, with advancements in prediction technology, several methodologies were developed to come up with susceptibility maps. In this research, the index entropy method was applied based on the work performed by Chen *et al.* (2017) and Wu *et al.* (2020).

2 METHODS AND RESULTS

Index Entropy Model, which is a binary statistical model performed by Vlčko *et al.* (1980), was used to calculate the area percentages at all levels and weight of debris-flow impact factors according to Eqs. (1)–(6).

$$P_{ij} = \frac{A_{sd}}{A_t} \quad (1)$$

$$(P_{ij}) = \frac{P_{ij}}{\sum_{j=1}^{S_j} P_{ij}} \quad (2)$$

$$H_j = -\sum_{i=1}^{S} (P_{ij}) log_2(P_{ij}) \qquad j = 1, \ldots n \quad (3)$$

$$H_{jmax} = log_2(S_j) \quad (4)$$

$$I_j = \frac{H_{jmax} - H_j}{H_{jmax}} \quad (5)$$

$$W_j = I_j \times P_{ij} \quad (6)$$

where A_t = area of each level for the first classification per factor; A_{sd} = area of debris flow at all levels per factor; P_{ij} = area percentage of debris flow at all levels per factor; H_j and H_{jmax} = entropy; S_j = factor level number; I_j = information coefficient; and W_i = total weight of the factor.

Besides, geographic information system (GIS) was applied to create a debris-flow inventory map and maps of impact factors (slope gradient, slope aspect, precipitation, NDVI, geology, and developmental stages of catchment), then the debris-flow susceptibility assessment was performed (Figure 1).

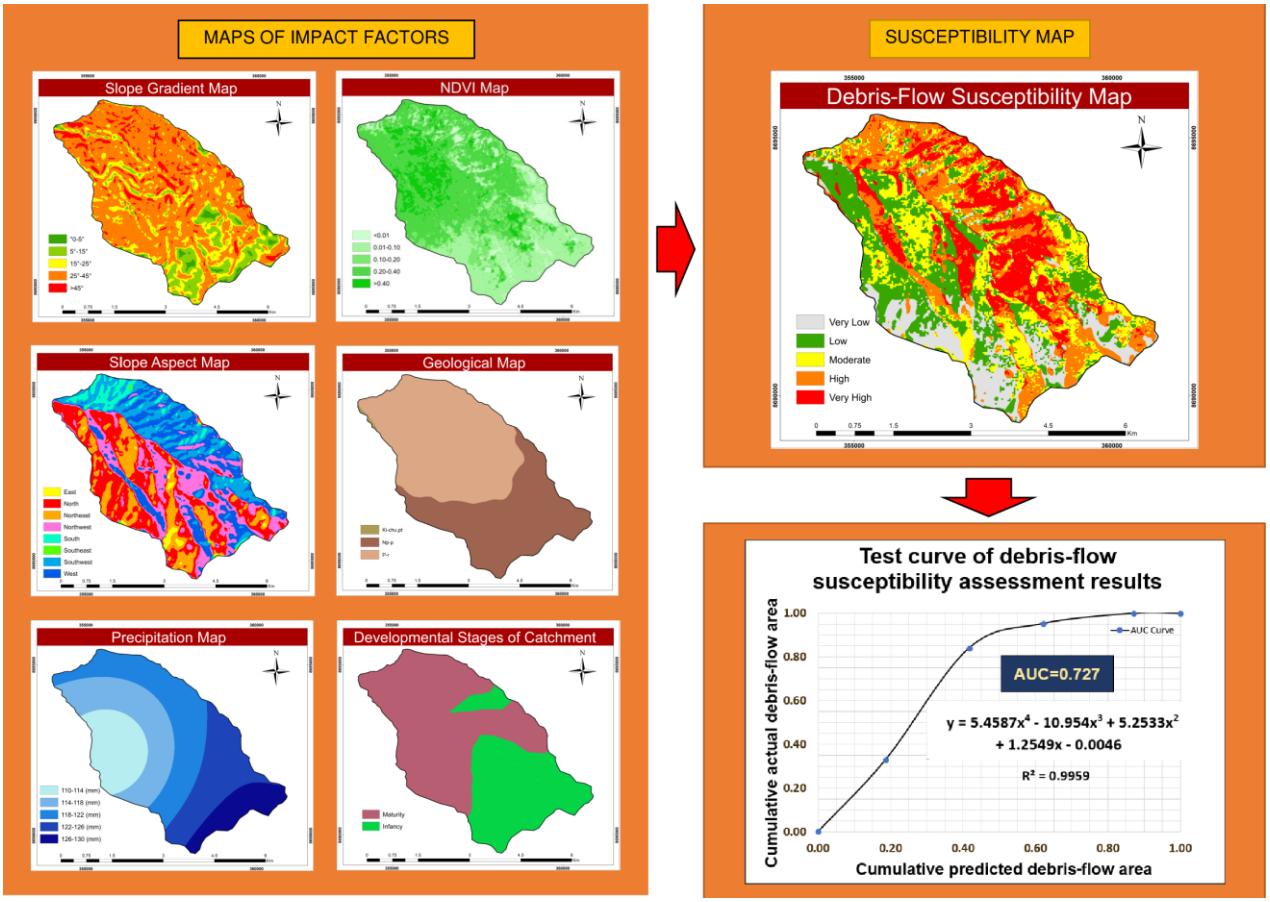

Figure 1: Maps of impact factors, susceptibility map, and cross-validation AUC test.

Finally, the area under the curve (AUC), which assesses the goodness of fit between the actual debris flow and the prediction model, worked out at 0.727.

3 CONCLUSIONS

From the susceptibility zonation results, the extreme and high debris-flow susceptibility areas are mainly distributed in Viso catchment on its right bank. Slope aspect, NDVI, and developmental stages of the Viso catchment are the most dominant factors influencing on debris-flow events after applying the index entropy model. A cross-validation AUC test was performed to assess the accuracy of the model, thus getting an encouraging success rate of debris flow prediction of 72.7%.

References

Chen J., Li Y., Zhou W., Iqbal J., Cui Z. (2017). Debris-flow susceptibility assessment model and its application in semiarid mountainous areas of the southeastern tibetan plateau. *Natural Hazards Review 18*(2), 05016005.

Vlčko J., Wagner P., Rychlikova Z. (1980). Evaluation of regional slope stability. *Mineralia Slovaca 12*(3), 275–283.

Wu S., Chen J., Xu C., Zhou W., Yao L., Yue W., Cui Z. (2020). Susceptibility assessments and validations of debris-flow events in meizoseismal areas: Case study in china's longxi river watershed. *Natural Hazards Review 21*(1), 05019005.

Proceedings of the 1st IAHR
Young Professionals Congress
17-18 November 2020

EXPERIMETNAL STUDY ON TRANSPORT OF MICROPLASTIS IN COASTAL SEDIMENT WITH AN OSCILLATING WATER TUNNEL

Dongwook Hwang [1], Yong Sung Park [*1,2] & Jeongin Kim [1]

[1] Department of Civil and Environmental Engineering, Seoul National University, Seoul, South Korea
[2] Integrated Research Institute of Construction and Environment, Seoul National University, Seoul, South Korea
* Email : dryspark@snu.ac.kr

ABSTRACT

This paper focuses on the characteristics of transport of microplastics in coastal sediment through experiment. For it, it uses a new form of oscillating water tunnel(OWT) with detachable sediment basin. It makes it possible to consider the change of depth of the sediment in high Reynolds number flow. The experiment was designed to turn out how the plastic particles embedded in coastal sediment get transported under wave forcing. After the system is being subjected to the wave forcing, the distribution of the beads is measured. Moreover, the relation between the wave and the seabed is studied by utilizing a particle image velocimetry(PIV) system. As a result, the transport of microplastics is expected to be related to wave forcing, physical properties of the plastic and the sediment particle, and relative depth of plastics within the sediment layer.

Keywords: experimental study, microplastics, oscillating water tunnel, wave forcing, particle image velocimetry

1 INTRODUCTION

Increasing use of plastics due to industrial development has caused serious plastic pollution (PlasticsEurope, 2016). The most of them returns to shores and coastal regions, and are fragmented (Brennan, 2018; Willis, 2017). The plastic debris ranging from 1um to 5mm in size are called 'microplastics'. They are nowadays found prevalent around the world (GESAMP, 2016; G20, 2017). There are lots of needs for the study on how they are going into the ocean, how they interact hydro-dynamically with others, and where and how they are distributed. Although they are regarded as the main destroyer of the marine environment, there is a dearth of the research due to the complex mechanism for transport of these fine and large amount of the plastics interacting with sediment and waves. Therefore, this paper investigates the transport of plastics in coastal sediment, and it will contribute to preventing and managing the marine microplastic pollution. The main goal of this experimental study is to figure out the effects of physical factors in the transport of microplastics in coastal sediment.

2 METHODOLOGY

For the purposes of the study, the experiment has been proceeding using a newly-built oscillating water tunnel equipped with a detachable sediment basin. The Reynolds number based on the maximum free-stream velocity and the maximum displacement of water particle is on the order of $O(10^5)$, which is well within the turbulent regime. It is higher than the 2-D wave basin. Also, the equipment makes it possible to consider the horizontal velocity only.

Prior to start the experiment, we utilize a particle image velocimetry system to assess the equipment. It is to figure out the precise flow velocity and to observe the relation between the wave and the seabed. The system shows the boundary layer flow due to the friction of the seabed. In the system, PIV particle is used with the mixture of two different sizes of $\emptyset 10\ \mu m$ and $\emptyset 20\ \mu m$. The system is conducted on the flat surface without the sediment basin first.

The sediment basin is filled with the mixture of sediment and plastic beads. The beads that have different diameters of $6\ mm$ and $8\ mm$ and four different colors are used as substitutes of plastic debris in the experiment. The sediment in the basin is divided into four sections, and distributions of the beads in each section are measured with different input velocities. Each section has 110 pieces of beads which 100 pieces are in the sediment and others are on the sediment.

3 RESULTS

The analysis of the PIV system shows boundary layer thickness of $1.7\ mm$. The free stream velocity and the wave period are $0.028\ m/s$ and about $0.28 sec$, respectively, in the steady motion with the input velocity of $0.1\ m/s$ and the stroke length of $0.26\ m$.

Figure 1. A shot image of PIV system

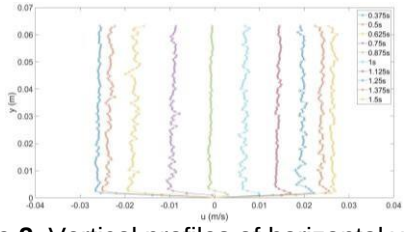

Figure 2. Vertical profiles of horizontal velocity

When the system in the input of $1\ m/s$, the distributions of the beads are indicated in Table 1.

Table 1. A shot image of PIV system

Case1 of $\emptyset 6\ mm$	Red	Blue	White	Yellow	Case2 of $\emptyset 8\ mm$	Red	Blue	White	Yellow
Section ①	53	-	-	-		82	-	-	-
Section ②	-	42	1	-		-	73	-	-
Section ③	-	-	49	52		-	-	74	-
Section ④	-	-	1	16		-	-	-	81
Left	40	38	21	16		25	26	13	6
Right	17	30	38	42		3	11	23	23
Sum	110	110	110	110		110	110	110	110

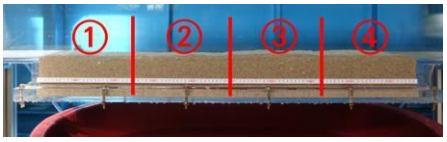

Figure 3. Indication of each section

The $\emptyset 6mm$ beads are more out of the sediment than $\emptyset 8mm$. Also, they move to the both ends of the tunnel as quick as they come out. Within 2 minutes of the start, the beads on the sediment go to the ends.

4 CONCLUSIONS

This paper introduces an experimental study for investigating the transport of microplastics in coastal sediment. It shows initial stages of the experiment. The results of the distributions of the beads indicate the smaller and lighter debris can be come out of the sediment. Also, they move to both and sides of the tunnel. Thus, they microplastics in the coastal and marine environment can travel very far quickly, and the properties of the microplastics is important to their transport movement. For further works, the more various sizes of beads will be dealt and the effects of roughness and bedform of the sediment will be studied.

ACKNOWLEDGEMENTS

This work was supported by the National Research Foundation of Korea (NRF) grant funded by the Korea government (MSIT) (No. NRF-2020R1F1A1070390).

※ MSIT : Ministry of Science and ICT

REFERENCES

Eriksen, M., Lebreton, L.C.M., Carson, H.S., Thiel, M., Moore, C.J., Borerro, J.C., Galgani, F., Ryan, P.G., and Reisser, J. (2014). Plastic pollution in the world's oceans: more than 5 trillion plastic pieces weighing over 250,000 tons afloat at sea. *PloS one,* 9 (12), e111913.

G20 (2017). Annex to G20 Leaders Declaration: G20 Action Plan on Marine Litter. *G20 Summit 2017: Hamburg, Germany (7-8 July), Federal Ministry for the Environment, Nature Conservation, Building and Nuclear Safety,* 7 pp.

GESAMP (2015). Sources, fate and effects of microplastics in the marine environment: a global assessment. *IMO/FAO/UNESCO-IOC/UNIDO/WMO/IAEA/UN/UNEP/UNDP Joint Group of Experts on the Scientific Aspects of Marine Environmental Protection,* Ed. P.J. Kershaw, Rep. Stud. GESAMP, 90, 96 pp.

GESAMP (2016). Sources, fate and effects of microplastics in the marine environment: part two of a global assessment. *IMO/FAO/UNESCO-IOC/UNIDO/WMO/IAEA/UN/UNEP/UNDP Joint Group of Experts on the Scientific Aspects of Marine Environmental Protection,* Ed. P.J. Kershaw and C.M. Rochman, Rep. Stud. GESAMP, 93, 220 pp.

PlasticsEurope (2016). Plastics–the Facts 2016 An analysis of European plastics production, demand and waste data. *Plastics Europe, Association of Plastic Manufacturers Brussels.*

Willis, K., Hardesty, B.D., Kriwoken, L., and Wilcox, C. (2017). Differentiating littering, urban runoff and marine transport as sources of marine debris in coastal and estuarine environments. *Scientific reports*, 7, 44479.

Proceedings of the 1st IAHR
Young Professionals Congress
17-18 November 2020

INFLUENCE OF SURGE WAVE ON CARRYING CAPACITY AND TRANPORT OF MACROPLASTICS

Preet Patel [1], Magdalena Krol [2] & Shooka Karimpour [3]

[1, 2, 3] Department of Civil Engineering, Lassonde School of Engineering, York University, Toronto, Canada,
[1] e-mail Preet26@my.yorku.ca
[2] e-mail Magdalena.krol@lassonde.yorku.ca
[3] e-mail Shooka.karimpour@lassonde.yorku.ca

ABSTRACT

Plastic use has increased steadily over the last few decades which has led to significant plastic production, followed by substantial plastic waste. Rivers and storm events near coastal regions are responsible for transporting millions of tons of plastic waste to marine environments. The coastal transport of plastic wastes is influenced by mixing and turbulent behaviors in surge waves. The plastic debris are transported by breaking bores, which is affected by the surge wave properties including their Froude numbers. Since polyethylene and polypropylene are common pollutants in the marine environment, for this research macro-sized pieces composed of these plastics will be introduced in a surge wave generated in a hydraulic flume. Particle movement will be tracked with multiple Raspberry Pi cameras and their trajectory and velocity will be determined by in-house particle tracking velocimetry (PTV) software.

Keywords: surge waves, coastal plastic waste, macroplastics, turbulence, Froude number.

1 INTRODUCTION

One of the UN Sustainable Development Goals is that “life below water must be a priority since majority of the resources required to sustain a life are regulated by the sea”. Unfortunately, more than a million seabirds and over 100,000 marine mammals are killed due to plastic waste (UNESCO, 2017) as plastics account for 70% (Kornei, 2017) to 80% (Thevenon & Carroll, 2015) of total marine waste. It is estimated that over 90% of plastic produced globally is not recycled (Parker, 2018a). Nearly 50% of global plastic production (359 million tons) comprises of polyethylene (30%) and polypropylene (20%), and therefore polyethylene and polypropylene are also predominant in marine waste (Plastics Europe & EPRO, 2019). Coastal regions are significant contributors of marine plastic waste, and they are responsible for transporting 8.2 million tons of plastic waste each year (Parker, 2018b), similarly, riverine systems can transport 1.15 to 2.41 million tons of plastic waste yearly (Lebreton et al., 2017). Shoaling effects on solitary waves can generate a bore with a steep front in shallow water and a surge on dry bed; this phenomenon can be observed in rivers and narrow waterways. Tidal bores have substantial influence on the river mouth, where debris is suspended due to wave motion and the advected material is transported due to a breaking bore, and as a result bed erosion takes place beneath the bore front (Docherty & Chanson, 2012; Koch & Chanson, 2008). Furthermore, coastal wastes can be transported through mixing induced by breaking waves. In a laboratory setting, bores are generated by sudden closure or removal of a sluice gate. The characteristics of a surge wave, including air entrainment, their turbulent kinetic properties, and transport capacity directly depends on the surge wave Froude number, Fr_s. The motive of this research is to analyze the impact of this most important dimensionless number that dominates surge properties and understand how it affects plastic transport.

2 OBJECTIVE

Abundance, and fate and transport of microplastics and macroplastics have been studied extensively. However, the transport of plastic waste due to surge waves has been mostly overlooked. Since a majority of plastic debris found in the aquatic environment are buoyant with material densities smaller than water, turbulent mixing directly impacts the transport pathways, residence, and accumulation of plastic debris. Breaking surge waves and bores

are highly turbulent phenomena and the turbulent kinetic energy across the wave front impacts the plastic mobilization from coastlines and their transport pathways. These surge properties can be captured using the surge wave Froude number. Therefore the objective of this research is to investigate the impact Fr_s has on surge transport capacity, and the movement of mesoplastics (5 mm – 20 mm) and macroplastics (20 mm – 100 cm) due to mixing patterns in the surge waves' front.

3 METHODOLOGY

Surge waves with various Fr_s will be generated in a GUNT hydraulic flume, by controlling flowrate and bed angle. Plastic spheres made up of polyethylene, polypropylene, and polystyrene (polystyrene were considered to mimic floating debris which have density marginally higher than of water) will be introduced in the flume and their trajectory will be observed using Raspberry Pi cameras. Multiple Raspberry Pi boards will be synchronized to enable simultaneous recording and the data will be analyzed using an in-house particle tracking velocimetry (PTV). PTV is a Lagrangian approach where the focus is on individual particles during the flow. Open-source PTV software (PTVReseach) was tested and optimized using experimental data obtained from an in-house hydraulic flume, Figure 1.

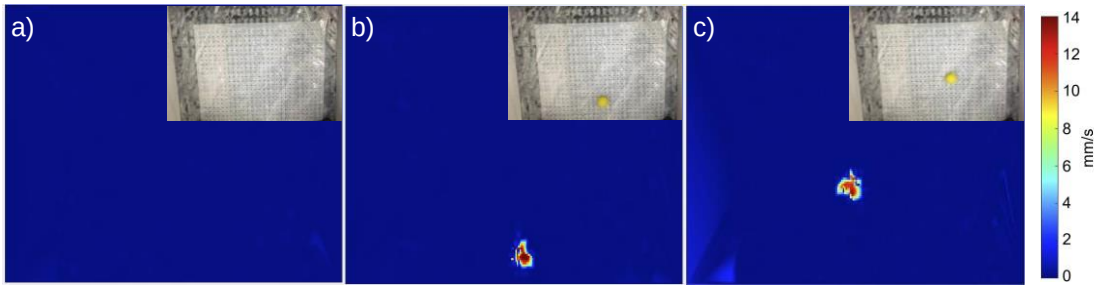

Figure 1. Sequence of frames displaying vector length of a particle in motion. Picture in top right corner shows the unprocessed image. Time, t: a) 0s; b) 0.17s; c) 0.50s

4 ANTICIPATED OUTCOMES AND INITIAL FINDINGS

Exploratory findings may yield new insights and lead to improved mitigation plans to cope with growing plastic pollutions and improve rivers and coastal infrastructures to reduce transport of plastic debris. This research may promote further investigation into transport and mobilization of plastic waste through other pathways.

REFERENCES

Docherty, N. J., & Chanson, H. (2012). *Physical Modeling of Unsteady Turbulence in Breaking Tidal Bores*. *138*(May), 412–419. https://doi.org/10.1061/(ASCE)HY.1943-7900.0000542

Koch, C., & Chanson, H. (2008). Turbulent Mixing beneath an Undular Bore Front. *Journal of Coastal Research*, *244*, 999–1007. https://doi.org/10.2112/06-0688.1

Kornei, K. (2017). *Plastic makes up nearly 70% of all ocean litter*. 10.1126/science.aal0998

Lebreton, L. C. M., Van Der Zwet, J., Damsteeg, J. W., Slat, B., Andrady, A., & Reisser, J. (2017). River plastic emissions to the world's oceans. *Nature Communications*, *8*(June), 1–10. https://doi.org/10.1038/ncomms15611

Parker, L. (2018a). *A whopping 91% of plastic isn't recycled*. National Geographic. https://www.nationalgeographic.com/news/2017/07/plastic-produced-recycling-waste-ocean-trash-debris-environment/#close

Parker, L. (2018b). *Fast facts about plastic pollution*. National Geographic. https://www.nationalgeographic.com/news/2018/05/plastics-facts-infographics-ocean-pollution/

Plastics Europe, & EPRO. (2019). *Plastics - the Facts 2019*. 38. https://www.plasticseurope.org/en/resources/market-data

Thevenon, F., & Carroll, C. (2015). Plastic debris in the ocean: the characterization of marine plastics and their environmental impacts, situation analysis report. In *Plastic debris in the ocean: the characterization of marine plastics and their environmental impacts, situation analysis report*. https://doi.org/10.2305/iucn.ch.2014.03.en

UNESCO. (2017). *Facts and figures on marine pollution*. UNESCO. http://www.unesco.org/new/en/natural-sciences/ioc-oceans/focus-areas/rio-20-ocean/blueprint-for-the-future-we-want/marine-pollution/facts- and-figures-on-marine-pollution/

Proceedings of the 1st IAHR
Young Professionals Congress
17-18 November 2020

BALANCING FLUSHING EFFICIENCY AND DURATION: PROOF OF CONCEPTS

Giulia Stradiotti, Maurizio Tavelli, Giuseppe Roberto Pisaturo, Maurizio Righetti

Free University of Bozen-Bolzano, Bozen-Bolzano, Italy

*Correspondance : gstradiotti@unibz.it

ABSTRACT

Dams interrupt the river continuity, affecting sediment transport. Prevented from going downstream, sediments deposit in the reservoir, which ultimately becomes silted. Not only this deprives rivers of their natural sediment load, but it also causes reservoirs to lose storage and water regulation capacity. Especially in alpine-type reservoirs, sediment flushing is applied as a common management practice to restore the original storage volume. However, from a hydro-power plant standpoint, this results in the periodic loss of energy production. In this work, we compared numerically the sediment flushing carried out in the Rio di Pusteria reservoir (Italy) in May 2019 with alternative flushing scenarios, with the aim of proposing more efficient operations from the manager's perspective. Results show that lower reservoir filling can lead to shorter flushing periods, and to a minor stored water consumption.

Keywords: sediment management, reservoirs, flushing, numerical simulation.

1 INTRODUCTION

Sediment flushing is a widespread practice which aims at restoring the lost capacity in hydro-power reservoirs (Kondolf *et al.* (2014)). However, this management strategy affects the ecosystem downstream of the dam. One key-aspect is the flushing duration, both from a managing and an environmental perspective. As a matter of fact, a longer flushing costs in terms of energy production, and it produces a longer stress on the downstream ecosystem, whose resistance to a disturbance has been linked to the duration of the exposure (Newcombe et Jensen (1996)). In this work, we discuss whether more frequent flushing operations can be overall more efficient compared to fewer but longer flushings.

2 FLUSHING EVENT OF MAY 2019

This study is related to the Rio di Pusteria hydro-power reservoir (Italy), managed by Alperia Greenpower srl, whose original capacity is 1 690 000 m^3. Due to the deposition of silt and sand, it periodically undergoes drawdown flushing. The last flushing took place in May 2019, five years after the previous one (June 2014). The difference between the 2014 after-flushing DEM and the 2019 before-flushing DEM highlighted a deposition of 538 995 m^3 of sediments, equal to a sedimentation rate of 107 799 m^3/year. The deposited sediments were entirely removed by the 2019 flushing [Difference of DEM before-flushing and after-flushing = 580 542 m^3 (V_{ref})]. The end of the flushing, identified as the moment in which the concentration value at the bottom outlets tends to nearly zero-values, was reached in 10 days.

3 MATERIAL AND METHODS

The flushing event carried out in May 2019 was numerically compared with three alternative scenarios with different initial sediment filling in the reservoir: 25%, 50%, 75% of the volume of the sediments in the reservoir before the 2019 flushing, equal to V_{ref} . V_{ref} was set as the reference volume (100%) because it is the volume of sediments flushed at the current flushings periodicity. The comparison was carried out through the 3D version

Scenario	Flushing frequency	Flushing duration	Days of flushing in 10 years	Final stored water
100% 75%	5 years 4 years	10 days 9.5 days	20 days 24 days	~0 m^3 ~200 000 m^3
50%	3 years	7 days	23 days	~400 000 m^3
25%	1 year + 2 years	4.5 days	31.5 days	~500 000 m^3

Table 1: Main features for the different flushing scenarios. In the 25% scenario, flushing is alternated between 1 and 2 years.

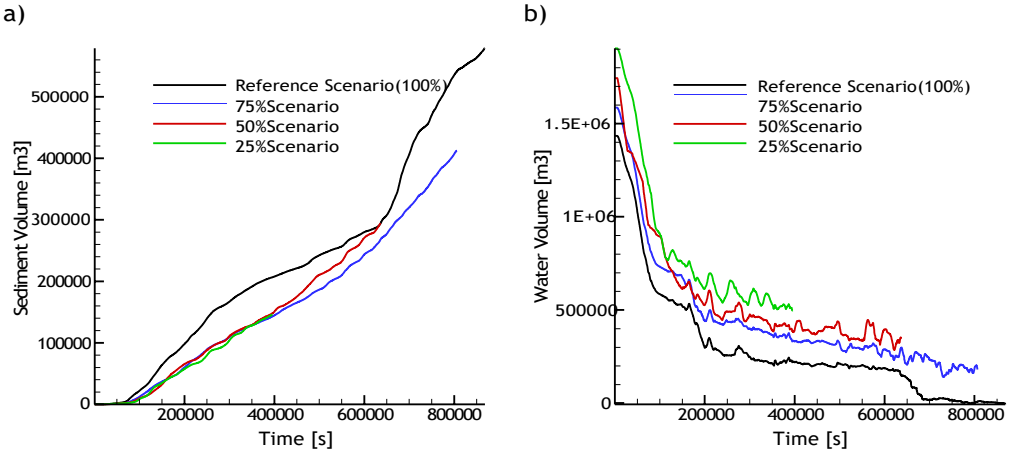

Figure 1: a) Volume of flushed sediments over time. b) Volume of stored water over time.

of a semi-implicit numerical solver of the Navier-Stokes equations (Tavelli *et al.* (2020)).

4 RESULTS

The end of the flushing in the three alternative scenarios was set as the moment in which 25%, 50%, or 75% of the reference sediments volume was flushed. As Figure 1a shows, the relation between the flushing duration and the initial filling level in the reservoir is non-linear. Indeed, a lower filling of sediments in the reservoir implies a higher volume of water and a higher inertia, which slows down the erosion process. Differences in the erosion velocity among the scenarios are also due to the requirement for the mean concentration at the outlet not to exceed 1.5%, for which the bottom gates were temporary closed in the simulations (i.e., the boundary condition for the outlet discharge was set as 0) whenever the value was about to be overcome. However, in all the alternative scenarios the water volume in the reservoir at the end of the flushing is higher (Figure 1b). At the current sedimentation rate, the amount of sediment flushed in the reference scenario accumulates in 5 years, 75% of it accumulates in 4 years, 50% in 2.5 years, and 25% in 1.5 years (Table 1). Therefore, looking at the 10-years framework, the reference scenario is the one that requires the least flushing days (twice per decade, 10 days long each). However, the 50% scenario is really close to it and it allows for a saving of about 25% of the stored water every time. Furthermore, being shorter, it is less stressful for the downstream ecosystem.

5 ACKNOWLEDGEMENTS

This work was supported by the project Sediplan-r (FESR1002). The authors would like to thank Alperia Green-power srl for sharing the data from the flushing operations.

References

Kondolf G. M., Gao Y., Annandale G. W., Morris G. L., Jiang E., Zhang J., Cao Y., Carling P., Fu K., Guo Q., Hotchkiss R., Peteuil C., Sumi T., Wang H.-W., Wang Z., Wei Z., Wu B., Wu C., Yang C. T. (2014). Sustainable sediment management in reservoirs and regulated rivers: Experiences from five continents. *Earth's Future 2*(5), 256–280. doi:10.1002/2013EF000184.

Newcombe C. P., Jensen J. O. (1996). Channel suspended sediment and fisheries: A synthesis for quantitative assessment of risk and impact. *North American Journal of Fisheries Management 16*(4), 693–727. doi:10.1577/1548-8675(1996)016¡0693:CSSAFA¿2.3.CO;2.

Tavelli M., Piccolroaz S., Stradiotti G., Pisaturo G. R., Righetti M. (2020). A new mass-conservative, two-dimensional, semi-implicit numerical scheme for the solution of the navier-stokes equations in gravel bed rivers with erodible fine sediments. *Water 12*(3). doi:10.3390/w12030690.

Proceedings of the 1st IAHR
Young Professionals Congress
17-18 November 2020

EFFICIENCY OF SEDIMENT FLUSHING FOR DIFFERENT SEDIMENT MIXTURES

Sebastián Guillén Ludeña [1], Jorge Toapaxi Álvarez [1, 2] & Luís G. Castillo [1]

[1] Hidr@m group, Department of Mining and Civil Engineering, Universidad Politécnica de Cartagena, Cartagena, Spain
sebastian.guillen@upct.es

[2] Civil and Environmental Engineering Department, Escuela Politécnica Nacional, Ecuador,

ABSTRACT

Sediment flushing has been reported as an efficient measure for reservoir desiltation. However, the efficiency of flushing varies depending on factors such as bed material, initial water head and capacity of dam outlets. This study aims to assess the influence of the initial water head and of the sediment size on the flushing efficiency. Efficiency is defined as the ratio between the volume of sediments evacuated to that of water released. For that purpose, 60 laboratory experiments were conducted in a rectangular flume. Ten pairs $h_s - h_w$ were tested for two different reservoir volumes and for three sands, so-called fine, medium and coarse. h_s and h_w stand for the initial sediment and water elevations, respectively. Measurements consisted in lateral videos to characterize the evolution of the water and bed surfaces during the experiments. The flushing efficiency decrease as h_s decreases and as h_w and V_w increase, irrespective of the sediment size.

Keywords: sediment flushing, flushing efficiency, reservoir sedimentation, sediment management.

1 INTRODUCTION

Sedimentation in reservoirs is a major issue for dam operators and owners. The accumulation of sediments in reservoirs progressively reduces their storage capacity, it alters the sediment balance of the river and, in extreme circumstances, it may block totally or partially the operational structures of the dam (water intakes and bottom outlets) (Annandale et al. 2016, Fan et al. 1992). To prevent and mitigate these negative effects, several techniques can be used to evacuate sediments from reservoirs thought with very different efficiency (Fan et al. 1992).

This study focuses in the sediment flushing technique, which consists in evacuating sediments from the reservoir by emptying it through the bottom outlets. Flushing has been reported as one of the most efficient techniques for reservoir desiltation (Atkinson 1996, Fan et al. 1992), though the efficiency of flushing varies significantly depending on factors such as the geometry of the reservoir, the initial water head, and the sediment properties (Atkinson 1996, Fan et al. 1992). In this context, this study aims to assess the efficiency of sediment flushing for varying initial conditions and for different sediment mixtures. Efficiency is herein defined as the ratio between the volume of sediment evacuated to that of the water released ($\eta = V_s / V_w$). The study is based on the analysis of the results obtained from 60 experiments, conducted in the Hydraulic Laboratory of Universidad Politécnica de Cartagena, Spain.

2 METHODS

The experiments were conducted in a 12.5 m long and 0.30 m wide horizontal rectangular glass flume. To enforce critical flow at the downstream end of the channel, the bottom was elevated 0.15 m along 6 m from the downstream end. Upstream, the flume is equipped with a sluice gate to control the volume of water stored. Downstream, the channel is equipped with a 0.30 m wide tilting gate that allows a sudden opening, and with a sediment trap to collect the sediments evacuated during the experiments. Figure 1 shows a sketch of the experimental facility.

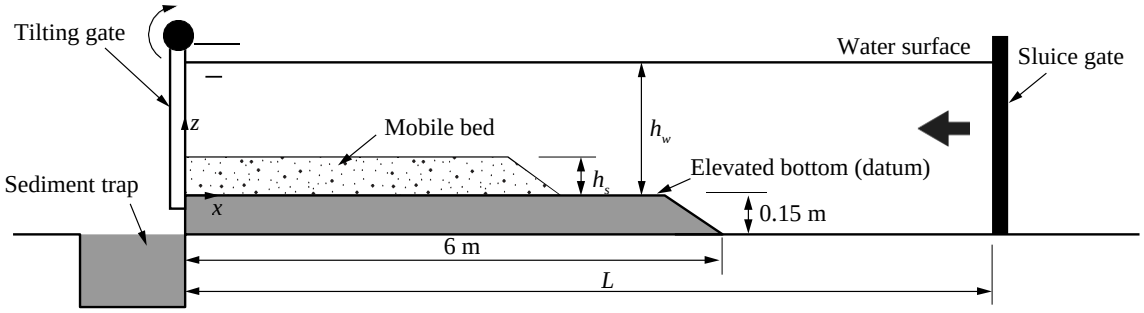

Figure 1. Sketch of the experimental facility (not to scale).

In this experimental setup, three different sands, so called fine (d_{50} = 0.39 mm), medium (d_{50} = 0.80 mm) and coarse (d_{50} = 1.54 mm), were tested. For each sand, 20 experiments were run by covering 10 values of the ratio h_w / h_s (from 1.25 to 5.00) and 2 values of L (6.00 m and 12.05 m). h_w and h_s stand for the initial water head and for the initial sediment height, respectively. The measurements consisted of: i) Lateral videos to characterize the evolution of the bed and water surfaces during the experiments. ii) Discrete monitoring of the water surface by means of ultrasonic limnimeters. iii) Weighing of the sediment evacuated during the experiments.

3 RESULTS

The results show a good correlation between the flushing efficiency and the parameters $h_w \cdot h_s^{-1}$ and $V_w^{1/3} \cdot h_s^{-1}$, which represent the initial potential energy of the reservoir and its inertia, respectively. Figure 2 illustrates that the efficiency decreases as the initial potential energy and the inertia of the reservoir increase, irrespective of the sediment size.

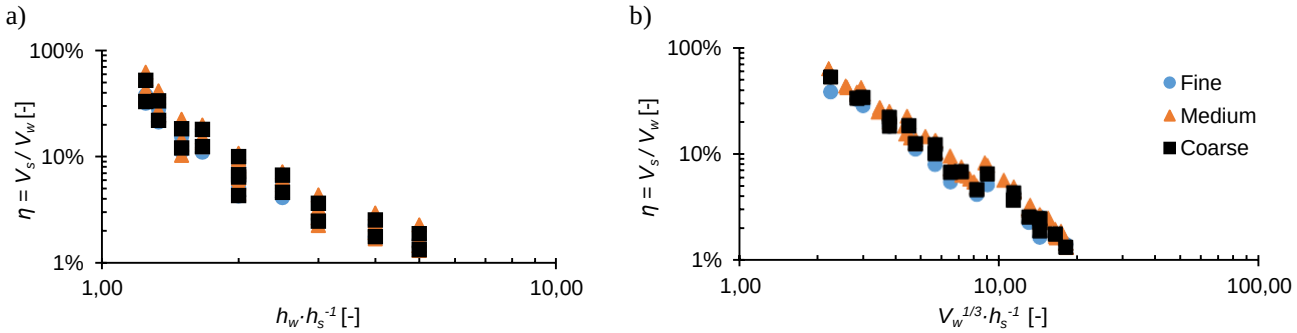

Figure 2. Flushing efficiency for different sands and for varying values of: a) $h_w \cdot h_s^{-1}$, and b) $V_w^{1/3} \cdot h_s^{-1}$

4 CONCLUDING REMARKS

Within the range of values adopted in this study, the influence of variables such as the initial height of sediment and the initial water head on the efficiency of flushing is significant, in comparison to the negligible influence of the sediment size.

ACKNOWLEDGEMENTS

This study is part of the project EFISED (20403/SF/17) funded by the Fundación Séneca from Región de Murcia (Spain). The second author thanks Universidad Politécnica de Cartagena (Spain), Escuela Politécnica Nacional (Ecuador) and Fundación Carolina (Spain) for the financial aids received for his doctoral studies.

REFERENCES

Annandale, G. W., Morris, G. L., & Karki, P. (2016). *Extending the Life of Reservoirs: Sustainable Sediment Management for Dams and Run-of-River Hydropower*. https://doi.org/10.1596/978-1-4648-0838-8

Atkinson, E. (1996). *The feasibility of Flushing Sediment from Reservoirs. Report OD 137*.

Fan, J., & Morris, G. L. (1992). Reservoir Sedimentation. II: Reservoir Desiltation and Long- Term Storage Capacity. *Journal of Hydraulic Engineering*, *118*(3), 370–384. https://doi.org/10.1061/(ASCE)0733-9429(1992)118:3(370)

IAHR AIRH

International Association for Hydro-Environment Engineering and Research

Hosted by
Spain Water and IWHR, China

Session 8

Transient Flows and Hydraulic Machinery

IAHR YPN

Hosted by
Spain Water and IWHR, China

Proceedings of the 1st IAHR
Young Professionals Congress
17-18 November 2020

STUDY OF TURBULENT STRUCTURES AND AIR ENTRAINMENT PATTERNS IN SURGE WAVES

ZHUORAN LI [1], SHOOKA KARIMPOUR [2]

[1,2] York University, Toronto, Canada
e-mail: zli29@my.yorku.ca

ABSTRACT

Surge waves are commonly observed in numerous hydrodynamic events such as dam breaks, tidal bores, and tsunami due to abrupt flow change. The research to-date emphasizes the high turbulence, sharp discontinuity of pressure and velocity, and air entrainment properties of the surge waves. The objective of this study is to investigate the impact of surge Froude number on turbulent mixing and air entrainment patterns. With the numerical tool OpenFOAM, two $k-\varepsilon$ and one Large Eddy Simulation (LES) models are applied to simulate the turbulent breaking wave. Significant difference in flow patterns are observed between three models. Time series of velocity components capture the passage of surge waves and identify maximum fluctuation levels behind surge waves.

Keywords: surge waves, dam break waves, turbulent modelling, air entrainment.

1 INTRODUCTION

The surge waves will form as an abrupt variation that happened to the flow condition (Koch & Chanson, 2009). Surge waves are observed in engineering applications such as hydropower generation, which generates the dam break wave, or for the natural phenomena such as tsunami waves (Li & Chanson, 2018). Commonly, as noted by Li and Chanson (2018), hydrodynamic shocks are observed in the positive surges with the form of discontinuity in pressure and velocity fields, and with the extreme unsteady turbulence involved could bring consequences including sediments advection, contribution to the sediment's origin and contaminants transportation. Hence, understanding the turbulent characteristics of the surge waves is vital to mitigate environmental-related issues such as nutrient and sediment cumulation, habitat damage, debris transport, and ecological balance.

2 KEY LITERATURE REVIEWS AND PROBLEM DEFINITION

There are substantial studies of the turbulent structures in the surge waves such as Koch and Chanson (2009) conducted experiments to measure turbulence across surge wave front. Also, there are studies like Chanson's (2003) measured air entrainment in the surge waves experimentally. However, few papers have coupled between the two. The research aims to study the interconnection between turbulent structures and air entrainment patterns in the surge waves. For the numerical simulation, a volume of fluid method for interface capture by Hirt and Nichols (1981) was utilized in the preliminary dam break wave simulation for the phase profile. The air entrainment model by Hirt (2003), which was transferred to the OpenFOAM by Almeland (2018), was applied in the dam break wave simulation.

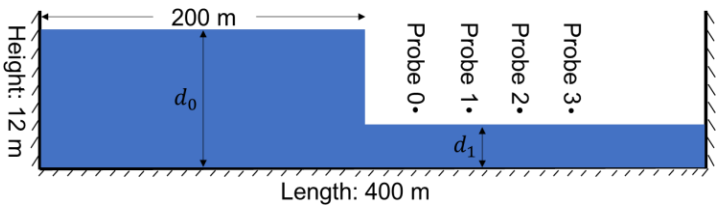

Figure 1. The schematic of the computational domain where the probes are evenly distributed downstream of the gate at every 30 meters, where $d_0 = 10\ m$ and $d_1 = 2\ m$.

3 METHODOLOGY

The simulation started with dam break waves by utilizing the Reynold Average Navier Stokes (RANS) version of "interFoam" solver and $k-\varepsilon$ model for the turbulence without air entrainment function. The interface is captured based on the volume of fluid method which assigns a volume fraction scalar for fully liquid ($\alpha_l = 1$) or gas ($\alpha_l = 0$) and the interface should have $0 < \alpha_l < 1$ (Hirt & Nichols, 1981). The simulated water depth profiles in the preliminary results in dam-break wave analysis were compared with the analytical solution using the Method of Characteristics (MOC), where the effect of bed friction is overlooked. Almeland (2018) developed the interAirEntFoam solver based on the Hirt (2003) method, which states the air entrainment incepts when the turbulent force is greater than the stabilizing force at the surface. The air entrainment is added as a source term in the void fraction equation in the solver.

4 RESULTS

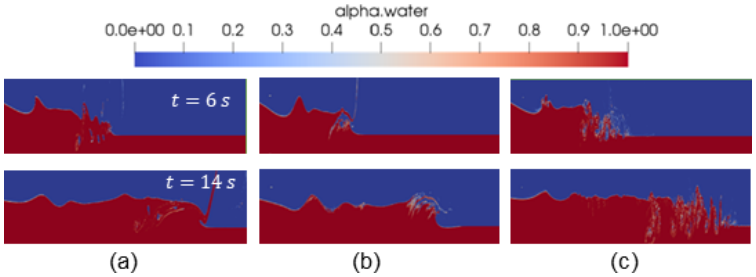

Figure 2. Phase distribution at $t = 6$ and $14\ s$ for surge wave Froude number, $Fr_s = \frac{c}{\sqrt{gd_1}} = 2.12$, where c is surge wave celerity, (a) $k-\varepsilon$ without source, (b) $k-\varepsilon$ with source, (c) LES.

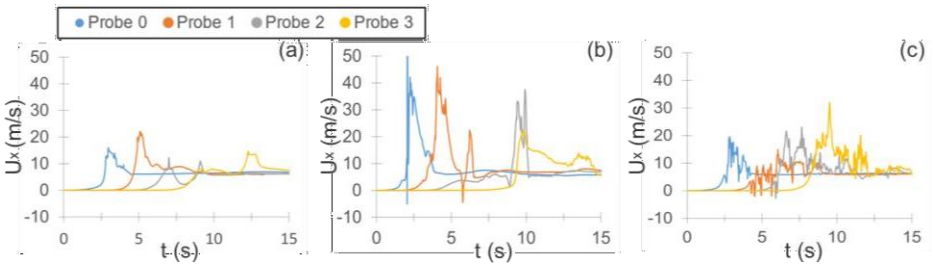

Figure 3. Time series of longitudinal velocity, U_x from $t = 0$ to $15\ s$, $Fr_s = 2.12$, (a) $k-\varepsilon$ without source, (b) $k-\varepsilon$ with source, (c) LES.

5 CONCLUSION

As demonstrated in Figure 2(b), adding the air source term to the $k-\varepsilon$ model, created the entrapment of finer air pockets at the interface. Furthermore, large scale air pockets are observed in Figure 2(a) which are no longer visible with implementation of source term in Figure 2(b). LES model, as it captures larger than grid-scale fluctuations, generates the most air entrainment behind the surge front. $\boldsymbol{U_x}$ plots across points 0 to 3 identify the arrival of surge waves. For point 0 one peak only exists for $\boldsymbol{U_x}$ in all three models, however, for points 1, 2 and 3 a secondary peak appears except for point 1 in model (a). LES model compared to $k-\varepsilon$ generates detailed fluctuations, but follows peak trends observed in $k-\varepsilon$. Adding the air source term, however, significantly impacts the results. Since three models generate different flow patterns, it is essential to validate them with available experimental data and select the most suitable model for the research.

6 REFERENCES

Almeland, S. K. (2018). *Proceedings of CFD with OpenSource Software, 2018, Edited by Nilsson H.* tfd.chalmers. http://dx.doi.org/10.17196/OS_CFD#YEAR_2018.

Chanson, H. (2003). Two-phase flow characteristics of an unsteady dam break wave flow.

Hirt, C. W. (2003). Modeling turbulent entrainment of air at a free surface. *Flow Science, Inc*.

Hirt, C. W., & Nichols, B. D. (1981). Volume of fluid (VOF) method for the dynamics of free boundaries. *Journal of computational physics*, *39*(1), 201-225.

Koch, C., & Chanson, H. (2009). Turbulence measurements in positive surges and bores. *Journal of Hydraulic Research*, *47*(1), 29-40.

Li, Y., & Chanson, H. (2018). Sediment motion beneath surges and bores.

Proceedings of the 1st IAHR
Young Professionals Congress
17-18 November 2020

NUMERICAL MODAL ANALYSIS OF A KAPLAN TURBINE RUNNER

RAFEL ROIG, OSCAR DE LA TORRE, ESTEVE JOU, XAVIER ESCALER

Universitat Politècnica de Catalunya, Barcelona, Spain
e-mail: rafel.roig@upc.edu

ABSTRACT

The aim of the research has been to investigate the change of dynamic behavior of a Kaplan turbine runner when submerged in still water. More specifically, the effects of the added mass on the modes of vibration have been quantified. For that, the modes of vibration of the runner in vacuum, in air and in water have been simulated with a coupled Acoustic-Structural modal analysis and, from their comparison, the reduction of the natural frequencies and the possible changes of the mode shapes have been determined. The results show that the typically assumed invariance of all the mode shapes of a structure when submerged in a dense fluid is not fully accomplished in this particular geometry. And regards to the frequency reduction ratios, they are found to be similar for the first six modes with an average value of about 37%.

Keywords: Kaplan runner, modal analysis, fluid structure interaction, frequency reduction ratio, mode shape.

1 METHODS

Up to now, the prediction of natural frequencies in hydraulic turbines has been performed by considering that the solid surface displacements and the fluid density variations are small, and by using an irrotational flow without mean velocity (J.P. Gauthier *et al.*, 2017; D.S. Braga *et al.*, 2013). Therefore, the use of the acoustic wave equation for pressure coupled to the structural one is deemed valid to carry out the modal analysis of a Kaplan turbine runner based on Equation 1:

$$\left.\begin{matrix}[M_s]\ddot{u} + [K_s]u = [R]p \\ [M_f]\ddot{p} + [K_f]p = -\rho[R]^T\ddot{u}\end{matrix}\right\} \quad [1]$$

where $[M_s]$ and $[M_f]$ are the structural and fluid mass matrices, respectively, $[K_s]$ and $[K_f]$ are the structural and fluid stiffness matrices, respectively, $[R]$ is the coupling matrix, p is the pressure, ρ is the density and u is the structural displacement.

The frequency reduction radio (FRR) between the natural frequencies of the structure in vacuum and in water has been computed using the Equation 2:

$$\text{FRR}\ (\%) = \frac{W_v - W_w}{W_v} 100 \quad [2]$$

where W_v is the natural frequency of the structure in vacuum and W_w in water.

The Modal Assurance Criterion (MAC) has been used to compare the modal vectors between the runner in vacuum, in air and in water (M. Pastor *et al.*, 2012) as defined by Equation 3:

$$\text{MAC}\ (\text{r},\text{q}) = \frac{|\{V_r\}^T\{V_q\}|^2}{(\{V_r\}^T\{V_r\})\ (\{V_q\}^T\{V_q\})} \quad [3]$$

where $\{V_r\}$ is the mode shape of the structure in vacuum and $\{V_q\}$ in air or water. The MAC can take a value between 0 and 1, with values larger than 0,9 indicating a consistent correspondence between two mode shapes, whereas small values suggest a poor resemblance between them.

2 RESULTS

In Table 1, the frequencies of the first six bending modes of the runner blades in vacuum, in air and in water are listed along with the FRRs between the frequencies in vacuum and water. Others studies which also investigated

the FRRs of the first bending mode of a Kaplan runner blade showed values ranging from 40 to 50 % (V.P. Zolotarevich *et al.*, 2017; J.P. Vialle *et al.*, 2008; M. Zhang *et al.*, 2019). The dispersion between results steam from the fact that the added mass depends on multiple factors such as geometry, dimensions, blade-hub assembly or nearby boundary conditions, which makes comparisons complicated.

Table 1. Runner natural frequencies in vacuum, air and water, and corresponding FRRs.

	Natural Frequency (Hz)			
Mode	**Vacuum**	**Air**	**Water**	**FRR(%)**
M1	1081	1081	736	32
M2	1257	1257	768	39
M3	1262	1261	775	39
M4	1269	1268	779	39
M5	1280	1279	833	35
M6	1285	1284	836	35

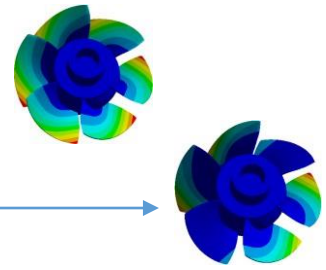

Despite of the common assumption that the mode shapes are invariant between structures in vacuum and water, it seems that this correlation is lost for complex structures which are submerged in a heavy fluid such as a Kaplan turbine runner.

Table 2 shows the MAC values for the vibration modes obtained by the numerical modal analysis of the present geometry. It can be observed that they are exactly 1 between vacuum and air, as expected, but they are significantly lower between vacuum and water, specially for *M6*.

Table 2. MAC values between mode shapes: vacuum-water and vacuum-air.

		Water					
		M1	*M2*	*M3*	*M4*	*M5*	*M6*
Vacuum	*M1*	0,8	0,7	0,7	0,6	0,7	0,6
	M2	0,5	0,9	0,4	0,2	0,3	0,2
	M3	0,9	0,8	0,9	0,3	0,7	0,3
	M4	0,5	0,4	0,6	0,8	0,6	0,3
	M5	0,8	0,5	0,9	0,4	0,8	0,3
	M6	0,3	0,4	0,3	0,7	0,3	0,4

		Air					
		M1	*M2*	*M3*	*M4*	*M5*	*M6*
Vacuum	*M1*	1	0,5	0,8	0,7	0,7	0,6
	M2	0,5	1	0,6	0,2	0,3	0,3
	M3	0,8	0,6	1	0,6	0,8	0,3
	M4	0,7	0,2	0,6	1	0,7	0,5
	M5	0,7	0,3	0,7	0,7	1	0,2
	M6	0,6	0,4	0,4	0,5	0,2	1

3 CONCLUSIONS

It has been found that the FRRs of a Kaplan turbine runner are slightly lower than the values provided by other authors, which might be attributed to the high sensitivity of the estimates to several factors such as the boundary conditions. With regards to the mode shape invariance which is generally assumed, it is shown in our particular case that the modes shapes when submerged in water are slightly different than the ones in vacuum, and specially for the highest order mode considered in the present study.

Acknowledgments

This project has received funding from the European Union's Horizon 2020 research and innovation programme under grant agreement No 814958. The authors also wish to acknowledge Vattenfall for the support.

REFERENCES

Braga, D.S., Coelho, D.F., Soeiro, N.S., Melo, G.S.V., Mesquita, A.L.A., 2013. Numerical simulation of fluid added mass effect on a Kaplan turbine runner with experimental validation. 22nd International Congress of Mechanical Engineering, Ribeirao Petro, Brazi, Nov. 3-7.

Gauthier, J.P., Giroux, A.M., Etienne, S., Gosselin, F.P., 2017. A numerical method for the determination of flow-induced damping in hydroelectric turbines. *J. Fluids Struct,* 69 (2017), 341-354.

Pastor, M., Binda, M., Harcarik, T., 2012. Modal Assurance Criterion. *Procedia Engineering,* 48 (2012), 543-548.

Vialle, J.P., Lowys, P.Y., Dompierre, F., Sabourin, M., 2008. Prediction of natural frequencies in water–Application to Kaplan runner. HydroVision, Sacramento, USA, Jul. 14-18.

Zhang, M., 2019. On the changes in dynamic behavior produced by the hydraulic turbine runner damage. PhD Thesis, Polytechnic University of Catalonia, Barcelona, Spain.

Zolotarevich, V.P., Salienko, A.E., Frumen, A.I., Yugov, N.V., 2017. Numerical and Experimental research of natural frequencies and mode shapes for runner of Francis turbine. P. Struct. Inte., 6 (2017, 224-227.

Proceedings of the 1st IAHR
Young Professionals Congress
17-18 November 2020

TSNet: Transient Simulation in Water Networks

Lu Xing[*1] **and Lina Sela**[1]

[1]Department of Civil, Architectural and Environmental Engineering, The University of Texas at Austin, Austin, United States

*Correspondance : xinglu@utexas.edu

ABSTRACT

Hydraulic modeling of pressure transients in water distribution networks (WDNs) has shown increasing promises in various applications, such as WDN design, fault detection, and risk assessment. To facilitate the integration of transient simulation in these simulation-based applications, this paper contributes the first, general, and open-source implementation of transient simulation software: Transient Simulation in water Networks (TSNet). TSNet is a Python package with the following capacities: (1) read EPANET INP files and establish initial conditions, (2) perform transient simulations under various conditions, i.e., valve and pump operations, leaks, and bursts, with and without surge protection devices, and (3) obtain, visualize, and post-process results. TSNet not only provides transparency needed by the research community, but also presents a platform where users and developers can further develop, improve and extend the existing transient model. This paper presents the capabilities of TSNet, an example application, and additional resources for TSNet.

Keywords: transient simulation; open-source software; Python; water distribution networks

1 INTRODUCTION

Aging infrastructure and growing water demand have imposed increasing challenges on the performance of water distribution networks (WDNs) to secure safe and reliable water supply. Facing with these challenges, various methods have been proposed to assess the pipeline conditions and detect anomalies (Xu et Karney, 2017). Model-based technique, exploiting the hydraulic behavior of WDNs, is one of the most popular approaches for tackling the problem of pipeline condition assessment and anomaly detection owing to its cost-efficiency and non-intrusiveness (Rajani et Kleiner, 2001). The core drivers of these model-based techniques are hydraulic models, including steady-state (Rossman *et al.*, 2000) and transient models (Wood *et al.*, 2005). Transient-based models are generally believed to be superior to steady-state models because a considerable amount of information about the state of the WDN can be revealed within a very short period of time as the transient wave travels rapidly through the pipe at wave speed (Xu et Karney, 2017).

The extensive transient-based applications, including system design, condition assessment, and anomaly detection, require efficient and accurate hydraulic transient simulation tools as core drivers. However, the lack of freely available, openly accessible, and easily interactive software impedes the applications of transient-based methods to complex pipe networks. As results, the previous transient-based applications are largely restricted to pipe segments, such as reservoir-pipeline-valve systems, and small networks of simple typologies. Although a number of commercial software exists for transient simulation in WDNs, such as Hammer (HAMMER, Bentley, 2019), Pipe 2018 (KyPipe, LLC, 2019), and InfoSurge (Innovyze, 2019), the use of these software for research purpose is limited. Ultimately, there is a clear gap between the currently available transient simulation capacities and ever growing demand in the flexibility, accessibility of transient simulation tools. Hence, the authors are motivated to develop an open-source package rendering easiness for interaction, modification, and extension of transient modeling and simulation. The Transient Simulation for water Networks (TSNet) is a Python package designed to (1) provide users with open source Python code for simulating transients in WDNs that can be integrated with other case specific applications, and (2) encourage users and developers to further develop and extend the current transient model.

2 PACKAGE CAPACITIES

TSNet, as a Python package for transient simulation in WDNs, is available in Python Package Index (PyPI). All source codes can be downloaded from the GitHub repository at https://github.com/glorialulu/TSNet. The online documentation, including detailed descriptions of the numerical scheme, installation instructions, setting-up and performing transient simulation, getting simulation results, and modeling conventions and limitations, are available at https://tsnet.readthedocs.io. The major capacities of the package includes: (1) read directly from an EPANET formatted water network model input file and create the corresponding transient model; (2) set up transient models by define transient-related features such as wave speed and time step; (3) define operational changes in valves and pumps as well as background leaks and pipe bursts; (4) perform transient simulation using method of characteristics (MOC) (Wylie *et al.*, 1993); (5) model open and closed surge tanks; and (6) obtain and visualize flow and pressure results.

3 APPLICATION AND RESULTS

The example application in this section demonstrates the multiple capabilities of TSNet Python package on an example network, which comprises 126 junctions, 1 reservoirs, 2 tanks, 168 pipes, 2 pumps, and 8 valves, as depicted in Figure 1. Wave speed for all pipes are set to be 1200m/s. Four scenarios (S1, S2, S3, and S4) were set up: S1 simulates pipe burst at Junction 73, which starts at 1s and takes 1s to fully develop to the final burst coefficient of $0.01 m^3/s/(mH_2O)^{0.5}$; S2 models the linear closure of Valve-1 within 1s; S3 predicts the impacts of PUMP-1 linear shut-off within 2s; and S4 simulates the background leak at Junction-20 with leak coefficient of $0.01 m^3/s/(mH_2O)^{0.5}$. The results of the four scenarios were reported at the chosen junctions, as by black dots, and presented in Figure 1, where pressure transients of different shapes and amplitudes can be observed.

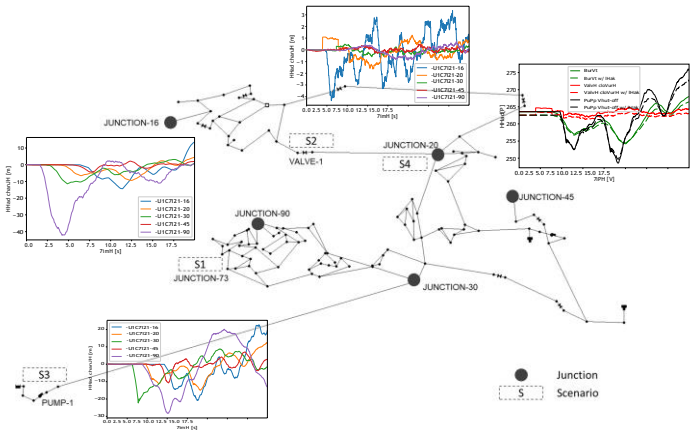

Figure 1: Example network for demonstrating TSNet usage and the results for four example scenarios.

The results of this example application demonstrate the simulation capacities of TSNet. More examples as well as all source codes, software documentation, example codes and networks, and contacting information for reporting bugs and questions are included in the GitHub repository (https://github.com/glorialulu/TSNet).

References

HAMMER, Bentley (2019). *Water Hammer and Transient Analysos Software*. URL: https://www.bentley.com/en/products/product-line/hydraulics-and-hydrology-software/hammer.

Innovyze (2019). *InfoSurge - User Giude*. URL: https://www.innovyze.com/en-us/products/infowater/infosurge.

KyPipe, LLC (2019). *Pipe 2018 Users Guide*. URL: http://kypipe.com/.

Rajani B., Kleiner Y. (2001). Comprehensive review of structural deterioration of water mains: physically based models. *Urban water 3*(3), 151–164.

Rossman L. A., *et al.* (2000). Epanet 2: users manual.

Wood D. J., Lingireddy S., Boulos P. F., Karney B. W., McPherson D. L. (2005). Numerical methods for modeling transient flow in distribution systems. *Journal-American Water Works Association 97* (7), 104–115.

Wylie E. B., Streeter V. L., Suo L. (1993). *Fluid transients in systems*, Volume 1. Prentice Hall Englewood Cliffs, NJ.

Xu X., Karney B. (2017). An overview of transient fault detection techniques. In *Modeling and monitoring of pipelines and networks*, pp. 13–37. Springer.

Proceedings of the 1st IAHR
Young Professionals Congress
17-18 November 2020

CHASING TRANSIENTS IN A WATER TRANSMISSION MAIN IN MILAN, ITALY

Caterina Capponi [1], Francesco Montoro [2], Massimo Chignola [3], Filomena Maietta [4], Bruno Brunone [5] & Silvia Meniconi [6]

[1,4, 5, 6] The University of Perugia, Perugia, Italy,
caterina.capponi@unipg.it, filomena.maietta@studenti.unipg.it, bruno.brunone@unipg.it, silvia.meniconi@unipg.it

[2,3] Gruppo CAP, Milan, Italy
francesco.montoro@gruppocap.it, massimo.chignola@gruppocap.it

ABSTRACT

Hydraulic transients can be due to different causes, such as pump switchings, customer demand changes, maneuvers on valves. They, in turn, may cause bursts and breaks in water supply systems. The Dorsale transmission main (TMs) in the north east of Milan, Italy, has been monitored during the night at two measurement sections with a high frequency rate, that allowed to detect transients with different characteristics. The data presented in this paper show the importance of monitoring towards a better management of TMs in order to reduce leakages and bursts.

Keywords: transients, monitoring, transmission mains, field tests, frequency rate.

1 INTRODUCTION

Hydraulic transients in water supply systems are an issue that in the last few years gained interest among water utilities. In fact, they are a constant presence in networks – as a result of customer demands, pump switching on and off, maneuvers on valves etc. (Meniconi et al., 2014; Mc Innis and Karney, 1995; Morris, 1967) – and they may cause bursts and breaks in pipelines. Monitoring networks and detecting transients can lead to a better management of the water supply systems and to a reduction of leakage and bursts, with a consequent reduction of all the inconvenience related to such phenomena. One of the crucial features of monitoring with the aim of detecting transients is the pressure acquisition rate (Rathnayaka et al., 2016), that must be high enough to capture rapid pressure variations. Such a feature is not ensured by the remote-control systems that the managers are equipped with.

In this paper, data from a field measurement campaign executed on the Dorsale transmission main (TM) in the north east of Milan, Italy, managed by CAP Holding SpA, are presented. Such measurements have been carried out during the night with an acquisition rate of 2048 Hz and reveal the presence of several transients.

2 FIELD MEASUREMENTS

The Dorsale TM connects the Pozzuolo Martesana well-field (WF) to a rising main (RM) that pumps water to a reservoir. It mainly consists of cast iron pipes (alternated with relatively short iron pipes) of three different nominal diameters: DN 800 for a length, L, of about 11666.08 m from the WF, DN 700 (L = 2571.67 m) and DN 600 (L = 1353.8 m), for a total length of about 15591.55 m. Between the WF and the RM there are seven active branches and two inactive ones, consisting of pipes of different materials and diameters. The operating pressure is between 8 and 10 bar, whereas the steady-state discharge is between 100 and 200 L/s. Two data-loggers have been placed at the WF and at the RM, with an elevation of 125.5 m a.s.l. and 195.58 m a.s.l., respectively. Such acquisition systems are equipped with a GPS antenna that allows the data synchronization even at several kilometers of distance.

As an example, the pressure signal, H, acquired between midnight and 1 a.m. on December 5, 2019 at the two measurement sections is shown in Fig. 1. It is evident the presence of several rapid pressure variations with a significant magnitude, especially at the WF section. For example, it is worthy of note that at 00:23 only one of the four pumps at the WF was operating and it has been switched off, generating a very large pressure variation of about 42 m. Then, at about 00:28, one pump has been switched on again. It can be observed that the magnitude of the other pressure oscillations registered at the WF section ranges between 15 and 20 m. On the

contrary, at the RM section, the pressure variations are smaller (around 4-5 m), but more numerous with respect to the WF section, and are characterized but a sort of periodicity. This is due to the fact that at RM four variable speed pumps are installed and the inverter effect reflects on the pressure signal.

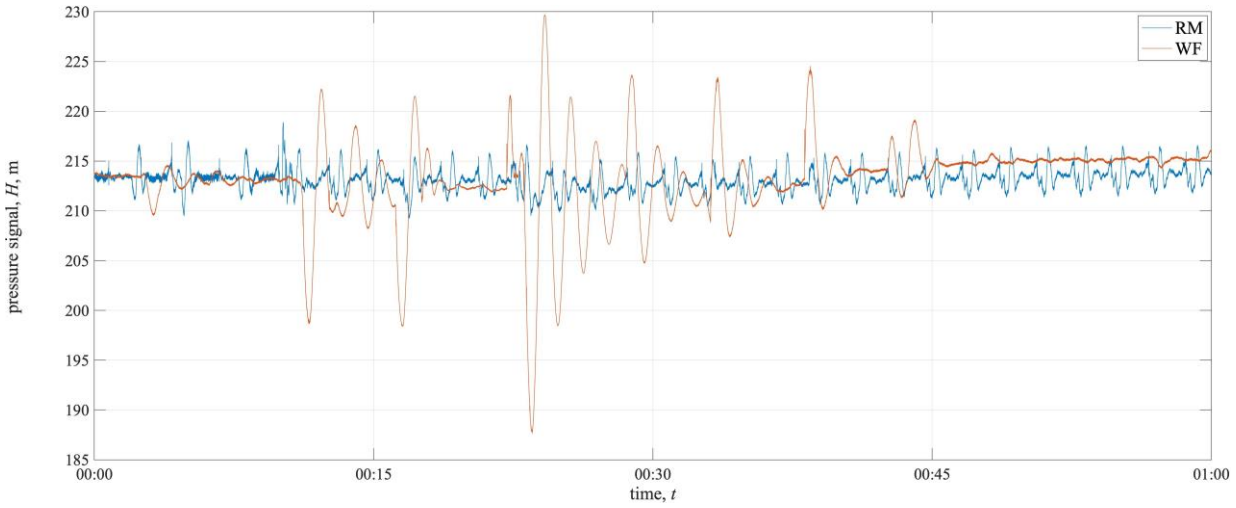

Figure 1. Pressure signal, *H (t)*, acquired at RM and WF sections between 00:00 and 01:00 a.m.

3 CONCLUSIONS

Data acquired synchronously with an acquisition rate of 2048 Hz at two measurement sections of the Dorsale transmission main in the north east of Milan, Italy have been shown. Within one hour of acquisition during the night, several transients have been detected and they can be distinguished in two types. On one hand, few transients due to the pump switching on and off at the Pozzuolo Martesana well-field, with large pressure variations (up to more than 40 m); on the other hand more numerous transients during the same time period, but with smaller variations and a repeated pattern, associated to the effect of the inverter installed at the rising main. Both types of transients can be potentially dangerous for the water system and surely need to be investigated by means of more field measurements and data analyses. For the first type of transients, further measurements in other sections would allow studying the propagation of the water hammer phenomenon in the network. For the second type of transients, the next step is the monitoring of stresses and strains over long periods of time in some critical points and their analysis by means of both time- and frequency-domain tools.

ACKNOWLEDGEMENTS

This research has been funded by the Hong Kong (HK) Research Grant Council Theme-Based Research Scheme and the HK University of Science and Technology (HKUST) under the project “Smart Urban Water Supply System” (Smart UWSS).

REFERENCES

Mc Innis D. and Karney B. W. (1995). Transients in distribution networks: field tests and demand models, *J. of Hydraulic Engineering*, 121(3), 218–231.

Meniconi, S., Brunone, B., Ferrante, M., Capponi, C., Carrettini, C.A., Chiesa, C., Segalini, D., and Lanfranchi, E.A. (2014). Anomaly pre-localization in distribution–transmission mains by pump trip: preliminary field tests in the Milan pipe system, Journal of Hydroinformatics, 17(3), 377–389.

Morris R. E. (1967). Principal causes and remedies of water main breaks, *J. American Water Works Association*, 59(7), 782–798.

Rathnayaka, S., Shannon, B., Rajeev, P., & Kodikara, J. (2016). Monitoring of pressure transients in water supply networks. *Water Resources Management*, 30(2), 471-485.

Proceedings of the 1st IAHR
Young Professionals Congress
17-18 November 2020

A PRELIMINARY LOW-FREQUENCY PRESSURE ANALYIS TOWARDS HIGH-FREQUENCY TRANSIENTS MONITORING IN THE PADUA WATER DISTRIBUTION SYSTEM

Andrea Rubin[1], Lorenzo Tirello[2], Caterina Capponi[3], Filomena Maietta[4], Silvia Favaro[5], Bruno Brunone[6] & Silvia Meniconi[7]

[1,2,5] AcegasApsAmga, Hera Group, Padua, Italy,
ARubin@acegasapsamga.it, ltirello@acegasapsamga.it, SFavaro@acegasapsamga.it
[3,4,6,7] The University of Perugia, Perugia, Italy,
caterina.capponi@unipg.it, filomena.maietta@studenti.unipg.it, bruno.brunone@unipg.it, silvia.meniconi@unipg.it

ABSTRACT

The water distribution system (WDS) of Padua, Italy, is a complex network of 1,246 km of pipes. In order to control and improve the efficiency of such a system, recently, AcegasApsAmga, the Padua water utility company, started monitoring transients. A preliminary analysis of the available pressure measurements provided by the existing remote-control system has been executed. These measurements, with a time step of 15 minutes, allows pointing out the most critical areas of the WDS, i.e., the ones exposed to the most severe pressurevariations.

Keywords: field tests, water distribution system, transients, monitoring.

1 INTRODUCTION

In Italy and worldwide, Water Distribution Systems (WDSs) are affected by several deficiencies leading to low level of service both from a quantitative and qualitative point of view. Particularly, in Italy WDSs are quite aged, with a very high average level of water leakage – approximately 41.9% of input water volume being dispersed (ARERA, 2017)**.** Transients are one of the key loads that act on the WDSs and contribute to the occurrence of leaks (e.g., Karney and Mc Innis, 1990). They are not only caused by an accidental pipe rupture due to external forces or power failure in a pumping station, but also by the normal variation in the drinking water demand patterns that trigger pump operations and valve manipulations (e.g., Marsili et al., 2020). In this paper, low-frequency pressure measurements, acquired by the manager in the network of Padua (Italy) within the remote-control system, are used to locate the areas of the network mainly exposed to the most severe pressure variations. Based on this preliminary study, it is possible to make decisions on where to put high-frequency mobile dataloggers to monitor transients in the system.

2 MATERIALS AND METHODS

The WDS of Padua, managed by AcegasApsAmga (Hera Group), has a total length of 1,246 km, five pumping stations with surge tanks and six storage tanks, with a total number of consumers of 290,000. The pipe diameter ranges from DN700 to DN50 (indicated with different colors and thickness in Figure 1), whereas material differs between steel, asbestos cement and polyethylene. The supply system has three transmission mains: a free surface concrete channel installed in 1890, a DN900 diameter concrete main, installed in 1958, and a steel line with a diameter DN1300, installed in 2000. All these mains convey water to three main pumping stations: Brentelle, Montà and Codalunga (Figure 1). From 2009, Padua WDS is divided into a series of District Metered Areas (DMAs), in order to keep the water loss level monitored and under control, and reduce the water pressure when consumptions are low. For this reason, the WDS has several permanent pressure measurement sections, indicated by white labels in Figure 1, with a time step of 15 min. In accordance to previous research in this area (e.g., Rathnayaka et al., 2016), the minimum acceptable value of the frequency acquisition is 20 Hz, much larger than that of the remote-control system. As a consequence, to measure pressure transients in the network properly and then to understand and localize their causes, a synchronized acquisition of pressure at high-frequency in some sections of the WDS is necessary. However, in this paper, the available low frequency data are preliminary analysed in details to guide and orient the main objective of the study: to measure the magnitude of pressure transients that occur in the Padua WDS due to various operational scenarios and understand the dynamics of the system.

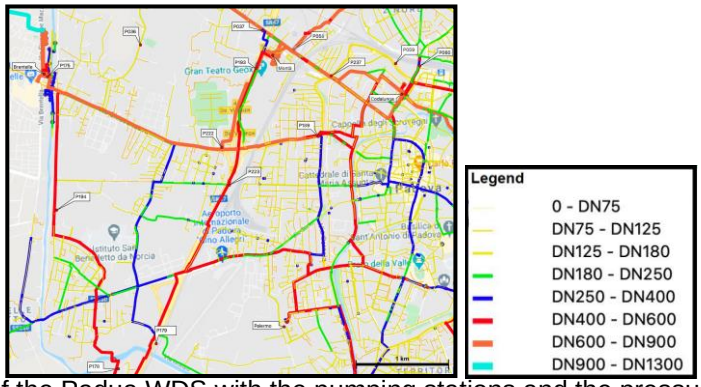

Figure 1. The west part of the Padua WDS with the pumping stations and the pressure measurement sections highlighted.

3 RESULTS

As an example, Figure 2a shows the pressure signals acquired on a normal (i.e., with no uncommon maneuvers executed) midweek day (July 15 2020) by the remote-control pressure sensors highlighted in Figure 1. The behavior of all the acquired pressure signals is extremely similar, with a maximum pressure value at about 7:15 and a minimum value at 14:30, even if they happen in very different pipe sections in an area of about 3 x 4 km. The histogram analysis of the pressure variations provides some insight into transient behavior in these sites, as reported in Figure 2b. The most severe pressure variations happen at the following sites: P036, P037, P058, P175, P193. Specifically, the measurement section P175 is located immediately downstream of the Brentelle pumping station in a steel DN700 pipe. Equivalently, sections P058, P193 (in two steel DN600 pipes), and P037 (in a HDPE DN315 pipe), are located downstream of the Montà pumping station. In addition, the P036 point shows quite large and stable pressure fluctuations, even if it is located in a residential area in a small plastic pipe (HDPE, DN160). Accordingly, such an area should be analyzed in a deeper detail.

As expected, the preliminary analysis of the low-frequency pressure measurements confirms that high-frequency measurements are needed to better understand the transient response of the systems. Moreover, they point out in which sites the high-frequency mobile data loggers should be preferably installed.

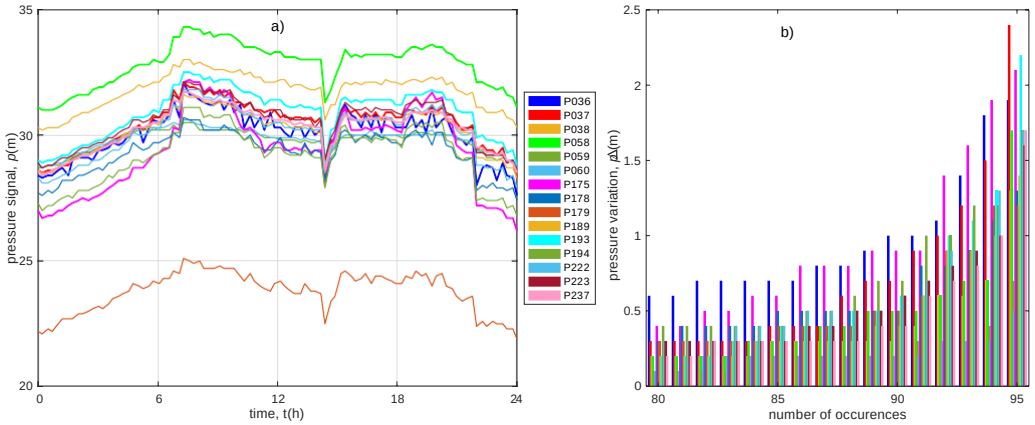

Figure 2. Pressure signals and histograms of head change rates for the measurement sections indicated in Figure 1.

ACKNOWLEDGEMENTS

This research has been funded in part by the Hong Kong (HK) Research Grant Council Theme-Based Research Scheme and the HK University of Science and Technology (HKUST) under the project “Smart Urban Water Supply System” (Smart UWSS).

REFERENCES

Italian Authority for Electric Energy, Gas, and Integrated Water Service (ARERA), 2017, Delibera 27 dicembre 2017 (917/2017/R/idr), Regolazione della qualità tecnica del servizio idrico integrato ovvero di ciascuno dei singoli servizi che lo compongono (in Italian).

Karney, B. W., and McInnis, D. (1990). Transient analysis of water distribution systems. *J. of the American Water Works Association*, *82*(7), 62–70.

Marsili, V., Meniconi, S., Alvisi, S., Brunone, B., and Franchini, M. (on print). Experimental analysis of the water consumption effect on the dynamic behaviour of a real pipe network. *J. of Hydraulic Research*.

Rathnayaka, S., Shannon, B., Rajeev, P., and J. Kodikara (2016). Monitoring of pressure transients in water supply networks. *Water Resources Management,* 30, 471–485.

Proceedings of the 1st IAHR
Young Professionals Congress
17-18 November 2020

UNSTEADY FRICTION COMPUTATION IN COMMERCIAL HYDRAULIC SOFTWARE

Omar M. Abdeldayem[1], David Ferràs[1], Sam van der Zwan[2] & Maria Kennedy[1]

[1]Department of Environmental Engineering and Water Technology, IHE Delft Institute for Water Education, Westvest 7, 2611 AX Delft, the Netherlands.

[2]Department Hydraulics for Infrastructure and Industry, Deltares, Delft, Netherlands.
Email: Omar.abdeldayem94@gmail.com

ABSTRACT

Up to date, transient analysis methods are mainly theoretical, and their implementation to real engineering problems is constrained due to several physical phenomena not accounted for, such as unsteady friction. This study investigated the behavior of different unsteady friction models in Python environment. The models have been compared based on well-developed criteria to be implemented in WANDA commercial software. Vítkovský's unsteady friction model was found to be the fittest one to be implemented in WANDA. The upgraded WANDA version was then tested on a simple hydraulic network. The newly implemented Vítkovský's friction model has significantly influenced the damping over the conventional quasi-steady friction.

Keywords: Transient analysis, unsteady friction, water hammer, WANDA

1 INTRODUCTION

Inverse transient analysis (ITA) offers the possibility of leak pinpointing from the perspective of a software-based approach, and it is now becoming an emerging technique for leakage detection. Even though this technique is well-defined in research papers, it is not yet adequately implemented in commercial software due to several fundamental aspects and assumptions used in the transient solvers (Lin and Yeh, 2019). Most hydraulic transient commercial software use steady friction in their computation, which might be valid for basic water-hammer analyses but not for complex analyses like transient based leakage detection techniques (Abdulshaheed et al., 2017). Hence, implementation of unsteady friction for transient events is mandatory to enhance the aptitudes of commercial software.

WANDA is a hydraulic based model software developed by Deltares which performs hydraulic analyses for steady and unsteady flow conditions in water networks. For transient analysis purposes, WANDA can be used to execute efficiently tasks that are dependent on the maximum pressure wave. However, the later pressure history is poorly simulated. This problem arises from the fact that WANDA relies on steady friction computation. This study aims to update the current transient solver in WANDA with an unsteady friction component, so that it can provide more accurate computations.

2 Methodology

The research plan included several steps that are featured in two different environments, Python and WANDA, respectively. In the Python environment, the water hammer numerical solution is first implemented and solved using the basic MoC with steady friction computation. Secondly, the quasi-steady friction and 3 different unsteady friction models were implemented in Python environment. The different implemented friction models were then compared with real experimental data using the setup used in Ferràs et al. 2016 research. Based on this comparison, the most-suited unsteady friction model for engineering practice is implemented in WANDA and tested for different synthetic networks.

A simple synthetic network was constructed to easily compare the effects of transient event simulation at the valve using unsteady friction with the previously installed quasi-steady friction model. The network is composed of an elevated tank, 5 pipes, 2 nodes, a butterfly valve, and the final reservoir. The valve closure occurred during 1 second. The network is illustrated in Figure 1 .

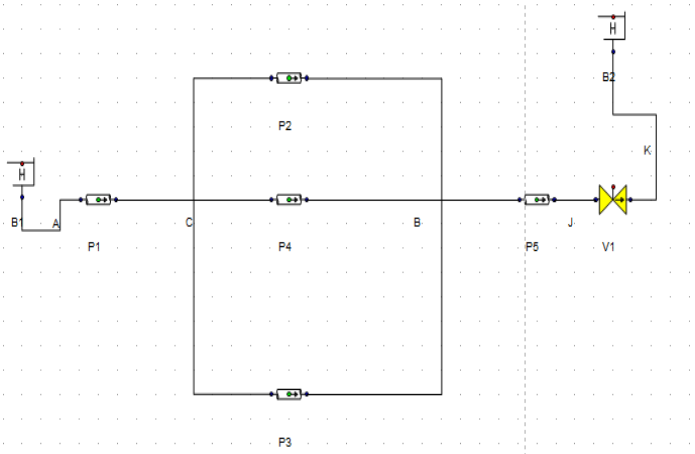

Figure 1 Simple network structure

3 RESULTS AND DISCUSSION

3.1 Simulation of different unsteady friction models

All the friction models were implemented and presented in Figure 2. The steady, quasi-steady first-order model and quasi-steady second-order model provided overall close results. Hino's model provided a slight improvement over the previous models due to the additional instantaneous mean flow velocity assumption (Hino et al., 1977). Daily's model provided more accurate results by using instantaneous mean flow velocity and local acceleration while estimating the friction. A significant improvement has already been deduced when using Brunone's model and further improved by Vítkovský's model (Vítkovský et al., 2006). These models depend on the instantaneous mean flow velocity, local acceleration, and convective acceleration./ Vítkovský's model provided higher accuracy than Brunone, and this is mainly attributed to the *sign* term which was introduced (Vítkovský et al., 2006). Finally, Vítkovský's model was chosen to be implemented in WANDA as it (i) doesn't need an input from user (ii) stable (ii) has moderate accuracy (iv) has highly moderate accuracy (v) accuracy is not case dependent

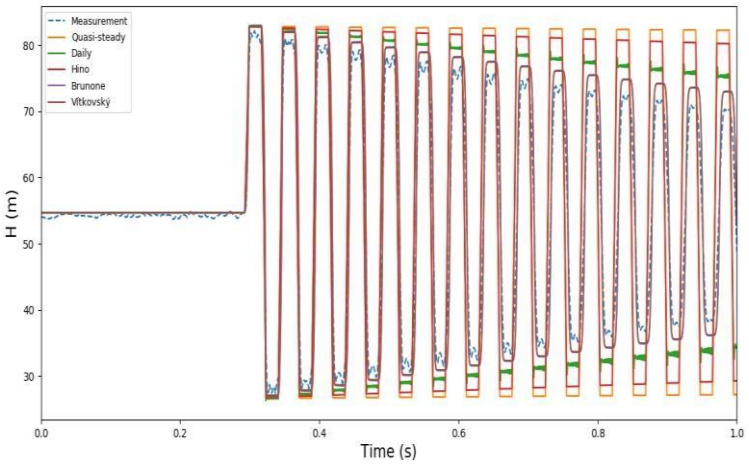

Figure 2 Simulation of different friction models compared to measurement

3.2 Simulation of unsteady friction in a simple pipe network

Information retrieved from Figure 3 confirms the fact that the quasi-steady friction gives a realistic approximation of the first few pressure peaks only. The first two pressure peaks are almost identical with the unsteady friction model; however, differences can be noticed from the third peak. Hence, the conventional quasi-steady friction model can be good enough for the applications that use the highest pressure peaks, for example, pipe bursts tests or pump trips. The WANDA's upgraded model provides a higher and more realistic damping rate than the conventional quasi-steady model. This is mainly credited to the addition of the previously neglected unsteady friction that counts for different factors like turbulence.

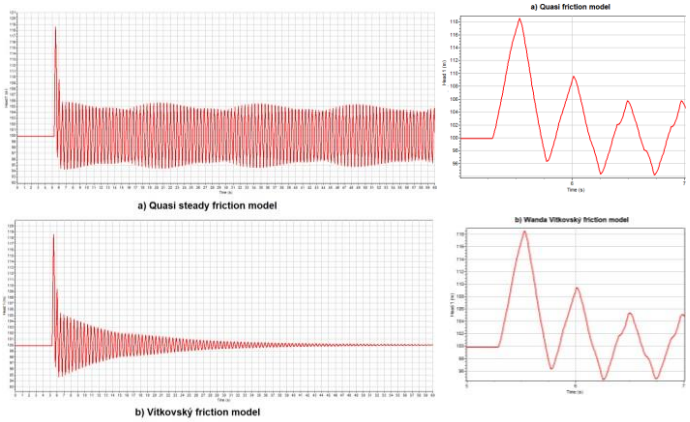

Figure 3 Pressure history in simple synthetic network using a) quasi-steady friction and b) Vítkovský friction

4 CONCLUSIONS

- Unsteady friction is significantly important for different applications and tasks executed by standard engineers
- Vítkovský friction was found to be the best-suited unsteady friction model to be implemented in WANDA according to the developed criteria mentioned in this study
- Unsteady friction improves the simulation significantly for standard pipes; however, it falls short for simulating PVC and HDPE pipes
- Vítkovský's friction provided affordable computational efforts and high moderate accuracy in the context of transient analyses in hydraulic networks

Acknowledgments

The authors would like to thank Prof. Silvia Meniconi from University of Perugia for the constructive comments. The authors acknowledge the contribution of Deltares consultancy in providing the means to test the research developments in WANDA software.

REFERENCES

Abdulshaheed, A., Mustapha, F., & Ghavamian, A. (2017). A pressure-based method for monitoring leaks in a pipe distribution system: A review. *Renewable and Sustainable Energy Reviews*, *69*, 902-911.

Ferràs, D., Manso, P. A., Schleiss, A. J., & Covas, D. I. (2016). Experimental distinction of damping mechanisms during hydraulic transients in pipe flow. *Journal of Fluids and Structures*, *66*, 424-446.

Hino, M., Sawamoto, M., & Takasu, S. (1977). Study on the transition to turbulence and frictional coefficient in an oscillatory pipe flow. *Transactions of JSCE*, *9*, 282-284.

Lin, C. C., & Yeh, H. D. (2019). An inverse transient-based optimization approach to fault examination in water distribution networks. *Water*, *11*(6), 1154.

Vítkovský, J. P., Bergant, A., Simpson, A. R., & Lambert, M. F. (2006). Systematic evaluation of one-dimensional unsteady friction models in simple pipelines. *Journal of Hydraulic Engineering*, *132*(7), 696-708.

Proceedings of the 1st IAHR
Young Professionals Congress
17-18 November 2020

THE EFFECT OF THE FUNCTIONING CONDITIONS ON THE TRANSIENT BEHAVIOUR OF A WATER DISTRIBUTION SYSTEM: LABORATORY TESTS

Filomena Maietta [1], Caterina Capponi [2], Bruno Brunone [3] & Silvia Meniconi [4]

[1,2,3,4]Dipartimento di Ingegneria Civile ed Ambientale, Università degli Studi di Perugia, Perugia, Italy,
filomena.maietta@studenti.unipg.it, caterina.capponi@unipg.it, bruno.brunone@unipg.it, silvia.meniconi@unipg.it

ABSTRACT

Water distribution systems (WDSs) often experience pressure transients. This paper shows some preliminary transient tests executed in a two-loop network installed at the Water Engineering Laboratory of the University of Perugia, Italy. Specifically, the effect of the functioning conditions during transient events is investigating.

Keywords: transients, networks, functioning conditions, water distribution systems, laboratory tests.

1 INTRODUCTION

Water distribution systems (WDSs) are complex, usually highly looped, infrastructures with thousands of elements such as pipes, pumps, and valves. The space-time variability of users' water demands and the operation of pressure regulating devices, cause sudden transients that are not normally detected by current pressure remote-control systems, designed to capture data every 5-15 minutes. For a given maneuver, the magnitude of a transient depends on the topology of the network, i.e., its geometrical and mechanical characteristics and boundary conditions. In the presence of very rapid and severe transients, generated for example by pump shutdown or valve closure (Gullick, 2004; Mc Innis, 1995; Morris, 1967; Jaeger, 1948), catastrophic damages can occur. On the contrary, transients characterized by small overpressures, as those generated by the operation of variable-speed pumps and pressure-reducing valves (Meniconi et al., 2017), as well as those linked to the dynamics of water consumptions, can cause collapse of the pipes due to fatigue. Such a feature, generally underestimated, is among the causes of network failure. The aim of this paper is to offer experimental evidence of the effect of the functioning conditions of a network on its transient response.

2 MATERIALS AND METHODS

The experimental setup is a pipe network with two loops simulating a District Metered Area (DMA) installed at the Water Engineering Laboratory (WEL) of the Department of Civil and Environmental Engineering (DICA) of the University of Perugia. The network (Figure 1b) consists of a 42.3 m long DN110 supply pipe connecting a pressure tank to the DMA. The first loop of the DMA has four DN75 pipes with a length L = 100 m, whereas the second one has four pipes: one in common with the first loop and the other three with DN50 and L = 100 m. DN25 short pipes (L = 0.75 m) with a solenoid valve (with a closing time of about 30 ms) at the downstream end section (terminals) are installed at nodes 4, 5, 6, 7, and 8 (Figure 1b) to simulate users. Pressure is monitored in eight measurement sections along the pipes (i.e., 23, 34, 47, 87, 45, 58, 65, and 36). A transient test has been generated by the almost instantaneous closure of valve 5, for two different operating conditions. In the first condition, the terminals 4, 6, 7, 8 are open simulating active users (hereinafter, such a network layout is referred to as "open network"), whereas in the second one they are close ("closed network").

3 RESULTS

The acquired pressure signals, h, are shown in Figure 2a and 2b in the long term for the open and closed network, respectively. Specifically, for the open network, the pressure wave generated by the closure of valve 5 (Δh_{58} = 10.96 m) is smaller than that occurring in the closed network (Δh_{58} = 18.16 m), because of the smaller initial discharge at valve 5 (2.60 L/s vs. 3.70 L/s). Moreover, the decay of the pressure oscillations is faster in the open network (the damping occurs in about 4 s) than that in the closed one. In the latter, the damping

happens in about 40 s due to reflections at the closed terminals. More details are offered in Figs 2c and 2d where the pressure changes with respect to the steady-state value, h_0, during the first two periods for the open and closed network are shown, respectively. For the closed network, pressure changes are larger than Δh_{58} in sections 87 and 47 (at a distance of about 120 m from valve 5): 29.46 m (~ 162% Δh_{58}) and 27.62 m (~ 152% Δh_{58}), respectively, because of the reflection of the pressure wave at the closed terminals. On the contrary, in these sections, the initial pressure variation decays rapidly in the case of the open network: at section 87 the pressure variation is 3.46 m (~32% Δh_{58}) and at section 47 it is 4.65 m (~ 42% Δh_{58}). Therefore, to identify the most exposed to transient areas (Starczewska, 2014), it is necessary to monitor not only the node where the transient is generated, since its effects can be emphasized by the topology of the system and functioning conditions.

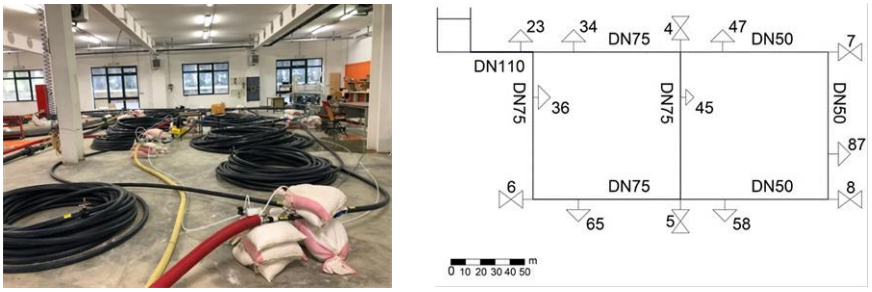

Figure 1. DMA at WEL: a) general view, and b) network layout.

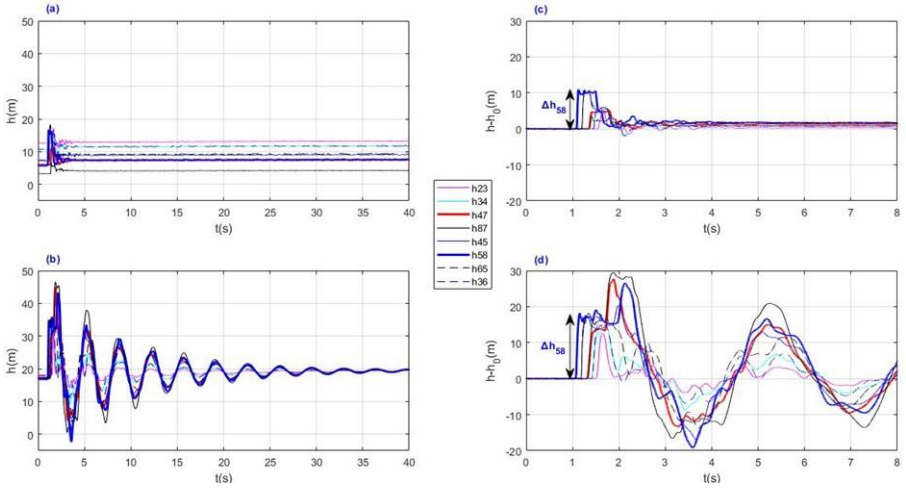

Figure 2. Pressure signals in the case of a) “open network”, and b) “closed network”.

ACKNOWLEDGEMENTS

This research has been funded by the Hong Kong (HK) Research Grant Council Theme-Based Research Scheme and the HK University of Science and Technology (HKUST) under the project “Smart Urban Water Supply System (Smart UWSS)”.

REFERENCES

Gullick R. W., LeChevalier M. W., Svindland R. C. and Friedman M. (2004). Occurrence of transient low and negative pressures in distribution systems, *J. American Water Works Association*, 96(11), 52–66.

Jaeger C. (1948). Water-hammer effects in power conduits: accidents due to water hammer, *J. of the Institution of Civil Engineers*, 29(4), 334–338.

Mc Innis D. and Karney B. W. (1995). Transients in distribution networks: Field tests and demand models, *J. of Hydraulic Engineering*, 121(3), 218–231.

Meniconi S., Brunone B., Mazzetti E., Laucelli D.B. and Borta G. (2017). Hydraulic characterization and transient response of Pressure Reducing Valves. Laboratory experiments. *J. of Hydroinformatics*, 19(6), 798–810.

Morris R. E. (1967). Principal causes and remedies of water main breaks, *J. American Water Works Association*, 59(7), 1967, 782–798.

Starczewska D., Collins R. and Boxall J. (2014). Transient behavior in complex distribution network: a case study, *Procedia Engineering*, 70, 1582–1591.

Proceedings of the 1st IAHR
Young Professionals Congress
17-18 November 2020

A well-balanced non-hydrostatic pressure model for steady and unsteady shallow flows

Isabel Echeverribar[*1,2], Pilar Brufau[1], Pilar García-Navarro[1]

[1]University of Zaragoza, Zaragoza, Spain
[2]Hydronia Europe S.L., Madrid, Spain

*Correspondance : echeverribar@unizar.es

ABSTRACT

A depth-averaged system for free surface flow based in non-hydrostatic pressure (NHP) assumptions is presented and analyzed for the numerical simulation of open channel flows. This research analyzes the numerical behaviour of the model when simulating both steady and unsteady for open channel flows. The NHP model is solved my means of a one-dimensional explicit-implicit finite volume method. A well-balance scheme must be designed for these models to solve some particular problems. The numerical results are validated with semi-analytical and experimental data.

Keywords: non-hydrostatic pressure, finite-volume, dispersive, steady, well-balanced.

1 INTRODUCTION

There is a wide range of geophysical flows that can be mathematically represented by the non-linear shallow water 1D equations involving hydrostatic pressure assumptions. In this context, the use of non-hydrostatic pressure (NHP) models have been restricted to coastal applications where vertical accelerations can not be neglected and the extra computational time is justified. These applications are generally focused unsteady wave propagation and the attentions has not been paid on problems where there is an steady state that must be balanced. This work is focused on the resolution of a one-dimensional NHP model and its application to analytical steady states, presenting the consequences of using one of the most common numerical strategies to solve these NHP equations: the Pressure Correction Method Anderson (1995).

2 GOVERNING EQUATIONS AND NUMERICAL MODEL

The 1D system of equations can be written (see Bristeau *et al.* (2015)) as:

$$\frac{\partial h}{\partial t}+\frac{\partial (hu)}{\partial x}=0;\qquad \frac{\partial (hu)}{\partial t}+\frac{\partial}{\partial x}\left[hu^2+\frac{1}{2}gh^2\right]=-gh\frac{\partial z_b}{\partial x}\underbrace{-\frac{1}{2}h\frac{\partial p_{nh}}{\partial x}+p_{nh}\frac{\partial (h+2z_b)}{\partial x}}_{\text{Non-hydrostatic terms}};\qquad (1)$$

$$\frac{\partial w}{\partial t}+u\frac{\partial w}{\partial x}=\frac{p_{nh}}{h};\qquad h\frac{\partial (hu)}{\partial x}+2hw+(hu)\frac{\partial}{\partial x}(h+2z_b)=0;$$

where h is water depth, u and w stand for depth-averaged velocity components in x and z directions, respectively, and p_{nh} represents the non-hydrostatic pressure at the bottom. The non-hydrostatic pressure is fully represented on the right hand side of the momentum equations in system 1 and is solved by means of a Pressure Correction Method (PCM), also called fractional step procedure Stelling et Zijlema (2003). First, a finite-volume scheme is used to explicitly solve the shallow water part of the system and get intermediate states, h^* and hu^*, assuming p_{nh} = 0 with an upwind finite-volume scheme Murillo et Garcia-Navarro (2010). The implicit PCM provides the new p_{nh} distribution. Finally, this non-hydrostatic distribution is used to update the final values of the new state, h^{n+1} and hu^{n+1}.

3 RESULTS

3.1 Wave propagation over irregular topography

The NHP model has been used to reproduced experimental waves on an open channel of 31.7 m length (L) that can be found in Beji et Battjes (1993). The Figure 1 shows the water depth distribution over time at probe 5

along the channel. In the graph, a comparison between experimental data, a SWE model and the NHP model can be seen and compared.

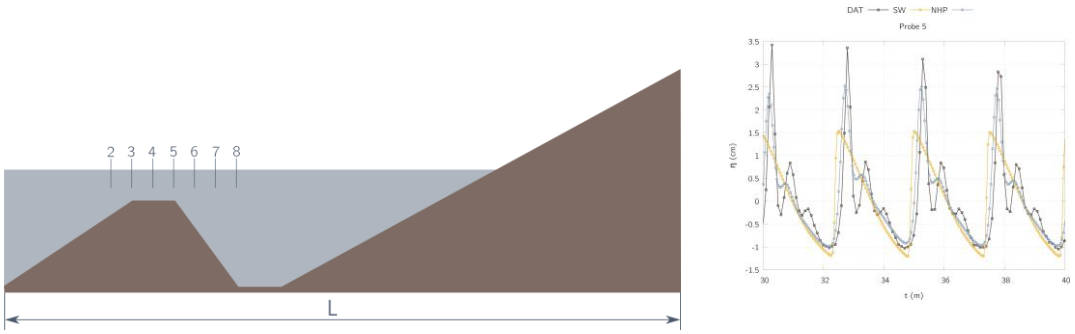

(a) (b)

Figure 1: Experimental layout scheme (a) and temporal evolution of water depth at point 5 (b) of the channel comparing experimental data (brown), simulation results with a SW model (orange) and with the NHP model (blue).

3.2 Stationary *quasi*-analytical solution

A *quasi*-analytical solution of the system 1 can be found in Bristeau *et al.* (2015). The NHP model presents numerical problems of spatial discharge conservation, as shown in Figure 2.

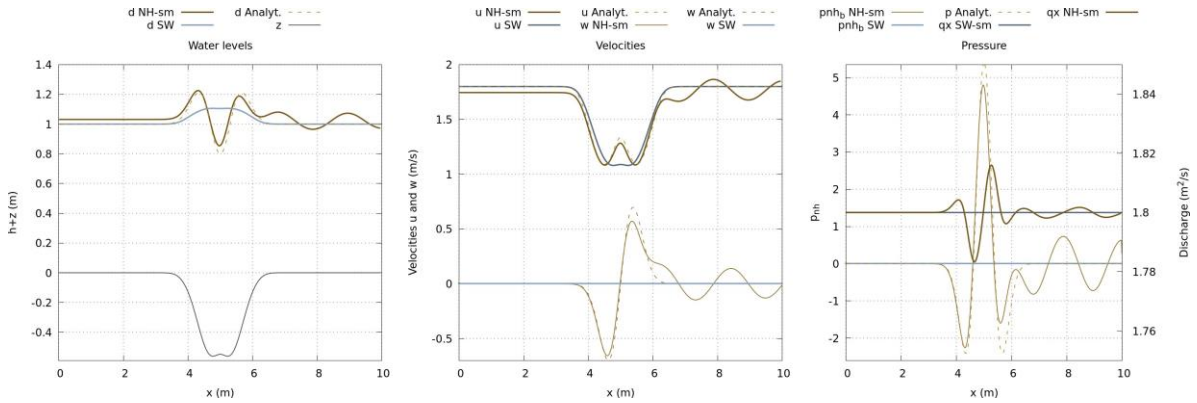

Figure 2: Spatial distribution of flow variables in an steady state over irregular topography, *z*.

4 CONCLUSIONS

The application of the fractional step procedure to solve a NHP model is very effective and robust, and presents accurate results when dealing with unsteady wave propagation, as can be seen in Fig. 1. However, the same method applied to an steady case shows the necessity of an equilibrium analysis of the scheme, since the numerical fluxes after the corrector step get unbalanced and the steady discharge is not able to remain spatially constant.

References

Anderson J. D. (1995). *Computational Fluid Dynamics: The Basics with Applications*. McGraw-Hill, Inc.

Beji S., Battjes J. A. (1993). Experimental investigation of wave propagation over a bar. *Coastal Engineering 19*, 151–162.

Bristeau M., Mangeney A., Sainte-Marie J., Seguin N. (2015). An energy-consistent depth-averaged euler system: Derivation and properties. *Discrete and Continuous Dynamical Systems Series B 20*(4).

Murillo J., Garcia-Navarro P. (2010). Weak solutions for partial differential equations with source terms: Application to the shallow water equations. *Journal of Computational Physics 229*(11), 4327–4368.

Stelling G., Zijlema M. (2003). An accurate and efficient finite-difference algorithm for non-hydrostatic free-surface flow with application to wave propagation. *Journal for Numerical Methods in Fluids 43*(1), 1–23.

Proceedings of the 1st IAHR
Young Professionals Congress
17-18 November 2020

Time reversal of waves in pressurized pipelines

Muhammad Waqar[*1], **Moez Louati**[1], **Mohamed S. Ghidaoui**[1]

[1]Department of Civil and Environmental Engineering, Hong Kong University of Science and Technology, Hong Kong

*Correspondance : mwaqar@connect.ust.hk

ABSTRACT

Time reversal (TR) of transient waves has been recently introduced as a powerful technique for defect detection in pipelines. However, there remains an unresolved paradox that although TR breaks down due to inevitable damping in real systems, TR based defect detection techniques are optimal in the sense of signal to noise ratio. This paper aims to address this paradox experimentally. The experiment is conducted in a simple pump-pipe-valve system and performed in two steps. In step 1, a transient wave is generated by rapidly opening the in-line side discharge valve, and the transient response of the system is recorded near the upstream and downstream side. In step 2, the measured signals are flipped in time and used as boundary conditions in the transient model. The results show that the time-reversed waves focus back on the source (i.e. side discharge valve), effectively proving the time-reversibility of waves in pipes. However, the amplitude of the refocused wave is much smaller than the original wave amplitude due to damping.

Keywords: Hydraulic transients, leak detection, time reversal, waterhammer, valve stroking.

1 INTRODUCTION

TR of waves is instrumental in many fields. For example, TR is used to destroy tumors and kidney stones, to detect defects in solids, and to perform long-distance communication (Fink, 1999; Anderson *et al.*, 2008). In the waterhammer field, the closest application to TR is the backward-in-time calculation used to perform valve stroking (Wylie *et al.*, 1993). Very recently, the principle of TR of the waterhammer equations is used to develop pipeline defect detection schemes (Waqar *et al.*, 2019; Wang *et al.*, 2019; Zouari *et al.*, 2020). What is most surprising and unexpected is that these TR schemes give excellent results in the presence of both distributed damping (e.g., friction and visco-elasticity) and discrete damping (e.g., leaks and discrete blockages) (see Wang *et al.* (2019); Zouari *et al.* (2020)). It must be emphasized that the wave equation is strictly not time reversible in the presence of damping. For instance, the waterhammer wave equation with linear frictional damping is written as

$$\frac{\partial^2}{\partial t^2} H(x,t) - a^2 \frac{\partial^2}{\partial x^2} H(x,t) - R \frac{\partial}{\partial t} H(x,t) = 0 \tag{1}$$

where $H(x, t)$ is the pressure head, t is the time, x is the position, a is the wave speed, and R is the damping coefficient. It is easy to verify that Eq. 1 (without last term) is time-reversible. However, with the damping term and changing t to $-t$ in Eq. 1 gives

$$\frac{\partial^2}{\partial t^2} H(x,-t) - a^2 \frac{\partial^2}{\partial x^2} H(x,-t) + R \frac{\partial}{\partial t} H(x,-t) = 0. \tag{2}$$

Note that the damping term in the time reversed equation has a positive sign implying that TR does not hold. In fact, the solution of such equation is unstable in the sense that small measurement and modeling errors grow exponentially with time. Yet, the approach in Zouari *et al.* (2020) and Wang *et al.* (2019) finds that TR works exceptionally well in the presence of damping. This paradox has already been noted in the classic waterhammer book by Wylie *et al.* (1993) in connection with the use of backward-in-time solution for valve stroking in the presence of damping. On page 223 they wrote: *"the [waterhammer] equations are remarkably*

robust in calculating backward in time, effectively regenerating a transient… [However] the idea of calculating backwards in time defies logic since it cannot be done physically. It cannot because of the irreversibility of losses in real systems." Here, we experimentally investigate the extent to which waterhammer waves are time reversible. In particular, the objective is to investigate how well the time-reversed waves refocus back at the source and reproduce the transient trace that was injected through a source.

2 EXPERIMENTAL SETUP AND METHODOLOGY

The test rig is situated in the Water Research Resources Laboratory of HKUST and comprised of (i) a pump at the upstream side, (ii) a 140 m long high-density polyethylene pipe, (iii) a side discharge valve at 98 m from the pump, and (iv) an open end at the downstream side. At steady-state (before transient event), the pressure head and flowrate at the downstream end are 19.95 m and 0.4 l/s, respectively. The TR experiment is performed in two steps. In step 1: a transient wave is injected by manually opening a side discharge valve (defined as a source) in 0.1 s and the response of the system is recorded near both ends of the pipe and near the source. In step 2: the recorded signals at both ends (in step 1) are reversed (flipped) in time such that the sequence of the elements in a signal is reversed. These time-reversed signals are used as boundary conditions in the transient model which incorporates frictional and visco-elastic damping effects.

3 RESULTS AND CONCLUSIONS

Figure 1a shows the pressure head profile versus space (solid line) at $t = 0.1$ s of step 2, actual source location (dashed line) and wave refocusing location (dotted line). This figure shows that the re-emitted waves refocus only at the correct source location (i.e. side discharge valve) and at the time of the source (i.e. $t = 0.1$ s). The localization error is about 0.97 m. Figure 1b gives a comparison of the experimental signal recorded near the source in step 1 and the signal recovered at the estimated source location from the transient model in step 2. It can be seen that both signals are in-phase, implying that re-emitted waves followed their past steps accurately. However, the amplitude of the recovered signal is less than the original signal. It is because the measured signals experienced additional damping due to both friction and visco-elasticity when re-emitted in step 2. It is concluded that various damping effects only affect the amplitude of the waves and do not alter the refocusing property of waves. In future work, a correction to the damped wave amplitude will be applied using a mathematical transformation, proposed by Zouari *et al.* (2020).

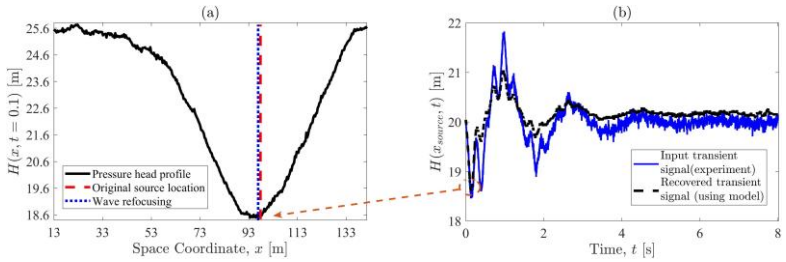

Figure 1: (a) Waves refocusing at the source location, and (b) transient pattern of the injected and refocused transient wave

References

Anderson B. E., Griffa M., Johnson P. A., Larmat C., Ulrich T. J. (2008). Time reversal. *Acoustical Society of America 28*(4), 5–16.

Fink M. (1999). Time-reversed acoustics. *Scientific American 281*(5), 91–97.

Wang X., Lin J., Keramat A., Ghidaoui M. S., Meniconi S., Brunone B. (2019). Matched-field processing for leak localization in a viscoelastic pipe: An experimental study. *Mechanical Systems and Signal Processing 124*, 459–478.

Waqar M., Louati M., Ghidaoui M. S. (2019). Leak localization using time reversal technique. In *the proceedings of the 38th IAHR World congress held in Panama*.

Wylie E. B., Streeter V. L., Suo L. (1993). *Fluid transients in systems*, Volume 1. Prentice Hall Englewood Cliffs, NJ.

Zouari F., Louati M., Meniconi S., Blåsten E., Ghidaoui M. S., Brunone B. (2020). Experimental verification of the accuracy and robustness of area reconstruction method for pressurized water pipe system. *Journal of Hydraulic Engineering 146*(3), 04020004.

Zouari F., Nasraoui S., Louati M., Ghidaoui M. S. (2020). Transformation between damped and undamped waterhammer waves. *Journal of Sound and Vibration*, 115706.

IAHR AIRH

International Association for Hydro-Environment Engineering and Research

Hosted by
Spain Water and IWHR, China

Session 9
Flood Risk Management

IAHR YPN

Hosted by
Spain Water and IWHR, China

Proceedings of the 1st IAHR
Young Professionals Congress
17-18 November 2020

BEYOND INNER SLOPE INSTABILITY: A METHOD TO QUANTIFY THE RESIDUAL DIKE STRENGTH BY WAVE OVERTOPPING

Vincent Verdonk[1*], Vera van Bergeijk[1], Jord Warmink[1] & Suzanne Hulscher[1]

[1] University of Twente, Water Engineering and Management, Enschede, the Netherlands

*Correspondence: v@1verdonk.nl

ABSTRACT
Climate change increases the risk of grass dikes to breach as warm weather can weaken the grass cover while more frequent high water is present. This may cause initial damage to the dike cover; in which case the dike does not breach. Understanding the residual dike strength is essential from a flood risk management perspective to design dikes efficiently against extreme events. This study assesses the residual dike strength by wave overtopping at three locations across a dike profile by evaluating a newly developed framework for the failure probability of overtopping waves of grass-covered river dikes. A method is next presented to derive failure probabilities and fragility curves. To extend on current Dutch safety standards obtained fragility curves by wave overtopping are to be combined with follow-up failure mechanisms for dikes with inner slope instability.

Keywords: damaged dyke, residual dike strength, macro-instability, wave overtopping, failure probability.

1 INTRODUCTION

Understanding dike failure is essential for flood protection in a country like the Netherlands, where a quarter of the land surface lies below sea level. Within the current Dutch safety assessment, the degree of flood protection is classified according to a flooding probability for the hinterland. In the case of failure by the mechanism macro-instability, where the dike slides along a slip plane, not all slope instabilities result in flooding causing the evaluated failure probability to be very conservative (Van Der Krogt et al., 2019). To define the actual breach probability, the residual profile that remains to offer its protective function must be examined against follow-up mechanisms. However, there is not yet a method to evaluate follow-up mechanisms besides slope-instability and, as a result, it is not possible to determine the actual strength of a dike. Figure 1 (l.) outlines a typical dike with slope-instability for a homogeneous clay top layer covered with a grass cover layer. The schematized dike core consists of sand but can also consist of clay or peat. The follow-up mechanism wave overtopping (Figure 1 r.) can occur after the macro-instability of a dike profile, which can cause a dike failure. This mechanism occurs for extreme wave conditions when waves overtop the dike crest causing the inner grass cover layer of a dike to erode. Extensive erosion results in instability, after which a dike breach results.

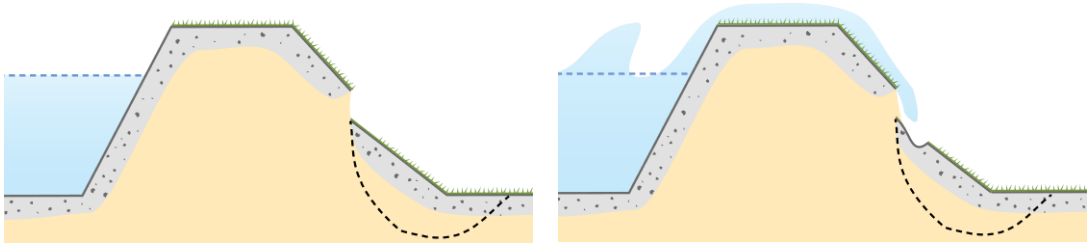

Figure 1. (l.) Failure processes by macro-instability (r.) with the erosion of the grass cover by overtopping.

Aim of this research is to assess the residual dike strength after a slope instability for wave overtopping. A new framework is developed to determine the failure probability of wave overtopping for grass-covered river dikes. The framework allows the occurrence of critical erosion failure to be evaluated during storms with high wind speeds combined with variable water levels. This framework is applied to a river dike near Millingen aan de Rijn in the Netherland to determine the failure probability for the original dike profile and for different types of slope instabilities (Verdonk, 2020).

2 METHODOLOGY

The probability of failure at multiple water levels is computed using the new framework for the original dike profile and the profile after a slope instability. Firstly, the local geometry and bathymetry data are acquired from Hydra-NL WBI 2017 software. Next, the overtopping characteristics at the start of the dike are calculated using the Bretschneider equations in combination with the extreme wind statistics and run-up equations. These overtopping characteristics are used as input for the analytical grass erosion model (Van Bergeijk et al., 2019) for the flow velocity and erosion depth across the dike. New relations for additional turbulence at a slope instability were derived to simulate the effect of jet impact at this location (Verdonk, 2020). The failure probability is calculated using a Monte-Carlo-Analysis with the wind speed and grass strength as stochastic variables. Failure is defined as the exceedance of 20 cm erosion depth according to the Dutch safety standards. Model runs are performed for varying grass quality, clay quality, wave characteristics and locations across the dike. The failure probability of erosion by overtopping at varying water heights is calculated, resulting in fragility curves to compare the failure probability of a dike profile with macro-instability relative to a regular dike profile.

3 RESULTS

The fragility curves show that no wave overtopping occurs for free crest heights larger than 1 m (Figure 2). The clay quality of the cover layer significantly affects the failure probability. Slipped profiles are more vulnerable for wave overtopping with a failure probability that is 2-12 times larger than a regular profile depending on the cover characteristics. Instabilities on the upper and middle inner slope are most vulnerable for wave overtopping.

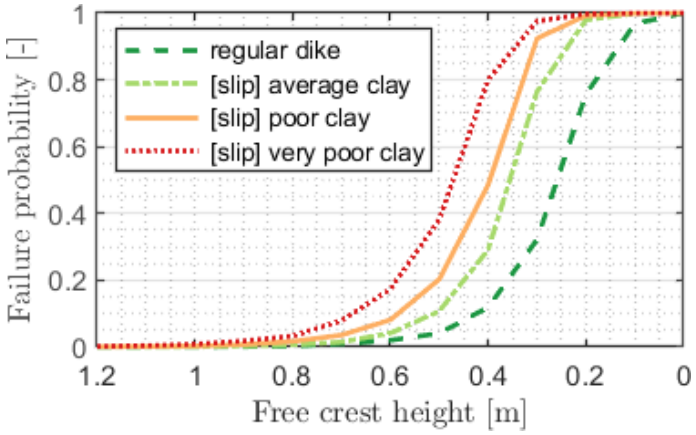

Figure 2. Failure occurrence by overtopping for a dike with macro-instability [slip] at the upper slope section and a regular dike at a varying free crest height.

4 CONCLUSIONS

The new framework is developed to calculate the failure probability of wave overtopping for grass-covered river dikes with a slope-instability. Therefore, this framework is a valuable tool to assess the residual dike strength after a slope instability. We showed that the failure curves for overtopping show a steep gradient for an increasing water level and slipped profiles are up to 12 times more vulnerable for wave overtopping. Combining the failure mechanisms macro-instability and wave overtopping will lead to more accurate strength assessments of flood defences, which can save costs and improve future designs.

ACKNOWLEDGEMENTS

This work is part of the research programme All-Risk, with project number P15-21, which is (partly) financed by the Netherlands Organisation for Scientific Research (NWO).

REFERENCES

Van Bergeijk, V.M., Warmink, J.J., Frankena, M., & Hulscher, S.J.M.H. (2019). Modelling Dike Cover Erosion by Overtopping Waves: The Effects of Transitions. *Hydraulic Engineering Repository*, 1097–1106. https://doi.org/https://doi.org/10.18451/978-3-939230-64-9_110

Van Der Krogt, M.G., Schweckendiek, T., & Kok, M. (2019). Do all dike instabilities cause flooding? *13th International Conference on Applications of Statistics and Probability in Civil Engineering, ICASP 2019*.

Verdonk, V.A. (2020). The impact of overtopping on the failure probability of slipped river dikes. *Master Thesis, University of Twente*. https://www.utwente.nl/en/et/wem/education/msc-thesis/2020/Verdonk.pdf

Proceedings of the 1st IAHR
Young Professionals Congress
17-18 November 2020

FLOOD DISASTER AND ADAPTATION MEASURES IN BRISBANE AUSTRALIA

Usman Khalil [1], Shuqing Yang [2] & Muttucumaru Sivakumar [3] Mariam Sajid [4]

[1,2,3] University of Wollongong, Australia [4]University of Engineering and Technology Lahore, Pakistan

[1]uk998@uowmail.edu.au [2]shuqing@uow.edu.au.com [3]siva@uow.edu.au.com [4]maryamsajidmalik@hotmail.com

ABSTRACT

This study selects the region of Brisbane, River to analyse the adaptation measures against the 2011 flood through a Coastal Reservoir (CR) technique. A numerical model based on MIKE-21 is used to investigate the feasibility of the proposed CR after being calibrated and validated. The results show that the gate operation of the CR shows that the flood level can be reduced up to 13% and under the joint operation of CR and Wivenhoe dam its can be reduced to 28% at the Brisbane city, which can safeguard infrastructure damage. This study is of interest and could provide useful information on flood management for the regional community.

Keywords: Flood mitigation, Coastal Reservoir, MIKE-21, Estuary, Gate operation

1 INTRODUCTION

Analyzing and adaptation of future flooding risks in Brisbane Australia is essential for coastal planning and management (Pellikka et al., 2018). Coastal Reservoir technique is used for flood adaptation in Brisbane River Estuary (BRE) (Khalil et al., 2020) and may be used to store water for Brisbane City water supply. Coastal Reservoir area is selected based on available bathymetry and has a storage capacity of 900GL (surface area 75 km^2 and the water depth approximately 12 m). The reservoir dike with hydraulic gates to regulate the river flows into CR as shown in Figure 1.

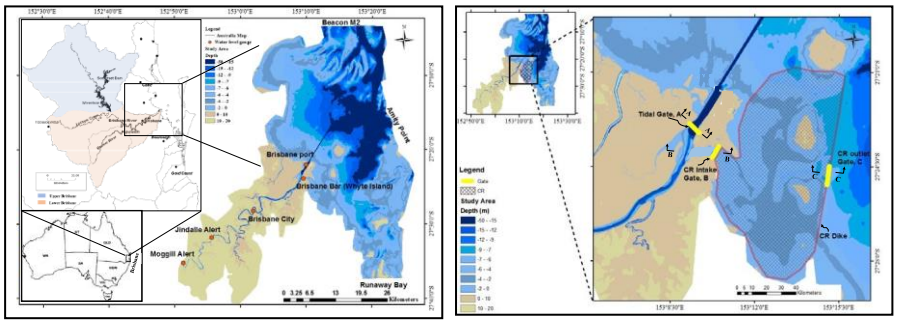

Figure 1. Brisbane River and Moreton Bay with marked boundary conditions data and Costal Reservoir gates in Moreton Bay

2 METHODS

MIKE 21 FM hydrodynamic module is used to model the flow in the Brisbane River and to study the coastal reservoir effects on the flooding process in the Brisbane River. The MIKE 21 FM hydrodynamic model is set up with topographic data, Manning's roughness coefficients, water level and tidal data for the year 2011. The model is calibrated and validated well to match flood inundation extent with 85% accuracy as shown in Figure 2. The optimum gate operation during the 2011 flood hydrograph is shown in Figure 3.

Gate location and size is optimized according to the width of the river mouth. Gate A and B operation is optimized to allow water inside the CR and to stop the tidal water entering the estuary as shown in Figure 3. During high flood, water could be diverted into the CR, which will cause decrease in upstream flood level as there will be no resistance from tidal water and all flow will move to CR. While during low flow season, water will be discharged towards the Brisbane bar by closing the CR gate without storage.

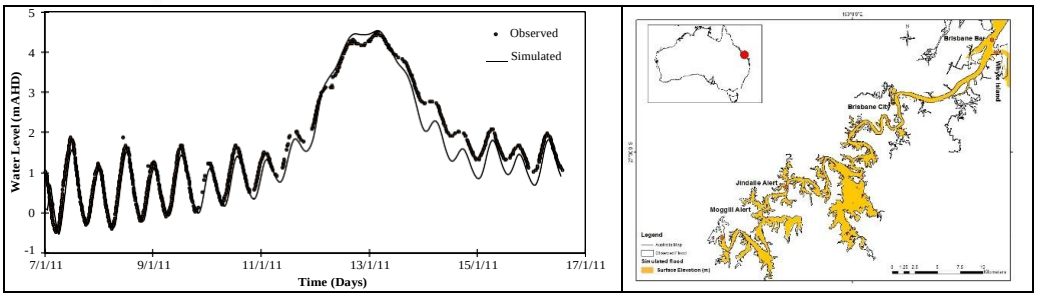

Figure 2. Simulated and observed water levels at Brisbane City; and simulated and observed inundation area

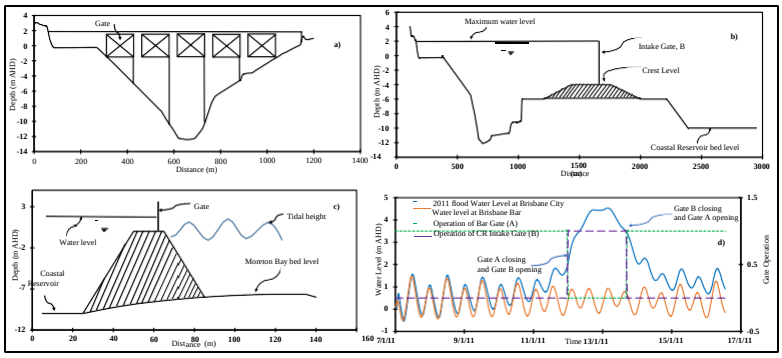

Figure 3. Gate *sections and* operation for the 2011 flood mitigation

3 RESULTS AND DISCUSSION

The water level remains unaffected before the gate operation. As the gate start operating at 12 January 2011 12:05 am, the water level starts decreasing in the Brisbane River and it reduces the peak water level at Brisbane city gauge from 4.46 m AHD to 3.95 m AHD, with overall 0.51 m reduction in peak water level as shown in Figure 4. This reduction in water level will save the infrastructure damage. Further, with improved flood management of the Wivenhoe Dam, the releases will be controlled and the water level at Brisbane city would be reduced below the major flood level.

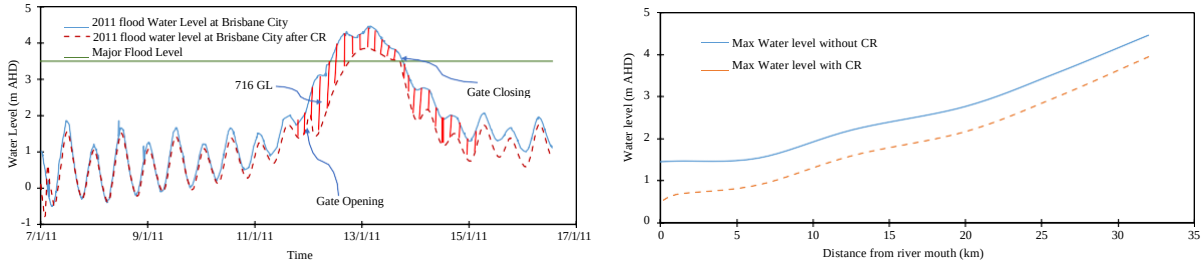

Figure 4. The water level during the 2011 flood in BRE with and without CR.

4 CONCLUSIONS

To enhance flood disaster mitigation in BRE, we analyzed the feasibility of a proposed CR at the river mouth. The major flood of 2011, was simulated and CR operation was analyzed using MIKE 21. The operation of the CR intake gate shows that the 2011 observed flood level (4.46 m AHD) can be reduced to 3.88 m AHD (13% reduction). While under the improved management of Wivenhoe dam, flood level will be (4 m AHD), by suitable operation of CR gate, flood level can be reduced to 2.87 m AHD (28.3% reduction) at the Brisbane city, The CR has great prospects to adapt to the flood of the Brisbane catchment and thus to mitigate BRE the flood disaster.

REFERENCES

Khalil, U. et al., 2020. Investigating an Innovative Sea-Based Strategy to Mitigate Coastal City Flood Disasters and Its Feasibility Study for Brisbane, Australia. Water, 12(10). DOI:10.3390/w12102744

Pellikka, H., Leijala, U., Johansson, M.M., Leinonen, K., Kahma, K.K., 2018. Future probabilities of coastal floods in Finland. Continental Shelf Research, 157: 32-42. DOI:10.1016/j.csr.2018.02.006

Proceedings of the 1st IAHR
Young Professionals Congress
17-18 November 2020

STATISTICAL ANALYSIS OF PRECIPITATION DATA FOR HYDROLOGICAL AND HYDRAULIC MODELING OF FLASH FLOODS

Uqubai Gessessew [1,2], Franziska Tügel [1], Zebrhan Measho [3], Kifle Weldearegay [2], Reinhard Hinkelmann [1]
[1] Technische Universität Berlin, Chair of Water Resources Management and Modeling of Hydrosystems, Germany
e-mail: uqub2002@gmail.com
[2] Mekelle University, Ethiopia
[3] Technische Universität Berlin, Campus El Gouna

Abstract

In hydrological and hydraulic modeling, identification and evaluation of the rainfall pattern and extreme events for a specific probability of occurrence is considerably important. The purpose of this research was to identify patterns of precipitation data and analyse extreme events for a time series of 6939-point data from 2001-2019. The Mann-Kendall trend test is used to detect the trend in the data at 5 % level of significance. Log Pearson Type III and Gumbel are applied for the analysis of the extreme rainfall events. Outlier testing was carried out and high and low outliers were observed in the data with values 68.24 mm and 20.74 mm, respectively and were removed. As the computed p - value < 0.0001 is lower than the significance level alpha = 0.05, the null hypothesis Ho should be rejected, and the alternative hypothesis Ha should be accepted. As the alternative hypothesis Ha is accepted, it is concluded that there is a significant trend component in the time series data.

Key words: precipitation data, trend analysis, Ethiopia, extreme events, outliers.

1 Introduction

This study is part of the research on modeling of flash floods in ungauged catchment areas for semi-arid regions in northern part of Ethiopia. Though several areas are frequently affected by such hydrological hazards, this study has focused on Wukro town which is surrounded by mountainous terrains with sparse vegetation cover and which has been under dynamic land use/land cover change due to urbanization and degradation.

Hydrological and hydraulic models are used to simulate the hydrological behaviour of the catchment and model the hydraulic surface runoff of the flash floods in a specific area.

The rainfall-runoff correlation of the area is examined using Hydrologic Engineering Centre Hydrological Modeling System (HEC-HMS) which is a physically based semi-distributed model designed to simulate rainfall-runoff processes of dendritic watershed systems (Scharffenberg, 2010). It was developed by the US Army Corps of Engineers and since then it has been widely applied for humid, tropical, subtropical, and arid watersheds to simulate and forecast streamflow. Many studies conducted in the previous times with HEC-HMS showed its ability to simulate and forecast streamflow based on different datasets and catchment types (Anderson et al. 2002; Bournaski et al. 2009).

The most severe urban areas could be simulated using a high resolution hydrodynamic numerical 2D model called hydroinformatics modeling system (hms) solving the shallow water equations. hms is a Java-based object-oriented software framework that has been developed at the Chair of Water Resources Management and Modeling of Hydrosytems, Technische Universität Berlin since many years (Simons et al. 2014).

This paper focuses on the statistical analysis of available precipitation data which is an essential input for the above-mentioned models. Trend identification in the time series is tested using the parametric and non-parametric Mann-Kendall trend test (Durn, 2010). In this contribution, Mann-Kendall non – parametric trend test is used.

Null and alternative hypotheses are applied to identify the presence or absence of the trend component in the time series. The null hypothesis (Ho) assumes that the time series data have no trend while the alternative hypothesis (Ha) expects, there is a significant trend in the time series (Bainchi et al., 1998). As the precipitation data is one of the main inputs for the hydrological modelling (HEC – HMS), the trend component was identified and evaluated using statistical methods. Presence of outliers in the data creates difficulties when analysing the trend of the data. The method of Grubbs and Beck (1972) could be used to pinpoint high and low outliers.

2 Results and discussions

Long term precipitation historical records were used to identify the presence or absence of precipitation trend for the period of 2001 to 2019.Having done the precipitation data analysis using the statistical methods, the statistical parameters of the data are: maximum = 59.733 mm, minimum = 0 mm, mean = 1.5948 mm, standard deviation = 4.6923 mm, p-value < 0.0001, and alpha = 0.05.

As the computed p - value is lower than the significance level alpha = 0.05, the null hypothesis Ho was rejected, and the alternative hypothesis Ha was accepted. Thus, there was a significant trend component in the time series

as shown in Figure 1. The risk to reject the null hypothesis Ho while it is true is lower than 0.01%. This implies that there is a significant trend component in the time series data.

Precipitation frequency analysis for different return periods was carried out for 19-year data from 2001 to 2019 using Gumbel's and Log Pearson Type III methods. The probable maximum precipitations for 10, 50, 100 and 200 years recurrence periods (mm) for Gumbel (mean = 39 mm and standard deviation = 9.93 mm) and Log Pearson Type III (mean = 1.58 mm, standard deviation =0.11 mm and skewness= 0.153) were 55, 71, 77, 84 and 53, 65, 69, 74 respectively.

The peak values for Gumbel's method are a bit higher than for the Log Pearson Type III. This could be caused by the transformation of the data into logarithm.

For the same precipitation data used in the precipitation frequency analysis, outlier test was carried out between ± 0.4 for high and low outliers, and the results found were 68.24 and 20.74 mm for +0.4 and -0.4. The maximum and minimum values of the data were 60 and 24 mm, respectively. It was concluded that both outliers were found. Therefore, it was important to remove the outliers from the data before using for further analysis.

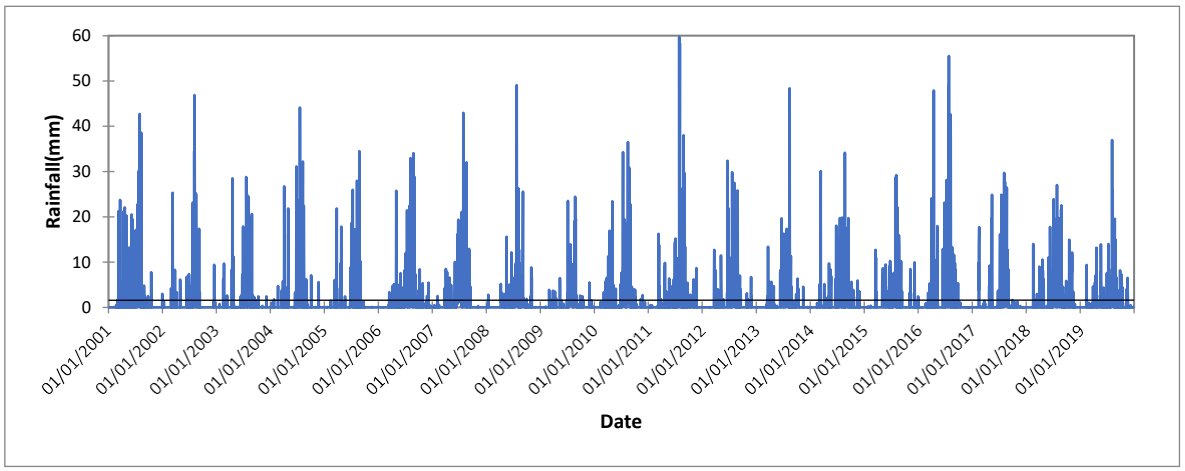

Figure 1: Trend analysis using Mann-Kendall trend test

Having determined the pattern and trend of the historical time series precipitation data, appropriate methods could be selected and applied for prediction or forecasting of the precipitation time series which will be the input for the hydrological and hydraulic modeling of flash floods in ungauged catchment areas in a semi-arid region in the Northern part of Ethiopia.

Acknowledgement

Our heartfelt gratitude goes to DAAD and Ethiopian Ministry of Science and Education for financial support.

References:

Anderson, M. L., Chen, Z.-Q., Kavvas, M. L., and Feldman, A. (2002). Coupling HEC-HMS with atmospheric models for prediction of watershed runoff. J Hydrol Eng 7:312–318.

Bianchi, L., Jarrett, J., and Choudary Hanumara, R. (1998). Improving forecasting for telemarketing centres by ARIMA Modeling with intervention. Int J Forecast 14:497–504.

Bournaski, E., Iliev, R., and Kiriloy, L. (2009). HEC-HMS modeling of rainstorm in a catchment. The mesta case study. Comptes Rendus de L'Academie Bulgare des Sciences 62:1141–1146.

Burn, D. (2010). Detection of trend in hydrological extremes for Canadian watershed. hydrological process 24, 1781-1790.

Grubbs, F., and Beck, G. (1972). ''Extension of Sample Sizes and Percentage Points for Significance Tests of Outlying Observations'', Technometrics, Vol. 14 (4), pp. 847-854.

Simons, F., Busse, T., Hou, J., Özgen, I., and Hinkelmann, R. (2014). A model for overland flow and associated processes within the Hydroinformatics Modelling System. https://doi.org/10.1007/s12665-015-4726-7

Scharffenberg, W., Ely, P., Daly, S., Fleming, M., and Pak J. (2010). Hydrologic modeling system (HEC-HMS): physically based simulation components.

Proceedings of the 1st IAHR
Young Professionals Congress
17-18 November 2020

SIMULATION OF HYDROLOGICAL AND MORPHODYNAMICAL PROCESSES IN A MOUNTAIN CATCHMENT OF THE CENTRAL PYRENEES

Javier Fernández-Pato[*1,2], Sergio Martínez-Aranda[1,3], Noemí Lana-Renault[4], Pilar García-Navarro[1,3]

[1]Fluid Mechanics, University of Zaragoza, Zaragoza, Spain
[2]Hydronia-Europe S.L., Madrid, Spain
[3]LIFTEC-CSIC, Zaragoza, Spain
[4]Departament of Human Sciences, University of La Rioja, Logroño, Spain

*Correspondance : jfpato@unizar.es

ABSTRACT

An efficient and properly calibrated computational model represents a useful tool to provide insight into the catchment dynamics at hydrological and geomorphological levels. In addition, it allows to develop detailed risk management and conservation plans. In this work, we present a coupled hydraulic-morphodynamical distributed flow model and its application to a well characterized experimental catchment (Arnás basin). The calibration of the water flow model response to rainfall is performed by means of the fitting to experimental outlet hydrographs. On the other hand the calibration of a suspended and bed load model is also addressed by means of the fitting to experimental outlet sedigraphs. The numerical results show a good agreement between numerical and observed hydrographs and sedigraphs, significantly improving previous published simulations. Additionally, the need to repeat the simulations in the calibration processes is no longer an unapproachable problem.

Keywords: Shallow flows, Mountain catchment, Sediment transport, Infiltration, Coupled models.

1 INTRODUCTION

Environmental-related sciences have evolved in the last decades due in part to the introduction of simulation techniques at catchment scale Singh (2018). Most of the processes participating in the hydrological cycle can be considered, in a distributed way by discretizing the spatial domain in as many computational cells as necessary, conforming the discrete mesh. Each cell works as a water and sediment control volume where the net surface water flow and sediment transport inputs/outputs, the rainfall input, the infiltration/exfiltration fluxes and the changes in bed level due to erosion/deposition processes are taken into account. In this work, data from a sub-Mediterranean experimental mountain catchments (Arnás) is used. It has been widely studied and characterized from an experimental point of view by researchers from the IPE/CSIC (Instituto Pirenaico de Ecología) Lana-Renault et Regüés (2007). This catchment has also been studied from a numerical perspective in the past, focusing on the calibration of the infiltration component of the model Fernández-Pato *et al.* (2018).

2 GOVERNING EQUATIONS

Free surface flows are usually described in Hydraulics by means of the depth-averaged 2D Shallow Water Equations (SWE),

$$\frac{\partial \boldsymbol{U}}{\partial t} + \frac{\partial \boldsymbol{F}}{\partial x} + \frac{\partial \boldsymbol{G}}{\partial y} = \boldsymbol{S} \tag{1}$$

$$\boldsymbol{U} = (h, q_x, q_y)^T, \qquad \boldsymbol{F} = \left[q_x, \frac{q_x^2}{h} + \frac{1}{2} g h^2, \frac{q_x q_y}{h} \right]^T, \qquad \boldsymbol{G} = \left[q_y, \frac{q_x q_y}{h}, \frac{q_y^2}{h} + \frac{1}{2} g h^2 \right]^T \tag{2}$$

with h representing the water depth and $q_x = hu$ and $q_y = hv$ the unit discharges, u and v the depth averaged components of the velocity vector $\boldsymbol{u}$ along the x and y coordinates, respectively, and the acceleration due to gravity is represented with g. The source term $bf\ S$ on the right hand side of the equations is written as

$$\boldsymbol{S} = (R - f - \xi \omega_s (\varphi - \varphi^*), gh(S_{0x} - S_{fx}), gh(S_{0y} - S_{fy}))^T \tag{3}$$

where the mass source term includes the rainfall intensity R, the soil infiltration/exfiltration rate f, computed by a Fractional-Order Green-Ampt method (FOGA) Fernández-Pato *et al.* (2018) and the net solid exchange flux between the flow and the static bed $\xi \omega_s(\varphi - \varphi^*)$, being ω_s the settling velocity of the solid particles, φ the actual depth-averaged volumetric concentration of the sediment transported in suspension, φ^* the equilibrium or capacity volumetric concentration for the suspended solid phase, $\xi = 1/(1 - p)$ and p the porosity of the bed layer. S_{0x}, S_{0y} and S_{fx}, S_{fy} represent the bed and energy slopes along the x and y direction, respectively, and are given in terms of the bed elevation z_b and the Manning roughness coefficient n. The suspended solid phase conservation is modeled by an advection equation, leaving aside the consideration concerning diffusion terms:

$$\frac{\partial (h\varphi)}{\partial t} + \frac{\partial}{\partial x}(q_x \varphi) + \frac{\partial}{\partial y}(q_y \varphi) = -\omega_s (\varphi - \varphi^*) \tag{4}$$

3 RESULTS AND CONCLUSIONS

Figure 1 shows the combined fit for numerical hydrograph and sedigraph. The results corresponding to the classical Green-Ampt (GA) model are also depicted for both liquid and solid discharges. In the light of the numerical results, several conclusions can be drawn: 1) The GA infiltration model predicts excessive infiltration in the early period of the storm, leading to a wrong reproduction of the outlet hydrograph; 2) A wrong fit of the outlet hydrograph generates a wrong numerical outlet sedigraph. In other words, a correct estimation of the infiltration along the whole catchment is essential in order to carry out an adequate sediment transport computation. 3) The use of the FOGA infiltration law improves significantly both hydrograph and sedigraph fits.

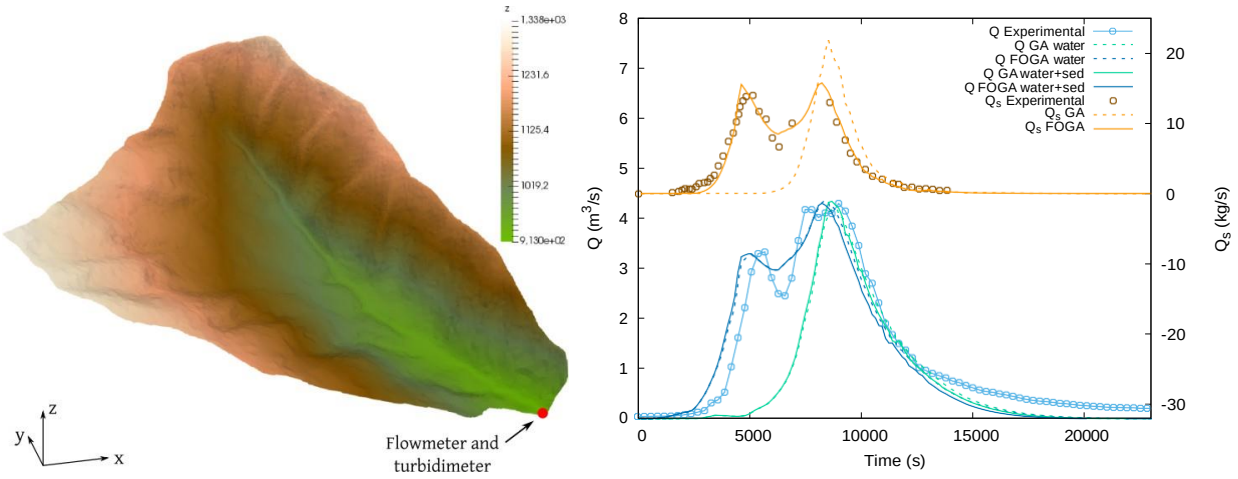

Figure 1: Arnás catchment hypsometry map (left) and numerical fit to observed hydrograph and sedigraph.

References

Fernández-Pato J., Gracia J. L., García-Navarro P. (2018, 04). A fractional-order infiltration model to improve the simulation of rainfall/runoff in combination with a 2D shallow water model. *Journal of Hydroinformatics 20*(4), 898–916.

Lana-Renault N., Regüés D. (2007). Bedload transport under different flow conditions in a human-disturbed catchment in the central spanish pyrenees. *Catena 71*, 155–163.

Singh V. (2018). Hydrologic modeling: progress and future directions. *Geoscience Letters 5*(15).

Proceedings of the 1st IAHR
Young Professionals Congress
17-18 November 2020

EVALUATION OF FLOODPLAINS ALONG THE DANUBE IN AUSTRIA WITH THE FLOODPLAIN EVALUATION MATRIX - COMPARISON OF 1D AND 2D MODELS

Lena Ferstl[*1], Markus Eder[1], Sabrina Scheuer[1], Helmut Habersack[1]

[1]Institute of Hydraulic Engineering and River Research (IWA), Department of Water, Atmosphere and Environment, University of Natural Resources and Life Sciences, Vienna, Austria

*Correspondance : lena.ferstl@outlook.com

ABSTRACT

For the preservation of floodplains within integrated flood risk management, the evaluation of floodplains and their effectiveness in flood risk reduction is of great significance. To apply the Floodplain Evaluation Matrix (FEM), hydrodynamic-numerical modeling results are needed. This work compares 1D/2D HEC-RAS models with HYDRO AS-2D model results regarding the sufficient reproduction of floodplain retention during extreme flood events. The simplified FEM evaluation assigns high performance to all parameters and leads to the conclusion that all of the studied models are valid for the assessment.

Keywords: Flood risk reduction, floodplain evaluation method, floodplain retention, HEC-RAS.

1 INTRODUCTION

Due to the multifold uses on floodplains, conflicts between different sectors arise (flood protection, ecology and socio-economics). In order to effectively balance the distinct needs and to determine the floodplains which are highly relevant for different sectors, a methodology for an integrated evaluation of floodplains was developed (Floodplain Evaluation Matrix, Habersack *et al.* (2015)). The parameters are based on results from hydrodynamic-numerical modeling. Whenever overbank flows are of interest, 2D modeling is recommended to correctly represent the complex processes of overland flow. Due to insufficient data basis or financial reasons, often 1D software is used. This work aims to compare 1D and 2D models and their capability to reproduce observed floodplain retention. The modeling results from the different models are used to determine the performance of the parameters.

2 METHODS

A 76 km long stretch of the Austrian Danube upstream of Vienna is modeled using HEC-RAS with 1D elements and a 2D Flow Area. An existing model of the commonly used license-based software HYDRO AS-2D serves as reference (Riocom/Pöyry, adapted by IWA). The three models are based on the same DTM and are calibrated to observed retention during the flood event of 2013 (>HQ100). The results are compared and a 100-year flood wave is used to determine the FEM-parameters. The simplified FEM-approach applied in this case focuses on hydrological parameters only. The relevant parameters are flood peak reduction (ΔQ_{rel}) and flood wave translation (Δt). For the relative parameter ΔQ_{rel} (%) the absolute value of flood peak reduction (m^3/s) is put into relation with the peak value and the bankfull discharge. According to the resulting values and defined thresholds the performance class (high, medium or low) of the floodplain is determined.

The calibrated HEC-RAS models were able to reproduce the 2013 flood peak at the end of the floodplain with only small variations. The inundation outlines coincide with all models. The 100-year simulations show similar results of all models (Table 1, Figure 1). All parameters performed high. The defined thresholds for high performance are $\Delta Q_{rel} > 2\,\%$ for the parameter Flood peak reduction and $\Delta t > 5$ h for the parameter Flood wave translation).

Table 1: Comparison of FEM parameters

	ΔQ_{rel} (%)	Δt (h)
HEC-RAS 1D	11.8	13.0
HEC-RAS 2D	12.6	18.0
HYDRO_AS-2D	12.3	20.5

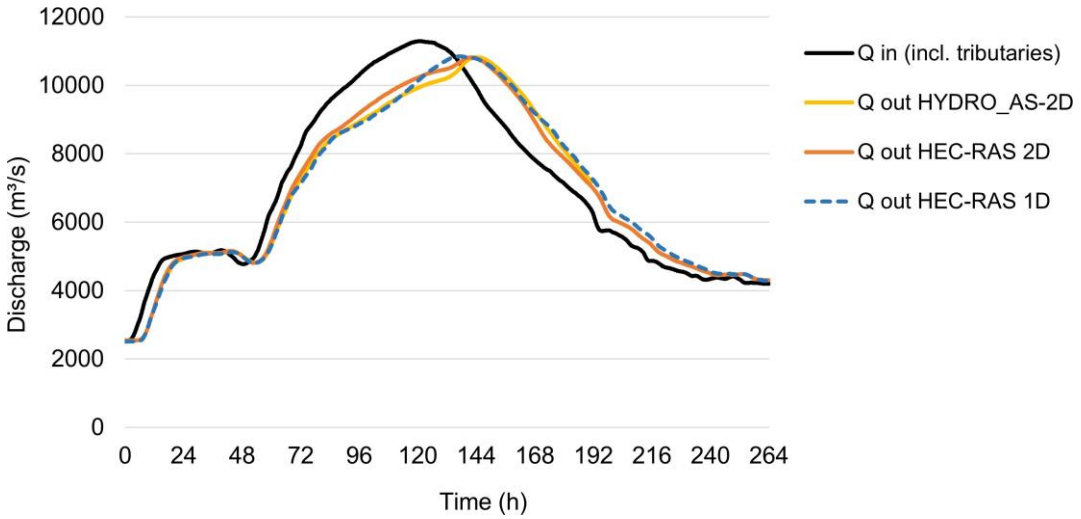

Figure 1: Comparison of modeled retention of 100-year event (scaled event 2013)

4 CONCLUSIONS

Generally, it is possible to sufficiently reproduce the resulting retention of certain floodplains using the tested alternative models. Since all evaluated parameters were assigned to the same performance class according to FEM parameters, all models are applicable for floodplain evaluation in the context of retention effects. HEC-RAS allows easy and fast generation of a 2D computational mesh. HEC-RAS models generally allow for a more detailed calibration, due to considerably lower computational times compared to HYDRO AS-2D (several hours vs. days) which primarily result from different mesh sizes. HEC-RAS 1D geometry for unsteady simulation and heterogeneous flow patterns produces instability to a high extent. When stable, models can be calibrated thoroughly assigning varying flow roughness values from lower to higher flows, varying coefficients of lateral structures, floodplain roughness and ineffective flow areas. It can be observed, that in 1D model assigning extensive ineffective flow areas instead of high manning values leads to improved results regarding flood peak reduction and flood wave translation. However, several other processes might influence these parameters and the performance of the model. Deviations in modeled vs. observed hydrographs could be a consequence of the simplified incorporation of weir geometry and gate operation at power plants, and the quite rough manning values in the impounded sections, which are necessary to reproduce the elevated water levels at the overflow sections in order to assure outflow at certain flow rates. In what way this affects retention processes of the whole modeled stretch is a topic of further discussion. Furthermore, it would be interesting to analyze HEC-RAS performance on retention reproduction at floodplains where retention is less dependent on weir operation. Also, 1D and 2D geometry elements could be combined in order to benefit from advantages that were observed for the individual HEC-RAS models.

References

Habersack H., Schober B., Hauer C. (2015, sep). Floodplain evaluation matrix (FEM): An interdisciplinary method for evaluating river floodplains in the context of integrated flood risk management. *Natural Hazards 75*(S1), 5–32. doi:10.1007/s11069-013-0842-4.

Proceedings of the 1st IAHR
Young Professionals Congress
17-18 November 2020

A PROCEDURE FOR HUMAN SAFETY ASSESSMENT DURING HYDROPEAKING EVENTS

Giuseppe R. Pisaturo[*1], Maurizio Righetti[1], Claudio Castellana[2], Michele Larcher[1], Andrea Menapace[1], Georg Premstaller[3]

[1]Free University of Bozen-Bolzano, Faculty of Science and Technology, Bolzano, Italy
[2]Department of Civil, Environmental and Mechanical Engineering, Trento, Italy
[3]Department of Engineering & Consulting Alperia plc, Bolzano, Italy

*Correspondance : gpisaturo@unibz.it

ABSTRACT

A method for human safety assessment on a hydropeaked river reach is proposed and applied to an Alpine river. The proposed procedure is characterized by the combination of hydraulic simulations with a human safety analysis. Human safety can be assessed in two different ways: one is by studying human stability during hydropeaking events and the other is exploring the possibility of a "target person" leaving the reach during hydropeaking waves, adapting proper escape strategies. For the escape strategy Dijkstra's algorithm is used, where the distance between adjacent nodes is defined as the difficulty (penalty) of moving from one node to the other. The results show that the areas where the human safety is very low are mainly located in the central part of the watercourse. The present work proposes a possible investigational tool to evaluate and parameterize the risk for the population during hydropeaking events through quantitative indices.

Keywords: open channel flow, hydropeaking, escape route, human stability, human safety.

1 INTRODUCTION

High-head Hydropower Plants (HPPs) have an important role in peak energy supply but storage hydropower plants (hydropower plants with a storage basin to support peak energy production) can have several negative effects on the ecosystems of the downstream watercourses. The intermittent operation of the storage hydropower plants induces artificial and sudden changes of the downstream flow rate (hydropeaking) (Meile *et al.* (2011)). Together with environmental issues, there is also another aspect of increasing interest, but not yet properly debated and analyzed in the scientific literature: the human safety during hydropeaking events. The present work focuses in detail on the interaction between hydropeaking and human safety and on the conditions for which a person can safely withstand a hydropeaking wave ramping and, if feasible, can escape from the river itself.

2 METHOD

The procedure proposed for risk assessment is structured into two steps. In the first one, hydraulic simulation of the hydropeaking are performed. Secondly, Dijkstra's algorithm (Cormen *et al.* (2009)) is applied defining the penalty functions for the distance parameter for each cell in which the reach is subdivided.

The relative penalty values of these have been assigned according to the following scheme:

- higher penalty value was assigned to steep uphill paths;
- higher penalty values for cells containing trees or bushes and cells containing large boulders;
- hydrodynamic limit values (hydraulic parameter) have been proposed by Bischof *et al.* (2002) and the most penalizing values are assigned to hydrodynamic parameters that exceeds the higher risk threshold

It is possible to evaluate for each computational cell the escape route that minimizes the difficulty of escape from a given cell in the reach, to the banks (that are considered safe), for a given flow rate.

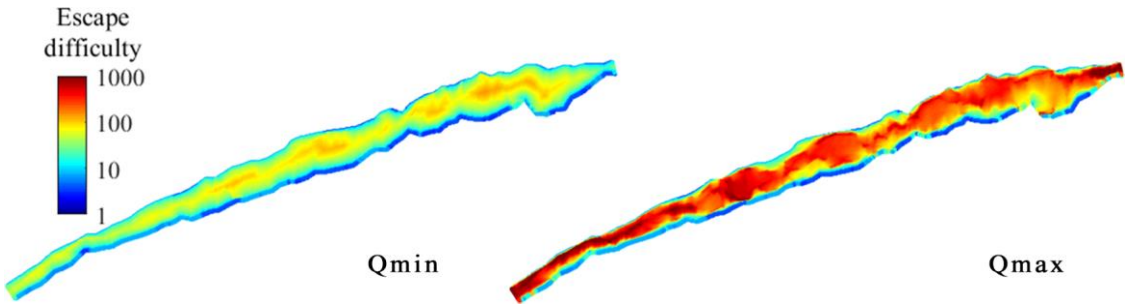

Figure 1: Escape difficulty for the minimum flow (Qmin) and maximum flow (Qmax) .

In the map concerning the minimum flow (Figure 1), it can be noted that the difficulty is low for the entire reach. The difficulty of escape only increases in the few areas that are distant from the banks and when the water depth is quite high. In addition, the escape map for the minimum flow rate can also be read as the map of ease of access to the watercourse so it also represents which areas are most easily accessible by the population. These easily reached areas, could then become a trap during the flow rate increase. Observing Figure 1 for Qmax, in fact, it can be observed that the areas with good and excellent escape readiness are located exclusively along the river banks. In the central areas of the river the escape readiness is very low and in some areas it is totally impossible to leave the river. This trend is given by two factors of equal importance. Since the difficulty to escape was defined as the sum of the difficulty of the individual segments along the path, the increase in the difficulty of escape from the center of the river bed is obviously a direct consequence of the increase in the distance to travel necessary to exit the riverbed. A second aspect to take into consideration also concerns the hydraulic aspect linked to the difficulty of escape. In fact, in the central part of the watercourse, higher values of water depth and flow velocities are present, which cause an increase in the difficulty of escape. This aspect is evident in the red areas that, despite the relative proximity to the banks, are extremely difficult to leave for high flow rates. This is almost exclusively due to the hydraulic characteristics of those areas with high water depths and flow velocities. These areas are in fact located in areas of the river where a wet section narrowing is present.

4 CONCLUSIONS

The present work aims at proposing a possible investigational tool for understanding the risk for the population during hydropeaking events. The method proposed is based on hydraulic simulations and on the capacity to assign a realistic value to the penalty values. This last aspect is the main source of uncertainty in our research and would be better investigated with information from field experts and local security bodies such as firemen in future studies. However, the method proposed is able to provide indications about the possibility of using rivers for recreational purposes. In fact, the approach can define which areas can be safely reached and abandoned if the flow rate increases during hydropeaking. Moreover, the same maps can be used during the people recovery phases who are blocked in the water course. Finally, the method can be also utilized to evaluate the efficiency against human safety of typical mitigation measures adopted to increase the level of good habitat in the stream.

5 ACKNOWLEDGEMENTS

Part of this work was supported by the projects HSAH (RTD Call 2018) and CRC project HM: Hydropeaking mitigation, financed by the Free University of Bozen-Bolzano.

References

Bischof R., Hauenstein W., Kalt L., Müller R. W., Pougatsch H., Raboud P.-B., Vetterli W. (2002). Sicherheit der Stauanlagen - Basisdokument zu den Unterstellungskriterien. Technical report.

Cormen T. H., Leiserson C. E., Rivest R. L., Stein C. (2009). *Introduction to algorithms - 3rd edition*. London: The MIT Press.

Meile T., Boillat J. L., Schleiss A. J. (2011). Hydropeaking indicators for characterization of the Upper-Rhone River in Switzerland. *Aquatic Sciences*, 171–182. URL: http://link.springer.com/article/10.1007/s00027-010-0154-7, doi:10.1007/s00027-010-0154-7.

Proceedings of the 1st IAHR
Young Professionals Congress
17-18 November 2020

ASSESSMENT OF LAND COVER CHANGES OF MARIKINA WATERSHED, PHILIPPINES TO RIVER RUNOFF AND FLOODING

Patricia Mae J. Paraiso [1], Ma. Flordeliza P. Del Castillo [2] & May Celine T.M. Vicente [2]

[1] University of the Philippines Los Baños, Laguna, Philippines
pjparaiso@up.edu.ph
[2] Manila Observatory, Quezon City, Philippines
fpdelcastillo@observatory.ph, celine@observatory.ph

ABSTRACT

Land cover in Marikina Watershed has been changing in the past years and have influenced the hydrological parameters in the area especially the runoff of Marikina River. Land cover data of 2009 and 2018 were used in determining the effect of land cover changes on peak discharge and timing of runoff. A Typhoon Ketsana scenario-based hydrologic and hydraulic models were generated with HEC-HMS and HEC-RAS. Flood model results showed increases in both peak discharge (500 m^3/s) and volume of flood (40 mm). Modelled peak discharge for land cover of 2018 happened 15 minutes earlier than in 2009. Flood extent in the downstream areas also increased by an estimated of 7 km^2. The increase in areas converted to built-up raised the risk of flooding downstream. Forest cover should be protected to mitigate flooding and flood modelling is recommended as a potential early warning system and tool in disaster risk planning.

Keywords: flood model, HEC-HMS, HEC-RAS, land cover change, watershed management

1 INTRODUCTION

Flooding is considered as one of the most common and most destructive natural hazards. In the Philippines, these are caused by increasing typhoon activity where an average of 19 typhoons enter the Philippine Area of Responsibility (Cinco et al., 2016). Land cover also plays an important role in influencing the hydrologic response of watersheds in multiple ways (Dwarakish & Ganasri, 2015). In September 2009, typhoon Ketsana (Ondoy) brought in a record 448.5 mm of rain in 12 hours leading to 10.99 m increase in the water level of Marikina River (NOAH, 2009). Flooding in parts of the watershed was repeated in the next few years during wet season.

The main objective of the study is to determine how urban development in the Marikina Watershed would affect flood characteristics of a Tropical Storm Ketsana-type rainfall in 2009. Hydrologic-hydraulic models were done using land covers of 2009 and 2018. Both the precipitation and estimated discharge of 2009 are used as scenarios and constant in both models. The study is limited to HEC-HMS Hydrologic Engineering Center - Hydrologic Modeling System (HEC-HMS) and HEC-River Analysis System (HEC-RAS) programs of the United States Army Corps of Engineers. The Nash-Sutcliffe Coefficient of Model Efficiency (NSE) was used for the validation of hydrologic models.

2 RESULTS AND DISCUSSION

The delineated watershed for Marikina River has a total area of 535.5 km^2 making it the largest watershed draining to the Laguna Lake. Its slope ranges from 4-51° and the elevation ranges from 2 -1403 meters above sea level. Overall, 439.8 km^2 (82.3 %) of Marikina Watershed was unchanged and 33.27 km^2 was urbanized from 18.8 km^2 of open forest and 12.8 km^2 of grassland. This means that urbanization is the main direction of change leading to 4.5% increase in impervious surface. The watershed has 45 sub-basins, 22 junctions and 22 reaches. It has a computed shape factors of 0.21- 7.22 among its sub-basins and has a semi-circular shape, circular at the upstream with some elongation near the outlet.

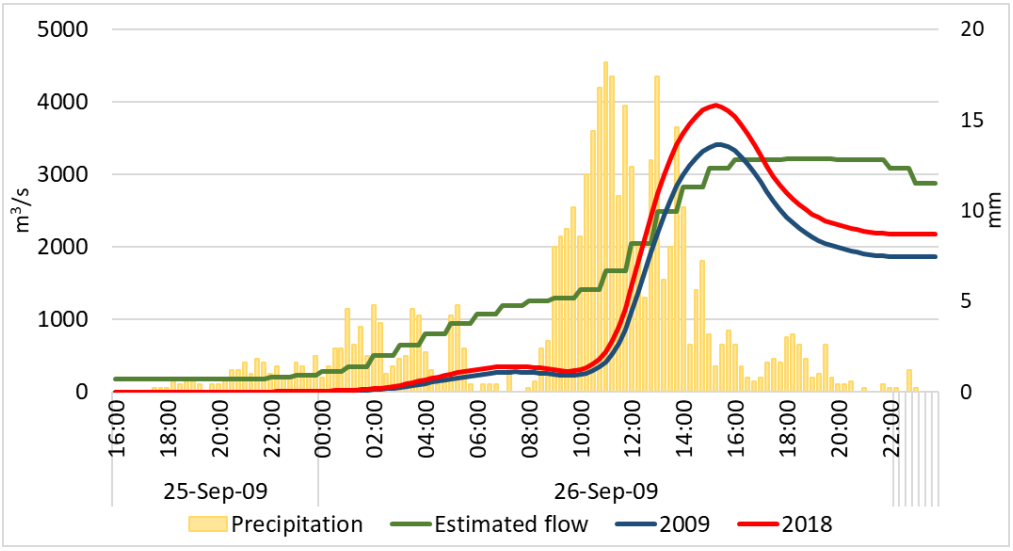

Figure 1. Hydrograph models of 2009 and 2018.

The streamflow data (m^3/s) is estimated from Marikina River's hourly water level (Sto. Niño station) data up to September 26, 2009 because the monitoring device was damaged the following day. The peak discharge and volume of flow of 2009 model corresponded to 3,414.9 m^3/s (September 26 at 15:30) and 205.76mm (Figure 1). For the 2018 model, the peak discharge is 3,951.1 m^3/s (September 26 at 15:15) which is higher and 15 minutes earlier than the result for 2009. This suggests that the land cover changes, mainly urbanization and the decreased vegetal cover, affected the peak runoff by more than 500 m^3/s. The volume flow of 242.74mm is also higher than the previous model. The NSEs for both 2009 and 2018 models increased after calibration to 0.641 and 0.717 indicating the difference between the simulated and estimated flows was minimal and the models were considered more than satisfactory.

The 4-hour time difference between the peak rainfall and peak discharge can be utilized for evacuation. Flood extents covering approximately 36.20 km^2 for 2009 while 43.03 km^2 for 2018 were generated. The model maps were overlain to Marikina 5-, 25- and 100- Year Flood Hazard Maps and they overlapped inside the flooded area. They were also in accordance with the flood reports during Typhoon Ketsana.

3 CONCLUSIONS

In the Marikina Watershed, urban area expanded by 5% from 2009 to 2018 and the tree-covered surface was reduced by roughly 5% as well. The computed results for the 2018 scenario follow the same pattern but is higher and 15 minutes earlier than 2009. This concludes that land cover changes affected the response of Marikina River. Using the hydrograph produced, the flood model in the downstream areas also increased by an estimated of 7 km^2 for 2018 scenario. Land cover change can be considered in flood mitigation and disaster risk planning. Vegetal cover should be increased by allocating green spaces. Hydrologic and hydraulic modelling are effective tools in decision making for watershed management.

ACKNOWLEDGEMENTS

This study is part of Coastal Cities at Risk in the Philippines: Investing in Climate and Disaster Resilience Project (CCARPH). It is implemented by Ateneo de Manila University and Manila Observatory, in partnership with National Resilience Council and with support from International Development Research Centre (IDRC).

REFERENCES

Cinco, T., Guzman, R., Ortiz, A.M., Delfino, R.J., Lasco, R., Hilario,F., and Ares, E. (2016). Observed trends and impacts of tropical cyclones in the Philippines. *International Journal of Climatology*, https://doi.org/10.1002/joc.4659.

Dwarakish, G.S., and Ganasri, B.P. (2015). Impact of land use change on hydrological systems: A review of current modeling approaches. *Cogent Geoscience*, 1(1), 1115691. https://doi.org/10.1080/23312041.2015.1115691.

National Operational Assessment of Hazards (NOAH) (2009). Ondoy (2009), Floods in Marikina City, Metro Manila, Disaster Timeline. Retrieved from https://center.noah.up.edu.ph/ondoy-flood-metro-manila/.

Proceedings of the 1st IAHR
Young Professionals Congress
17-18 November 2020

COUPLED HYDRODYNAMIC AND HYDROLOGIC MODELLING USING TELEMAC-2D

Nitesh Godara[1], Michal Pavlíček[2], Oddbjørn Bruland[3]

[1,2] PhD Scholar, Norwegian University of Science and Technology, Trondheim, Norway
[3] Professor, Norwegian University of Science and Technology, Trondheim, Norway
e-mail : nitesh.godara@ntnu.no

ABSTRACT

Floods and other hydrological processes are difficult to estimate because of complex relationship between various meteorological and basin parameters, extreme rainfall events and complex topography such as steep slopes within the catchment. Telemac-2D model is used for rainfall- runoff modelling in a steep and small (10.5 km2) catchment in Møre og Romsdal county in western Norway. Telemac-2D is a hydrodynamic model and the SCS curve number method can be used in the rainfall-runoff module of this model to extend it to a Hydrodynamic Rainfall-Runoff Model (HDRRM). This paper focuses on the coupling of the hydraulic model and the hydrologic model to extract the hydrograph at any point in the catchment. The implemented hydrological scheme is quite simple, and the simulation is inaccurate and quite slow from the hydrologic point of view because of coupling with the hydraulic model. The purposes of this work are to improve the hydrological scheme in Telemac-2D, increasing the accuracy of the coupled model and reducing the simulation runtime.

Keywords: Hydrology, steep catchment, floods, Telemac-2D, rainfall-runoff modelling.

1 INTRODUCTION

Telemac-2D is a hydrodynamic model solving the shallow water equations. Since telemac-2D has a supplement to include Soil Conservation Curve Number (SCS-CN) it can be extended with a hydrodynamic rainfall-runoff model. The SCS - method was developed by USA's Soil Conservation Services. This method is widely used throughout the world because it is very stable and based on the empirical data (Ligier; 2016). SCS-CN method is very simple and easy to use as the infiltration losses depend only on one parameter curve number which is based on the land- use and hydrologic soil group present in the catchment.

2 METHODS

2.1 Input data collection and preparation

The area chosen for this study is Sleddalen catchment which lies in Møre og Romsdal county of Norway. The catchment is very steep whose elevation drops from 1379m to 77m and its approximate area is 10.5 km^2. The digital elevation model (DEM) for the catchment was downloaded from høydedata.no which is obtained by red lidar scan of the area. The curve number file used as input was extracted from the GCN250, new global gridded curve numbers (Jaafar et al.,2019). The main meteorological data required for the rainfall-runoff modelling using Telemac-2D is the precipitation data in the form of a hyetograph text file. Precipitation data for the catchment was downloaded from the website senorge.no, where the hourly precipitation data was available from 2018 mid-October to the present date. The triangular mesh for the geometry file was generated using Bluekenue.

2.2 Running the simulations

The main input files required for running the simulation are geometry file containing the information about the basin characteristics and curve numbers, boundary condition file, hyetograph file and the simulation file. The model was tested by running the simulations for the different time periods between October 2018 and September 2020 using different scenarios such as changing the mesh sizes in the river and the catchment, curve numbers, AMC conditions and the temporal scale of the precipitation data.

3 FINDINGS AND ARGUMENTS

The main result is presented in Figure 1 (on the left). The model responds to the rainfall, but there are large discrepancies between observed and simulated. In this simulation, a mesh size of 10m in the river and 500m in the remaining catchment was used.

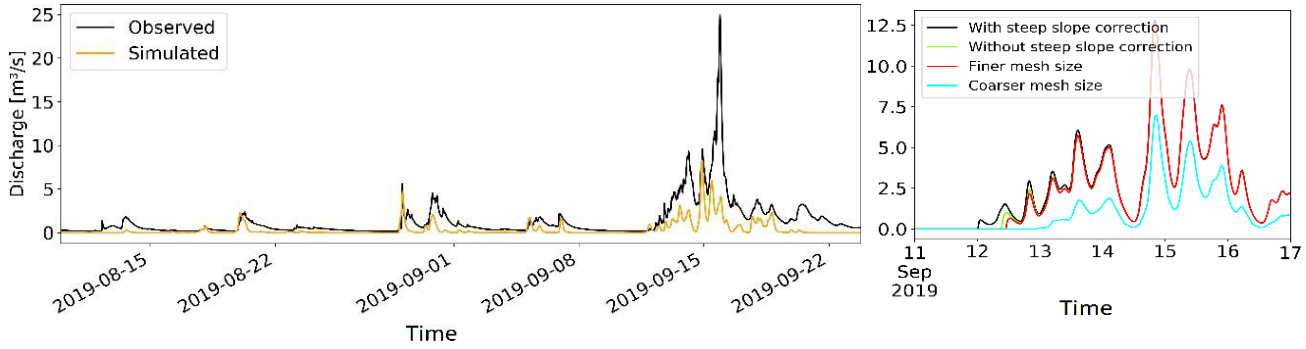

Figure 1. Observed and simulated discharge for a longer period with a coarse mesh size (on the left), Effect of steep slope correction and the mesh size (on the right).

The effects of changing the antecedent moisture conditions (AMC) and the curve number were as expected i.e. increasing the curve number throughout the catchment gave the higher runoff volume and changing the AMC conditions from AMC3 (wet conditions) to AMC1 (dry conditions) decreased the runoff volume. Some studies have shown that increasing the catchment slope increases the runoff volumes (Taccone et Antoine; 2015). The average catchment slope is approx. 48% but the catchment has sudden drops making it more than 100% at some places. Hence the correction for steep slope was applied. Figure 1 (on the right) shows that the effect was significant only in the beginning of the simulation time period.

To make the simulations faster, coarser mesh was generated in the catchment and the river. The benefit of this was that the simulation runtime was decreased many-fold, but it did not represent the true geometry of the river. Using the coarser mesh in the river also made it difficult to catch the exact volume of the water in the river which resulted in the lower volume of the water than the actual. 3m triangular mesh size was used for the river and 5m mesh size was used for the remaining catchment as the finer mesh size while, 10m mesh size was used for the river and 500m was used for the remaining catchment as the coarser mesh size. The effect of mesh size on the results are shown in Figure 1 (on the right).

4 CONCLUSION

A steep and small Norwegian catchment was chosen for the rainfall-runoff simulation. Hydrologic model was coupled with the hydraulic model using the SCS-curve number rainfall- runoff module present in telemac-2D model. The simulations were very fast in terms of hydraulic modelling but quite slow in the hydrologic point of view. Running the simulation for a longer time period (with course mesh size) showed that currently the results for peak discharges are not very good for the coarser mesh size, but the volume of the water can be made more precise with the finer mesh size. In the future work, more sophisticated hydrologic models and methods including a snow routine will be implemented in telemac-2D to improve the simulation results. In addition to that, the aim will be to further reduce the simulation runtime.

REFERENCES

Jaafar H. H., Ahmad F. A., El Beyrouthy N. (2019). Gcn250, new global gridded curve numbers for hydrologic modeling and design. Scientific data 6(1), 1–9.

Ligier P.-L. (2016). Implementation of a rainfall-runoff model in telemac-2d. In *Proceedings of the XXIIIrd TELEMAC-MASCARET User Conference 2016, 11 to 13 October 2016, Paris, France*, pp. 13–19.

Taccone F., Antoine G. (2015). Numerical modeling of sediment transfers at the catchment scale with telemac. In *Proceedings of the XXII TELEMAC-MASCARET Technical User Conference October 15-16, 2044*, pp. 18–27.

Proceedings of the 1st IAHR
Young Professionals Congress
17-18 November 2020

OPTIMIZATION AND VISUALIZATION OF NUMERICAL MODELS OF FLASH FLOODS IN STEEP NORWEGIAN RIVERS

Adina Moraru[*1], Andrew Perkis[1], Oddbjørn Bruland[1], Nils Rüther[1]

[1]Norwegian University of Science and Technology (NTNU), Trondheim, Norway

*Correspondance : adina.moraru@ntnu.no

ABSTRACT

Visualizing results is more important than ever in scientific dissemination. The analysis and communication of complex phenomena such as flash floods requires new approaches. The target is using a state-of-the-art model with a fast and robust predictive capability, which has been tested in small, steep rivers affected by recent flash floods, and visualizing this model in a relatable manner. To do so, this research project aims to achieve optimized simulations that could be carried out in the prototype of a serious gaming engine. The incentive for such optimized simulations is that complex hydraulic modelling is data- and computationally costly. This clashes with the need for low complexity solutions in the real-time based scenarios that an immersive experience and on-site decision-making requires.

Keywords: flash floods, steep rivers, hydraulic modelling, optimization techniques, visualization of numerical models.

1 RESEARCH MOTIVATION

Visualizing the dynamics during a flash flood based on hydraulic modelling, as well as enabling more efficient numerical simulations, would enhance flood risk assessment and its communication. Available models for floods in steep Norwegian rivers do not convey the estimated risk based on a user-friendly and three-dimensional real world. Moreover, 3D visualizations that could be used for educational or training purposes are often not based on precise hydraulic data.

The target is to implement the optimized numerical models into the prototype for a serious gaming flood platform (e.g. Virtual Reality or Augmented Reality). Thus, the flood scenario will be complimented by gamification, storytelling and immersive narrative techniques, which will provide a better user experience and improved risk perception. The current paper provides an overview of ongoing research, where several methods have been implemented to address the need for faster hydrodynamic models in two steep Norwegian rivers.

2 METHODOLOGY

The following modelling techniques were implemented in two Norwegian rivers, namely Byrteåi in Tokke- and Storelva in Utvik municipalities (south and west of Norway, respectively):

- Parallel CPU-based computing of 2D models;
- GPU-based computing of 2D models;
- Machine Learning (ML) for 1D emulation models.

River Byrteåi (in Tokke), which was flooded in 2009, was used to identify critical areas based on geomorphic indexes and parallel CPU-based 2D numerical modelling. The river's geometry was modified and its slope was virtualized into constant values along the modelled reach to identify the influence of other parameters in the river response. The results of such study and its applications are described in detail in (Moraru *et al.*, 2019, 2020). Such critical areas have the potential of being further combined into a locally refined, yet faster-solving, model.

The flash flood that affected Storelva river (in Utvik) in 2017 (Bruland, 2020) has been modelled in 2D (i.e. HEC-RAS, Iber; 1(a)) and also visualized in 3D (i.e. Blender, Unity, Autodesk 3ds Max). The focus of the 2D models was to understand the dynamics during the flood event in comparison to on-site documentation of the flood, as well as searching for an optimal numerical method for small and steep rivers. The HEC-RAS model was carried out on multiple parallel CPU threads, while the Iber numerical model was carried out on both CPU (single and multi-thread), as well as on GPU (1(b)). Furthermore, the obtained 2D Iber model was used as input data for a ML emulation model, and their performance was subsequently compared by Son (2020). Section 3 highlights especially the outcome of using Iber CPU- and GPU-based computing in Storelva in Utvik.

3 PRELIMINARY RESULTS: CPU VS GPU FOR THE 2017 FLASH FLOOD

GPU computing, as well as the use of ML, are state-of-the-art optimization techniques (Moraru *et al.*, 2020). The computing tool used for numerical modelling will determine greatly the performance of the model, nevertheless. For instance, preliminary results of a comparison of the computing performance of different CPUs and GPUs in a small model of the 2017 flash flood (1(a)) shows that GPU-based computing is generally quicker than CPU-based computing and that the dispersion of the data is larger in the CPU tests than in the GPU tests (1(b)).

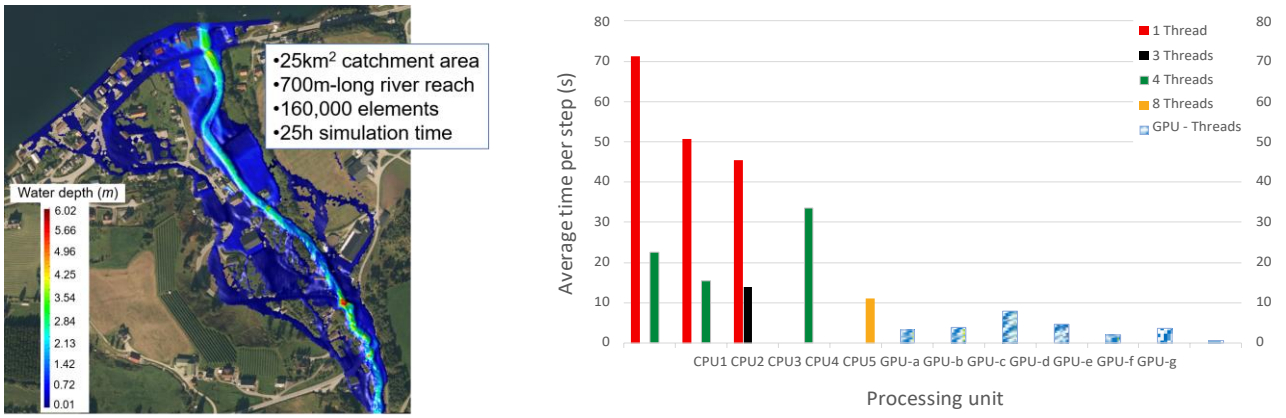

(a) Utvik flash flood modelled on GPU

(b) Preliminary CPU and GPU comparison for Utvik study case

Figure 1: (a) Study case, (b) average computing time per step for different CPUs (single- and multi-thread) and GPUs.

CPU- and GPU-based simulations need different computational effort based on the number of threads available in the processing unit, i.e. the CPUs shown in 1(b) have from 1 to 8 threads, whereas the respective GPUs have from 384 to 4352 threads. As the simulation will experience a speedup until all threads are fully used, the speedup will be larger in GPU-based simulations than in CPU-based ones. In conclusion, this makes a personal computer with a GPU suitable for fast hydrodynamic simulations of flash floods in steep Norwegian rivers.

Acknowledgements

The authors wish to thank an anonymous reviewer for the valuable feedback. This publication is part of the World of Wild Waters (WoWW) project, which falls under the umbrella of Norwegian University of Science and Technology (NTNU)'s Digital Transformation initiative.

References

Bruland O. (2020). How extreme can unit discharge become in steep Norwegian catchments? *Hydrology Research 51*(2), 290–307. doi:10.2166/nh.2020.055.

Moraru A., Rüther N., Bruland O. (2020). Current trends in the optimization of hydraulic flood simulations in ungauged steep rivers. In W. Uijttewaal *et al.* (Eds.), *10th International Conference on Fluvial Hydraulics (River Flow 2020)*, Delft, the Netherlands, pp. 1231–1238. Taylor & Francis Group, ISBN 978-0-367-62773-7.

Moraru A., Usman K. R., Bruland O., Alfredsen K. (2019). River idealization for identification of critical locations in steep rivers using 2D hydrodynamic modelling and GIS. In *22nd Northern Research Basins Workshop and Symposium*, Yellowknife, Canada, pp. 144–153. doi:10.13140/RG.2.2.13276.64647.

Son S. (2020). *Optimization of hydraulic flood simulations in steep rivers using GPU and Machine Learning*. Msc thesis, Universitat Politecnica de Catalunya - Norwegian University of Science and Technology.

IAHR AIRH

International Association for Hydro-Environment Engineering and Research

Hosted by
Spain Water and IWHR, China

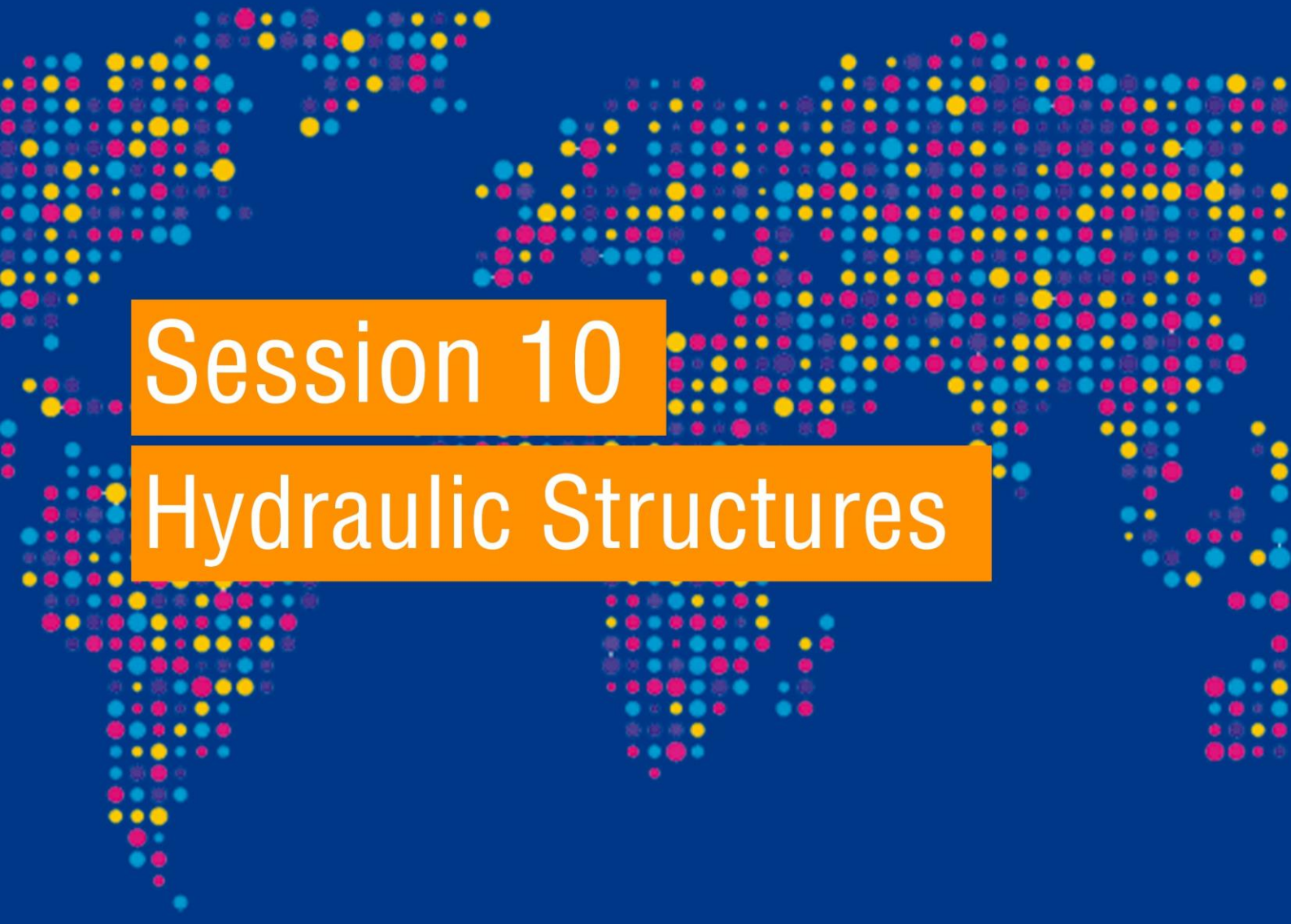

Session 10
Hydraulic Structures

IAHR YPN

Hosted by
Spain Water and IWHR, China

Proceedings of the 1st IAHR
Young Professionals Congress
17-18 November 2020

MEASUREMENT OF VOID FRACTION AND VELOCITY PROFILES IN RECTANGULAR FREE-FALLING JETS

Patricio R. Ortega[1,2], José M. Carrillo [1], Luis G. Castillo [1] & Juan T. García[1]

[1] *Hidr@m Group, Civil Engineering and Mining Engineering School, Universidad Politécnica de Cartagena, Cartagena, Spain.*
[2] *Civil and Environmental Engineering Department, Escuela Politécnica Nacional, Quito, Ecuador*.
patricio.ortega@epn.edu.ec, jose.carrillo@upct.es, luis.castillo@upct.es, juan.gbermejo@upct.es

ABSTRACT

Air entrainment generates energy dissipation in turbulent free-falling jets, where self-aeration processes reduce the velocity and increment the jet thickness. This experimental study presents an analysis of some air-water properties in rectangular free-falling jets. Two specific flows were considered with falling distances up to 1.2 m. A conductivity phase-detection probe was used for measuring the void fraction distributions, while a Pitot-Prandtl tube was used for measuring the velocity profiles. The jet thickness was also analyzed during the fall. The results show the evolution of the inner jet core with slight differences in the upper and lower nappe, the aeration increment, and a small reduction of the velocity field during the fall.

Keywords: *free-falling jets, air entrainment, phase-detection probe, air-water flow, laboratory model*.

1 INTRODUCTION

Dams are essential hydraulic structures whose design must guarantee safety hydraulic operations in different loading scenarios. During the past few years, the increase in design flood flows and the new requirements in hydraulic and structural design criteria have demanded a re-evaluation of the current capacity of the dams. For instance, many large dams in Spain were built for the maximum spillway capacity for flow returns of 500 years (Spanish Dams Instruction of 1967). Later, the design flow return was increased to 5,000 years in gravity dams and 10,000 years in embankment dams. During extreme events, those dams might be overtopped (Wahl, 2008). Turbulent water jets discharging into the atmosphere are also used in hydraulic structures to improve self-aeration and the energy dissipation process. According to Ervine and Falvey (1987), turbulence is the principal mechanism of air entrainment in turbulent jets, as turbulent fluctuations affect the jet spread, the deformation of the free surface, and the inner jet core disintegration. The mechanisms of energy dissipation in rectangular free-falling jets may be divided into: aeration of the jet and disintegration of the inner water core during the fall; air entrainment and diffusion of the jet into the plunge pool; impact with the bottom; and recirculation in the dissipation basin (Castillo et al., 2015). A better knowledge of the free-falling jets will allow us to understand their energy dissipation mechanisms and how they interact with the plunge pools.

2 MATERIALS AND METHODS

Measurements were carried out in an experimental device located at the Universidad Politécnica de Cartagena (Spain). The experimental setup has a mobile inlet channel of 4.00 m length and 1.05 m width that ends in a rectangular sharp-crested weir. The weir crest is located at vertical falling distance *Z* of 2.20 m from the bottom of the plunge pool (Fig. 1). Further information may be found in Carrillo et al. (2020).

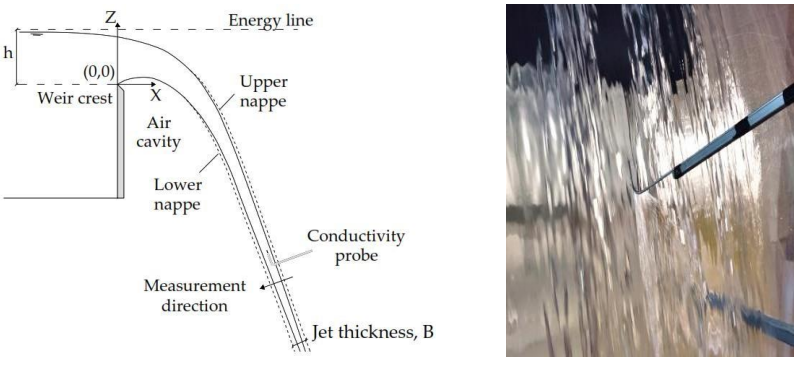

Figure 1. Scheme of the rectangular jet (left), and rectangular free-falling jet with air-water probe (right).

Cartagena. The probe tip was made of platinum wire with a diameter of 0.25 mm. As our previous analyses have shown that at least 30 s are needed for obtaining an uncertainty of about ±1% in the void fraction, each measurement was sampled at 20 kHz for 45 s. The conductivity probe was used for measuring the local void fraction distributions and bubble frequency at different points of the cross sections. For analyzing the local velocity in different positions of the cross sections, a Pitot-Prandtl tube with back-flushing system was used. For this study, different dimensionless falling distances between 5.0 < Z/h < 16.5 were tested, with specific flows q = 0.048 and 0.072 m³/s/m. The cross sections were measured with a spatial resolution of 1.0 mm.

3 RESULTS AND DISCUSSION

During the rectangular free-falling jet, the amount of air that enters into the jet tends to increase. It modifies the cross-section profile and the jet thickness *B.* Air entrainment and the interaction with the boundary's turbulent layer tend to reduce the inner jet core. Figure 2 shows the void fraction distribution and the velocity profile for both specific flows, being B_{90} the jet thickness with $C \leq 0.90$. The behavior between the upper and lower nappe shows slight differences in the void fraction and velocity distributions. For falling distances ratios $Z/h \leq -11.0$ the inner jet core showed non-aerated water (C = 0); for falling distances $Z/h > -11.0$, the air entrainment reaches the center of the jet (minimum void fractions between 0.08 and 0.25). The maximum velocities are similar to their correspondent gravitational velocities. However, the velocity tends to rapidly reduce outside of the non-aerated core. Although the falling distance is relatively small (up to 1.20 m), a slight velocity reduction effect has been observed during the fall in the jet´s core.

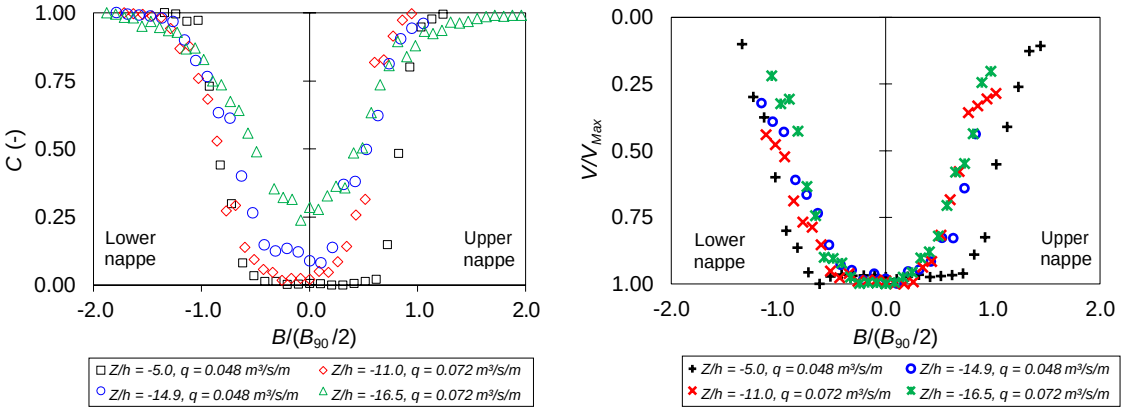

Figure 2. Void fraction distributions and velocity profiles for different dimensionless falling distance.

ACKNOWLEDGMENTS

The authors express their gratitude for the financial aid received from the "Ministerio de Ciencia, Innovación y Universidades" (MCIU), the "Agencia Estatal de Investigación" (AEI) and the "Fondo Europeo de Desarrollo Regional" (FEDER), through the Project "La aireación del flujo en el vertido en lámina libre por coronación de presas a nivel de prototipo y su efecto en cuencos de disipación de energía", grant number RTI2018-095199-B-I00, and by the "Comunidad Autónoma de la Región de Murcia" through the "Programa Regional de Fomento de la Investigación Científica y Técnica (Plan de Actuación 2019) de la Fundación Séneca, Agencia de Ciencia y Tecnología de la Región de Murcia", grant number 20879/PI/18.

REFERENCES

Carrillo, J.M., Ortega, P.R., Castillo, L.G., García, J.T. (2020). Experimental characterization of air entrainment in rectangular free falling jets. *Water*, 12, 1773; doi:10.3390/w12061773.

Castillo, L.G., Carrillo, J.M., and Blázquez, A. (2015). Plunge pool mean dynamic pressures: a temporal analysis in nappe flow case. *Journal of Hydraulic Research*, 53(1), 101–118; doi:10.1080/00221686.2014.968226.

Ervine, D. A., Falvey, H. (1987). Behaviour of turbulent jets in the atmosphere and plunge pools. *Proc. of the Institutions of Civil Engineers* , 83(2), 295-314.

Ministerio de Obras Públicas (1967). Instrucción para el proyecto, construcción y explotación de grandes presas. Spain. (in Spanish).

Wahl, T.L., Frizell, K.H., Cohen, E.A. (2008) Computing the trajectory of free jets. *Journal of Hydraulic Engineering,* 134(2), 256–260.

Proceedings of the 1st IAHR
Young Professionals Congress
17-18 November 2020

INFLUENCE OF LENGTH OF MICRO GROINS ON BED MORPHOLOGY IN A STRAIGHT CHANNEL

Andreas C.T Müller [1], Frank Seidel [1] & Franz Nestmann [1]

[1] Karlsruhe Institute of Technology, Institute for River Basin Management, Karlsruhe, Germany, andreas.mueller@kit.edu

ABSTRACT

Micro groins are an alternative bank-protection method which uses small submerged installations in the river bed to direct the flow away from the bank. In order to assess the impact of micro groins on the bed morphology, physical model experiments with movable bed were designed. A reference experiment and five variants with micro groins having different lengths were conducted. Strong changes of the bed morphology with pronounced deposition along the groin's root and two erosion areas at the head of the groin and upstream its root were observed. The bed morphology became more accentuated with increasing length of the groins.

Keywords: *river restoration, micro groins, hydraulic experiments, bed morphology, bank protection*

1 INTRODUCTION

Micro groins are an alternative bank protection method that identifies the flow field as the cause for bank and bed erosion. Consequently, the flow velocity at the protected bank is reduced by inducing secondary flow with small submerged installations called micro groins in the river bed (Mende & Sindelar 2010). Compared to traditional, bank-hardening structures, e.g. river revetments, micro groins are more cost effective and offer ecological advantages, e.g. a better crosslinking of land and water habitats as riprap-protection. However, for the morphological impacts of micro groins only few studies exist so far (Möws & Koll 2014).

2 EXPERIMENTAL SETUP & METHODS

With reference to the conditions in a field project at the lowland river Alb near the Rhine port in Karlsruhe, Germany, physical model experiments with movable bed ,that was made of plastic granulate, were designed in the Theodor-Rehbock laboratory (Müller et al. 2020). Experimental runs were carried out in an acrylic flume with a length of 18 meter and a width of 1 m and a slope of 0.9 ‰. The scale of the experiments was set to 1:15. The 100-year flood of 88.44 l/s and a water depth of 22.5 cm were used as testing condition. Groins with an inclination angle α of 60°, a groin width w_{groin} of 7 cm and a height h_{groin} of 1/10 of the water level were selected (Fig 1). Five different projected lengths l_P with ¼, ⅓, ½, ⅔ and ¾ of the channel width w_{ch} were chosen for these experiments. Four groins were placed with the recommended relative distance d_{groin}= 6 or 4 m (Mende 2014) starting at X1= 2.5. A reference experiment without groins was analyzed as well.

According to previous results, the secondary current evoked by the micro groins will not fully develop until the third groin (Mende 2014). Therefore, the soil morphology was measured at groin n°3 from X= 8.5 m to X= 12.5 m by a Seatek Ultrasonic Ranging System compromising 31 transducers. Two extremely different states of the bed structures could be observed due to the dunes in the flume. Yet, all intermediate states in-between existed as well. The first characteristic state S1 was defined by low bed levels in the direct surroundings of the groin, whereas in the second state S2 much higher bed levels at the groin root were found as the crest of the dune was passing by. The bed topography from both states was used for the statistical analysis and the standard deviation from S1 and S2 was averaged. For more detail on the experiments see Müller et al. (2020).

3 RESULTS

In Figure 1 a comparison is shown between bed morphologies for the reference experiment and micro groins with lengths l_p of 1/3 and 2/3 in state 1. In the reference experiment the bed morphology is very homogenous and it's mainly influenced by dunes due to the fine bed material. The reduced bank-near flow velocity

downstream of the groin leads to a significant deposition along the protected bank. This further increases the bank protective effect. In the variant with l_p = 2/3, the extremes in the bed morphology are much more accentuated than for l_p = 1/3. This finding is supported by the statistical analysis which shows an increase of bed level variety with increasing length of the micro groins (Fig. 1). The micro groin with l_p = ¾ shows the biggest variance of the bed levels. For this variant the standard deviation of the bed level increases to 3.7 cm in comparison with 2.7 cm in the reference experiment.

Moreover, in all setups a scour can be found around half of the flume width downstream of the groin's head. Thus, the bed characteristics correspond well with results from Möws & Koll (2014) in a flume with gravel bed. However, in the investigated setup, a deep scour upstream of the groin root can be found as well. It roughly forms an equilateral triangle along the groin's axis. Thus, the groin's bank-protective effect is reversed in the upstream area. This area will have to be properly protected to ensure the structural integrity of the structure.

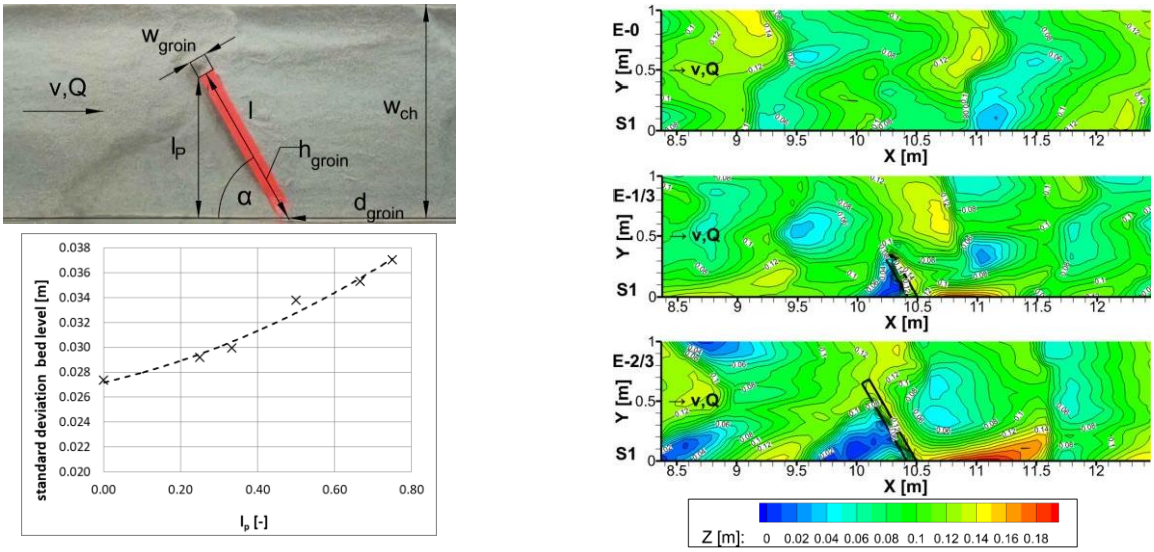

Figure 1. Design parameters of micro groins (Müller et al. 2020, left side up) and statistical analysis of the bed level variety (left side down) and comparison of bed morphology for state 1 between the reference experiment and experiments with micro groin of lengths l_p = ⅓ and ⅔ (right side)

4 CONCLUSIONS

With the presented study it could be shown that micro groins have a strong effect on the river bed structures. A deposition along the adjacent bank improves the bank protection effect. The effect is augmented with increasing length of the structure. However, an erosion area directly upstream of the groin counteracts the bank protection. Considering the high variety of bed morphology during the experiments more systematic investigations and repeated experiments will have to be analyzed in order to further quantify these findings.

ACKNOWLEDGEMENTS

The authors like to thank M.Sc. Larissa Ortrun Pereira Ziesmann for conducting of some of the experiments and analyses as a part of her final thesis. This work was supported by the Hector Fellow Academy, Germany.

REFERENCES

Mende, M. 2014. Naturnaher Uferschutz mit Lenkbuhnen – Grundlagen, Analytik und Bemessung. Dissertation, Fakultät für Architektur, Bauingenieurwesen und Umweltwissenschaften der Technischen Universität Braunschweig.

Mende, M. & Sindelar, C. 2010. Instream River Training - Lenkbuhnen und Pendelrampen. In: 15. Gemeinschafts-Symposium der Wasserbau- Institute TU München, TU Graz und ETH Zürich vom 1.-3. Juli 2010 in Wallgau, Oberbayern, 35-44.

Möws, R. & Koll, K. 2014. Influence of a Single submerged groyne on the bed morphology and the flow field. Proceedings of the International Conference on Fluvial Hydraulics, RIVER FLOW 2014. doi: 10.1201/b17133-193.

Müller, A., Seidel, F., Nestmann, F. (2020): Assessment of the effect of micro groins on riverbed structures – Comparison of the velocity distribution between experiments with fixed and mobile bed. In: River Flow 2020 – Uijttewaal et al (eds). Taylor & Francis Group, London.

Proceedings of the 1st IAHR
Young Professionals Congress
17-18 November 2020

THE INFLUENCE OF BERMS AND ROUGHNESS ON WAVE OVERTOPPING AT ROCK-ARMOURED DIKES

Alberto Marconi[1], Weiqiu Chen [2,3], Marcel R.A. van Gent[3], Jord J. Warmink[2] & Suzanne J.M.H. Hulscher[2]

[1] Department of Civil Engineering, University of Roma Tre, Rome, Italy, alb.marconi@stud.uniroma3.it

[2] Department of Marine and Fluvial Systems, University of Twente, Enschede, The Netherlands, w.chen-6@utwente.nl; j.j.warmink@utwente.nl; s.j.m.h.hulscher@utwente.nl

[3]Department of Coastal Structures & Waves, Deltares, Delft, The Netherlands, marcel.vangent@deltares.nl

ABSTRACT

Average overtopping discharge is a crucial parameter for design and reinforcement of dikes. Rock armours and berms are widely used to reduce wave overtopping discharge by introducing slope roughness and energy dissipation. Since methods for estimating the influence of a rock berm and roughness of rock armour at dikes on the average overtopping discharge still need to be developed and/or validated, this study aims to empirically develop better quantification of the reductive influence of rock armour on wave overtopping, compared to existing procedures. That is derived based on the analysis of experimental data from physical model tests. Moreover, the influence of roughness of a rock armour applied only on part of waterside slopes is estimated by introducing location weighting coefficients. Results show that the newly derived methods for evaluating the influence of berm and roughness for rock-armoured dikes lead to significantly better predictions of the average wave overtopping within the tested ranges compared to existing ones.

Keywords: dikes, coastal structures, wave overtopping, physical model tests, rocks.

1 INTRODUCTION

Dikes protect coastal areas from flooding due to wave overtopping. With the background of climate change and sea-level rise, existing dikes may require reinforcement. Berms and roughness elements (e.g. rocks) are often applied to dikes, which can effectively reduce the average overtopping. Accurate estimations of the berm and roughness influence on overtopping discharge would help the cost-effective design and safety assessment of a dike. TAW (2002) and EurOtop (2018) provide empirical formulae for the average overtopping discharge (q), both characterised by the structure $q = A \exp(-B\ R_c)$, taking the effect of berms and roughness on wave overtopping discharge into account by introducing the dependence of A and B on berm and roughness influence factors (γ_b and γ_f). Those are 1.0 when no influence is present, while smaller values indicate a larger reductive influence due to a berm or slope roughness. R_C is the crest freeboard.

For the roughness influence factor, values are provided for various types of roughness elements (e.g. γ_f=0.55 for rocks on an impermeable core). Further research showed that γ_f varies with wave conditions and structure configuration and that there is still no validated method to evaluate that for rock armours. For the estimation of the berm influence, TAW (2002) and EurOtop (2018) provide equations to calculate γ_b for impermeable berms, but there are no validated ones for permeable rock berms. Chen et al. (2020a) developed new expressions for γ_b and γ_f, taking all those aspects into account for slopes covered by concrete blocks.

2 DEVELOPMENT OF NEW METHODS

This research aims to recalibrate and adapt empirical coefficients of the following Eqs. [1]-[2]-[3] by Chen et al. (2020a) to the case of permeable slope revetment made of rocks.

$$\gamma_b = 1 - b_0 \frac{r_b(1-r_{dh})}{\sqrt{S_{m-1,0}}} \qquad 0.6 < \gamma_b < 1.0 \qquad [1]$$

$$\gamma_f = 1 - c_0 \frac{R_c}{H_{m0}\ \xi_{m-1,0}} \qquad [2]$$

$$\gamma_f = \frac{\alpha_1\gamma_{f,1}L_1 + \alpha_2\gamma_{f,2}L_2 + \alpha_3\gamma_{f,3}L_3}{\alpha_1 L_1 + \alpha_2 L_2 + \alpha_3 L_3} \qquad [3]$$

where b_0 and c_0 are empirical coefficients affected by the type of armour layer. A larger value of b_0 (c_0) means a larger reductive influence of the berm (roughness) on the average overtopping discharge; $s_{m-1,0}$ is the wave steepness; r_b and r_{dh} can be calculated as given by TAW (2002) and EurOtop (2018). Eq. [3] is used for varying roughness along the slopes (L is the effective length).

Physical model tests (139 in total) have been performed in the Pacific Basin (Deltares, Delft, The Netherlands) in order to collect a database to set up a calibration and validation process of influence factors expressions. Different roughness configurations were tested, as rocks were applied alternatively on the whole slope, on the upper slope only, on the upper slope and berm and on the berm only. Irregular wave conditions were applied to all physical model tests, based on JONSWAP spectrum and characterised by a wave steepness range of 0.013÷0.044. The crest freeboard varied between 0.12÷0.2m. The berm width was fixed (0.2m) for all configurations, except for the one with a larger berm (0.5m). The wider berm was tested to investigate how the proposed expressions for influence factors behave for such a different structure. More details on the tests are provided in Chen et al. (2020b).

3 CONCLUSIONS

Test results confirm that the application of a berm and rock armour significantly reduces the average overtopping discharge compared to that at smooth straight slopes. New expressions for berm and roughness influence factors of rock-armoured dikes are derived based on experimental data by calibrating the empirical coefficients in [1]-[2] as b_0=0.19 and c_0=0.70. It was also found that, for Eq. [3], the values of location weighting coefficients as proposed by Chen et al. (2020a) (α_1=0.65, α_2=0.22, α_3=0.13) for structures with other slope protections, appear to be valid for rock-armoured slopes as well.

The performance of new methods has been validated by using experimental data with wider ranges of test conditions, getting an improvement (from *NSE*=-1.32 to *NSE*=0.7) on estimates of average overtopping discharge over the structure with rock armour applied on the upper slope. For the structure with a wider berm ($\frac{B}{H_{m0}}$> 3.7), there is no improvement using new methods compared to TAW (2002). The influence of roughness on rock-armoured slopes needs further investigation for smaller relative freeboards ($\frac{Rc}{H_{m0}}$ < 1.1) in combination with wide berms ($\frac{B}{H_{m0}}$> 3.7). Overall, new methods to account for the influence of berms and roughness of rock-armoured dikes significantly improve predictions of average overtopping discharges as shown in Figure 1, where each data point corresponds to 1 test (shape and colour indicate the different test conditions) with *NSE*=0.8 within tested ranges.

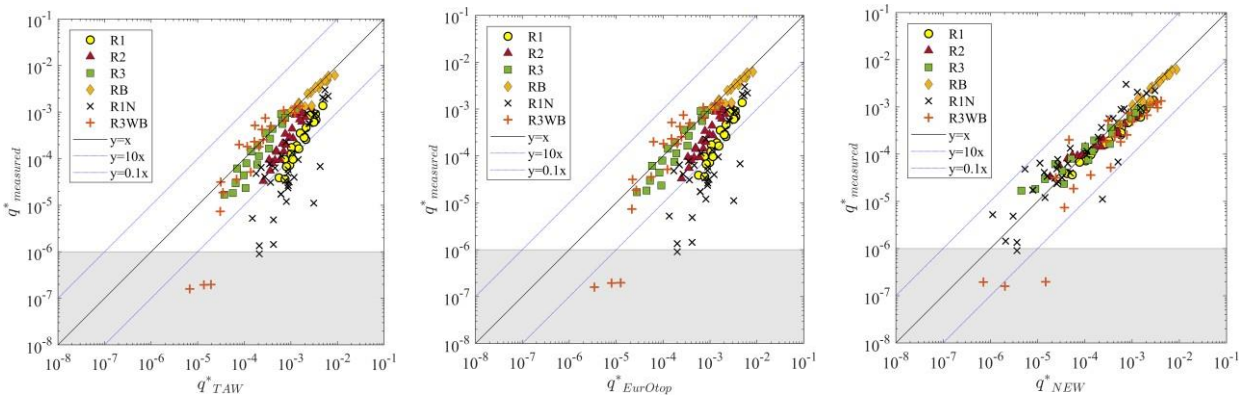

(a) (b) (c)

Figure 1. Measured and calculated dimensionless overtopping discharges for all datasets, using (a) TAW (2002), (b) EurOtop (2018) and (c) new methods for the estimation of influence factors.

REFERENCES

Chen, W., van Gent, M.R.A., Warmink, J.J., Hulscher, S.J.M.H. (2020a). The influence of a berm and roughness on the wave overtopping at dikes. Coastal Engineering, 156, 103613.

Chen, W., Marconi, A., van Gent, M.R.A., Warmink, J.J., Hulscher, S.J.M.H. (2020b). Experimental study on the influence of a berm and roughness on the wave overtopping at rock-armoured dikes. Journal of Marine Science and Engineering. 8, 446.

EurOtop (2018). Manual on Wave Overtopping of Sea Defences and Related Structures.

TAW (2002). Technical Report Wave Run-Up and Wave Overtopping at Dikes. Technical Advisory Committee on Flood Defence, The Netherlands.

Proceedings of the 1st IAHR
Young Professionals Congress
17-18 November 2020

Numerical modelling of impulse wave forces on dams

Tommaso Attili[1], **Valentin Heller**[1], **Savvas Triantafyllou**[2]

[1]Environmental Fluid Mechanics and Geoprocesses Research Group, Faculty of Engineering, University of Nottingham, Nottingham, UK
[2]Institute for Structural Analysis and Aseismic Research, School of Civil Engineering, National Technical University of Athens, Athens, Greece

*Correspondance: tommaso.attili@nottingham.ac.uk; valentin.heller@nottingham.ac.uk; savtri@mail.ntua.gr

ABSTRACT

Large impulse waves are generated in reservoirs by, e.g., landslides and iceberg calving. Impulse waves result in significant forces when impacting dams and it is important to take these forces into account when designing a dam. The prediction of forces due to extreme waves is still subject to large uncertainties. Analytical models are available for wind waves, while empirical equations, relying on a limited number of experiments, are employed for more extreme waves. These equations are validated in the present study through numerical modelling with the open source toolbox solids4foam in foam-extend. The model is successfully validated with available laboratory measurements and an analytical model for two experiments. A computational example is presented for a hypothetical, yet realistic, case, revealing a good agreement between the numerical results and predictions based on an existing empirical equation.

Keywords: foam-extend, impulse wave forces, long waves, numerical modelling, wave-structure interaction.

1 BACKGROUND

Impulse waves in reservoirs generated by, e.g., landslides and iceberg calving may generate large additional forces on dams. Sainflou (1928) and Tadjbakhsh and Keller (1960) analytically derived the wave pressure acting on rigid walls under idealised conditions. These models may be generally applied for wind waves, while for more extreme impulse waves such as solitary waves, Heller et al. (2009) approximated the total force F_{tot} for both the wave and hydrostatic pressure combined with

$$F_{tot} = [1 - 1.5(a/h)]^{1/6} \rho g (2a + h)^2/2 \quad (1)$$

Eq. (1) was derived from the interpolation of a small number of experiments of Ramsden (1996) for $0 \leq a/h \leq 0.6$, where a is the wave amplitude, h the water depth, ρ the water density and g the gravitational acceleration. The present study aims to provide a numerical investigation of impulse waves impacting on dams to validate and extend the existing prediction method for a wide range of wave conditions and types. A recently developed numerical model is validated with laboratory measurements and an analytical solution. This model is then applied to estimate F_{tot} for a hypothetical, yet realistic, case and the force is compared with Eq. (1).

2 NUMERICAL MODEL

The toolbox solids4foam (Cardiff et al., 2018) was used to model two-dimensional wave forces on dams in the present study. This toolbox was compiled in foam-extend 4.0 and implemented on the High Performance Computing cluster Augusta at the University of Nottingham. solids4foam is capable of solving fluid-solid interaction with several models for both the fluid and solid. Their governing equations are discretised into a set of algebraic equations based on the spatial and temporal partition of the domain using the cell-centred Finite Volume Method (Cardiff et al., 2018). These are separately solved and coupled through a partitioned approach. The coupling within each time step consists of (i) solving the fluid domain, (ii) passing the fluid interface forces to the solid interface, (iii) solving the solid domain and (iv) passing the solid interface velocities to the fluid interface. The library waves2Foam (Jacobsen et al., 2012) was used for wave generation in the numerical wave tank.

3 RESULTS AND DISCUSSION

3.1 Validation of the numerical model

The numerical model was validated with laboratory measurements of Mallayachari and Sundar (1995) and the analytical solution of Tadjbakhsh and Keller (1960) for two selected tests with linear waves. The numerical simulations were conducted with the identical set-up as in the laboratory and two mesh resolutions were investigated. The dimensionless wave pressure $p/(\rho g H)$ versus z/h at the vertical dam, with the wave height H, period T and the vertical coordinate z, is compared between the present study, the experimental, and the analytical models in Fig. 1. In both cases the numerical model captures the experimental data and the analytical model well, with a normalised root mean square error ($nRMSE$) of 0.14 and 0.08 in Figs. 1a,b, respectively, for the experimental data, and $nRMSE$ = 0.07 to 0.14 and 0.02 to 0.21 in Figs. 1a,b, respectively, for the analytical solution at $z \leq 0$.

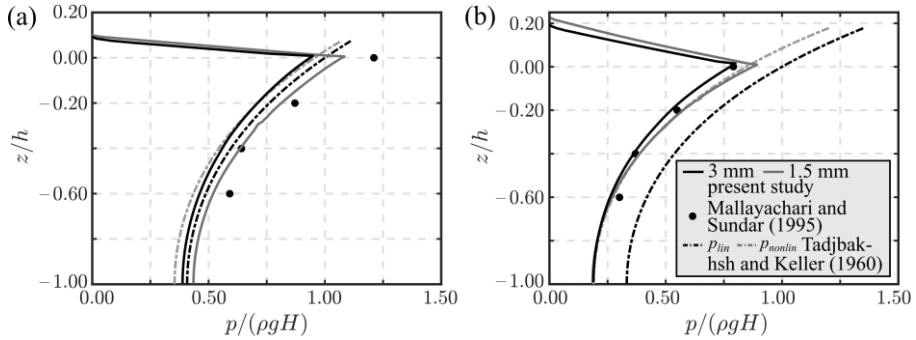

Figure 1: Comparison of the numerical pressure $p/(\rho g H)$ versus z/h with Mallayachari and Sundar (1995) and Tadjbakhsh and Keller (1960) for two tests at h = 0.315 m with (a) H = 0.023 m and T = 0.950 s and (b) H = 0.048 m and T = 0.873 s.

3.2 Computational example

The numerical model was further applied to estimate F_{tot} on a 50 m high dam due to a solitary wave. A 800 m long numerical wave flume was used. With h = 25 m and a/h = 0.38, F_{tot} = 8.01 · 10^6 N/m resulted. This is approximately 2.6 times the hydrostatic force $\rho g h^2/2$ = 3.07 · 10^6 N/m, confirming the relevance of impulse wave forces. The total force from Eq. (1) is F_{tot} = 8.30 · 10^6 N/m, resulting in a deviation of only 3.6%.

4 CONCLUSIONS

Impulse waves impacting dams may result in significant additional forces to the hydrostatic force. The investigation of this wave-structure interaction phenomenon is still a major challenge. In the present study an available numerical model has been applied to investigate impulse waves impacting dams. Comparisons with laboratory measurements and an analytical model confirmed that the numerical model captures wave pressures on rigid dams well. A hypothetical, yet realistic, case was simulated, showing an excellent agreement with predictions from an empirical equation. Detailed numerical investigations of impulse waves impacting dams for a wide range of conditions will be conducted in future work to support impulse wave hazard assessment in reservoirs.

References

Cardiff, P., Karač, A., Jaeger, P. D., Jasak, H., Nagy, J., Ivanković, A. and Tuković, Z. (2018), An open-source finite volume toolbox for solid mechanics and fluid-solid interaction simulations, *ArXiv Prepr ArXiv180810736*.

Heller, V., Hager, W. H. and Minor, H.-E. (2009), *Landslide-generated impulse waves in reservoirs: basics and computation*, R. Boes (Ed.), VAW-Mitteilung 211, ETH Zurich, Zurich.

Jacobsen, N. G., Fuhrman, D. R. and Fredsøe, J. (2012), A wave generation toolbox for the open-source CFD library: OpenFOAM, *Int. J. Numer. Meth. Fl.* **70**(9), 1073 – 1088.

Mallayachari, V. and Sundar, V. (1995), Standing wave pressures due to regular and random waves on a vertical wall, *Ocean Eng.* **22**(8), 859 – 879.

Ramsden, J. D. (1996), Forces on a vertical wall due to long waves, bores, and dry-bed surges, *J. Waterw. Port, Coast. Ocean Eng.* **122**(3), 134 – 141.

Sainflou, M. (1928), Essai sur les digues maritimes verticales, *Annales des Ponts et Chaussées* **98**, 5 – 48.

Tadjbakhsh, I. and Keller, J. (1960), Standing surface waves of finite amplitude, *J. Fluid Mech.* **8**(3), 442 – 451.

Proceedings of the 1st IAHR
Young Professionals Congress
17-18 November 2020

EXPERIMENTAL AND NUMERICAL METHODS IN INVESTIGATIONS OF SUSTAINABLE DEEP SCOURS AS FISH HABITAT

CHRISTIN KANNEN [1], FRANK SEIDEL [1] & FRANZ NESTMANN [1]

[1] Karlsruhe Institute of Technology, Karlsruhe, Germany
Christin.Kannen@kit.edu
Frank.Seidel@kit.edu
Franz.Nestmann@kit.edu

ABSTRACT

Former regulative measures on water bodies have highly affected structural diversity and thus the habitat quality for fish fauna. In a 3-year research project, funded by the Fisheries Department of the state of Baden-Württemberg, hydraulics and morphodynamics of deep watercourses and scours will be investigated. The background and objectives of the project are explained and the scouring mechanisms are investigated with three different methods: flume experiments, numerical simulations and field studies.

Keywords: *scour, morphodynamics, sediment transport, fish habitat, ecohydraulics.*

1 INTRODUCTION

The aim of many revitalisation measures on watercourses is to improve the structural diversity and thus the habitat quality for the fish fauna. Through various measures for restoration of fish passage, in particular by removing bottom sills and cross-barriers, a degradation of local depth variation and disappearance of local scours can be seen. Moreover, water management often requires bank and river bed protection which is contrary to natural morphodynamics and depth variability. As a result, watercourses lose significant parts of their ecological functionality (e.g. adult habitats and wintering grounds for fish) and the climate change and the increasing water temperatures in summer aggravate the threat to the fish biocenosis (LUBW, 2019; Roberts et al, 2014). The goal of the research project is to fill the knowledge gap in terms of suitability and dimensioning of hydraulic engineering structures for the permanent creation of deep pools by investigating the hydraulic and the morphodynamic interaction. Based on the results, recommendations for practice will be derived with special regard to fish biology, hydraulics and morphodynamics.

2 FUNDAMENALS OF SCOURING PROCESSES

Deep pools in rivers are created by scouring processes. Scouring occurs when the transport capacity of sediment is locally higher than in other sections of the river. Leading processes are higher flow velocities, higher turbulence, secondary currents and combinations of the latter (Zanke, 1982). In general, there are three different types of scouring processes. The general scour occurs due to morphological processes in rivers. Constriction scours are caused by a reduction in the width of the river and thus increased flow velocity. The local scour occurs at structures in rivers such as bridge piers or groynes and superimposes the two previous scour types (Breusers and Raudkivi, 1991). Scours can also be divided in three categories according to their morphodynamic behavior (Breusers and Raudkivi, 1991). If the relation of local velocity U_o to the critical velocity of the bed material U_c is smaller than 0,5 no scour will occur. Clear-water scour conditions are present for $0,5 < U_o/U_c < 1$. Live-bed scour with a general sediment transport occurs for $U_o/U_c > 1$. According to various authors (see e.g. Breusers and Raudkivi (1991), Melville (2008) and Breusers (1977)) the influencing factors on scouring depth can be divided up into five groups:

- Parameters of the fluid: fluid density ρ, kinematic viscosity v
- Flow parameters: mean flow velocity U_o, depth of flow h, gravity g, overflow depth $h_{overflow}$
- Parameters of the bed material: geometric mean diameter d_{50}, geometric standard deviation σ_g, density of the sediment ρ_s, mean critical velocity U_c

- Geometry of the structure (shape, dimensions, surface condition)
- Time-depending processes

3 METHODS

To answer the previous research questions, different methods of hydraulic engineering research are applied. To explore the morphodynamic questions of the project, a flume experiment is currently being installed in the Theodor-Rehbock laboratory at KIT. The experimental setup will be used to investigate the complex three-dimensional flow processes that occur in scour formation and the interaction with local morphodynamics. The hydraulic and morphodynamic boundary conditions are based on local aspects of the state of Baden-Württemberg. Two exemplary sites in Schwarzenberg at river Murg and Criesbach at river Kocher were selected for hydraulic conditions. Discharges will mainly focus on the low flow and on the two year flood, which is often seen to be the morphodynamically significant discharge. Due to the predominantly disturbed bedload balance in the states rivers, clear-water scour conditions will be accomplished. The flume experiments will be carried out in a 7,8 m long, 0,79 m wide and 0,54 m deep flume corresponding to a model scale of approximately 1:25. The mean diameter of the sediment (d_{50}) was selected to 3 mm. Velocity measurements will be made with an LDA-system. The bottom topography will be captured with a Structure from Motion technique. The experiments in the laboratoy will be investigated further, first in a hydrodynamic and later in a hydromorphological numerical 3D approach. The physical and numerical model tests will be supported by the analysis of different case studies in Baden-Württemberg.

Table 1. Overview of application of model types.

PHYSICAL MODEL	NUMERICAL MODEL	FIELD STUDY
Movable bed experiments	Simulations with flat, rigid bed Simulations with scoured, rigid bed Simulations with movable bed with calibration values from the physical model	Validation in field study

4 CONCLUSIONS

The presented project investigates different measures and structures to initiate deep watercourses and scours that provide fish habitats especially at low flow conditions and high water temperatures. Flume experiments, numerical simulations and field studies are applied to answer the research questions. The focus of the project will be on hydraulic and morphodynamic aspects.

ACKNOWLEDGEMENTS

This work was funded by the Fisheries Department of the state of Baden-Württemberg.

REFERENCES

Akhlaghi, E., Babarsad, M. S., Derikvand, E., & Abedini, M. (2019). Assessment the Effects of Different Parameters to Rate Scour around Single Piers and Pile Groups: A Review. *Archives of Computational Methods in Engineering, (March)*. https://doi.org/10.1007/s11831-018-09304-w

Breusers, H. N. C., Nicollet, G., & Shen, H. W. (1977). Local Scour Around Cylindrical Piers. *Journal of Hydraulic Research*, 15(3), 211–252. https://doi.org/10.1080/00221687709499645

Breusers, H. N. C., & Raudkivi, A. J. (1991). *Scouring (VIII).* Rotterdam: Balkema.

LUBW. (2019). Zu warm, zu heiß, zu trocken? – Eine klimatische Einordnung des Jahres 2018 für Baden-Württemberg. Karlsruhe: LUBW Landesanstalt für Umwelt Baden-Württemberg.

Melville, B. (2008). The physics of local scour at bridge piers. In H. Sekiguchi (Hrsg.), *Proceedings 4th International Conference on Scour and Erosion (ICSE-4) (S. 28–40)*. Tokyo, Japan.

Roberts, M., Promny, M., & Vollmer, S. (2014). Klimaprojektionen für Sedimenthaushalt und Flussbettentwicklung. *Schlussbericht KLIWAS-Projekt 4.02*. KLIWAS-44/2014. https://doi.org/10.5675/Kliwas_44/2014_4.02

Zanke, U. (1982). *Grundlagen der Sedimentbewegung : mit 13 Tabellen (XII).* Berlin; Heidelberg [u.a]: Springer.

Proceedings of the 1st IAHR
Young Professionals Congress
17-18 November 2020

DAMPING OF SHIP-INDUCED WAVES IN GROYNE FIELDS

Rutger Pasman, Ralph Schielen, Jeremy Bricker, Arne van der Hout, Erik Mosselman, Wim Uijttewaal & Freek Huthoff

HKV, Delft, the Netherlands
f.huthoff@hkv.nl
Technische Universiteit Delft, Delft, the Netherlands
ralph.schielen@rws.nl

ABSTRACT

Ships in rivers create waves and these can have a negative impact on fish habitats along the river banks. A modelling study is carried out to investigate how these ship-induced waves can be damped in groyne fields by making structural modifications to the groynes. For this purpose, different types of openings (notches) are applied to the groynes. Next, hydro-ecologic indicators are used to assess the impact of notching of groynes on fish habitat suitability. The results suggest that relatively simple modifications can significantly improve the ecological value of the groyne fields.

Keywords: ship-induced waves, groyne field, ecological preservation, hydraulic modelling.

1 Introduction

Recent ecological studies (Collas et al., 2018) show that ship-induced waves can reduce suitability of fish habitats along the river banks. Specifically eggs and young fish are vulnerable to these waves (Wolter & Arlinghaus, 2003). For the river Waal in the Netherlands the breeding and growing season of this fauna is from April to September, which generally corresponds to flow conditions where the groynes in the river are not completely submerged. The living habitat of eggs and young fish is in the shallow zones close to the bank, which experience a high degree of hydrodynamic variability due to ship-induced waves.

The goal of this research is to explore whether fish habitat during the growing and breeding season can be improved by reducing the flow impact of passing ships through structural modifications ("notching") of groynes.

2 Method

A 2D hydrodynamic model is used to simulate ship-induced wave dynamics (XBeach, (Roelvink et al., 2015). The model consists of a straight river channel with groynes along the banks. In the main channel, a steady flow is imposed. Passing ships are included in the model by defining a moving pressure field. Various groyne geometries are considered to study the flow properties in the groyne field. Two hydro-ecologic indicators are defined for the assessment of habitat suitability in-between the groynes:

1. Water level range: the difference between the highest water level and the lowest water level when a ship is passing.
2. Flow velocity range: the maximum change of the velocity vector during a ship is passing.

Both of these parameters are calculated for a 60-second time interval centered around the passing of a ship. The 'Flow velocity range' takes into account the magnitude as well as the direction of the flow field, as illustrated in Figure 1. The figure shows the two horizontal components of the velocity vector (u and v-velocity), for a specific fixed location in the groyne field during the 60 second time interval. A circle is fitted around these velocity points, of which the diameter is the 'Flow velocity range'. This calculation is carried out for each location in the groyne field.

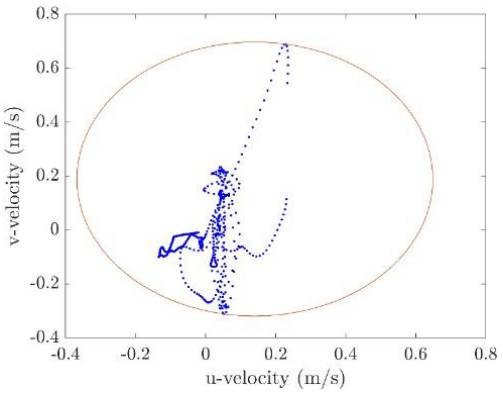

Figure 1: plot of the u- and v- directed velocity values during ship passing to determine the maximum velocity range.

3 Results

Figure 2 shows the results of the 'Flow velocity range' for two different groyne-configurations. The top plot shows the velocity range for a sequence of traditional impervious groynes. The middle plot shows the velocity range when the groynes are "notched", i.e. when a 10 m opening is created in the groynes. The bottom plot shows the difference in 'Flow velocity range' between the two situations. Herein, a negative value (blue) indicates regions where the notching has reduced the flow velocity range, and, hence, where fauna habitability has improved. In general, the velocity range has improved near the tips of the groynes, the center of the groyne field and close to the river banks, which is the area of interest for fauna habitat. When a ship passes the modified groyne field, the largest flow velocities occur within the notches (see middle plot). Immediately next to the notch, the velocity range improves the most. Additional simulation runs with changes in notch location and notch size have shown that notches close to the bank appear to be most effective in reducing the 'Flow velocity range' in the groynes field (see (Pasman et al., 2020), results not shown here).

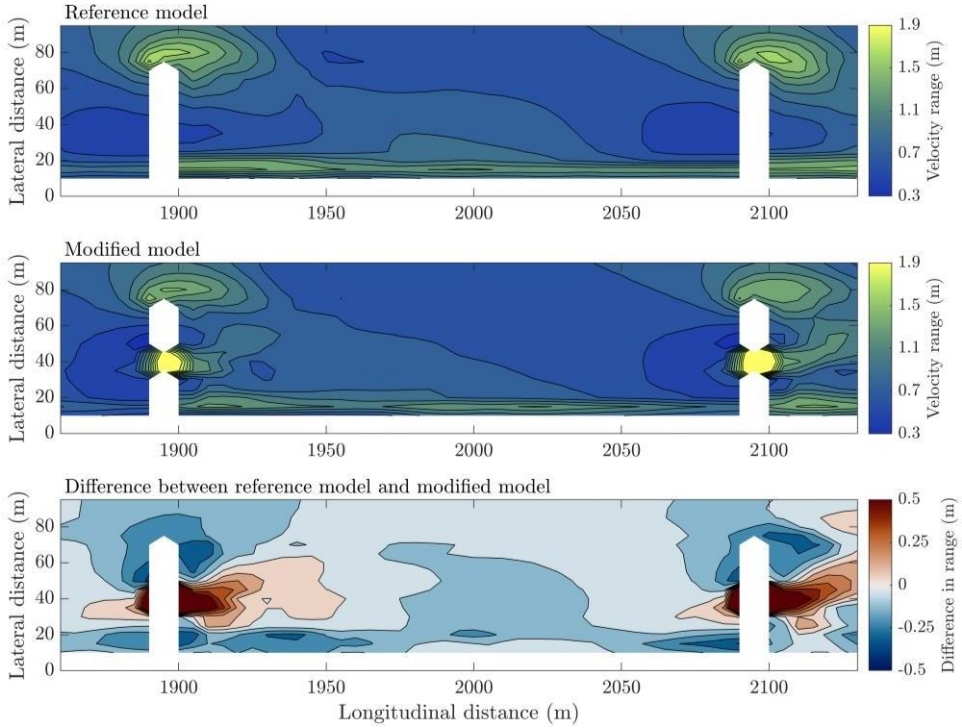

Figure 2: Flow velocity range during passing of a ship (travelling upstream). The base flow in the main channel is from left to right.

4 Conclusions

Results from the modelling study show that a notched groyne can have a positive influence on the fish habitat in rivers. Close to the notch, the fish habitat may locally become less suitable because of the higher flow velocities associated with flow through the notch. However, in large parts of the groyne field the flow variability is reduced, because of the inter-connection between neighbouring groyne fields. This makes most of the areas in the groyne fields more suitable for fish habitats. An optimal location of the notch for creating hospitable fish habitat appears to be close to the bank with a wide but shallow notch shape.

REFERENCES

Collas, F. P. L., Buijse, A. D., van den Heuvel, L., van Kessel, N., Schoor, M. M., Eerden, H., & Leuven, R. S. E. W. (2018). Longitudinal training dams mitigate effects of shipping on environmental conditions and fish density in the littoral zones of the river Rhine. *Science of the Total Environment*, *619–620*.

Pasman, R., Schielen, R. M. J., Bricker, J., van der Hout, A. J., & Huthoff, F. (2020). *Damping of ship induced waves by modifying groynes with the aim of increasing quality of fauna habitats*.

Roelvink, D., van Dongeren, A., Mccall, R., Hoonhout, B., van Rooijen, A., van Geer, P., de Vet, L., & Nederhoff, K. (2015). *Xbeach Manual*. 138.

Wolter, C., & Arlinghaus, R. (2003). Navigation impacts on freshwater fish assemblages: The ecological relevance of swimming performance. *Reviews in Fish Biology and Fisheries*, *13*(1), 63–89.

Proceedings of the 1st IAHR
Young Professionals Congress
17-18 November 2020

ENERGY DISSIPATION FOR FLOW OVER THE GABION WEIR

Ali Shariq [1], Muhammed Hashid [2], Ajmal Hussain [3] & Zulfequar Ahmad [4]

[1,3] Department of Civil Engineering, Zakir Hussain College of Engineering & Technology, Aligarh Muslim University, Aligarh, India
[1]e-mail: alishariq@zhcet.ac.in
[3]e-mail: ajmalamin.iitr@gmail.com

[2,4] Department of Civil Engineering, Indian Institute of Technology Roorkee, Uttarakhand, India.
[2]e-mail: mhashid@gmail.com
[4]e-mail: zulfifce@gmail.com

ABSTRACT

Gabion weirs are the simplest form of rectangular broad crested porous weirs very low negative impact on the environment. The objective of this paper was to investigate the relative energy dissipation for flow over the rectangular broad crested gabion weir. A series of laboratory experiments were conducted for the rectangular broad crested gabion weir having 0.3 m length, 0.225 m crest height, 0.5 m width. Three types of gabion materials were used in the present study. It is observed that the ratio of head over the weir to length of gabion weir, ratio of the diameter of gabion material to crest height of gabion weir and ratio of downstream depth to upstream depth are the affecting parameters for the energy dissipation. The developed model predicts relative energy dissipation within a maximum of ±10% error for almost all data set, which is considered satisfactory from practical consideration.

Keywords: Gabion weir, relative energy dissipation, discharge, gabion material.

1 INTRODUCTION

Gabion weirs are the simplest form of rectangular broad-crested porous weirs that usually span the full width of a river. The flow that passes through the boulders or rocks of gabion weirs allows enhancing the dissolved oxygen due to turbulence, which makes it ecologically and environmentally friendly structure.

Many experimental and numerical studies have been conducted related to the energy dissipation on the gabion stepped weir and solid stepped weir (Peyras et al. 1992; Pagliara and Palermo 2013; Wuthrich and Chanson 2014). Shariq et al. (2020) provided the discharge equation for the rectangular broad crested gabion weir for through flow condition. Fathi-Moghaddam et al. (2018) numerically investigate the hydraulic performance of triangular and trapezoidal gabion weir and provide an equation to estimate the relative energy dissipation. The objective of this paper was to investigate the relative energy dissipation on the rectangular broad crested gabion weir. The relative energy dissipation between the upstream and the downstream section of the gabion weir can be calculated as

$$\Delta E / E_1 = (E_1 - E_2) / E_1 \quad (1)$$

$$E_1 = y_1 + (v_1^2 / 2g) \quad (2)$$

$$E_2 = y_2 + (v_2^2 / 2g) \quad (3)$$

where, E_1 *and* E_2 represents the energy at upstream and downstream sections, g is the acceleration due to gravity, v_1 is the averaged velocity at upstream section, v_2 is the averaged velocity at downstream section, y_1 is upstream depth and y_2 is upstream depth of the gabion weir.

2 DIMENSIONAL ANALYSIS

There are different parameter that effects the relative energy dissipation on the rectangular broad crested gabion weir. These parameters are upstream depth (y_1, m), downstream depth (y_2, m), mean diameter of

gabion material (*d*, m), crest height of the gabion weir (*P*, m), crest length of the gabion weir (*L*, m), head over the gabion weir (*H*, m). The geometrical and flow parameters of the gabion weir are shown in Figure 1.

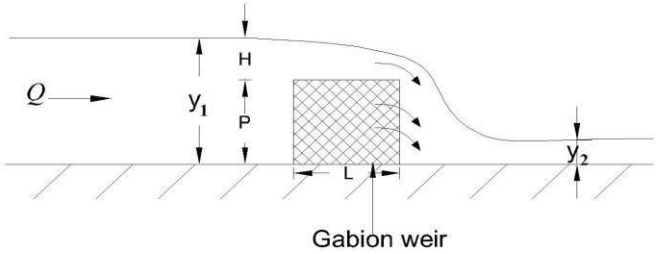

Figure 1. The definition sketch of the model used in the experiment.

The functional relationship for the relative energy dissipation on gabion weir may be represent as follows:

$$\Delta E / E_1 = f\left(H / L, d / P, y_2 / y_1\right) \tag{4}$$

A series of laboratory experiments were conducted for the rectangular broad crested gabion weir having 0.3 m length, 0.225 m crest height, 0.5 m width. Three types of gabion materials were used in the present study.

3 PROPOSED RELATIONSHIP FOR RELATIVE ENERGY DISSIPATION ON GABION WEIRS

An equation for relative energy dissipation is developed herein using the present study experimental data and relating it with parameters given in Eq. (4). The regression analysis was carried out for the estimation of relative energy dissipation, using 80% of the data collected in the present study and 20% data used for validation. The following empirical relationship was obtained.

$$\Delta E / E_1 = 0.624 - 1.185(H / L) + 0.662(d / P) + 0.768(y_2 / y_1) \tag{5}$$

The accuracy of the proposed equations (5), the value of R is (0.958) while APE, STDV, and SI values are as low as -1.469, 6.82, and 0.105, respectively. Details of performance parameters can be found in Shariq et al. (2018) and Ansari et al. (2019). It was observed that Equation (5) estimates relative energy dissipation within a maximum of ±10% error for almost all data.

4 CONCLUSION

Experimental and analytical studies related to the relative energy dissipation for flow over the gabion weir in open channels have been reported in this paper. It was found that the *H/L, d/P* and y_2/y_1 are the important dimensionless parameter, effects the relative energy dissipation on gabion weir. The proposed relative energy dissipation model was found to estimates results with a maximum error of ±10% for almost data. The qualitative performance of the relative energy dissipation model indicates that it has the low APE (-1.469), STDV (6.82), SI (0.105) and high R (0.958) values.

REFERENCES

Ansari, M.A., Hussain, A., Shariq, A., and Alam, F. (2019). Experimental and numerical study for the estimation of coefficient of discharge for side compound weir. *Canadian Journal of Civil Engineer*ing. 46(10): 887-895.

Fathi-Moghaddam, M., Tavakol-Sadrabadi, M., Rahmanshahi M. (2018). Numerical simulation of the hydraulic performance of triangular and trapezoidal gabion weirs in free flow condition. *Flow Measurement and Instrumentation*, 62; 93–104.

Pagliara, S., Palermo, M., (2013). Rock grade control structures and stepped gabion weirs: scour analysis and flow features. *Acta Geophys.* 61 (1), 126–150.

Peyras, L., Royet, P. and Degoutte, G. (1992). Flow and energy dissipation over stepped gabion weirs, *Journal of Hydraulic Engineering-ASCE*, 118 (5), 707-717.

Shariq, A., Hussain, A. and Ansari, M.A. (2018). Lateral flow through the sharp crested side rectangular weirs in open channels. *Flow Measurement and* Instrumentation, Vol. 59; 8-17.

Shariq, A., Hussain, A., & Ahmad, Z. (2020). Discharge equation for the gabion weir under through flow condition. *Flow Measurement and Instrumentation*, 74; 101769.

Wuthrich, D. and Chanson, H. (2014), Air Entrainment and Energy Dissipation on Gabion Stepped Weirs, in *"Hydraulic Structures and Society – Engineering Challenges and Extremes*", *Proceedings of the 5th IAHR International Symposium on Hydraulic Structures (ISHS2014)*, 25-27 June 2014, Brisbane, Australia.

Proceedings of the 1st IAHR
Young Professionals Congress
17-18 November 2020

LEVEL SET BASED MODELING OF LOCAL SCOURING IN THE VICINITY OF A SUBMERGED ARCH BRIDGE

Gábor Fleit [1], Sándor Baranya [2] & Hans Bihs [3]

[1,2] *Budapest University of Technology and Economics, Budapest, Hungary*
fleit.gabor@epito.bme.hu, baranya.sandor@epito.bme.hu

[3] *Norwegian University of Science and Technology, Trondheim, Norway*
hans.bihs@ntnu.no

ABSTRACT

Three-dimensional (3D) computational fluid dynamics (CFD) is more and more frequently used to solve various hydraulic engineering related problems, such as prediction of complex flow conditions or local scouring. While 3D models offer the solution of complex flow patterns determining the morphodynamic conditions (e.g. coherent turbulent structures), most of the available software is single-phased, thus bounded to simpler free surface conditions (i.e. flows with single local free surface elevations (depth)). In this study, the level set method (LSM) based, multiphase hydro- and morphodynamic model REEF3D was tested for the simulation of local scouring in the vicinity of a submerged arch bridge, where the sediment transport is mostly driven by the prevailing pressurized flow conditions under the bridge deck. The LSM showed robust performance in the treatment of the combined free surface/pressure flow problem as well as in the tracking of bed elevation changes.

Keywords: CFD, level set method, free surface, local scour, submerged bridge.

1 INTRODUCTION

Due to the rapid, continuous increase of available computational resources and the development of the related computer sciences, computational fluid dynamics (CFD) modeling is more and more frequently used within the hydroscience community. These models offer solutions to hydraulic engineering tasks in various scales – from laboratory up to river system scale – with different spatiotemporal resolutions, and as a function of the adopted abstractions and simplifications. Formerly, physical models were the only tools for investigating complex flow and morphodynamic problems, where classical formulas or simpler numerical models were no longer applicable. With the recent developments in CFD, the point has been reached, where numerical models can very well mimic real-life flow conditions, and thus can compete with the conventionally used, time demanding and expensive physical model experiments.

In this study an open-source CFD tool (REEF3D) is employed to solve the local scouring problem in the direct vicinity of a submerged arch bridge. The geometrical complexity and the prevailing pressurized flow conditions call for a multiphase modeling approach, which in this study is performed by utilizing the level set method (LSM).

2 NUMERICAL FRAMEWORK AND SETUP

The open-source CFD tool REEF3D (Bihs et al., 2016) was used for the numerical simulations. The model solves the incompressible Reynolds-averaged Navier–Stokes (RANS) equations along with the continuity equations using conservative finite differences. The stability and accuracy of the solver is ensured by high-order spatial (5^{th}-order WENO) and time (3^{rd}-order Runge-Kutta) schemes. Turbulence closure is achieved with the standard k-ω model. The LSM (Sussman, 1994) is used to numerically treat the interface between air and water (i.e. free surface), as well as between the water phase and the mobile sediment bed, while bed load transport is approximated using van Rijn's semi-empirical formula. The numerical setups were built up to mimic the laboratory experiments performed by Martín-Vide (2005).

3 RESULTS AND DISCUSSION

On the left side of **Fig. 1**, flow field around the submerged arch bridge is presented with velocity vectors. The high velocities observed in the pressurized region under the bridge deck suggest increased erosion potential, leading to the predicted scour presented on the right side of the figure.

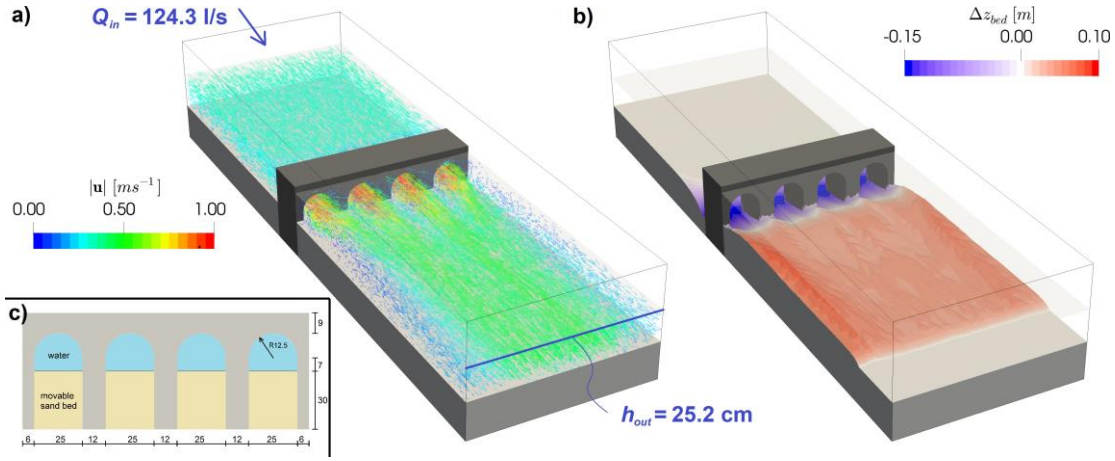

Figure 1. a) Velocity vector field for the rigid bed simulation with boundary conditions; b) morphodynamic result after 8 hours of sediment simulation time (right); c) bridge geometry.

The predicted bed topography shows realistic features: while intense scouring is observed at the bridge openings, the consequent sediment deposition is also represented on the downstream side of the obstacle.

Although the first results (presented in **Fig. 1**) are promising and the model has already been successfully applied to even more complex free surface flow problems (see e.g. Kamath et al. (2019)), additional model testing is required to see the effect of i) different bed load transport formulas; ii) different critical shear stress reduction formulas; and iii) other sediment related parameters and numerical methods, as they can reportedly determine the very nature of such morphodynamic simulations.

4 CONCLUSIONS

The LSM based modeling framework offers the robust numerical simulation of complex hydro- and morphodynamic conditions, making REEF3D and other competent CFD models valuable tools to complement or partially replace expensive and time demanding physical model experiments. It is noted, that due to the far from generalized theoretical background of bedload transport, additional numerical tests and sensitivity analyses are required in general, and in this particular case as well.

ACKNOWLEDGEMENTS

The first and the second authors acknowledge the support of the ÚNKP-20-3 and ÚNKP-20-5 New National Excellence Programs of the Ministry of Innovation and Technology, respectively. The second author acknowledges the support of the Bolyai János research fellowship of the Hungarian Academy of Sciences.

REFERENCES

Bihs, H., Kamath, A., Chella, M.A., Aggarwal, A., Arntsen, Ø.A. (2016) A New Level Set Numerical Wave Tank with Improved Density Interpolation for Complex Wave Hydrodynamics. *Computers and Fluids*, 140, 191-208.

Martín-Vide, J.P. (2005) Backwater of arch bridges under free and submerged conditions. *Journal of Hydraulic Research*, 43(5), 515-521.

Kamath A., Fleit G., Bihs H. (2019) Investigation of Free Surface Turbulence Damping in RANS Simulations for Complex Free Surface Flows. *Water*, 11, 456, 26p.

Sussman M. (1994) A level set approach for computing solutions to incompressible two-phase flow. *Journal of Computational Physics*, 114, 146-159.

Proceedings of the 1st IAHR
Young Professionals Congress
17-18 November 2020

FORMULAE TO ESTIMATE PEAK EFFLUENT FLOWS FROM BRASILIAN DAMS BREAK IN 21TH CENTURY

Carolina del Pilar Icho Castillo [1], Rodolfo Martins [2] & Jose Carlos de Melo Bernardino [3]

[1,] MSc Candidate [2] Associate Professor ,[3] Assistant Professor, School of Engineering, University of São Paulo
carolina.icho@usp.br

ABSTRACT

To predict the flood after a dam failure, many computational and empirical approaches have been developed throughout history. All those includes a certain number of parameters and are intended to help engineers in quick estimates and planning more detailed studies. In this article we aimed to evaluate the different empirical formulas proposed by researchers to estimate the outflow peak dambreak situations and compare the results in two different case studies, the overtopping and piping failure of Jurumirim and Chavantes dams. In this study, Hec-Ras software was implemented and used as reference to calculate the discharge peaks. Considering the large amount of available formulas, a statistical analysis where employed to evaluate and classify the results. Finally, the pertinence and range of application of the formulas is discussed.

Keywords: Dam break, flood propagation, Hec-Ras computational modeling, dam safety, rupture parameters.

1 INTRODUCTION

To minimize the losses associated with the failure of a dam, the National Dam Safety Policy of 2010 requires the elaboration of the Risk Plan involved **(ANA, 2010)**. The Risk Plan includes estimating the potential impacts of a dam disruption and the Emergency Action Plan (EAP) for projects under construction. The EAP contains information such as the inundation maps and the procedures to be performed in cases of emergency **(Lauriano, 2009).** Its execution is based on the forecast and calculation of maximum flooded levels, water velocities and maximum discharges resulting from the rupture. With the objective of reducing human, infraestructure and biodiversity losses by doing a number of anticipated activities. On the other hand, in order to guarantee the safety of hydraulic structures, the Brazilian Dam Safety Law requires a constant update of the Dam Safety Manual **(ANA, 2016)** which describes the dam safety inspection procedure. That is why it is more than justified the need to develop useful tools to classify the hazard, plan emergency actions, map and assess the risk **(Graham, 1998)**. One of these tools is the modeling of the full effluent of the dam rupture using empirical, mathematical and computational approaches. Computational modeling uses mathematical models and computation techniques. The use of computational models has shown to be an important tool for predicting hydraulic and hydrological phenomena. A computational model is the Hec- Ras software which requires little input data and presents a simplified view of one-dimensional constant flow studies, unidimensional and bidimensional unsteady flow calculations, sediment transport / moving bed calculations and modeling of temperature and water quality for a complete network of natural and/or artificial channels. Furthermore, it is free and works with small simplifications of the Saint Venant equation, using an implicit method of finite difference, which provide a high degree of precision and reliability **(Mbajiorgu, 2017).** Hence, this work will use the Hec-Ras software and formulas proposed by researchers in the area, to estimate the peak flow from a dam rupture by Piping and Overtopping. You will need the help of this HecRas software to simulate the rupture of the dam in a non-permanent 1-D flow regime. The calculation processes for the study of emergency scenarios will result in information about the characteristics of the gap, formation time and peak flow with the respective rupture hydrographs. In addition, with the flow analysis we will be able to identify the flooding areas and the time of arrival of the flood wave at points of interest located downstream from the dam.

Thus, this project aims, mainly, to identify and predict the scope of some of the effects of the rupture of the Jurumirim and Chavantes dams through a reliable computational modeling, which in this case will be the Hec-Ras software.

2 METHODOLOGY

The formulas proposed by various authors were compiled and organized to calculate the peak flow **(Figure 1)** and be compared with the results obtained by the Hec-Ras software. This software will have as input data the geometric information of the cross section of the dam, the breach, and the river channel **(Figure 2).** However, these results will vary depending on boundary conditions and gap geometry. So, we can divide the results generated into 4 categories:

- Jurumirim Dam with rupture by Overtopping
- Jurumirim Dam with rupture by Piping
- Chavantes Dam with rupture by Overtopping
- Chavantes dam with piping rupture

3 FIGURES

Figure 1: Number of formulas analyzed vs. Number of input variables

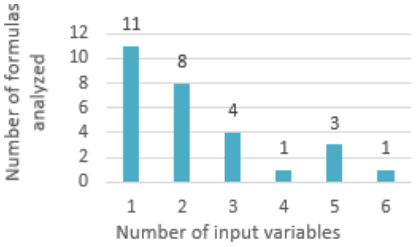

Figure 2: Implementation of the HEC-RAS software in Chavantes dam and Jurumirim dam. **Source:** FCTH.

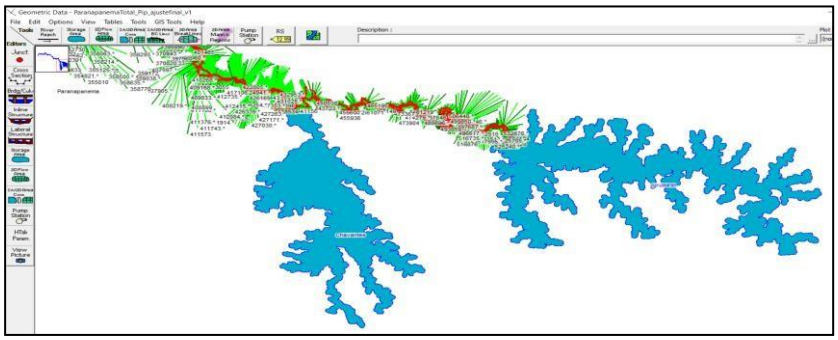

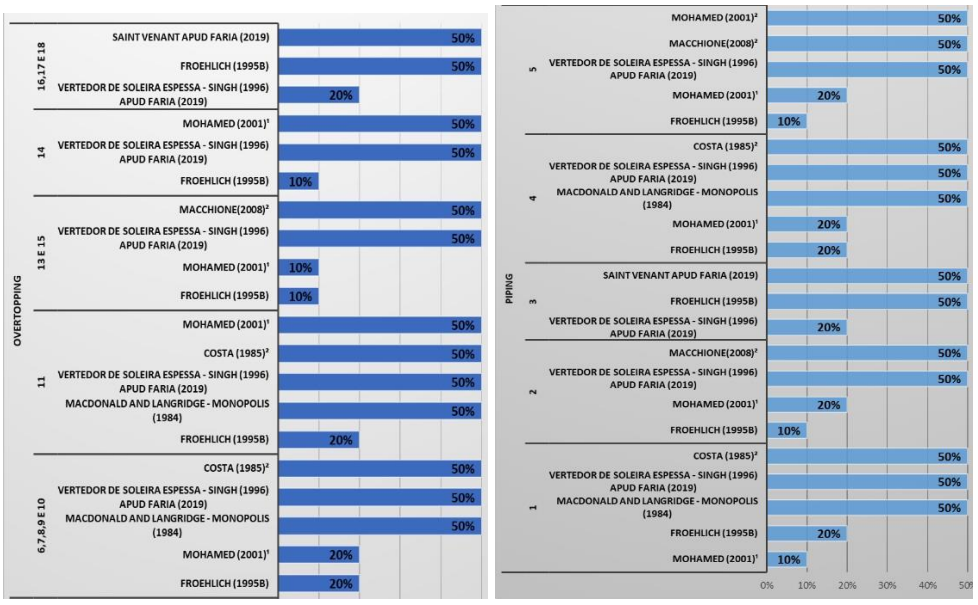

Figure 3 and Figure 4. Degree of uncertainty between the results provided in each case by the HEC-RAS software and those generated by the proposed in formulas in Jurumirim dam. **Source:** Author

Figure 5. Degree of uncertainty between the results provided in each case by the HEC-RAS software and those generated by the proposed in formulas in Jurumirim dam. **Source:** Author

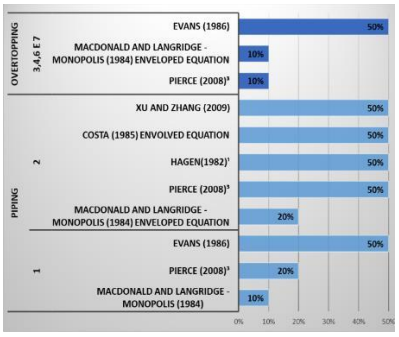

4 RESULTS AND CONCLUSIONS

From the results obtained we can conclude that (Figure 7) (Figure 8) and (Figure 9), in the Jurumirim dam, the most accurate formulas in all cases are the formulae proposed by Froehlich (1995B) and Singh (1996). Second, the formula proposed by Mohamed (2001) 1 is accurate in most of the cases analyzed. Third, the formulas proposed by the U.S. Army corps of Engineering, by Macchione, by Costa (1985) 2 and by MacDonald (1984) are met in some cases.

On the other hand, in the case of the Chavantes dam, the most precise formula in all cases is the one proposed by Pierce (2008)3. Second, the formula proposed by Evans (1986) and MacDonald Enveloped equation (1984) is fulfilled in most of the cases analyzed. Third, in some cases of Piping rupture there are the formulas of Xu and Zhang (2009), Costa (1985) enveloped equation, Hagen (1982) and MacDonald (1984).

ACKNOWLEDGEMENTS

This project was supported by the Unified Scholarships Program of the University of Sao Paulo

REFERENCES

ANA, Agencia Nacional de Águas. Manual de Políticas de Segurança de Barragens para Entidades Fiscalizadoras, 2016.
LAURIANO, A. W. Estudo de Ruptura da Barragem de Funil: comparação entre os modelos FLDWAV e HEC-RAS. 2009.
GRAHAM, W., Channel and Valley Changes Resulting from Dam Failure. Proceedings of the 2nd CADAM Workshop, Munique, Alemanha, 1998.
MBAJIORGU, C. C. Flood Inundation Simulation using HEC-RAS Hydrologic Model: A Case Study of Oyun River, Nigeria; 2017.

IAHR AIRH

International Association for Hydro-Environment Engineering and Research

Hosted by
Spain Water and IWHR, China

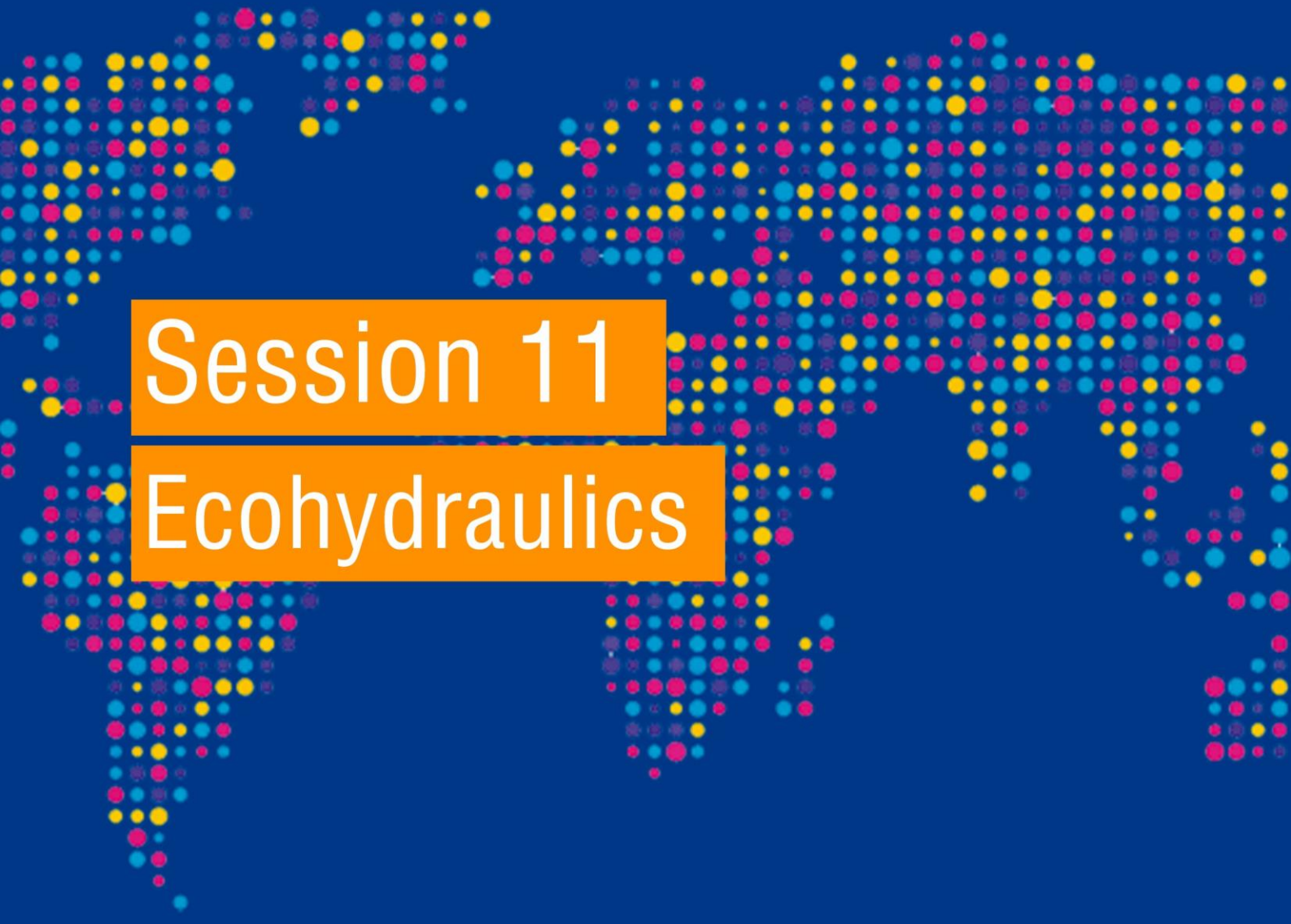

Session 11
Ecohydraulics

IAHR YPN

Hosted by
Spain Water and IWHR, China

Proceedings of the 1st IAHR
Young Professionals Congress
17-18 November 2020

ESTIMATING THE RESISTANCE OF A POROUS MEDIA THAT NUMERICALLY REPRESENTS A FLOATING TREATMENT WETLAND

Taís Natsumi Yamasaki [1] & Johannes Gérson Janzen [1]

[1] Federal University of Mato Grosso do Sul, Campo Grande, Brazil,
taisnatsumi@gmail.com, johannesjanzen@gmail.com

ABSTRACT

Floating treatment wetlands (FTWs) are an important nature-based solution to treat water, wastewater and stormwater. Their roots grow hydroponically, through which they absorb nutrients, metals and dissolved matter, retain suspended solids and improve water turbidity. Moreover, FTWs constitute a green infrastructure because of their added ecological value. Numerically, FTWs can be represented as a porous media, in which the resistance is usually estimated by fitting the simulation to measured data. This study presents a new approach to estimate the viscous and inertial resistance factors of the porous media. The FTW is treated as a packed bed, for which the Ergun equation is applied, but in the vertical direction (flow parallel to the roots) the root diameter is estimated as a hydraulic diameter, which creates a non-isotropic resistance. This approach resulted in better agreement with the experiments than the fitting strategy, for a simulation case.

Keywords: wetlands, CFD, porous media, validation.

1 INTRODUCTION

From a hydrodynamic perspective, the treatment performance of a FTW can be influenced by the contact time and mass flux entering the root zone (Liu et al., 2019). That is why recent studies have been employing Computational Fluid Dynamics (CFD) to assess hydrodynamic interactions between the flow and the FTW (Xavier et al., 2018; Rao et al., 2016). In CFD, there is a known difficulty in representing the vegetation structure as it is due to the high computational cost required. For FTWs, one alternative is to represent the roots as a porous media (Xavier et al., 2018; Rao et al., 2016), which requires determining the viscous ($1/\alpha$) and inertial (C_2) resistance factors. The goal of this study is to present a more physically-tied approach to estimate $1/\alpha$ and C_2, instead of estimating the factors by fitting the simulation to measurements.

2 METHODS

The FTW root zone is represented by a porous media, in which a sink term is added to the momentum equation, according to Darcy's Law. The porous media is treated as a packed bed, for which the Ergun equation estimates $1/\alpha$ and C_2:

$$\frac{1}{\alpha} = \frac{150\,(1-\epsilon)^2}{D_p^2}\frac{}{\epsilon^3} \qquad [1]$$

$$C_2 = \frac{3.5\,(1-\epsilon)}{D_p}\frac{}{\epsilon^3} \qquad [2]$$

in which D_p is the mean particle diameter and ϵ is the void fraction. In the horizontal direction (flow perpendicular to the roots), D_p can be assumed as the root cylinder (d). However, in the vertical direction (flow parallel to the roots), D_p can be estimated as the hydraulic diameter (d_h), which is dependent on the spacing: diameter ratio (s/d) of the roots (Oldham & Sturman, 2001):

$$d_h = d\left(\frac{4(s-d)^2}{\pi} - 1\right) \qquad [3]$$

and this will lead to a non-isotropic resistance in the FTW.

This approach was tested on a CFD model that recreated laboratory-scale experiments from Liu et al. (2019), who built FTWs based on *E. crassipes* arrangements and placed them in a flume. The FTW length, width and depth were, respectively, L_{FTW} = 25.6 cm, W_{FTW} = 18 cm and h = 10.5 cm (approximately half of the channel depth), and it presented d = 0.36 cm and ϵ = 0.93. A single FTW was placed 300 cm downstream of the channel inlet, and it was attached to one of the channel walls. Then, three other similar FTWs were placed in series, with a spacing of $2L_{FTW}$ between one another. For brevity, details on mesh, boundary conditions and solver configuration were omitted. A fitted resistance was obtained for comparison.

3 RESULTS

The first comparison regards the flow adjustment past a single FTW (Figure 1a). The longitudinal profile of x-velocity (u) normalized by the initial velocity (U_0) was obtained in the centerline (= $W_{FTW}/2$) and mid-depth (= $h/2$) of the FTW. The FTW is located at x/L_{FTW} = 0 and 1. The best-fitted resistance was $1/\alpha = 10^{-6}$ m^{-2}. The calculated resistance was $1/\alpha$ = 70507.2 m^{-2} and C_2 = 73.2 m^{-1} in the horizontal direction, and $1/\alpha$ = 365.2 m^{-2} and C_2 = 6.1 m^{-1} in the vertical direction. The calculated resistance (continuous line) and the fitted resistance (dashed line) had similar behavior, and they agreed with the measurements (open circles) especially in the FTW, where the steep velocity reduction occurred. When comparing FTWs in series, the calculated resistance showed better precision (Figure 1b). The fitted resistance (open triangles) matched the measurements (filled diamonds) in the first and second FTWs, but underestimated the flow reaching the third and fourth FTWs. The calculated resistance (open squares) showed consistent agreement with the measurements for all FTWs.

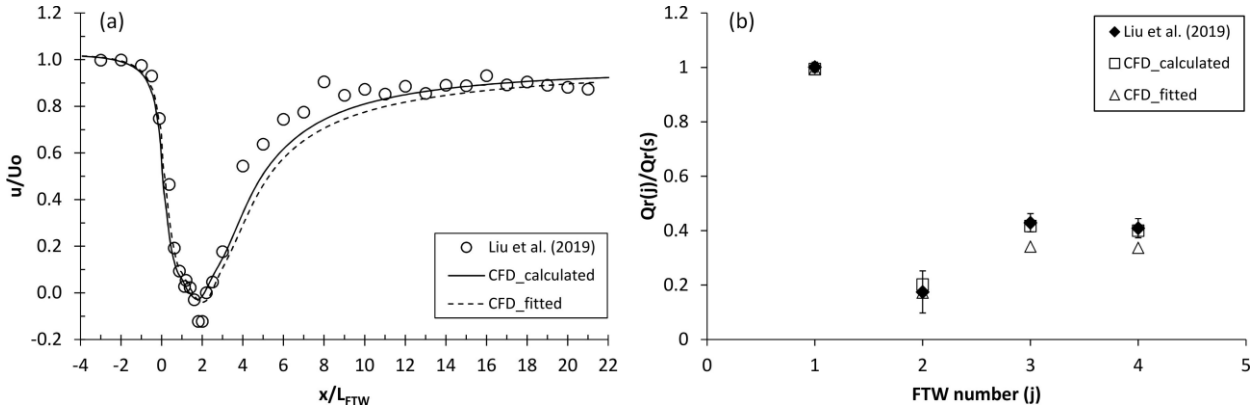

Figure 1. (a) Longitudinal profile of u/U_0 in the centerline and mid-depth of the FTW. The FTW is located at x/L_{FTW} = 0 and 1. (b) Flow entering the jth FTW ($Q_{r(j)}$) normalized by the flow rate entering the first FTW ($Q_{r(s)}$).

4 CONCLUSIONS

The Ergun equation combined with the hydraulic diameter approach in the vertical flow direction (Oldham & Sturman, 2001) showed to be a reliable method to estimate porous media resistance in the FTW.

REFERENCES

Liu, C., Shan, Y., Lei, J., and Nepf, H. (2019). Floating treatment islands in series along a channel: The impact of island spacing on the velocity field and estimated mass removal. *Adv. Water Resour.*, 129, 222-231.

Oldham, C.E., and Sturman, J.J. (2001). The effect of emergent vegetation on convective flushing in shallow wetlands: Scaling and experiments. *Limnol. Oceanogr.*, 46 (6), 1486-1493.

Rao, L., Wang, P., Lei, Y., and Wang, C. (2016). Coupling of the flow field and the purification efficiency in root system region of ecological floating bed under different hydrodynamic conditions. *J. Hydrodyn.*, 28 (6), 1049-1057.

Xavier, M.L.M., Janzen, J.G., and Nepf, H. (2018). Numerical modeling study to compare the nutrient removal potential of different floating treatment island configurations in a stormwater pond. *Ecol. Eng.*, 111, 78-81.

Proceedings of the 1st IAHR
Young Professionals Congress
17-18 November 2020

Plastics in streams: transport dynamics and open questions

Arianna Varrani[*1] **and Paweł M. Rowiński** [1]

[1]Institute of Geophysics - Polish Academy of Sciences, Warsaw, Poland

*Correspondance : avarrani@igf.edu.pl

ABSTRACT

The presence of plastic debris in lotic environments is well reported. Rivers and streams are recognised to be mostly pathways for plastic litter, and the increasing number of evidences proves how widely plastics and their by-products (namely macro-, micro- and nanoplastics) have permeated the natural environment. Though, the transport process itself has not yet been completely resolved. With the aim to partially fill this gap, this short contribution outlines the plastics transport issue, with a particular focus on microplastics, and few available studies on plastic bedload. Moreover a research thread is presented, which will be further developed in the next years by the Authors.

Keywords: microplastics, river, sediment transport, bedload.

1 INTRODUCTION

Only in the year 2020, 185 papers (according to Scopus database as of August) have been published, containing the keywords ”microplastics” and ”river”. This should ring a bell on how much the problem is perceived as actual and compelling, and demands attention. Moreover, the ongoing COVID-19 pandemia is inevitably exhacerbating this issue (Fadare et Okoffo, 2020; Prata *et al.*, 2020), in that single-use products are not always disposed correctly, thus adding plastic litter to the environment, and eventually to rivers. Albeit the increasing body of literature regarding microplastics in riverine environments, very few attention has been devoted, to date, to the transport processes which contribute to the yield of small plastic debris to their sinks (namely lakes, seas and ocean). From the pioneering studies by Venrick *et al.* (1973); Wong *et al.* (1974) reporting the presence of plastic debris in the ocean, to most recent paper highlighting the seepage of plastic particles into the bed sediment layer Frei *et al.* (2019), literature on plastic debris in the environment reports, with increasing level of detail, how such material is ubiquitous in all the environmental compartments. Concerning plastic fragments with dimensions in the range 1 µm - 5 mm, namely microplastics-MP, they have been extensively found in rivers, and it is widely accepted that rivers and streams function as pathways for such materials to reach their final sink (Rochman, 2018; Waldschläger *et al.*, 2020). While the ecotoxicological effects of MP are being meticulously explored, as the main concern is the future harm and hazard they pose to the ecosystems and eventually our society and health (Li *et al.*, 2018; Laskar et Kumar, 2019), much less attention has been devoted to the understanding of the transport processes and fate of MP in rivers (Akdogan et Guven, 2019). Most straightforwardly, microplastics (MP) are assumed to be transported sediments alike, as washload, suspended or bedload, mostly depending upon their dimensions and density. Indeed, while light particles (with grain density ρ_S smaller than that of water ρ_W) are transported downstream by the current, heavier ones ($\rho_S > \rho_W$) tend to deposit and be buried or rest on the bed surface until they are re-mobilised again by a change in the hydrodynamic conditions. Heavier plastic particles can be threrefore generally considered to be transported as bedload, but to which extent such assumption can be valid is yet to be proven, as, to date, the ”sediment” transport mechanism of non-natural particles moving at the bed has not been exhaustively addressed. Until very recent times, indeed, it has been neither necessary, nor scientifically relevant. At the laboratory scale, on the other hand, plastic granules have been used to mimic natural material in bedload studies, see among others (Campagnol *et al.*, 2013; Hosseini-Sadabadi *et al.*, 2016), since such materials are easily available, more colourful and, in general, lighter, thus allowing to be transported with lower hydrodynamic conditions. These studies could now bridge the gap in terms

of consistency of the aforementioned assumption on the equivalence of the transport processes of natural and plastic grains at a stream bed.

2 METHODOLOGY OUTLINE

Transport of particles at the bed initiates as they detach from the bed surface: these coditions are referred to as "incipient motion" and they set the lower limit for transport to occur. Therefore,the identification of incipient motion conditions is essential in the characterisation of MP transport. Following the basic idea outlined in Waldschläger et Schüttrumpf (2019) to identify erosional behaviour of MP particles lying on different types of bed sediments, a series of experiments will be carried out in the new Hydrodynamics Model Laboratory in Warsaw, to investigate the role of bed composition (in terms of both type of sediments and percentage of MP particles) on the incipient motion conditions of MP. For this reason, image-analysis techniques will be used to identify bed-surface changes in time, coupled with acoustic measurements of the near-bed hydrodynamics.

3 WHAT NEXT?

The combination of optical and acoustic measurements aims at validating the abovementioned assumption of equivalence of MP and sediments in terms of bedload transport.

4 ACKNOWLEDGEMENTS

This work was supported within statutory activities No. 3841/E-232 41/S/2020, Ministry of Science and Higher Education of Poland.

References

Akdogan Z., Guven B. (2019). Microplastics in the environment: A critical review of current understanding and identification of future research needs. *Environmental Pollution 254*, 113011.

Campagnol J., Radice A., Nokes R., Bulankina V., Lescova A., Ballio F. (2013). Lagrangian analysis of bed-load sediment motion: database contribution. *Journal of Hydraulic Research 51*(5), 589–596.

Fadare O. O., Okoffo E. D. (2020). Covid-19 face masks: A potential source of microplastic fibers in the environment. *The Science of the total environment 737*, 140279.

Frei S., Piehl S., Gilfedder B., Löder M., Krutzke J., Wilhelm L., Laforsch C. (2019). Occurence of microplastics in the hyporheic zone of rivers. *Scientific reports 9*(1), 1–11.

Hosseini-Sadabadi S. A., Radice A., Ballio F. (2016). An analysis of entrainment and deposition rate fluctuations in weak bed load transport. In *Hydrodynamic and mass transport at freshwater aquatic interfaces*, pp. 333–342. Springer.

Laskar N., Kumar U. (2019). Plastics and microplastics: A threat to environment. *Environmental technology & innovation 14*, 100352.

Li J., Liu H., Chen J. P. (2018). Microplastics in freshwater systems: A review on occurrence, environmental effects, and methods for microplastics detection. *Water Research 137*, 362–374.

Prata J. C., Silva A. L., Walker T. R., Duarte A. C., Rocha-Santos T. (2020). Covid-19 pandemic repercussions on the use and management of plastics. *Environmental Science & Technology 54*(13), 7760–7765.

Rochman C. M. (2018). Microplastics research—from sink to source. *Science 360*(6384), 28–29.

Venrick E., Backman T., Bartram W., Platt C., Thornhill M., Yates R. (1973). Man-made objects on the surface of the central north pacific ocean. *Nature 241*(5387), 271–271.

Waldschläger K., Lechthaler S., Stauch G., Schüttrumpf H. (2020). The way of microplastic through the environment–application of the source-pathway-receptor model. *Science of The Total Environment 713*, 136584.

Waldschläger K., Schüttrumpf H. (2019). Erosion behavior of different microplastic particles in comparison to natural sediments. *Environmental Science & Technology 53*(22), 13219–13227.

Wong C., Green D. R., Cretney W. J. (1974). Quantitative tar and plastic waste distributions in the pacific ocean. *Nature 247*(5435), 30–32.

Proceedings of the 1st IAHR
Young Professionals Congress
17-18 November 2020

Tracking fish swimming behaviour in response to a vertical axis turbine

Stephanie Müller[*1], Valentine Muhawenimana[1], Pablo Ouro[1,3], Jo Cable[2], Catherine Wilson[1]

[1]Hydro-Environmental Research Center, School of Engineering, Cardiff University, Cardiff, CF24 3AA, Wales, UK
[2]School of Biosciences, Cardiff University, Cardiff, CF10 3AX, Wales, UK
[3]School of Mechanical, Aerospace and Civil Engineering, University of Manchester, Manchester, M13 9PL, UK

*Correspondance : MullerS1@Cardiff.ac.uk

ABSTRACT

Hydrokinetic vertical axis turbines (VAT), suitable for rivers and estuaries, are a promising alternative to traditional hydropower schemes to meet the increasing global energy demand while minimising environmental impacts. To date, there are major research gaps in quantifying the impact of VAT turbulent wake hydrodynamics on fish swimming behaviour and passage. Here, we investigate fish behavioural responses to a single VAT in a confined laboratory environment by relating fish body position and swimming kinematics to the surrounding flow field. Initial results show that although fish passed from downstream into the upstream area, they spent most time within the turbine wake area, which was characterised by a region of low momentum immediately downstream of the VAT and regions of high momentum on either side of the turbine. These experimental observations will contribute to the commercial development of VATs as sustainable renewable energy technology with low environmental impact.

Keywords: renewable energy, vertical axis turbine, Acoustic Doppler Velocimetry, fish behaviour, motion tracking

1 INTRODUCTION

Due to rising energy consumption, an urgent need for sustainable and environmentally friendly energy technologies exists. So far only 11% of the world's consumption is provided by renewable energies with hydropower being the second largest source (REN21, 2020), yet its full potential is not used. The environmental impact of traditional, large-scale hydropower projects has driven the development of small-scale alternatives such as vertical axis turbines (VAT). These turbines can operate in low to medium velocity flows, making them suitable for shallower waters typically found in rivers and estuaries. Their versatile deployment may be particularly beneficial for small, remote communities in low-middle income countries with limited access to the energy grid, allowing the generation of continuous sustainable energy. Despite the potential of VAT, only a few studies have examined their impact on fish passage and swimming behaviour. These studies reported changes in passage, spatial, and schooling behaviour (Castro-Santos et Haro, 2013; Molloy *et al.*, 2017) but no injuries when colliding with turbine blades (Castro-Santos et Haro, 2013), which may be attributed to the turbine's open design and low rotational speed. Behaviour changes might be associated with noise and near wake alterations (Molloy *et al.*, 2017), however, much remains unknown about their extent and causes. This research examines the interaction between hydrodynamic flow structures generated in the near-wake of a single VAT and swimming behaviour of juvenile rainbow trout (*Oncorhynchus mykiss*) in a confined laboratory environment using motion tracking.

2 METHODS

A first set of experiments were undertaken in a recirculating flume in the hydraulic laboratory at Cardiff University, UK. The experimental set-up comprised of a $10m$ long, $0.3m$ wide and $0.3m$ deep flume with a constant discharge of $0.0013m^3s^{-1}$ and flow depth of $0.23m$. At $4m$ downstream of the flume inlet, a three-bladed vertical axis turbine with diameter and height $0.12m$ and NACA0015 blades of chord length $0.03m$, was mounted in the centre of the flume, constantly rotating at $59rpm$ for an optimum tip speed ratio of 1.9. A test section of $0.75m$ was delimited by honeycomb flow straighteners $0.25m$ upstream and $0.5m$ downstream of the turbine (Figure 1) and illuminated with spot lights on either side of the test section. A camera (60fps, 1920x1080px) was mounted approx. $1m$ above the flume to record the behaviour of fish swimming individually ($5cm$ standard length) for $5min$. A $0.01m$ thick Perspex plate was placed on top of the water surface, ensuring a clear view of the test section. Fish behaviour was analysed using an adapted version of the Matlab-based Sensory Orientation Software (Gomez-Marin *et al.*, 2012), to identify the fish centre of mass (COM), as well as head ($y_{head}(t)$) and tail ($y_{tail}(t)$) position

in each frame (Figure 1 (right)). Based on these time-dependent variables, we recorded spatial preference, head and tail kinematics, covered distance, and swimming speed. Near-wake hydrodynamics for this VAT were measured in a $10m$ long, $1.2m$ wide and $0.3m$ flume under similar flow and rotational conditions, using Acoustic Doppler Velocimetry (sampling time $180 - 300s$, sampling rate $200Hz$).

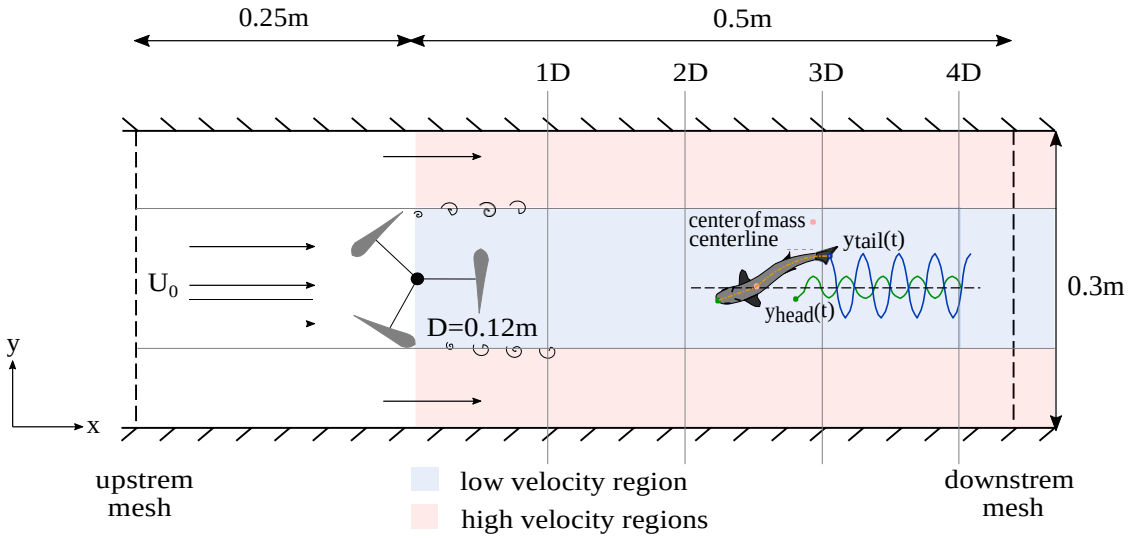

Figure 1: Flume test section used for fish behaviour experiments, comprising a single VAT, upstream and downstream mesh. Individual fish were released furthest downstream. Fish behaviour and kinematics were recorded over time, including the lateral position of the head and the tail, and centre of mass (COM).

3 WAKE HYDRODYNAMICS AND FISH BEHAVIOUR

Wake velocity measurements showed a region of low momentum immediately downstream of the turbine, with a wake asymmetric about its centreline. This region was accompanied by an increase in velocity on either side of the turbine, as indicated in Figure 1. Blade induced vortices were convected downstream along the edges of the low-velocity region. Although fish spent most time downstream of the turbine within the low velocity region, they also occupied both low- and high-velocity regions. Despite the increased streamwise mean velocities on either side of the turbine, fish passed from downstream into the upstream area. So far, no avoidance behaviour concerning the turbine was observed as fish swam even close to the rotating turbine. Tip and dynamic stall vortices, generated during the upstroke and downstroke rotations of the turbine, did not negatively impact swimming stability.

4 CONCLUSIONS

The application of a motion tracking algorithm generated useful insights into fish behaviour adaptations in response to a single VAT, namely spatial preference, attraction and avoidance behaviours. Fish occupied both the low- and high- momentum areas of the VAT near wake and swam unimpeded when passing the turbine. This may help to improve turbine arrangements, operation, and design, and to foster VATs as an environmental-friendly technology. Future research will test more fish and analyse swimming behaviour in the wake of VAT for a range of discharges and turbine rotational speeds.

5 ACKNOWLEDGEMENTS

Funding was provided by the Engineering and Physical Science Research Council (EPSRC) Global Challenges Research Fund and the Water Informatics Science and Engineering Centre for Doctoral Training (WISE CDT) under a grant from the EPSRC (EP/L016214/1.1).

References

Castro-Santos T., Haro A. (2013). Survival and Behavioral Effects of Exposure to a Hydrokinetic Turbine on Juvenile Atlantic Salmon and Adult American Shad. *Estuaries and Coasts 38*(1), 203–214. doi:10.1007/s12237-013-9680-6.

Gomez-Marin A., Partoune N., Stephens G. J., Louis M. (2012). Automated tracking of animal posture and movement during exploration and sensory orientation behaviors. *PLoS ONE 7* (8). doi:10.1371/journal.pone.0041642.

Molloy S., Batt J., Eddington J., Mahon-hodgins L., MacNeil A. M., Kregting L., Bibeau E. (2017). Tidal Turbine Marine Life Interaction study: Fish. pp. 24.

REN21 (2020). *Renewables 2020 Global Status Report*. URL: http://www.ren21.net/resources/publications/.

Proceedings of the 1st IAHR
Young Professionals Congress
17-18 November 2020

BURSTING PHENOMENA DOWSNTREAM AQUATIC PLANTS GROWING IN NATURAL CONDITIONS

Łukasz Przyborowski [1], Anna Maria Łoboda [2]

[1,2] Institute of Geophysics, Polish Academy of Sciences, Warsaw, Poland
lprzyborowski@igf.edu.pl

ABSTRACT

The studies of ecohydraulics are essential for discovering complex processes occurring in natural aquatic ecosystems. Investigation of the turbulence downstream submerged vegetation is essential to evaluate the effect of plants on the water mixing and sediment transport. The experiments in natural river were performed, where the velocity field was measured downstream single patches of submerged plants. Increased $\overline{u'w'}$ Reynolds stress outlined the spatial reach of wake area and signalized the presence of the coherent structures in the flow, which transported momentum and mass. The combined results from different measuring points showed that downstream the plant patch, the magnitude of bursting events depended on the distance and relative position to the vegetation height. The use of thresholding in the detection of coherent structures revealed that the passage of roller vortices was visible at the upper boundary of the plant's wake.

Keywords: turbulence, bursting events, coherent structures, quadrant analysis, aquatic vegetation.

1 INTRODUCTION

Consideration of the role of aquatic plants in the water resources management is related to the study of interactions between flow, aquatic vegetation and sediment at various scales. The use of acoustic doppler velocimetry and data about morphological and biomechanical traits can be merged to take a more detailed look into those connections. Such approach is important in the field of ecohydraulics, where different elements of ecosystems are taken into analysis. For example, laboratory tests implied that movements of flexible stems are the same as the frequency of ambient turbulences (Siniscalchi and Nikora, 2013). Therefore, plant traits have an impact on the vegetation induced drag and turbulences, which then influence momentum transport and fluxes (Nikora, 2010). Furthermore, Marjoribanks et al. (2017) showed in simulation that turbulent events in even quadrants are correlated with the presence of roller vortices and that two types of events dominate in flow through the submerged vegetation. Continuing the investigations of flow-plant-sediment interactions (Przyborowski et al., 2019), the focus on bursting events induced by the presence of flexible vegetation may reveal more about the sediment transport and scouring effect downstream such obstacles in natural river habitats.

2 METHODOLOGY

To study flow-plant-interactions, experiment in the unaltered, sandy bedded lowland river in central Poland, the Świder River, was conducted. Naturally occurring flexible aquatic plants growing from the riverbed were identified and described in terms of their morphological traits, further supplemented by the information of their biomechanical traits. Two different plant species, *M. spicatum* L. and *P. crispus* L., growing in patches of similar dimensions (i.e., about 1 meter long, submerged of about 15 centimeters height), were chosen for the experiment. Acoustic Doppler velocimeters were installed downstream of the plants on a wide platform (more details on the poster) to stabilize probes and guarantee the precision of positioning. The recorded velocity time series were filtered out of spikes using a variety of methods specially fitted for that purpose. The quadrants analysis method with the modification described by Ferreira et al. (2009) was used to enhance the detection of the events. To calculate the magnitude of events above threshold of h = 1.8, the total value of $\overline{u'w'}$ Reynolds stress from each detected event in each quadrant was normalized by the whole length of measurement period.

3 RESULTS

Downstream both plants, increased values of Reynolds stresses marked the area of turbulent mixing between free flow and the wake. In the case of *M. spicatum* at the maximal height of the floating plant stems, the greatest turbulence was visible around 0.3 meter downstream (Fig. 1), farther than in the case of *P. crispus*. Closer to the plant, the strong sweep events, which were marked in the fourth quadrant, were the most numerous and further away from the plant's edge, the strong ejections made its appearance. More detailed description of the results are presented in the conference poster.

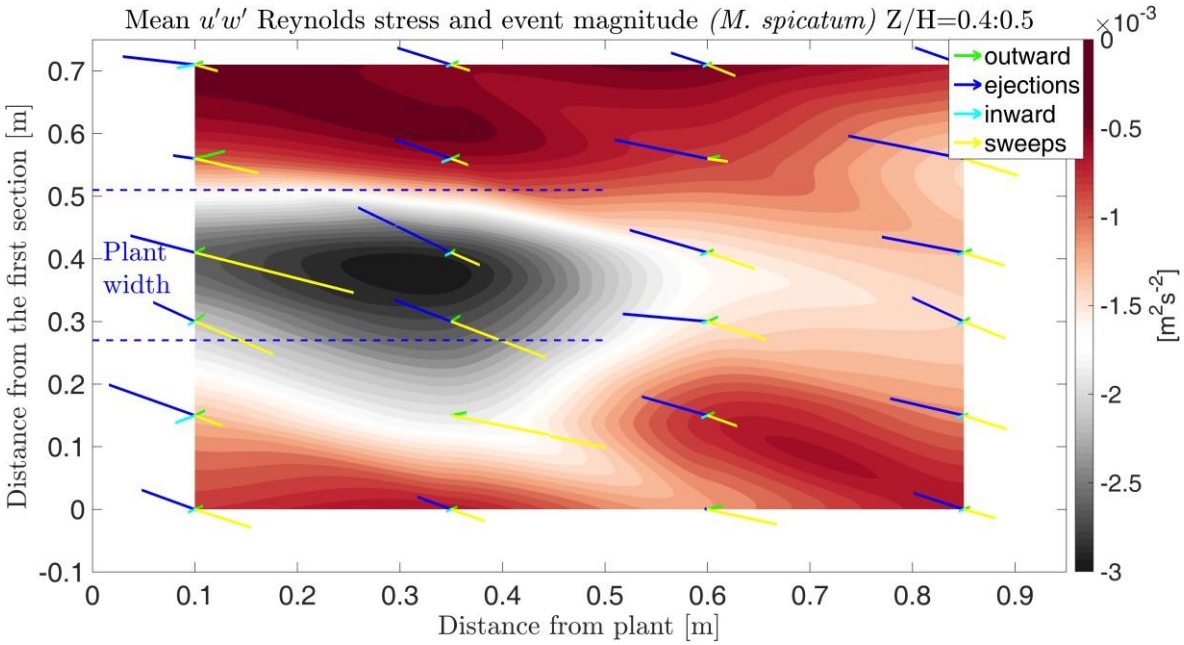

Figure 1. Interpolated field of $\overline{u'w'}$ Reynolds stress and magnitudes of four types of events in the measured points downstream of *M. spicatum* patch at the height of the vegetation top.

4 CONCLUSIONS

The pattern in the magnitude of strong bursting events downstream the submerged patch indicated the presence of roller vortices, which was in line with the simulations done by Marjoribanks et al. (2017) for a submerged plant canopy. It is worth noting that biomechanical tests proved the *M. spicatum* stems to be less flexible but still undergo swaying motions. Further time analysis of coherent structures occurrence should then reveal the length and frequency of the detected event sequences possibly matching the swaying frequency of the plant stems.

ACKNOWLEDGEMENTS

This work was supported by the National Science Centre, Poland, Grant No. UMO-2014/13/D/ST10/01123 "Field experimental investigation of hydrodynamics of water flow–vegetation–sediment interactions at the scale of individual aquatic plants."

REFERENCES

Ferreira, R.M.L., Franca, M.J., Leal, J.G.B., Cardoso, A.H. (2009). Organized turbulence over mobile and immobile hydraulically rough boundaries. In proc. 35 rd IAHR Congress, Vancouver, British Columbia, Canada, 36-43.

Marjoribanks, T.I., Hardy, R.J., Lane, S.N., Parsons, D.R. (2017). Does the canopy mixing layer model apply to highly flexible aquatic vegetation? Insights from numerical modelling. *Environmental Fluid Mechanics*, 17(2), 277-301.

Nikora, V. (2010). Hydrodynamics of aquatic ecosystems: an interface between ecology, biomechanics and environmental fluid mechanics. *River research and applications*, 26(4), 367-384.

Przyborowski, Ł., Łoboda, A.M., Bialik, R.J., Västilä, K. (2019). Flow field downstream of individual aquatic plants—Experiments in a natural river with Potamogeton crispus L. and Myriophyllum spicatum L. *Hydrological Processes*, 33(9), 1324-1337.

Siniscalchi F., Nikora V. (2013). Dynamic reconfiguration of aquatic plants and its interrelations with upstream turbulence and drag forces. *Journal of Hydraulic Research*, 51(1), 46–55.

Proceedings of the 1st IAHR
Young Professionals Congress
17-18 November 2020

ECO-HYDRAULIC IMPACT OF PLASTIC FLOW OVER THE MOUTH OF THE MAGDALENA RIVER AND ADJACENT BEACHES

Carlos Julio Hernández[1], Giovanna María Cera [2], Jerson Javier Rodríguez [3]

[1,2,3] Fundación Universidad del Norte, Puerto Colombia, Colombia,
[1]carlosjh@uninorte.edu.co, [2]giovannetig@uninorte.edu.co, [3]vjerson@uninorte.edu.co

ABSTRACT

Plastic debris are an important issue due to the environmental impact it induces at the aquatic ecosystems. Since most of plastics come from land-based sources, rivers play an important role in transporting plastic patches. The Magdalena river, the most important river in Colombia ranks among the most contaminated rivers by plastic in the world. This contribution analyzes in situ data recorded during beach and river cleaning events, among of them stands out the data obtained from a coastal garbage island. The latter allowed estimating the plastic mass input of the Magdalena. This analysis could be used to raise societal attention on this eco-hydraulic problem and to highlight the need of an engineered plastic patches management plan and field measurements.

Keywords: plastic, Magdalena River, Garbage Island, eco-hydraulics.

1 INTRODUCTION

The Magdalena River is both the main fluvial system and a national symbol of Colombia as it constitutes the largest fluvial waterway that runs from the center of the country to the Caribbean Sea and holds around 80% of the Colombian population (Galvis & Mojica, 2007). It is also the habitat for several flora and fauna species. In recent years, the Magdalena has exhibited a marked increase in plastics flow. Plastic litter is detrimental for river biota as it can be ingested by aquatic animals and affect plant species such as mangrove forest trees (Tim and Schwarz, 2020). In average, Colombia produces 24 kilograms of plastic per capita per year (Greenpeace, 2018), which is not adequately disposed. A global model of plastic inputs by Lebreton et al. (2017) ranks the Magdalena river as 15th World's watercourse that discharges higher amounts of plastics into the ocean (1.67x10^4 ton/year midpoint plastic mass). However, to date there is not information related to field measurements and/or plastic classification at the Magdalena mouth.

The amount of waste transported in rivers has increased worldwide for several years because of plastic dependence in cities (Plastics Europe, 2016). Barranquilla (population 1.2 million) is located at the Magdalena mouth and is the largest river city. Since the year 2015 beach and river cleanups at the Magdalena mouth during the winter season (May-July) have been frequently conducted. Thus, plastic islands at the river channel and the coastal area have been identified. This study posits that yearly mass estimates of plastic mass can be obtained by analyzing these islands.

2 DATA AND METHODS

A review of data from cleaning events in the adjacent zone of the river mouth has been conducted starting from 2015 (Fig. 1). In Sabanilla, Puerto Colombia, during a beach cleaning event in mid-June 2015, about 25 tons of garbage were collected, which contained a high percentage of plastics (Limpieza en Sabanilla, 2015). Another cleaning event took place on the riverbank, near the Gran Malecón of Barranquilla, in October 2018. Around 3 tons of garbage that contained 3 kilograms of recyclable material were removed (Limpieza en el río Magdalena, 2018). In June 2019, an environmental emergency arose in the department of Atlántico, since an island of garbage boarded the beaches of Puerto Colombia, which are among the most crowded in the region. The island (Fig. 2) contained more than 1050 tons of garbage. Parts of this debris were plastics (volume ~ 20%), non-biodegradable waste, branches and logs coming from many of the streams that cross the city of Barranquilla (Playas de Puerto Colombia, 2019). This island was formed in a period of two – four days, initiating the accumulation of garbage on May 27th and being fully formed on May 31th. By analyzing data from

satellite images and videos, we estimated that the approximate daily mass of plastics (assuming a LDPE density of 940 kg/m^3) that entered the island in this time interval (3 days midpoint) was 65 tons. This estimation demanded delimiting the surface of the garbage island, by rebuilding in Qgis the affected area captured in drone videos. A subsequent correction, comparing several newspaper images, was carried out to find the real dimensions of the debris island.

Finally, an annual projection of this rate results in 2.37 x 10^4 ton/year, which approaches both the midpoint (1.67 x 10^4 ton/year) and upper mass inputs (2.95 x 10^4 ton/year) estimated by Lebreton et al., (2017) for the lower Magdalena.

Figure 1. Geographic location of the cleaning events.

Figure 2. Island of garbage in Puerto Colombia in June 2019.

3 CONCLUSIONS

The data reviewed confirm the incidence of plastic flow in the lower Magdalena river that significantly affects both the biota and the community welfare. Although preliminary, our results suggest that garbage patches volumes may be used as proxy information to estimate the plastic mass inputs. Likewise, underline the need for further research concerning eco-hydraulic impact of plastics.

ACKNOWLEDGEMENTS

We appreciate the cooperation and efforts of the IAHR Fundación Universidad del Norte YPN, as well as the mentoring of one of our advisors, Dr. Ronald R. Gutierrez. We also value the mentoring and improvement ideas suggested by MSc. Francisco J. Gómez.

REFERENCES

EL HERALDO. (2015). En Primer Día De Limpieza En Sabanilla, CRA Retira 25 Toneladas De Basura. https://www.elheraldo.co/local/en-primer-dia-de-limpieza-en-sabanilla-cra-retira-25-toneladas-de-basura-197764.

EL HERALDO. (2018). Jornada De Limpieza En El Río Magdalena: Recogen 3 Toneladas De Basura. https://www.elheraldo.co/barranquilla/jornada-de-limpieza-en-el-rio-magdalena-recogen-3-toneladas-de-basura-542380.

Elpais.com.co. (2019). Playas De Puerto Colombia, En Riesgo Por Toneladas De Basura. https://www.elpais.com.co/medio-ambiente/toneladas-de-basura-ponen-en-emergencia-a-playas-de-puerto-colombia.html.

Galvis, G., and Mojica, I. (2007). The Magdalena River fresh water fishes and fisheries. *Aquatic ecosystem health & management*, 10(2), 127-139.

Greenpeace Colombia. (2018). Greenpeace Anuncia Campaña Para Frenar El Avance Del Plástico En Colombia - *Greenpeace Colombia.* https://www.greenpeace.org/colombia/noticia/issues/contaminacion/greenpeace-anuncia-campana-para-frenar-el-avance-del-plastico-en-colombia/.

Lebreton, L. C., Van Der Zwet, J., Damsteeg, J. W., Slat, B., Andrady, A., and Reisser, J. (2017). River plastic emissions to the world's oceans. *Nature communications*, 8, 15611.

Plastics Europe. (2016). Plastics–the facts 2016: an analysis of European plastics production, demand and waste data. http://www.plasticseurope.org.

Tim, E., & Schwarz, A. (2020). Plastic debris in rivers. *WIREs Water, 7*, 24.

Vanguardia. (2019). Una 'isla' de basura amenaza las playas de Puerto Colombia. https://www.vanguardia.com/colombia/una-isla-de-basura-amenaza-las-playas-de-puerto-colombia-GF1025109.

Proceedings of the 1st IAHR
Young Professionals Congress
17-18 November

PHYTOREMEDIATION OF CONTAMINATED SOIL WITH HEAVY METALS APPLYING PLATEAU NATIVE SPECIES: *FUERTE SIMALVA ECHINATA* AND *LUPINUS BALLIANUS*

Jhoana Herrera [1], Claudia Medina [2]Alejandra Tancara [3]

[1,2,3]*Centro de Investigación en Agua, Energía y Sostenibilidad (CINAES), Universidad Católica Boliviana "San Pablo", La Paz - Bolivia.*
[1]jhoana64.herrera@gmail.com [2] claummontecinos@gmail.com [3]moraleta1698@gmail.com

ABSTRACT
Milluni Valley is located at the beginning of the Katari basin, Bolivia, where mining caused heavy metal pollution in soil and water bodies, including Milluni reservoir, which is partially destined for human consumption throughout two important cities. Moreover, this basin drains towards Titicaca Lake, polluting the highest lake in the world. Therefore, this research assesses the use of *Fuertesimalva Echinata* and *Lupinus Ballianus*, plateau native species, for the phytoremediation technique of the soil. Plants were kept in greenhouse conditions and planted in pots with different proportions of polluted soil from Milluni Valley and potting soil. We measured pH and conductivity, as parameters to assess the soil status, and microscopical observation of the leaves at the end of the study period. Results showed a maximum increment of 53,2% in pH and a maximum reduction of 61,14% in conductivity over time. *Fuertesimalva Echinata* demonstrated more resistance against toxicologic effects than *Lupinus Ballianus.*

Keywords: Phytoremediation, heavy metals, soil pollution, water management.

1 INTRODUCTION

Controlless intense mining activities were carried out along the Milluni Valley, Bolivia, causing unattended environmental passives due to the acid mine drainages (Salvarredy et al., 2008). Hence, Milluni Grande and Milluni Chico lagoons, which are partially destined for human consumption throughout La Paz and El Alto cities, were polluted with high concentrations of heavy metals (Campanini, 2019). These lagoons are significant sources of pollution in the Katari basin, which finally drains into Titicaca Lake, an important Bolivian plateau water resource. The exchange of heavy metals cations in the interface between the water and soil led to the impoverishment of the soil quality (Cunningham, 1997). Phytoremediation is a mitigation measure that could be applied in this context, because it bases on the partial or total remotion of contaminants from a medium, reducing its concentration and toxic effects (Pivetz, 2001). The aim of the study was to assess the employment of *Fuertesimalva Echinata (FE)* and *Lupinus Ballianus (LB)* as plateau native species in the soil phytoremediation technique for the Milluni Grande area.

2 MATERIALS AND METHODS

Simple samples were taken from the Milluni Grande area on October 25th of 2018, along the edge of the lagoon, where the soil has an orange characteristic color. We followed a zig-zag sequence in order to obtain a composed sample, which then was mixed with potting soil and distributed in six pots, according to the proportions: M1 (0,00%), M2 (58,33%), M3 (67,74%) and L1 (0,00%), L2 (28,57%), L3 (60,00%); where M1, M2, and M3 correspond to *FE,* and L1, L2, L3 to *LB.* We kept them in greenhouse conditions during the study period, from October 27th to November 27th of 2018, in order to maintain the soil temperatures in the range of 21ºC to 26ºC.

Control tests were carried out once a week, in which we measured the parameters of pH, temperature and conductivity from the soil of each pot. We considered pH as an indicator of the acid conditions of the soil, and conductivity to assess the presence of ions in the soil. We took samples of 75 g of soil, which were mixed with 150 ml of distilled water. A multimeter HANNA HI 9828 was used to take the data of pH and conductivity from the mix, and a Mercury Thermometer for the temperature. At the end of the study period, we extracted some leaves from *FE* (M2 and M3) to observe with the microscope the presence or absence of chloroplasts using methylene blue. Finally, percentage differences were used to analyse the evolution of soil status over time and Analysis of Variance was applied to study three sources of variability: the species of plants with six different concentrations, the time and random error, with an alpha value of 5%.

3 RESULTS

Analysis of Variance and percentages differences were performed for pH and conductivity. We detected statistical differences among the treatments and a pH increment and a conductivity reduction over time. Results are shown on Table 1. During the microscopic observation of the leaves' chloroplasts of each *FE*, we did not observe any sign of chlorosis effect. On the other hand, *LB* showed a periodic decay until the end of the study period, thus, the microscopic observation was not performed for this species.

Table1. Weekly data and percentage differences between W1 and W3**.**

TIME (WEEK)	TREATMENT (PH MEASUREMENTS)					
	L1	L2	L3	M1	M2	M3
W1	4,06	2,45	2,03	4,14	2,6	2,4
W2	5,06	3,22	3,03	6,26	3,43	2,6
W3	4,98	3,29	3,11	4,77	3,6	3,1
TOTAL INCREMENT (%)	22,66	34,29	53,20	15,22	38,46	29,17
TIME (WEEK)	**TREATMENT (CONDUCTIVITY MEASUREMENTS, µS/ cm^2)**					
	L1	L2	L3	M1	M2	M3
W1	1327,67	2507,67	3411,33	542,33	2025,33	2328,67
W2	1062,33	1547,33	1467,67	352	1419	1278
W3	1153,33	1240	1325,67	263	858,67	1197,67
TOTAL REDUCTION (%)	51,51	57,60	48,57	13,13	50,55	61,14

4 DISCUSSION

Results suggest that the absorption of metallic ions from the soil by the plant's roots may have occurred. We cannot ensure the process of translocation of these ions within the plant's system, since we did not perform an analysis of the stems. The absence of chlorosis in the *FE* leaves can be attributed to either one of two phenomena: 1) During the study period, the translocation of metals towards the upper parts of the plant did not occur. 2) The *FE* species is resistant to the accumulation of heavy metals. Although *FE* species demonstrated a slower remediation of the contaminated soil, it did not show any visual toxicologic effect. On the other hand, even though *LB* showed the greatest improvement of the soil status, its periodic decay of *LB* may be assumed as a toxicologic effect of the heavy metal ions on the plant, which turns the use of *LB* unsustainable over time.

5 CONCLUSIONS

- *FE* may be considered as a phytoremediator plant due to the absence of toxicologic effects during the study period.
- *LB* employment can be discarded for this remediation technique since its periodic decay could be understood as a toxicologic effect of the heavy metals on its system.
- The performance of this study in the environmental conditions of Milluni Valley would be necessary for a better assessment of the phytoremediation effectiveness.

ACKNOWLEDGEMENTS

This work was supported by the CINAES. We acknowledge Ana Gonzales for her technical knowledge of the subject.

REFERENCES

Campanini, O. (2019). *Desechos de Comsur aún contaminan la represa de Milluni*.
Cunningham, S. (1997). *Phytoremediation of Contaminated Water and Soil*.
Peña, J, Gómez, J, Montoya, H, Chanco, M, Mariano, M, Cano, N. (2014) *Phytoremediation capacity of five high andean species from soils contaminated with heavy metals*.
Pivetz, B (2001). *Phytoremediation of Contaminated Soil and Ground Water at Hazardous Waste Sites*.
Salvarredy, M. Probst, A. Roulet, M. Isaure, M.(2008) *Applied Geochemistry*: *Contamination of surface waters by mining wastes in the Milluni Valley (Cordillera Real, Bolivia): Mineralogical and hydrological influences*

Proceedings of the 1st IAHR
Young Professionals Congress
17-18 November 2020

Velocity profiles on a grass-lined spillway in supercritical flow

Hanwen Cui[*1,2], **Matthias Kramer**[1], **Stefan Felder**[2]

[1]UNSW Canberra, School of Engineering and Information Technology (SEIT), Canberra, ACT 2610, Australia
[2]Water Research Laboratory (WRL), School of Civil and Environmental Engineering, UNSW Sydney, NSW 2052, Australia

*Correspondance : hanwen.cui@adfa.edu.au

ABSTRACT

Grass-lined spillways represent an environmental friendly solution for flow conveyance in mildly-sloped water ways. The grass linings act as roughness elements that facilitate the stability of the soil and the safe conveyance of flows. Velocity profiles of grass-lined open channel flows have been extensively studied under subcritical flow conditions, whereas experiments in supercritical flows are limited. Herein, velocity profiles and flow resistance on a mildly sloped chute with artificial grass were experimentally investigated using a Prandtl Pitot tube. The velocity profiles exhibited the development of the boundary layer along the chute achieving uniform flow conditions towards the chute's end. The results revealed similarities of the velocity profiles to a previously proposed velocity decomposition and provided insights into point flow resistance.

Keywords: Boundary layer; Eco-friendly hydraulic structures; Flow resistance; High-velocity flows

1 INTRODUCTION AND METHODOLOGY

The velocity profile of a channel equipped with Kikuyu grass was first studied by Eastgate (1966), indicating that the velocity distribution in subcritical flow follows the logarithmic profile. Recent development considered the separation of soil and grass and revealed substantially more complex distributions (Nepf et Vivoni, 2000; Nikora *et al.*, 2004; Nepf, 2012; Nikora *et al.*, 2013), comprising the following regions: (i) uniform velocity distribution layer with almost constant velocity, (ii) mixing layer with appearance of an inflection point, (iii) logarithmic layer that follows the logarithmic growth of the velocity, and (iv) wake region. These four regions are characterized by the velocities U_{UD}, U_{ML}, U_{LL} and U_{WF}, where the near bed boundary layer has been omitted.

Historic developments and mentioned contemporary velocity models were established in subcritical flow, which may be different from high-velocity flows characterized by free-surface roughness and air entrainment. Given the common occurrence of supercritical flows over grass-lined conveyance and embankment protection structures, detailed investigations of velocity and shear stresses are essential and results are presented herein.

New experiments with flow rates ranging from Q = 25 l/s to 250 l/s were conducted at the UNSW Water Research Laboratory (WRL), which corresponds to the Froude numbers of $F_r = U/\sqrt{gH}$ = 1.46 to 3.42 in the uniform region, where U is the mean velocity, H is the water depth and g is the gravitational acceleration. A 0.8 m wide, 8 m long flume was inclined at θ = 10.8° and the flume's bed was equipped with artificial grass elements, generating self-aerated flows (Fig. 1a).

The measured supercritical velocity profiles (Pitot tube) were fitted to a semi-analytical model of Nikora *et al.* (2013), who proposed to decompose the time-averaged velocity U as follows:

$$U = \underbrace{\left(\frac{2gS_0}{C_D a}\right)^{0.5}}_{U_{UD}} + \underbrace{(U_i - U_{UD})\left(1 + \tanh\left(\frac{y - y_i}{L_e}\right)\right)}_{U_{ML}} + \underbrace{u_{*m}\frac{1}{\kappa}\ln\left(\frac{y-d}{z_0}\right)}_{U_{LL}} + \underbrace{\frac{2\Pi}{\kappa}\sin^2\left(\frac{\pi y}{2H}\right)}_{U_{WF}} \quad (1)$$

where S_0 is the bed slope, C_D the drag coefficient, a the frontal vegetation area per unit volume, U_i the velocity at the inflection point, y the vertical coordinate, y_i the elevation of the inflection point, L_e the mixing length scale,

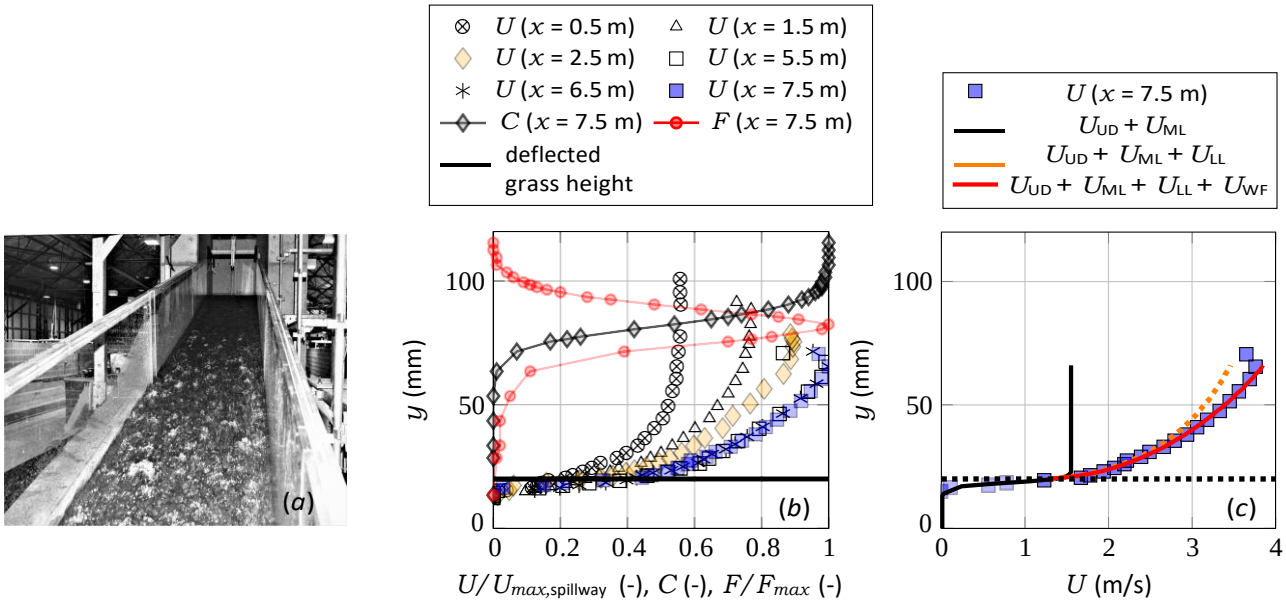

Figure 1: Experimental setup and and preliminary results (a) Grassed spillway with self-aerated flows at 125 l/s;(b) Velocity profiles along the channel at Q = 150 l/s; (c) Velocity profile fitting example at x = 7.5 m for Q = 150 l/s;

u_{*m} the shear velocity at the canopy top, d the hydraulic roughness length scale, z_0 the zero-plane displacement, κ the Von-Karman constant and Π the wake strength parameter.

2 RESULTS

Volumetric air concentrations (C) and particle count rates (F) were measured with a phase-detection probe, indicating self-aeration in the upper flow region (Figs. 1a,b). Mean velocity profiles (Pitot tube) are shown for Q = 150 l/s at different measurement points along the flume (Fig. 1b), revealing the boundary layer development along the chute as well as the presence of uniform flow conditions towards the chute's end. The velocity profiles resembled the four regions with distinct shapes in the mixing layer and logarithmic layer (Fig. 1c), while the uniform flow layer appeared to have zero contribution to the velocity structure. The inflection point between the mixing layer and logarithmic layer could clearly be identified, enabling the fitting of the velocity profiles to Eq. (1). The comparison of the measured velocity profile with Nikora *et al.* (2013)'s model, as Fig. 1c suggests, clearly demonstrated similarities between subcritial and supercritical flow, allowing to evaluate the shear stress at the canopy top of the grass elements u_{*m} and Coles' wake strenght parameter Π.

3 CONCLUSION

The velocity profiles of a grass-lined spillway were systematically investigated under high-velocity supercritical flow conditions. With the current configuration, the intermittent level of self-aeration did not exert significant influence on the structure of the velocity profile, which was demonstrated through comparison with a model developed for subcritical flows. Through data fitting, the velocity profiles were used to estimate the indicative shear stress at the canopy top u_{*m}, which allowed for a decomposition of the flow resistance. These findings aim to provide a better understanding of flow resistance of supercritical flows on grass-lined spillways.

References

Eastgate W. I. (1966). *Vegetated stabilisation of grassed waterways and dam bywashes*. Thèse de doctorat, University of Queensland.

Nepf H., Vivoni E. (2000). Flow structure in depth-limited, vegetated flow. *Journal of Geophysical Research Atmospheres 105*(28), 547–558.

Nepf H. M. (2012). Flow and Transport in Regions with Aquatic Vegetation. *Annual Review of Fluid Mechanics 44*(1), 123–142. doi:10.1146/annurev-fluid-120710-101048.

Nikora N., Nikora V., O'Donoghue T. (2013). Velocity Profiles in Vegetated Open-Channel Flows: Combined Effects of Multiple Mechanisms. *Journal of Hydraulic Engineering 139*(10), 1021–1032.

Nikora V., Koll K., McEwan I., McLean S., Dittrich A. (2004). Velocity distribution in the roughness layer of rough-bed flows. *Journal of Hydraulic Engineering 130*(10), 1036–1042.

Proceedings of the 1st IAHR
Young Professionals Congress
17-18 November 2020

ATTRACTING SILVER PERCH INTO A TUBE FISHWAY: PRELIMINARY RESULTS

Maryam Farzadkhoo[1*], Stefan Felder[1], Iain M Suthers[2], William L Peirson[1], Richard T Kingsford[2] & John H Harris[2]

[1] Water Research Laboratory, School of Civil and Environmental Engineering, UNSW Sydney, Australia
*e-mail: maryam.farzadkhho@unsw.edu.au
[2] Centre for Ecosystem Science, School of Biological, Earth and Environmental Sciences, UNSW Sydney, Australia

ABSTRACT

Fishways are common approaches to restore habitat fragmentations. A novel fishway design, the UNSW tube fishway, has been developed recently. A detailed understanding of methods for fish attraction into a tube is essential for the operation of the tube fishway. Herein, systematic fish attraction experiments were conducted to find suitable fish attraction conditions for silver perch (Bidyanus bidyanus), an Australian native fish species. Groups of five naïve silver perch were attracted into the tube irrespective of the attraction flow velocities, with the highest entry rate for velocities of 0.15 to 0.4 m/s. Streamlining of the entry geometry increased the entry rate and reduced the first entry time. The preliminary results show that hatchery-bred juvenile silver perch can be attracted reliably into a closed conduit, paving the way for field deployment of the UNSW tube fishway.

Keywords: attraction velocity, fishway entrance, fish attraction, silver perch, tube fishway.

1 INTRODUCTION

Many natural and anthropogenic barriers fragment habitat for freshwater organisms. Fishways are the most viable solution to facilitate fish migration (Katopodis et al., 2001). However, long-term observations over 50 years of fish passage indicated that numbers of silver perch, an Australian native fish species, declined by up to 95–100% (Mallen-Cooper et al., 2007). While fish entrances are of utmost importance for fishway effectiveness, knowledge of their design requirements is incomplete (Wilkes, et al., 2018). There is a need to better understand fish attraction mechanisms, reflecting fish behavior and preference. A new type of fishway, the UNSW tube fishway, was recently introduced (Harris et al., 2020). A key process is the volitional attraction of fish into the tube fishway before hydraulically lifting fish across a barrier. To facilitate successful field deployment of the tube fishway it is important to understand and optimize the attraction of fish into a tube. Our study had the objectives: (1) to assess the possibility of attracting fish into a tube with a slotted entrance and (2) to identify the most favorable flow velocity at the slotted entrance for fish attraction into the tube.

2 METHODOLOGY

A fish attraction facility was established in an open channel flume of 6 m length, 0.6 m width and 0.6 m height at the UNSW Water Research Laboratory. At one end of this flume, the attraction tube is placed, consisting of a slot of 0.03 m width across the full height of the tube of 0.4 m diameter and 0.7 m length (Fig.1). Outflows from the pipe into the observation zone via the slotted entrance provided the attraction flows. A skylight above the tube maintained ambient light for attracted fish (Harris et al., 2020). At the start of each experiment, groups of 5 naïve silver perch (mean total length TL = 70 mm ± 1.58 SE) were placed in the observation zone. Three GoPro cameras were installed at the top and side of the observation zone to monitor any fish movements and fish entry into the tube via the slotted entrance.

Five attraction flow velocities at the slotted entrance between 0 and 0.5 m/s were tested. An additional configuration with a more streamlined entrance was also tested by blocking the corners next to the slotted entrance with angled plates (not shown). For all flow conditions, the water depth at the slotted entrance was kept at 80% of the tube diameter. Downstream of the observation zone, water exited the test section via a weir (Fig. 1). Based upon pilot tests, the fish were acclimated in the observation zone for one hour without attraction flow and with the entrance slot blocked. After acclimation, the entrance slot was opened, and the attraction flow established. Fish entry was then monitored for one hour. All captured videos were manually analyzed, providing information about the number of fish that entered the tube as well as details of the time of first entry, the

maximum number of fish inside the tube at any given time and the duration that fish stayed in the tube. Fish entry patterns was observed to better understand fish behavior, including entry height and entry patterns.

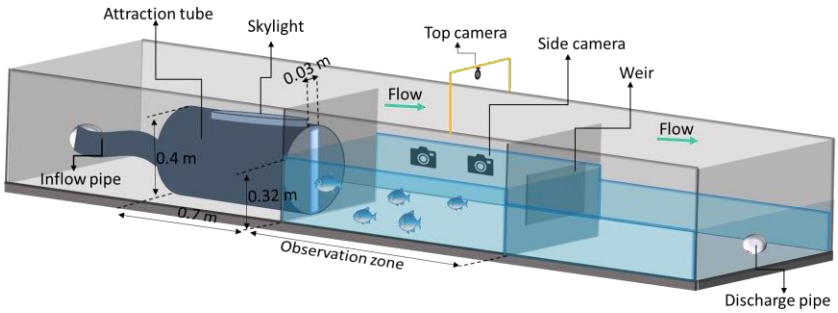

Figure 1- 3-D schematic view of the setup of the attraction experiments; flow direction from left to right through the slotted entrance of the tube,

3 RESULTS AND DISCUSSION

Figure 2 illustrates the accumulative number of fish inside the tube over the duration of the experiment for three attraction flow velocities of 0.15, 0.4, and 0.5 m/s. The results indicate that groups of five naïve silver perch were attracted to the entrance for all flow conditions, with strongest fish attraction for velocities of 0.15 m/s. Groups of 5 silver perch tended to stay in the tube for longer duration at a lower discharge (0.15 m/s). These findings emphasize the importance of providing low attraction flow velocity to stimulate silver perch of this size range to enter and stay in the attraction tube. Streamlining of the entry geometry increased the entry rate and reduced the time taken for fish to enter the tube for the first time by up to 28%.

These preliminary experiments demonstrated favorable conditions for attracting naïve silver perch into a tube, paving the way for prototype deployment of the tube fishway. The attraction flow research is ongoing involving repeated experiments with naïve silver perch using different tube sizes to test the scalability of the tube fishway.

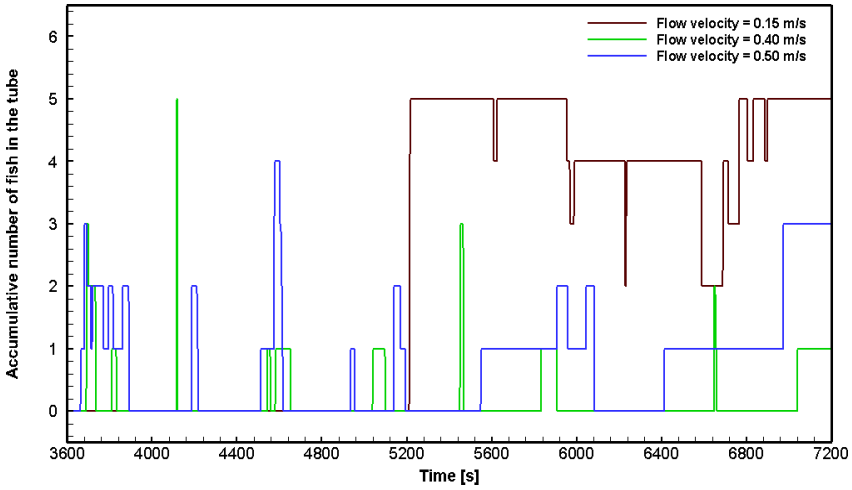

Figure 2. Accumulative number of fish in the tube for attraction velocities of 0.15, 0.4 and 0.5 m/s

REFERENCES

Harris, J.H., Peirson, W.L., Mefford, B., Kingsford, R.T., and Felder, S. (2020). Laboratory testing of an innovative tube fishway concept. *J. Ecohydraulics*, 5(1), 84-93.

Katopodis, C., Kells, J.A., and Acharya, M. (2001). Nature-like and conventional fishways: alternative concepts?. *Can. Water Resour. J.*, 26(2), 211-232.

Mallen-Cooper, M., and Brand, D.A. (2007). Non-salmonids in a salmonid fishway: what do 50 years of data tell us about past and future fish passage? *Fish. Manag. Ecol*, 14(5), 319-332.

Wilkes, M.A., Mckenzie, M., and Webb, J.A. (2018). Fish passage design for sustainable hydropower in the temperate Southern Hemisphere: an evidence review. *Rev. Fish Biol. Fish*, 28(1), 117-135.

Proceedings of the 1st IAHR
Young Professionals Congress
17-18 November 2020

HYDRO-ENVIRONMENT

Ana Karolina Valencia

Universidad Tecnológica de Panama, Panama City, Panama
Valekarol13@gmail.com

ABSTRACT

Hydro-environment is composed by two words hydro and environment. the concept of hydro-environment was first introduced at the IAHR World Congress at Vancouver in 2009. but is currently used in the scientific community because it involves the new trends of hydrology and environmental themes which nowadays most important is pollution.

Keywords: hydro-environment, hydrology, environment, eco-hydraulics, hydraulics.

1 INTRODUCTION

Defining both words, starting with “hydro” from the Greek which means “Water”; and environment as the elements, factors, conditions or influences in the surroundings. However, nowadays when must people talk or refer to Environment, immediately they focus on trees, rivers, mountains, etc. Therefore, today, they forget what these landforms are made of, climate, and their physical and chemical features.
There are different sciences and subjects that have been studying the water bodies for many years. Mainly to mention is the Hydrology.
Hydrology is the science that studies the water’s properties on the Earth’s surface and below it, including all the physical and chemicals processes and components, also all factors, cycles and changes of matter in the water. All other sciences and auxiliary sciences have their basics principles in Hydrology such as the hydrodynamics, oceanography, hydrography, limnology, etc.

2 HYDRO-ENVIRONMENT, ANA KAROLINA VALENCIA.

3 WHAT IS HYDRO-ENVIRONMENT?

Based on the interview with Mr. Joseph Hun-Wei posted on the IAHR News Portal, president of the IAHR, the concept of hydro-environment was first introduced at the IAHR World Congress at Vancouver in 2009. This word is not officially recognized either in Merriam-Webster Dictionary nor Oxford English Dictionary but is currently used in the scientific community because it involves the new trends of hydrology themes.

The most common topics today are environmental problems and based on the approach mentioned in the first paragraph hydro-environment responds to today’s issues.

Hydrodynamic studies the movement of the fluids in all known spaces. As we are in a living world all matter is constantly in change and motion, that is why the water or fluids arise. Based on that statement is why hydrodynamic is very relevant to environmental studies.

Both sciences hydrodynamics and hydrology are very helpful in our modern times because they allow us to know the behavior of the water in our environment. This is reflected in this interesting article written by R. J. W. Nooij et al entitled “*The Importance of Hydrodynamics for Protected and Endangered Biodiversity of*

Lowland Rivers", in which the importance of hydrodynamics along rivers and ecosystems is mentioned in various taxonomic groups.

Knowing all different uses of water, it is almost impossible not to have damages and consequences that cause a lot of pollution to the water bodies and other side effects such as contaminant transport and interaction. This is one of the major ways of damaging of contamination, for instance when someone throws a plastic wrap on the street, suddenly it rains and this tiny piece of plastic gets into the drain and so to the channel, then to the river, and finally to the sea: A simple way of contaminant transport. Therefore, unchain some other effects in soil and ground water, all this because of water flow.

It is good to highlight the importance of following modern trends on the care of the environment, and in this specific case of the hydro-environment. This trend leads us to develop new sciences or new modalities of the existing ones, for example eco-hydrology and eco-hydraulics, which help us to create new ways of sustainable uses of our water bodies according to environmental policies and international regulations.

CONCLUSIONS

We should learn from the existing worldwide situation of pandemic to get more involved, encouraged, and supported researches and studies in order to anticipate problems that will affect more our environment and thus be better prepared to solve them. So does famous people from scientific community as Bill Gates who wrote on his blog a post in which he mentions one of his recent books "My plan to avoid a climate disaster". Like the tittle, it mentions a variety of ideas to treat some environmental problems that we actually have and some we may have in the future if we do not pay the proper attention in the way we take care of our environment.

REFERENCES

R. J. W. Nooij et al (2016). *The Importance of Hydrodynamics for Protected and Endangered Biodiversity of Lowland Rivers*. 6500 GL Nijmegen, The Netherland

Bill Gates(2020) . The Blog Of Bill Gate-www.gatesnotes.com*, A plan for climate Change.*

IAHR Talks (2019). IAHR News Portal*. Interview with Joseph Hun-Wei Lee*. A vision for IAHR.

UNESCO (2004). *Ecohydrology Guidelines Book.*

Proceedings of the 1st IAHR
Young Professionals Congress
17-18 November 2020

LEAST DISTURBED RIVERS IN THE ALTAI MOUNTAINS CAN REVEAL ENVIRONMENTAL GUIDING PRINCIPLES FOR ALPINE RIVERS: A CASE STUDY FROM THE BIYA RIVER

Lisa Schmalfuß*[1], Martin Schletterer [2] & Christoph Hauer [1]

[1] Institute of Hydraulic Engineering and River Research, University of Natural Resources and Applied Life Sciences, Vienna, Austria
[2] Institute of Hydrobiology and Aquatic Ecosystem Management, University of Natural Resources and Applied Life Sciences, Vienna, Austria,

*Correspondence: lisa@schmalfuss.at

ABSTRACT

Anthropogenic stressors have altered the hydromorphological characteristics of many rivers worldwide, including those in the European Alps. Environmental guiding principles are essential for the planning of sustainable river restoration measures. The goal of this study is to elaborate such guidelines and to support process understanding. The alpine river Biya, located in the Russian Altai mountains, represents a least disturbed hydromorphological reference system. The present work aims to analyze planform hydromorphological patterns for selected reaches along the Biya based on topographic maps and satellite data. These parameters will be set in relation with changes in slope and interactions with the surrounding floodplain area. The obtained characteristics will be discussed alongside historical topography maps of selected segments of comparable alpine rivers in Europe in order to demonstrate that the dataset from the Biya can be used as an assisting tool in the planning process of restoration measures in the European Alps.

Keywords: hydromorphology, sinuosity, reference conditions, alpine rivers.

1 INTRODUCTION

Throughout the history of human societies, the exploitation of natural resources has been a basis for increasing wealth and rising standards of living. River systems have undergone a particularly strong process of degradation, resulting from river straightening and other regulation measures. Over the past decades, there has been growing demand to reorganize anthropogenic use of watercourses and the surrounding floodplains, in order to improve ecological functionality (Muhar, 2000; Muhar, 1996). Efficient river restoration approaches are needed to meet both ecological goals and legal requirements like the EU Water Framework Directive (WFD, 2000/60/EC). For this purpose, it is vital to have a predefined restoration goal in mind. This is usually expressed by a so-called reference condition, which represents the state a river would have without anthropogenic disturbances. Due to the lack of rivers that have remained free from anthropogenic impacts in the Alps (Comiti, 2012), reference sites must be found elsewhere. This approach follows the premise, that reference sites at currently undisturbed rivers are preferable to historically reconstructed reference conditions (Wyżga et al., 2012). A river basin (including its 'reference situation') should not be understood as something static: A wide range of influencing factors makes changes over time unavoidable (Newson and Large, 2006). The goal is not to recreate a past situation, but to reach a self-sustaining status under the given circumstances, instead of recreating a past situation that may no longer be supported by current environmental conditions. This ideally requires little management interventions while retaining a desirable status. The mountain river Biya, located in the Russian Altai region, is regarded as one such undisturbed example. It has been researched regarding hydrological properties (Chalov and Ermakova, 2011) as well as its geological origins (Baryshnikov et al., 2016). Together with the Katun (Seidl, 2020), the Biya is one of the two headstreams of the river Ob. It shares its history of past glaciation with European alpine rivers (Baryshnikov et al., 2016), which suggests a certain degree of comparability.

The underlying hypothesis of this first part of the study is, that the river Biya is (over a wide range) free from anthropogenic disturbances and exhibits a natural succession of hydromorphological patterns. This leads to the

assumption that the hydromorphological characteristics observed at selected sub-stretches of the Biya can be used to describe reference sites. It is further assumed that the hydromorphological characteristics of the Biya are comparable to those found at alpine rivers in Europe with similar topographic conditions. This makes the reference sites described at the Biya applicable for river restoration planning in the Alpine region.

2 METHODS

The 301 km of the river Biya will be divided into morphological sub-stretches, which will be the basis for this hydromorphological study. The required data will consist mainly of satellite imagery and topographic maps, which will be processed using Geographic Information Systems (GIS software). Sinuosity will be assessed based on the definitions provided by Mueller (1968). Channel width will be determined for cross sections along the river. Additionally, the longitudinal gradient of grain size distributions is assessed based on the random Wolman (1954) pebble count method using data from sampling sites on the riverbanks between the river's source and its confluence with the Katun. The aim is to make qualitative statements about the changes along the river. Research suggests that channel sinuosity is tightly linked to variations in channel width (Ferrer-Bolx et al., 2016; Luchi et al., 2010). There is also a close connection between topographic parameters, especially slope and channel geometry (Belmont, 2011; Pitlick and Cress, 2002). For these reasons, channel planform parameters will be related to changes in slope along the river course. A catalogue of hydromorphological characteristics will be established for the Biya. This systematic compilation of hydromorphological parameters will ideally serve as ecological guiding principle for river restauration planning in the European Alps.

3 OUTLOOK

The initial focus of the study lies on establishing a descriptive inventory of morphological parameters along the Biya. This represents the starting point of a longer analysis that will go more into detail:

- Interactions between the main channel and the surrounding floodplains are of integral ecological importance and will consequently be modeled by applying a 1-D model (HEC-RAS).
- The proposed study will eventually provide an example of the application of the proposed guiding principles for an anthropogenically impacted Alpine river in Europe.

REFERENCES

Baryshnikov, G., Panin, A. and Adamiec, G. (2016). Geochronology of the late Pleistocene catastrophic Biya debris flow and the Lake Teletskoye formation, Altai Region, Southern Siberia. *International Geology Review*, 58(14), 1780-1794.

Belmont, P. (2011). Floodplain Width Adjustments in Response to Rapid Base Level Fall and Knickpoint Migration. *Geomorphology*, 128, 92-102.

Chalov, S. and Ermakova, G. (2011). Fluvial response to climate change: a case study of northern Russian rivers. Cold Region Hydrology in a Changing Climate. *IAHS*, 346, 111-119.

Comiti, F. (2012). How Natural are Alpine Mountain Rivers? Evidence from the Italian Alps. *Earth Surface Processes and Landforms*, 37, 693-707.

Ferrer-Bolx, C., Chartrand, S.M., Hassan, M.A., Martín-Vide, J.P., and Parker, G (2016). On how Spatial Variations of Channel Width Influence River Profile Curvature. *Geophysical Research Letters*, 43, 6313-6323.

Luchi, R., Hooke, J.M., Zolezzi, G., and Bertoldi, W. (2010). Width Variations and Mid-Channel Bar Inception in Meanders: River Bollin (UK). *Geomorphology*, 119, 1-8.

Mueller, J. E. (1968). An Introduction to the Hydraulic and Topographic Sinuosity Indexes. *Annals of the Association of American Geographers*, 58(2), 371-385.

Muhar, S., S. Schwarz, S. Schmutz and M. Jungwirth (2000). Assessing rivers with high habitat integrity: methodological approach and applications. *Hydrobiologia* 422/423, 343-358.

Muhar, S. (1996). Bewertung der ökologischen Funktionsfähigkeit von Fließgewässern auf Basis typspezifischer Abiotik und Biotik. Wasserwirtschaft, 86 (5), 238-241.

Newson, M.D. and Large, A.R.G. (2006). 'Natural' Rivers, 'Hydromorphological Quality' and River Restoration: A Challenging New Agenda for Applied Fluvial Geomorphology. *Earth Surface Processes and Landforms*, 31, 1606-1624.

Pitlick, J. and Cress, R. (2002). Downstream Changes in the Channel Geometry of a large Gravel Bed River. *Water Resources Research*, 38(10), 34-1-34-11.

Seidl, F. (2020). Untersuchungen zur Hydromorphologie großer Gletscherflüsse. Master Thesis. Technische Universität, München.

Wolman, M.G. (1954). A Method of Sampling Coarse River-Bed Material. *Transactions, American Geophysical Union*, 35(6), 951-956.

Wyżga, B., Zawiejska, J., Radecki-Pawlik, A., and Hajdukiewicz, H. (2012). Environmental Change, Hydromorphological Reference Conditions and the Restoration of Polish Carpathian Rivers. *Earth Surface Processes and Landforms*, 37, 1213-1226.

IAHR AIRH

International Association for Hydro-Environment Engineering and Research

Hosted by
Spain Water and IWHR, China

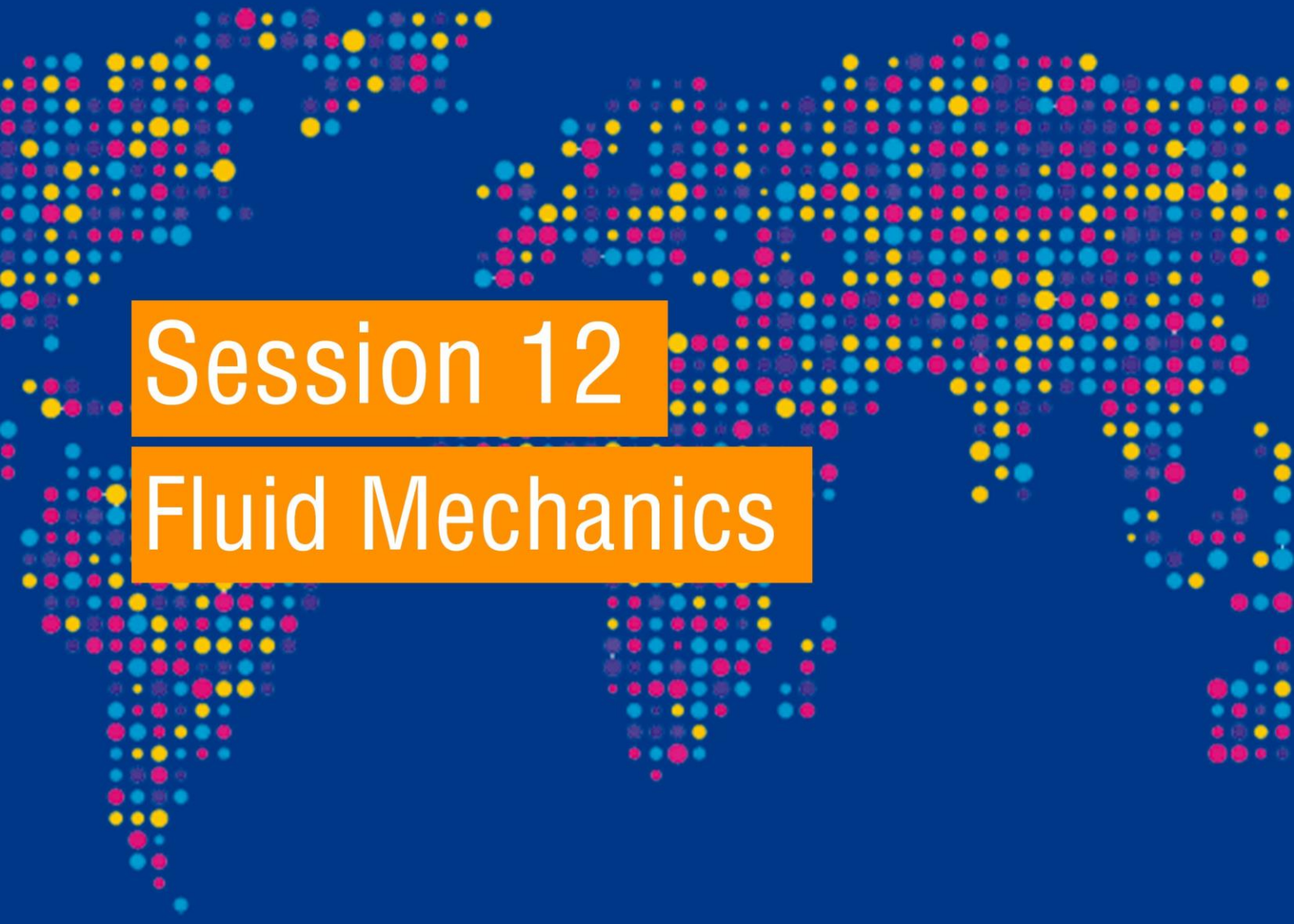

Session 12
Fluid Mechanics

IAHR YPN

Hosted by
Spain Water and IWHR, China

Proceedings of the 1st IAHR
Young Professionals Congress
17-18 November 2020

Concepts for performance improvements of shallow water flow simulations

Lennart Steffen[*1], **Finn Amann**[1], **Reinhard Hinkelmann**[1]

[1]Technische Universität Berlin, Chair of Water Resource Management and Modeling of Hydrosystems, Berlin, Germany

*Correspondance : lennart.steffen@wahyd.tu-berlin.de

ABSTRACT

Flow simulations with the depth-averaged shallow water equations are applicable to many naturally occurring surface water flows, such as open channel flow or floods. Improving the performance of simulation software enables a higher resolution, larger computational domain or more runs with different parameters within the same time frame, or less time required to obtain results and lower energy consumption for the same simulation. To explore avenues for performance improvements of shallow water flow simulations, an open-source C++ framework for explicit finite-volume-method solvers was designed and a robust shallow water equations solver based on a previous in-house development was implemented. First results show the expectable performance improvements from vectorisation of cell-based calculations, and preliminary tests show measurable speedups from reordering edge flux computations to reduce cache misses and locks between threads. Furthermore, a simple load rebalancing scheme for distributed computations is introduced and two load criteria are compared.

Keywords: shallow water equations, finite volume method, high performance computing.

1 INTRODUCTION

The depth-averaged shallow water equations (SWE) are a simplification of the Navier-Stokes equations and are applicable to a wide range of surface water flows, such as open channel flow and floods. Numerical SWE solvers are an important tool for modelling such flows. Improving the performance of such solvers allows for higher resolutions, longer simulated time frames, larger computational domains or more runs with different test parameters for the same computational cost, or shorter computation times and energy costs for the same simulation. Especially in time-critical applications, such as when the decision making process for a flood event requires modelling of different scenarios, time savings can be greatly beneficial.

At the Chair of Water Resource Management and Modeling of Hydrosystems at TU Berlin, a robust solver for the SWEs has been developed since 2005, as part of a Java framework called the *Hydroinformatics Modeling System* (*hms*) (Simons *et al.*, 2013).

To make full use of high-performance compute libraries as well as distributed computing with MPI, a new C++ framework named *hms++* is being created. It provides an expressive interface to create explicit solvers for the finite volume method (FVM) on arbitrary meshes, but with a focus on structured ones (both rectangular and non-rectangular). The well-tested SWE solver from *hms* has been reimplemented in this new framework, to investigate two main approaches for performance improvements:

Firstly, the code implementing the solver logic is restructured to improve general metrics such as cache utilisation, vectorisation, branch prediction and parallelism (specifically wait times for locks or atomic operations). Results obtained here are likely applicable to any (explicit) FVM solver. Secondly, SWE simulations with both wet and dry regions can cause load imbalances between threads and/or nodes, because some calculations can be skipped for dry cells. Therefore, to maximise utilisation, dynamic intra- and inter-node load balancing is another key area of investigation.

2 GENERAL PERFORMANCE IMPROVEMENTS FOR FVM SOLVER FRAMEWORK

By using existing and mature linear algebra libraries, non-interdependent computations on contiguous data can be optimised with relative ease. The library used here, called *eigen*, provides expression templates for both matrix and coefficient-wise array operations, which are internally resolved to vectorisable loops. For calculations that only require single-cell-based data, using such expressions typically results in significant speedups over per-cell function calls. This was observed in the calculations of the maximum stable time step, source terms and new state variables. After a rewrite of these steps to allow vectorisation, they take up only 10–15 % of the computation time per time step, as opposed to about 50 % before. Overall computation time was roughly halved.

However, the flux calculation of FVM solvers requires data of at least two cells per flux over one edge, and can therefore not easily be expressed as a set of matrix or array operations. Given that this step now takes up 85–90 % of the computation time, it is the focus of further optimisation efforts.

For structured meshes, including non-rectangular ones, the concept is, to investigate different orders in which edges are traversed and the corresponding fluxes are calculated. These traversal methods define the order in which cell-based data is accessed. This can be used to improve data locality and thus cache usage, as well as minimising wait times for parallel write access to shared memory. Preliminary investigations indicate that removing atomic write accesses may reduce flux calculation times by around 20 %, while traversing edges in blocks can reduce flux calculations by another 10 %, likely due to higher retention of relevant data in the cache. However, results are still subject to change, as the relevant code sections are still being worked on.

3 DRY CELL EXPLOITATION AND DYNAMIC LOAD BALANCING

Ginting et Mundani (2019) found dry cells to require only about half the computational effort of wet cells in SWE simulations. However, depending on both implementation and the simulated case, dry cells may not lead to less computation time overall: While they reduce the load of the corresponding thread, this may simply lead to higher idle times. Therefore, static and dynamic thread scheduling are compared and wet/dry aware thread spawning methods (i.e. skipping large dry regions altogether) are explored.

For distributed memory computations, dynamic load balancing requires mesh and data redistribution. Here, a simple and fast two-stage scheme for rebalancing structured meshes is introduced, which is portrayed in Fig. 1. Furthermore, two criteria for load imbalance are compared: average processor load per node is used as an aggregate criterion, while wet/dry flags per cell are used as a more highly resolved criterion. First results indicate that rebalancing quality, measured by the sum of load deficits over all nodes, is similar between both criteria, while the computational cost of the aggregate criterion is much lower. Nevertheless, these results are still preliminary and are only meant as a proof of concept.

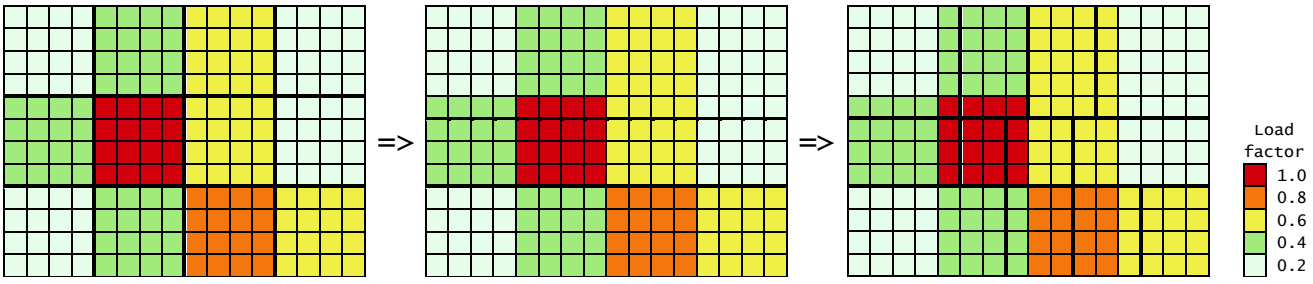

Figure 1: Two-stage scheme for rebalancing structured meshes. First, the mesh is divided into bands with similar loads, then these bands are divided again to form partitions with similar loads.

References

Ginting B. M., Mundani R.-P. (2019, 5). Parallel flood simulations for wet–dry problems using dynamic load balancing concept. *Journal of Computing in Civil Engineering 33*(3), 04019013. doi:10.1061/(asce)cp.1943-5487.0000823.

Simons F., Busse T., Hou J., Özgen I., Hinkelmann R. (2013). A model for overland flow and associated processes within the hydroinformatics modelling system. *Journal of Hydroinformatics*, 375–391. URL: https://iwaponline.com/jh/article/16/2/375/3479/ A-model-for-overland-flow-and-associated-processes, doi:https://doi.org/10.2166/hydro.2013.173.

Proceedings of the 1st IAHR
Young Professionals Congress
17-18 November 2020

BOTTOM GRAVITY CURRENTS AND STRATIFIED EXCHANGE FLOWS IN A ROTATING CHANNEL

Maria Chiara De Falco[1], Claudia Adduce [2], Alan Cuthbertson [3], Maria Eletta Negretti [4], Janek Laanearu [5], Daniela Malcangio [6], Katrin Kaur [7] & Joel Sommeria [8]

[1,2] Roma Tre University, Italy,
e-mail: mariachiara.defalco@uniroma3.it, claudia.adduce@uniroma3.it

[3] University of Dundee, UK,
e-mail: a.j.s.cuthbertson@dundee.ac.uk

[4,8] Laboratory of Geophysical and Industrial Flows, France,
e-mail: eletta.negretti@legi.cnrs.fr, Joel.sommeria@legi.cnrs.fr

[5,7] Institution Tallinn University of Technology, Estonia,
e-mail: janek.laanearu@taltech.ee, katrin.kaur@taltech.ee

[6] Polytechnic University of Bari, Italy,
e-mail: daniela.malcangio@poliba.it

ABSTRACT

Large-scale laboratory experiments on bottom gravity currents and stratified exchange flows have been conducted at the CNRS Coriolis Rotating Platform at LEGI. Both rotating and non-rotating experiments were performed in a trapezoidal cross section channel and different configurations were considered by varying both the upper fresh water volume fluxes and the channel rotation rates. Detailed velocity fields were measured by 2D Particle Image Velocimetry in different vertical planes spanning the width of the channel. Results highlight the role that both ambient rotation and net-barotropic forcing have on the geostrophic adjustment of the dense outflowing. As the rotation rate increases, the tilt of the interface between lower salty and upper fresh water flow increases, generating a meandering pattern within the salty layer along the trapezoidal channel.

Keywords: Geophysical Flows, Rotation, Stratified flow.

1 INTRODUCTION

Bottom gravity currents and stratified exchange flows develop in submerged channels, such as sea straits and estuaries, when two water masses with horizontal density differences (i.e. baroclinic forcing) or pressure gradient (i.e. barotropic forcing), meet. Earth rotation can affect the flow dynamics by introducing a geostrophic adjustment of the internal fluid flow, with resulting cross channel variations in velocity and density profiles, and by inducing secondary flows (Cossu et al., 2010; Cuthbertson et al., 2011). Additionally, the nature of these buoyancy-driven flows depends on strong topographic controls imposed by seafloor bathymetry and channel shape, playing a significant role in flow dynamics (Laanearu et al., 2014; De Falco et al., 2020). In the present study, the behavior of bottom gravity currents and stratified exchange flows along a trapezoidal-shaped channel is investigated to determine the relative influence of the net-barotropic forcing and Coriolis forces on the lateral distribution of the (counter-) flowing water masses. The experimental apparatus and the exchange flow dynamics at the interface, with particular focus on the observed lateral variations in cross-channel dense interface are discussed.

2 EXPERIMENTAL APPARATUS

The experiments were conducted in the CNRS Coriolis Rotating Platform a 13 m in diameter and 1.2 m deep circular tank with a rotation period that can be rotated in a anti-clockwise or clockwise direction at a constant angular velocity Ω to simulate the Coriolis forces experienced in the Northern and Southern hemispheres. The rotation of the Coriolis Platform was varied with four angular velocities Ω tested (i.e. Ω= 0,0.05,0.1,0.2 rad·s^{-1}). Bottom gravity currents and stratified exchange flows of a saline solution and fresh water were reproduced in a trapezoidal cross section channel, 6.5 m long placed in the center of the platform (Figure 1a). The channel had a 2.0 m top and 1.0 m bottom width and a total depth of 0.5 m with side slopes of α_s=45°. Two slopes with α_b=26.57° connected the channel to the inlet saline water basin (B), and the outlet fresh water basin (A). The circular tank was filled with fresh water at initial density ρ_F in order to have in the channel the submergence

depth H_{ch}=0.4 m. A constant saline water discharge Q_2=4.4 l/s at density ρ_S, was then fed into basin B to establish a stable, bottom gravity current along the trapezoidal channel. Two water pumps in the upper part of Basin B were employed to provide a constant fresh water flux Q_1, which was increased over a range of values (Q_1=0, 8, 20 l·s^{-1}, i.e. q*= Q_1/Q_2=0, 1.8, 4.5), to generate a stratified exchange flow. Two-dimensional Particle Image Velocimetry (PIV) was used to obtain high temporal and spatial resolution velocity fields across the channel, within a central 1 m-long section of the channel (Figure 1a). In particular, the velocity fields were acquired in 11 vertical sections (XZ) at lateral positions ranging between -79.2 cm < y < 20.8 cm (Figure 1b).

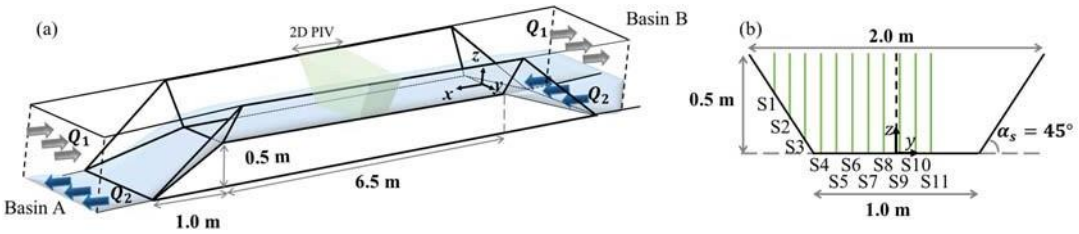

Figure 1. (a) 3D schematic representation of the trapezoidal cross section channel placed in the Coriolis Rotating Platform. (b) Trapezoidal channel side view and PIV fields of view (green vertical lines).

3 RESULTS

Detailed information on the spatial flow structure of the upper and lower layers across the channel were obtained by PIV measurements. In particular, the cross channel variation in zero-velocity interface elevation is shown in Figure 2 in the measured PIV sections for the three q* values tested.

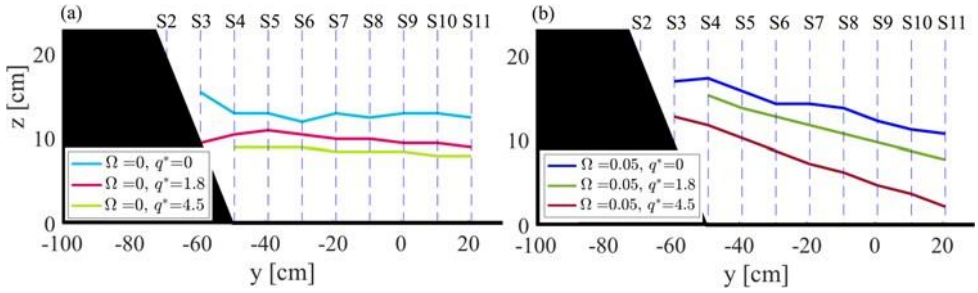

Figure 2. Cross channel zero-velocity interface, for different q* and angular velocity (a) Ω=0 rad·s^{-1} and (b) Ω=0.05 rad·s^{-1}.

The non-rotating experiments (Figure 2a) are compared with the experiments with an angular velocity Ω=0.05 rad·s^{-1} (Figure 2b). For Ω=0 rad·s^{-1}, the increasing upper fresh water flow (i.e. increasing q*) causes the reduction of the lower layer thickness (Figure 2a) defined as the zero-velocity interface. Whereas, when the angular rotation Ω plays a key role in the counter-flowing water masses (i.e. for Ω =0.05 rad·s^{-1}, Figure 2b), a tilt in the interface is observed and is coupled with the effect of the increasing q*, causing a significant deflection of the saline outflow on the right hand side of the trapezoidal channel. In conclusion, the rotation causes the deflection of the current to the right hand side of the trapezoidal channel and the exchange flows are geostrophically adjusted to the channel rotation. In the rotating stratified exchange flows, the coupled effect of an increase of both rotation and upper fresh water flow enhances the tilt of the interface up to generate a meandering pattern in the trapezoidal channel.

ACKNOWLEDGEMENTS

This project has received funding from the European Union's Horizon 2020 research and innovation programme under grant agreement No 654110, HYDRALAB+. This research was also funded by the Italian Ministry of Education, University and Research (MIUR) through the Departments of Excellence 2018-2022 Program.

REFERENCES

Cossu R., Wells M.G. & Wåhlin A.K. (2010). Influence of the Coriolis force on the velocity structure of gravity currents in straight submarine channel systems, J. Geophy. Res., 115, C11016.

Cuthbertson A.J.S, Laanearu J., Wåhlin A.K. & Davies P.A. (2011). Experimental and analytical investigation of dense gravity currents in a rotating, up-sloping and converging channel. *Dyn. Atmos. Oceans*, 52(3), 386-409.

De Falco M.C., Ottolenghi L. & Adduce C. (2020). Dynamics of gravity currents flowing up a slope and implications for entrainment. *J. Hydraul. Eng*., 146(4):04020011.

Laanearu J, Cuthbertson A.J.S & Davies P.A (2014). Dynamics of dense gravity currents and mixing in an up-sloping and converging vee-shaped channel. *J. Hyd. Res*., 52(1), 67-80.

Proceedings of the 1st IAHR
Young Professionals Congress
17-18 November 2020

INTERACTION OF GRAVITY CURRENTS WITH SLOPES AND OVERHANGS

Maria Rita Maggi[1], Claudia Adduce [1] & Gregory Francis Lane-Serff [2]

[1] Roma Tre University, Rome, Italy,
mariarita.maggi@uniroma3.com, claudia.adduce@uniroma3.com
[2] University of Manchester, Manchester, United Kingdom,
gregory.f.lane-serff@manchester.ac.uk

ABSTRACT

The dynamics of gravity currents interacting with sloping and overhanging barrier are investigated by laboratory experiments. Gravity currents are generated in a tank and an image analysis technique is applied to evaluate the instantaneous density fields. A wide range of slope angles are tested. The position of the incoming gravity currents and outgoing bores for flows reflected is evaluated and discussed. The analysis performed showed how a complex topography strongly affects the dynamics of the dense current. Despite the initial development of the dense flow exhibiting a similar behaviour for both cases, when the dense current approaches the foot of the barrier, the deceleration of the current is larger for overhangs than slopes. Consequently, the reverse flow develops a different dynamics.

Keywords: gravity currents, stratified flows, complex topography.

1 INTRODUCTION

Gravity currents, also known as density currents, are flows driven by a density difference due to a temperature or a salinity difference or the presence of suspended particulates. These flows often occur both in the natural environment and in man-made situations (Simpson, 1998). For this reason, gravity currents have been the subject of intensive research over the last decades. Despite several studies investigating gravity currents propagating on a horizontal boundary (Ottolenghi et al., 2018; Inghilesi et al., 2018), generally those flows develop over natural surfaces characterized by complex geometries (De Falco et al., 2020). Salt wedges in estuaries as well as sea-breeze are typical examples of gravity currents interacting with an up-sloping or overhanging topography.

The aim of this work is precisely to investigate the interaction of gravity currents with slopes (S runs) and overhang barriers (O runs) using laboratory experiments.

2 EXPERIMENTAL PROCEDURE

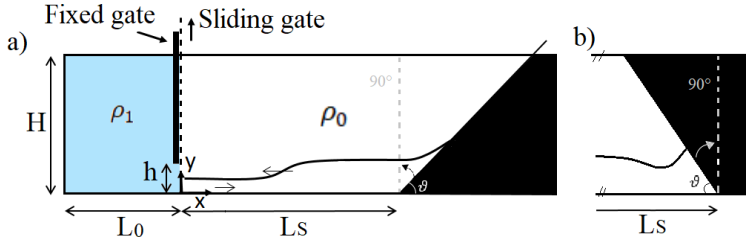

Figure 1. Sketch of the tank used to perform laboratory experiments respectively a) slope and b) overhang barrier cases.

Several laboratory experiments are conducted in a $3m$ long, $0.2m$ wide and $0.3m$ deep Perspex tank. Using an experimental set-up, similar to the one described in Lane-Serff et al. (1955) (Fig.1), a fixed gate is placed at $L_0 = 0.4m$ leaving a rectangular opening at the bottom across the width of the tank. A $4mm$ thick, removable, gate is inserted vertically to cover the opening, thus forming a lock region filled with salty water at density ρ_1 while the rest of the tank is filled with an ambient fluid of density $\rho_0 < \rho_1$. A controlled quantity of dye is added to the salty water in order to allow the visualization of the dense current during the experiment. A Perspex slope is placed at $L_S = 0.85m$ from the fixed gate with different angles ϑ, in order to represent up slopes or overhanging barriers cases. For all experiments an electronic density meter is used to obtain a density difference equal to

$\Delta\rho$=40 $\mathrm{Kg/m^3}$, with $\Delta\rho = \rho_1 - \rho_0$. The run starts with the sudden removal of the sliding gate, causing an exchange flow through the opening. The dense fluid collapses under the lighter one forming a gravity current. The experiment stops when a reflected dense flow, generated by the presence of the slope, has reached the opening of the fixed gate. The experiments are recorded by a camera. Images are extracted from the acquired movie and for each experiment the instantaneous density fields are evaluated using an image analysis technique.

3 RESULTS

In order to study the instantaneous front position and the reflected bore position of the dense current, the instantaneous dimensionless density $\rho^*(x, y, t)$ is defined by Eq. [1]:

$$\rho^* = \frac{\rho(x,y,t)-\rho_0}{\rho_1-\rho_0} \qquad [1]$$

The experimental front position is obtained by using the non-dimensional iso-density contours at $\rho^* = 2\%$, while the reflected current position is defined as the first point identified using a non-dimensional iso-density contours at $\rho^* = 50\%$. The dimensionless front/outgoing bore position, $x^* = x/L_0$, versus the dimensionless time, $t^* = t/t_0$, for the Up-Slope cases and the Overhangs cases are shown in Fig.2. In the Up-Slope cases (Fig.2a), the current is characterized by a constant front speed until it reaches the slope where it starts to decelerate as it flows up the slope. At the same time, t_{b0}, a reflected bore propagates back upstream. Differences in the time t_{b0} can be observed for different angles, the smaller is ϑ the grater is t_{b0}. In the overhang case, the current decelerates as it approaches the foot of the barrier being affected by its presence. In this case the reflection starts in a close range of time t_{b0} for all the experiments. Furthermore, the density fields analysis emphasizes a more complex dynamics in overhangs due to the presence of the barrier. In conclusion, this work shows how the dynamics of the gravity current are strongly affected by the nature of the barrier and then on the topographic features of the domain.

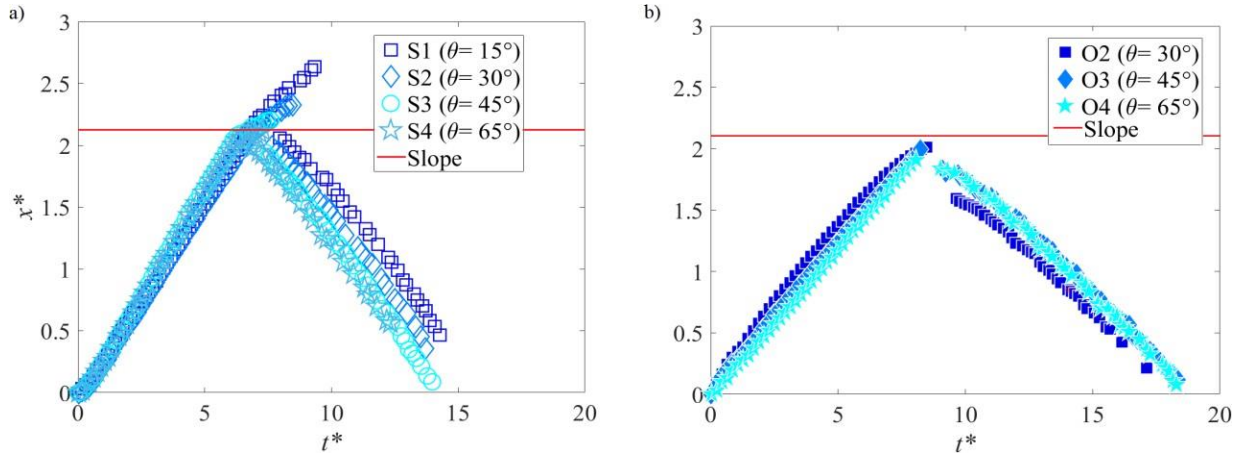

Figure 2. The dimensionless front position and outgoing bores for flows reflected from Up-Slopes a) and Overhangs b).

ACKNOWLEDGEMENTS

This research was also funded by the Italian Ministry of Education, University and Research (MIUR) through the Departments of Excellence 2018-2022 Program.

REFERENCES

De Falco, M.C., Ottolenghi, L., Adduce, C. Dynamics of gravity currents flowing up a slope and implications for the entrainment. *Journal of Hydraulic Engineering,* 46(6), 04020011.

Inghilesi, R., Adduce, C., Lombardi, V., Roman, F., Armenio, V. (2018). Axisymmetric three-dimensional gravity currents generated by lock exchange. *Journal of Fluid Mechanics,* 851, 507-544.

Lane-Serff, G.F., Beal, L.M., Hadfield, T.(1995). Gravity current flow over obstacles. *J. Fluid Mech*., 292, 39-53.

Ottolenghi, L., Prestininzi, P., Montessori, A., Adduce, C., and La Rocca, M. (2018). Lattice Boltzmann simulations of gravity currents. *on European Journal of Mechnics-B/Fluids,* 67, 125-136.

Simpson, J.E., and Manga, M. (1998). Gravity currents in the environment and the laboratory. *Physics Today,* 51(4), 63.

Proceedings of the 1st IAHR
Young Professionals Congress
17-18 November 2020

The influence of a grid structure on hydraulic river modelling outcomes of schematised river meanders

E. Bilgili[*1,2], A. Bomers[1], J. van Lente[2], F. Huthoff[1,2], S. J. M. H. Hulscher[1]

[1]University of Twente, Enschede, The Netherlands
[2]HKV lijn in water, Lelystad, The Netherlands

*Correspondance : e.bilgili@student.utwente.nl

ABSTRACT

Flow simulations in rivers are typically carried out using spatially-averaged quantities, which are affected by choice of grid structure. To isolate these effects, we set-up schematised river meanders with a flat bed in the transverse flow direction. We considered curvilinear and triangular grids with a high, medium and low resolution for cases where floodplains are excluded. Next, curvilinear, triangular and hybrid (combination of curvilinear and triangular cells) grids with a high and medium resolution are applied in schematised rivers where floodplains are present. The analysis showed that lower depth-averaged flow velocities and higher water depths are simulated with coarser grids. The numerical effects by the coarser grids are substantially larger in cases with distinct flow changes, such as in sharper river bends, and areas with high discharges per unit width. With the presence of floodplains, the latter decreases, leading to a damping of the numerical effects created by the grid.

Keywords: Grid resolution, Grid shape, Numerical diffusion, false diffusion, Two-dimensional depth-averaged model.

1 INTRODUCTION

To evaluate the efficacy and impact of river interventions a detailed insight in flow patterns in rivers is essential. A common approach to investigate such processes is by making use of hydrodynamic simulations, which solve the (depth-averaged) shallow water equations. In these models, fully triangular and fully curvilinear grids are commonly applied to discretise study areas. A combination of both grid shapes is also possible, which is known as a hybrid grid. Bomers *et al.* (2019) have shown that the accuracy and computation time of depth-averaged models is substantially influenced by the grid structure.

In Caviedes-Voullième *et al.* (2012) and Bomers *et al.* (2019), it has been highlighted that in river models, grid coarsening and poor alignment between grid and the direction of the flow, lead to a smoothed hydrograph, resulting in a lower depth-averaged flow velocities and hence higher water depths. These generated effects by a grid are referred as respectively numerical diffusion and false diffusion. Nonetheless, in these studies, grid effects are interrelated with how well the bathymetry is captured by a grid. Consequently, it is unclear to what extent effects by grid generation choices influence hydraulic river modelling outcomes, especially in river bends. The objective of this study is to understand under which conditions effects by grid generation choices affect hydraulic river modelling outcomes in schematised meander bends.

2 MODEL SET-UP

The schematised rivers are set-up based on the characteristics of the Grensmaas river, which is a section of the Meuse River, the Netherlands. The Grensmaas river consists of both mild and sharp bends with large local variations in floodplain width. To capture the extremes of these geometrical characteristics in the Grensmaas river, four idealised river schematisations are set-up which can be differentiated by a mild or sharp bend and the presence/absence of floodplains with all a total length of 50km (Fig. 1).

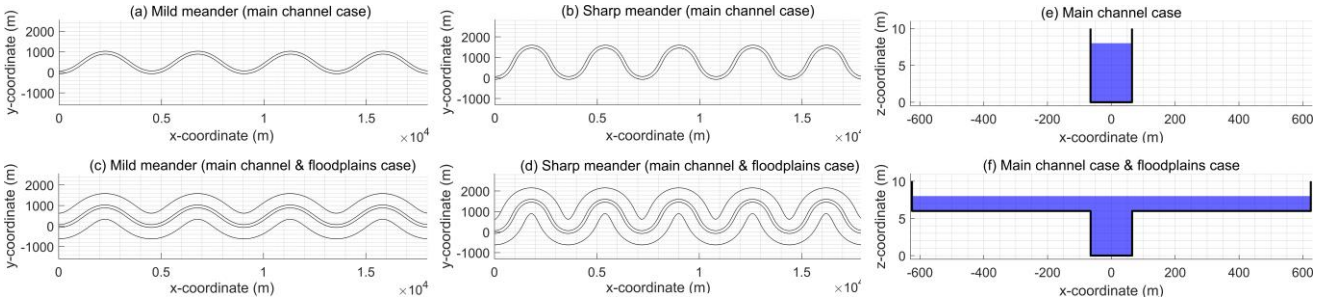

Figure 1: In (a-d) a top-view of a section of the four schematised rivers and (e-f) the applied cross-sections in the absence/presence of floodplains respectively.

For the cases with floodplains, a floodplain height of 6m is considered with respect to the bed level of the main channel (Fig. 1). For all idealised models a valley slope of 4.49×10^{-4}m/m is applied, which is the slope along a straight line through the meanders bends. Except for the transition between main channel and floodplains a constant bed level in transverse flow direction is used. All four rivers are forced at $x = 0$ with a constant discharge until similar water levels are obtained between the cases. Three flow scenarios are calculated with each lasting 10 days: (i) low; (ii) mid and (iii) high discharge range. The downstream boundary conditions are set by predefined rating curves based on steady uniform flow considerations.

Curvilinear and triangular grids are considered with three different grid resolutions (high, medium and low) in case a and b (Fig. 1). Regarding the resolution in the main channel of the curvilinear grids, 20, 10 and 5 grid cells are placed in the transverse flow direction for respectively the high, medium and low resolution. For the triangular grids, 8, 4 and 3 cells in the transverse flow direction are placed for respectively the high, medium and low resolution. In cases c and d (Fig. 1), curvilinear and triangular grids, as well as hybrid grids, are used with only a high and medium grid resolution. D-Flow FM is used as the software to perform the computations.

3 RESULTS

The analysis showed that lower depth-averaged flow velocities and hence higher water depths are obtained with coarser grids in the schematised river meanders in the absence of floodplains. Even larger deviations are simulated in the sharper bend, as rapid flow changes have to be captured by the grids. These differences are more evident at higher discharges. Regarding the differences between grid shapes, a higher false diffusion is obtained with curvilinear grids at lower resolutions than triangular grids. The opposite is observed at highest resolution of both grids.

In contrast to the cases without floodplains, negligible differences are obtained in terms of the water level in case c and d (Fig. 1). This is a consequence of relatively less deviations in depth-averaged flow velocity differences throughout the spatial domain even though considerable differences are present in the main channel.

4 CONCLUSIONS

The results showed that the generated numerical diffusion and false diffusion become larger in the case of higher discharges and hence higher depth-averaged flow velocities, and under circumstances in which rapid flow changes occur (i.e. for cases with sharp river bends). The influence of the generated numerical diffusion and false diffusion is dampened by the presence of floodplains. This indicates that the numerical effects are proportional to the discharge per unit width.

References

Bomers A., Schielen R., Hulscher S. (2019, 2). The influence of grid shape and grid size on hydraulic river modelling performance. *Environmental fluid mechanics 19*(5), 1273–1294. Springer. doi:10.1007/s10652-019-09670-4.

Caviedes-Voullième D., Garcia-Navarro P., Murillo J. (2012, 07). Influence of mesh structure on 2d full shallow water equations and scs curve number simulation of rainfall/runoff events. *Journal of Hydrology s 448–449*, 39–59. doi:10.1016/j.jhydrol.2012.04.006.

Proceedings of the 1st IAHR
Young Professionals Congress
17-18 November 2020

Numerical Study of Meandering Effect on Confluence Channel Flow by openFoam

Minjae Lee[1] **and Yong Sung Park**[*1,2]

Department of Civil and Environmental Engineering, Seoul National University, Seoul, Korea
Integrated Research Institute of Construction and Environment, Seoul National University, Seoul, Korea

*Correspondance : dryspark@snu.ac.kr

ABSTRACT

Confluence channel flow is complex and it is important in river flow such as mixing and sediment transport. Confluence channel flow changes depending on geometry and hydraulic conditions. Through numerical simulations, effects of tributary channel location and discharge ratio (also, momentum ratio) on meandering confluence channel flow have been investigated. Depending on location of tributary channel, flow pattern in meandering channel is greatly influenced. Shear lay er mode is examined through vorticity and Kelvin-Helmholtz mode is shown when velocity of tributary channel is high.

Keywords: Confluence channel flow, Meandering, Flow pattern, Separation, Shear layer

1 INTRODUCTION

Representative geometry features in natural rivers are confluence and meandering channel. These show noticeable flow patterns, for example, separation zone, deflection, mixing layer, and secondary flow can be seen in confluence channel and the features for meandering channel flow are asymmetric horizontal velocity distribution and secondary flow. These characteristics have great effects on natural river such as mixing, sediment transport, and morphology change. In this study, the flow in meandering confluence channel has been investigated by numerical simulation using openFoam. The main goal of this study is understanding the flow structure shown in confluence channel with curvature of downstream channel. Also, we aim to understand is how flow regime changes depending on the location of tributary channel and the discharge ratio (also, momentum ratio).

2 METHODOLOGY

2.1 Description of the model

3-dimensional numerical simulations have been conducted to simulate the complex flow structure by openFoam which is the open source CFD tool. Large eddy simulation with Smargorinsky for subgrid scale model has been applied. The numerical models have been constructed and validated according to previous experimental study Lee (2013). The experiment (Lee (2013)) examined flow structures in confluence channel under various conditions including bed elevation difference between main channel and tributary channel.

2.2 Description of the simulation cases

Downstream channel of the confluence model has strong curvature which is similar to Nakdong River and Geumho River confluence, South Korea. It is expected that the flow structure is changed by inflow direction from tributary, so that, four models with different tributary channel location are constructed. Different mean velocities are used at inlet of main channel to control the discharge ratio ratio and mean velocity at inlet of tributary channel is maintained.

3 RESULTS

It can be seen that flow in meandering channel is disturbed by flow from the tributary channels and different velocity distributions after the junction are shown depending on the location of tributary channel (Fig 1). Height of separation zone is similar in case of same discharge ratio. It infers that the height is related to flow deflection marked black dotted line in Fig 1 affected by discharge ratio. The location of tributary channel does not have great effect on separation zone size, however, it has effect on shear layer. The length of shear layer becomes shorter as the tributary channel moves to the center of meandering channel. It is due to that the velocity along the outer bank increases as the curve progresses. In the meandering confluence channel, confluence channel flow characteristics is affected by meandering channel flow distribution. It can be seen that Kelvin-Helmholtz instability occurs at junction and the vorticity develops strongly along the shear layer when the discharge ratio increases. The mode of shear layer can be classified as Kelvin-Helmholtz mode.

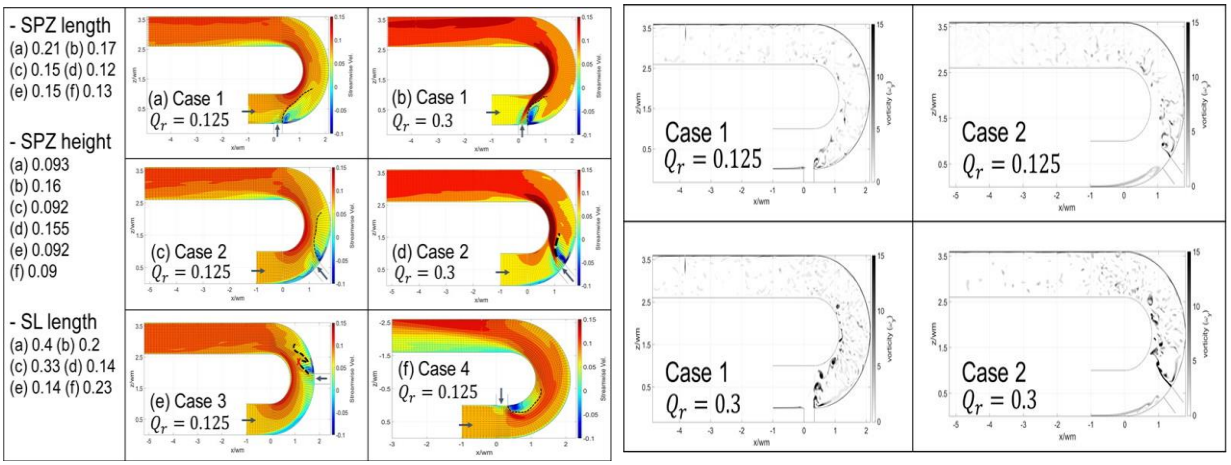

(a) Streamwise Velocity (b) Vorticity

Figure 1: Comparing numerical simulation results of Streamwise velocity and vorticity

4 CONCLUSIONS

Effects of two parameters, namely (i) the radial location of the joint in half-circular channel and (ii) the discharge ratio (also, momentum ratio) have been investigated. The location of tributary channel and discharge ratio have greater influence on shear layer. On the other hand, separation zone is affected by discharge ratio rather than the branch location. Flow pattern along the meandering channel is affected by location and velocity of tributary channel since distribution of flow velocity in meandering channel is spatially varied. Shear layer mode in confluence channel is classified into wake mode and Kelvin-Helmholtz mode (Constantinescu *et al.* (2016)) which can be decided according to vorticity fields. Shear layer tends to develop in Kelvin-Helmholtz mode when flow velocity of tributary channel is increased.

5 ACKNOWLEDGEMENTS

This study was funded by Korea Environment Industry & Technology Institute (KEITI) as Service Program for Demand-Responsive Water Supply, funded by Korea Ministry of Environment (MOE).(2020002650001)

References

Constantinescu G., Miyawaki S., Rhoads B., Sukhodolov A. (2016). Influence of planform geometry and momentum ratio on thermal mixing at a stream confluence with a concordant bed. *Environmental Fluid Mechanics 16*(4), 845–873.

Lee J. (2013). Experimental investigation of flow characteristics in a confluent channel with bed elevation difference. master thesis, Seoul National University.

Proceedings of the 1st IAHR
Young Professionals Congress
17-18 November 2020

A well-balanced DG scheme for the resolution of the shallow water equations

Pablo Solán-Fustero [*1], **Adrián Navas-Montilla**[1,2], **Javier Murillo**[2], **Pilar García-Navarro**[2]

[1]Universidad de Zaragoza, Zaragoza, Spain
[2]Centro Universitario de Defensa, Zaragoza, Spain

*Correspondance : psolfus@unizar.es

ABSTRACT

In this work, a novel framework for the construction of Discontinuous Galerkin schemes using augmented Riemann solvers for the resolution of the shallow water equations is proposed. The benefits of this family of solvers lie in the exact preservation of the Rankine Hugoniot (RH) condition at cell interfaces at the discrete level, ensuring the preservation of equilibrium solutions (i.e. the well-balanced property) without requiring extra corrections of the numerical fluxes.

Keywords: shallow water, augmented solver, high order, source terms, Discontinuous Galerkin

1 INTRODUCTION

Many engineering and environmental problems that involve steady and transient free surface water flows can be described by the Shallow Water Equations (SWE). High order methods are becoming increasingly popular in shallow water flow modelling motivated by their high computational efficiency. In particular, Discontinuous Galerkin (DG) schemes Reed et Hill (1973); Cockburn et Shu (1989) are very well suited for the resolution of the SWE, due to their many advantages: high accuracy, inherent conservativeness, compactness, high parallel efficiency, flexibility for hp-adaptivity and possibility of using arbitrary geometry and meshes.

When considering the SWE with bottom topography, numerical schemes must preserve a relevant equilibrium state called quiescent equilibrium, also known as “lake at rest”, where the water surface elevation is constant. Numerical schemes satisfying such equilibrium state are called well-balanced methods Bermudez et Vázquez-Cendón (1994); J.M. Greenberg (1996); V. Caleffi (2015). In this work, the DG formulation is combined with augmented Riemann solvers to design a well-balanced arbitrary order discretization of the SWE.

2 NUMERICAL METHOD

The x-split SWE can be expressed as $\boldsymbol{U}_t + \boldsymbol{F}_x = \boldsymbol{S}$, where $\boldsymbol{U} = (h, hu, hv)^T$, $\boldsymbol{F} = (hu, hu^2 + 0.5gh^2, huv)^T$, $\boldsymbol{S} = (0, -ghz_x, 0)^T$, with h the water depth, hu and hv the discharges, g the acceleration of gravity and z the bed elevation.

The DG method is based on the approximation of the solution by a linear combination of basis functions $\{\varphi_l\}_{l=0,\dots,N_d}$ as follows $\boldsymbol{U}(x,t) \approx \boldsymbol{U}_i(x,t) = \sum_{l=0}^{N_d} \hat{\boldsymbol{U}}_{i,l}(t)\varphi_l(x)$. This allows to express the updating scheme for the unknown degrees of freedom as $\hat{\boldsymbol{U}}_{i,k}(t)$

$$\frac{\partial \hat{\boldsymbol{U}}_{i,k}}{\partial t} = -\frac{1}{a_k}\left[\int_{\Gamma_i} \varphi_k \mathbf{F}^{Y,-} d\Gamma - \int_{\Omega_i} \boldsymbol{F}\cdot\frac{\partial \varphi_k}{\partial x} dx - \int_{\Omega_i} \varphi_k \boldsymbol{S} dx\right], \tag{1}$$

where $\boldsymbol{F}$ is the matrix of physical fluxes, $\mathbf{F}^{Y,-}$ stands for the numerical flux in the x-direction and $\boldsymbol{S}$ is source term. Numerical fluxes are usually computed by means of the resolution of the Riemann Problem (RP) at cell interfaces in order to obtain accurate numerical solutions. Augmented Riemann solvers were introduced in an attempt to represent the effect of the source term in the solution of the RP and automatically fulfill RH conditions Navas-Montilla *et al.* (2020).

Second and third order Discontinuous Galerkin (DG2 and DG3) schemes with Strong Stability Preserving third order Runge-Kutta (SSPRK3) integrator will be compared with a first order Godunov’s scheme.

3 NUMERICAL RESULTS

Three different cases are tested. First of all, Case 1 is an evaluation of the convergence rates of the well-balanced DG3-SSPRK3 scheme with smooth topography. Table 1 shows its error norms and convergence rates. Cases 2 and 3 are Riemann Problems, designed as a dam break the first one and as an equilibrium representing an ideal shear layer (contact wave) the second one, whose initial conditions are provided in Table 2. The solution for the water surface elevation of Case 2 is plotted in Figure 1a. It is observed that the intermediate states are accurately predicted, as well as the location of the shock wave and rarefaction wave.

	h				hu			
Meshes (N_j/N_{j+1})	$L_1(h)$	O_{L_1}	$L_\infty(h)$	O_{L_∞}	$L_1(hu)$	O_{L_1}	$L_\infty(hu)$	O_{L_∞}
160/320	4.17e-09	3.48	2.97e-08	3.54	1.86e-08	3.48	1.40e-07	3.571
320/640	4.72e-10	3.14	3.30e-09	3.17	2.11e-09	3.14	1.55e-08	3.17
640/1280	5.74e-11	3.03	4.00e-10	3.04	2.57e-10	3.03	1.88e-09	3.04
1280/2560	7.12e-12	3.01	4.93e-11	3.02	3.19e-11	3.01	2.33e-10	3.01

Table 1: Convergence rates for Case 1 for the water depth and discharge, h and hu, associated to the L_1 and L_∞ error norms.

Label	h_L	h_R	hu_L	hu_R	hv_L	hv_R	z_L	z_R	T	N
RP1	1.0	0.1614067989	0.0	0.0	1.0	0.1614067989	0.0	0.05	0.02	320
RP2	1.0	1.0	0.0	0.0	1.0	2.0	0.0	0.0	0.032	160

Table 2: Initial condition for Cases 2 and 3. Units in m, m^2/s and s.

In Case 3, Figure 1b shows that the 1-st order scheme adds a large amount of numerical diffusion, which would involve a strong mixing between the left and right regions in the context of the resolution of a shear layer. The DG2-SSPRK3 scheme reproduces a sharper transition across the contact discontinuity. Its performance is much better than the first order version of the augmented Riemann solver and even than other higher order schemes.

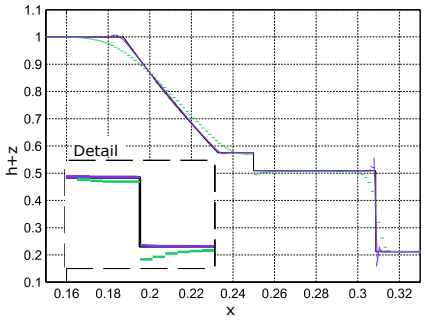

(a) Case 2. Numerical solution for $h + z$.

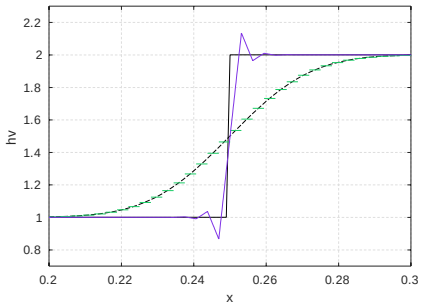

(b) Case 3. Numerical solution for hv.

Figure 1: Cases 2 and 3 are computed by the well-balanced first order Godunov's scheme (green) and DG2-SSPRK3 (purple), compared with the exact solution (black solid line), and the analytical solution in Case 3 (dashed line). Units are given in m and m/s.

4 CONCLUSIONS

It is herein evidenced that DG schemes are automatically well-balanced when using augmented solvers, provided: (i) the use of an exact quadrature rule for the surface and volume integrals and (ii) the reconstructed data satisfy the discrete equilibrium. The numerical results evidence that the proposed scheme achieves the prescribed convergence rates and preserves the equilibrium states of relevance with machine precision.

Our immediate goals are the limitation of shock oscillations and the correct resolution of dry/wet fronts. Also the parallelization of the 2D scheme using CUDA/OpenACC to solve it in the GPU is within the next steps.

References

Bermudez A., Vázquez-Cendón M. (1994). Upwind methods for hyperbolic conservation laws with source terms. *Comput. Fluids 23*, 1049–1071.

Cockburn B., Shu C.-W. (1989). Tvb runge-kutta local projection discontinuous galerkin finite element method for conservation laws ii: General framework. *Math. Comput. 52*, 411–435.

J.M. Greenberg A. L. (1996). A well-balanced scheme for the numerical processing of source terms in hyperbolic equations. *SIAM J. Numer. Anal. 33*, 1–16.

Navas-Montilla A., Solán-Fustero P., Murillo J., García-Navarro P. (2020, 04). Discontinuous Galerkin well-balanced schemes using augmented Riemann solvers with application to the shallow water equations. *Journal of Hydroinformatics*.

Reed W., Hill T. (1973). *Triangular mesh methods for the neutron transport equation*. National topical meeting on mathematical models and computational techniques for analysis of nuclear systems. University of California.

V. Caleffi, A. Valiani G. L. (2015). A comparison between bottom-discontinuity numerical treatments in the dg framework. *Appl. Math. Model.*.

Proceedings of the 1st IAHR
Young Professionals Congress
17-18 November 2020

TURBULENT FLOW STRUCTURE UPSTREAM OF AN ISOLATED BOULDER: IMPLICATIONS FOR SEDIMENT DEPOSITION

Micah A. Wyssmann [1], James G. Coder [2] & John S. Schwartz [3]

[1] Dept. Civil and Env. Engineering, The University of Tennessee, Knoxville, TN, USA
e-mail mwyssman@vols.utk.edu

[2] Dept. Mech., Aerospace and Biomedical Engineering, The University of Tennessee, Knoxville, TN, USA
e-mail jcoder@utk.edu

[3] Dept. Civil and Env. Engineering, The University of Tennessee, Knoxville, TN, USA
e-mail jschwart@utk.edu

ABSTRACT

In mountainous gravel-bed rivers, boulders tend to stimulate the development of unique bed morphological features in their vicinity due to their effects on local flow structure. The important role of boulder submergence on the location of depositional patches has also been highlighted in recent research. However, limited studies have provided quantitative measurements of turbulence structure upstream of boulders for different submergence conditions to help explain this behavior. This study is motivated by this research gap and provides results from new laboratory particle image velocimetry (PIV) measurements focused upstream of an isolated spherical boulder in a laboratory flume. The mean flow velocity results for a fully submerged boulder are presented and may explain in part the sediment deposition observations made in previous studies at similar conditions.

Keywords: turbulent flows, boulders, relative submergence, gravel-bed rivers, sediment deposition

1 INTRODUCTION

In mountainous gravel-bed rivers, large and relatively immobile boulders exert a significant influence on turbulent flow structure in their vicinity as they cause flow acceleration and deceleration and the formation of vortex structures. As a result, boulders tend to stimulate deposition and erosion of sediment in their vicinity and thereby affect the morphology of the surrounding riverbed (Monsalve and Yager, 2017; Schömer et al., 2020).

A key parameter that has been recently found to affect the characteristics of sediment depositional features around boulders is the relative submergence, which is defined as the ratio of the flow depth to the boulder height (Papanicolaou et al., 2018). Specifically, sediment has been observed to preferentially deposit either upstream or downstream of boulders depending on the relative submergence. A clear explanation for this behavior has not been developed, however, largely due to the limited amount of quantitative data documenting turbulent flow structure upstream of boulders under different submergence conditions. The present study is motivated by this research gap and aims to provide new turbulence measurements in the vicinity of boulders.

2 METHODS

The experimental setup is developed at the Hydraulics and Sedimentation Lab (HSL) at the University of Tennessee by using a recirculating laboratory flume to provide well-controlled conditions for examining turbulence structure upstream of an isolated boulder. The flume bed is covered with five layers of well-packed spherical particles (18.5-mm diameter) to represent a porous gravel sediment bed with an idealized geometry. The isolated boulder used in this study is a 55-mm diameter sphere, which is mounted and secured atop the bed (Papanicolaou et al., 2018).

Experiments are conducted for a fully submerged flow condition where the ratio of the water depth, H_w, to the boulder height, H_b, is equal to 2.18. The key experimental parameters are summarized in Table 1, which include the bed slope, S_0, bulk velocity, U, Froude number, Fr, channel Reynolds number, Re, and boulder Reynolds number, Re_b. A TSI, Inc. volumetric, three-component particle image velocimetry (PIV) system is utilized to document turbulent flow statistics within a control volume located upstream of the spherical boulder.

Table 1. Conditions for fully submerged boulder experiments.

H_w/H_b (-)	H_w (m)	S_0 (-)	U (m/s)	Fr (-)	Re (-)	Re_b (-)
2.18	0.12	0.0052	0.822	0.76	3.9×10^5	4.5×10^4

3 RESULTS

Mean streamwise velocity, $\bar{u}$ and mean vertical velocity, $\bar{w}$ profiles (with respect to the vertical direction, z) are plotted in Figure 1, which are taken from the streamwise-vertical plane along the boulder centerline. Streamwise locations, x, of the profiles are normalized with the boulder width, W_b (and x = 0 is at the spherical boulder's most upstream point). The $\bar{u}$ profiles show a gradual flow deceleration within the region below and just above the boulder height as the boulder is approached. The lowest flow velocities are observed near the stagnation point on the boulder (i.e., x = 0 mm at the height indicated in Fig. 1) and no near-bed mean flow recirculation region is observed for $x/W_b \leq 0$. The relatively high near-bed velocities may partly explain the limited deposition in this region observed by Papanicolaou et al. (2018) for similar conditions. The $\bar{w}$ profiles exhibit inflection points at the height of the stagnation point, with upward directed flow above this height and downward directed flow below it. The significant downward flow velocity near the bed at the base of the boulder ($\bar{w}/U \approx$ -0.2) may also suggest flow intrusion into the porous gravel bed (e.g., Apsilidis et al. 2016).

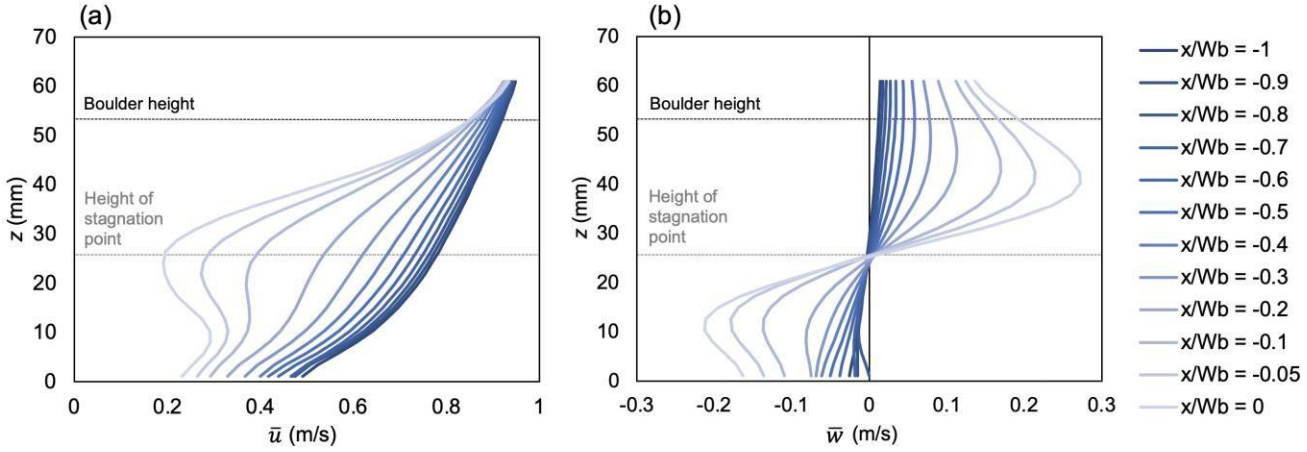

Figure 1. Mean velocity profiles upstream of the boulder. (a) Mean streamwise velocity, $\bar{u}$ and, (b) mean vertical velocity, $\bar{w}$

4 CONCLUSIONS

Laboratory experiments documenting turbulent flow structure upstream of a fully submerged, spherical boulder are performed. These measurements can provide improved understanding of flow structure around boulders and insights into the characteristics of sediment deposition and mobilization.

ACKNOWLEDGEMENTS

M.A.W. thanks funding support from the Chancellor's Fellowship and the Dept. of Civil and Environmental Engineering at the University of Tennessee, Knoxville. Input from Dr. Thanos Papanicolaou as well as Drs. Matthew Stegmeir and Dan Troolin from TSI in the development of the experimental setup is acknowledged.

REFERENCES

Apsilidis, N., Diplas, P., Dancey, C.L., Bouratsis, P. (2016). Effects of wall roughness on turbulent junction flow characteristics. *Exp. Fluids*, 57, 12.

Monsalve, A., and Yager, E. (2017). Bed surface adjustments to spatially variable flow in low relative submergence regimes. *Water Resour. Res.*, 53, 9350-9367.

Schlömer, O., Herget, J., Euler, T. (2020). Boundary condition control of fluvial obstacle mark formation – framework from a geoscientific perspective. *Earth Surf. Process. Landforms*, 45 (1), 189-206.

Papanicolaou, A.N., Tsakiris, A.G., Wyssmann, M.A., and Kramer, C.M. (2018). Boulder array effects on bedload pulses and depositional patches. *J. Geophys. Res.: Earth Surf.*, 123 (11), 2925-2953.

Proceedings of the 1st IAHR
Young Professionals Congress
17-18 November 2020

APPLICABILITY OF TELEMAC-3D FOR FINE-SCALE HYDRAULICS

Jorge Santamaría[1,2], Matthieu De Linares [1] & Olivier Bertrand [1]

[1] ARTELIA, Echirolles, France
jorge.santamaria@arteliagroup.com; Matthieu.DELINARES@arteliagroup.com; Olivier.BERTRAND@arteliagroup.com

[2] Ecole Nationale Supérieure de l'énergie, l'eau et l'environnement de l'Institut Polytechnique de Grenoble, Grenoble, France.
jorge-andres.santamaria-chamorro@grenoble-inp.org

ABSTRACT

TELEMAC-3D is an open source software created by Electricité de France (EDF) applied for Computational Fluid Dynamics (CFD) in the area of Hydraulics. This software is constantly tested and improved by academic and private organizations such as ARTELIA, engineering group which continually collaborates with enhancements and practical applications of TELEMAC-3D. At the moment, ARTELIA is interested in employing this software for simulating scour, and the first step is to study the fine-scale hydraulic phenomena. Therefore, this work focuses on evaluate TELEMAC-3D for fine-scale-hydraulics based on two cases: Flat-Bed-Channel and Flow-Around-Pile, both have been analyzed and compared with other published experimental studies.

Keywords: Hydraulic-Numerical-Modelling, Computational-Fluid-Dynamics CFD, TELEMAC-3D, Fine-Scale-Hydraulics.

1 INTRODUCTION

For future TELEMAC-3D applications in scour, it is necessary to explore the fine-scale phenomena. This work evaluates the fine-scale hydrodynamics based on two cases: Flat-Bed-Channel and Flow-Around-Pile. For the first case, simulations varying turbulence model and mesh are presented and compared with experimental measurements obtained by (MF Tachie, 2003). For the second case, the results of the simulations are compared with studies carried out by (Roulund, 2005) and (Nagel, 2018). Flat-Bed-Channel aims to evaluate the influence of turbulence model and mesh, while Flow-Around-Pile is presented as an application example. In addition to TELEMAC-3D, BlueKenue and ParaView have been used for Pre- and Post-Processing.

2 FLAT BED CHANNEL and FLOW AROUND PILE

Flat-Bed-Channel results are compared with vertical velocity profiles obtained in an open channel with smooth surface by (M.F. Tachie, 2003). For the simulations run in the present study, horizontal element size is about 0.05 m for meshes MA and MA3. Concerning vertical element size, MA elements has a constant size of 0.01 m, while MA3 elements grow from the bottom to the water surface locating its first vertical element at 0.0002 m. In addition, each mesh has been simulated with two turbulence models: k-epsilon and k-omega. This first case explores how turbulence model and mesh influence the dimensionless wall distance y^+. Regarding the second case, (Roulund, 2005) and (Nagel, 2018) mainly evaluate scour around a pile. However, in the first place both of them analyzed the hydrodynamics over a rigid bed. The Flow-Around-Pile case utilizes this rigid bed configuration for the comparison. Geometry and Mesh was provided by Damien Pham-Van-Bang (Zhang, Zapata, Bai, Pham-Van-Bang, & Nguyen, 2019). The horizontal element size varies from 0.2 m to 0.003 m. Water depth was divided into 32 horizontal levels (vertical element size=0.01 m). Concerning turbulence model, k-epsilon has been chosen due to its practicality.

3 RESULTS AND DISCUSSION

3.1 Flat-Bed-Channel

As expected, inside the viscous sublayer, a higher mesh resolution better approximates physical measurements. MT_4 (MA3 and k-omega model) presents the most acceptable behavior. This be in accord

with the fact that k-omega model works well as long as the first element is ubicated on the viscous sublayer. In contrast, inside the logarithmic sublayer, MT_2 (MA3 and k-epsilon model) presents furthest behavior from the measurements. This would suggest that k-epsilon needs the first element to be found in the logarithmic sublayer. In fact, TELEMAC theory and user guide establish this as a hypothesis for k-epsilon algorithm (Leroy, 2018) (Mattic, 2018) (Hervouet, 2007). In general, there is a better consistency for the logarithmic sublayer.

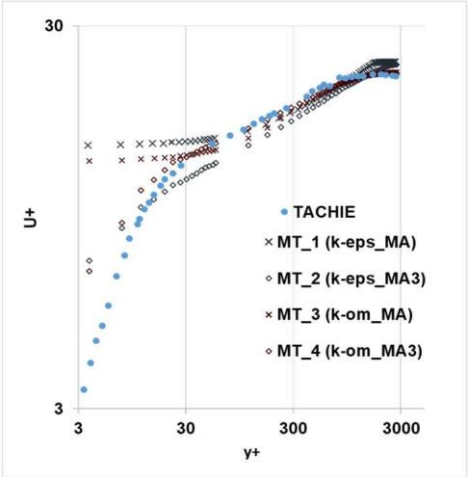

Figure 1. Flat-Bed-Channel comparison inside boundary layer.

3.2 Flow-Around-Pile

With regard to flow velocities ***u***, at elevation z=20 cm there is a good agreement with the other studies. For vertical velocities ***w*** it could be said that TELEMAC 3D is closer to Roulund numerical model (**Rou-Num**). In general, none of the numerical models perfectly approximates the phenomena either upstream or downstream, but there is an acceptable concordance in order of magnitude.

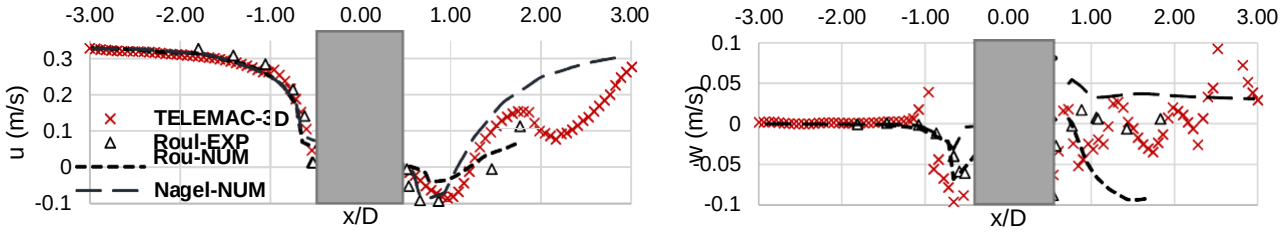

Figure 2. Mean-stream u (left) and vertical velocity w (right) at z=20cm

4 CONCLUSIONS

The Flat-Bed-Channel is a suitable example for analyzing a wall function behavior. Results confirm that a wall function only “transmits” viscosity effect to the main flow but without simulating it. For obtaining the “direct” representation of the viscosity, it would require elements smaller than the thickness of the viscous sublayer.
From the two cases with their respective comparisons, it can be seen that TELEMAC-3D is certainly capable of representing phenomena close to the boundary layer in order of magnitude, as well as vertical velocities. Deeper code changes would allow for better results.

ACKNOWLEDGEMENTS

This work would not have been possible without the support of Hydraulics Numeric team of ARTELIA, to whom I extend my sincere gratitude. I also extend my thanks to Damien Pham-Van-Bang, who provided information on their work for the completion of this study.

REFERENCES

Andreas Roulund, M. S. (2005). Numerical and experimental investigation of flow and scour around a circular pile. Journal of Fluid Mechanics, 351-401.
Hervouet, J. M. (2007). Hydrodynamics of Free Surface Flows. Wiley-Blackwell.
M.F. Tachie, D. B. (2003). Roughness effects in low-Reh open-channel turbulent boundary layers. In Experiments in Fluids (pp. 338–346).
Nagel, T. (2018). Numerical study of multi-scale flow-sediment-structure. Université Grenoble Alpes.

Proceedings of the 1st IAHR
Young Professionals Congress
17-18 November 2020

OPTIMIZATION OF THE TRANSPORT VELOCITY FOR ALE-SPH SCHEME

Pietro Rastelli[1]*, Renato Vacondio[1] & Jean-Christophe Marongiu[2]

[1] Dipartimento di Ingegneria Civile e Architettura, Università di Parma, Parma, Italy
*e-mail: pietro.rastelli@unipr.it

[2] R&D Department, ANDRITZ Hydro, Vevey, Switzerland

ABSTRACT

Smoothed Particle Hydrodynamic (SPH) is a Lagrangian meshless numerical scheme suited to simulate complex flows with fragmented interfaces and/or moving boundaries. In the present work, a novel formulation has been developed in the framework of Arbitrarily Lagrangian-Eulerian SPH schemes to improve the particle distribution and, consequently, the accuracy. A fictitious pressure has been introduced to overcome the limitation of other existing corrections for the transport velocity. The new formulation has been tested against the inviscid Taylor-Green flow and its capability of preserving good quality in particle distribution without introducing significant overheads has been demonstrated and it can be applied to a wide range of fluid simulations.

Keywords: ALE-SPH: Arbitrarily Lagrangian-EulerianSmoothed Particle Hydrodynamics, PST: Particle Shifting Technique.

1 INTRODUCTION

The Smoothed Particle Hydrodynamics (SPH) numerical scheme has been originally introduced by Gingold et al. (1977) in astrophysics and later it has been adapted to solve the Navier-Stokes equations (Monaghan, 1994). Despite the success of SPH models to simulate complex flows, there are still some fundamental issues related to their mathematical properties which require further investigations. For this reason, different corrections to the pure Lagrangian trajectories of the particles have been proposed in literature to improve the particle distribution. One of the most effective approach is the shifting formulation originally introduced by Lind et al. (2012) for Incompressible SPH schemes. In the present work a shifting correction has been introduced for the transport velocity of the ALE-SPH formulation (Vila, 1999), to achieve an adequate accuracy of the SPH interpolation, ensuring mass and momentum conservation.

2 METHODOLOGY

In ALE-SPH schemes the particle position update is controlled by the transport velocity, $\mathrm{d}\boldsymbol{x}_i / d\mathrm{t} = \boldsymbol{v}_{0i}$, (Oger et al., 2016), which is completely independent from the fluid velocity $\boldsymbol{v}$. Neuhauser (2014) proposed to compute the $\boldsymbol{v}_0$ as follow:

$$\boldsymbol{v}_0(\boldsymbol{x}_i) = \boldsymbol{v}(\boldsymbol{x}_i) - \delta\boldsymbol{v}(\boldsymbol{x}_i) \quad [1]$$

where $\delta\boldsymbol{v}(\boldsymbol{x}_i)$ is a correction defined as:

$$\delta\boldsymbol{v}(\boldsymbol{x}_i) = \sum_{j\in D_i} \omega_j \left[\frac{p_{ref}}{\rho_0} + \frac{c_0}{2}(\boldsymbol{v}_0(\boldsymbol{x}_i) - \boldsymbol{v}_0(\boldsymbol{x}_j)) \cdot \boldsymbol{n}_{ij}\right] \nabla W_{ij} \quad [2]$$

where $p_{ref} = \rho_0 {c^2}_0 / \gamma$ is a constant background pressure field, ρ_0 and c_0 are respectively the reference density and speed of sound, ω_j is the particle volume, ∇W_{ij} is the kernel function gradient and $\boldsymbol{n}_{ij}$ is the unit vector between particle *i-th* and particle *j-th*. In Weakly-Compressible SPH the speed of sound c_0 is usually defined as 10-20 times the maximum expected velocity U_{max} (corresponding to Mach number on the order of 0.1). As defined in Eq [2] the magnitude of $\delta\boldsymbol{v}(\boldsymbol{x}_i)$ is proportional to c_0. In order to obtain satisfactory results for most demanding test cases, in the framework of ALE-SPH, the speed of sound c_0 had to be increased up to 50-100 U_{max}, leading to a very small time integration interval Δt, remarkably increasing the computational cost. In the present work a new approach for the $\delta\boldsymbol{v}_0$ correction, is proposed with the aim to overcome the issue above

described. A fictitious pressure field, P^F, (that has no influence on physical quantities), has been defined as follow:

$$P^F = \frac{\rho_0 c_0'}{\gamma} + \frac{\rho_0 c_0'}{\gamma}\left[\left(\frac{\omega_0}{\omega}\right)^{\gamma} - 1\right] \quad [3]$$

Substituting Eq [3] in Eq [2] (with γ being an arbitrary dimensionless coefficient) the correction $\delta\boldsymbol{v}(\boldsymbol{x}_i)$ becomes:

$$\delta\boldsymbol{v}(\boldsymbol{x}_i) = \sum_{j\in D_i} \omega_j \left[\frac{1}{\rho_0}\frac{P^F{}_i + P^F{}_j}{2} - \frac{c_0}{2}\left(\boldsymbol{v}_0(\boldsymbol{x}_i) - \boldsymbol{v}_0(\boldsymbol{x}_j)\right)\cdot \boldsymbol{n}_{ij}\right]\nabla W_{ij} \quad [4]$$

This correction has the capability to couple the kinematics equations of ALE scheme (volume variation and particle position). The quality of particle spatial distribution has been evaluated measuring the particle concentration with the so-called Error Closed Box magnitude (ECB) (Neuhauser, 2014) defined as:

$$ECB_i = \sum_{j\in D_i} \omega_j \nabla W_{ij} \quad [5]$$

High values of ECB can show the presence of clusters or holes in particle distribution that affect negatively the accuracy of the SPH interpolation. The inviscid Taylor Green Vortex (TGV) test case with $U_{ref} = 1m/s$ has been used to evaluate the capability of Eq [4] to maintain high quality of particle distribution (i.e. low values of ECB). Main results, $ECB\ L_2$ norm and computational time, for different simulations using Eq [2], with c_0 value equal to $10U_{ref}$ and $100\ U_{ref}$ and simulation using Eq [4] with c_0 equal to $10U_{ref}$ are shown in Figure 1.

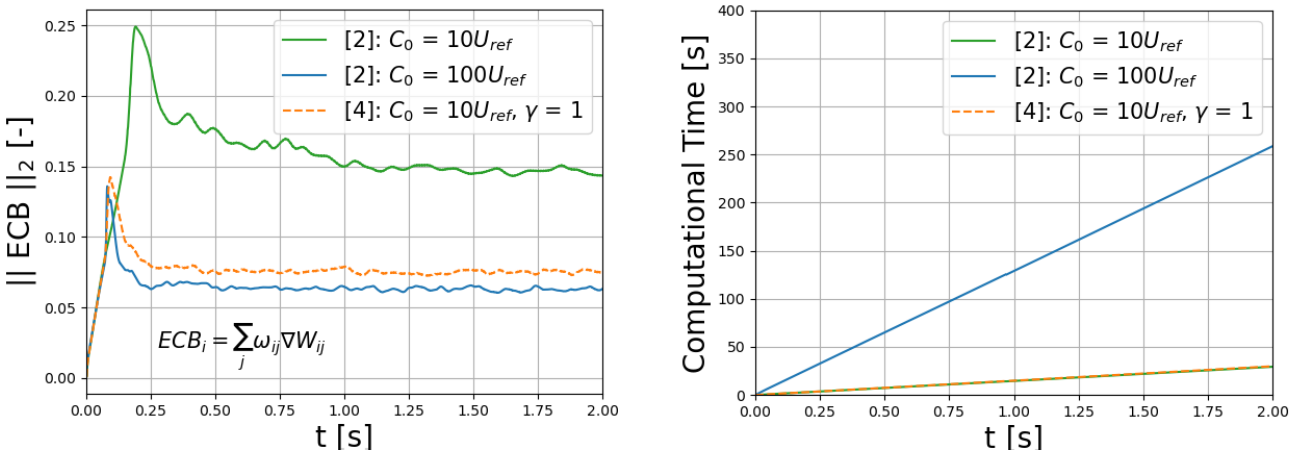

Figure 1. TGV simulations. $ECB\ L_2$ norm (left). Computational time (right) Note: computational time for simulations with same c_0 are almost coincident and overlapped in figure.

3 CONCLUSIONS

In the present work a novel formulation for the transport velocity $\boldsymbol{v}_0$ of ALE-SPH schemes has been proposed and tested for the inviscid Taylor Green flow in which the particles, following counter-rotating trajectories, tend to create hole or cluster in the domain. Ensuring a uniform particle concentration is necessary to guarantee the accuracy of the SPH spatial interpolations in the continuity and momentum equations. The formulation herein proposed guarantees a constant particle concentration, as observed with $ECB\ L_2$ norm (Figure 1 (left)) without introducing any additional computational cost (Figure 1 (right)).

REFERENCES

Gingold, R.A. & Monaghan, J. J. (1977). Smoothed particle hydrodynamics: theory and application to non-spherical stars. Monthly notices of the royal astronomical society, 181(3):375-389.

Lind, S., Xu, R., Stansby, P. & Rogers, B. D. (2012). Incompressible smoothed particle hydrodynamics for free-surface flows.. Journal of Computational Physics, 231(4), 1499-1523.

Monaghan, J.J. (1994) Simulating free surface flows with SPH. Journal of Computational Physics,110, 399-406.

Neuhauser, M. (2014). Development of a coupled SPH-ALE/Finite Volume method for the simulation of transient flows in hydraulic machines. PhD thesis, Ecole centrale de Lyon (France).

Oger, G. et al (2016). SPH accuracy improvement through the combination of a quasi-Lagrangian shifting transport velocity and consistent ALE formalisms. Journal of Computational Physics, 313, 76-98.

Vila, J. (1999). On particle weighted methods and smooth particle hydrodynamics. Mathematical models and methods in applied sciences, 9(02), 161-209.

IAHR YPN

Young Professionals Network

Hosted by
Spain Water and IWHR, China

IAHR AIRH

International Association for Hydro-Environment Engineering and Research

Hosted by
Spain Water and IWHR, China

IAHR Madrid Secretariat

Paseo Bajo Virgen del Puerto 3. 28005, Madrid, SPAIN

Tel: +34 913357908

IAHR Beijing Secretariat

A-1 Fuxing Road, Haidian District, 100038, Beijing, CHINA

Tel: +86 1068781808